THE EFFECTS OF FUTURE EXTREME PRECIPITATION EVENTS ON STREAM HYDROLOGY AND HYDRAULICS OF STREAM CROSSING STRUCTURES

BY

DANIEL R. GAMBILL

DISSERTATION

Submitted in partial fulfillment of the requirements
for the degree of Doctor of Philosophy in Agricultural and Biological Engineering
in the Graduate College of the
University of Illinois at Urbana-Champaign, 2016

Urbana, Illinois

Doctoral Committee:

Professor Prasanta K. Kalita, Chair
Professor Richard A. Cooke
Research Associate Professor Momcilo Markus
Assistant Professor Rabin Bhattarai
Wade Wall, PhD

Abstract

Army field training exercises are conducted to replicate real-world combat requirements and are inherently subject to the effects of the prevailing climate and weather conditions. Adapting to variability of climate is part of realistic training and extreme storm events and associated flooding risks can temporarily limit access to training lands and other training features such as water crossings. If an increase in intensity and incidence of extreme precipitation events is realized, installations associated with river systems are likely to have increased flood risk and associated prevention and mitigation costs. Low water crossings (LWCs) are especially susceptible to changes in intensity and incidence of extreme precipitation events with regards to infrastructure usability, resilience, and safety. The June 2, 2016 incident at Fort Hood, TX where five soldiers from the 3rd Battalion, 16th Field Artillery Regiment, 2nd Armored Brigade Combat Team, 1st Cavalry Division drowned when their troop carrier overturned at a flooded LWC, shows the safety risks associated with LWCs.

The first objective of this study is to examine the stationary assumption of total annual precipitation, total annual wet days and wet hours, and regional frequency analysis for a range of design storms and extreme events. Both parametric and non-parametric statistical tests were used to detect trends. In addition, precipitation frequency estimates were calculated for the 0.5-, 1-, 2-, 5-, 10-, 25-, 50-, and 100-year Annual Return Interval (ARIs) and durations of 1-, 2-, 3-, 6-, 12-, and 24-hr; and 2-, 5-, and 10-days for three different time periods 1970-1989, 1980-1999, and 1990-2009. The results suggest the assumption that precipitation is stationary over time with regards to total annual rainfall and storm frequency is not valid for the three Midwest regions, Central Indiana, East Central Illinois, and Central Michigan.

The second objective is to analyze projected precipitation data from four climate models with regards to total annual precipitation, total annual wet days and wet hours, and regional frequency analysis for a range of design storms and extreme events and compare findings to analyses of historic precipitation data. Four dynamically downscaled CMIP5 global climate models were bias corrected using quantile mapping. The average projected (2080-2099) design storm of the four climate modeols across all locations, durations, and return periods is larger than the corresponding observed design storm and usually significantly larger based on the standard deviation of the model results, especially for return periods greater than 1 year. The four models provided bias-corrected precipitation output that agreed in general trends, however, the precise levels of precipitation increases varied substantially, especially for the 2040-2059 projected timeframe.

The third objective is to apply projected climate model precipitation to hydrologic models to determine projected stream flow characteristics and compare to current stream flow characteristics. The result indicate increases in peak flood events across all return periods for the projected timeframes compared to observed conditions. In Indiana and Michigan the projected (2080-2099) peak flow events are larger than the projected (2040-2059) peak flows while in Illinois the projected (2080-2099) peak flow events are larger than or equal to the former events. Analysis of the number of days projected stream flow exceeds the 0.5-, 1-, and 10-yr design flows during the 20-yr simulation showed a wide range of results between the two models representing the upper and lower bounds of maximum precipitation estimates for a majority of return periods for each projected timeframe at each location. Generally there was an increase in exceedances during the projected timeframes compared to current conditions, but on a yearly average basis the increase were minimal.

The fourth objective is to route projected design flow and continuous stream flow hydrographs through hydraulic models to determine usability and sustainability of current structures and feasibility of alternative designs for projected flow regimes. The results indicate the riverine crossing structures considered for this study are projected to see an increase in the magnitude and frequency of high flow events by the end of this century. The projected (2080-2099) 10-yr event is on the order of the present 50-yr (sometimes 25-yr or 100-yr) event for many of the studied streams, suggesting possible future conditions should be considered when designing new infrastructure. Unfortunately the uncertainty inherent in the climate modeling makes it difficult to develop specific recommendations on how to revise current LWC design criteria with regards to climate change in the study regions. The continuous model simulations and projections proved to underestimate average yearly flow durations for small flow events with very frequent return periods. Special care must be taken when using and applying frequent events from dynamically downscaled climate model precipitation data. An investigation into the timing and intensity of very frequent observed and simulated precipitation events could be needed before applying similar climate model data to hydrologic and hydraulic models.

Overall, they study showed that the riverine crossing structures considered for this study are projected to see an increase in the magnitude and frequency of high flow events by the end of this century. The changes in hydrologic flows were constant with changes in projected precipitation. The four climate models provided bias-corrected precipitation output that agreed in general trends but the precise levels of precipitation increases varied substantially, especially for the 2040-2059 projected timeframe.
In addition, watershed specific variables, such as those found in Michigan, can add a great deal of uncertainty to modeling results. The projected increases in precipitation and subsequent changes in peak flood events are large enough that corresponding impacts on stormwater infrastructure design

should be considered, however, the uncertainty of the future projections makes it difficult to develop specific design recommendations.

Acknowledgements

I would like to thank everyone who has offered support, guidance, and words of encouragement to me during the duration of my doctoral work. Your assistance played an important role in my completion of this study.

I would like to express gratitude to my advisor, Dr. Prasanta Kalita, for allowing me to pursue this project under his guidance. He is a pleasure to work with and learn from and his guidance has been appreciated since by freshman year of college.

I want to thank Dr. Momcilo Markus for his direction with regards to this project and other projects at the Illinois State Water Survey. His input and help was truly appreciated. Thank you. Thanks also to Dr. Wade Wall for his willingness to collaborate with me on this project and others at the USACE ERDC-CERL.

I also want to thank my committee members Dr. Richard Cooke and Dr. Rabin Bhattarai, for taking time to review my dissertation and provide suggestions and comments for improvement.

A special thanks to Heidi Howard at ERDC-CERL for employing me as a grad student when I was working on my master's degree and encouraging me eight years later to work at CERL fulltime. I couldn't have finished this work without those opportunities. I sincerely appreciate it.

Thanks to Emily Jenkins for deciding that working on a doctorate degree wasn't completely ridiculous and partnering with me on numerous class projects. Thanks to Greg Byard, Chen Zhang, and Sudip Gautam for technical help with various models and coding.

A tremendous amount of gratitude goes to my mom, Vicki Allen, for teaching me that life is a result of the choices you make, so I always try to make the best ones. Also thanks to Chris Wise and Dixie and Steve Packard for their encouragement… and for helping with Steven.

I would like to give a special thanks to my wife, Donna, for supporting me during this process. You make this crazy, busy life a pleasure. I can't imagine being on this adventure without you by my side. And thanks goes to my son, Steven, for putting up with his parents' being continuously students for all of his life. You two are why I work hard and play hard.

Dedication

To Donna, my love

To Steven, my treasure

Table of Contents

Chapter 1 – INTRODUCTION

1.1 Background

The job of the Department of Defense (DOD) is to defend the country and protect its interests. To meet this goal, the DOD trains and deploys all branches of the armed forces to meet and resist any threat. Maintaining a high level of efficiency and readiness is required for the US Army to complete its mission. To this end, US Army continually undergoes realistic and effective training on military installations around the United States and the World. For the specific case of the United States Department of the Army, there are 11 million acres of land in active use (OUSD, 2014). Effectively moving soldiers and heavy vehicles and equipment across maneuver lands is essential to military training (Samples et al., 1998). Stream crossings, specifically, low water crossings (LWCs), are present within military training lands at any location where unimproved roads and trails intersect the stream network and stream size is small enough to permit the use of such a fording structure. Maneuver areas, tank trails, and range course roads are all examples where LWCs are suitable (USACE, 2006a). A low water crossing (LWC) is any crossing used as a means to traverse an intermittent or low flowing perennial stream and is designed so that its hydraulic capacity is insufficient one or more times during a year of normal rainfall (Carstens and Woo, 1981). The many different LWC designs are divided into three main groups: unvented fords, vented fords, and low-water bridge (USACE, 2011).

While providing high quality and realistic training is the top priority, maintaining long-term training sustainability requires environmental stewardship. Army Regulation 200-1 (Dept. of the Army, 1997) states that the Army must execute an environmental policy that: 1) focuses efforts on pollution prevention where and when possible to reduce or eliminate pollution at the source, 2) conserve and preserve natural and cultural resources so they will be available for present and future generation to

use, 3) give priority to sustained compliance with all applicable environmental laws, and 4) continue to restore previously contaminated sites deemed as a threat to human health and the environment. While movement throughout a military installation is paramount, training access needs must be balanced to offset erosion and habitat impact. Because military vehicles can access locations typically unsuited to LWCs, it is common for these fords to occur in sub-optimal locations within the stream system (USACE, 2011). Issues stemming from LWCs (erosion, aggregation, ponding, scour, etc.) can disrupt stream equilibrium, cause water quality problems, and lead to potential infrastructure failure and safety concerns. Beyond environmental costs, reduced training access, the need for ongoing maintenance, and potential safety issues present negative monetary and mission impacts (USACE, 2011). By improving crossing design and implementation, both the military maneuvers and the ecosystem can function more successfully.

Beyond environmental and mission threats due to stream-crossing infrastructure in the near-term, the DOD is beginning to consider the threats created by climate change. Executive Order No. 13,514 (2009) required agencies to evaluate climate change risks and vulnerabilities to manage the effects of climate change on the agency's operations and mission in both the short and long term. Executive Order No. 13,653 (2013) required agencies to modernize federal programs to support climate resilient investment and manage lands and waters for climate preparedness and resilience. As a result, the US Army Corps of Engineers (USACE) began working on climate change preparedness and resilience in all activities to help enhance the resilience of built and natural water-resource infrastructure and the effectiveness of its military support mission, and to reduce potential vulnerabilities to the effects of climate change and variability (USACE, 2014). USACE is working on climate preparedness and resilience by focusing on infrastructure resilience, vulnerability assessments, risk-informed decision-making for climate change,

and developing new policy and guidance to support adaptation implementation based on the best available and actionable science. Of specific note is the issue of stationarity, or the assumption that the statistical characteristics of hydrologic time series data are constant through time, which enables the use of well-accepted, simplified statistical methods in water resources planning and design. Climate change has shown this assumption to be invalid (USACE, 2014).

Field training exercises are conducted to replicate real-world combat requirements and are inherently subject to the effects of the prevailing climate and weather conditions (OUSD, 2013). Adapting to variability of climate is part of realistic training and extreme storm events and associated flooding risks can temporarily limit access to training lands and other training features such as water crossings (USACE, 2013). If an increase in intensity and incidence of extreme precipitation events is realized, installations associated with river systems (which are most Midwest installations) are likely to have increased flood risk and associated prevention and mitigation costs. LWCs are especially susceptible to changes in to intensity and incidence of extreme precipitation events with regards to infrastructure usability, resilience, and safety. The June 2, 2016 incident at Fort Hood, TX where five soldiers from the 3rd Battalion, 16th Field Artillery Regiment, 2nd Armored Brigade Combat Team, 1st Cavalry Division drowned when their troop carrier overturned at a flooded LWC, shows the safety risks associated with LWCs.

This project aims to determine if the assumption of stationarity with regards to historical precipitation records is valid at Camp Atterbury Joint Maneuver Training Center near Edinburg, Indiana; Camp Grayling Joint Maneuver Training Center near Grayling, Michigan; and Edger County in east central Illinois. Future precipitation will also be projected based on climate change models and compared to

historical trends. Climate model simulations have an inherent amount of uncertainty in the results, due to the limitations of the physics of numerical modeling, in the spatial and temporal resolution, and in the details of phenomena that interact in complex ways, such as clouds, radiation, ecosystems, and carbon absorption (IPCC, 2000). As a result, each climate model produces different simulations of present and future climate, but there are some consistent features in the climate projections across most models, suggesting greater confidence in these features: the large-scale temperature increase across the U.S., the decrease in precipitation (mostly in summer) in the southwest U.S., and the increase in precipitation in the northern tier of U.S. (west, central, and north) (IPCC, 2000). This project will analyze four climate models due to the uncertainty of associated with the projected precipitation of each. The projected precipitation will be applied to hydrologic and hydraulic models to determine the effects of projected stream flow events on the usability and sustainability of existing LWCs at the three locations and to determine future design implications.

1.2 Objective and Scope of Research

The hypothesis of this project is: Climate models can be useful in the assessment of existing low water crossing structures and design of alternative structures with regards to a changing environment.

Overall objective: Determine if, and to what degree, regional climate model precipitation projections can be used as inputs to stream hydrologic models to determine subsequent impacts at stream crossing structures.

Specific objectives:

1) Examine trends in historic precipitation data with regards to total annual precipitation, total annual wet days and wet hours, and regional frequency analysis for a range of design storms and extreme events (Chapter 4).
2) Bias correct and analyze projected precipitation data from four climate models with regards to total annual precipitation, total annual wet days and wet hours, and regional frequency analysis for a range of design storms and extreme events and compare findings to analyses of historic precipitation data (Chapter 5).
3) Apply projected climate model precipitation to hydrologic models to determine projected first-order stream flow characteristics and compare to current stream flow characteristics (Chapter 6).
4) Route projected design flow and continuous stream flow hydrographs through hydraulic models to determine usability and sustainability of current structures and feasibility of alternative designs for projected flow regimes (Chapter 7).

1.3 Organization of Dissertation

The format of this paper encompasses four stand-alone papers as individual chapters (Chapters 4, 5, 6, and 7). Each chapter addresses one specific objective, as indicated in the above list. A final summary of all objectives and proposed next steps are incorporated as the final chapter (Chapter 8) of this paper. Chapters 2 and 3 include a review of literature and detail study site specifics, respectively.

Chapter 2 – LITERATURE REVIEW

2.1 Low Water Crossings

2.1.1 Low Water Crossing Types

A low water crossing (LWC) is a term used to describe any crossing used as a means to traverse an intermittent or low flowing perennial stream and is designed so that its hydraulic capacity is insufficient one or more times during a year of normal rainfall (Carstens and Woo, 1981). The many different LWC designs are divided into three main groups: unvented fords, vented fords, and low-water bridge (Figure 2.1) (USACE, 2011). Unvented fords are usually located on ephemeral streams (streams with temporary flow during or after a precipitation event) or streams with shallow base flows that are safe to drive through. Fords can be unimproved (simple) or improved (hardened). Simple fords are unprotected, requiring the vehicle to drive on the natural channel bottom and are most frequently found on ephemeral and low-flowing streams with rock, gravel, or sand stream bottoms (USACE, 2011). Hardened LWCs have a stable driving surface of rock, concrete, asphalt, concrete blocks, concrete planks, gabions, geocells, or a combination of materials. On some structures, a small channel is included at the structure's low point to pass low flows or aquatic animals (USDA, 2006).

Vented crossings have a driving surface elevated above the channel bottom with culverts (vents) that allow low flows to pass beneath, keeping vehicles out of the water during low flow (USDA, 2006). Culverts utilized can included any number, combination, and size of corrugated or concrete pipe, concrete boxes, or corrugated or concrete open-bottom arches (USACE, 2011). The total vented area is determined by design requirements and stream flow characteristics of a given site and defined by the vent-area ratio (VAR). A low VAR refers to a small vented area relative to bankfull channel area while high VAR refers to a vented area equal to or greater than bankfull channel area (USDA, 2006). Leopold

et al. (1964) defines bankfull flow as that flow that just overtops the streambanks and begins to flow out over the floodplain.

Low-water bridges are defined as open-bottom structures with elevated desks and a total span of at least 20 feet (USDA, 2006). They may include one or more piers with abutments and are structurally very similar to other bridges except they are built lower. Low-water bridges generally have greater capacity and are able to pass higher flows underneath the driving surface than most vented fords, however, they are designed and installed with the expectation they will be under water at higher flows (USACE , 2011).

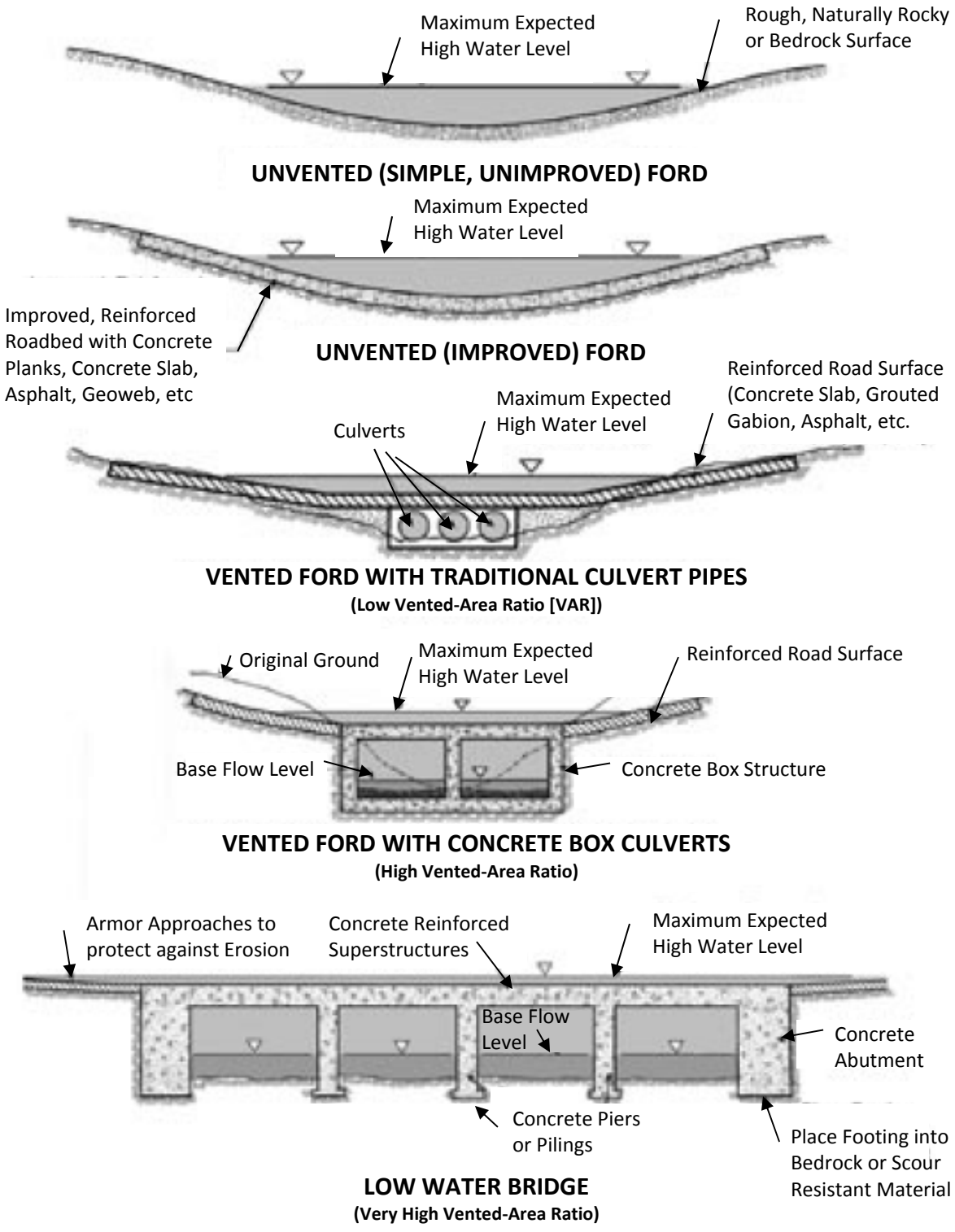

Figure 2.1. Types of common LWCs (from USDA, 2006).

2.1.2 Low Water Crossing Design Considerations

Choosing the type of structure for any crossing is highly site-dependent (Sample et al., 1998). In general, regardless of site specifics, the main advantages of low-water crossings over culverts and bridges may include the following: lower construction and maintenance costs; less channel and flood plain blockage; less susceptible to failure during high flow events (USDA, 2006). Each type of LWC provides possible benefits and introduces potential liabilities, as discussed in more detail below. Low-water crossings are generally less expensive to construct, designs are less complicated, construction is quicker, and fewer materials are involved than for a traditional culvert or bridge crossing, especially regarding unvented fords (USACE, 2011). Although the initial cost of more complex low-water crossings may exceed those of simple culvert installations, the lower long-term maintenance and repair costs may still make selecting a complex low-water crossing more economical (USDA, 2006).

Though LWCs afford an economical alternative to the replacement of a bridge with another bridge in many instances, the potential liability that might be incurred from the use of LWCs has served as a deterrent to their use (Carstens and Woo, 1981). For example, it only takes about 0.61 m (2 ft) of water to float most cars and, in some cases, less (Balke et al., 2011). Where the current is swift, the bottom hard and smooth, and the car's body low to the ground, as little as 0.3 m (1 ft) of water with a speed of 9.7 kpm (6 mph) will move most cars. Part of the reason why some drivers enter flooded roadway sections is that they have trouble judging the speed and depth of the water. Static warning signs on the approach to a LWC, markers along the edge of hardened surfaces, and water depth gauges are required for the safety of those using a crossing (USACE , 2011; Balke et al., 2011; Lohnes et al., 2001);

Additional environmental liabilities must also be considered when contemplating the use of LWCs. Unvented ford crossings are the most inexpensive, but not necessarily the safest or most

environmentally friendly for the stream if the traffic load surpasses the load the crossing is capable of handling (USACE , 2011). Brown (1994) determined that sediment is contributed to the river at simple LWCs by five major processes: 1) the creation of wheel ruts and concentration of surface runoff, 2) the existence of tracks and exposed surfaces, 3) the compaction and subsequent reduction in the infiltration rate of soils leading to increased surface runoff, 4) backwash from the vehicle, and 5) undercutting of banks by bow wave action. Fords, especially simple, unhardened crossings, are prone to runoff and gullies at the ingress and egress of the crossing. As heavy vehicles (tanks, trucks) ford streams, they can contribute greatly to area streambank erosion and area soil erosion due to excessive vegetation loss and soil disturbance (USACE, 2006a; USACE, 2011). Kidd et al. (2014) studied multiple use trail (hiking, mountain biking, and horseback riding) LWCs and found downstream changes in macroinvertebrate-based indices indicated water quality was lower downstream from crossings than in upstream reference reaches. Also, recreational stream crossing approaches have the potential to deliver sediment into adjacent streams, particularly where best management practices (BMPs) are not being implemented. Some solutions to these issues have been studied.

USACE (2006) stressed that improving streambank stabilization techniques and improving low-water ford substrate materials would enhance LWC longevity and reduce nearby erosion. Wang et al. (2013) determined that most of the sediment that enters streams following road construction is from the stream crossings and approaches to the crossings. When approach fill slopes became re-vegetated, they stabilize, and annualized sediment loads decline, however, sediment exports remained above pre-disturbance levels. Wear et al. (2013) showed varies stream crossing best management practice treatment could effectively reduce erosion and total suspended sediment loads near LWCs.

Field studies of hardened LWCs have proven that, when implemented properly, these crossings maintain stream water quality, reduce stream habitat fragmentation, and decrease maintenance outlays over the unimproved fords (Sample et al., 1998; USACE, 2006a). Brown et al. (2013) found LWC approaches or the section of road immediately adjacent to the stream crossing, represented primary sources and nearly direct pathways for sediment delivery to stream channels. Annual sediment delivery rates from bare approaches were 7.5 times higher than those from gravel (hardened) approaches. The findings suggested that corrective best management practices such as hardening and appropriate spacing of water control structures can reduce sediment delivery to streams.

Hardened LWCs are susceptible to scouring on the approaches and the downstream edge of the crossing, especially when perched above the channel bottom (USACE, 2011). Also, the hardened fords should be built so as not to narrow the main flow channel, causing flow velocities to increase. USGS (2002) studied the potential effects on stream habitat, water quality, and periphyton at hardened (cable-concrete) LWCs at the Fort Polk Military Reservation, Louisiana. Little change between crossing sites and natural reaches were observed for properly construction crossings. In this case, properly constructed crossings were crossing built flush with the channel bottom and protected from scour. Additional design elements will be discussed in the follow selection. Geomorphic channel units at the properly hardened LWCs were similar to those observed at the upstream and downstream reaches. The height and grade of the LWCs allowed movement of sand, silt, and gravel in the crossings, similar to bed sediment movement observed in the upstream and downstream reaches. However, improperly constructed (perched) crossings caused restricted flow and an increase in velocity across the hardened crossing, an increase in depth at the upstream end of the reach, and dissolution of the carbonate foundation material. USGS (2007), a follow up to the Fort Polk study, confirmed that average water-

quality values and sediment concentrations were similar upstream and downstream of the properly installed established hardened (cable-concrete) fords.

Furthermore, Malinga (2007) assessed the impact of simple LWCs on stream stability at Fort Riley, Kansas and found that poorly located stream crossings can alter the direction of stream flow, causing bank erosion on areas immediately below stream crossings while backwater pools upstream of the fords acted as sinks for sediment, which disrupted transport of sediment to the downstream reaches of the stream. In addition, there is a need to constantly modify simple LWCs relative to the level of stream instability at the site and such crossing can contribute to further stream geomorphological instability. USDA (2006) and Castro (2003) suggested vented LWCs can function as grade-control structures in situations where a headcut is moving upstream, controlling stream instability. Vented LWCs also keep vehicle tires dry during base flow conditions, keeping soils and other pollutants from vehicles from entering the stream (USACE, 2011). Hardened, elevated approaches also prevent erosion down them. Unfortunately, heavy military vehicles can crush any exposed culvert ends, requiring ongoing maintenance. Also, vented LWCs can cause the stream to lose its natural hydrological properties and culverts can clog from debris or sediment, which is less prone to occur at fords (USACE, 2011).

Additionally, Bouska et al. (2014) found stream crossings may alter the form and function of stream ecosystems and habitat and prohibit the movement of aquatic organisms. The geomorphic response of streams at vented fords (concrete slabs with one or more culverts) as Fork Riley, KS included: mean riffle spacing upstream of the LWCs was double that of downstream reaches, greater deposition of fine sediments occurred directly upstream, and incised channels downstream. The vented fords also slowed or blocked the transportation of water, sediments, and debris downstream during bankfull flows. Lane

and Sheridan (2002) determined there was a statistically significant difference in turbidity and total suspended solids downstream of unsealed vented crossings during baseflow conditions, but the quality of the water column remained good during non-rain periods. Rainfall events led to decreases in water quality downstream of the crossing and principal sediment sources were the fillslope that contributed coarse bedload material through rill erosion and unprotected toe scour.

Low water bridges are also susceptible to clogging and they can be more expensive to design and build (USACE, 2011). For example, the US Forest Service requires that all low water bridges receive specific hydrologic, hydraulic, structural, and foundation design in accordance with latest version of the American Association of State Highway Transportation Officials (AASHTO) Standard Specifications for Highway Bridges (USDA, 2006). However, low water bridges have an elevated driving surface, maintain a more natural streambed, allow more natural sediment and aquatic organism movement than culverts, and are the best LWC type for fish passage (USDA, 2006).

Warren and Pardew (1998) assessed movement for 21 fish species in seven families through culvert, slab, open-box, and ford crossings and through natural reaches and found that overall fish movement was an order of magnitude lower through culverts than through other crossings or natural reaches. Bouska and Paukert (2010) looked at fish passage at five concrete box culverts and five low-water crossings (concrete slabs vented by culverts) as well as 10 control sites (below a natural riffle) and found culverts to be barriers to fish movement. Changes in stream hydrology and velocity occur when the geometry of the stream is altered, such as when it is funneled through a culvert, which inhibits the movement and may prevent the establishment of many fish and invertebrates species (Cocchiglia et al., 2012). The degree to which aquatic organism passage is hindered is likely due in large part to the design, geometry, and condition of the low water crossings and negative effects of road crossings are

minimized if they mimic the form and function of the adjacent stream. (Bouska and Paukert, 2010; Cocchliglia et al., 2012). Fords sometimes included slots or small channel to allow aquatic organism passage during very low flows and generally provide little hindrance to organism passage if they mimic the form of the reach (USACE, 2011; USDA, 2006).

2.1.3 Low Water Crossing Design Guidelines

Allowing for the liabilities and design considerations of LWCs given above, the design guidelines for site selection, hydrology, hydraulics, and protection are provided. LWCs are generally appropriate at sites that are stable, the proposed design matches channel geometry and bed material, and flow characteristics conform to safety and usage/access requirements. Traffic load, traffic speed, detour length, debris load, channel conditions, and flow variability, duration, and frequency should all also be considered during LWC site selection (USDA, 2006). Table 2.1 provides quantitative site selection criteria from a survey of transportation engineers from several different states.

Table 2.1. LWC site selection transportation criteria (from Motayed et al., 1983)

Criteria	Most favorable for LWC	Least favorable for LWC
Average daily traffic (ADT)	Less than 5 vehicles/day	More than 200 vehicles/day
Average annual flooding	Less than 2 times/year	More than 10 times/year
Average duration of traffic interruption per occurrence	Less than 24 hours	More than 3 days
Extra travel time for alternate route	Less than 1 hour	More than 2 hours
Possibility of danger to human life	Less than 1 in 1 billion	More than 1 in 100,000
Property damage	None	1 million dollars
Frequency of use as an emergency route	None	Once/month

A partial list of key design elements for LWCs include (USDA, 2006):

- Do not cause significant aggradation in the channel upstream of the structure, or degradation or downcutting downstream of the structure.
- Do not confine or narrow the normal (bankfull) flows.
- Do not increase the natural stream channel velocity.
- Accommodate major flood flows without significant drops in the water surface profile.
- Align structures perpendicular to the stream channel.
- Maintain natural streambed substrate material, roughness, slope, and form through all or part of the structure (when possible).
- Straight reach and LWC alignments.

Design constraints for LWC design and construction are provided in Table 2.2 and Table 2.3.

Table 2.2. General design constraints for all LWC (Lohnes et al., 2001)

Considerations	Criteria
Overtopping flow depth	Less than or equal to 6 inches during Design Discharge
Vertical curve at dip (approach grades)	Less than 10%
Stream bank height	Less than 12 ft.
Orientation of Structure	Straight, avoid skew
Approach Distance	750 ft. minimum sight distance for warning signs
Height of crossing above streambed	Less than 4 ft.
Erosion from flows overtopping crossing	Elevation difference between crossing and streambed kept to minimum. LWC surface material extended in both directions away from structure. Downstream slope 4:1 or middleer.
Core material protection	Provide cutoff walls and sidewalls
Stream bank protection	Establish vegetation

Table 2.3. Design constraints for specific LWC (Lohnes et al., 2001)

Considerations	Criteria
Unvented ford design considerations	
Precast concrete panels	Should include a proper filter to prevent piping and consequent undermining of the crossing.
Erosion protection	End walls and/or gabion protection may be desirable; wide, sloped shoulders downstream may be helpful
Markers	Provide markers to help drivers spot the limits of the roadway when flooded
Vented ford design considerations	
Depth of cover above pipes	Minimum 1 ft recommended.
Exit velocity of pipes (vents)	Limit exit velocity of the flow not to exceed 10 ft/s.
Pipes	Pipes should be anchored in the ground; both ends beveled or mitered to reduce debris accumulation. Minimum size 1-ft diameter.
Guard rails	Guard rails are not recommended to avoid catching debris and floating materials during a flood.
High streamflow	Road surface is raised above streambed to accommodate the flow.
Streambed erosion protection	Riprap placed upstream and downstream to reduce the scour in erodible channel.
Low water bridge design considerations	
Surface	Decks must be heavy to withstand drag, uplift and lateral forces due to overflow and upstream water; upstream and downstream edges should be rounded
Height of piers	To reduce the risk of overturning, the height of piers should be limited to approximately 10 ft

Two methods have been used to determine the hydrologic design of LWCs. Lohnes et al. (2001) used flow-duration curves for Iowa to estimate the amount of time a LWC would be closed during an average year. A flow-duration curve is a cumulative frequency curve that show the percent of time specified discharges were equaled or exceeded during a given period (USGS, 1959). A LWC is closed when a design discharge, Q_e, is equaled or exceeded and results in LWC overtopping by more than 6 inches. The acceptable closing percent of time per year (e) is called the design exceedence probability (Lohnes et al., 2001). The State of Iowa applies an exceedence probability of 2% or about 7 days (McDonald and

Anderson-Wilk, 2003). This method enables crossing to be designed so that they are closed, on average, a certain number of days per year.

The second method, and the method used to design most standard stream crossings, uses a flood-frequency analysis, which identifies the probability of exceeding different peak flow levels, but does not estimate the timeframe the road may be closed during inundation (USDA, 2006). The design discharge is typically defined by the return period. The return period can be expressed as the expected recurrence interval such as the 1-yr or 5-yr events. The 1-yr event is expected to be exceeded, on average, once a year while the 5-yr event is expected to be exceeded, on average, once every 5 years, and has a 20-percent chance of occurring in any single year. The US Forest Service suggests using a recurrence interval of 0.5-yr to 2-yr to design LWCs with regards to vehicle usage and safely requirements and a recurrence interval of 50-yr to 100-yr for scour protection (USDA, 2006). Barnard et al. (2013) states acceptable conditions for fish passage must be satisfied 90 percent of the time so the 10-percent exceedance flow (10-year event) should be considered for LWC design with regards to aquatic passage. Common design flow estimation methods for LWC design include regional regression analysis (eg. Soong, 2004), gauge data analysis (eg. USWRC, 1981), and rainfall-runoff modeling (also called design storm approach). Rainfall-runoff modeling often uses hydrologic software packages such as HEC-HMS, to facilitate complex calculations (USACE, 2000).

Hydraulic modeling methods for LWC design are selected based on the type of LWC to be designed. Manning's equation is often used for fords flush to the channel bottom while perched fords are treated at broad crested weirs, in order to determine flow depth, flow velocity, etc for a given design flow . (Lohnes et al., 2001). Vented fords are typically analyzed as culvert structures with weir flow over the

road as required (eg. FHWA, 2012b). The hydraulic design and analysis of low water bridges is the same for all other bridges, with special consideration given to overtopping flows (eg. FHWA, 2012c). As noted previously, scour at and near LWCs can cause structural failure, safely concerns, and degrade water quality and habitat (USACE, 2006b). All LWC designs should incorporate consideration and design guidelines for scour (FHWA, 2012a), stream stability (FHWA, 2012d), and appropriate scour countermeasures (FHWA, 2009).

Numerous hydraulic models are available for modeling bridges and LWCs and include 1-dimentional, 2-dimentioanl, and 3-dimentional modeling with steady and/or unsteady flow regimes. FHWA (2012c) provides an extensive review of the differences between the various types of numerical modeling approaches. Most bridge hydraulic studies use 1-D analysis methods though 2-D models are becoming common and 3-D models are used to analyze complex flow fields. 1-D models are best suited for in-channel flows and when floodplain flows are minor. They are also frequently applicable to small streams and for extreme flood conditions, 1-D models generally provide accurate results for narrow to moderate floodplain widths. They can also be used for wide floodplains when the degree of bridge constriction is small and the floodplain vegetation is not highly variable. In general, where lateral velocities are small one-dimensional models provide reasonable results. The HEC-RAS model (USACE, 2010) is the most widely used 1-D model in the US (Zevenbergen et al., 2012). Leahy (2014) used HEC-RAS to model LWCs at a US Army Installation in Indiana. Two-dimensional models should be used when flow patterns are complex and 1-D model assumptions are significantly violated, however, data requirements are much higher. Examples of 2-D models include FST2DH (FHWA 2003) and RMA-2 (USACE 2009).

2.2 Climate Change

2.2.1 Historical Trends in Precipitation

Historical records indicate the frequency and intensity of heavy precipitation events have likely increased in certain regions of the world (IPCC, 2014). Groisman et al. (2005) observed increase in the number and intensity of large precipitation events (the upper 0.3% of daily precipitation events) around the world. For North America, Melillo et al. (2014) and Karl and Knight (1998) found that since 1900 average annual precipitation over the U.S. has increased by roughly 5% to 10%. There are important regional differences. For instance, the amount of rain falling in very heavy precipitation events has been significantly above average since 1991 (relative to 1901-1960) in the Northeast, Midwest, and southern Great Plains, while much of the Southeast and Southwest had a mix of areas of increases and decreases (Melillo et al., 2014).

Groisman et al. (2012) looked at changes in precipitation in the Midwest and Central Plains and found little change in the number of storms between 12.7 to 25.4 mm (½ to 1 inches). However, the frequency of heavy storms (25.4 to 76.2 mm [1 to 3 inches]), very heavy storms (76.2 or more mm [3 or more inches]), and extreme precipitation (more than 152.4 mm [more than 6 inches]) increased. Also, the extreme precipitation events increased by as much as 40% during the second half of the study period (1979-2009) compared to the first half of the study period (1948-78). Madsen and Figdor (2007) and Pryor et al. (2009) also found increases in the intensity of larger events in the Northeast and Midwest, respectively. IDNR (2015) reported that the statewide Illinois average precipitation has increased from 36 to 40 inches or 10% over the last century.

It is important to note that the increase in precipitation discussed above reflects, in part, the major droughts of the 1930s and 1950s, which made the early half of the record drier (Groisman et al., 2005). Kunkel et al. (1999) explained that there were lengthy periods of a below-average number of events in the 1930s and 1950s and an above-average number of events in the early 1940s, early 1980s, and 1990s. Also, for the Midwest, there is evidence of significant variability on the timescale of a century and attribution of the cause of the recent upward trend in precipitation should consider potential natural forcing factors that may make a significant contribution. There is no implication in these results that the upward trends will necessarily continue; however, evidence from some studies suggests that the most recent 5 to 15 years are the best predictor of conditions for the next 1 to 5 years, so current trends are likely to continue at least in the short term (Easterling, Angel, & Kirsch, 1990).

2.2.2 Changes in Design Storms

Design storm events are typically defined by rainfall duration, total rainfall amount, and temporal distribution of rainfall, in addition to the return period, and are conveyed as intensity-duration-frequency (IDF) curves (IDNR, 2015). IDF curves are based on statistical analyses of long-term rain gauge data. Though several data sets predate it, the National Weather Service's "Technical Paper No. 40" (TP-40) was a widely used rainfall intensity-duration data set (Hershfield, 1961). The rain gauge records spanned 1938-1958 and covered the continental United States. Updated rainfall intensity-duration estimates have been published by the National Oceanic and Atmospheric Administration's "Atlas 14: Precipitation-Frequency Atlas of the United States" (eg. Bonnin et al., 2006 & Perica et al., 2013). The rain gauge records spanned 1891-2010 and covered most the continental United States except the Northeast, Northwest, and Texas. Other rainfall intensity duration data sources include "Bulletin 70" (Huff and Angel, 1989), "Bulletin 71" (Huff and Angel, 1992), and "Hydro 35" (Frederick et al., 1977) which cover Illinois, the Midwest, and the Eastern United States, respectively.

Since rainfall intensity-duration estimates are based on gauge data, the length and time period from which the data was obtained can greatly affect results (Kunkel et al., 2003; INDR, 2015). For example, Huff and Angel (1989) found a general increase from 1901-1940 to 1941-1981 in Illinois of the 24-hr and 48-hr maximum rainfall amounts for recurrence intervals of 2, 5, 10, and 25 yrs. Huff and Angel (1992) extended the analysis to Indiana, Iowa, Kentucky, Michigan, Minnesota, Missouri, Ohio, and Wisconsin and found a general increase in rainfall amounts for the later time period, except for Wisconsin, central Missouri, and Southern Illinois and Indiana. Rosenburg et al. (2010), Fowler et al. (2003), Madsen et al. (2009), and Lucero (1998) used similar approaches to analyze changes in design storms for sub daily durations in Washington State, the United Kingdom, Denmark, and Argentina, respectively. Rosenburg et al. (2010) found no statistically significant changes in the historical record while Fowler et al. (2003) found significant decadal-level changes in 5- and 10-day events. Madsen et al. (2009) found a 10% increase in storm intensity for durations of 0.5 hrs – 3 hrs, but the increase was not statistically significant. Lucero (1998) found an increase in the annual mean rainfall but no change in rainfall intensity for various durations.

Such studies suggest that the assumption of a stationary time series for fitting statistical distributions to historical precipitation data may be invalid (Huff and Angel, 1992). However, the causes of the changes in precipitation are still under debate. Kunkel et al. (2003) suggested the elevated frequencies of intense precipitation events were most likely a consequence of naturally forced variability, although possible influences from land-use changes cannot be ruled out. Huff and Angel (1992), however, thought the increases in precipitation appeared to be greater than expected from natural climatic variability. Increasingly, climate change is considered the main driver of recorded changes in

temperature and precipitation over the last century, primarily due to increases in global greenhouse gas concentrations (Melillo et al., 2014; IPCC, 2014).

2.2.3 Future Changes in Precipitation and Streamflow

Denault et al. (2006) extrapolated historical trends to project future precipitation scenarios, but climate models are now the primary tool used to project the effects of increasing concentrations of greenhouse gasses on future climates. Global climate models (GCMs) simulate interactions of the atmosphere, oceans, land surface and ice, and project future climates for various greenhouse gas concentration scenarios (IDNR, 2015). Recent studies applying GCMs (IPCC, 2014) project surface temperatures to rise over the 21st century under all assessed emission scenarios. Also, heat waves are likely to occur more often and last longer, and extreme precipitation events will become more intense and frequent in many regions. Melillo et al. (2014) projects winter and spring precipitation in the Midwest by late this century (2071-2099) to increase 10%-20% relative to 1971-2000. Summertime precipitation is projected to decrease an average of 8% in 2041-2062 relative to 1971-2000, but the frequency and intensity of extreme precipitation events are projected to increase.

Unfortunately, the typical GCM output grid-cell size is approximately 50×70 miles and the temporal scale in also large, which poorly represent local scale precipitation (IDNR, 2015). GCM data must be downscaled to spatial and temporal increments appropriate for local (or point) precipitation and flood studies (Olsson et al., 2012). Two methods (statistical and dynamical) are used to downscale GCMs to finer spatial and temporal resolutions. Statistical downscaling uses transfer functions (e.g., regression relationships) representing observed relationships between larger-scale atmospheric variables and local quantities such as daily precipitation and/or temperature (Wilby and Fowler, 2010). Dynamic downscaling is based on regional climate models (RCMs) (usually just the atmospheric part) that have

finer horizontal grid resolution of surface features such as terrain (Castro et al., 2005). Currently, GCM data with sub daily temporal scales is only available through dynamical downscaling methods. Also, dynamical downscaling has the main advantage of responding in a physically consistent way to external forcing, since in an RCM all vertical levels of the atmosphere are considered to impact upon local climate and should therefore be more physically realistic (Fowler et al., 2007).

The recent availability of higher spatial and temporal resolution (sub daily) climate data, as produced by RCMs through dynamical downscaling, has facilitated impact assessments (Zhu, 2013). However, dynamically downscaled data often requires bias correction, the aim of which is to correct systematic error in RCM output, such as disparities in the frequency of rain events, total amount of rainfall, and seasonality, and have been found to be an important aspect of using such output for small-scale hydrologic modeling (Fowler et al., 2007). Many different methods can be used for such bias correction, analog methods, delta-change, gamma-gamma transformation, and quantile mapping (Ehret et al., 2012). Downscaled GCM and RCM data has been used in numerous studies to project changes in precipitation and runoff at the local level.

Forsee and Ahmad (2011), Mailhot et al. (2007), Markus et al. (2012), Moglen and Rios Vidal (2014), Rosenberg et al. (2010), Vavrus and Behnke (2014), and Zhu (2013) used downscaled climate models to project changes in IDF curves and design storm depth for Las Vegas NV, Southern Quebec, Chicago IL, the Mid-Atlantic Region, Washington, Wisconsin, and several US urban centers, respectively. Most of the studies found that future climate projections suggested an increase in the intensity of extreme storms for a given return period and duration, but with strong regional variations. The projected precipitation was applied within various hydrology models, including HEC-HMS, to determine the effects

of climate change on urban and natural drainage systems. Again, the studies found that peak discharges will increase in magnitude and the frequency of potential exceedences of current design standards for select storm-water infrastructure components will increase as well. However, the increase in precipitation and flow were not always statistically significant.

Wright et al. (2012) used daily precipitation statistics from four climate models and three greenhouse gas (GHG) emissions scenarios (A2, A1B, and B1) to projected changes in streamflow for HUC 8 watersheds across the US. They found significant increases in flow from the 100-year, 24-hr precipitation event that imply that the entire frequency distribution of flows may shift in the future. For example, what once was a 100-year event may be a 50-year event in the future. The shift of the entire frequency distribution because of climate change could have important implications for the life-cycle costs of maintaining stormwater infrastructure, as discussed in more detail below. Fowler and Kilsby (2007) used dynamically downscaled RCM precipitation output as input to hydrological models to simulated daily flow distributions in eight catchments. Results suggested RCM data can be used with some confidence to examine future changes in flow regime and suggested changing seasonality of flow regimes compared to historic observations.

2.2.4 Effects on Infrastructure

Runoff from increased precipitation intensity and quantity may have a significant impact of related infrastructure (Huff and Angel, 1992). Numerous studies have looked at the impact of climate change and the corresponding changes in precipitation on urban stormwater infrastructure (eg. Rosenberg et al., 2010; Fortier and Mailhot, 2015; Kirshen et al., 2015). With regards to riverine crossing structures, increases in the frequency and quantity of high flow events will increase bridge/culvert capacity exceedances (causing upstream flooding to occur), increase overtopping and scouring problems to

structures, increase flood plain inundatation occurrences, and increase the occurrences of culverts become blocked by debris (Scottish Executive, 2005; USDOT, 2014). The Transportation Research Board (TRB, 2008) suggested low-lying bridges will be more susceptible to flooding, thousands of culverts could be undersized, and runoff from increased precipitation levels will also affect stream flow and sediment delivery in some locations, with potentially adverse effects to bridge foundations. Most bridge failures in the United States are due to problems relating to scour, which causes stabilizing material, i.e. the riverbed, to move away from the bridge substructure, causing instability in the bridge's foundation (Wright et al., 2012). Scour typically occurs because the water flow is significant enough to move the sand or gravel away from the bridge's foundation.

Savonis et al. (2009) investigated potential climate change impacts on the transportation system in the Gulf Coast area and found increases in temperature, sea level, and precipitation intensity would cause an increase in the expected costs of maintaining the transportation networks and, at the same time, diminish the expected useful life of the system. Chinowsky et al. (2013) found climate change will increase maintenance cost for roads due to (1) rutting of paved roads from precipitation, (2) rutting of paved roads caused by freeze–thaw cycles, (3) cracking of paved roads during periods of high temperatures, and (4) erosion of unpaved roads from precipitation. Proposed bridge adaption and maintenance scenarios with regards to climate change, including scour mitigation (FHWA, 2009) and bridge elevation, were analyzed by Neumann et al. (2014). They found that climate change will affect the sustainability of long-lived infrastructure and require costly infrastructure upgrades or adaptations.

2.2.5 Design Guideline Modifications

Because infrastructure design relies on the assumption that past events can be used to predict future events, no change in the frequency of extremes over time is considered in manuals used by engineers and hydrologists (eg. Perica et al., 2013; Soong et al., 2004). However, as described previously, the frequency of extremes has been changing and is likely to continue changing in the future. Therefore, it is necessary to account for the nonstationary nature of precipitation and flooding when estimating the magnitudes and frequencies of future events (IDNR, 2015). Watt and Marsalek (2013), who reviewed the design storm concept with regards to climate change, concluded that design practices would be well served by adopting a comprehensive approach considering all design storm event characteristics (eg. duration, distribution, areal reduction factor, etc.) and their sensitivity to climate change and inherent uncertainties in the existing IDF relations. For example, if the spatial-temporal correlations of rainfall change in the future, areal reduction factors and the temporal distribution of rainfall (often assumed to be static) may also change. Dewar and Wachs (2006) proposed a robust approach that considers a wide range of possible situations due to the uncertainty of climate change modeling, to produce designs that do well across a broad range of plausible futures.

Arisz and Burrell (2006) suggested the design of minor and major drainage systems should accommodate the expected effects of climate change by incorporating the potential to upgrade the hydraulic capacity of the drainage system while minimizing the associated costs and proposed this can best be achieved through the designation of space for remedial measures when available and the flood-proofing of existing development and infrastructure where possible. Mailhot and Duchesne (2010) and Hennegriff (2007) proposed a procedure to revise the design criteria of drainage infrastructures by integrating information about climate projections for extreme rainfall, expected level of performance,

and expected lifetime of the infrastructure/system and produced a method that treats return periods as a function of time. For example, if a proposed system needs to have a 100-yr capacity at some point in the future, 133-year capacity is required based on current design return periods. Scottish Executive (2005) proposed a similar method of insuring a structure is designed to meet a future desired performance level by simply amending the design storm from a return period of 100 years to 200 years.

2.2.6 Climate Modeling and Uncertainty

Climate modeling and downscaling climate models for use as inputs for hydrologic assessments includes and introduces uncertainty. Wuebbles et al. (2014) and Janssen et al. (2014) found that many of the Coupled Model Intercomparison Project Phase Five (CMIP5) GCMs underestimate the historical observed trend in extreme precipitation and thus underestimate the projected extremes. While observations, historical simulations, and future projections agree on increases in heavy precipitation events consistent across a range of indicators, there are large differences between model simulations in the rate of heavy precipitation increase. Model spread is large and in most cases bigger than the model signal (trend) itself (Janssen et al., 2014). Climate modeling involves the interactive influences of the land, atmosphere, oceans and lakes, and continental glaciers over all time scales, with inherent uncertainty of the numerical representation of each real-world physical interaction within the model (Pielke, 2002 and Pielke et al., 2012). There is also uncertainty about what some GCM inputs, such as land cover, various water resources, and atmospheric CO2 concentrations will be for the duration of the model time scale (Fowler and Kilsby, 2007).

Downscaling (statistical and dynamical) also introduces uncertainties. Fowler and Wilby (2010) warn that finer and time-space-based downscaled information can be “misconstrued as accurate,” but the ability to get this finer-scale information does not necessarily translate into increased confidence in the

downscaled scenario. For statistical downscaling, the statistical relationship(s) between predictor(s) and predictants are not necessarily static and can be expected to change in the future and the same premise of stationarity (or lack thereof) also applies to the parameterized schemes within regional climate models (Pielke and Wilby, 2012). None the less, the stationarity of these statistics and schemes is assumed during statistical downscaling (Watt and Marsalek, 2013). Pielke (2002) suggests uncertainty of dynamical downscaling grows as more climate variables must be predicted by regional climate models (RCMs) rather than obtained from observations.

Fowler and Kilsby (2007) concluded that if RCM data are to be used directly as input to hydrologic models, there is a need for bias-correction. However, common bias-correction methods suffer from varying degrees of the assumption of variable stationarity. For example, the quantile mapping method assumes that the rainfall distribution will be the same in the future as in the control climate (Folwer and Kilsby, 2007). Other common stationarity assumptions include the areal reduction factor and number of wet days or wet hours (Watt and Marsalek, 2013). Typically, climate researchers address climate model uncertainty by analyzing a number of different GCM's and/or emission pathways to provide a range of possible projections and upper and lower bounds based on the highest and lowest model outputs (Fowler and Kilsby, 2007; Pielke et al., 2012). Unfortunately the substantial computational cost of downscaling numerous GCM sometimes limits the number of data sets available for analysis. As noted by Rosenberg et al. (2010), the range of predicted changes depends greatly on the underlying GCM simulations and the differences between climate model simulations (upper and lower bounds) is often too large to provide a single engineering design recommendation based on future projected precipitation.

Chapter 3 – STUDY SITES

The three regional areas and individual riverine-crossing structures and watersheds analyzed in this study are explored in greater detail below. The three study areas and studied streams include Camp Atterbury Joint Maneuver Training Center near Edinburg, Indiana (Nineveh Creek upstream of Hendricks Ford Road), Camp Grayling Joint Manever Traning Center near Grayling, Michigan (Portage Creek upstream of confluence with Manistee and East Branch Au Sable River upstream of West Karen Lake Road), and Edgar County, Illinois (North Fork Embarras River upstream of North 200th Street and East Fork Big Creek upstream of East 300th Road).

3.1 Camp Atterbery Joint Maneuver Training Center (Indiana)

Camp Atterbury Joint Maneuver Training Center (Camp Atterbury) was established in 1942 as a training facility and prisoner of war camp and is located about 40 miles south of Indianapolis near Edinburg, IN. Camp Atterbury is now an Indiana National Guard and U.S. Army Reserve training facility that accommodates a wide range of training for military forces and regional police (Svendsen, 2005). The majority of Camp Atterbury is located within the northwest corner of Bartholomew County with portions located within southern Johnson County and western Brown County. Camp Atterbury covers an area of approximately 13560 hectares (33500 acres), measuring 19 km from north to south, and 11.5 km from east to west at the widest point (Figure 3.1).

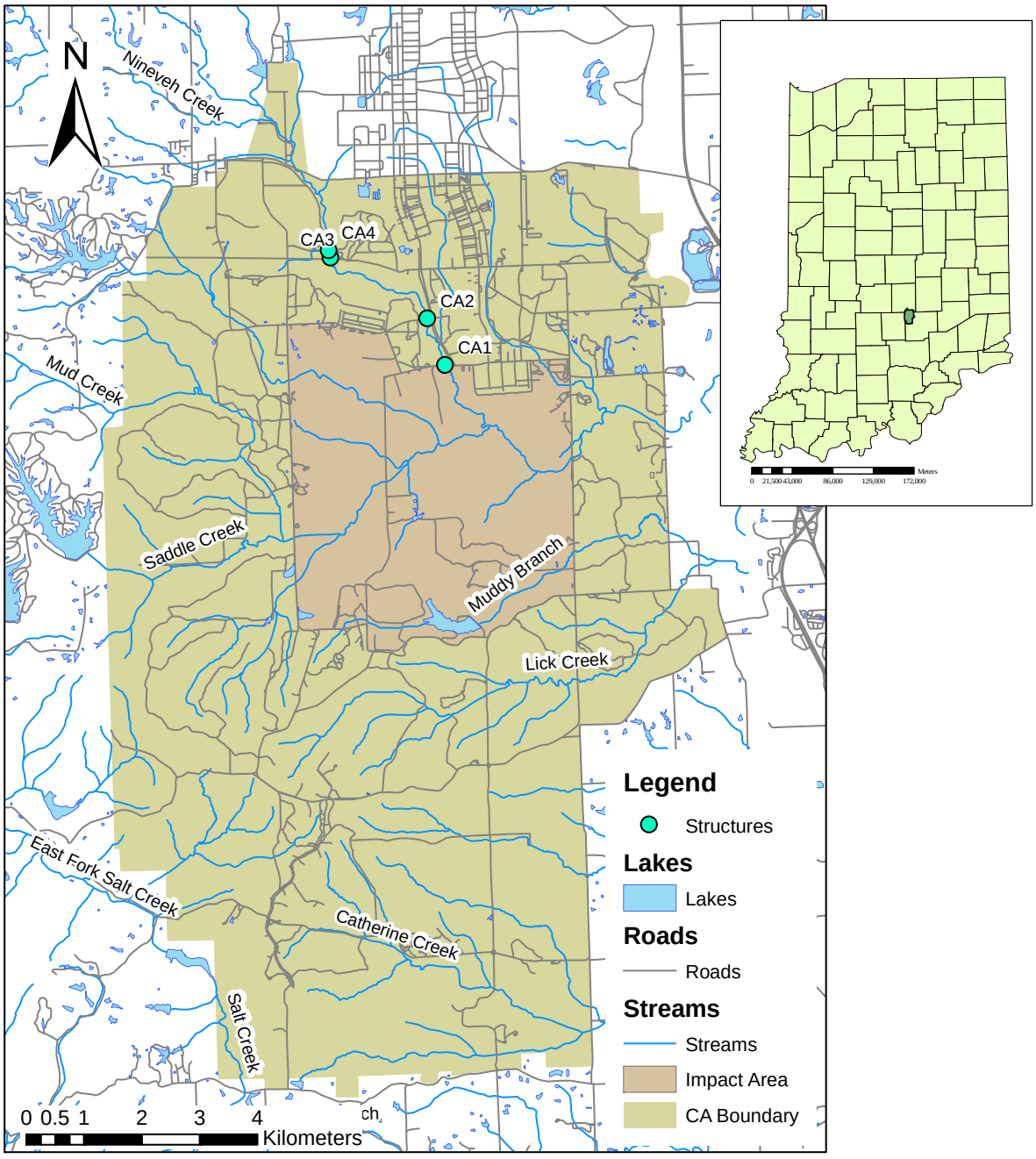

Figure 3.1. Camp Atterbury Location Map

3.1.1 LWC Sties

Two LWC fords and two, three span bridges with two pile bent piers were modeled and analyzed for this project, all of which cross Nineveh Creek upstream (north) of the Impact Area. Starting at the

downstream end (at Impact Area northern border), the two bridges carry Hendricks Ford Road (CA1) and Wilder Road (CA2) across Nineveh Creek and are located approximately 980m apart. The former is a secondary asphalt road and the latter is a tertiary unpaved road. Located approximately 2,300m upstream of Wilder Road is the first (CA3) LWC ford and the second (CA4) is a further 135m (north) upstream. LWC CA3 was installed in 2010 and CA4 was installed in 2002, both by installation staff. Both are hardened with 2.44 m x 4.88 m (8 ft x 16 ft) cable-concrete pads manufactured by US Construction Fabrics LLC. The pads weight 220 kg/sq. m (45 lb/sq. ft) and the individual concrete blocks are 292.1 mm (top) x 393.7 mm (base) x 139.7 mm (height) [11.5 in x 15.5 in x 5.5 in] trapezoids connected by stainless steel cable with 12.7 mm (0.5 in) spacing at the base. Each block weights 36.29 kg (80 lb). See Figure 3.1 for structure locations and Figure 3.2 for structure pictures.

The hardened LWCs are both 4.88 m (16 ft) wide and protrude from the streambed 0-5 cm (0-2 in) on average and so were installed partially within the streambed. The egress/ingress ramps are also hardened with the same cable-concrete at a slope of approximately 10H:1V, with the stream banks excavated as required. Significant sediment has deposited on CA3 since construction (the downstream LWC).

Figure 3.2. Nineveh Creek crossings CA1-CA4 (starting at upper left and going clockwise)

3.1.2 Hydrology

Nineveh Creek is a tributary of the Driftwood River within the Driftwood HUC-8 watershed. The tributary is approximately 18.4 km in length, approximately 11.5 km of which is upstream of the Impact Area. The watershed upstream of the Impact Area is 33.4 km^2 (12.9 mi^2). The watershed is predominately forest and agricultural areas in the headwaters and drains parts of the urbanized Camp Atterbury cantonment area (Figure 3.3). The rest of the watershed within Camp Atterbury is forested.

The study reach contains a downstream slope of approximately 0.003(V/H). The stream was classified using Chow (1959) to determine the appropriate Manning's n value of the reach. The value assigned for Manning's n was 0.04 within the channel and 0.1 for floodplain dominated by heavy timber stands.

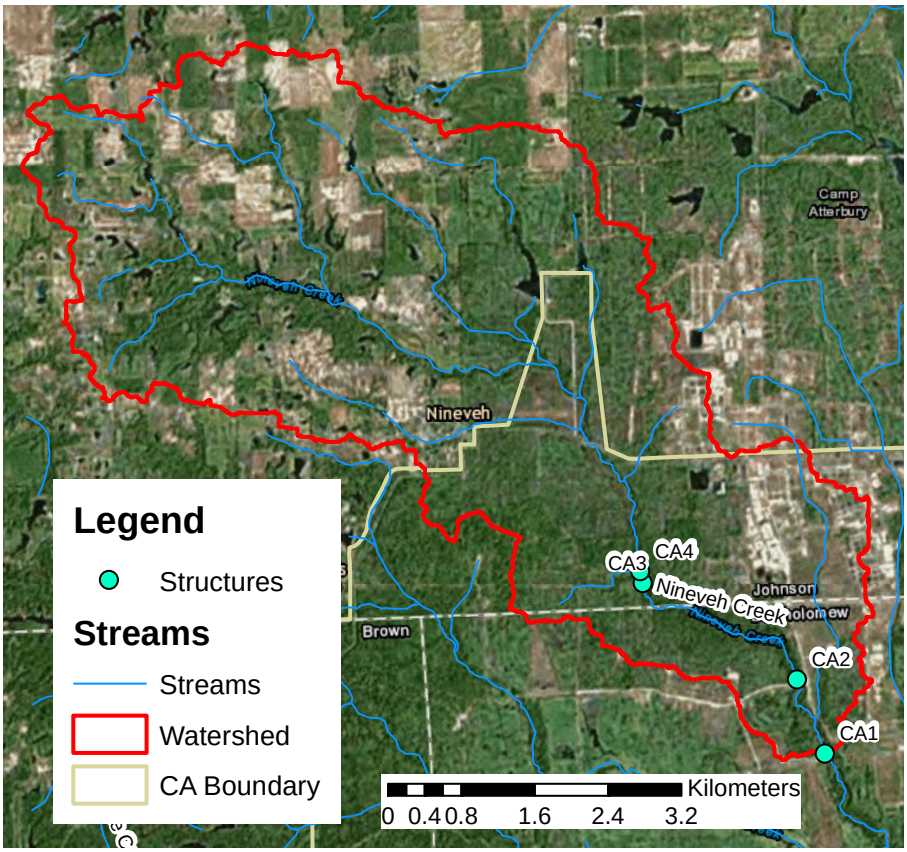

Figure 3.3. Nineveh Creek watershed overview

3.1.3 Soils

The majority of the Nineveh Creek watershed has soils in the "C" or "C/D" hydrologic group (see Figure 3.4 and Table 3.1) (USDA, 1986). Soil groups with drainage characteristics affected by a high water table are indicated with a "/D" designation, where the letter preceding the slash indicates the hydrologic group of the soil under drained conditions. Half of all land designated with row crop land use was assumed to be under drained. Note how the main drainage way is comprised primarily of "B" soils affected by a high water table ("B/D").

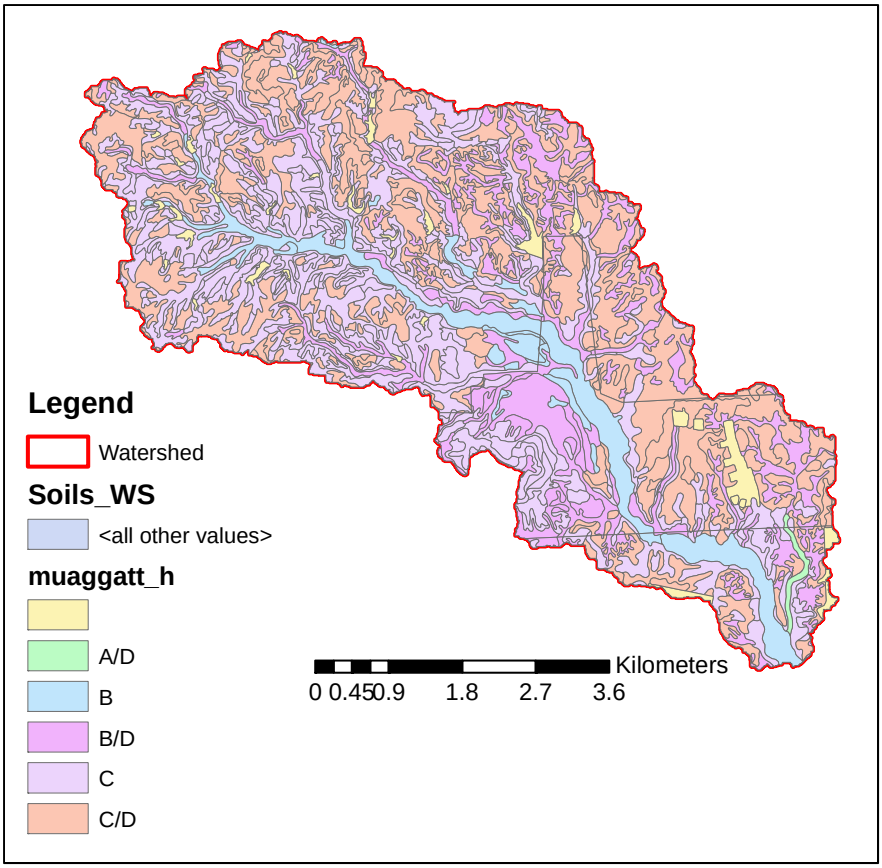

Figure 3.4. Nineveh Creek watershed hydrologic soil groups

Table 3.1. Nineveh Creek watershed hydrologic soil groups by percent area

% Area	Hydrologic Soil Type
2.4%	water
0.3%	A/D
7.9%	B
16.7%	B/D
36.4%	C
36.4%	C/D

3.1.4 Land Use

Land cover within the Nineveh Creek watershed is primarily deciduous forest and agricultural land (row crops and pasture) with several small open water bodies and developed areas primarily to the southeast (See Figure 3.5 and Table 3.2) (Homer et al., 2015).

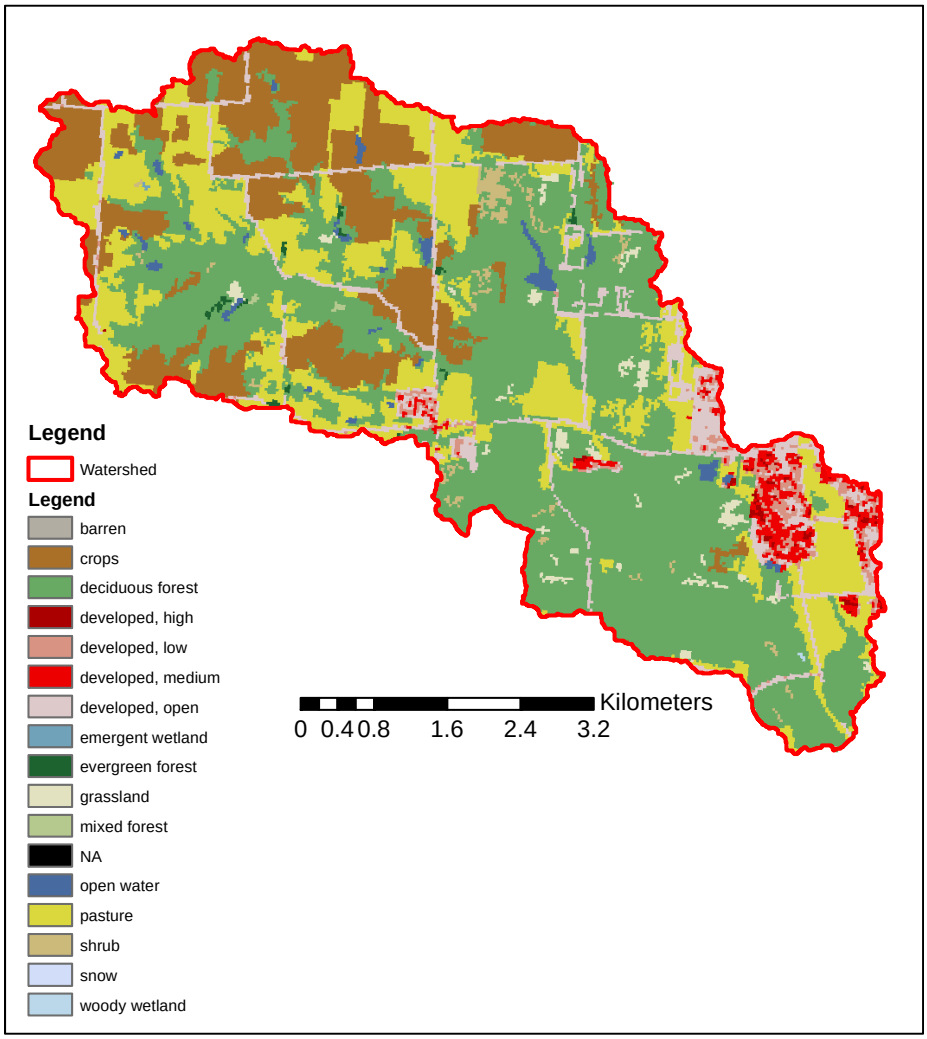

Figure 3.5. Nineveh Creek watershed NLCD land cover

Table 3.2. Nineveh Creek watershed NLCD land cover by percent area

% Area	NLCD Land Cover	% Area	NLCD Land Cover
1.00%	Open Water	0.10%	Mixed forest
6.80%	Developed, open	0.90%	Shrub
1.80%	Developed, low	1.20%	Grassland
1.80%	Developed, medium	22.10%	Pasture
0.30%	Developed, high	17.80%	Crops
46.00%	Deciduous forest	0.00%	Woody wetland
0.20%	Evergreen forest	0.00%	Emergent wetland

Specific combinations of land use and soil type were linked to Curve Number (CN) values as described in Section 6.2.3 (USDA, 1986). A GIS raster file was created for Nineveh Creek watershed to digitize the CN values for use in HEC-geoHMS. Figure 3.6 shows the distribution of CN values throughout the watershed.

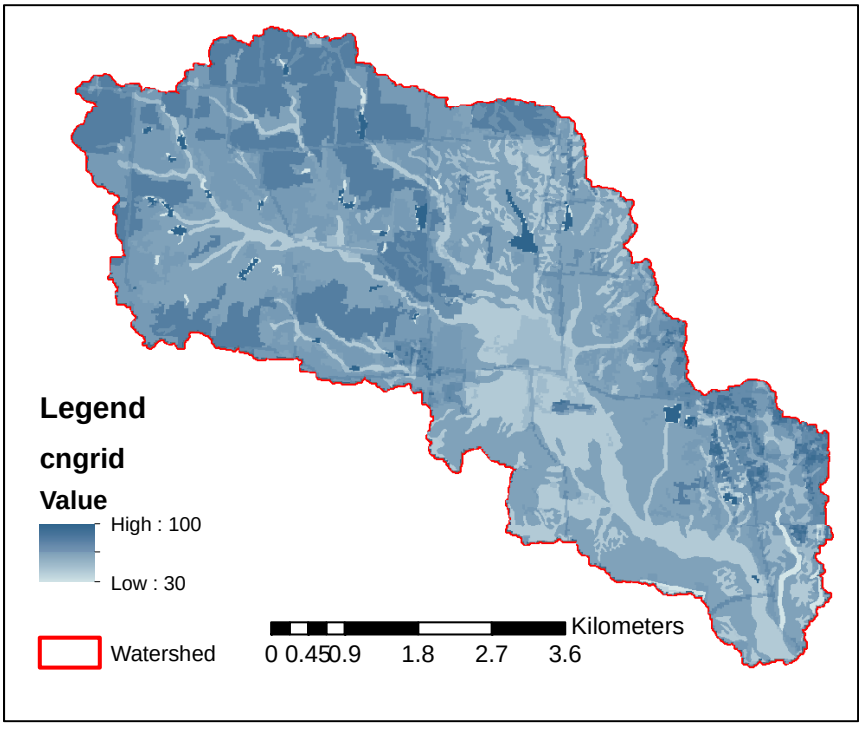

Figure 3.6. Nineveh Creek watershed curve numbers

3.1.5 Topography and Survey

Topography of Nineveh Creek watershed was developed from light detection and ranging (LiDAR) data generated from a LiDAR mission provided for the Army's Sustainable Range Program (SRP). A digital elevation model (DEM) was developed based upon the LiDAR data (Figure 3.7). The DEM is in meters. Survey of study sites was completed April 21-22, 2015 by the USACE. Survey included structure measurement, channel topography up to top of bank, and other relevant data.

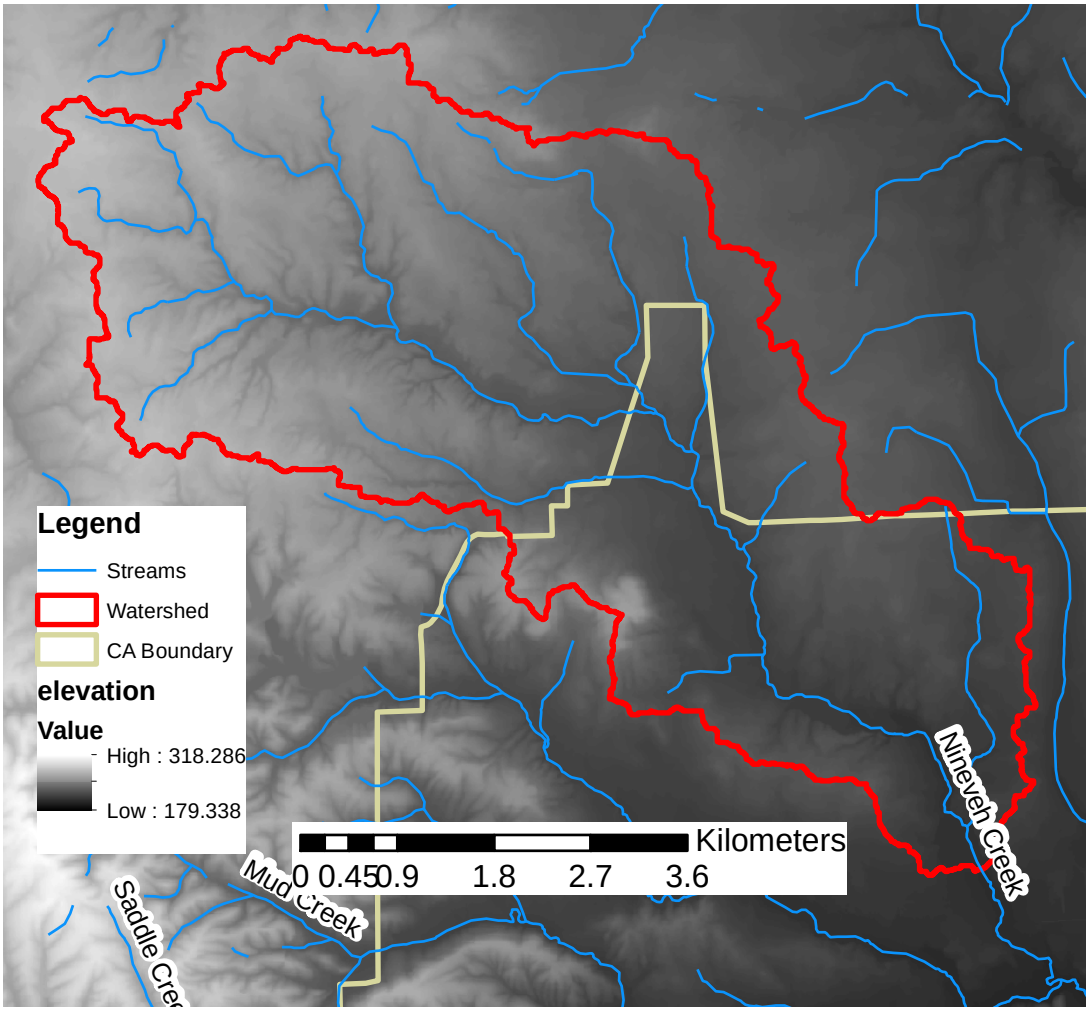

Figure 3.7. Nineveh Creek watershed topography (from LiDAR)

3.1.6 Precipitation Data

Precipitation measurements were obtained from the NWS Cooperative Observer Program's database maintained by the National Oceanic and Atmospheric Administration's (NOAA) National Climatic Data Center (NCDC). The location of each gauge is show in Figure 3.8 and the ID and record length are show in Table 3.3.

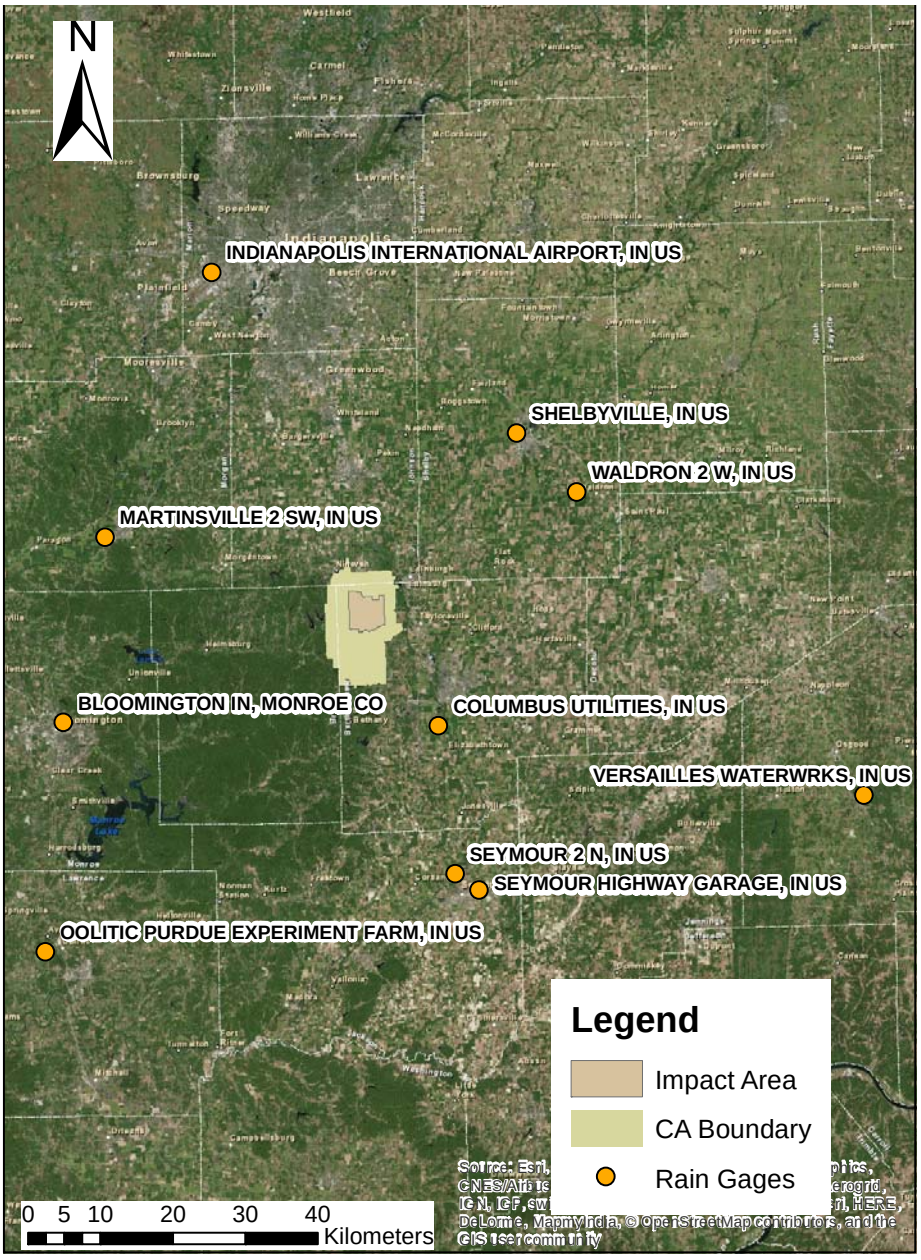

Figure 3.8. Central Indiana rain gauge locations

Table 3.3. Central Indiana rain gauge information

Name	Network	ID	Lat/Lon	Elevtaion	Start Date	End Date	Coverage
BLOOMINGTON INDIANA UNIVERSITY, IN US	GHCND	USC00120784	39.1742°, -86.5214°	253 m	15/11/1895	Present	97%
COLUMBUS, IN US	GHCND	USC00121747	39.166°, -85.9227°	186.8 m	1/1/1893	Present	99%
GREENSBURG, IN US	GHCND	USC00123547	39.3475°, -85.4891°	285.6 m	1/5/1896	Present	97%
INDIANAPOLIS INTERNATIONAL AIRPORT, IN US	GHCND	USW00093819	39.7318°, -86.2788°	240.8 m	10/6/1942	Present	93%
MARTINSVILLE 2 SW, IN US	GHCND	USC00125407	39.4039°, -86.4531°	180.4 m	12/21/1922	Present	97%
NORTH VERNON 2 ESE, IN US	GHCND	USC00126435	39.0017°, -85.5997°	225.6 m	1/1/1938	Present	94%
SEYMOUR HIGHWAY GARAGE, IN US	GHCND	USC00127930	38.9616°, -85.8608°	182.9 m	7/1/1948	Present	95%
SEYMOUR 2 N, IN US	GHCND	USC00127935	38.9822°, -85.8988°	173.7 m	1/2/1893	12/3/2013	98%
SHELBYVILLE, IN US	GHCND	USC00127999	39.5282°, -85.7914°	228.6 m	1/1/1893	Present	92%
WALDRON 2 W, IN US	GHCND	USC00129174	39.4538°, -85.6963°	251.8 m	2/2/1949	Present	95%

3.1.7 Past Studies

Leahy (2014) investigated the effect of the LWC orientation relative to the stream with regards to the performance of the hardened crossings and maintenance requirements. The LWCs on Nineveh Creek were included in the study. The study found that a perpendicular orientation performed the best with respect to the least amount of sediment accumulated at the crossing over the study period.

3.2 Camp Grayling Joint Maneuver Train Center (Michigan)

Camp Grayling Joint Maneuver Training Center (Camp Grayling) was established in 1913 as a training facility and is located about adjacent to Grayling, Michigan. Camp Grayling is now a Michigan National Guard and U.S. Army Reserve training facility that accommodates a wide range of training for military

forces and regional police. The majority of Camp Grayling is located within Crawford County with portions located in southeastern Kalkaska County and southern Otsego County. Camp Grayling covers an area of approximately 59500 hectares (147000 acres) (Figure 3.9).

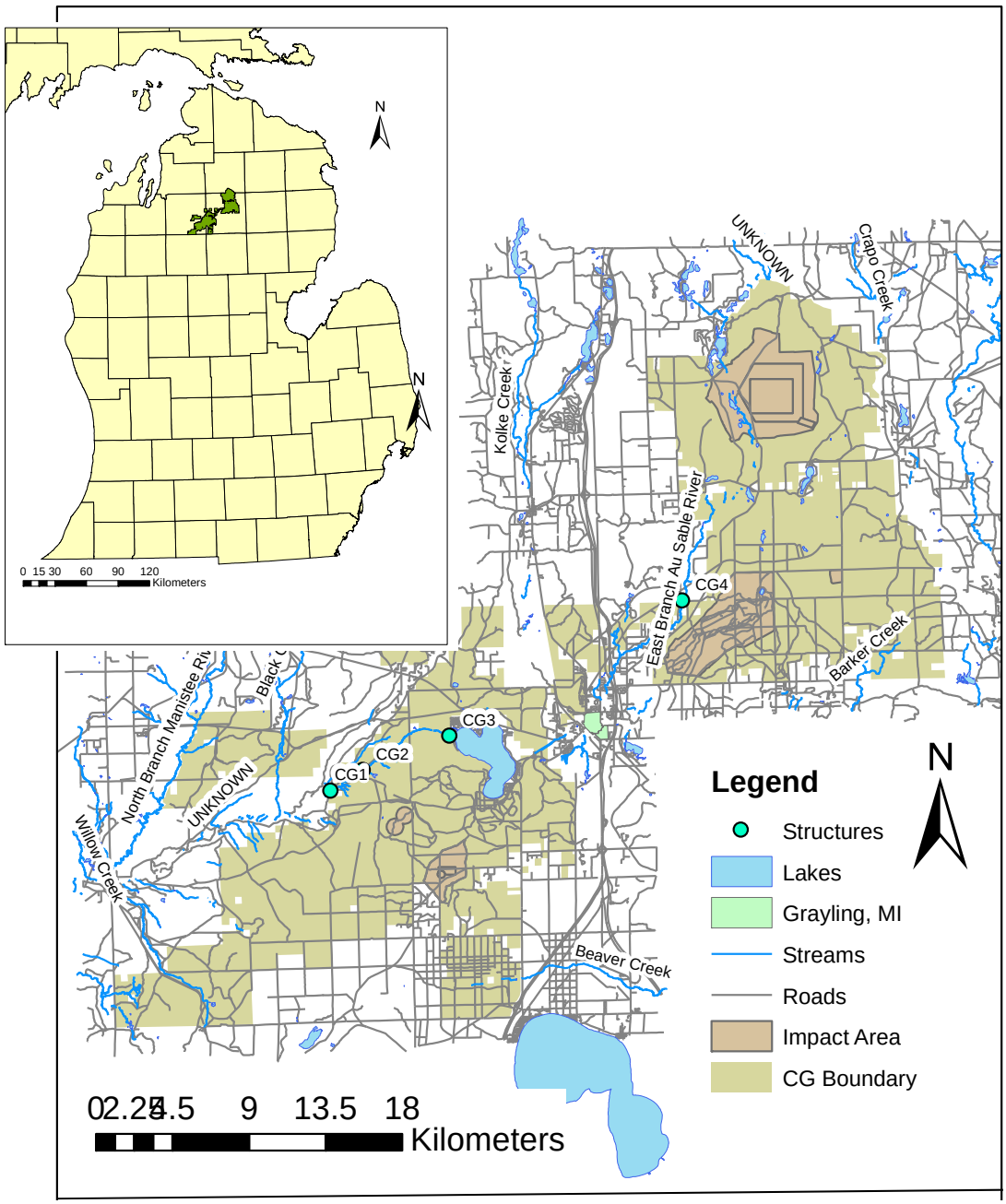

Figure 3.9. Camp Grayling Location Map

3.2.1 LWC Sites

Three vented LWCs and one single span bridge were modeled and analyzed for this project, one of which crosses East Branch Au Sable River and three of which cross Portage Creek. The LWC over East Branch Au Sable River (CG4) is vented with four iron pipe culverts (0.81 m in diameter) carrying W Karen Lake Road. Starting at the downstream end of Portage Creek a double corrugated metal pipe culvert (2 m is diameter) (CG1) carries Portage Lake Road over Portage Creek. Approximately 3100m upstream a single span bridge with spill-thru abutments carries an unnamed road over Portage Creek. Approximately 7000m further upstream a single corrugated metal pipe (1 m in diameter) carries Euclid Avenue over Portage Creek. All are secondary asphalt or concrete roads. See Figure 3.9 for structure locations and Figure 3.10 for structure pictures.

Figure 3.10. Camp Grayling crossings CG1-CG4 (starting at upper left and going clockwise)

3.2.2 Hydrology

East Branch Au Sable River is a tributary to Au Sable River within the Au Sable HUC-8 watershed. The tributary is approximately 26.6 km in length, approximately 20.8 km of which is upstream of W Karen Lake Road. The watershed upstream of the LWC is 102.8 km^2 (39.7 mi^2). East Branch Au Sable River confluences with the Au Sable River at Grayling Michigan, which flows into Lake Huron to the east. The study watershed is predominately forest and shrub land/grassland (Figure 3.11). The study watershed and stream reach is swampy with numerous natural inline ponds in the upper reaches. USGS Gauge 04135600 operated 1958-1984 on East Branch Au Sable River near Grayling, MI (downstream of the LWC) just upstream of the confluence with the Au Sable River. The drainage area at the gauge location is 198 km^2 (76 mi^2). USGS Gauge 04135500 operated 1942-1993 on the Au Sable River near Grayling, MI just upstream of the confluence with the East Branch Au Sable River. The drainage area at the gauge location is 284.9 km^2 (110 mi^2).

The study reach contains a downstream slope of approximately 0.002 (V/H). The stream was classified using Chow (1959) to determine the appropriate Manning's n value of the reach. The value assigned for Manning's n was 0.045 within the channel and 0.1 for floodplain dominated by heavy timber stands.

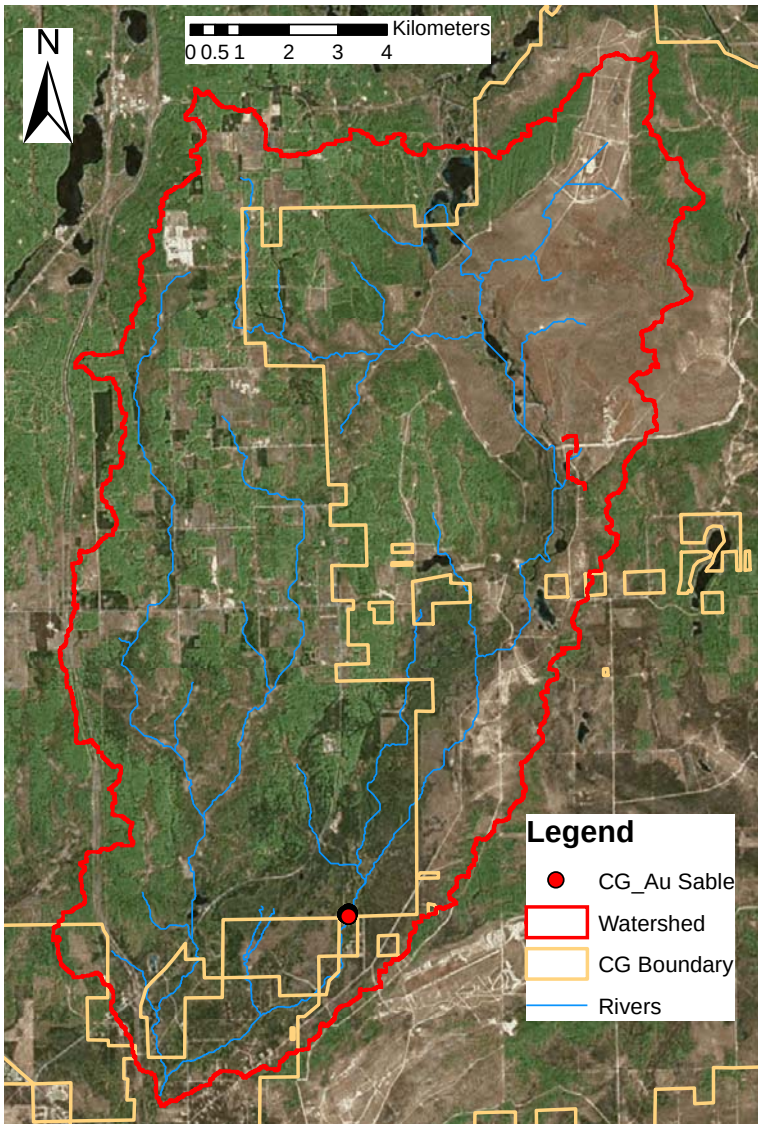

Figure 3.11. East Branch Au Sable River watershed overview

Portage Creek is a tributary to the Manistee River within the Manistee HUC-8 watershed. The tributary is approximately 11 km in length and the source is Lake Margrethe. The watershed at the Lake Margrethe outlet is 38.6 km^2 (14.9 mi^2) and the watershed at Portage Lake Road is 87.8 km^2 (33.9 mi^2). Portage Creek confluences with the Manistee River at just downstream of Portage Lake Road, which flows into Lake Michigan to the west. The study watershed is predominately forest, forested wetland, and Lake Margrethe (Figure 3.12). The study watershed and stream reach is swampy. Lake Margrethe has a pool surface area of 780 ha (1920 ac) and outflow is controlled by the Portage Creek Dam. The

Dam is a concrete structure with three at-grade gates over which wood boards can be raised and lowered. Unobstructed outflow is allowed from November 1 to May 1 during which the lake maintains a pool elevation of 345.55 m (1133.7 ft). During the rest of the year wood boards are lowered to maintain a pool elevation of 345.77 m (1134.4ft).

The study reach contains a downstream slope of approximately 0.001 (V/H). The stream was classified using Chow (1959) to determine the appropriate Manning's n value of the reach. The value assigned for Manning's n was 0.045 within the channel and 0.1 for floodplain dominated by heavy timber stands.

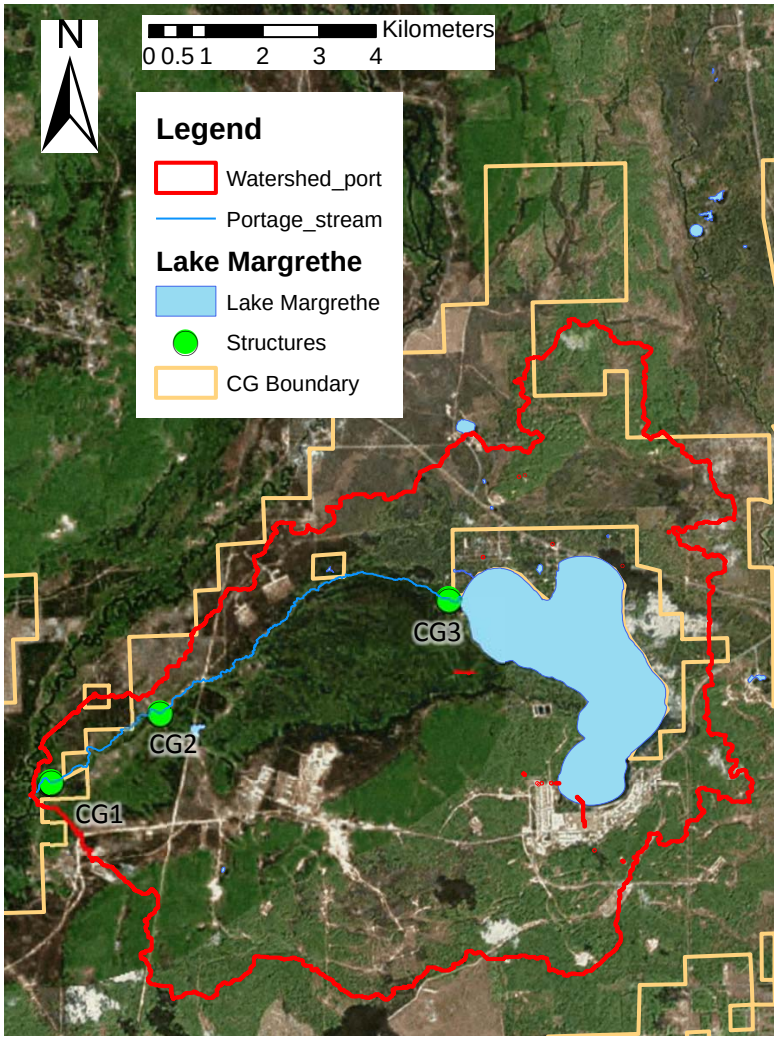

Figure 3.12. Portage Creek watershed overview

3.2.3 Soils

The majority of the East Branch Au Sable River and Portage Creek watersheds have soils in the "A" or "A/D" hydrologic group (see Figure 3.13, Figure 3.14, Table 3.4, and Table 3.5) (USDA, 1986). Soil groups with drainage characteristics affected by a high water table are indicated with a "/D" designation, where the letter preceding the slash indicates the hydrologic group of the soil under drained conditions.

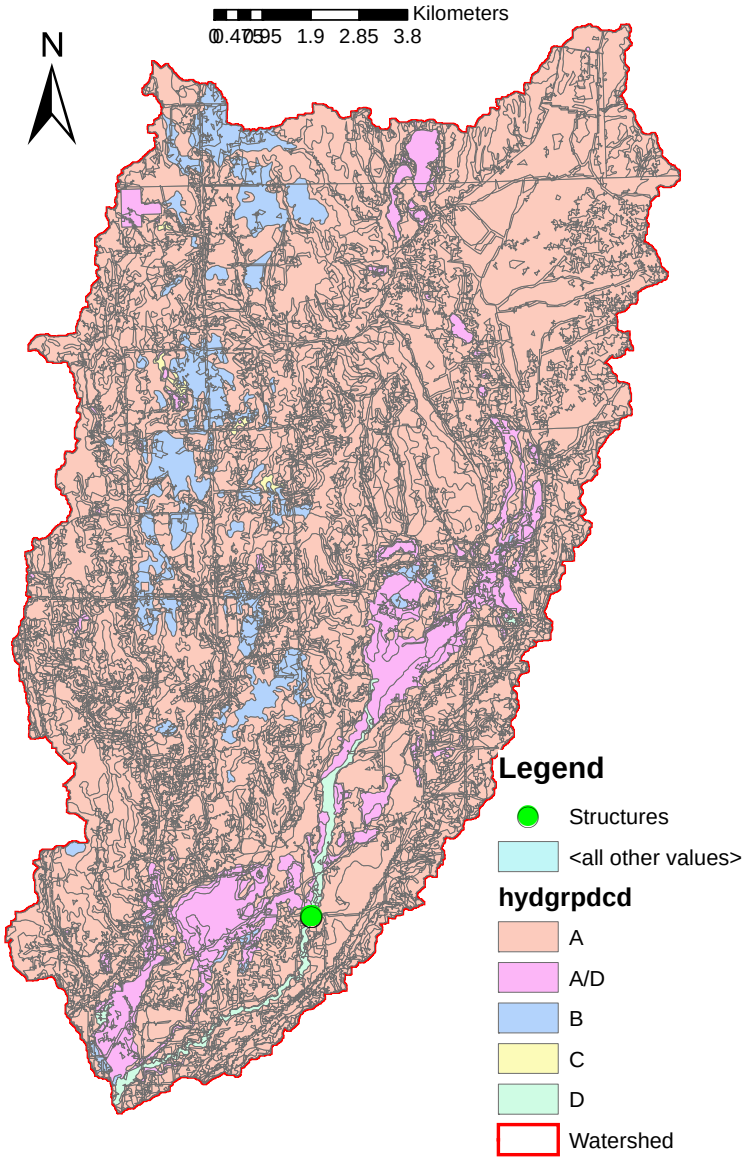

Figure 3.13. East Branch Au Sable River watershed hydrologic soil groups

Table 3.4. East Branch Au Sable River watershed hydrologic soil groups by percent area

% Area	Hydrologic Soil Type
86.92%	A
6.86%	A/D
5.30%	B
0.15%	C
0.77%	D

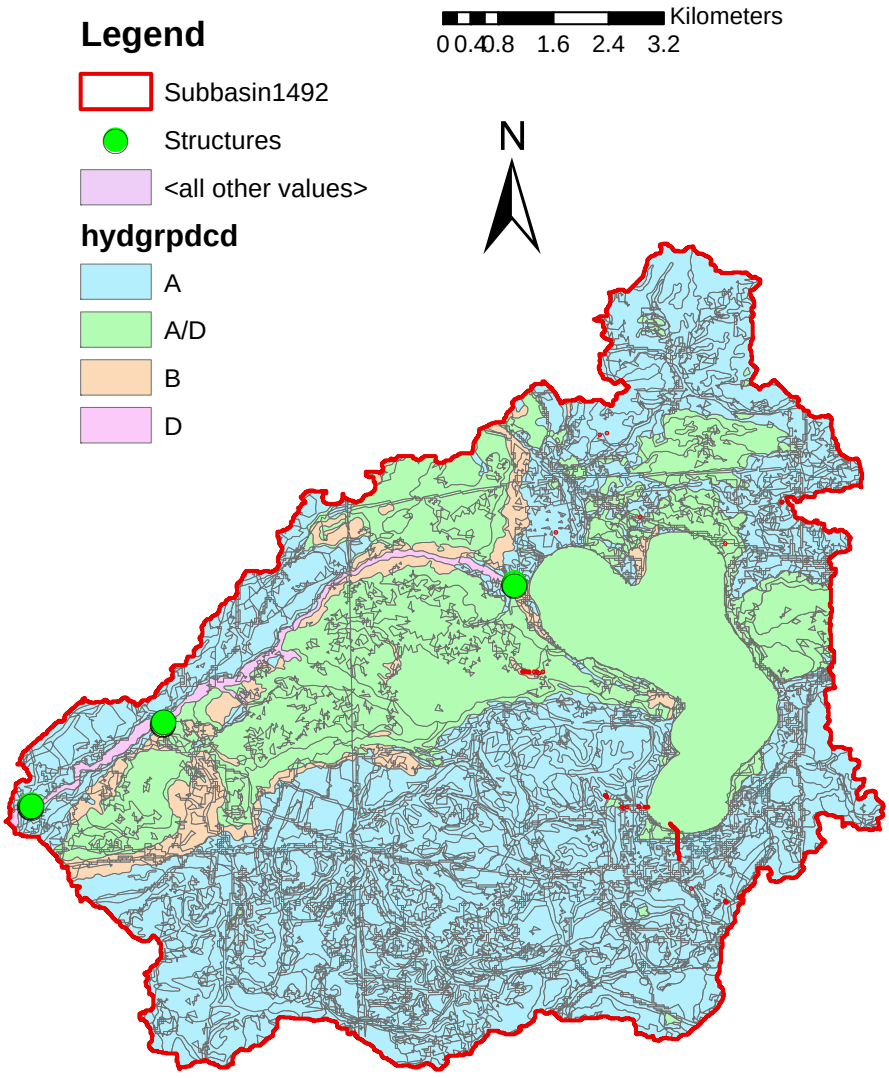

Figure 3.14. Portage Creek watershed hydrologic soil groups

Table 3.5. Portage Creek watershed hydrologic soil groups by percent area

% Area	Hydrologic Soil Type
71.36%	A
18.51%	A/D
3.58%	B
0.81%	D
5.74%	Water

3.2.4 Land Use

Land cover within the East Branch Au Sable watershed is primarily deciduous/evergreen forest, shrub/grassland, and wetland with several inline open water bodies in the upland areas (See Figure 3.15 and Table 3.6) (Homer et al., 2015). Land cover within the Portage watershed is primarily deciduous/evergreen forest and wetland with several inline open water bodies in the upland areas (See Figure 3.16 and Table 3.7). The shrub/grasslands in both watersheds are primarily military training ranges within Camp Grayling. The urbanized cantonment area of Camp Grayling is also located on the south side of Lake Margrethe.

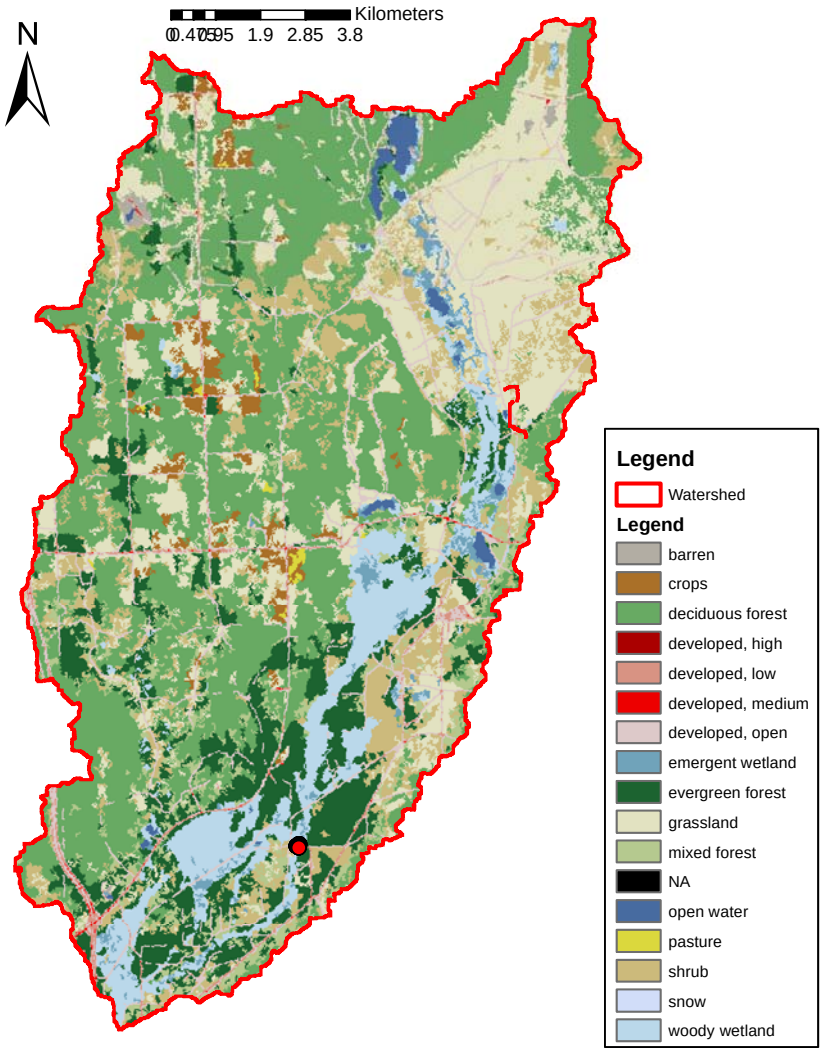

Figure 3.15. East Branch Au Sable River watershed NLCD land cover

Table 3.6. East Branch Au Sable River watershed NLCD land cover by percent area

% Area	NLCD Land Cover	% Area	NLCD Land Cover
0.77%	Open Water	3.97%	Mixed forest
5.11%	Developed, open	10.76%	Shrub
1.01%	Developed, low	17.31%	Grassland
0.07%	Developed, medium	0.14%	Pasture
0.00%	Developed, high	1.63%	Crops
41.41%	Deciduous forest	6.51%	Woody wetland
10.09%	Evergreen forest	1.22%	Emergent wetland

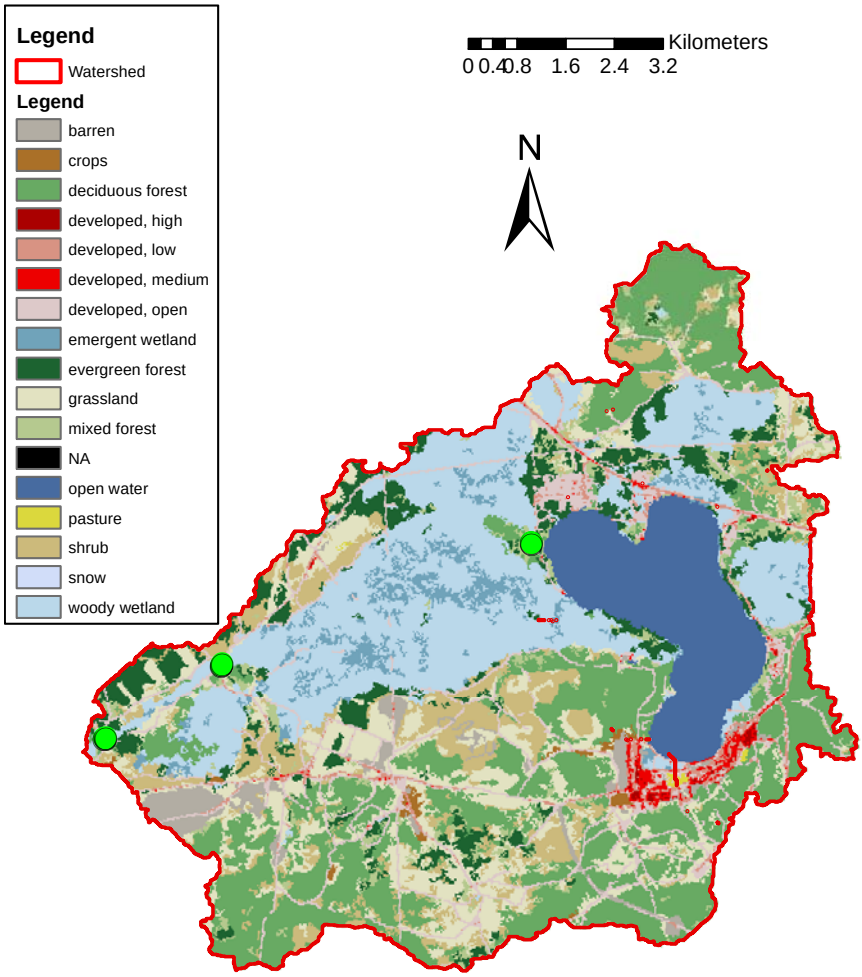

Figure 3.16. Portage Creek watershed NLCD land cover

Table 3.7. Portage Creek watershed NLCD land cover by percent area

% Area	NLCD Land Cover	% Area	NLCD Land Cover
5.99%	Open Water	2.94%	Mixed forest
6.02%	Developed, open	7.73%	Shrub
1.32%	Developed, low	10.46%	Grassland
0.47%	Developed, medium	0.07%	Pasture
0.10%	Developed, high	0.27%	Crops
39.41%	Deciduous forest	16.91%	Woody wetland
6.30%	Evergreen forest	2.02%	Emergent wetland

Specific combinations of land use and soil type were linked to Curve Number (CN) values as described in Section 6.2.3 (USDA, 1986). A GIS raster file was created for East Branch Au Sable and Portage watersheds to digitize the CN values for use in HEC-geoHMS. Figure 3.17 and Figure 3.18 show the distribution of CN values throughout the East Branch Au Sable and Portage watersheds, respectively.

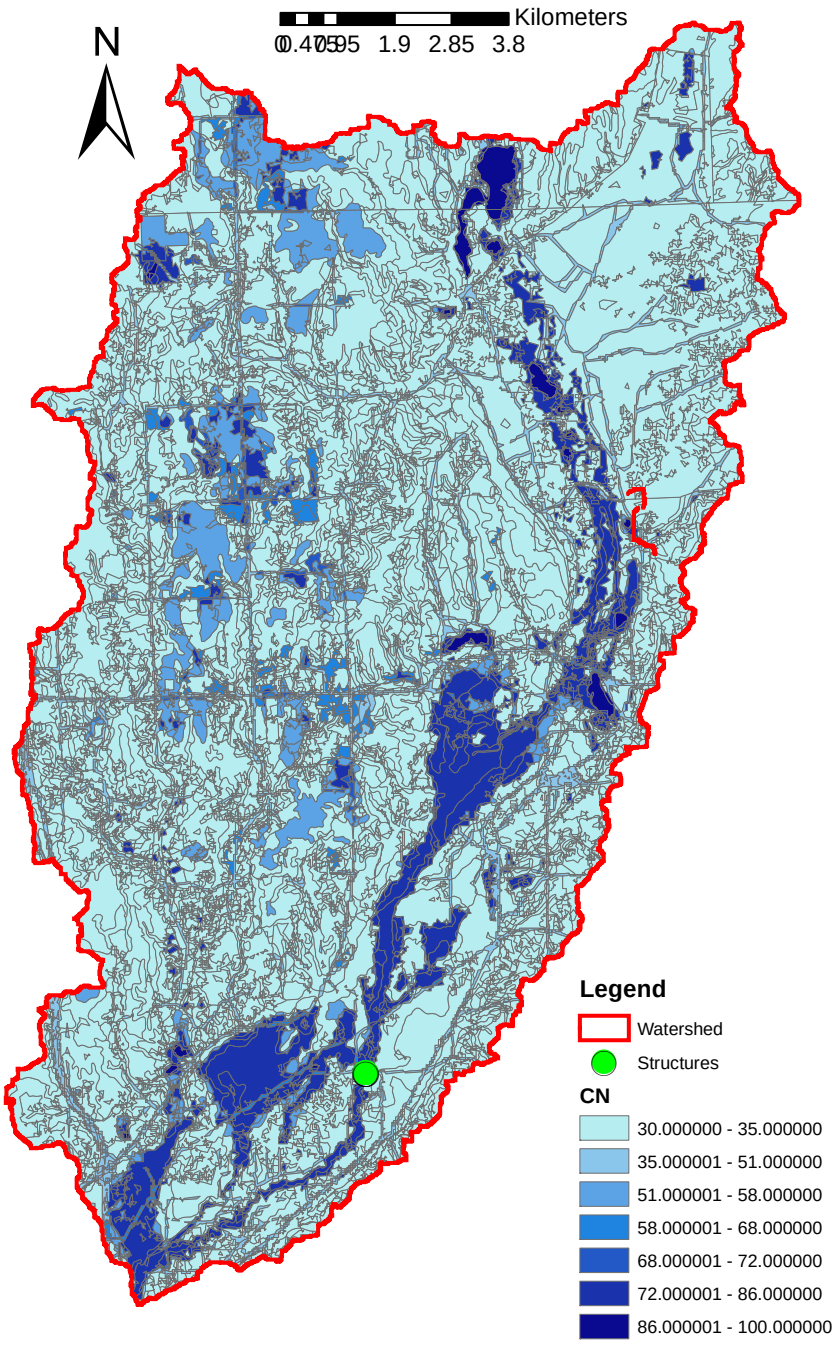

Figure 3.17. East Branch Au Sable River watershed curve numbers

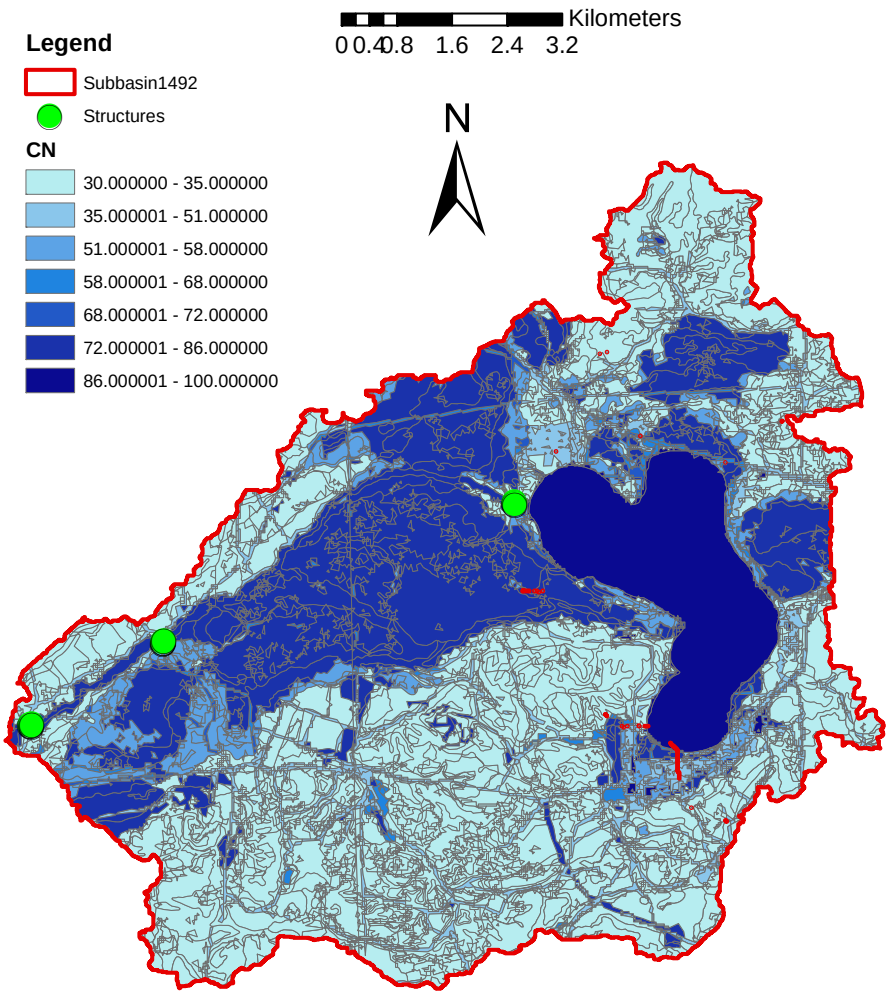

Figure 3.18. Portage Creek watershed curve numbers

3.2.5 Topography and Survey

Topography of East Branch Au Sable River and Portage Creek watersheds were developed from light detection and ranging (LiDAR) data generated from a LiDAR mission provided for the Army's Sustainable Range Program (SRP). A digital elevation model (DEM) was developed based upon the LiDAR data (Figure 3.19 and Figure 3.20). The DEMs are in meters. Survey of study sites was completed May 18-20, 2015 by the USACE. Survey included structure measurement, channel topography up to top of bank, and other relevant data.

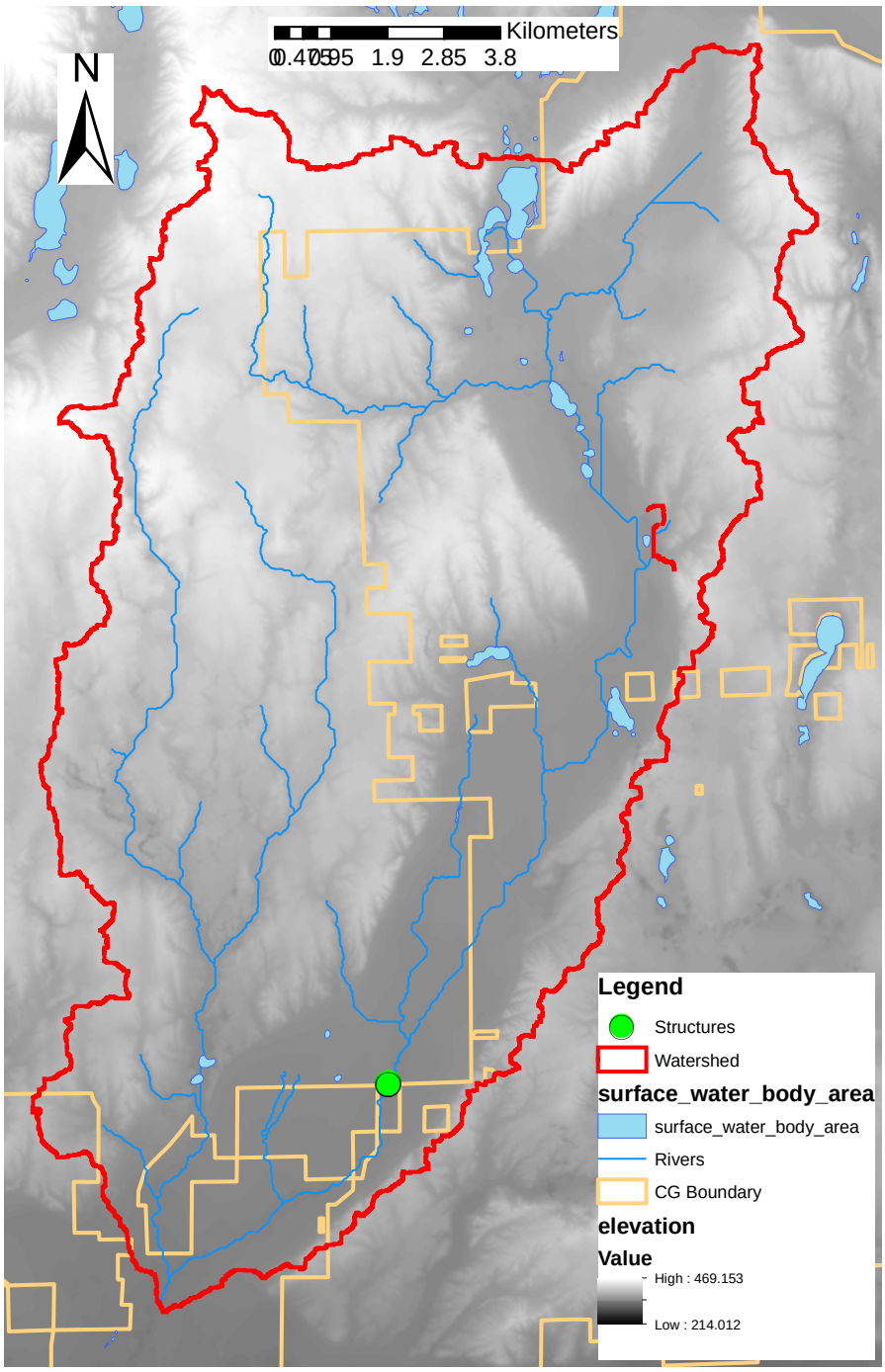

Figure 3.19. East Branch Au Sable River watershed topography (from LiDAR)

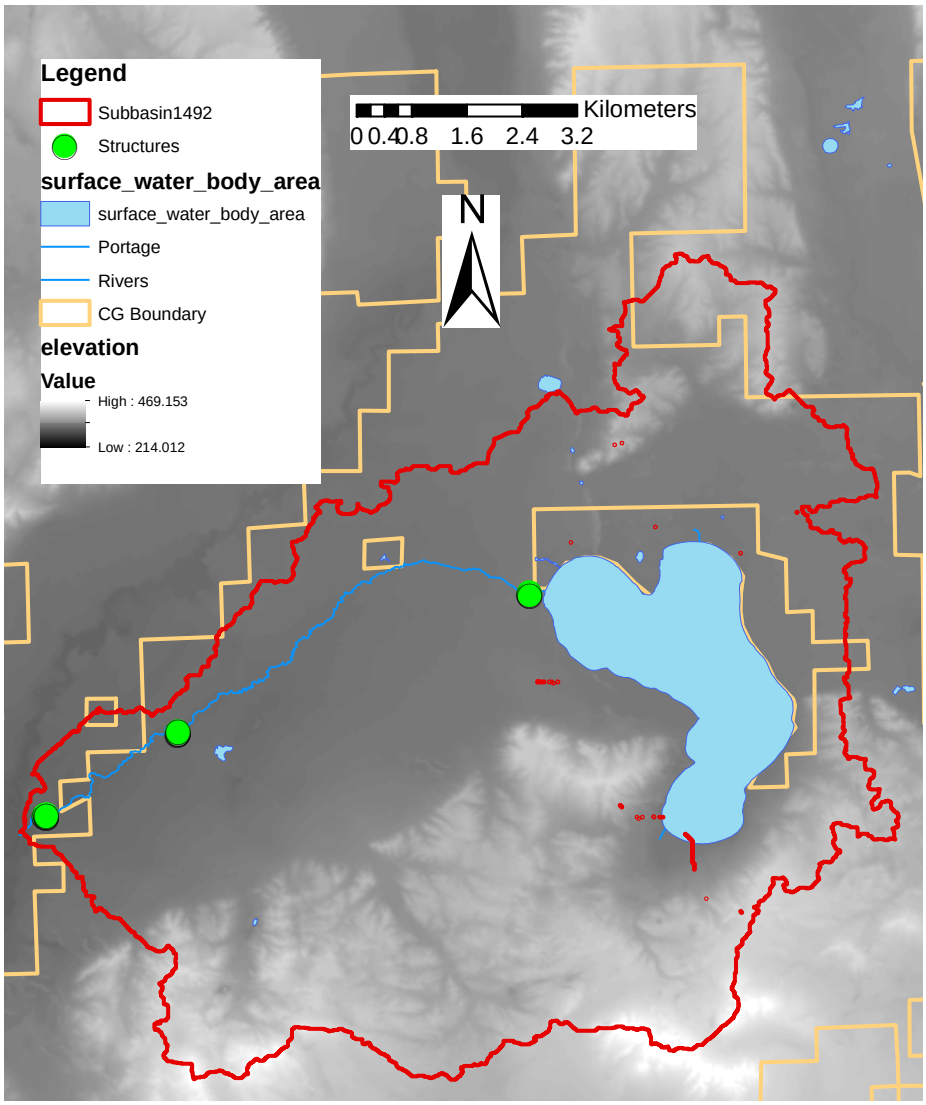

Figure 3.20. Portage Creek watershed topography (from LiDAR)

3.2.6 Precipitation Data

Precipitation measurements were obtained from the NWS Cooperative Observer Program's database maintained by the National Oceanic and Atmospheric Administration's (NOAA) National Climatic Data Center (NCDC). The location of each gauge is show in Figure 3.21 and the ID and record length are show in Table 3.8.

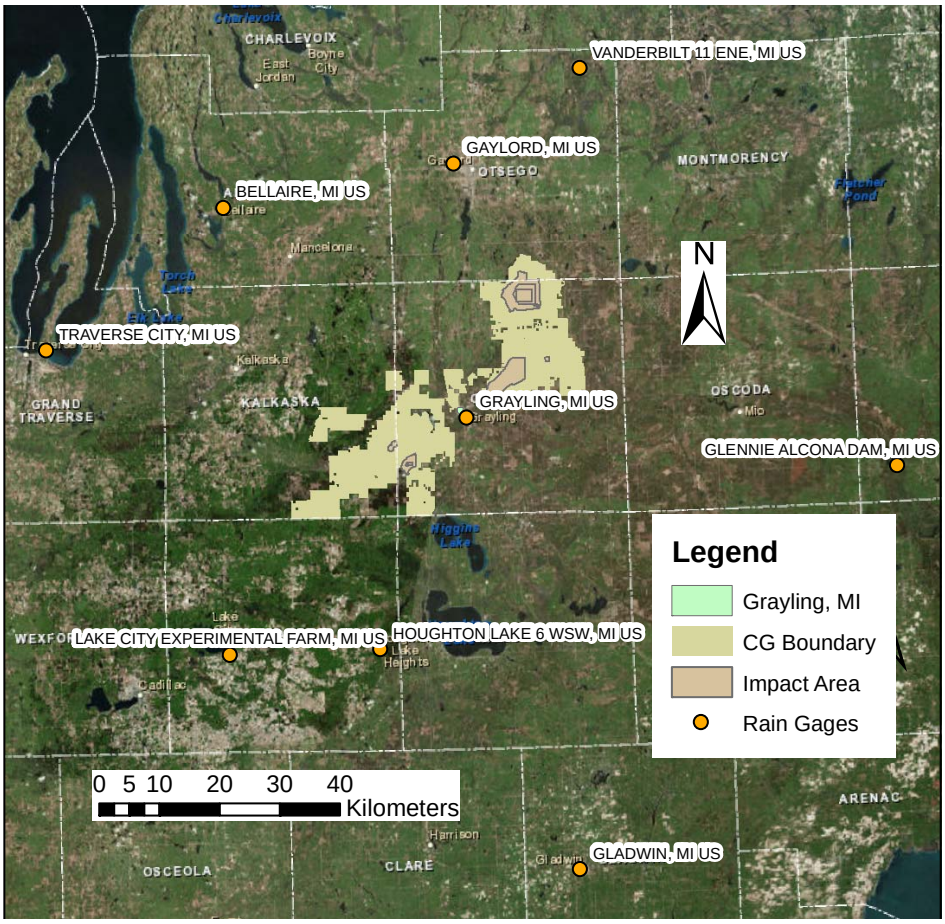

Figure 3.21. Central Michigan rain gauge locations

Table 3.8. Central Michigan rain gauge information

Name	Network	ID	Lat/Lon	Elevtaion	Start Date	End Date	Coverage
BELLAIRE, MI US	GHCND	USC00200662	44.9758°, -85.198°	190.5 m	7/1/1948	Present	98%
GAYLORD, MI US	GHCND	USC00203096	45.0332°, -84.7113°	401.7 m	1/1/1893	Present	78%
GRAYLING, MI US	GHCND	USC00203391	44.6541°, -84.6994°	346.3 m	1/1/1891	Present	97%
HOUGHTON LAKE 6 WSW, MI US	GHCND	USC00203932	44.3119°, -84.8922°	345.9 m	12/3/1912	Present	95%
KALKASKA, MI US	GHCND	USC00204257	44.728°, -85.1727°	315.5 m	12/1/1938	Present	99%
LAKE CITY EXPERIMENTAL FARM, MI US	GHCND	USC00204502	44.3088°, -85.205°	374.9 m	7/1/1892	Present	78%
MIO HYDRO PLANT, MI US	GHCND	USC00205531	44.6613°, -84.1316°	292.6 m	5/1/1892	12/31/2006	86%
VANDERBILT 11 ENE, MI US	GHCND	USC00208417	45.1702°, -84.4397°	275.8 m	2/1/1913	Present	97%

3.2.7 Past Studies

A 2008 study of the Lake Margrethe outlet dam and water levels was conducted by the Northwest Design Group of Petoskey, Michigan to address high year-around water levels in the lake. The study recommended dredging of Portage Creek between the lake and the outlet dam, which was subsequently completed. Survey data, flow data, and outlet dam geometry provided in the Northwest Design Group study report were incorporated into this study. A watershed assessment of Portage Creek watershed is also under contract with the Camp Grayling Environmental Office as of summer 2016, but no work has been completed.

3.3 Edger County, Illinois

Edgar County is located in East-Central Illinois, bordering Indiana to the east. The county seat is Paris, Illinois (Figure 3.22). The county is primarily agricultural with little relief except in the southern part of

the county, which also contains some forests. The eastern half of the county drains to the Wabash River via various smaller tributaries, while the western half drains to the Wabash River via the larger Embarras River. The two LWCs are located in the southern part of Edgar County.

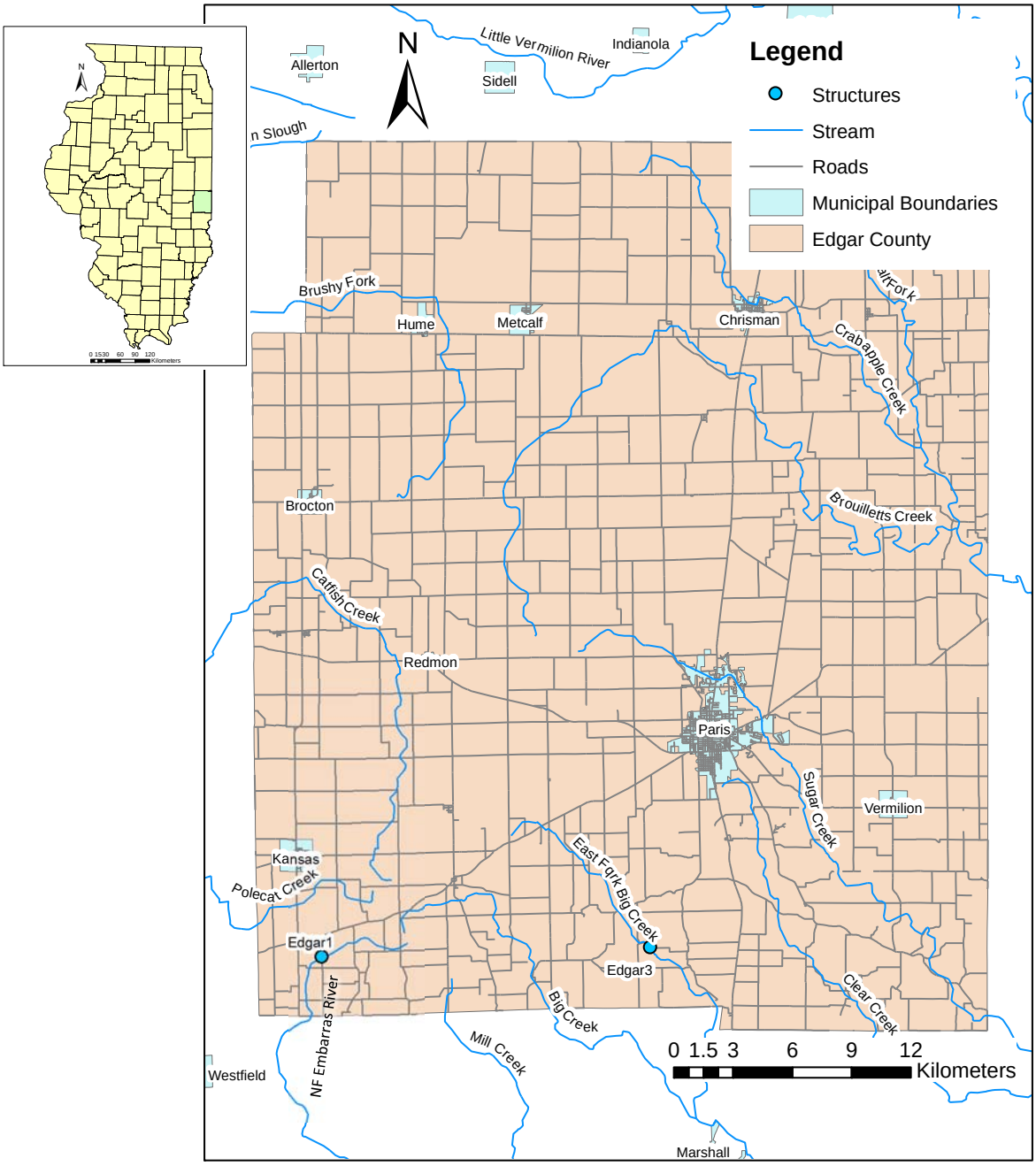

Figure 3.22. Edgar Country Location Map

3.3.1 LWC Sites

Two vented LWCs were modeled and analyzed for this project, one crossing the North Fork Embarras River and the other crossing East Fork Big Creek. The LWC over North Fork Embarras River (Edgar1) is vented with one corrugated metal arch culvert carrying N 200th Street. The arch culvert is 2.67 m wide and 0.76 m tall (8.75 ft x 2.5 ft). The LWC over East Fork Big Creek (Edgar3) is vented with two 0.31 m (1 ft) diameter corrugated metal culverts carrying E 300th Road. Both are secondary oil and chip roads while the LWCs are poured concrete slabs. See Figure 3.23 for structure pictures and Figure 3.24 and Figure 3.25 for structure locations.

Figure 3.23. Edgar County crossings Edgar1 and Edgar3 (top and bottom, respectively)

3.3.2 Hydrology

North Fork Embarras River is a tributary to the Embarras River within the Embarras HUC-8 watershed. The tributary is approximately 4.4 km in length upstream of 200th Street. The watershed upstream of the LWC is 11.3 km^2 (4.4 mi^2). North Fork Embarras River confluences with the Embarras River near Sainte Marie, Illinois , which flows into the Wabash River between Vincennes, Indiana and St. Francisville, Illinois. The study watershed is predominately row crop (Figure 3.24). The study watershed and stream reach is a dredged trapezoidal channel in the upper reaches and a natural channel within the forested reach.

The study reach contains a downstream slope of approximately 0.0034 (V/H). The stream was classified using Chow (1959) to determine the appropriate Manning's n value of the reach. The value assigned for Manning's n was 0.04 within the channel and 0.04 or 0.1 for floodplain dominated by either row crops or heavy timber stands.

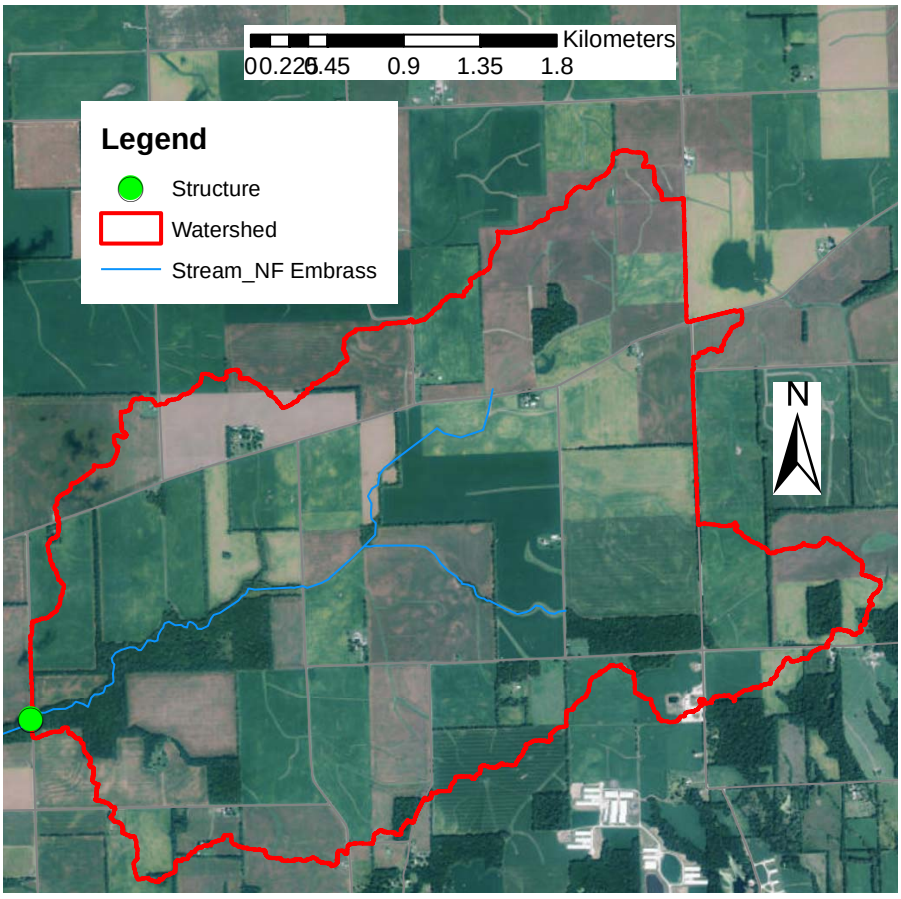

Figure 3.24. North Fork Embarras River watershed overview

East Fork Big Creek is a tributary to Big Creek within the Big Creek HUC-8 watershed. The tributary is approximately 10.5 km in length upstream of E 300th Road. The watershed upstream of the LWC is 34.7 km^2 (13.4 mi^2). East Fork Big Creek confluences with West Fork Big Creek north of Marshall, Illinois to form Big Creek, which flows into the Wabash River between Terre Haute, Indiana and Hutsonville, Illinois. The study watershed is predominately crow crop with forest along the floodplains (Figure 3.25). The study watershed and stream reach is a dredged trapezoidal channel in the upper reaches and a natural channel within the forested reach. USGS Gauge 03341700 operated 1961-1975 on an Unnamed Tributary to East Fork Big Creek at N 925th Street south of Route 16. The gauge location corresponds to J115 of the HEC-HMS model.

The study reach contains a downstream slope of approximately 0.0029 (V/H). The stream was classified using Chow (1959) to determine the appropriate Manning's n value of the reach. The value assigned for Manning's n was 0.04 within the channel and 0.04 or 0.1 for floodplain dominated by either row crops or heavy timber stands.

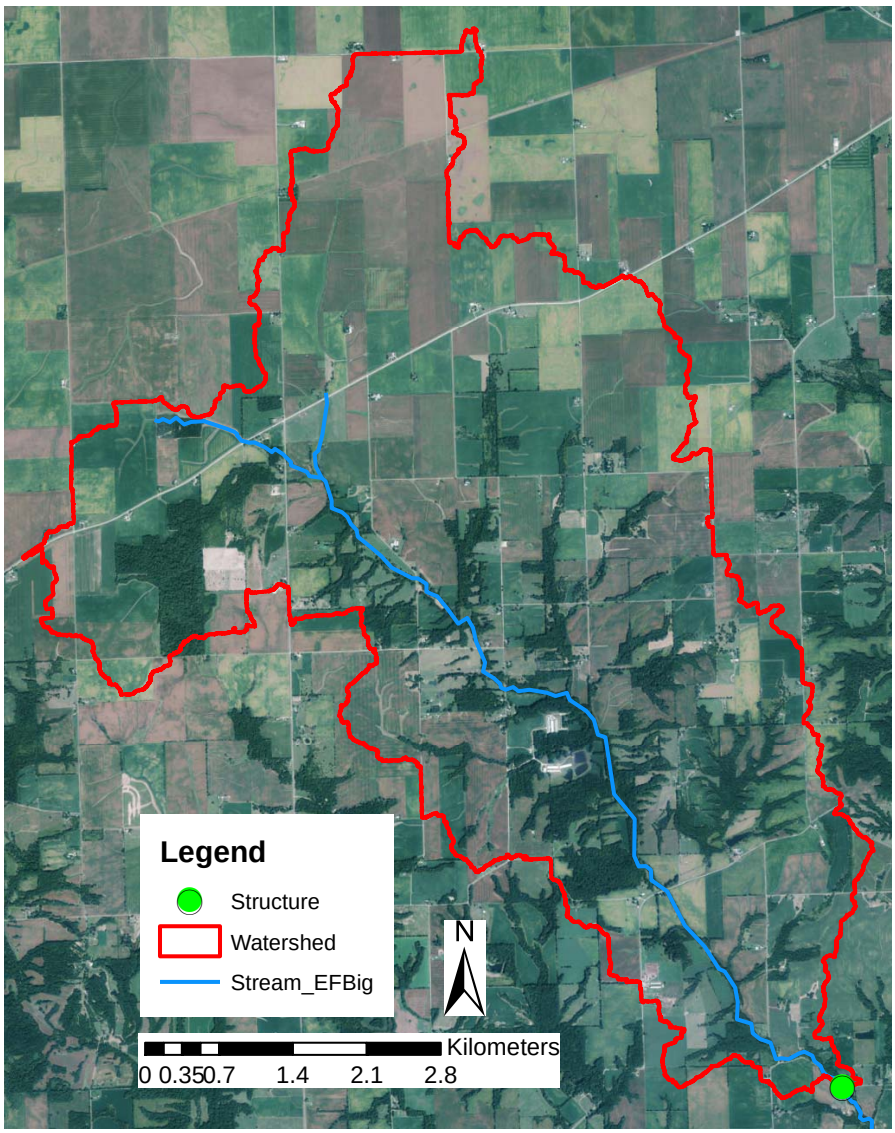

Figure 3.25. East Fork Big Creek watershed overview

3.3.3 Soils

The majority of the North Fork Embarras River and East Fork Big Creek watersheds have soils in the "B/D" or "C" hydrologic group (see Figure 3.26, Figure 3.27, Table 3.9, and Table 3.10) (USDA, 1986). Soil groups with drainage characteristics affected by a high water table are indicated with a "/D" designation, where the letter preceding the slash indicates the hydrologic group of the soil under drained conditions. Half of all land designated with row crop land use was assumed to be under drained.

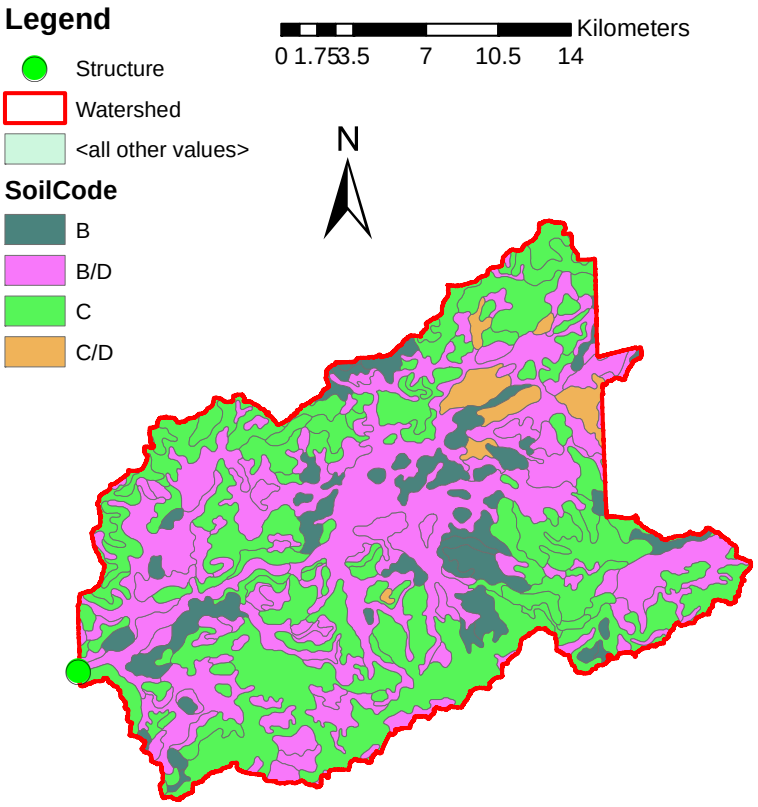

Figure 3.26. North Fork Embarras River watershed hydrologic soil groups

Table 3.9. North Fork Embarras River watershed hydrologic soil groups by percent area

% Area	Hydrologic Soil Type
7.85%	B
50.20%	B/D
40.24%	C
1.71%	C/D

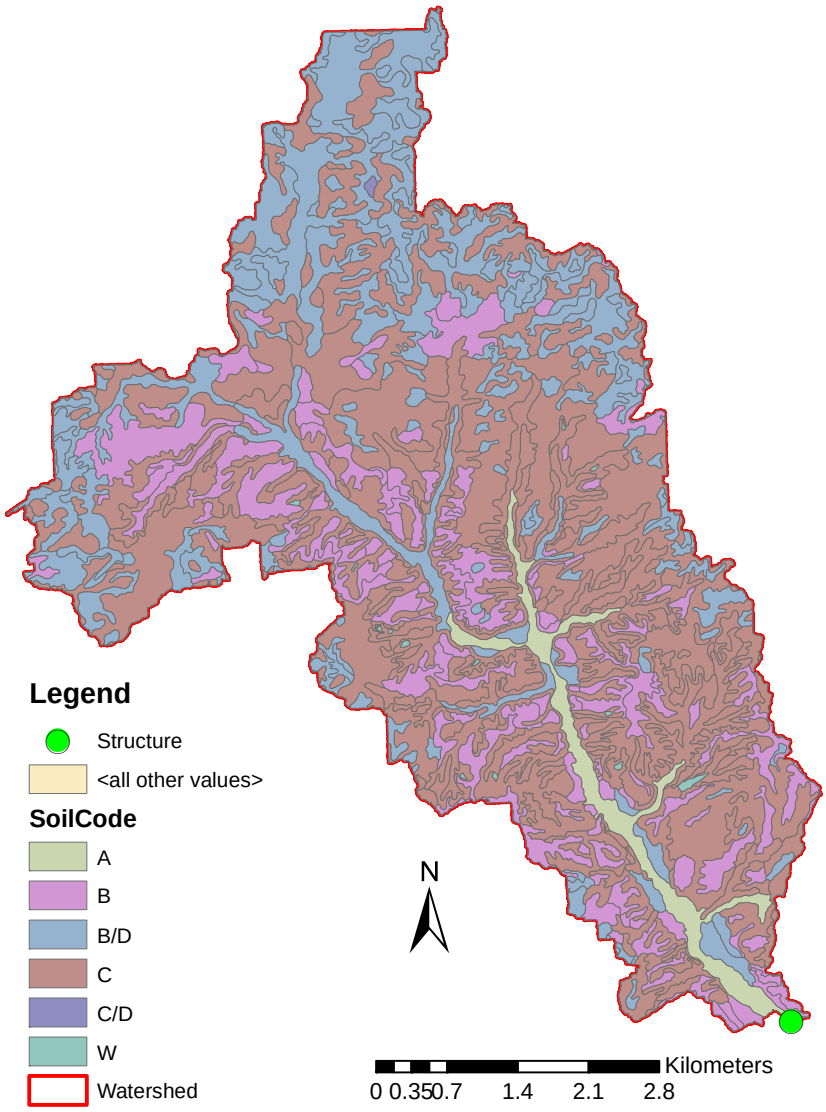

Figure 3.27. East Fork Big Creek watershed hydrologic soil groups

Table 3.10. East Fork Big Creek watershed hydrologic soil groups by percent area

% Area	Hydrologic Soil Type
4.89%	A
7.86%	B
57.70%	B/D
29.27%	C
0.06%	C/D
0.21%	Water

3.3.4 Land Use

Land cover within the North Fork Embarras River watershed is primarily row crop agriculture with deciduous forest along the river floodplain (See Figure 3.28 and Table 3.11) (Homer et al., 2015). Land cover within the East Fork Big Creek watershed is also primarily row crop agriculture with deciduous forest along the river floodplain (See Figure 3.29 and Table 3.12). Roads account for the only developed areas.

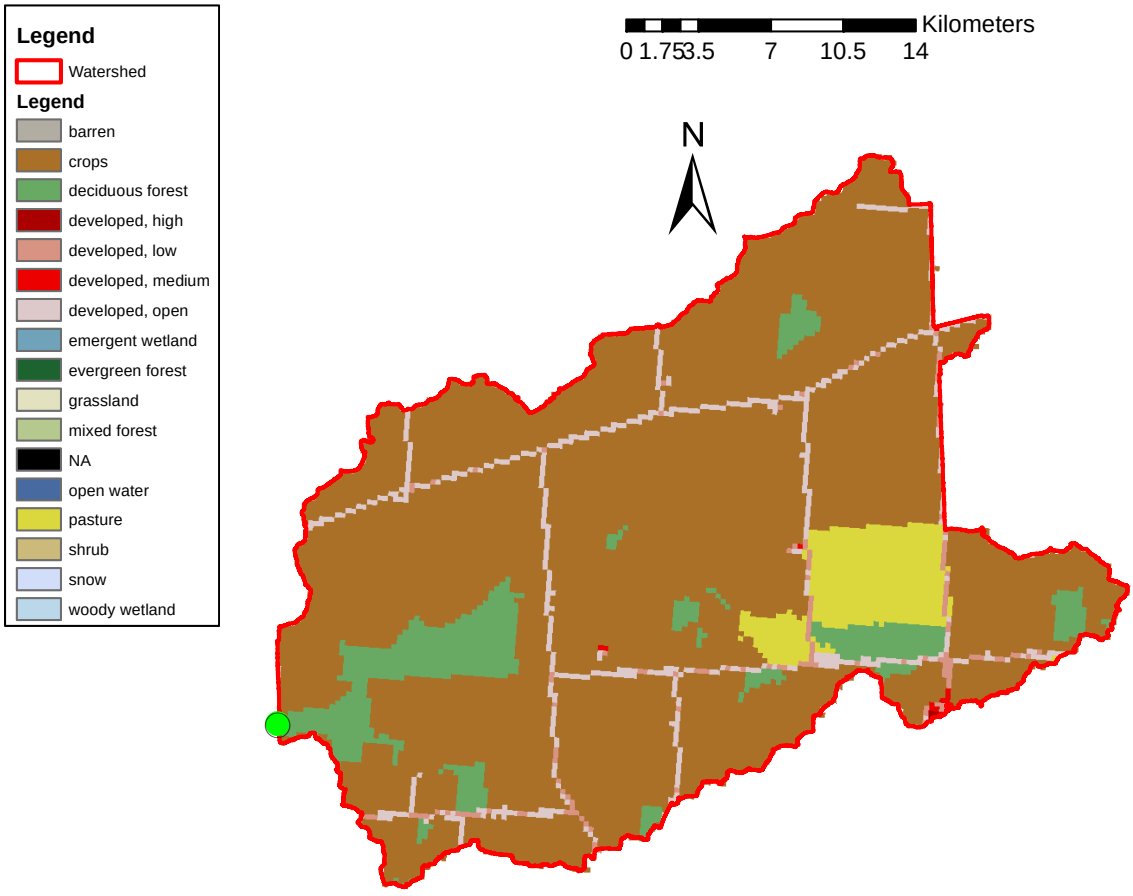

Figure 3.28. North Fork Embarras River watershed NLCD land cover

Table 3.11. North Fork Embarras River watershed NLCD land cover by percent area

% Area	NLCD Land Cover	% Area	NLCD Land Cover
0.00%	Open Water	0.00%	Mixed forest
2.61%	Developed, open	0.00%	Shrub
0.73%	Developed, low	0.00%	Grassland
0.08%	Developed, medium	3.02%	Pasture
0.03%	Developed, high	88.77%	Crops
4.77%	Deciduous forest	0.00%	Woody wetland
0.00%	Evergreen forest	0.00%	Emergent wetland

Table 3.12. East Fork Big Creek watershed NLCD land cover by percent area

% Area	NLCD Land Cover	% Area	NLCD Land Cover
0.00%	Open Water	0.00%	Mixed forest
4.96%	Developed, open	0.00%	Shrub
1.69%	Developed, low	0.36%	Grassland
0.02%	Developed, medium	6.37%	Pasture
0.00%	Developed, high	80.26%	Crops
6.33%	Deciduous forest	0.00%	Woody wetland
0.00%	Evergreen forest	0.00%	Emergent wetland

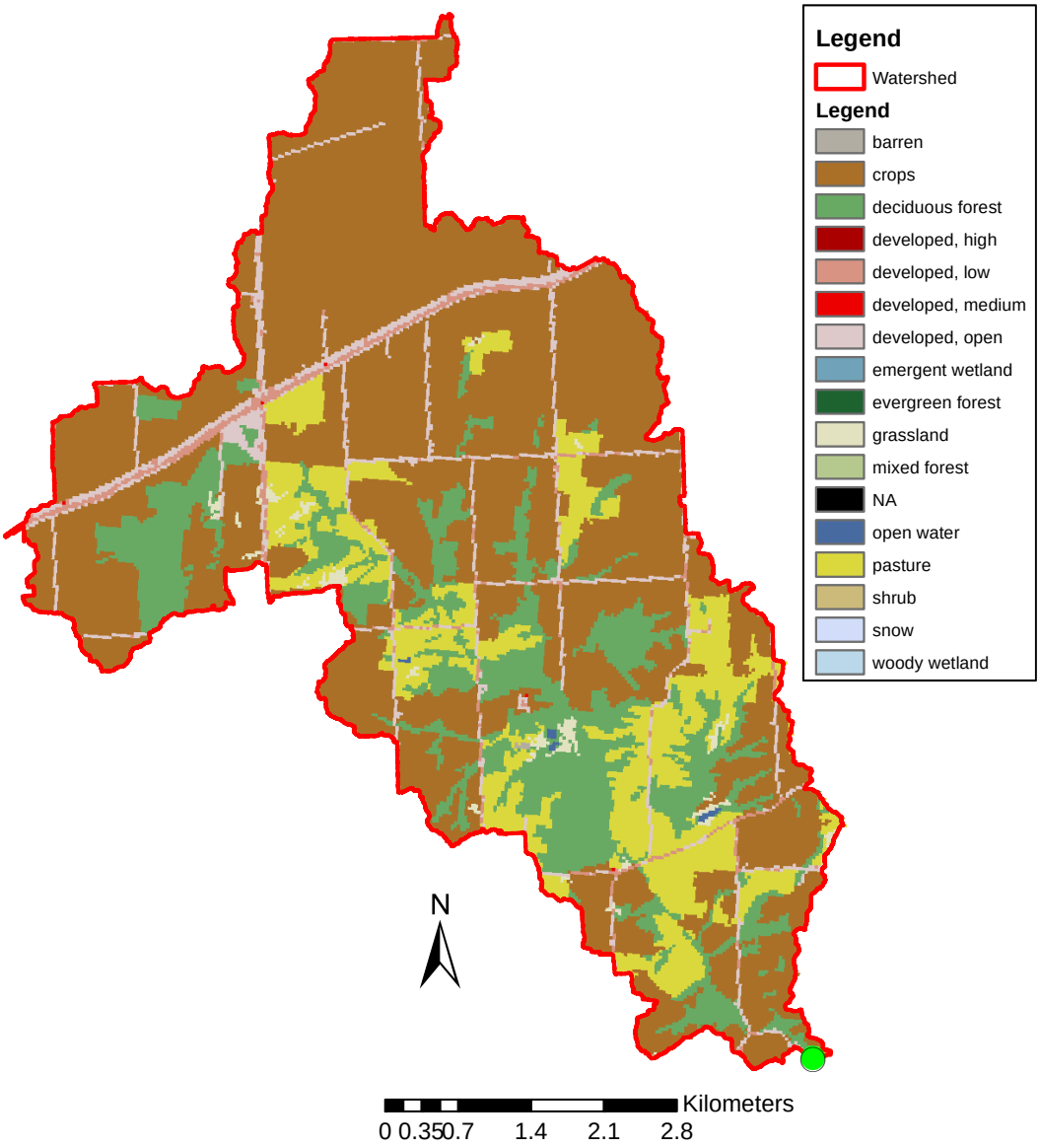

Figure 3.29. East Fork Big Creek watershed NLCD land cover

Specific combinations of land use and soil type were linked to Curve Number (CN) values as described in Section 6.2.3 (USDA, 1986). A GIS raster file was created for North Fork Embarras River and East Fork Big Creek watersheds to digitize the CN values for use in HEC-geoHMS. Figure 3.30 and Figure 3.31 show the distribution of CN values throughout the North Fork Embarras River and East Fork Big Creek watersheds, respectively.

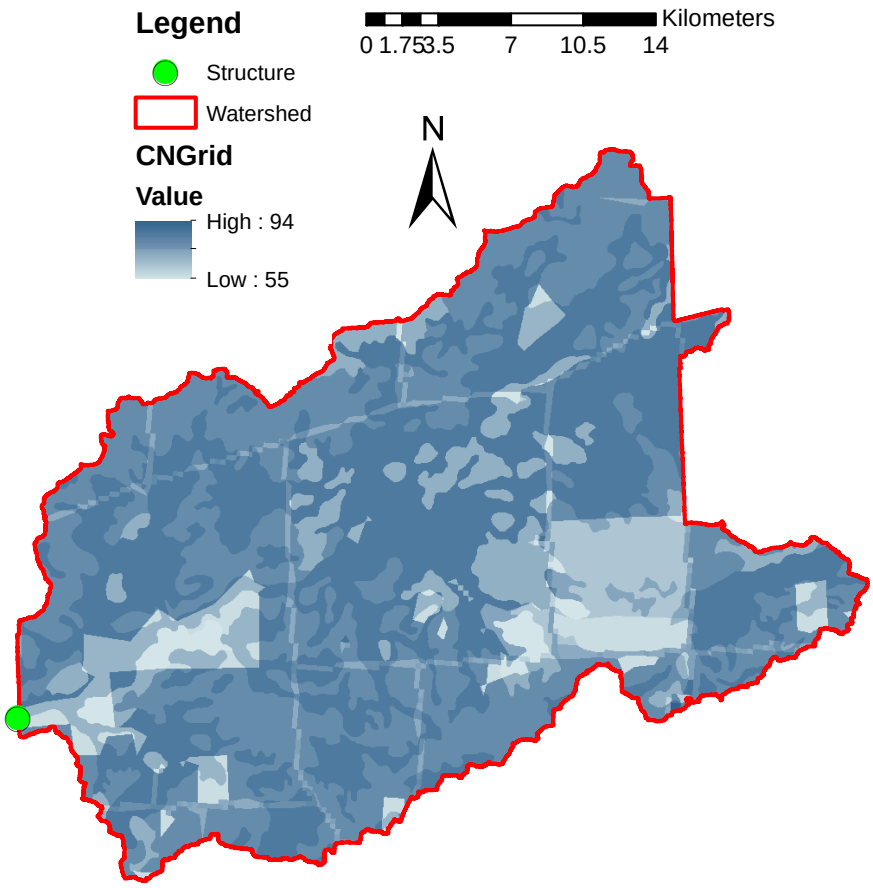

Figure 3.30. North Fork Embarras River watershed curve numbers

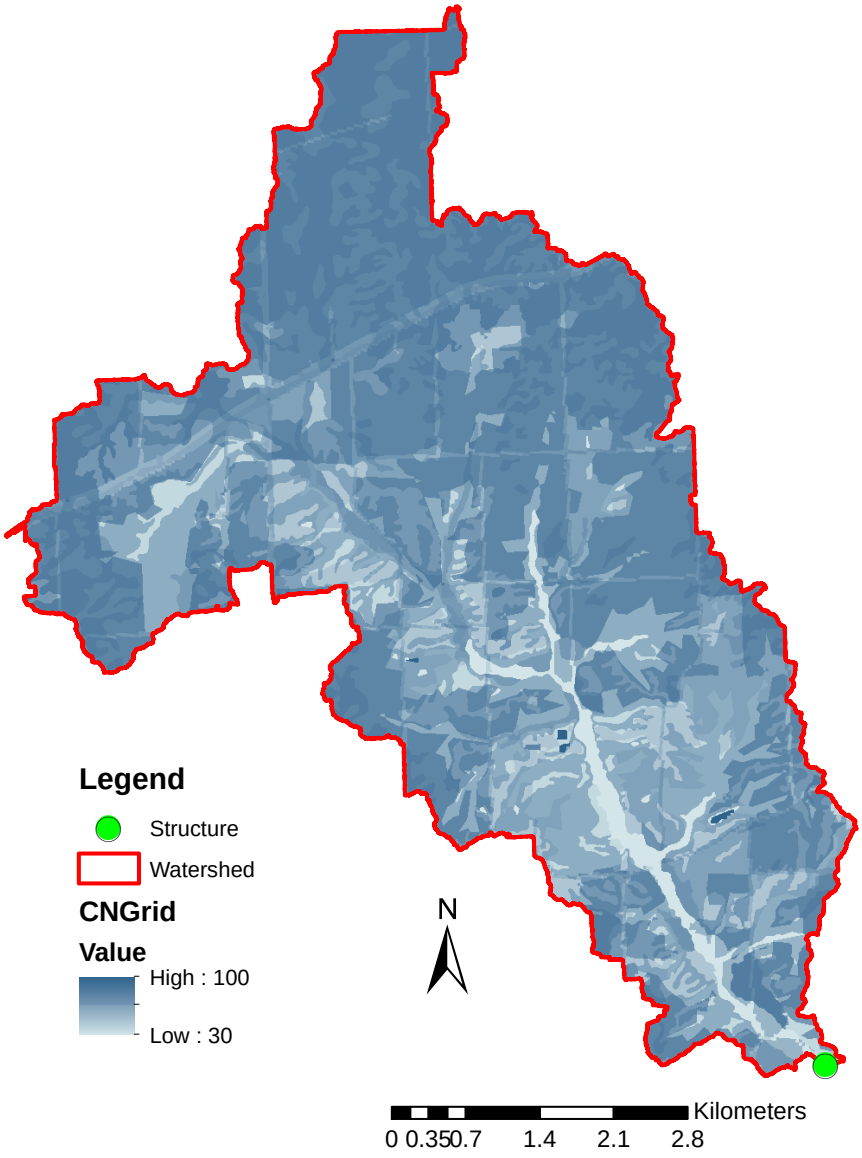

Figure 3.31. East Fork Big Creek watershed curve numbers

3.3.5 Topography and Survey

Topography of North Fork Embarras River and East Fork Big Creek watersheds were developed from light detection and ranging (LiDAR) data generated from a 2012 LiDAR mission provided for the Illinois Department of Transportation as part the of the Illinois Height Modernization Program. A digital elevation model (DEM) was developed based upon the LiDAR data (Figure 3.32 and Figure 3.33). The

DEMs are in meters. Survey of study sites was completed July 7, 2015 by the USACE and the Agricultural and Biological Engineering Department at the University of Illinois. Survey included structure measurement, channel topography up to top of bank, and other relevant data.

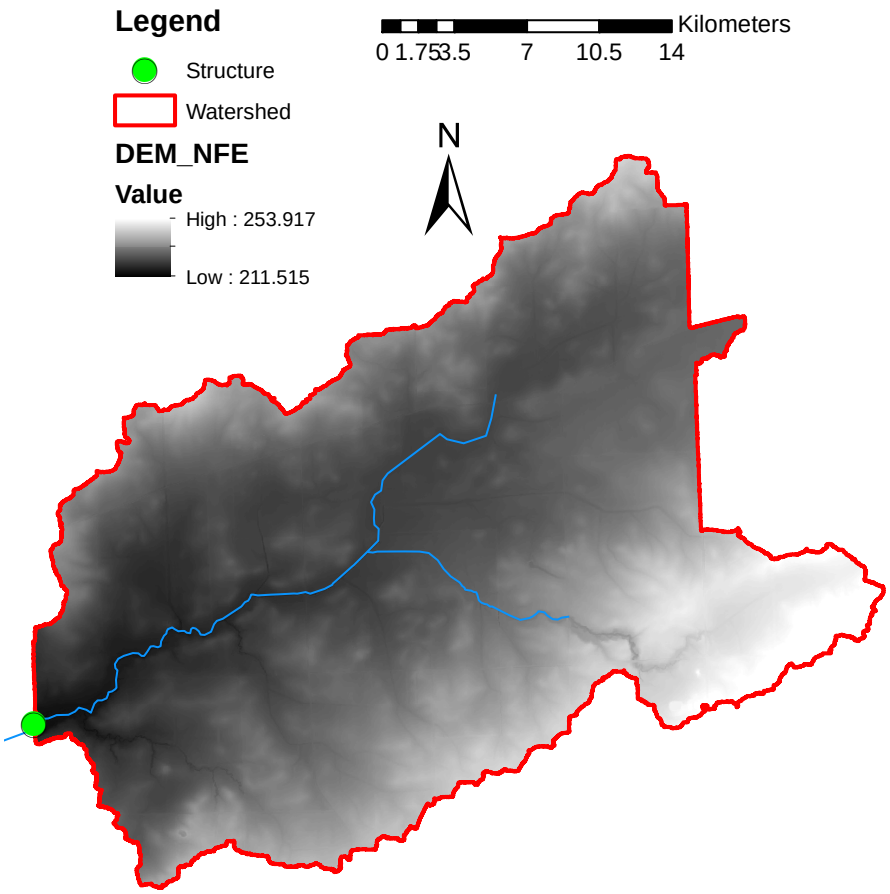

Figure 3.32. North Fork Embarras River watershed topography (from LiDAR)

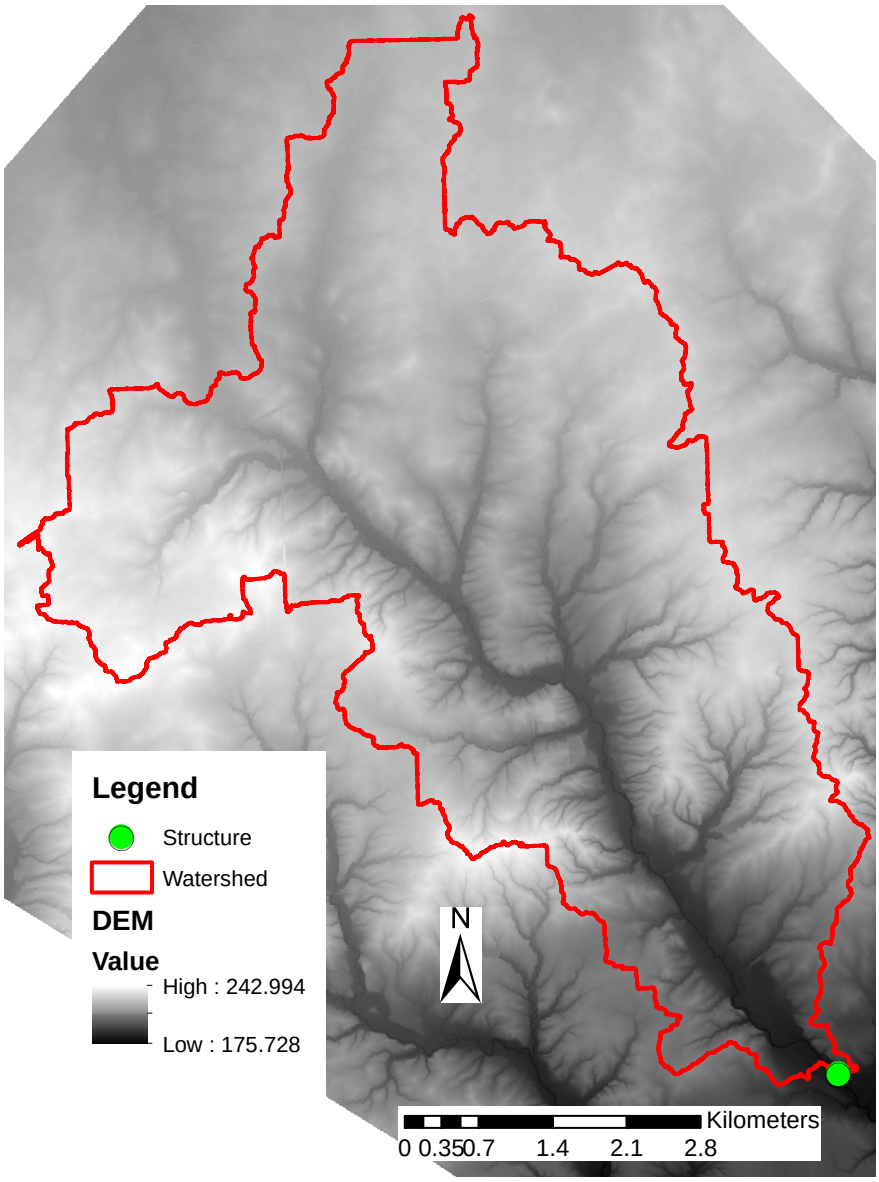

Figure 3.33. East Fork Big Creek watershed topography (from LiDAR)

3.3.6 Precipitation Data

Precipitation measurements were obtained from the NWS Cooperative Observer Program's database maintained by the National Oceanic and Atmospheric Administration's (NOAA) National Climatic Data Center (NCDC). The location of each gauge is show in Figure 3.34 and the ID and record length are show in Table 3.13.

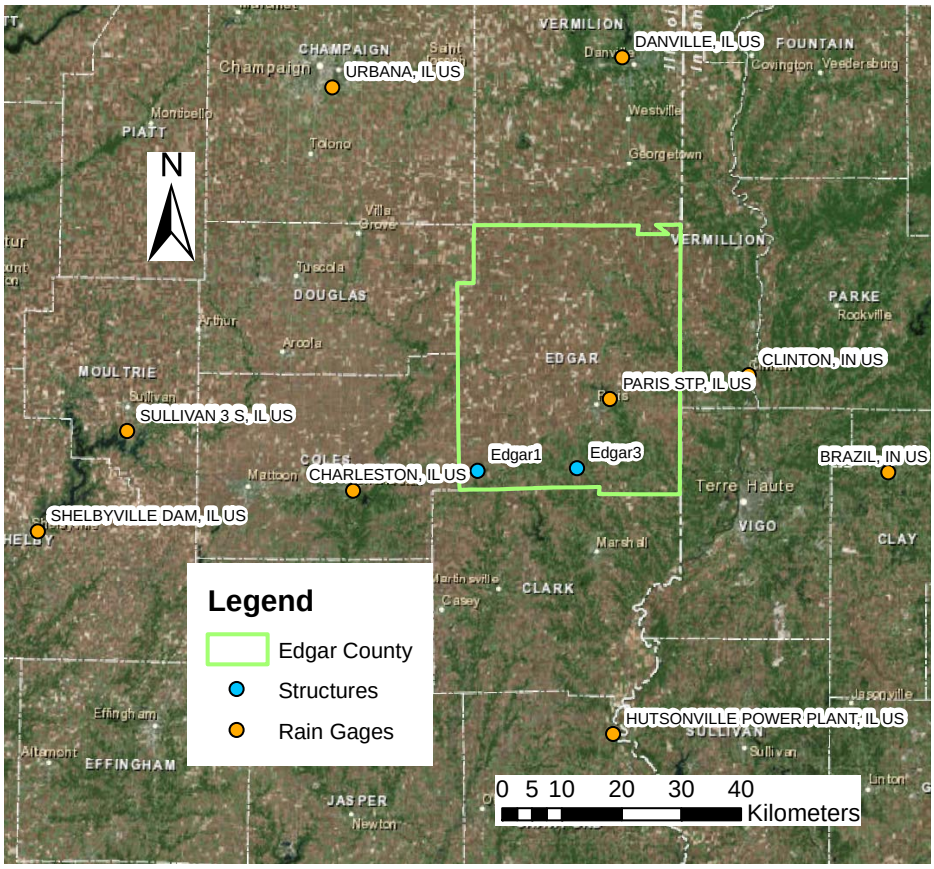

Figure 3.34. East-Central Illinois rain gauge locations

Table 3.13. East-Central Illinois rain gauge information

Name	Network	ID	Lat/Lon	Elevtaion	Start Date	End Date	Coverage
CHARLESTON, IL US	GHCND	USC00111436	39.4762°, -88.1652°	213.4 m	1/1/1896	Present	97%
GREENUP 3 SE, IL US	GHCND	USC00113683	39.2283°, -88.1261°	166.1 m	6/1/1942	8/31/2003	93%
HUTSONVILLE POWER PLANT, IL US	GHCND	USC00114317	39.1138°, -87.6563°	134.1 m	5/3/1946	Present	97%
MATTOON, IL US	GHCND	USC00115430	39.4726°, -88.3545°	212 m	1/1/1893	Present	63%
PARIS STP, IL US	GHCND	USC00116610	39.6185°, -87.6672°	199 m	4/1/1893	Present	98%
SIDELL 4 N, IL US	GHCND	USC00117952	39.9677°, -87.8228°	204.8 m	9/1/1913	Present	71%
TUSCOLA, IL US	GHCND	USC00118684	39.7946°, -88.2909°	199.6 m	3/1/1893	Present	94%
ROCKVILLE, IN US	GHCND	USC00127522	39.7594°, -87.2269°	211.2 m	1/1/1893	Present	97%
TERRE HAUTE INDIANA STATE, IN US	GHCND	USC00128723	39.4708°, -87.408°	154.5 m	9/1/1954	Present	90%

3.3.7 Past Studies

No known studies have been completed on or near the two study reaches.

3.4 Climate Change Models

This study utilizes climate models provided by the Center for Climate Research at the University of Wisconsin-Madison. Four global climate models (GCMs) from the Coupled Model Intercomparison Project Phase Five (CMIP5) were dynamically downscaled to 25-km grid spacing according to the representative concentration pathway 8.5 (RCP8.5) scenario using the Abdus Salam International Centre for Theoretical Physics (ICTP) Regional Climate Model Version Four (RegCM4) (Notaro et al., 2015). The four CMIP5 GCMs downscale by RegCM4 include the Centre National de Recherches Meteorologiques Coupled Global Climate Model Version Five (CNRM-CM5) (Voldoire et al., 2012), the Model for Interdisciplinary Research on Climate Version Five (MIROC5) (Watanabe et al., 2010), the Institute Pierre

Simon Laplace Coupled Model Version Five-Medium Resolution (IPSL-CM5-MR) (Dufresne et al., 2013), and the Meteorological Research Institute Coupled Global Climate Model Version Three (MRI-CGCM3) (Yukimoto et al., 2012). These models will be denoted as CNRM, IPSL, MIROC, and MRI, respectively. The GCMs and the RCM are reviewed in more detail in Section 5.2.1 Climate Models.

Chapter 4 – PRECIPITATION TRENDS 1950-2009

Abstract

The stationary assumption of total annual precipitation, total annual wet days and wet hours, annual maximum series (AMS) (1-hr and 24-hr), and extreme storm frequencies (roughly the 95th – 99th percentile were tested for regions centered around central Indiana, central Michigan, and east central Illinois. Precipitation series data were plotted over time at each gauge site to determine possible visual trends. Both parametric and non-parametric statistical tests were used to detect trends. In addition, precipitation frequency estimates were calculated for the 0.5-, 1-, 2-, 5-, 10-, 25-, 50-, and 100-year ARIs and durations of 1-, 2-, 3-, 6-, 12-, and 24-hr; and 2-, 5-, and 10-days for three different time periods 1970-1989, 1980-1999, and 1990-2009.

The results suggest the assumption that precipitation is stationary over time with regards to total annual rainfall and storm frequency and intensity is not valid for the three Midwest regions. Total annual precipitation has increased over the past century as well as average annual wet days in Michigan and Illinois, while average annual wet hours have remained the same or slightly decreased in some areas. The intensity of large events has generally stayed neutral across the region, but have shown increases and decreases at individual gauges for durations of 24- and 1-hr, respectively. Finally, the frequency of large storm events (24-hr duration) has increased across the region. Results indicate the frequency of extreme events up to the 95th but less than 99th percentile storms are increasing in Michigan and Illinois while the frequency of extreme events up to about the 99th percentile storm are increasing in Indiana. For the 1-hr duration, the frequency of extreme events up to the 95th percentile storm are increasing in Indiana, but are natural in the other regions.

Precipitation regional frequency analysis was used to estimate of how often specific events (for numerous return periods and durations) occur and how they changed between 1970-1989 and 1990-2009. Results were mixed, but indicate longer duration events (>12hrs) generally increase from the former to the latter time period across the Indiana and Illinois regions.

Keywords: Precipitation, stationarity, trend tests, precipitation regional frequency analysis

4.1 Introduction

Understanding the stationarity (or lack of stationarity) of precipitation is important for hydrologic and climate changes assessments. Stationarity, or the assumption that the statistical characteristics of hydrologic time series data are constant through time, enables the use of well-accepted, simplified statistical methods in water resources planning and design (USACE, 2014). If precipitation isn't stationary, fitting statistical distributions to historical precipitation data for regional precipitation analyses may be invalid (Huff and Angel, 1992). With regards to climate modeling, modeling subroutines, downscaling methods, and bias correction methods all suffer from varying degrees of the assumption of precipitation variable stationarity (Pielke and Wilby, 2012 & Folwer and Kilsby, 2007). The comparison of observed data at the same location over different time frames can inform the stationary assumption of precipitation magnitudes and frequencies.

The twentieth century marked the beginning of reliable, wide-spread rain gauge record keeping. Daily precipitation data is available in the Midwest from the turn of the last century while sub daily data became widely available starting between 1950 and 1970. Numerous studies have sought to quantify changes and tends in total precipitation (annual or seasonal) and precipitation intensity and frequency, especially focusing on long duration events of 1 – 7 days (eg: Groisman et al., 2005; Karl and Knight,

1998). Such work has also included regional precipitation frequency analyses considered for different time periods. Previous studies have generally found an increase in total annual precipitation. Groisman et al. (2012), Madsen and Figdor (2007), Pryor et al. (2009), and others have attributed the increases in annual precipitation to increases in the frequency of large storm events (durations of 1-7 days) while others (eg: Karl and Knight, 1998; Melillo et al., 2014) determined increases in both the frequency and intensity of large storm everts play a role (durations of 1-7 days).

The stationary assumption of total annual precipitation, total annual wet days and wet hours, AMS (1-hr and 24-hr), and storm frequency are tested for regions centered around central Indiana, central Michigan, and east central Illinois. Little work has been done to analyze sub daily precipitation data, and so to this end, both 24-hr and 1-hr data is analyzed. Precipitation series data are plotted over time at each gauge site to determine possible visual trends. Both parametric and non-parametric statistical tests are used to detect trends. In addition, precipitation frequency estimates were calculated for the 0.5-, 1-, 2-, 5-, 10-, 25-, 50-, and 100-year ARIs and durations of 1-, 2-, 3-, 6-, 12-, and 24-hr; and 2-, 5-, and 10-days for three different time periods 1970-1989, 1980-1999, and 1990-2009.

4.2 Methods

4.2.1 Rain Data

Precipitation measurements were obtained from the NWS Cooperative Observer Program's database maintained by the National Oceanic and Atmospheric Administration's (NOAA) National Climatic Data Center (NCDC). Stations were originally selected based on the availability of 1-hour duration data, the geographic location with regard to proposed LWC study sites, and a data record spanning at least 1980-1999. If both 1-hour and daily data was available at a station, only the 1-hour data was used in this

study as long as there was little differences between the datasets when the 1-hour data was converted to 24-hour data. Daily data was used for time periods preceding 1-hour data availability. Stations located within several miles of each other with complementary record periods and 1-hour data, were treated as a single station. Other precipitation data preprocessing, such as assessing and removing missing data, was completed using post-processed precipitation data provided by the Environmental Protection Agency's Basins 4.0 Meteorological Data sets, which consist of the same NCDC data at the same stations for the same time series as those utilized in this study (USEPA, 2013). Name, location, and record length of each station can be found in Chapter 3.

4.2.2 Trend Analysis

Precipitation frequency analysis methods are based on the assumption that annual maximum series (AMS) are stationary over time. An analysis of trends in historic precipitation data may provide insight and context for precipitation data for future time periods generated by climate change models. Total annual precipitation, precipitation event occurrences, and annual maximum series data were plotted over time at each gauge site to determine possible visual trends. Both parametric and non-parametric statistical tests were used to detect trends in the total annual precipitation and AMS mean and variance. Trends were examined at 1-hr and 24-hr durations and the null hypotheses was that there are no trends in totally annual precipitation and AMS means and/or variance. The 24-hr duration trends where tested at stations with at least 60 years of record. For the 1-hr duration trends, the record requirement was lowered to 40 years to increase sample size. The null hypotheses were tested at both the α = 5% and α = 10% levels of significance. McCuen (2016) suggested data analysis should include assessments of both statistical and hydrologic significance, where the latter is assessing how the findings might affect hydrologic design. Kirk (1996) explained that statistical significance is concerned with whether a research result is due to chance or sampling variability while practical (or hydrologic) significance is

concerned with whether the result is useful in the real world. Both the 95%-5% and the 90%-10% significance levels were tested as part of the trend analyses to assess both the statistical and hydrologic significance, respectively.

Levene's test (Levene, 1960) tests for the homogeneity of variances in the data. The test has been proven to be less sensitive to non-normality in data than some other commonly used tests (Perica et al., 2013). The test statistic (*W*) is given as (Levene, 1960):

$$W = \frac{(\mathrm{N}-\mathrm{k})}{(\mathrm{k}-1)} \frac{\sum_{i=1}^{k} \mathrm{N_i} \, (\mathrm{Z_{i.}} - \mathrm{Z_{..}})^2}{\sum_{i=1}^{k} \sum_{j=1}^{k} \mathrm{N_i} \left(\mathrm{Z_{ij}} - \mathrm{Z_{i.}}\right)^2}$$

Equation 4.1

where k is the number of sub-groups, N is the sample size, N_i is the sample size of the i^{th} subgroup, Y_{ij} is the value of the j^{th} sample from the i^{th} subgroup, and Z_{ij} is the absolute deviation of Y_{ij} from the mean of the i_{th} subgroup. The test rejects the hypothesis that the variances are equal if:

$$W > F_{a,k-i,N-k}$$

Equation 4.2

where $F_{a,k-i,N-k}$ is the upper critical value of the F distribution with k-1 and N-k degrees of freedom at α.

The Mann-Kendall test (Kendall, 1970) is a non-parametric test which compares the relative magnitudes of a data set. Non-parametric tests have advantages over parametric tests since they make no assumption of probability distribution, are performed without specifying whether the trend is linear or nonlinear, and are also more resilient to outliers in data, however, that they do not account for the magnitude of the data (Perica et al., 2013). If the annual value (total precipitation or annual maximum) is x_i for year t_i, the Mann-Kendall statistic (*S*) is given as:

$$S = \sum_{k=1}^{n-1} \sum_{i=k+1}^{n} sign(x_k - x_k)$$

Equation 4.3

The test statistic *Z* is computed using a normal approximation and standardization of *S* and the null hypothesis of no trend is rejected if $|Z|$ is greater than the critical value obtain from a standard normal distribution that has probability of exceedance of α/2 % (Perica et al., 2013). The sign of the statistic indicates the direction of the trend, positive or negative.

Parametric tests are generally more powerful than non-parametric tests when the data are approximately normally distributed and when the assumption of homogeneous variance holds but are less reliable when those assumptions do not hold (Perica et al., 2013). The parametric t-test for trends only considers the linear regression and therefore only checks for a linear trend in data. The test statistic is given as (Haan, 1977):

$$t = \frac{r\sqrt{n-2}}{\sqrt{1-r^2}}$$

Equation 4.4

where *r* is the Pearson correlation coefficient, and *n* in the record length. The null hypothesis is rejected if $|t|$ is greater than the critical value obtained from Student's distribution with (n - 2) degrees of freedom and exceedance probability of α/2 %, where α is the significance level (Perica et al., 2013). The sign of the *t*-statistic indicates the direction of the trend, positive or negative.

4.2.3 Precipitation Frequency Analysis

L-Moments

Precipitation frequency analysis is the estimate of how often a specific event occurs. In order to increase robustness and minimize uncertainty due to outliers at a single rain gauge, samples from

numerous gauges within a region are often used to generate regional precipitation frequency analyses. For this study a regional precipitation frequency analysis was completed for the three regions centered around Columbus, IN, Grayling, MI, and Paris IL using the L-Moments method (Hosking and Wallis, 1997) as implemented in the lmomRFA package (Hosking, 2015) in the statistical platform R (R Core Team 2014). The L-Moments method has been used in numerous studies to create IDF curves (eg. Bonnin et al., 2006; Perica et al., 2013; Markus et al., 2012) due to its robustness and distribution selection techniques.

The L-moments method uses linear combinations of ranked observations to produce estimates. L – moments have the theoretical advantages over conventional moments of being able to characterize a wider range of distributions and, when estimated from a sample, of being more robust to the presence of outliers in the data (Hosking, 1990). The L-moments method involves screening the precipitation data, assigning specified sites to a region, choosing a candidate distribution, and then applying that distribution to produce an estimate of the regional frequency distribution (Hosking and Wallis, 1997). Screening the precipitation data was accomplished for this study by applying the EPA Basins data described above. The regions to which the gauge sites are applied are not necessarily geographical, but instead consist of sites having similar values of those site characteristics that determine the frequency distribution (Hosking and Wallis, 1997). In the case of precipitation, regions are generally geographical, with occasional geographic outliers (Bonnin et al., 2006 & Perica et al., 2013).

L-moments used to calculate parameters of frequency distributions include 1st and 2nd order L-moments: L-locations (λ_1) and L-scale (λ_2), and the following L-moment ratios: L-CV (τ), L-skewness (τ_3), and L-kurtosis (τ_4). Let X be a random variable with a cumulative distribution function $F(x)$ and quantile

function $x(F)$, and let $X_{1:n} \leq X_{2:n...} \leq X_{k:n}$ be the order statistics of a random sample of size n drawn from the distribution X. The L-moments of a probability distribution are given in general as:

$$\lambda_r = r^{-1} \sum_{k=0}^{r-1} -1^k \binom{r-1}{k} \mathrm{E}(X_{r-k:r}), \qquad r = 1,2, \ldots$$

Equation 4.5

The specific L-moments are given as:

$$\lambda_1 = \mathrm{E}(X_{1:1})$$

Equation 4.6

$$\lambda_2 = \tfrac{1}{2}\mathrm{E}(X_{2:2} - X_{1:2})$$

Equation 4.7

$$\lambda_3 = \tfrac{1}{3}\mathrm{E}(X_{3:3} - 2X_{2:3} + X_{1:3})$$

Equation 4.8

$$\lambda_4 = \tfrac{1}{4}\mathrm{E}(X_{4:4} - 3X_{3:4} + 3X_{2:4} - X_{1:4})$$

Equation 4.9

The L-moment ratios are given as:

$$\tau = {}^{\lambda_2}/_{\lambda_1}$$

Equation 4.10

$$\tau_3 = {}^{\lambda_3}/_{\lambda_2}$$

Equation 4.11

$$\tau_4 = {}^{\lambda_4}/_{\lambda_2}$$

Equation 4.12

as per Hosking (1990).

The discordancy measure (D_i) indicates, for site i, the discordancy between the site's L-moment ratio and the unweighted regional average L-moment ratios (Hosking and Wallis, 1997). Large values indicate a possible error in the site data or can flag a site as an outlier within region. Some sites can be considered fits with multiple regions and D_i can be used to determine the region that is the best fit for a site. The critical values are dependent on the number of sites in a region, if there are 15 or more sites

the critical value is 3, but drops to 1.33 for a 5 site region (Hosking and Wallis, 1997). The discordancy measure is defined as:

$$\overline{\mathbf{u}} = N^{-1} \sum_{i=1}^{N} \mathbf{u}_i$$

Equation 4.13

$$\mathbf{A} = \sum_{i=1}^{N} (\mathbf{u}_i - \overline{\mathbf{u}}) \, (\mathbf{u}_i - \overline{\mathbf{u}})^{\mathrm{T}}$$

Equation 4.14

$$D_i = \tfrac{1}{3} N (\mathbf{u}_i - \overline{\mathbf{u}})^T \mathrm{A}^{-1} (\mathbf{u}_i - \overline{\mathbf{u}})$$

Equation 4.15

where $\mathbf{u}_i = \left[t^{(i)} \;\; t_3^{(i)} \;\; t_4^{(i)} \;\; \right]^{\mathrm{T}}$ is a vector containing sample L-moment ratios for site *i* with a region containing *N* total sites, $\overline{\mathbf{u}}$ is the unweighted group average, and **A** defines the matrix of sums of squares and cross-products (Hosking and Wallis, 1997).

Once a region has been tentatively established, the heterogeneity of the group of sites must be assessed to determine if the region can be treated as homogeneous. Heterogeneity measures (*H*) are based on between-site dispersion of L-moment ratios: weighted standard deviation of L-CV (*V*), average of L-CV/L-skew distances (V_3), and average of L-skew/L-kurtosis distances (V_4), however, *V* has been judged superior for between-site comparisons and *H*[1] is considered sufficient for making a determination on region homogeneity (Hosking and Wallis, 1997). A value of *H*[1]<1 indicates a homogenous region. The heterogeneity measure is defined as:

$$t^R = \sum_{i=1}^{N} n_i \, t^{(i)} \Big/ \sum_{i=1}^{N} n_i$$

Equation 4.16

$$V = \left\{ \sum_{i=1}^{N} n_i \left(t^{(i)} - t^R \right)^2 \Big/ \sum_{i=1}^{N} n_i \right\}^{1/2}$$

Equation 4.17

$$H = \frac{V - \mu_v}{\sigma_v}$$

Equation 4.18

where the proposed region has *N* sites, with site *i* having record of length n_i and sample L-moment ratio $t^{(i)}$, t^R is the regional average L-CV, and *V* is the weighted standard deviation of L-CV (Hosking and Wallis, 1997). Next, a kappa distribution is fitted to the regional average L-moment ratios and a large number of simulations are realized for which a *V* is calculated for each. From the simulations the mean and standard deviation of *V* is calculated, μ_v and σ_v, respectively (Hosking and Wallis, 1997).

The next step is to find a statistical distribution which best fits the region among the following 5 three-parameter distributions (Hosking, 2015): generalized logistic (GLO), generalized extreme value (GEV), generalized normal (lognormal) (GNO), Pearson type III (3-parameter gamma) (PE3), and generalized Pareto (GPA). For estimating p unknown parameters of a selected distribution, the method of L-moments obtains parameter estimates by equating first p sample L-moments to the corresponding population quantities. Hosking and Wallis (1997) provided expressions for distribution parameters in terms of the L-moments. All 5 distributions were used in this study, but GLO and GEV were utilized the most often, so example expressions are provided for them (See Hosking and Wallis (1997) for additional examples). The GLO distribution parameters, ξ (location), α (scale), and k (shape), are:

$$k = -\tau_3, \quad \alpha = \frac{\lambda_2 \sin k\pi}{k\pi}, \quad \xi = \lambda_1 - \alpha\left(\frac{1}{k} - \frac{\pi}{\sin k\pi}\right)$$

Equation 4.19

The probability density function, the cumulative distribution function, and the quantile function of the GLO distribution are given by:

$$f(x) = \frac{\alpha^{-1} e^{-(1-k)y}}{\left(1 + e^{-y}\right)^2}, \quad y = \begin{cases} -k^{-1} \log\{1 - k(x - \xi)/\alpha\}, & k \neq 0 \\ (x - \xi)/\alpha, & k = 0 \end{cases}$$

Equation 4.20

$$F(x) = 1/(1+e^{-y})$$

Equation 4.21

$$x(F) = \begin{cases} \xi + \alpha[1-\{(1-F)/F\}^{k}]/k, & k \neq 0 \\ \xi - \alpha \log\{(1-F)/F\}, & k = 0 \end{cases}$$

Equation 4.22

The GEV distribution parameters, ξ (location), α (scale), and k (shape), are:

$$k = 1/\delta, \quad \alpha = \beta/\delta, \quad \xi = \varsigma - \beta$$

Equation 4.23

The probability density function, the cumulative distribution function, and the quantile function of the GEV distribution are given by:

$$f(x) = \alpha^{-1} e^{-(1-k)y - e^{-y}}, \quad y = \begin{cases} -k^{-1}\log\{1-k(x-\xi)/\alpha\}, & k \neq 0 \\ (x-\xi)/\alpha, & k = 0 \end{cases}$$

Equation 4.24

$$F(x) = e^{-e^{-y}}$$

Equation 4.25

$$x(F) = \begin{cases} \xi + \alpha[1-\{-\log F\}^{k}]/k, & k \neq 0 \\ \xi - \alpha \log\{-\log F\}, & k = 0 \end{cases}$$

Equation 4.26

Each distribution is fit to the regional average L-moments 1, t^R, t_3^R, and t_4^R for a region with *N* sites and a large number of N_{sim} realizations. The bias of t_4^R is defined as:

$$B_4 = N_{sim}^{-1} \sum_{m=1}^{N_{sim}} \left(t_4^{(m)} - t_4^R \right)$$

Equation 4.27

where $t_4^{(m)}$ is regional average L-kurtosis for the *m*th simulated region (Hosking and Wallis, 1997). The standard deviations of t_4^R is defined as:

$$\sigma_4 = \left[\left(N_{sim}^{-1} - 1 \right)^{-1} \left\{ \sum_{m=1}^{N_{sim}} \left(t_4^{(m)} - t_4^R \right)^2 - N_{sim} B_4^2 \right\} \right]^{1/2}$$

Equation 4.28

and for each distribution the goodness-of-fit measure (Z^{DIST}) is defined as:

$$Z^{DIST} = \left(t_4^{DIST} - t_4^R + B_4 \right) / \sigma_4$$

Equation 4.29

where t_4^{DIST} is the fitted L-kurtoses for any distribution (Hosking and Wallis, 1997). N_{sim} is typically a large number, 1000 for this study, and a fit is declared adequate if the absolute value of Z^{DIST} is less than 1.64 (Hosking, 2015).

Once a homogeneous region has been identified and a single statistical distribution has been found to be the best fit, a single frequency distribution is determined for the region and then scaled appropriately at each site to estimate at-site frequency distributions and calculate design precipitation values (Hosking and Wallis, 1997). The exact equations for determining required parameters, probability density function, cumulative distribution function, quantile function, and calculate final estimates are dependent on which statistical distribution was determined to be the best fit (See Equations 4.19 – 4.26). Appendix A of Hosking and Wallis (1997) and Hosking (1990) provide specific forms for other distributions.

Calculation of heterogeneity and goodness-of-fit measures requires sampling variability of L-moment ratios, which are estimated by Monte Carlo simulation using N_{sim} realizations (Hosking and Wallis, 1997). Monte Carlo simulations are also used to construct confidence limits at a 95% confidence level. Confidence intervals constructed through this approach account for uncertainties in distribution parameters, but not for other sources of uncertainties (for example, distribution selection), that could also significantly impact the total error, particularly at more rare frequencies (Perica et al., 2013).

Partial Duration Series

AMS data consists of the largest event in each year. In many cases the second largest event in a year is larger than the largest event in another year. Partial duration series (PDS) data is generated by listing all events in order from largest to smallest for the highest N cases, where N is equal to the number of years in the record. PDS-based precipitation frequency estimates are generally higher than estimates based on AMS data due to the inclusion of all of the N highest events, especially for events with high probability of exceedance (low annual recurrence intervals [ARI]). AMS produce estimates of the average period between years when a particular value is exceeded while PDS gives the average period between cases of a particular magnitude (Bonnin et al., 2006). AMS and PDS estimates are numerically similar for rarer ARIs, but differ for ARIs of less than 20 years. PDS-based estimates are communally used for precipitation analyses due to common engineering design applications and have been used by numerous studies to create IDF curves (eg. Hershfield, 1961;Huff and Angel, 1992; Bonnin et al., 2006; & Perica et al., 2013).

PDS-based precipitation frequency estimates were calculated from AMS-based precipitation frequency estimates using Langbein's formula (Langbein, 1949) which transforms a PDS-based average recurrence interval (ARI) to annual exceedance probability (AEP):

$$\text{AEP} = 1 - e^{\left(-\frac{1}{\text{ARI}}\right)}$$

Equation 4.30

PDS-based frequency estimates were calculated for the same durations (1-, 2-, 3-, 6-, 12-, and 24-hr; and 2-, 5-, and 10-days) as AMS-based estimates for the 0.5-, 1-, 2-, 5-, 10-, 25-, 50-, and 100-year ARIs. The ARIs were converted to AEPs using Equation 4.30 and then precipitation frequency estimates were calculated for those AEPs following the same approach that was used in the AMS analysis. See Table 4.1 for the relationships between PDS and AMS ARIs as published by Langbein (1949).

Table 4.1. Relationship of annual recurrence interval between partial duration series and annual maximum series

Annual Recurrance Interval (ARI)	
PDS	AMS
0.5	1.16
1	1.58
2	2.54
5	5.52
10	10.5
25	25.5
50	50.5
100	100.5

Daily and Hourly Duration Corrections

Precipitation data from the cooperative network provides daily data based on the calendar day and hourly data based on the clock hour. The maximum precipitation totals often occur within 60-minute or 24-hour intervals that aren't constrained by the clock hour or calendar day. Hershfield (1961) developed and Bonnin et al. (2006) confirmed empirical conversion factors to convert calendar day rainfall to maximum 24-hour rainfall (1.13) and clock hour rainfall to maximum 60-minute rainfall (1.16). Huff and Angel (1992) provide conversion factors of 1.04, 1.02, and 1 for daily durations of 2-days, 5-days, and 10-days, respectively. These conversion factors were used in this study.

General

Precipitation frequency estimates were calculated for the 0.5-, 1-, 2-, 5-, 10-, 25-, 50-, and 100-year ARIs and durations of 1-, 2-, 3-, 6-, 12-, and 24-hr; and 2-, 5-, and 10-days. Available data for all regions and all durations spanned 1970-2009. The AMS data was analyzed at 20 year intervals, 1970-1989, 1980-1999, and 1990-2009. Analysis of differences between the intervals was limited to 1970-1989 vs 1990-2009 due to the generally minimal differences of the middle interval to either the former or latter interval. Heterogeneity and goodness-of-fit tests were completed for each region at each storm duration to ensure all L-moment analysis requirements were met.

4.3 Results

4.3.1 Total Annual Precipitation

The stationary assumption of total annual precipitation, total annual wet days and wet hours, and AMS (1-hr and 24-hr) were tested visually with graphs and statistically using the t-test, the Mann-Kendall test, and Levens's test.

Figure 4.1 and Figure 4.2 show total annual precipitation (mm/yr) for each rain gauge station near Camp Atterbury (see Section 3.1.6). Gauges shown in Figure 4.1 have records beginning 1900-1915 and the gauges shown in Figure 4.2 have records beginning after 1945. Figure 4.3 shows total average annual precipitation (mm/yr) for all 10 gauges. The graph begins in 1915 when at least five gauges could be averaged; subsequent gauges were added to the average at the start of each respective gauge record. All gauge stations show a positive linear trend in total annual precipitation, though Shelbyville, IN and Martinsville, IN show only a very small increase. The 10 year moving averages tend to fluctuate above and below the linear trend lines on 10-15 year cycles. An above average cycle has persisted at the gauges with longer records since about the turn of the latest century and the cycles tend to be consistent between these locations. The 10 year moving averages of the gauges with shorter records are less pronounced though similar among themselves.

Statistical tests and findings for trends in total annual precipitation are presented in Table 4.2. Of the nine gauges tested (Versailles excluded due to 56 year record length), 5 gauges plus the Indiana gauge average showed statistically significant (α = 5% and α = 10%) positive trends for both the t-test and MK test. Based on Levene's test, the hypothesis that variance did not change could not be rejected for any

of the stations. Perica et al. (2013) also found that that variance did not change at most studied gauges. This suggests that detected trends occur with minimal variances around the means of the two halves of the gauge record. The gauges with significant positive trends are those located on an east-west line with Camp Atterbury and several gauges directly south.

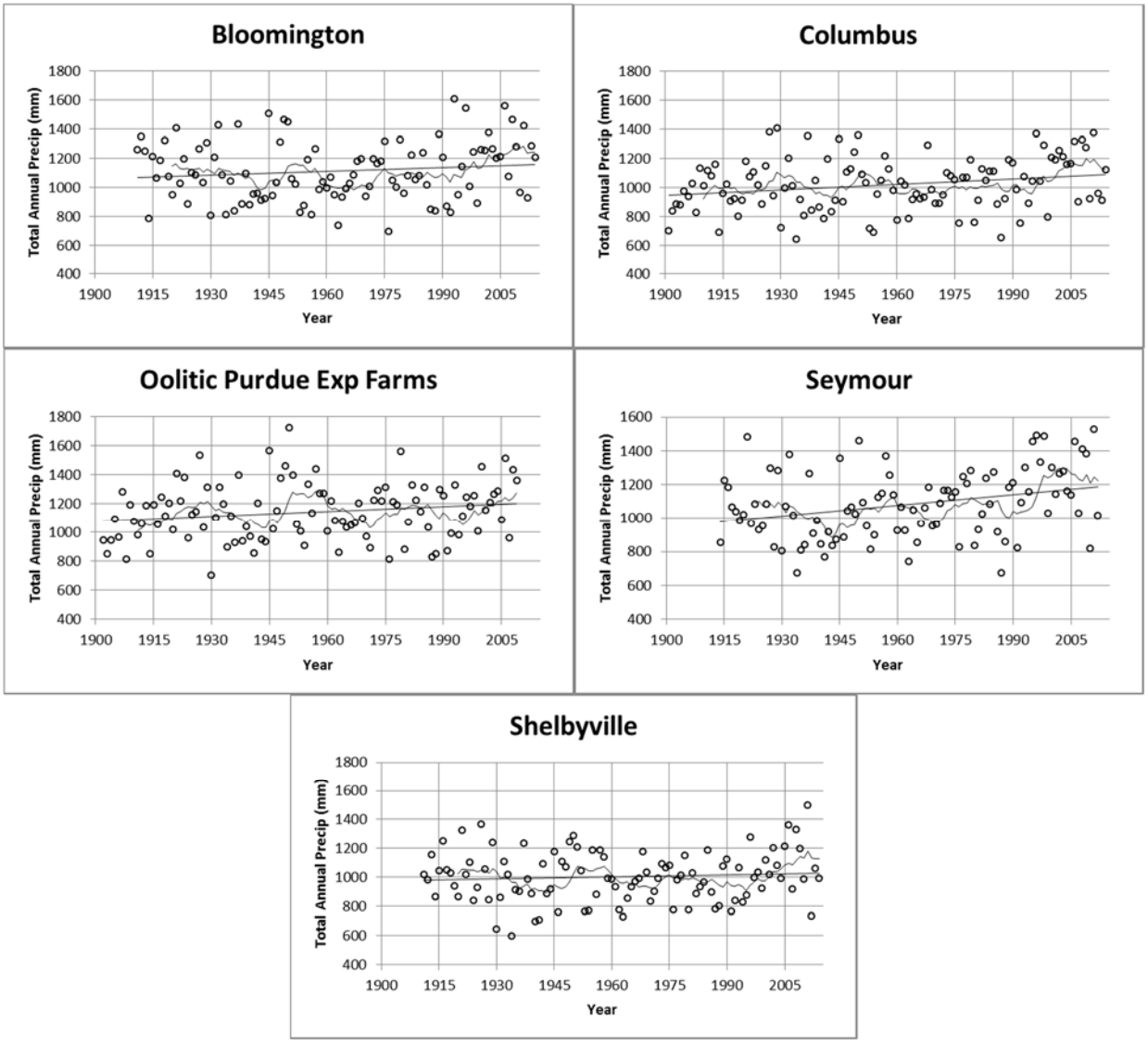

Figure 4.1. Total annual precipitation for several stations in Indiana with linear and 10 year moving average fits

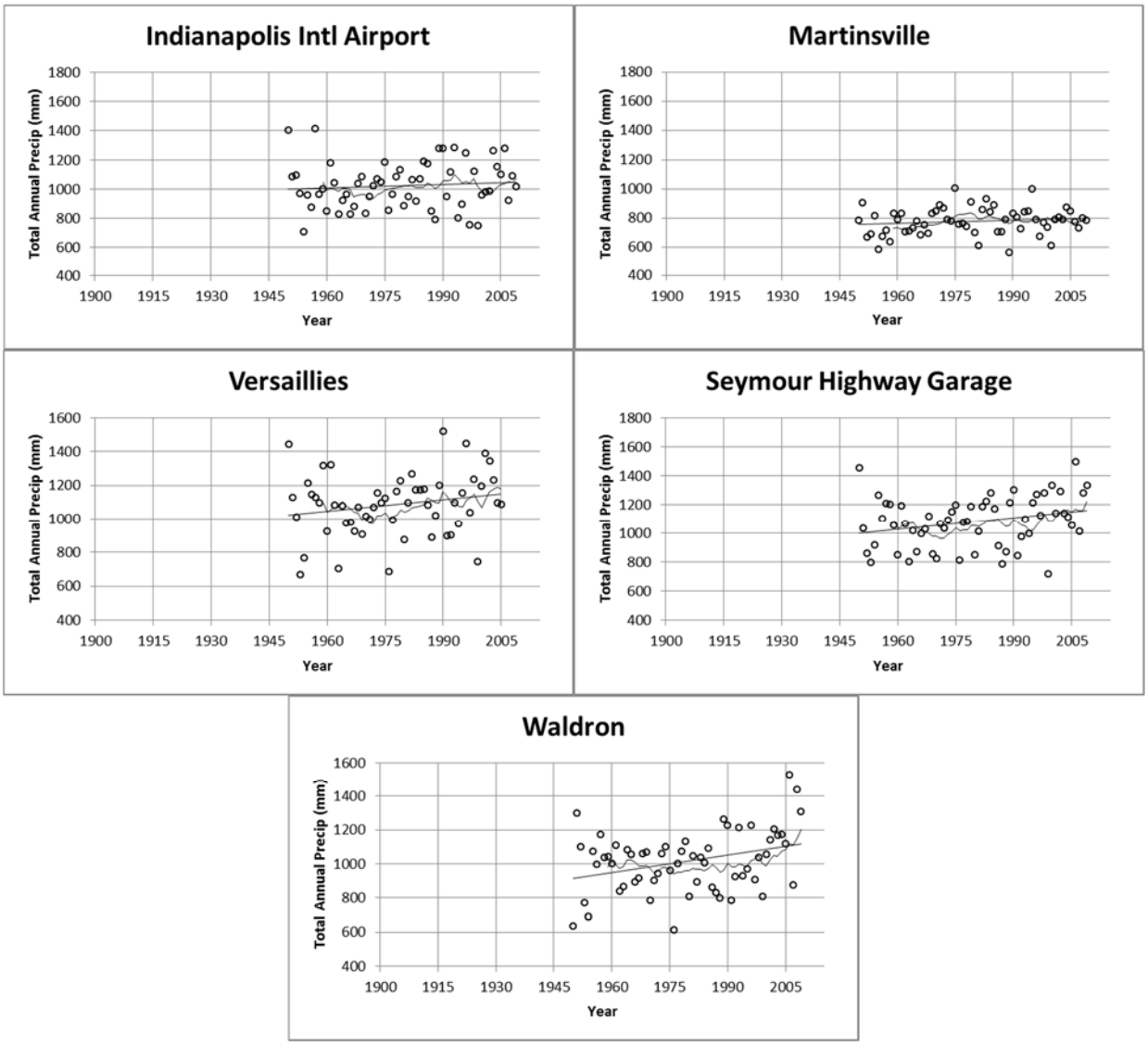

Figure 4.2. Total annual precipitation for several stations in Indiana with linear and 10 year moving average fits

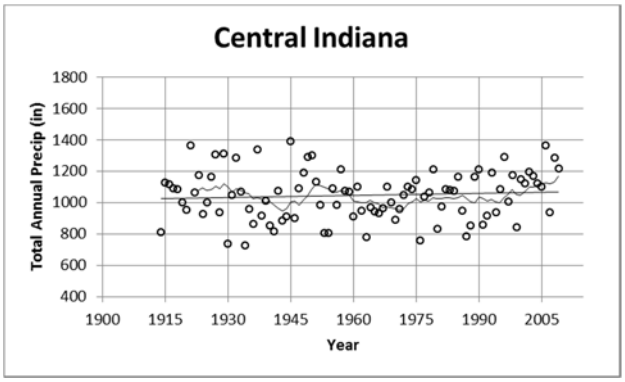

Figure 4.3. Total average annual precipitation for central Indiana region with linear and 10 year moving average fits

Table 4.2. Trend analysis results for total annual precipitation at individual Indiana stations and of average Indiana region

	Signif Level	Total Annual Precipitation		
		t-test	MK	Levene
BLOOMINGTON	95%-5%	**POS**	**POS**	NULL
	90%-10%			
COLUMBUS	95%-5%	**POS**	**POS**	NULL
	90%-10%			
INDIANAPOLIS IA	95%-5%	NULL	NULL	NULL
	90%-10%			
MARTINSVILLE	95%-5%	NULL	NULL	NULL
	90%-10%			
OOLITIC PURDUE EF	95%-5%	NULL	NULL	NULL
	90%-10%			
SEYMOUR HG	95%-5%	**POS**	**POS**	NULL
	90%-10%			
SEYMOUR	95%-5%	**POS**	**POS**	NULL
	90%-10%			
SHELBYVILLE	95%-5%	NULL	NULL	NULL
	90%-10%			
WALDRON	95%-5%	**POS**	**POS**	NULL
	90%-10%			
INDIANA AVERAGE	95%-5%	**POS**	**POS**	NULL
	90%-10%			

Figure 4.4 and Figure 4.5 show total annual precipitation (mm/yr) for each rain gauge station near Camp Grayling (see Section 3.2.6). Gauges shown in Figure 4.4 have records beginning prior to 1945 and the gauges shown in Figure 4.5 have records beginning after 1945. Figure 4.6 shows total average annual precipitation (mm/yr) for all 9 gauges. The graph begins in 1941 when at least four gauges could be averaged; subsequent gauges were added to the average at the start of each respective gauge record. All gauge stations show a positive linear trend in total annual precipitation, except for Glennie Alcona Dam, which shows a flat linear trend. The 10 year moving averages tend to fluctuate above and below the linear trend lines on 10-15 year cycles, much like the Indiana gauges. A below average cycle has

persisted at most the gauges since about the turn of the century and the cycles tend to be consistent between these locations; i.e. the timing and magnitudes of the cycles are similar.

Statistical tests and findings for trends in total annual precipitation are presented in Table 4.3. Of the seven gauges tested (Traverse City and Glennie Alcona Dam were excluded due to record lengths of less than 60 years), Lake City EF shows significant (α = 5% and α = 10%) trends for both the t-test and MK test and Gaylord shows a statistically significant trend for the t-test and practically significant trend for MK. Houghton Lake shows a practically significant increase for both tests. Based on Levene's test, the hypothesis that variance does not change could not be rejected for any of the stations. The gauges with significant positive trends are those located north and southwest of Camp Grayling.

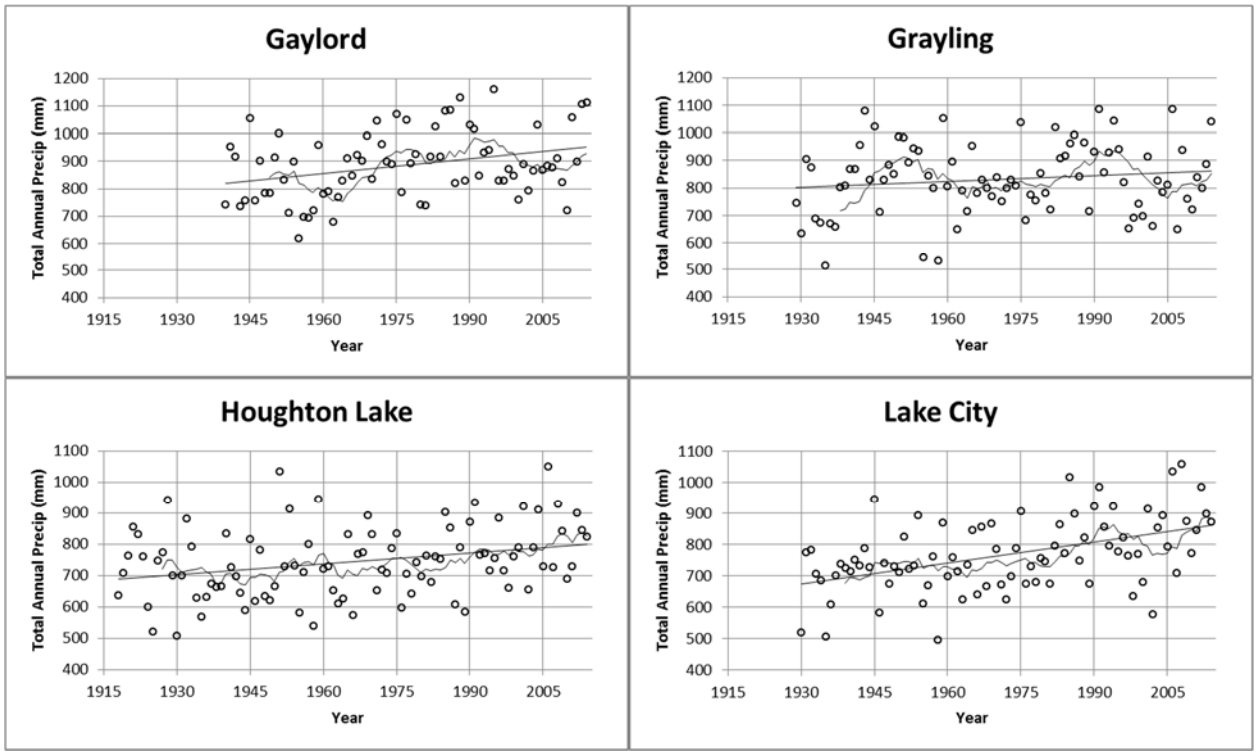

Figure 4.4. Total annual precipitation for several stations in Michigan with linear and 10 year moving average fits

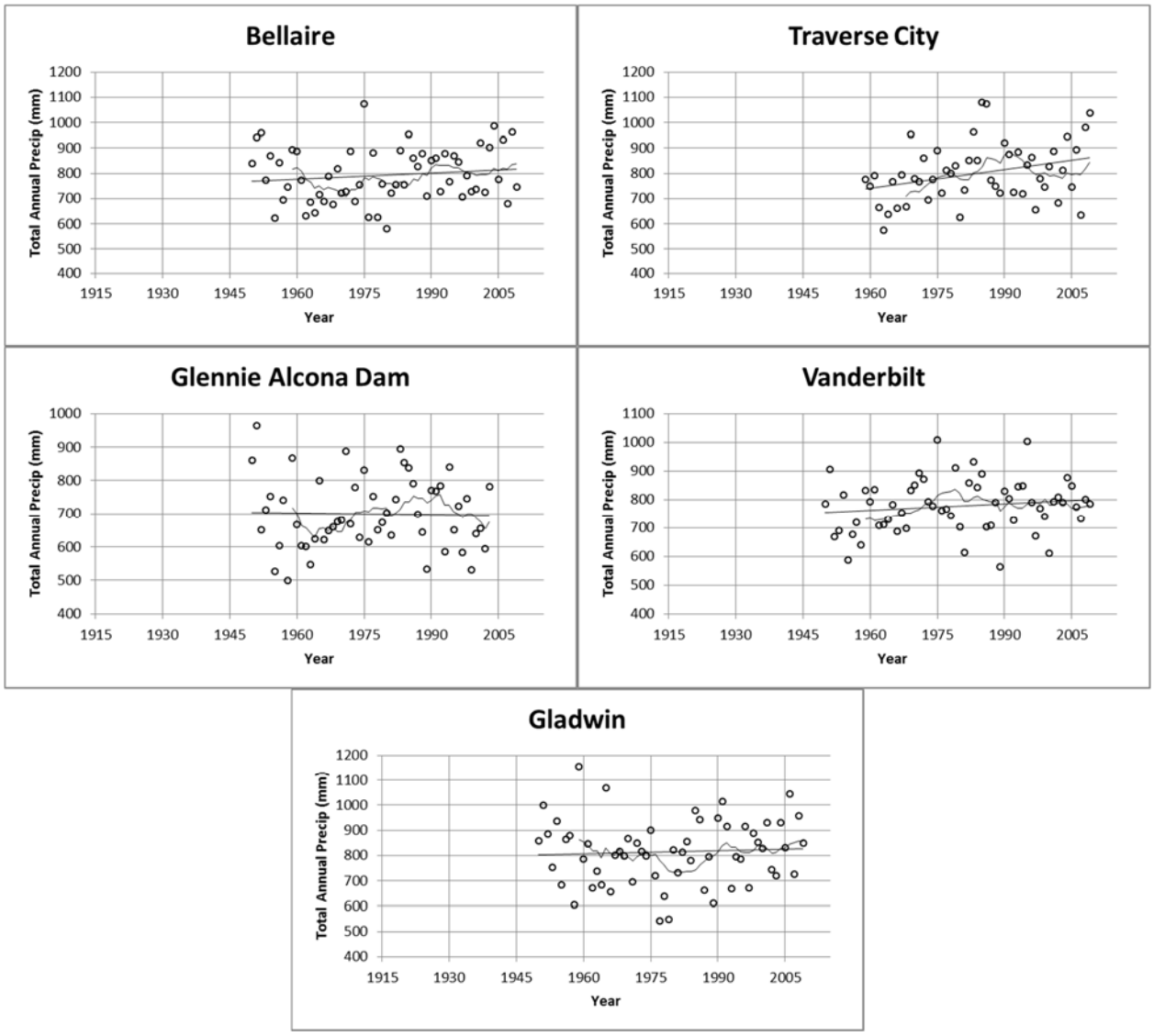

Figure 4.5. Total annual precipitation for several stations in Michigan with linear and 10 year moving average fits

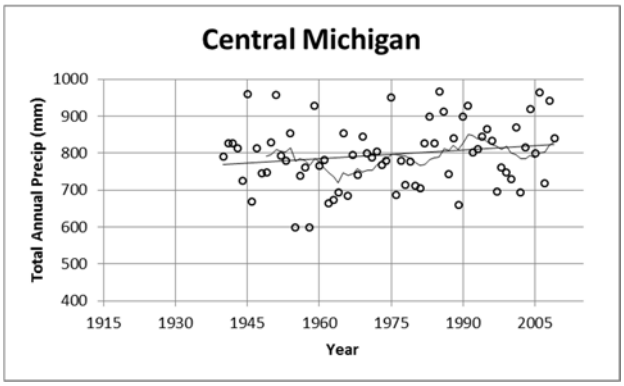

Figure 4.6. Total average annual precipitation for central Michigan region with linear and 10 year moving average fits

Table 4.3. Trend analysis results for total annual precipitation at individual Michigan stations and of average Michigan region

	Signif Level	Total Annual Precip		
		t-test	MK	Levene
BELLAIRE	95%-5%	NULL	NULL	NULL
	90%-10%			
GAYLORD	95%-5%	**POS**	NULL	NULL
	90%-10%		**POS**	
GLADWIN	95%-5%	NULL	NULL	NULL
	90%-10%			
GRAYLING	95%-5%	NULL	NULL	NULL
	90%-10%			
LAKE CITY EF	95%-5%	**POS**	**POS**	NULL
	90%-10%			
TRAVERSE CITY	95%-5%	-	-	-
	90%-10%			
VANDERBILT	95%-5%	NULL	NULL	NULL
	90%-10%			
HOUGHTON LAKE	95%-5%	NULL	NULL	NULL
	90%-10%	**POS**	**POS**	
MICHIGAN AVERAGE	95%-5%	NULL	NULL	NULL
	90%-10%	**POS**		

Figure 4.7 and Figure 4.8 show total annual precipitation (mm/yr) for each rain gauge station near Edgar County Illinois (see Section 3.3.6). Gauges shown in Figure 4.7 have records beginning 1900-1920 and

the gauges shown in Figure 4.8 have records beginning after 1945. Figure 4.9 shows total average annual precipitation (mm/yr) for all 9 gauges. The graph begins in 1920 when at least four gauges could be averaged; subsequent gauges were added to the average at the start of each respective gauge record. All gauge stations show a positive linear trend in total annual precipitation. The 10 year moving averages tend to fluctuate above and below the linear trend lines on 15-20 year cycles. A slightly below average cycle has persisted at most of the gauges since about 1995 and the cycles tend to be consistent between these locations.

Statistical tests and findings for trends in total annual precipitation are presented in Table 4.4. Of the six gauges tested (Shelbyville Dam, Sullivan, and Clinton, IN were excluded due to gauge record lengths of less than 60 years), 4 gauges plus the Illinois gauge average show statistically significant positive trends for both the t-test and MK test. Based on Levene's test, the hypothesis that variance did not change could not be rejected for any of the stations. The gauges with significant positive trends are located in every direction from Edgar County. The closest gauge station to the study sites, Paris, IL, shows a statistically insignificant positive trend.

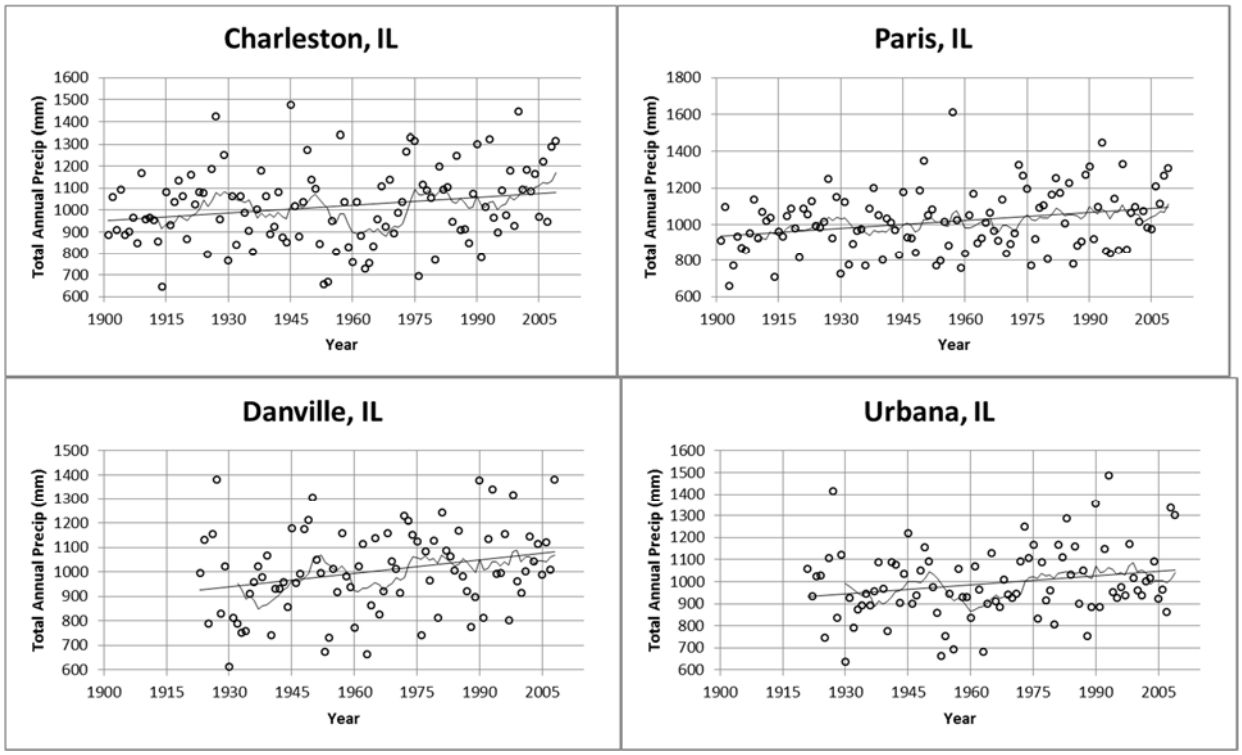

Figure 4.7. Total annual precipitation for several stations in Illinois with linear and 10 year moving average fits

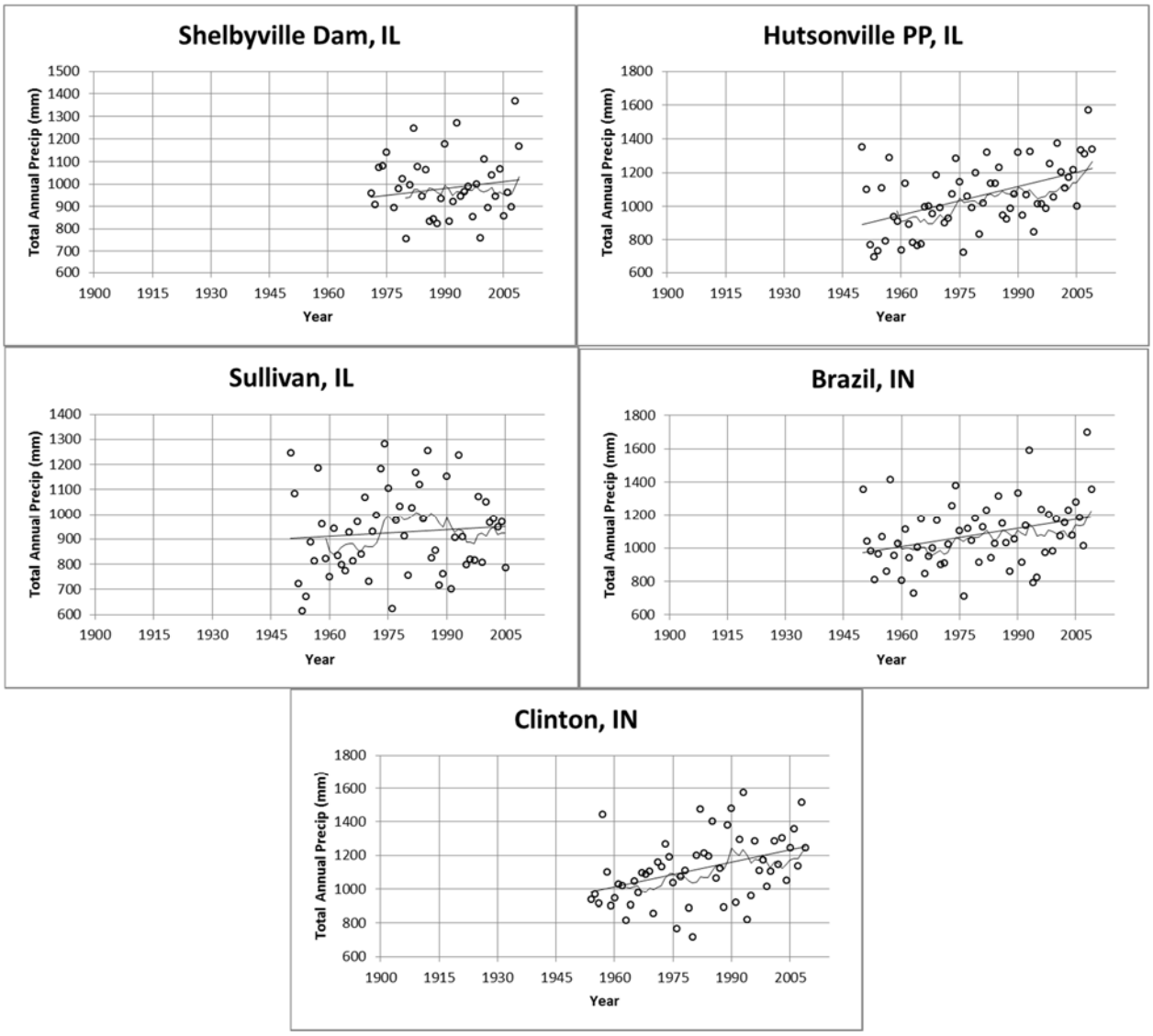

Figure 4.8. Total annual precipitation for several stations in Illinois and Indiana with linear and 10 year moving average fits

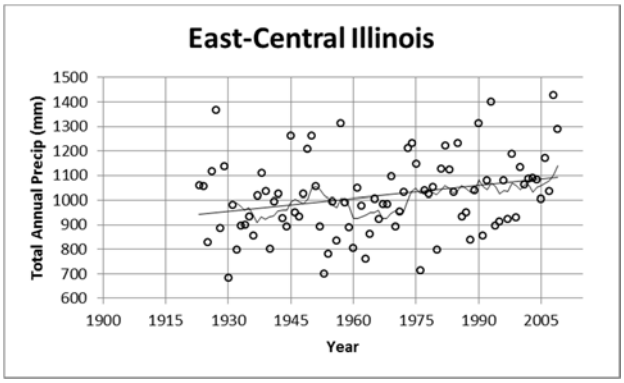

Figure 4.9. Total average annual precipitation for east central Illinois region with linear and 10 year moving average fits

Table 4.4. Trend analysis results for total annual precipitation at individual Illinois stations and of average Illinois region

	Signif Level	Total Annual Precip		
		t-test	MK	Levene
CHARLESTON	95%-5%	**POS**	**POS**	NULL
	90%-10%			
DANVILLE	95%-5%	NULL	NULL	NULL
	90%-10%			
HUTSONVILLE PP	95%-5%	**POS**	**POS**	NULL
	90%-10%			
PARIS	95%-5%	NULL	NULL	NULL
	90%-10%		**POS**	
URBANA	95%-5%	**POS**	**POS**	NULL
	90%-10%			
BRAZIL, IN	95%-5%	**POS**	**POS**	NULL
	90%-10%			
CLINTON, IN	95%-5%	-	-	-
	90%-10%			
ILLINOIS AVERAGE	95%-5%	**POS**	**POS**	NULL
	90%-10%			

4.3.2 Total Annual Wet Days

The trend of total annual wet days (calendar days) were assessed In order to check the validity of climate model bias correction with regards to precipitation thresholds. Any calendar day with at least 2.54 mm (0.1 in) were included.

Figure 4.10 and Figure 4.11 show total annual wet days for each rain gauge station near Camp Atterbury (see Section 3.1.6). Gauges shown in Figure 4.10 have records beginning 1900-1915 and the gauges shown in Figure 4.11 have records beginning after 1945. Figure 4.12 shows average annual wet days for all 10 gauges. Martinsville and Versailles show linear increases on the order of 5-8 days over about 55 years. Waldron shows a decrease of about 5 days over the same time period. All other gauges show no

trend and an average of 80 wet days per year. The 10 year moving averages tend to fluctuate above and below the linear trend lines on 10-15 year cycles and the cycles tend to be consistent between locations in timing but magnitude varies. An average of 80 wet days per year can be expected based on the historic gauge data with a range of 50-110 days.

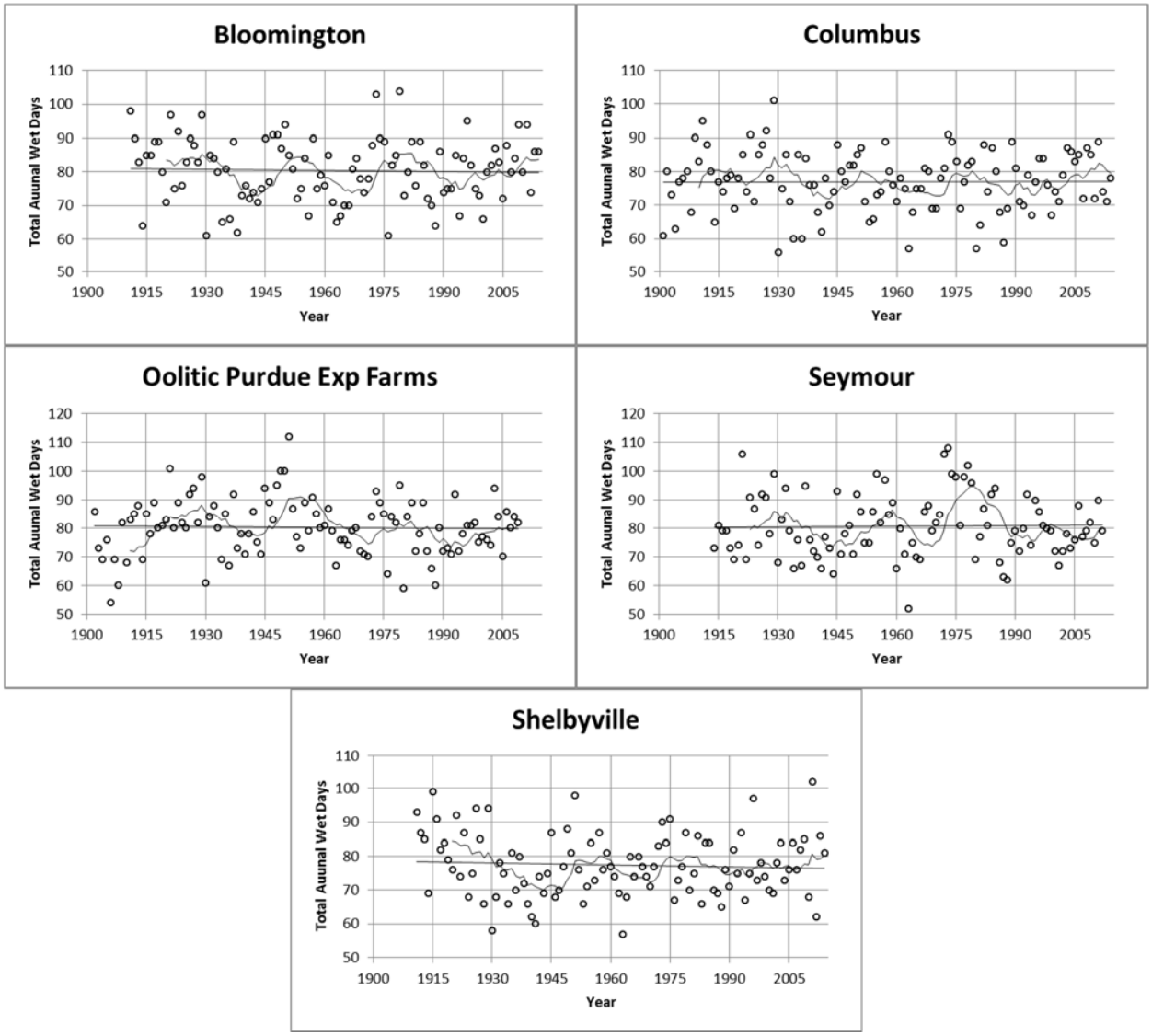

Figure 4.10. Total annual wet days for several stations in Indiana with linear and 10 year moving average fits

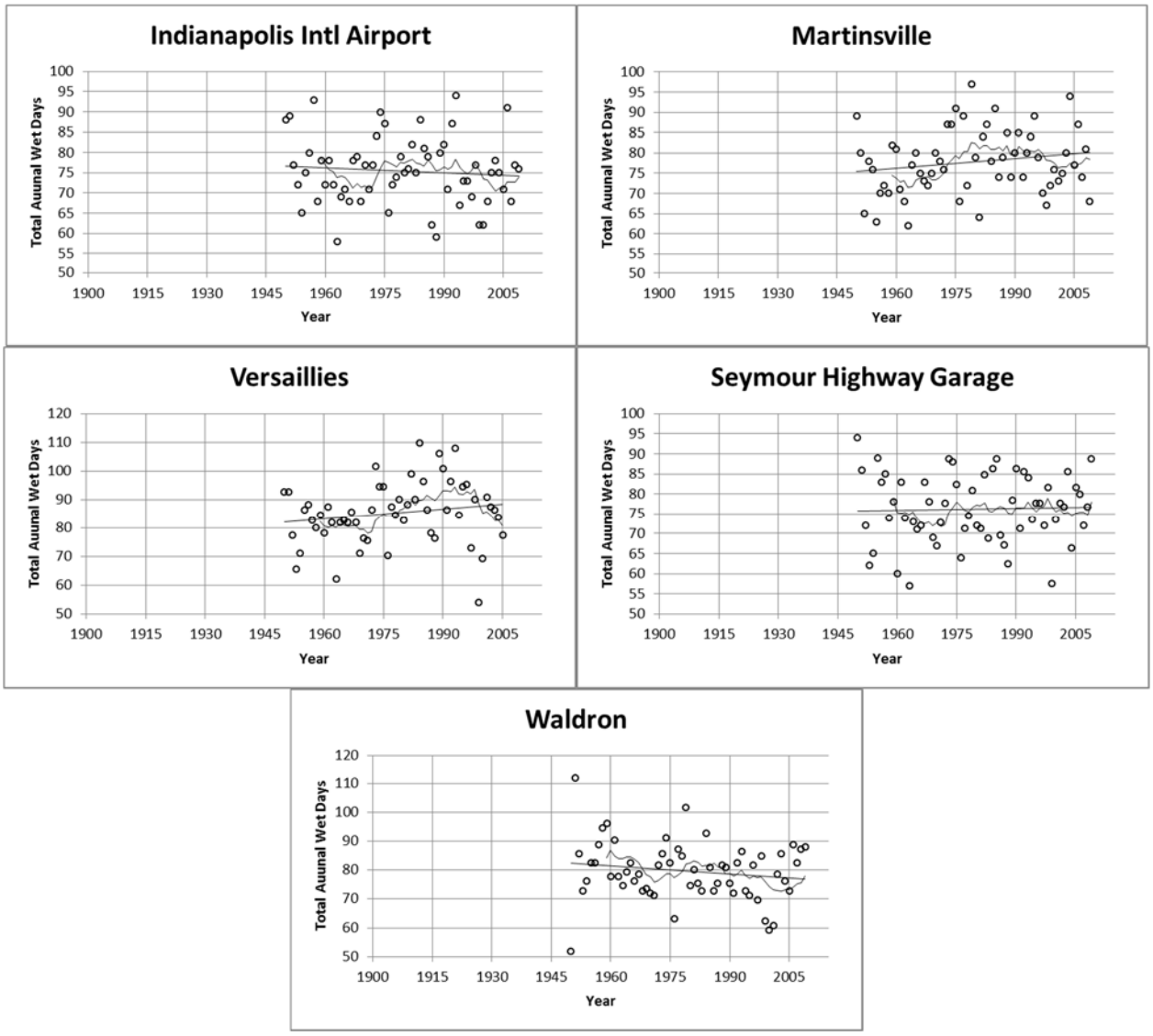

Figure 4.11. Total annual wet days for several stations in Indiana with linear and 10 year moving average fits

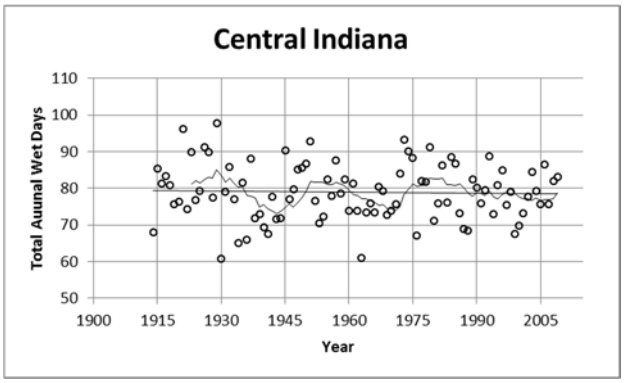

Figure 4.12. Total average annual wet days for central Indiana region with linear and 10 year moving average fits

Unlike the Indiana gauges, the number of wet days per year in Central Michigan seem to be increasing. Figure 4.13 and Figure 4.14 show total annual wet days for each rain gauge station near Camp Grayling (see Section 3.2.6). Gauges shown in Figure 4.13 have records beginning prior to 1945 and the gauges shown in Figure 4.14 have records beginning after 1945. Figure 4.15 shows total average annual wet days for all 9 gauges. The graph begins in 1941 when at least four gauges could be averaged; subsequent gauges were added to the average at the start of each respective gauge record. All gauge stations show a positive linear trend in total annual wet days of about 5 days since 1950. The 10 year moving averages tend to fluctuate above and below the linear trend lines on 10-15 year cycles, much like the Indiana gauges. An average of 78 wet days per year can be expected based on the historic gauge data with a range of 60-100 days.

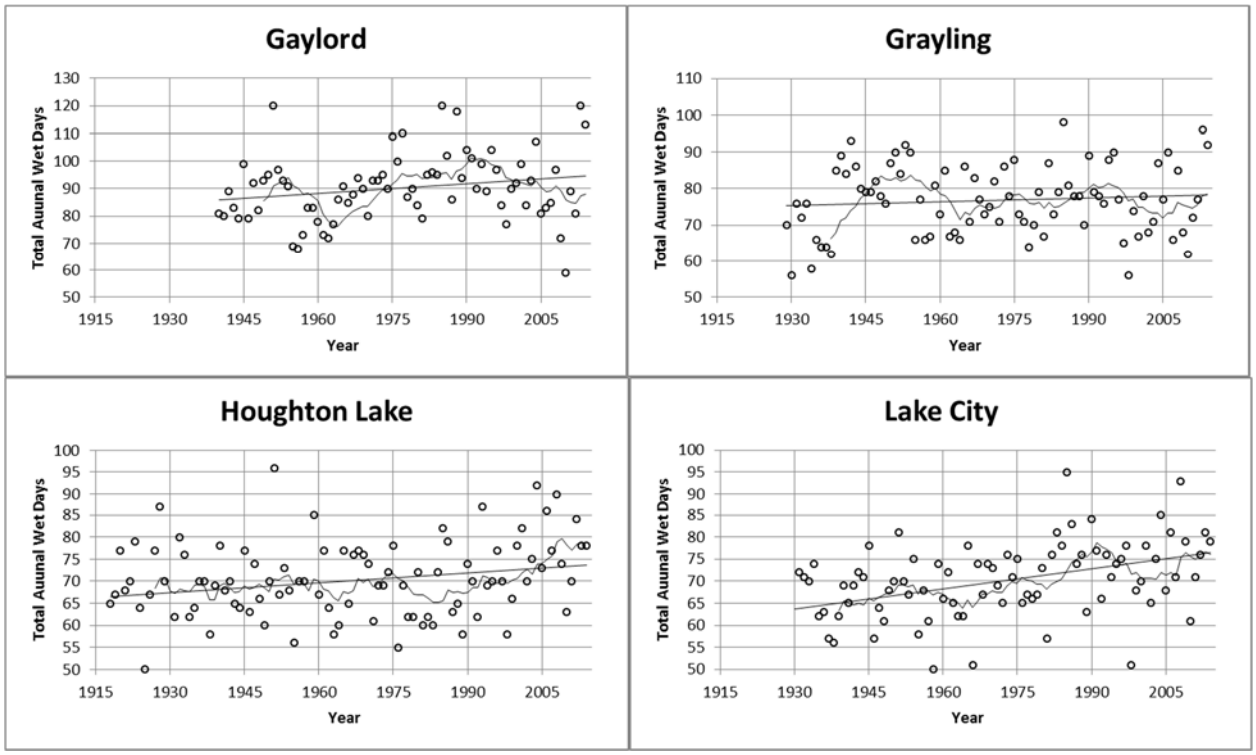

Figure 4.13. Total annual wet days for several stations in Michigan with linear and 10 year moving average fits

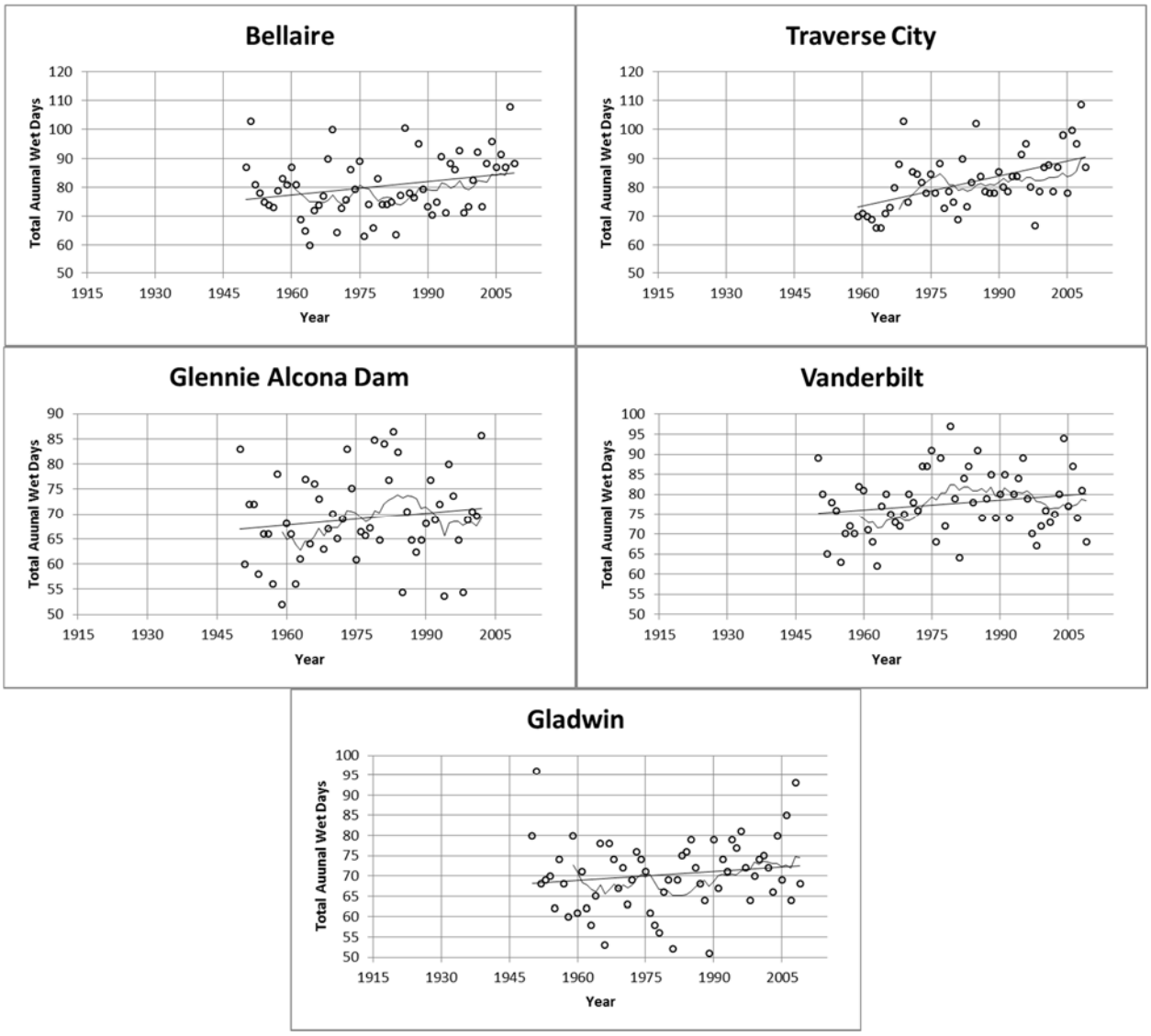

Figure 4.14. Total annual wet days for several stations in Michigan with linear and 10 year moving average fits

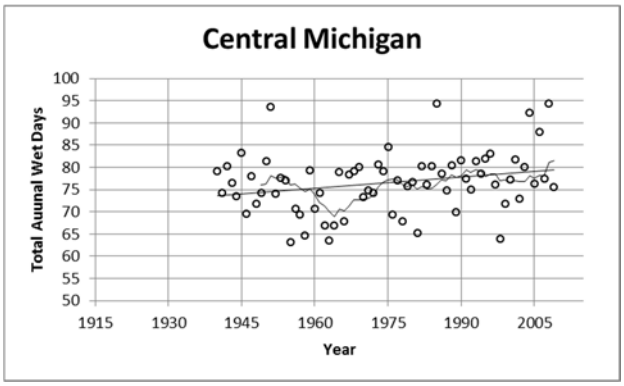

Figure 4.15. Total average annual wet days for central Michigan region with linear and 10 year moving average fits

Figure 4.16 and Figure 4.17 show total annual wet days for each rain gauge station near Edgar County Illinois (see Section 3.3.6). Gauges shown in Figure 4.16 have records beginning 1900-1920 and the gauges shown in Figure 4.17 have records beginning after 1945. Figure 4.18 shows total average wet days for all 9 gauges. The graph begins in 1920 when at least four gauges could be averaged; subsequent gauges were added to the average at the start of each respective gauge record. All gauge stations show a positive linear trend in total annual wet days of about 5-15 days since 1950 with an average of about 10 days. The 10 year moving averages tend to fluctuate above and below the linear trend lines on 10-15 year cycles, much like the Indiana gauges. An average of 75-80 wet days per year can be expected based on the historic gauge data with a range of 50-110 days.

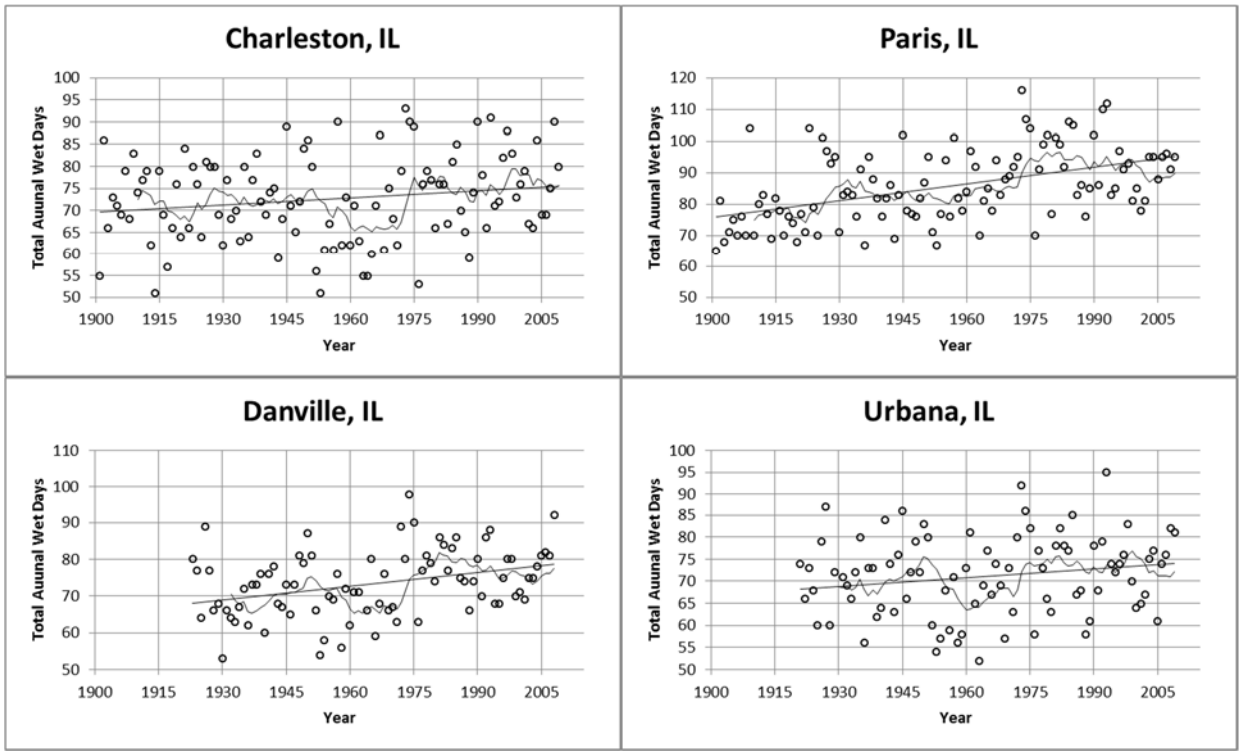

Figure 4.16. Total annual wet days for several stations in Illinois with linear and 10 year moving average fits

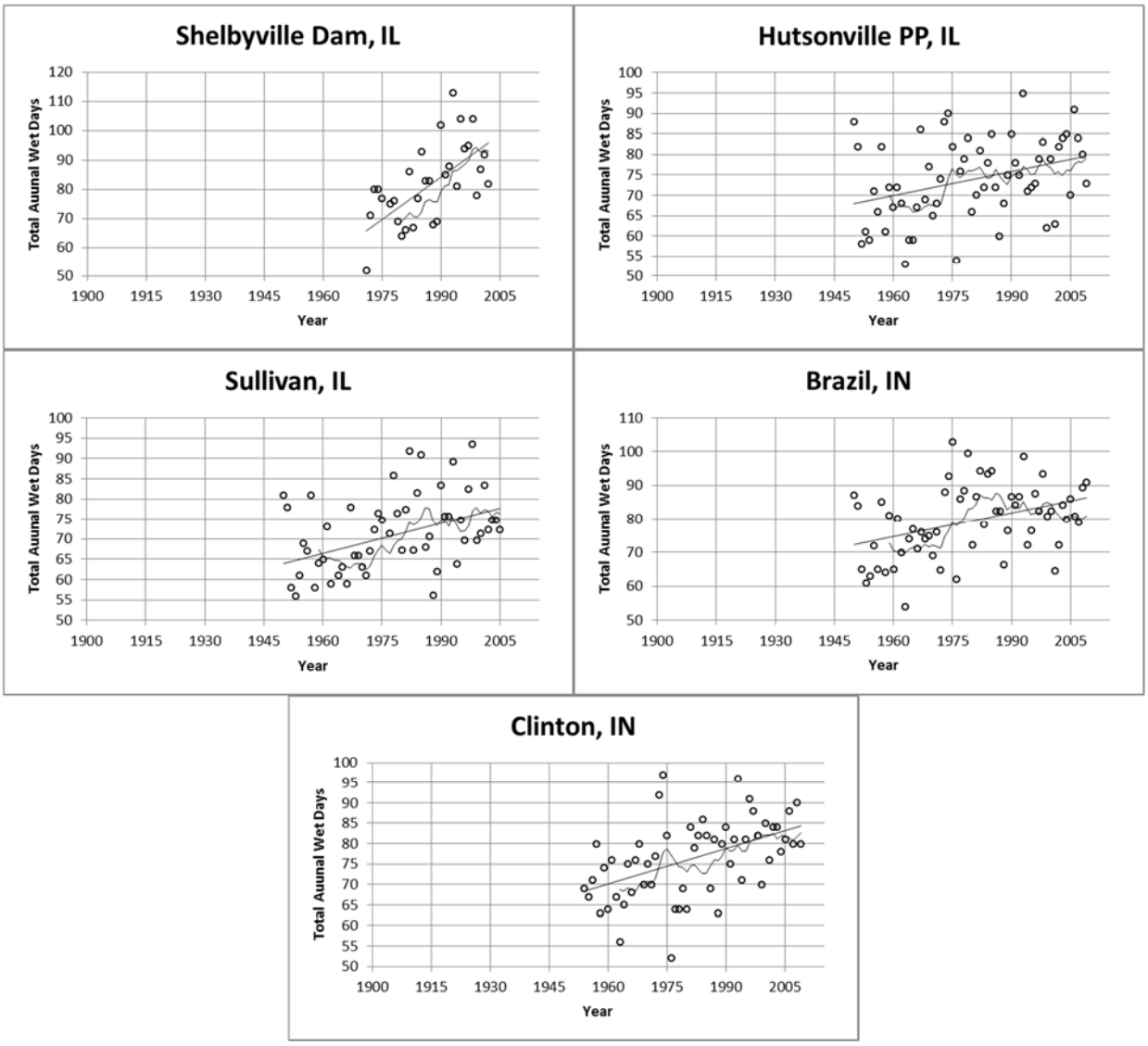

Figure 4.17. Total annual wet days for several stations in Illinois and Indiana with linear and 10 year moving average fits

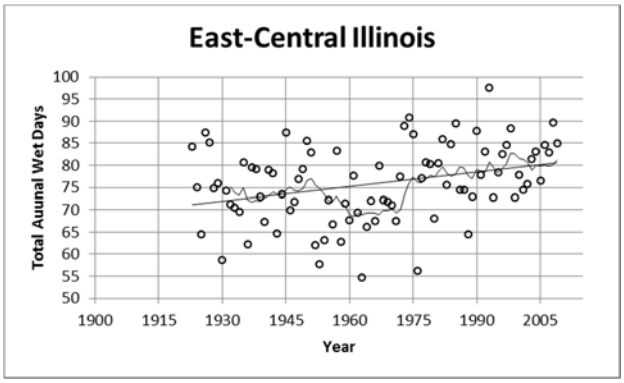

Figure 4.18. Total average annual wet days for east central Illinois region with linear and 10 year moving average fits

4.3.3 24-Hour Maximum Precipitation

For this study, PDS-based precipitation frequency estimates were calculated from AMS-based precipitation frequency, which were calculated using the L-moments method. An analysis of historic trends in AMS directly relates to trends in the estimated PDS. In order to analyze the trends in PDS more directly, precipitation event occurrences (number of events greater than or equal to the smallest AMS and the Atlas 14 1-yr event) were also graphed in time series. All units given in millimeters.

AMS

Figure 4.19 and Figure 4.20 show the 24-hr AMS for each rain gauge station near Camp Atterbury (see Section 3.1.6). Gauges shown in Figure 4.19 have records beginning 1900-1915 and the gauges shown in Figure 4.20 have records beginning after 1945. Figure 4.21 shows the average 24-hr AMS for all 10 gauges. The graph begins in 1915 when at least five gauges could be averaged; subsequent gauges were added to the average at the start of each respective gauge record. Most of the gauge stations show no linear trend in 24-hr AMS, though Oolitic Purdue Experimental Farm, Seymour, and Seymour Highway Garage show increasing linear trends. These locations are all south of Camp Atterbury on an east-west line. The 10 year moving averages tend to fluctuate above and below the linear trend lines but with no obvious pattern.

Statistical tests and findings for trends in 24-hr AMS are presented in Table 4.5. Of the nine gauges tested (Versailles excluded due to 56 year record length), only Seymour and the Indiana gauge average show statistically significant positive trends for both the t-test and MK test. Based on Levene's test, the hypothesis that variance did not change could not be rejected for any of the stations. The gauge with a significant positive trend is located south of Camp Atterbury.

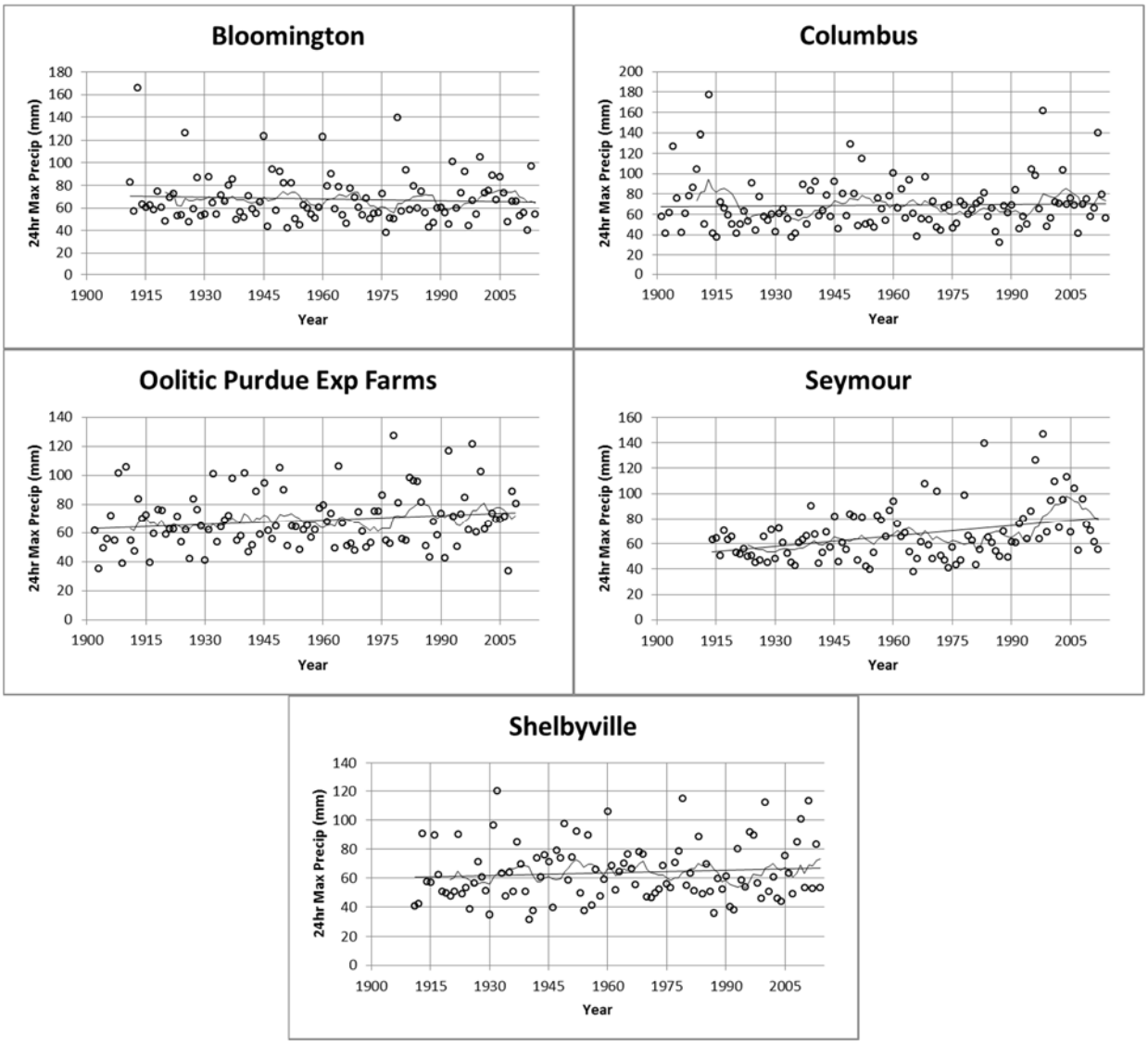

Figure 4.19. 24-hr AMS for several stations in Indiana with linear and 10 year moving average fits

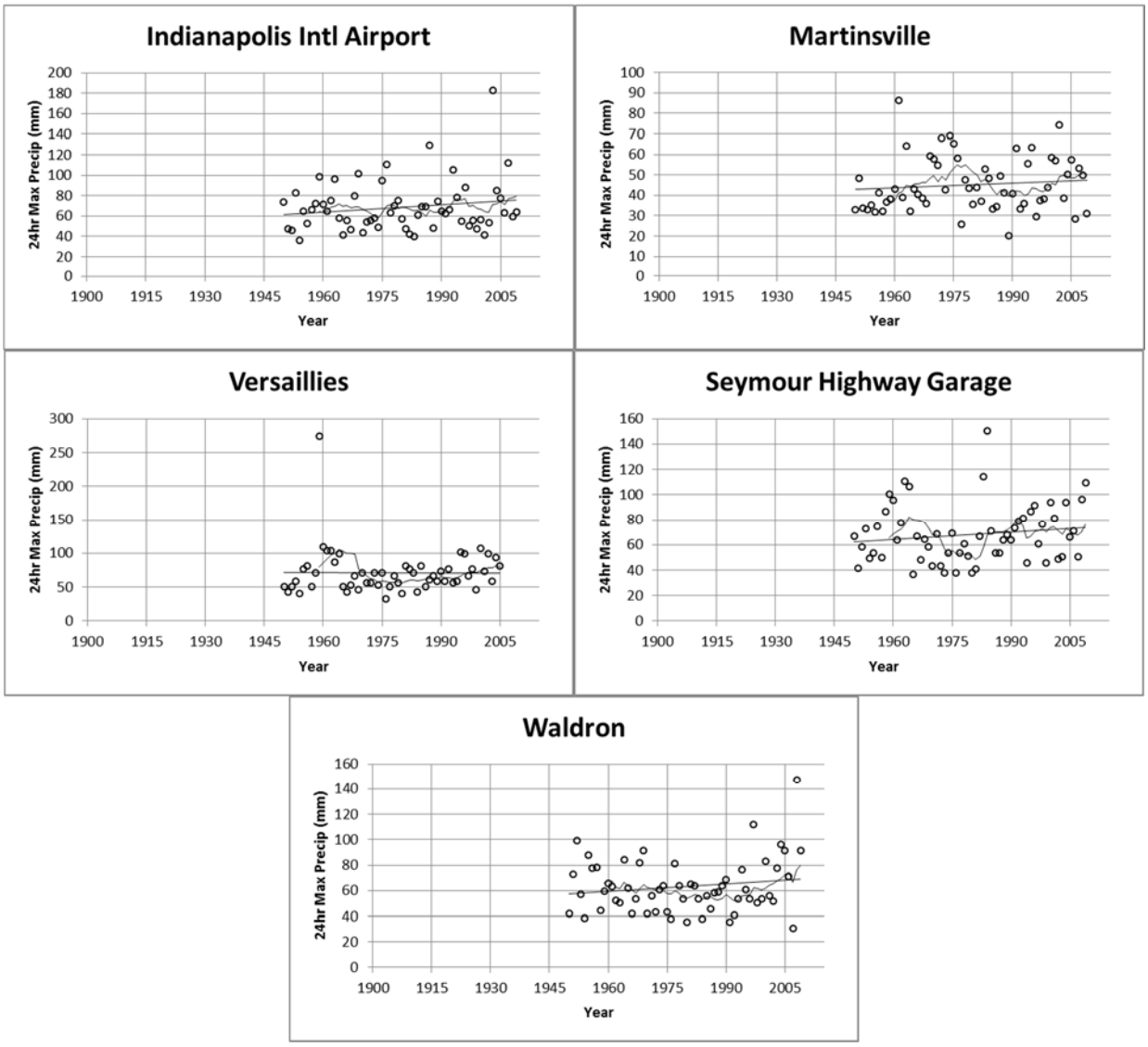

Figure 4.20. 24-hr AMS for several stations in Indiana with linear and 10 year moving average fits

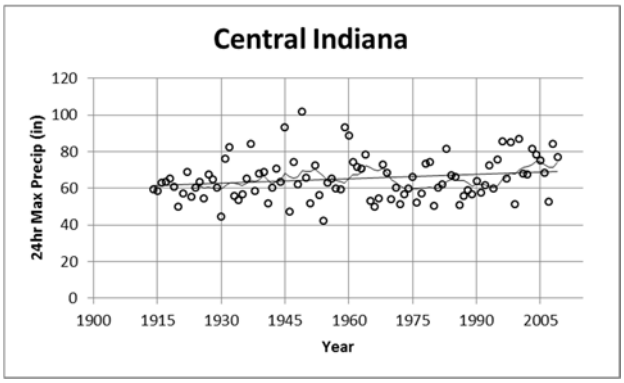

Figure 4.21. 24-hr average AMS for central Indiana region with linear and 10 year moving average fits

Table 4.5. Trend analysis results for 24-hr AMS at individual Indiana stations

	Signif Level	AMS 24-hr		
		t-test	MK	Levene
BLOOMINGTON	95%-5%	NULL	NULL	NULL
	90%-10%			
COLUMBUS	95%-5%	NULL	NULL	NULL
	90%-10%			
INDIANAPOLIS IA	95%-5%	NULL	NULL	NULL
	90%-10%			
MARTINSVILLE	95%-5%	NULL	NULL	NULL
	90%-10%			
OOLITIC PURDUE EF	95%-5%	NULL	NULL	NULL
	90%-10%			
SEYMOUR HG	95%-5%	NULL	NULL	NULL
	90%-10%			
SEYMOUR	95%-5%	**POS**	**POS**	NULL
	90%-10%			
SHELBYVILLE	95%-5%	NULL	NULL	NULL
	90%-10%			
WALDRON	95%-5%	NULL	NULL	NULL
	90%-10%			
INDIANA AVERAGE	95%-5%	NULL	**POS**	NULL
	90%-10%	**POS**		

Figure 4.22 and Figure 4.23 show the 24-hr AMS for each rain gauge station near Camp Grayling (see Section 3.2.6). Gauges shown in Figure 4.22 have records beginning prior to 1945 and the gauges shown in Figure 4.23 have records beginning after 1945. Figure 4.24 shows the average 24-hr AMS for all 9 gauges. The graph begins in 1941 when at least four gauges could be averaged; subsequent gauges were added to the average at the start of each respective gauge record. Most gauge stations show nearly constant linear trends in 24-hr AMS, except for Glennie Alcona Dam, which shows a positive trend, and Bellaire, which shows and negative trend. The 10 year moving averages tend to fluctuate only slightly above and below the linear trend lines and with not obvious pattern.

Statistical tests and findings for trends in 24-hr AMS are presented in Table 4.6. Of the seven gauges tested (Traverse City and Glennie Alcona Dam excluded due to record lengths of less than 60 years), none showed statistically significant trends (α = 5% or α = 10%) for either the t-test and/or MK test. Based on Levene's test, the hypothesis that variance did not change could only be rejected for Bellaire. Bellaire is located northwest of Camp Grayling and Glennie Alcona Dam is located east of Camp Grayling.

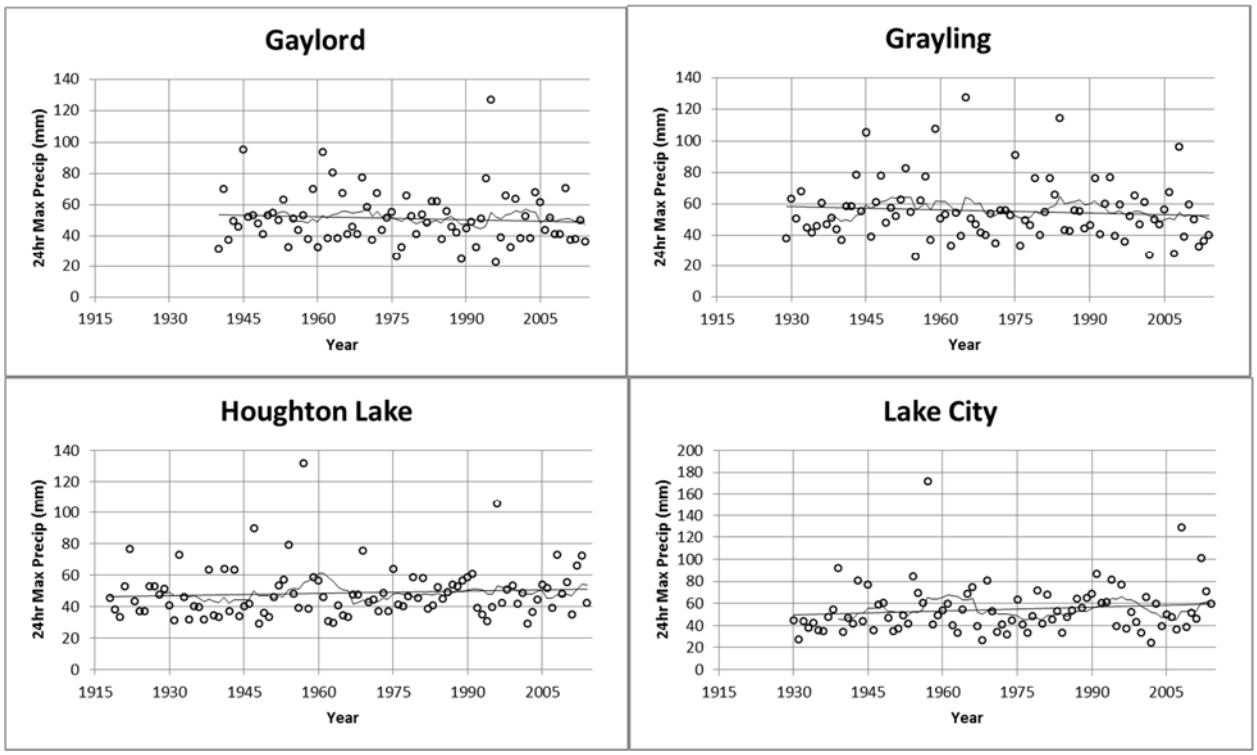

Figure 4.22. 24-hr AMS for several stations in Michigan with linear and 10 year moving average fits

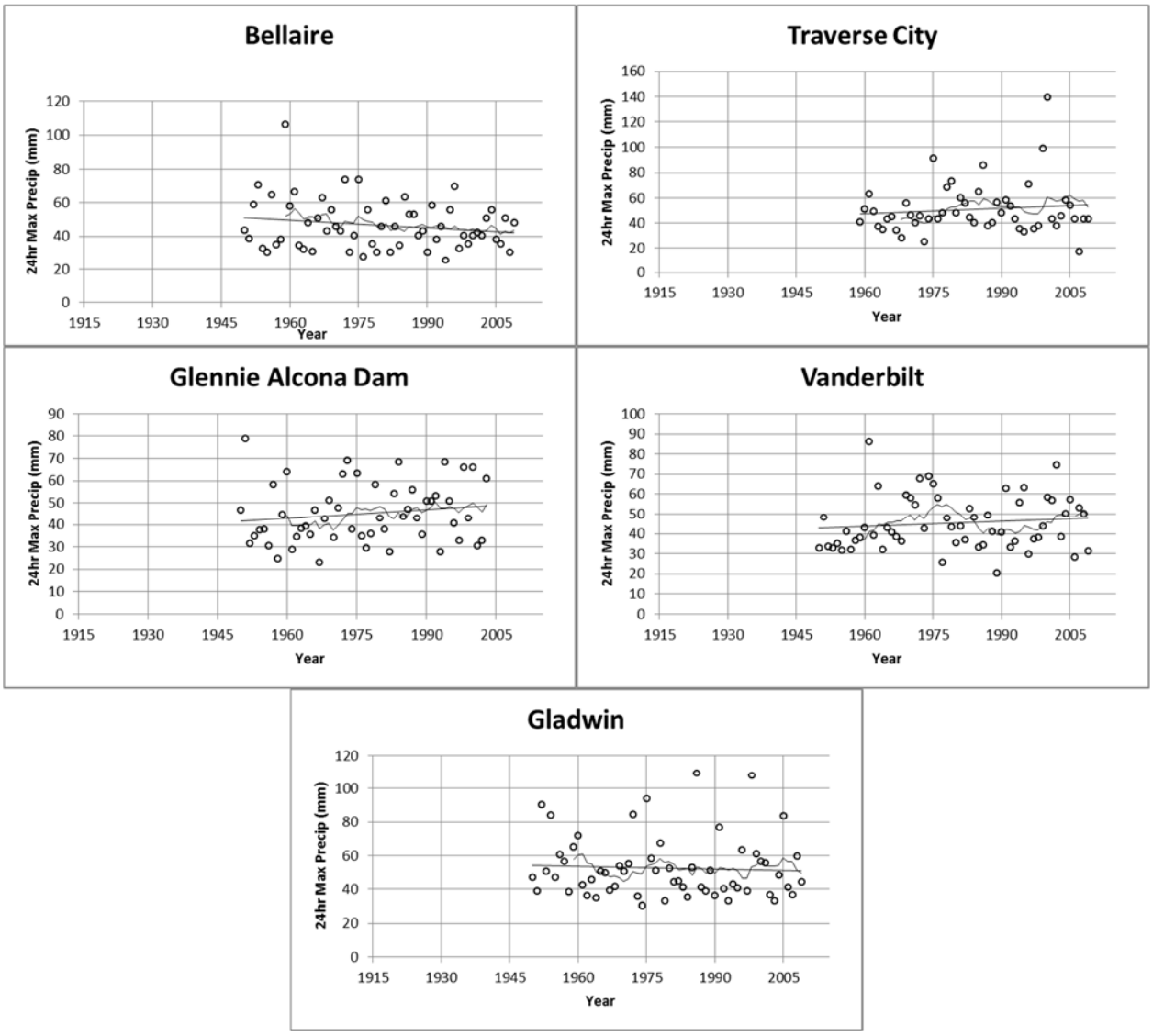

Figure 4.23. 24-hr AMS for several stations in Michigan with linear and 10 year moving average fits

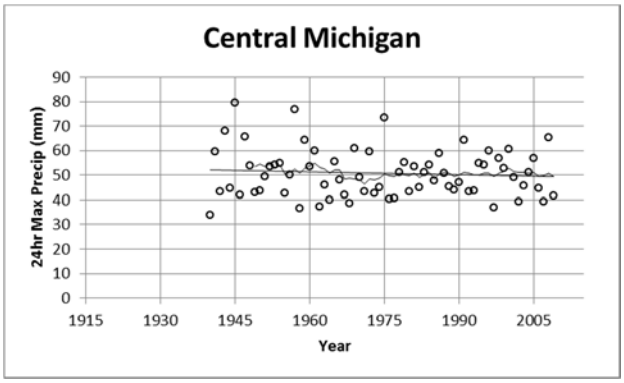

Figure 4.24. 24-hr average AMS for central Michigan region with linear and 10 year moving average fits

Table 4.6. Trend analysis results for 24-hr AMS at individual Michigan stations and of average Michigan region

	Signif Level	AMS 24-hr		
		t-test	MK	Levene
BELLAIRE	95%-5%	NULL	NULL	**HETERO**
	90%-10%			
GAYLORD	95%-5%	NULL	NULL	NULL
	90%-10%			
GLADWIN	95%-5%	NULL	NULL	NULL
	90%-10%			
GRAYLING	95%-5%	NULL	NULL	NULL
	90%-10%			
LAKE CITY EF	95%-5%	NULL	NULL	NULL
	90%-10%			
TRAVERSE CITY	95%-5%	-	-	-
	90%-10%			
VANDERBILT	95%-5%	NULL	NULL	NULL
	90%-10%			
HOUGHTON LAKE	95%-5%	NULL	NULL	NULL
	90%-10%			
MICHIGAN AVERAGE	95%-5%	NULL	NULL	NULL
	90%-10%			

Figure 4.25 and Figure 4.26 show the 24-hr AMS for each rain gauge station near Edgar County Illinois (see Section 3.3.6). Gauges shown in Figure 4.25 have records beginning 1900-1920 and the gauges shown in Figure 4.26 have records beginning after 1945. Figure 4.27 shows the average 24-hr AMS for all 9 gauges. Most of the gauge stations show a constant linear trend in 24-hr AMS, though Danville, IL and Hutsonville Power Plant, IL show increasing linear trends. The 10 year moving averages tend to fluctuate above and below the linear trend lines but with no obvious pattern.

Statistical tests and findings for trends in 24-hr AMS are presented in Table 4.7. Of the six gauges tested (Shelbyville Dam, Sullivan, and Clinton, IN were excluded due to gauge record lengths of less than 60 years), none showed statistically significant trends for the MK test while only Hutsonville PP showed a significant trend (α = 10%) for the t-test. Based on Levene's test, the hypothesis that variance did not change could only be rejected for Brazil, IN and Danville.

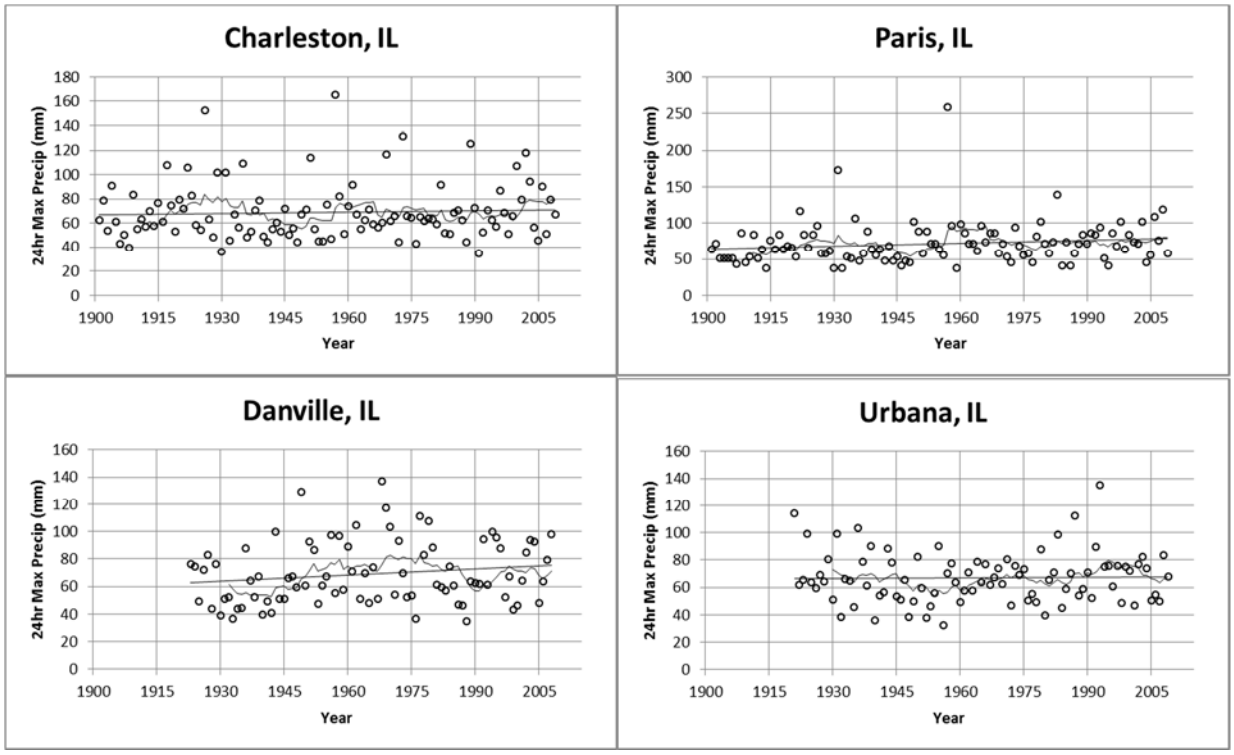

Figure 4.25. 24-hr AMS for several stations in Illinois with linear and 10 year moving average fits

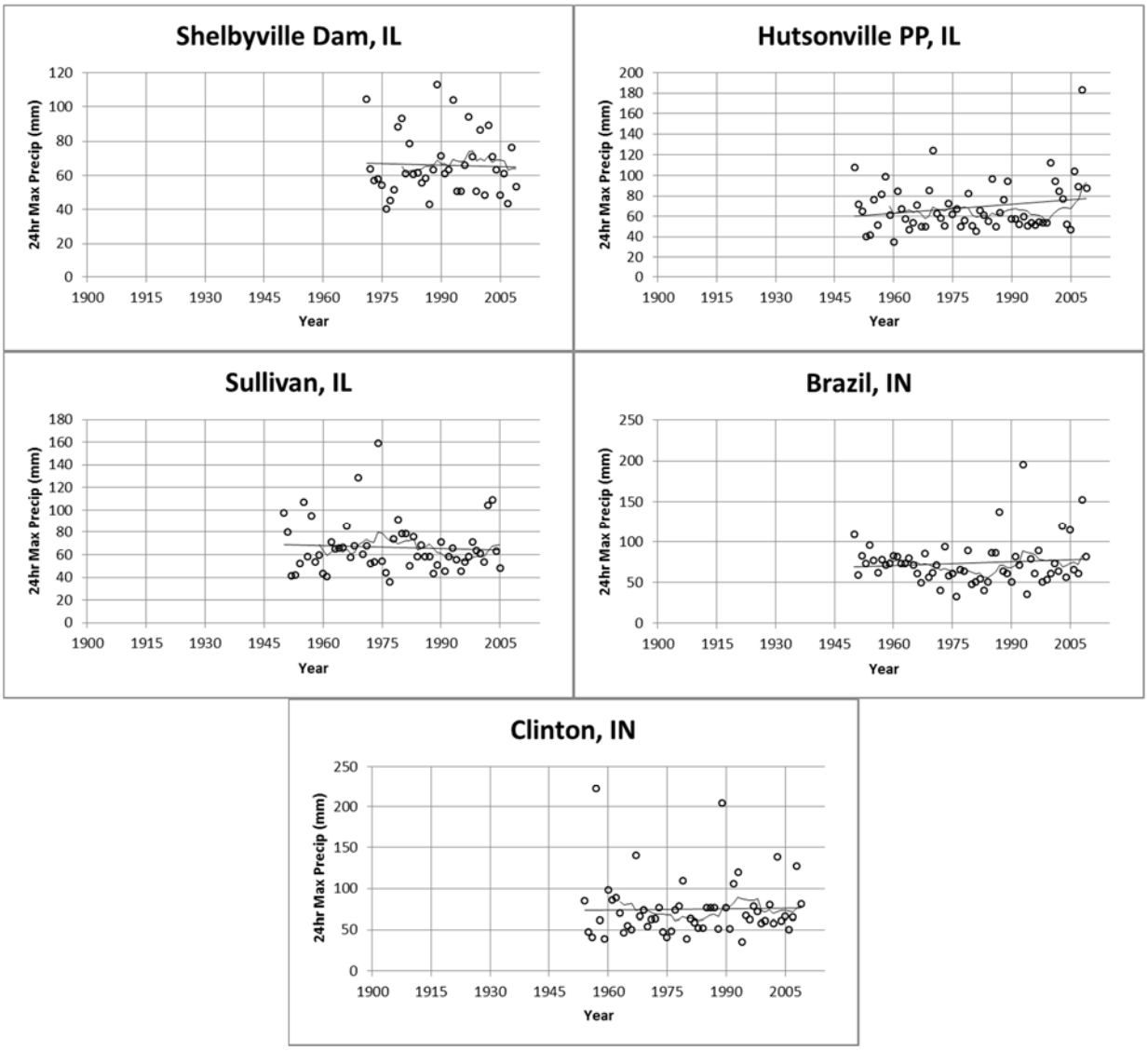

Figure 4.26. 24-hr AMS for several stations in Illinois and Indiana with linear and 10 year moving average fits

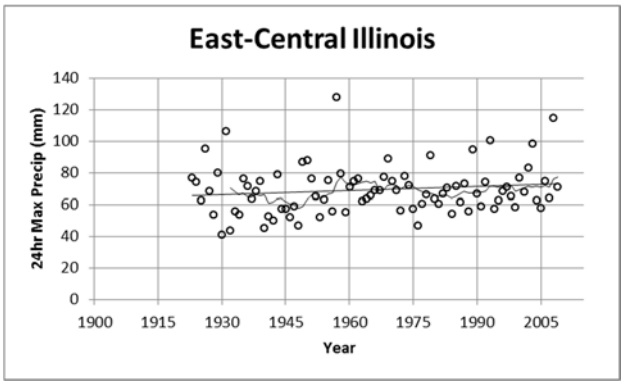

Figure 4.27. 24-hr average AMS for east central Illinois region with linear and 10 year moving average fits

Table 4.7. Trend analysis results for 24-hr AMS at individual Illinois stations and of average Illinois region

	Signif Level	AMS 24-hr		
		t-test	MK	Levene
CHARLESTON	95%-5%	NULL	NULL	NULL
	90%-10%			
DANVILLE	95%-5%	NULL	NULL	NULL
	90%-10%			**HETERO**
HUTSONVILLE PP	95%-5%	NULL	NULL	NULL
	90%-10%	**POS**		
PARIS	95%-5%	NULL	NULL	NULL
	90%-10%			
URBANA	95%-5%	NULL	NULL	NULL
	90%-10%			
BRAZIL, IN	95%-5%	NULL	NULL	**HETERO**
	90%-10%			
CLINTON, IN	95%-5%	-	-	-
	90%-10%			
ILLINOIS AVERAGE	95%-5%	NULL	NULL	NULL
	90%-10%			

Annual Occurrences Greater Than A Given 24-hr Event

In addition to an analysis the 24-hr AMS (the largest event per year), the trend of other large 24-hr events were considered. The annual number of occurrences of 24-hr rain events larger than or equal to

the gauge recorder's smallest 24-hr AMS were calculated and graphed in a time series. The Indiana, Michigan, and Illinois minimum 24-hr AMS for the gauges were 31.8 mm – 38.1 mm (1.25 in -1.5 in), 17.8 mm -33 mm (0.7 in – 1.3 in), and 33 mm – 40.6 mm (1.3 in -1.6 in), respectively. The minimum 24-hr AMS for each region corresponds to about half the value of the 1-yr, 24-hr Atlas 14 design storm for each region. In addition to the minimum AMS value for each gauge, the annual number of occurrences greater than or equal to the 1-yr, 24-hr Atlas 14 design storm for each region was also calculated and graphed in a time series for each gauges. The 1-yr, 24-hr Atlas 14 design storm for the Indiana, Michigan, and Illinois regions are 62.5 mm (2.46 in), 50.5 mm (1.99 in), and 65 mm (2.56 in), respectively. The number of rainfall occurrences greater than a given amount, can provide insight into the frequency of larger rainstorm events (PDS), which analysis of AMS can't provide.

Figure 4.28 and Figure 4.29 show the annual occurrences greater than the smallest 24-hr AMS for each rain gauge station near Camp Atterbury (see Section 3.1.6). Gauges shown in Figure 4.28 have records beginning 1900-1915 and the gauges shown in Figure 4.29 have records beginning after 1945. Figure 4.30 shows the average number of annual occurrences greater than the smallest 24-hr AMS for all 10 gauges. All the gauge stations show a positive linear trend in the number of occurrences greater than the smallest 24-hr AMS. The increasing trend is more evident if only the time series after 1960 is considered. Several long term gauges (i.e. Bloomington, Columbus, Seymour, and Shelbyville) show an evident increase is annual occurrences starting around 1990. The number of occurrences seems to increase after 1990 for many of the gauge station as shown by their 10 year moving averages. The increase in the number of occurrences is also reflected in the averaged occurrences time series. The region average shows a significant increase at the 95% confidence limit.

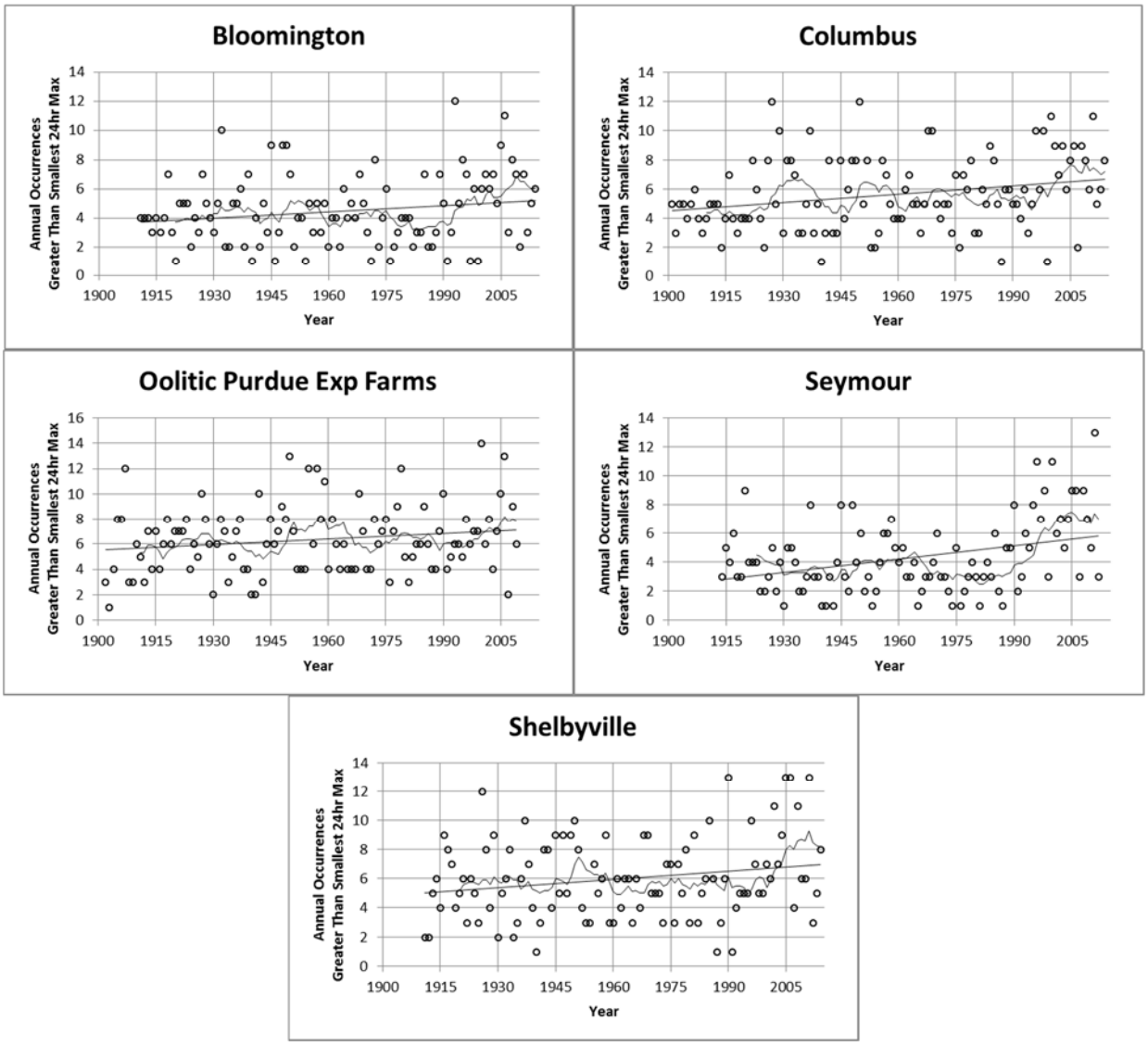

Figure 4.28. Annual occurrences greater than smallest 24-hr AMS for several stations in Indiana with linear and 10 year moving average fits

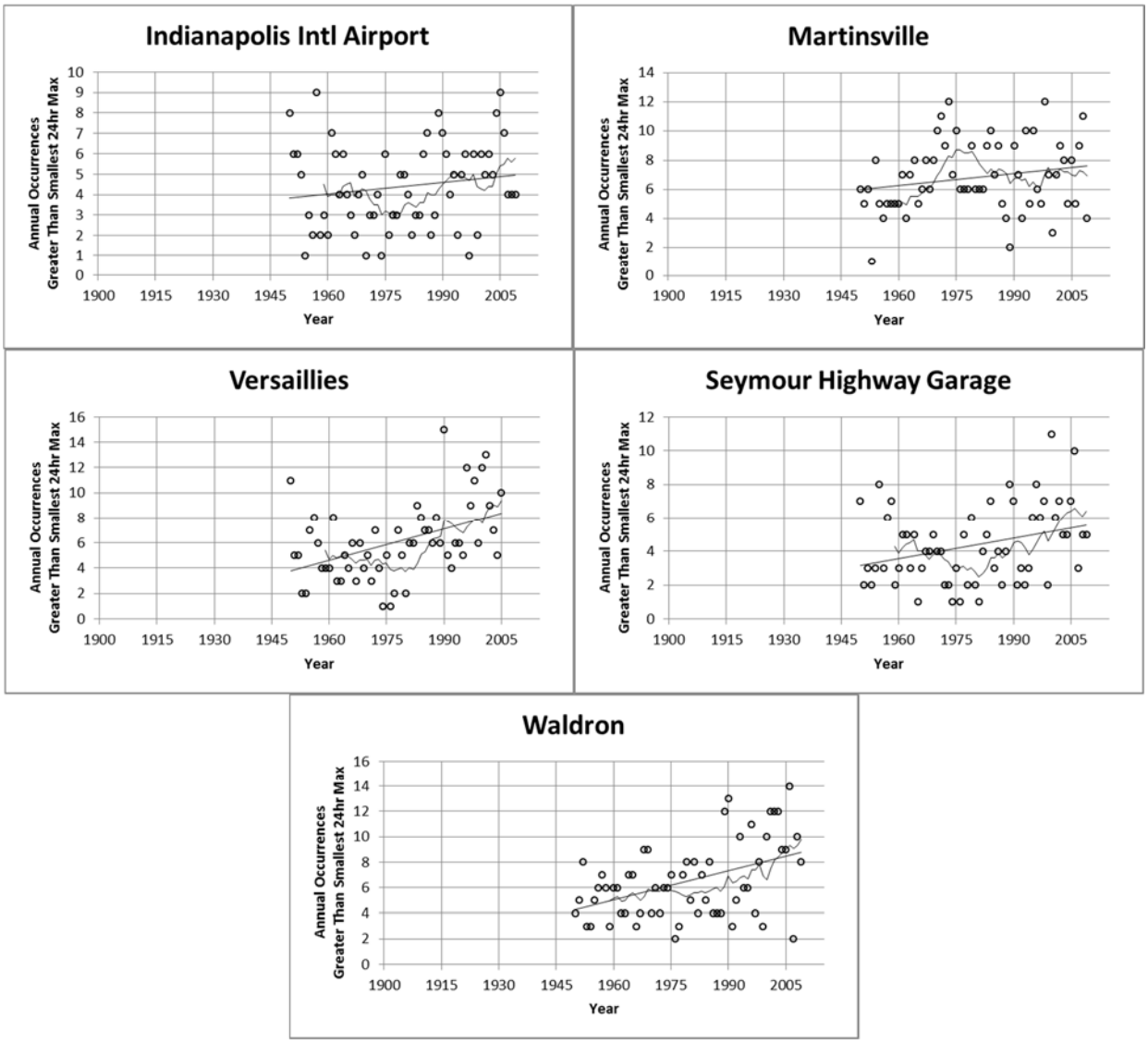

Figure 4.29. Annual occurrences greater than smallest 24-hr AMS for several stations in Indiana with linear and 10 year moving average fits

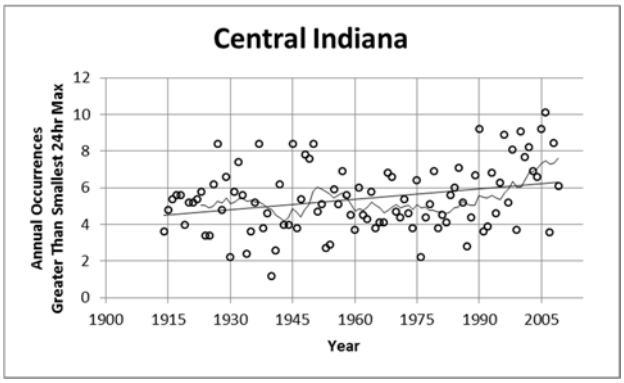

Figure 4.30. Annual average occurrences greater than smallest 24-hr AMS for central Indiana region with linear and 10 year moving average fits

Figure 4.31 and Figure 4.32 show the annual occurrences greater than the applicable 1-yr, 24-hr Atlas 14 design storm for each rain gauge station near Camp Atterbury (see Section 3.1.6). Gauges shown in Figure 4.31 have records beginning 1900-1915 and the gauges shown in Figure 4.32 have records beginning after 1945. Figure 4.33 shows the average number of annual occurrences greater than the applicable 1-yr, 24-hr Atlas 14 design storm for all 10 gauges. Most of the gauge stations show a positive linear trend in the number of occurrences greater than the 1yr-24hr Atlas 14 design storm while the other stations show no change over time. The region average shows a significant increase at the 95% confidence limit. The average number of occurrences per year is expected to be 1 given that reference storm is the 1-year event. The average number of annual occurrences increase from around 0.5 towards 1 during the time series.

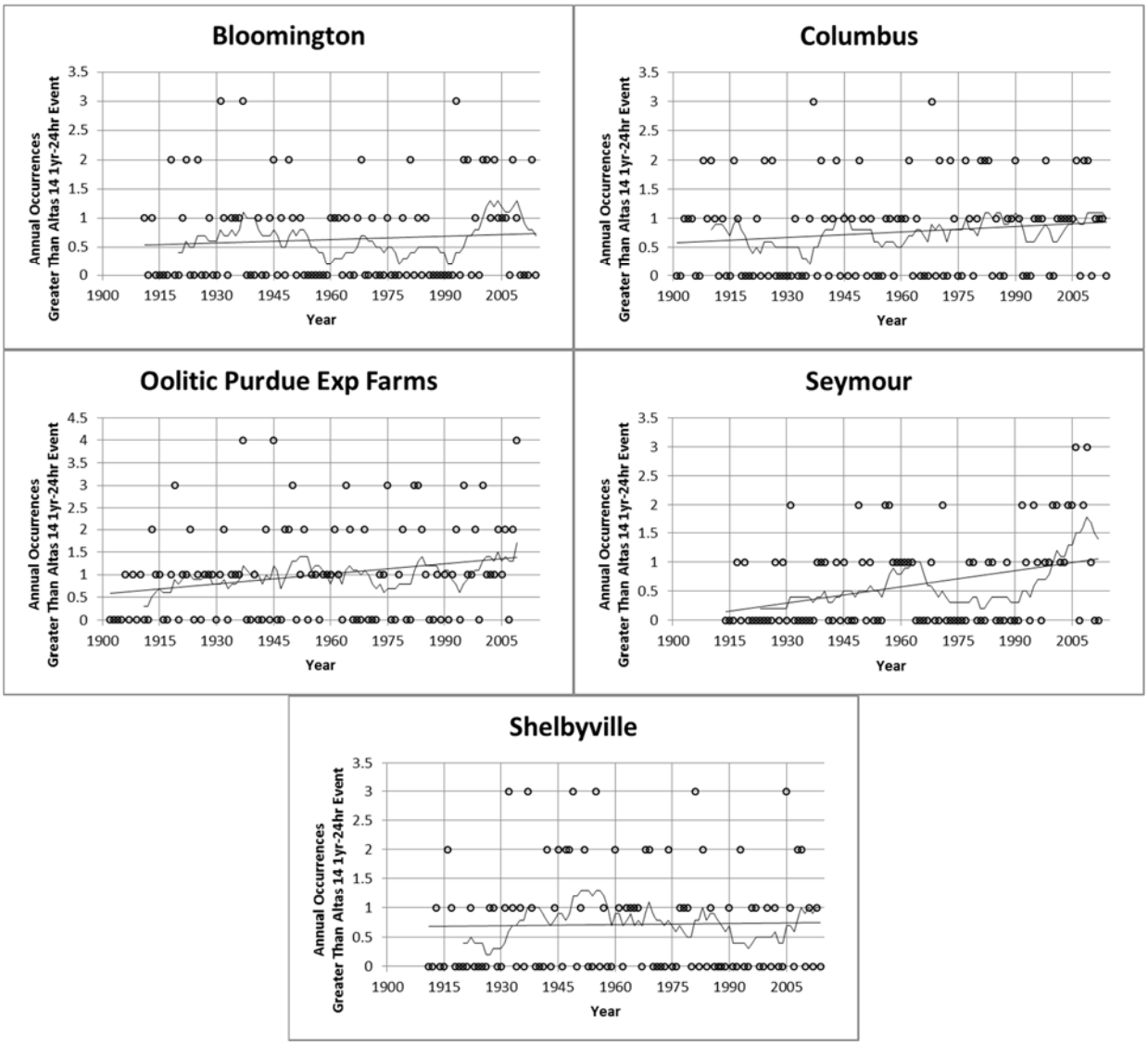

Figure 4.31. Annual occurrences greater than Atlas 14 1yr-24hr event for several stations in Indiana with linear and 10 year moving average fits

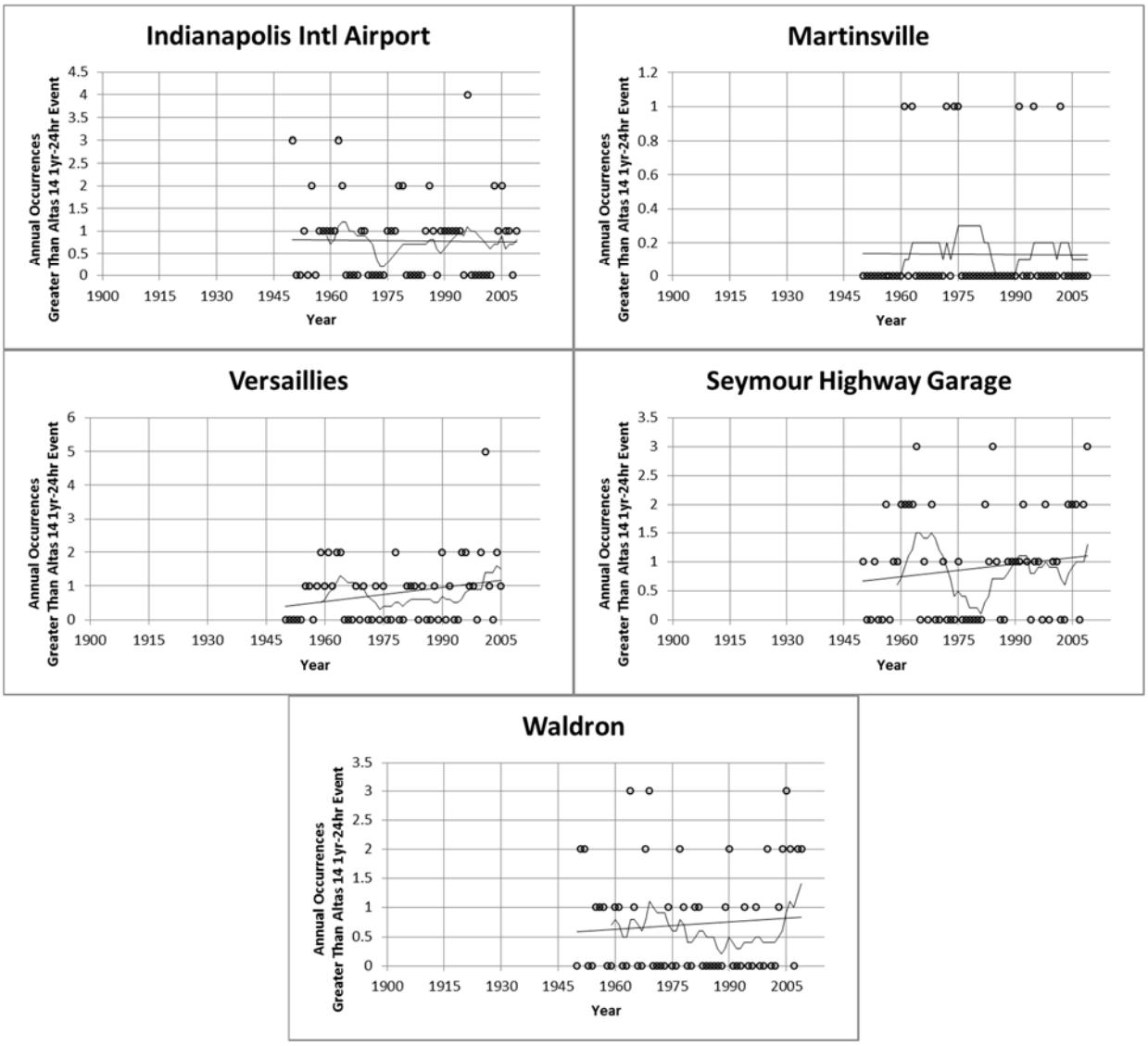

Figure 4.32. Annual occurrences greater than Atlas 14 1yr-24hr event for several stations in Indiana with linear and 10 year moving average fits

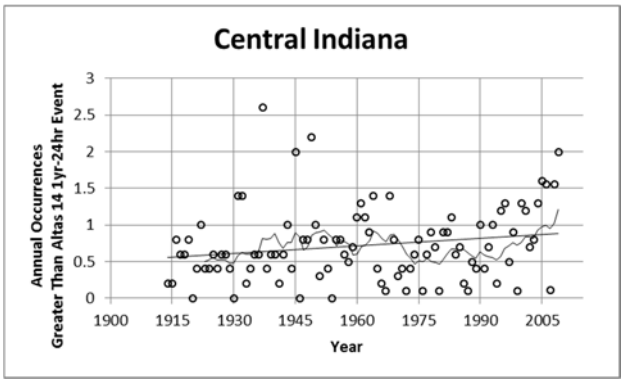

Figure 4.33. Annual average occurrences greater than Atlas 14 1yr-24hr event for central Indiana region with linear and 10 year moving average fits

Figure 4.34 and Figure 4.35 show the annual occurrences greater than the smallest 24-hr AMS for each rain gauge station near Camp Grayling (see Section 3.2.6). Gauges shown in Figure 4.34 have records beginning prior to 1945 and the gauges shown in Figure 4.35 have records beginning after 1945. Figure 4.36 shows the average number of annual occurrences greater than the smallest 24-hr AMS for all 9 gauges. Several gauges (Gaylord, Houghton Lake, Lake City, Traverse City, and Vanderbilt) show increasing trends, Grayling shows a decreasing trend, and the rest show no change in the number of annual occurrences over time. The gauges with increasing trends are located west and north of Camp Grayling, but the gauge closest to the installation (Grayling), shows a decreasing trend. The increase in the number of occurrences is also reflected in the averaged occurrences time series. The region average shows a significant increase at the 90% confidence limit.

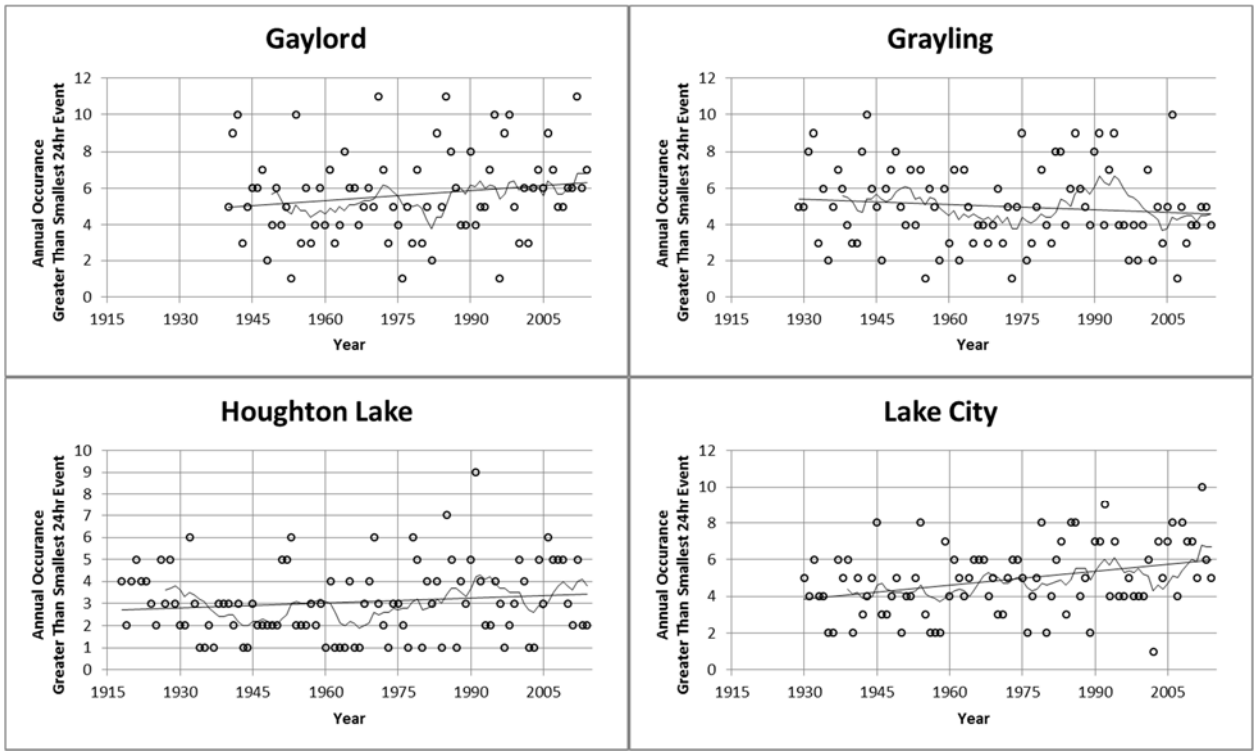

Figure 4.34. Annual occurrences greater than smallest 24-hr AMS for several stations in Michigan with linear and 10 year moving average fits

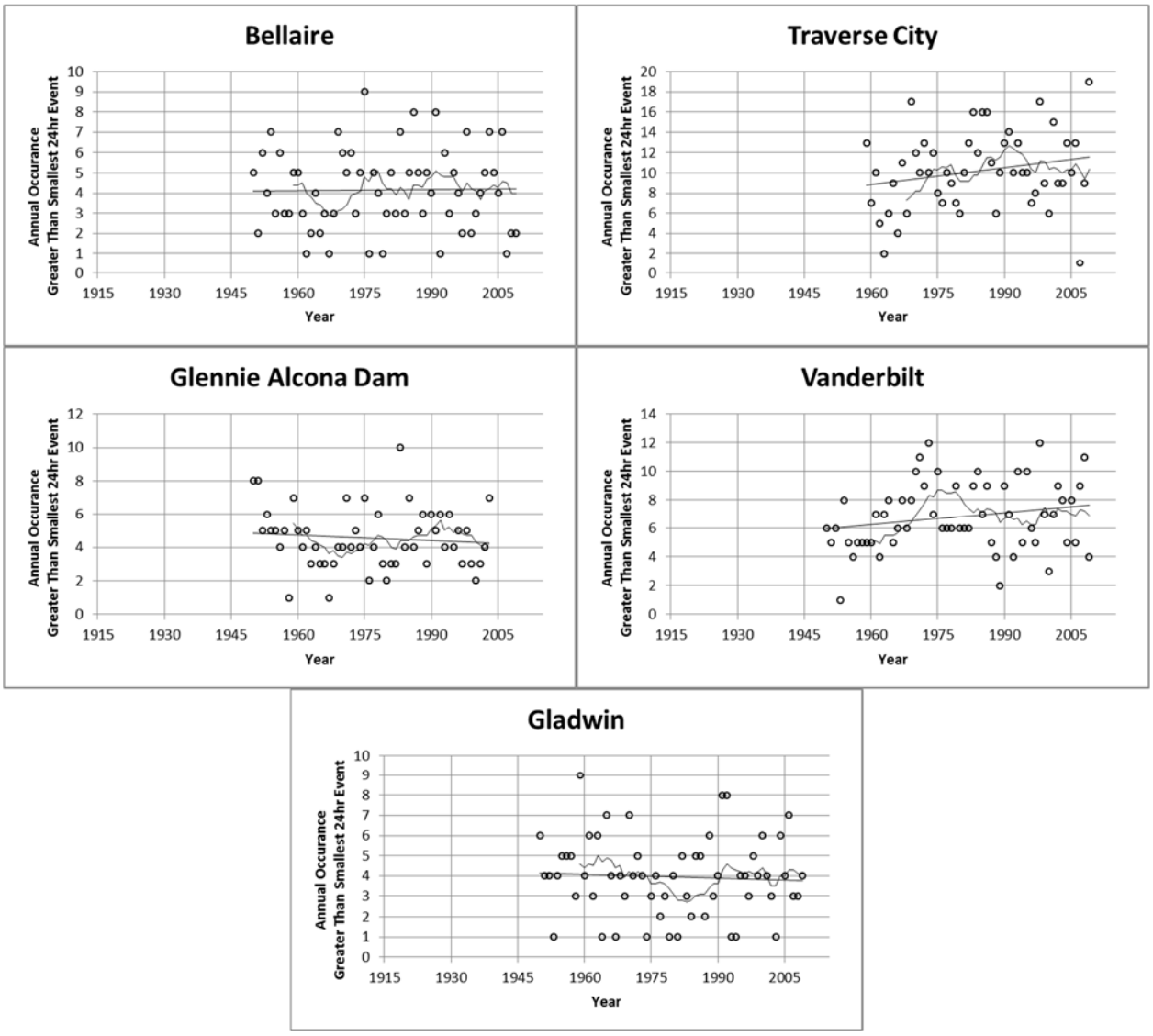

Figure 4.35. Annual occurrences greater than smallest 24-hr AMS for several stations in Michigan with linear and 10 year moving average fits

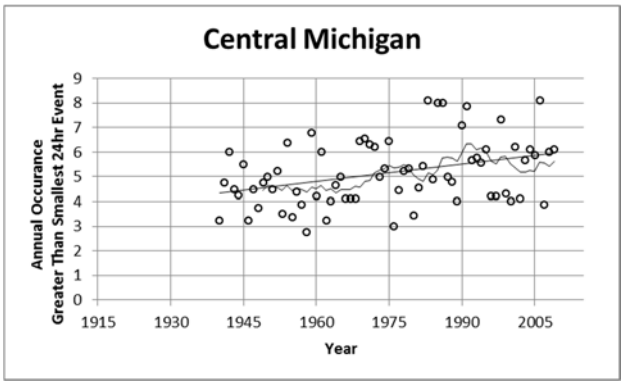

Figure 4.36. Annual average occurrences greater than smallest 24-hr average AMS for central Michigan region with linear and 10 year moving average fits

Figure 4.37 and Figure 4.38 show the annual occurrences greater than the applicable 1-yr, 24-hr Atlas 14 design storm for each rain gauge station near Camp Grayling (see Section 3.2.6). Gauges shown in Figure 4.37 have records beginning prior to 1945 and the gauges shown in Figure 4.38 have records beginning after 1945. Figure 4.39 shows the average number of annual occurrences greater than the applicable 1-yr, 24-hr Atlas 14 design storm for all 9 gauges. Half of the gauge stations (Houghton Lake, Lake City, Traverse City, Glennie Alcona Dam, and Vanderbilt) show slight increasing trends while the other stations show slight decreasing trends. The spatial distribution of the increasing and decreasing trend stations is mixed in relation to Camp Grayling. The average number of occurrences per year is expected to be 1 given that reference storm is the 1-year event. The average number of annual occurrences across the region is constant during the time series, which reflects the mixed results of the individual stations.

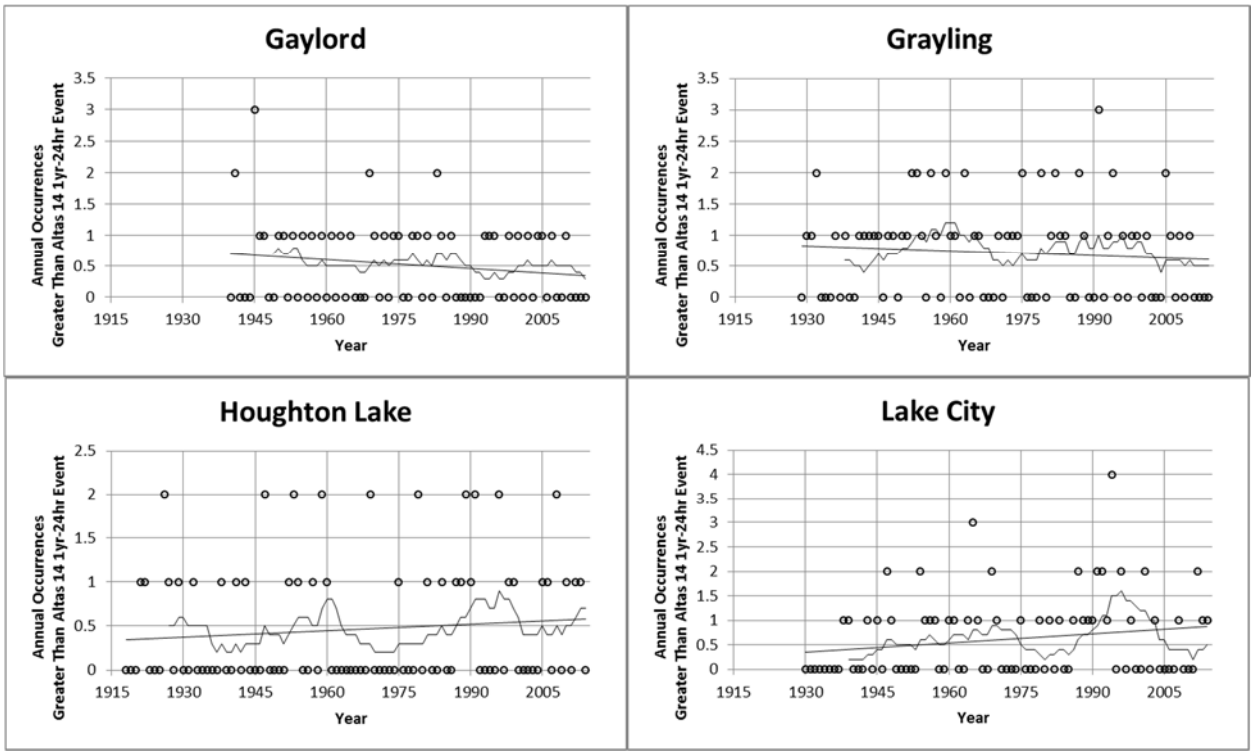

Figure 4.37. Annual occurrences greater than Atlas 14 1yr-24hr event for several stations in Michigan with linear and 10 year moving average fits

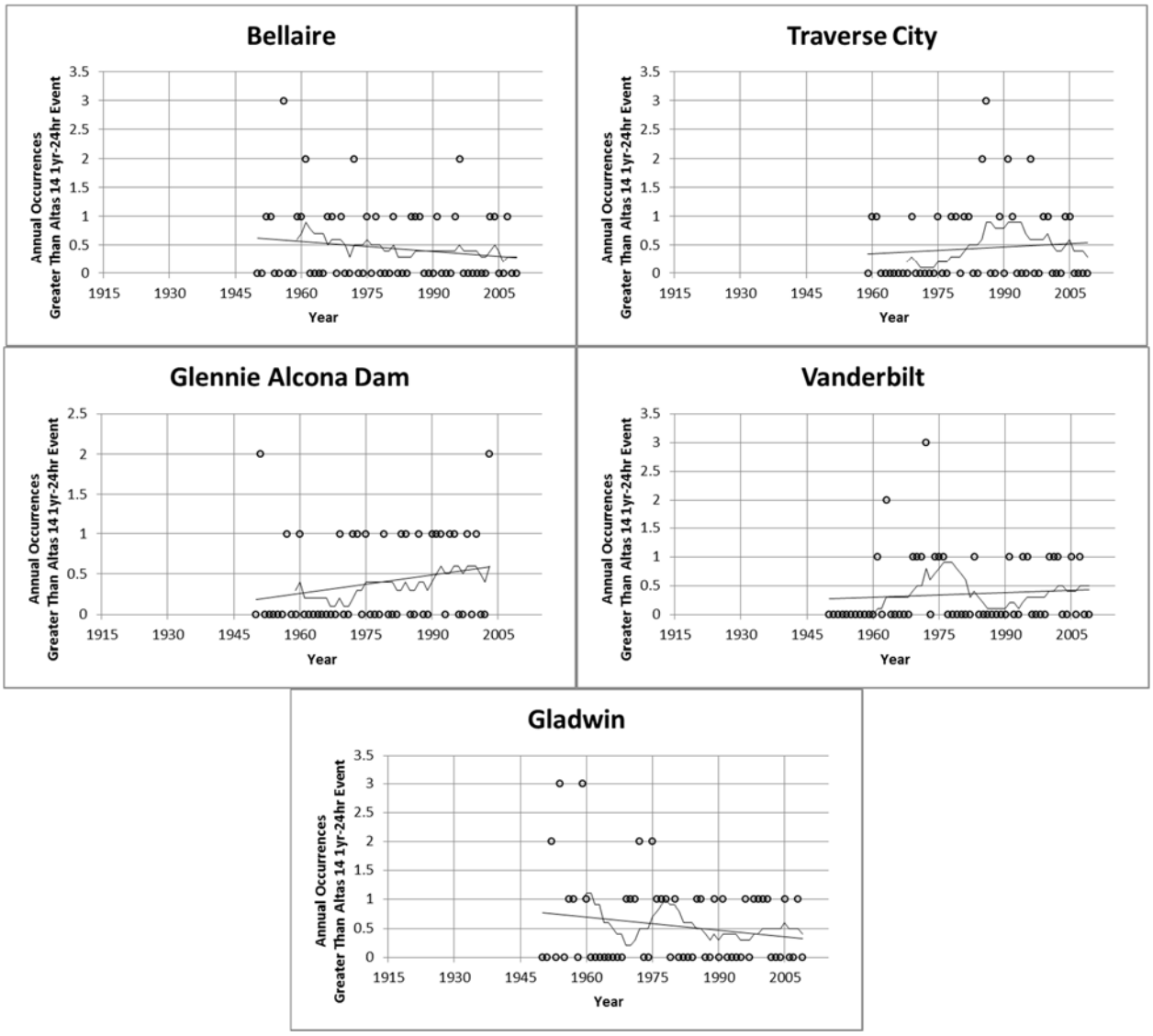

Figure 4.38. Annual occurrences greater than Atlas 14 1yr-24hr event for several stations in Michigan with linear and 10 year moving average fits

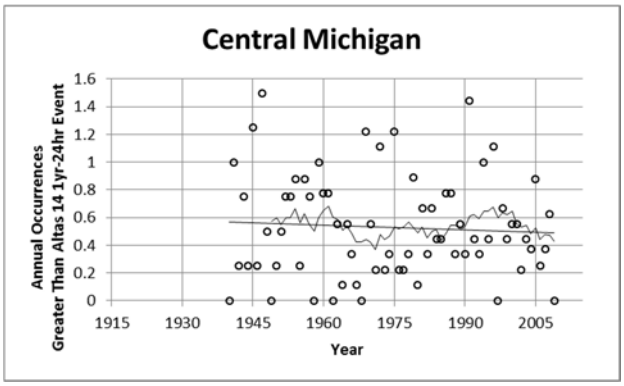

Figure 4.39. Annual average occurrences greater than Atlas 14 1yr-24hr event for central Michigan region with linear and 10 year moving average fits

Figure 4.40 and Figure 4.41 show the annual occurrences greater than the smallest 24-hr AMS for each rain gauge station near Edgar County Illinois (see Section 3.3.6). Gauges shown in Figure 4.40 have records beginning 1900-1920 and the gauges shown in Figure 4.41 have records beginning after 1945. Figure 4.42 shows the average annual occurrences greater than the smallest 24-hr AMS for all 9 gauges. Most of the gauge stations show no linear trend in annual occurrences greater than the smallest 24-hr AMS, though Hutsonville Power Plant, IL, Clinton, IN, and Brazil, IN show increasing linear trends and are located south and east of Edgar County. These gauges show trends similar to the nearby gauges in the central Indiana region (i.e. Bloomington, IN) for which the number of occurrences increase starting around 1990. The region average shows a significant increase at the 95% confidence limit.

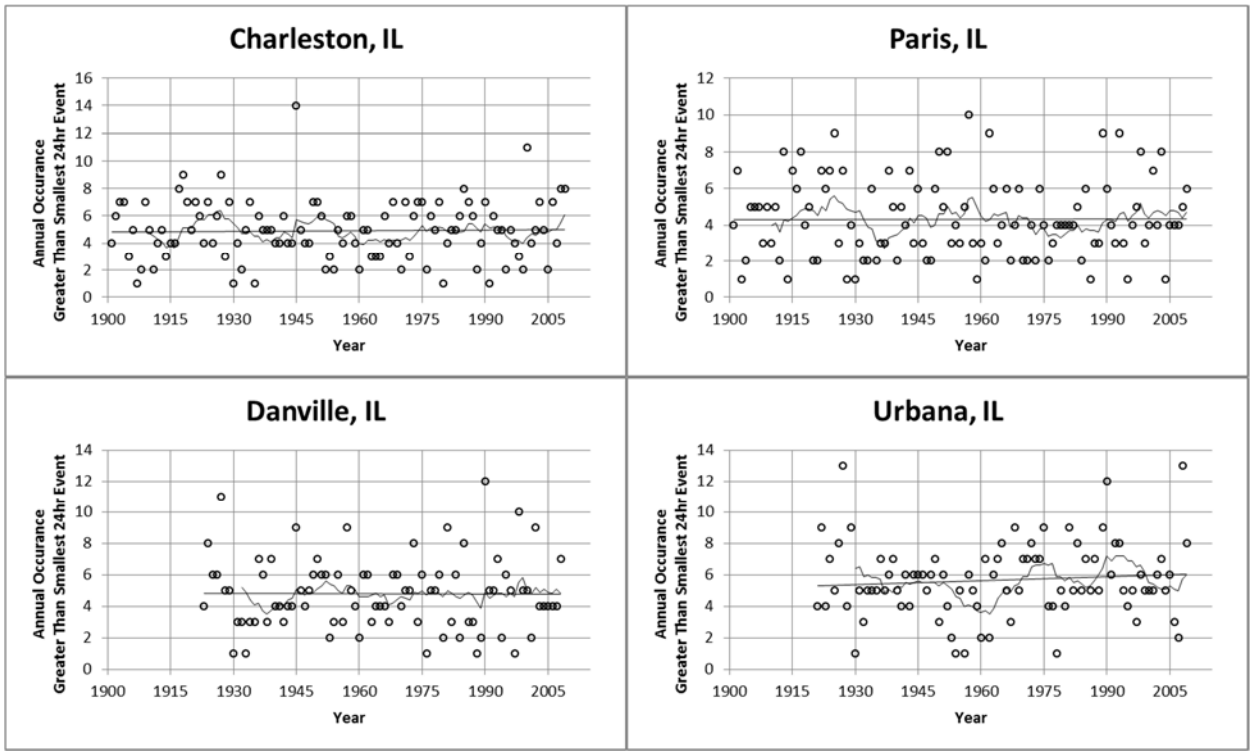

Figure 4.40. Annual occurrences greater than smallest 24-hr AMS for several stations in Illinois with linear and 10 year moving average fits

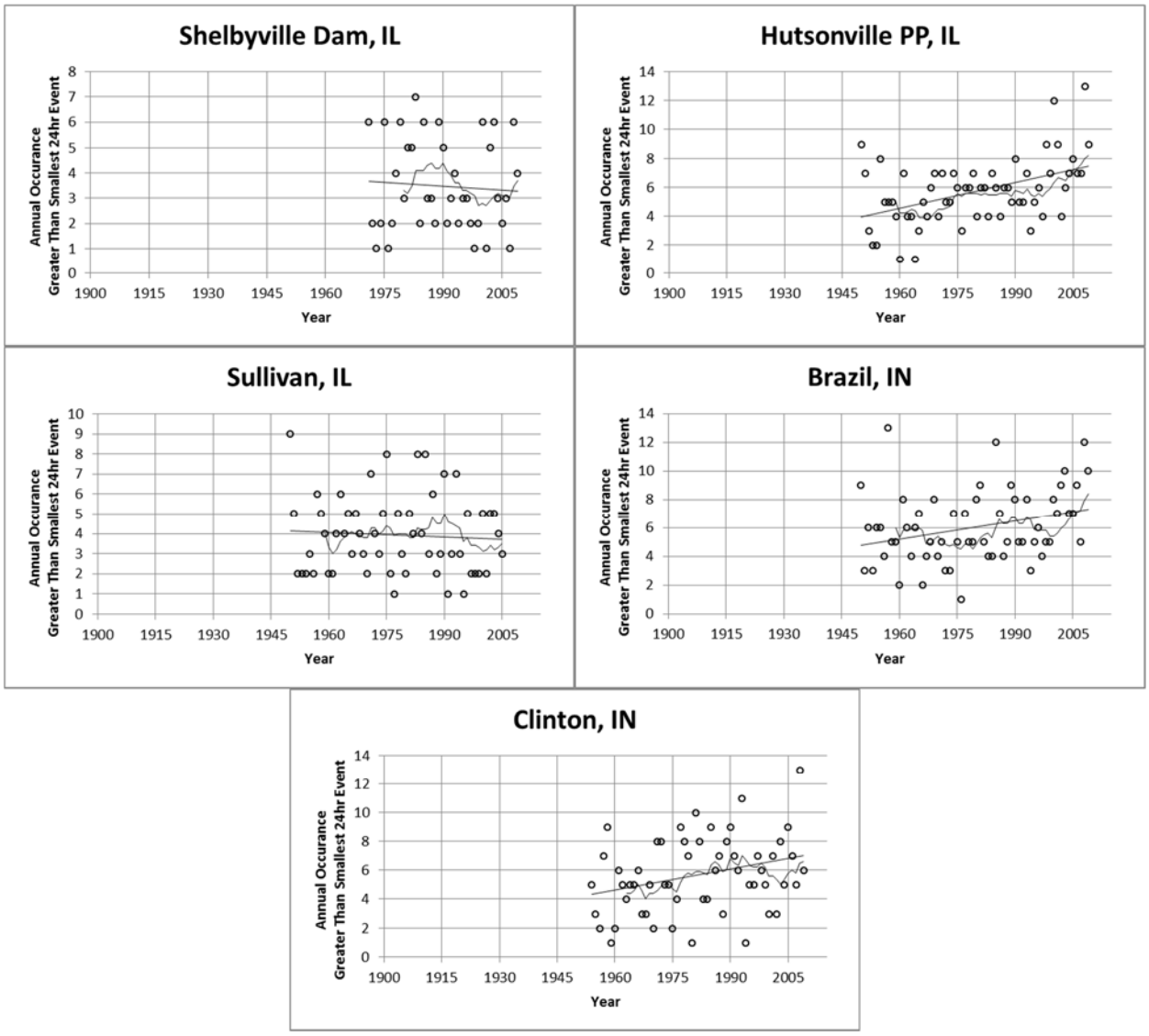

Figure 4.41. Annual occurrences greater than smallest 24-hr AMS for several stations in Illinois and Indiana with linear and 10 year moving average fits

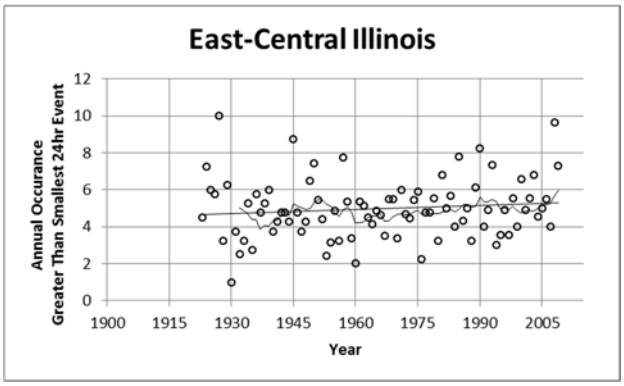

Figure 4.42. Annual average occurrences greater than smallest 24-hr average AMS for east central Illinois region with linear and 10 year moving average fits

Figure 4.43 and Figure 4.44 show the annual occurrences greater than the applicable 1-yr, 24-hr Atlas 14 design storm for each rain gauge station near Edgar County Illinois (see Section 3.3.6). Gauges shown in Figure 4.43 have records beginning 1900-1920 and the gauges shown in Figure 4.44 have records beginning after 1945. Figure 4.45 shows the average annual occurrences greater than the applicable 1-yr, 24-hr Atlas 14 design storm for all 9 gauges. Most of the gauge stations show no linear trend in 24-hr AMS, though Paris, IL and Hutsonville Power Plant, IL show increasing linear trends. The average number of occurrences per year is expected to be 1 given that reference storm is the 1-year event. The average number of annual occurrences increase from around 0.5 towards 0.8 during the time series.

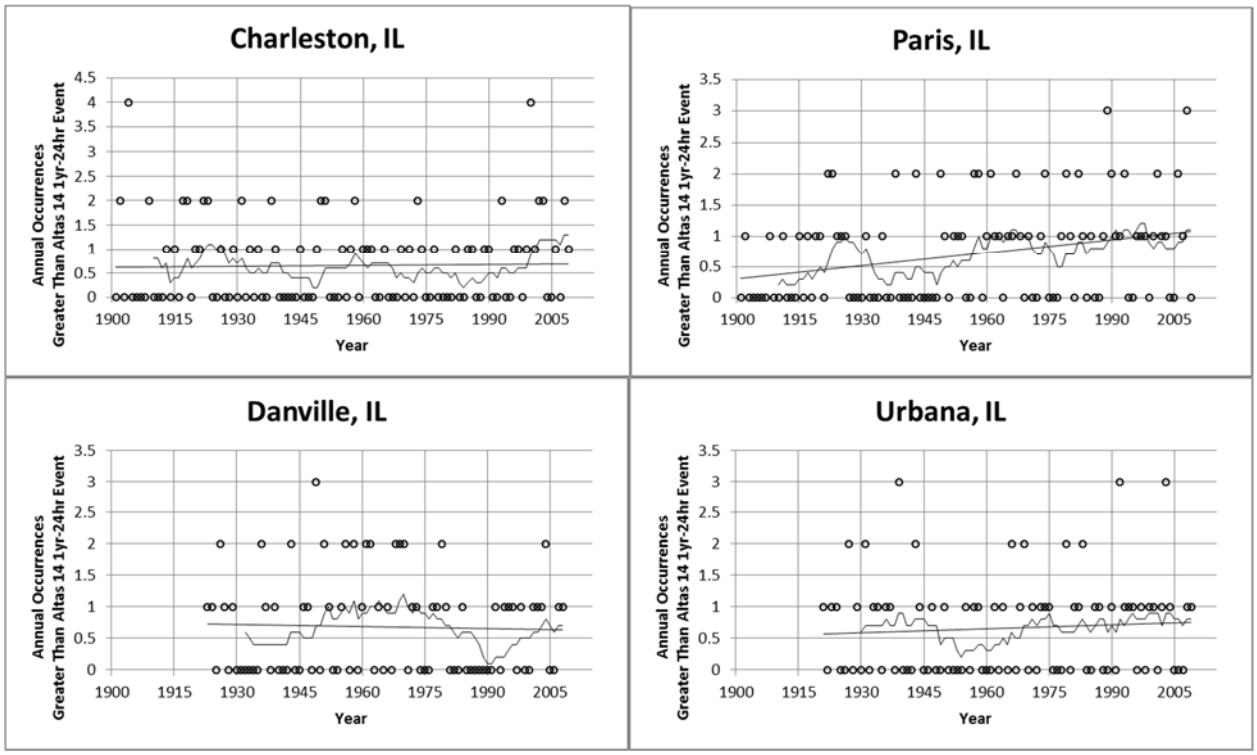

Figure 4.43. Annual occurrences greater than Atlas 14 1yr-24hr event for several stations in Illinois with linear and 10 year moving average fits

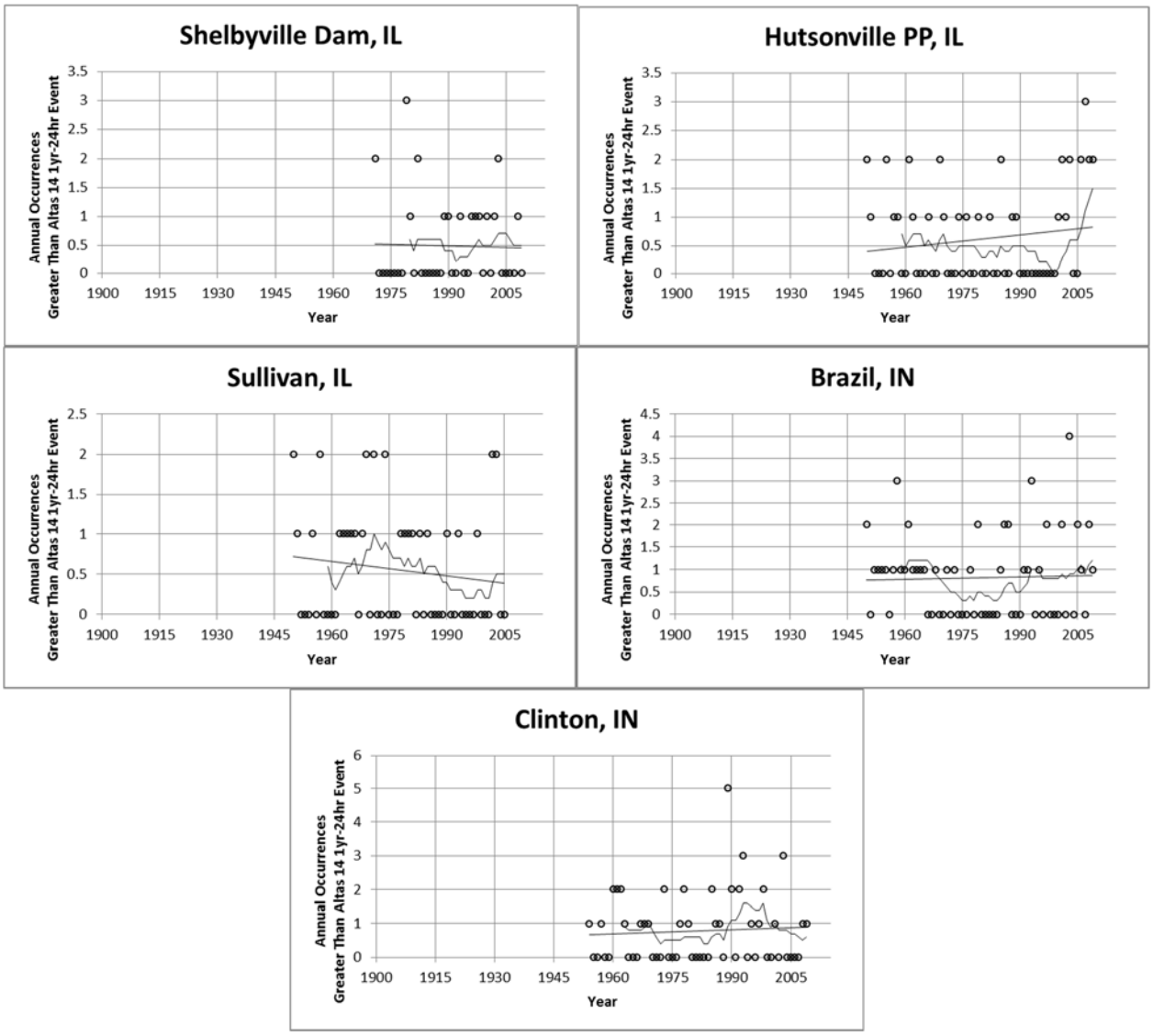

Figure 4.44. Annual occurrences greater than Atlas 14 1yr-24hr event for several stations in Illinois and Indiana with linear and 10 year moving average fits

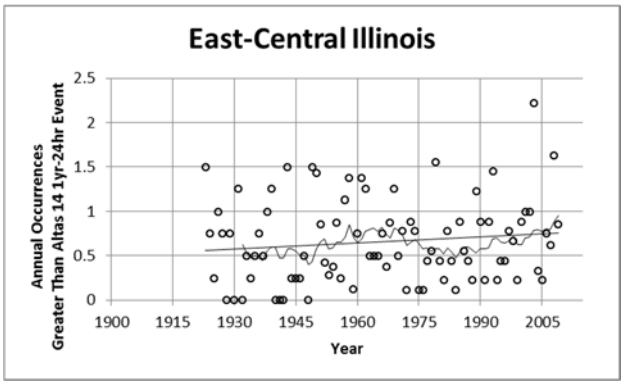

Figure 4.45. Annual average occurrences greater than Atlas 14 1yr-24hr event for east central Illinois region with linear and 10 year moving average fits

4.3.4 Total Annual Wet Hours

The trend of total annual wet hours (clock hours) were assessed in order to facilitate climate model bias correction with regards to precipitation thresholds. Any clock hour with at least 0.25 mm (0.01 in) were included.

Figure 4.46 and Figure 4.47 show total annual wet hours for each rain gauge station near Camp Atterbury (see Section 3.1.6). Gauge groupings for each figure are consistent with previous sections. Figure 4.48 shows average annual wet hours for all 9 gauges (the Seymour gauge recorded only 24-hr data). Shelbyville and Waldron, both located in Shelby County northeast of Camp Atterbury, show linear increases in annual wet hours while stations to the west (Indianapolis Airport, Oolitic Purdue Exp Farms, Martinsville, and Bloomington) show slight linear decreases. However, since 2000 there has been an increase. Bloomington and Columbus records show a 'U' shaped time series as evident by the 10 year moving averages, while the remaining time series have no discernable shape. The region has an average of 360 wet hours per year with a range of 200-500 hours.

Statistical tests and findings for trends in total annual wet hours are presented in Table 4.8. Of the seven gauges tested (Versailles and Shelbyville were excluded due 1-hr record lengths of less than 40 years and Seymour was due to the lack of 1-hr data), only Oolitic Purdue Experimental Farm showed statistically significant negative trend for both the t-test and MK test while Columbus showed a significant (α = 10%) negative trend for the t-test. The other stations showed no trends. Based on Levene's test, the hypothesis that variance did not change could be rejected (α = 10%) for Bloomington, Columbus, Martinsville, and Oolitic Purdue EF.

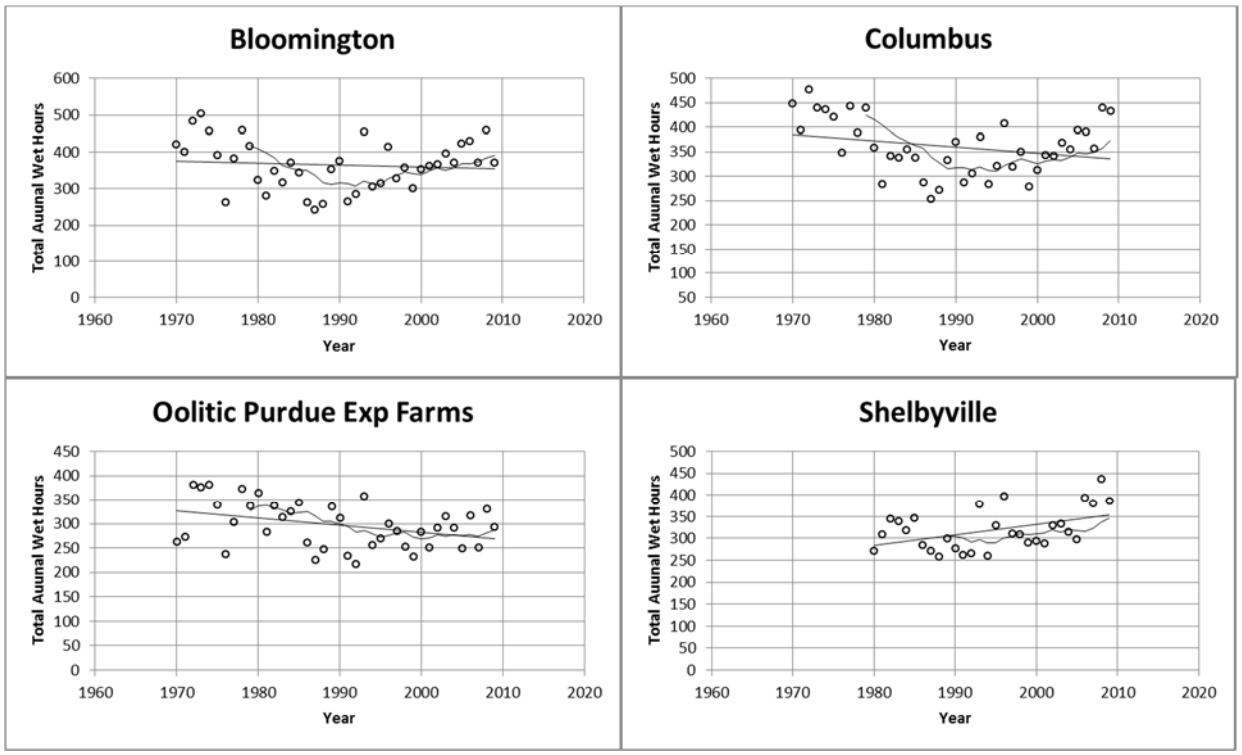

Figure 4.46. Total annual wet hours for several stations in Indiana with linear and 10 year moving average fits

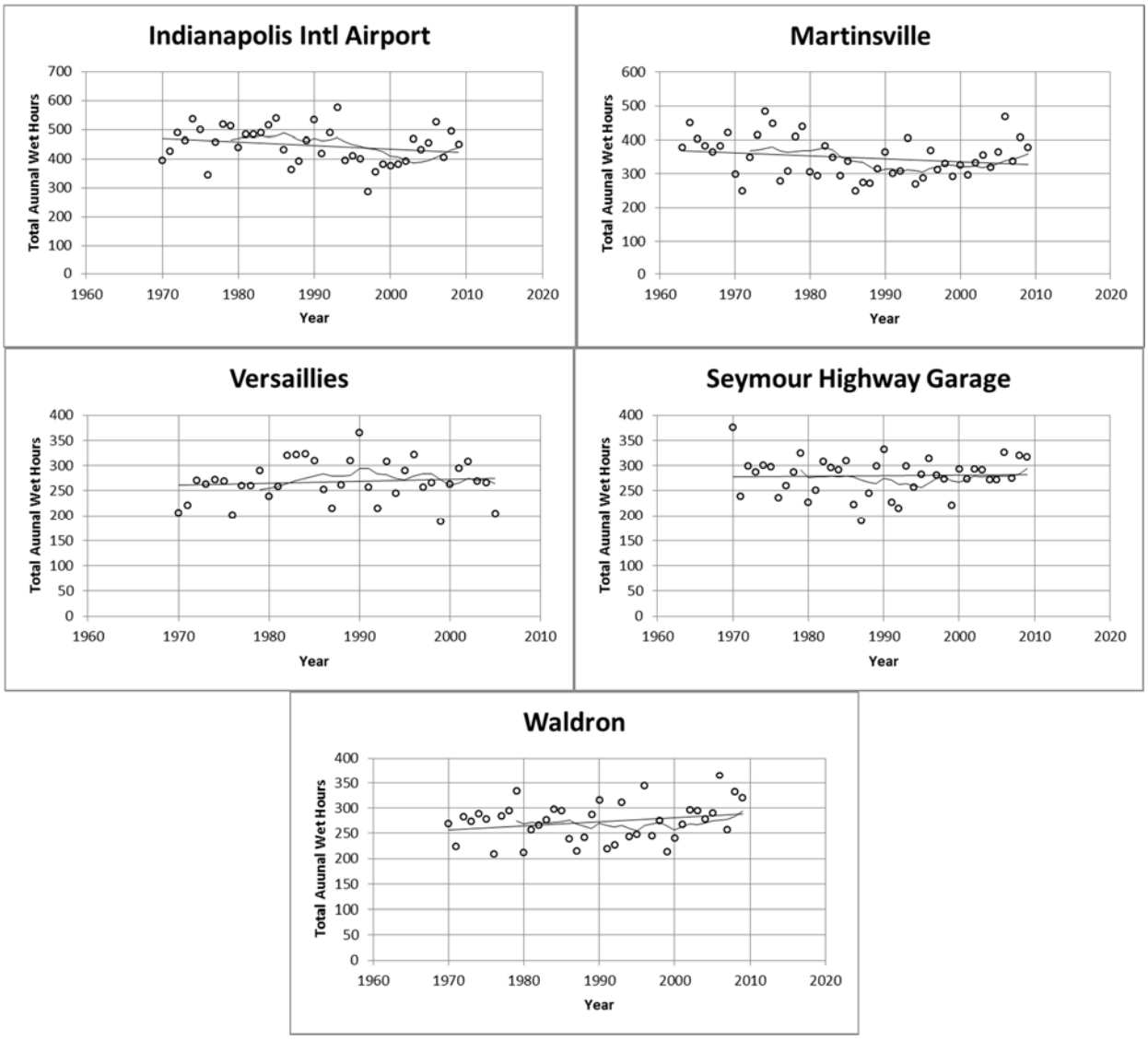

Figure 4.47. Total annual wet hours for several stations in Indiana with linear and 10 year moving average fits

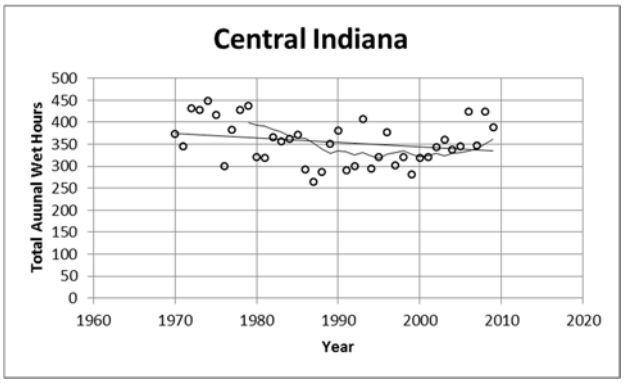

Figure 4.48. Total average annual wet hours for central Indiana region with linear and 10 year moving average fits

Table 4.8. Trend analysis results for total annual wet hours at individual Indiana stations and of average Indiana region

	Signif Level	Total Annual Wet Hours		
		t-test	MK	Levene
BLOOMINGTON	95%-5%	NULL	NULL	NULL
	90%-10%			**HETERO**
COLUMBUS	95%-5%	NULL	NULL	NULL
	90%-10%	**NEG**		**HETERO**
INDIANAPOLIS IA	95%-5%	NULL	NULL	NULL
	90%-10%			
MARTINSVILLE	95%-5%	NULL	NULL	NULL
	90%-10%			**HETERO**
OOLITIC PURDUE EF	95%-5%	**NEG**	**NEG**	NULL
	90%-10%			**HETERO**
SEYMOUR HG	95%-5%	NULL	NULL	NULL
	90%-10%			
WALDRON	95%-5%	NULL	NULL	NULL
	90%-10%			
INDIANA AVERAGE	95%-5%	NULL	NULL	NULL
	90%-10%			

The number of wet hours per year in Central Michigan seem to be decreasing. Figure 4.49 shows total annual wet hours for each rain gauge station near Camp Grayling (see Section 3.2.6). Figure 4.50 shows total average annual wet hours for all 7 gauges. Gaylord and Houghton Lake gauges don't have hourly

precipitation data. Lake City Experimental Farm, Traverse City, and Bellaire gauge stations (located west of Camp Grayling) show slightly positive linear trends in total annual wet hours while the remaining stations show decreasing trends. An average of 325 wet hours occur annually with a range of 200-500 hours. The 10 year moving averages tend follow closely to the linear trends. The average linear Michigan trend is decreasing, however, total average annual wet hours seem to be increasing since 2000.

Statistical tests and findings for trends in total annual wet hours are presented in Table 4.9. Of the five gauges tested (Gladwin and Glennie Alcona Dam were excluded due 1-hr record lengths of less than 40 years), Grayling showed a statistically significant negative trend for both the t-test and MK test while Vanderbilt and the Michigan region average showed a statistically significant negative trend for the t-test. Bellaire and the Michigan region average show (α = 10%) positive and negative trends for MK, respectively. Based on Levene's test, the hypothesis that variance did not change could be rejected for the Vanderbilt station and the Michigan region average time series.

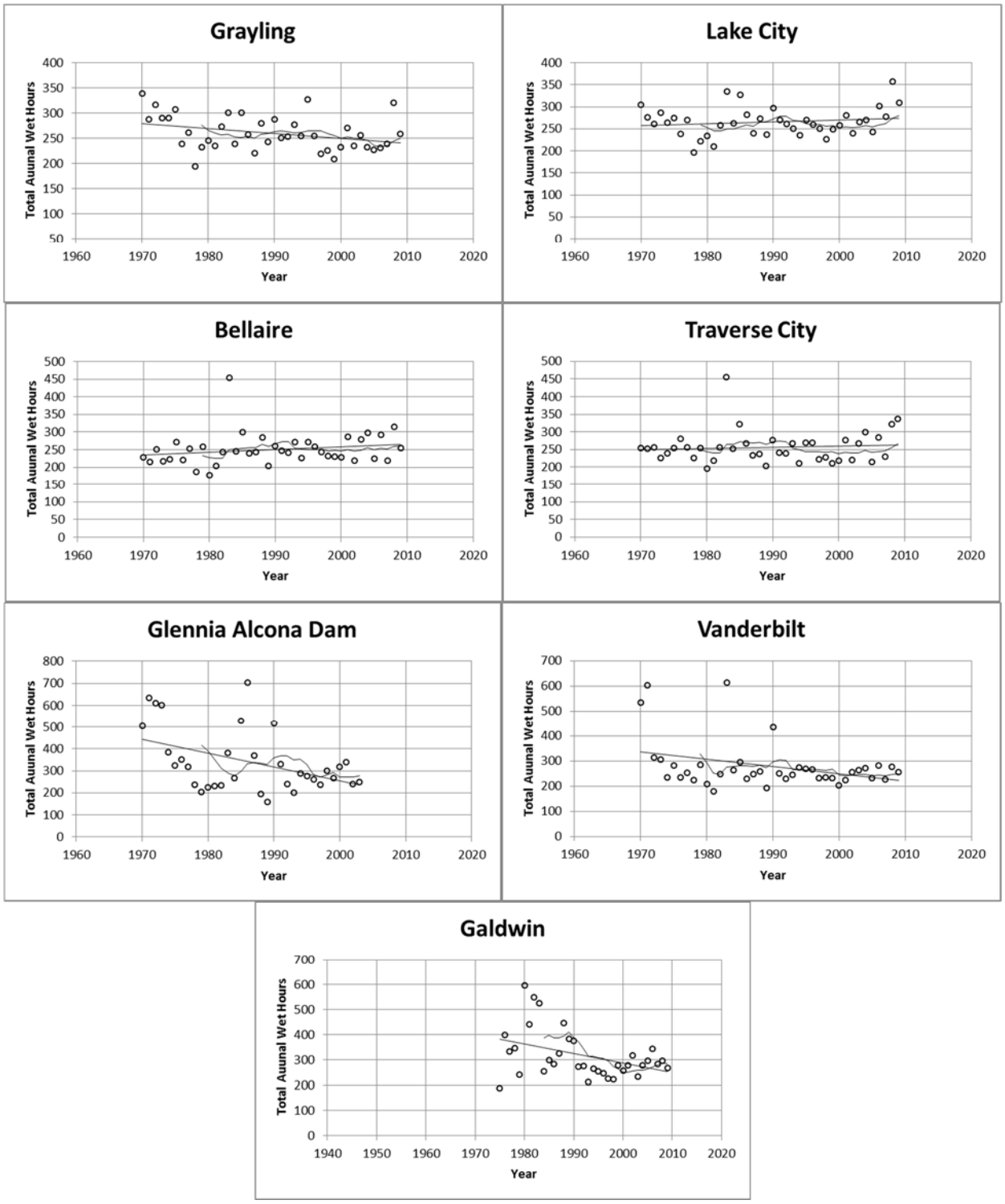

Figure 4.49. Total annual wet hours for several stations in Michigan with linear and 10 year moving average fits

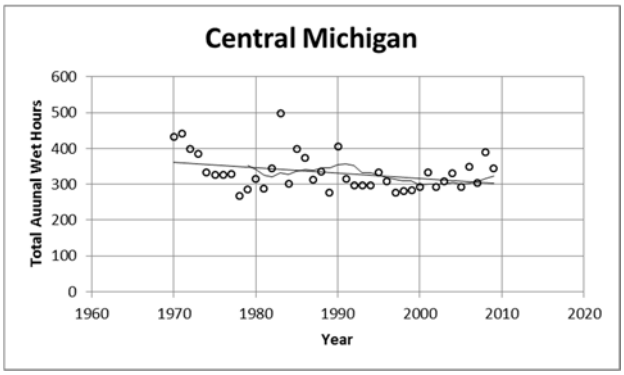

Figure 4.50. Total average annual wet hours for central Michigan region with linear and 10 year moving average fits

Table 4.9. Trend analysis results for total annual wet hours at individual Michigan stations and of average Michigan region

	Signif Level	Total Annual Wet Hours		
		t-test	MK	Levene
BELLAIRE	95%-5%	NULL	NULL	NULL
	90%-10%		**POS**	
GRAYLING	95%-5%	**NEG**	**NEG**	NULL
	90%-10%			
LAKE CITY EF	95%-5%	NULL	NULL	NULL
	90%-10%			
TRAVERSE CITY	95%-5%	NULL	NULL	NULL
	90%-10%			
VANDERBILT	95%-5%	**NEG**	NULL	**HETERO**
	90%-10%			
MICHIGAN AVERAGE	95%-5%	**NEG**	NULL	**HETERO**
	90%-10%		**NEG**	

Figure 4.51 show total annual wet hours for each rain gauge station near Edgar County Illinois (see Section 3.3.6). Figure 4.52 shows total average wet hours for all 8 gauges (the Charleston, IL gauge station only records daily precipitation data). Huntsonville Power Plant, IL and Clinton, IN show no slope of the linear trend while all of the other gauge stations show a decreasing linear trend in total annual wet hours. An average of 275-300 wet hours per year can be expected based on the historic gauge data

with a range of 200-500 hours. The 10 year moving average shows nothing of note. Annual wet hours at most stations have increased for the last 5-10 years.

Statistical tests and findings for trends in total annual wet hours are presented in Table 4.10. Of the six gauges tested (Sullivan, IL and Shelbyville Dam, IL were excluded due 1-hr record lengths of less than 40 years), Paris, IL showed a statistically significant negative trend for both the t-test and MK test while Brazil, IN showed a statistically significant negative trend for the t-test. Based on Levene's test, the hypothesis that variance did not change could be rejected for the Paris, IL and Brazil, IN stations at 95% confidence and for Urbana and Danville at 90% confidence.

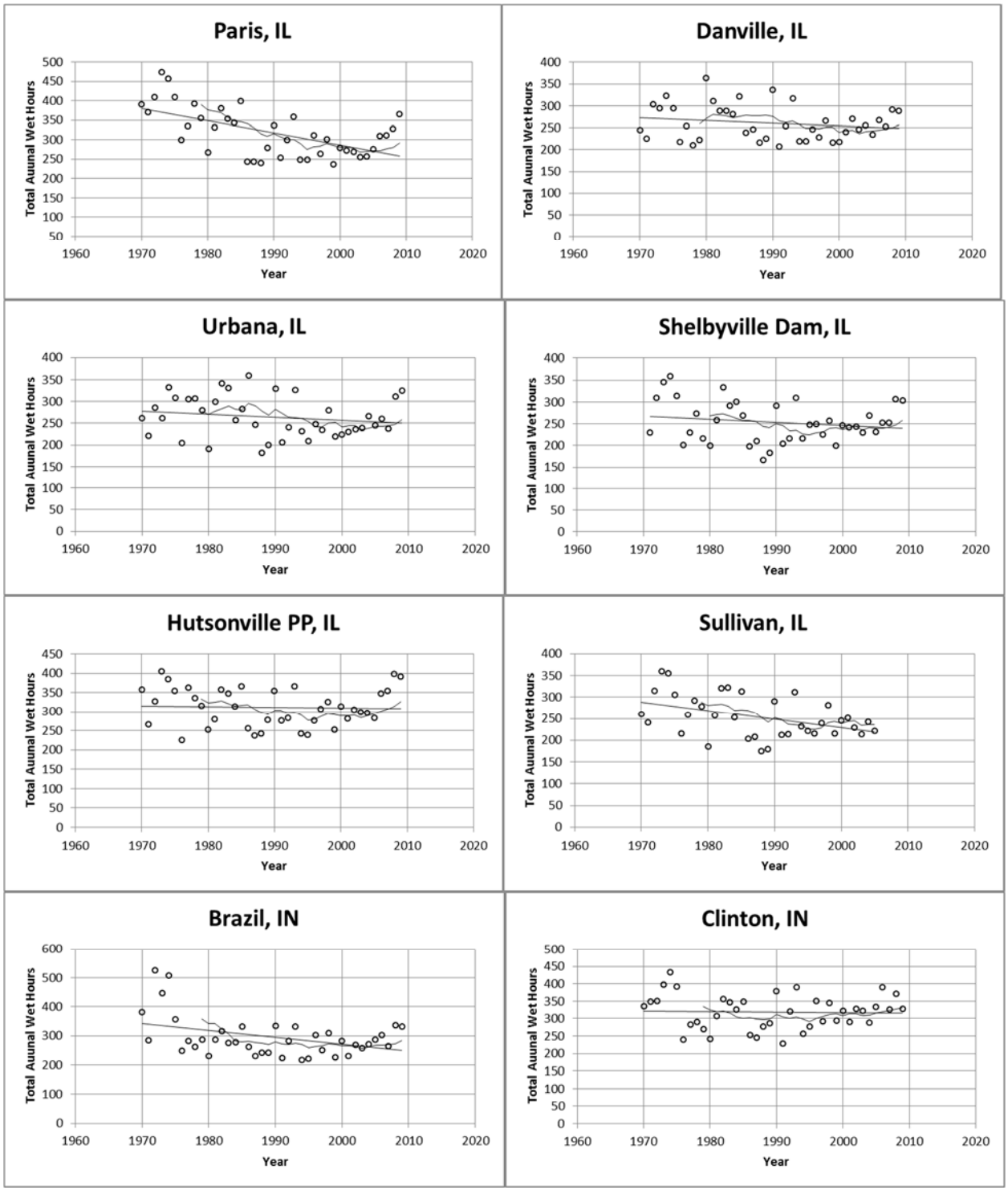

Figure 4.51. Total annual wet hours for several stations in Illinois and Indiana with linear and 10 year moving average fits

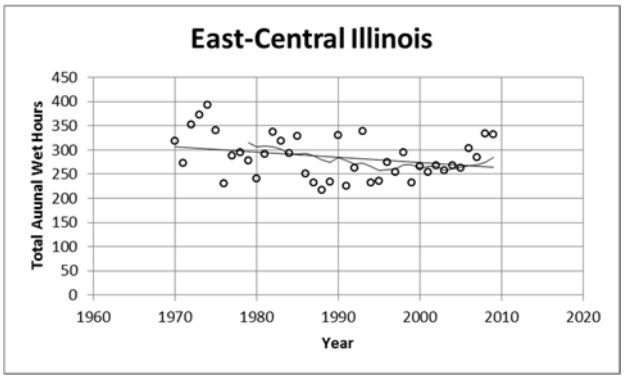

Figure 4.52. Total average annual wet hours for east central Illinois region with linear and 10 year moving average fits

Table 4.10. Trend analysis results for total annual wet hours at individual Illinois stations and of average Illinois region

	Signif Level	Total Annual Wet Hours		
		t-test	MK	Levene
DANVILLE	95%-5%	NULL	NULL	NULL
	90%-10%			**HETERO**
HUTSONVILLE PP	95%-5%	NULL	NULL	NULL
	90%-10%			
PARIS	95%-5%	**NEG**	**NEG**	**HETERO**
	90%-10%			
URBANA	95%-5%	NULL	NULL	NULL
	90%-10%			**HETERO**
BRAZIL, IN	95%-5%	**NEG**	NULL	**HETERO**
	90%-10%			
CLINTON, IN	95%-5%	NULL	NULL	NULL
	90%-10%			
ILLINOIS AVERAGE	95%-5%	NULL	NULL	NULL
	90%-10%	**NEG**		

4.3.5 1-Hour Maximum Precipitation

Maximum precipitation for 1-hr and 24-hr durations were analyzed in the same ways. An analysis of historic trends in AMS directly relates to trends in the estimated PDS, but in order to analyze the trends in PDS more directly, precipitation event occurrences (number of events greater than or equal to the

smallest AMS and the Atlas 14 1-yr event) were also graphed in time series. All units given in millimeters.

AMS

Figure 4.53 and Figure 4.54 show the 1-hr AMS for each rain gauge station near Camp Atterbury (see Section 3.1.6). Gauge groupings for each figure are consistent with previous sections. Figure 4.55 shows the average 1-hr AMS for all 9 gauges. Columbus and Indianapolis Airport show slight downward trends in 1-hr AMS while Shelbyville and Versallies show slight upward trends. However, most of the gauges show no trends. The 10 year moving averages show little movement from the linear trend line.

Statistical tests and findings for trends in 1-hr AMS are presented in Table 4.11. Of the seven gauges tested (Versailles and Shelbyville were excluded due 1-hr record lengths of less than 40 years and Seymour was due to the lack of 1-hr data), none showed statistically significant trends for either the t-test and MK test. Based on Levene's test, the hypothesis that variance did not change could not be rejected for any of the stations.

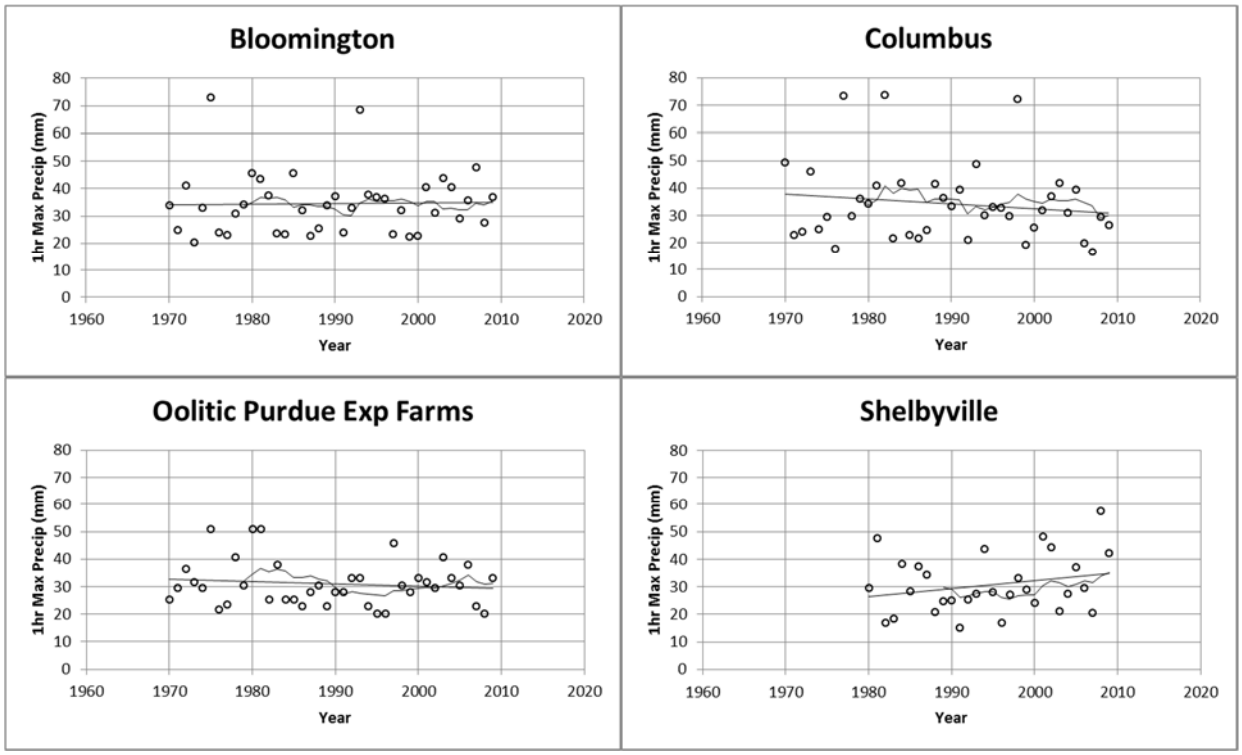

Figure 4.53. 1-hr AMS for several stations in Indiana with linear and 10 year moving average fits

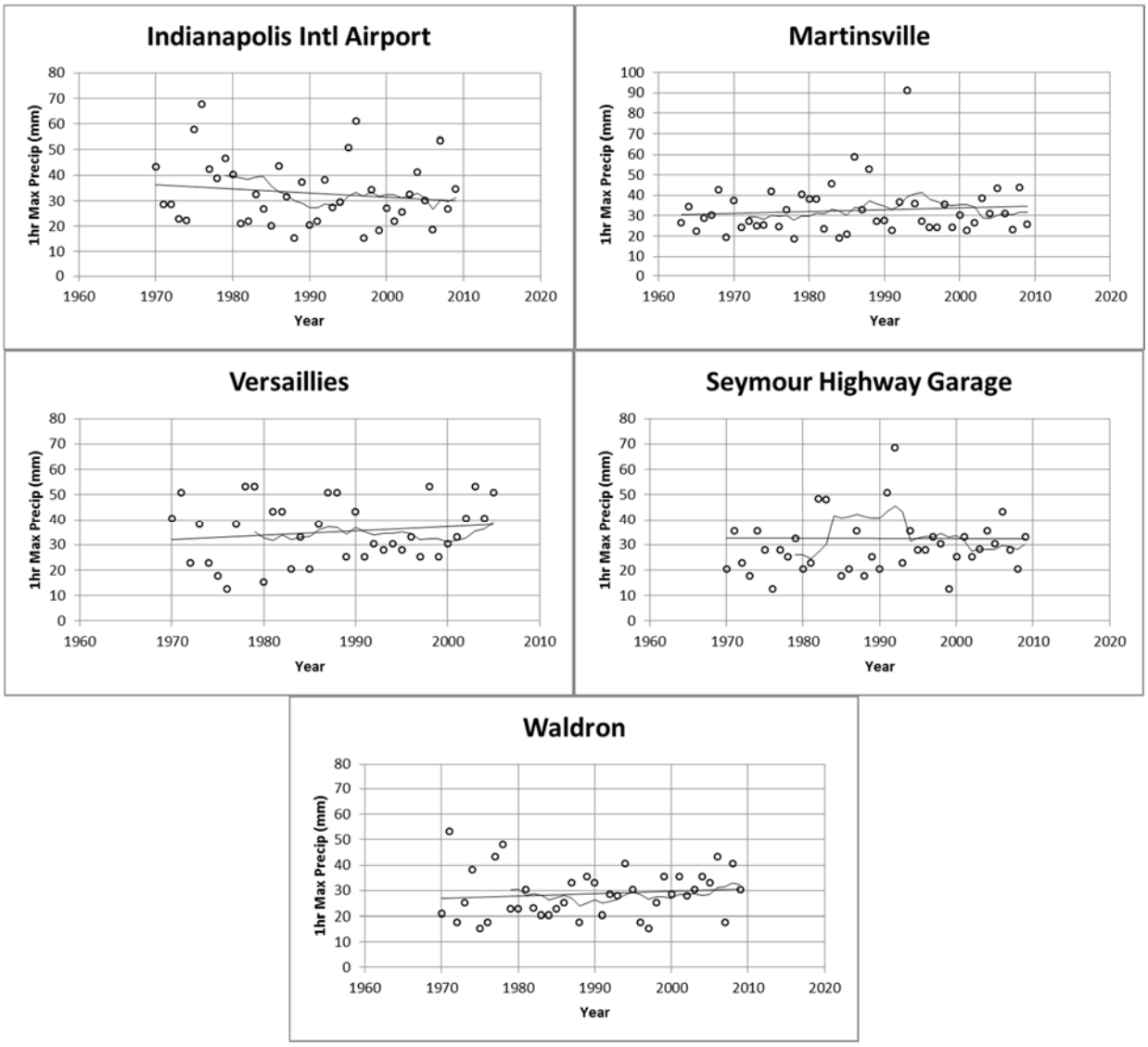

Figure 4.54. 1-hr AMS for several stations in Indiana with linear and 10 year moving average fits

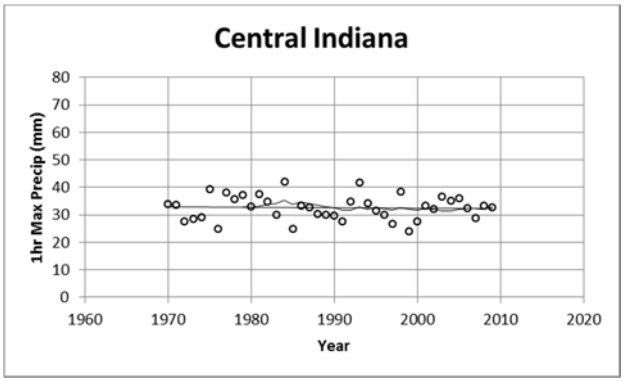

Figure 4.55. 1-hr average AMS for central Indiana region with linear and 10 year moving average fits

Table 4.11. Trend analysis results for 1-hr AMS at individual Indiana stations and of average Indiana region

	Signif Level	AMS 1-hr		
		t-test	MK	Levene
BLOOMINGTON	95%-5%	NULL	NULL	NULL
	90%-10%			
COLUMBUS	95%-5%	NULL	NULL	NULL
	90%-10%			
INDIANAPOLIS IA	95%-5%	NULL	NULL	NULL
	90%-10%			
MARTINSVILLE	95%-5%	NULL	NULL	NULL
	90%-10%			
OOLITIC PURDUE EF	95%-5%	NULL	NULL	NULL
	90%-10%			
SEYMOUR HG	95%-5%	NULL	NULL	NULL
	90%-10%			
WALDRON	95%-5%	NULL	NULL	NULL
	90%-10%			
INDIANA AVERAGE	95%-5%	NULL	NULL	NULL
	90%-10%			

Figure 4.56 shows total annual 1-hr AMS for each rain gauge station near Camp Grayling (see Section 3.2.6). Figure 4.57 shows total average annual 1hr-AMS for all 7 gauges. Gaylord and Houghton Lake gauges don't have hourly precipitation data. Lake City Experimental Farm shows a positive linear trend in 1-hr AMS while Grayling and Vanderbilt stations show decreasing trends. All others are constant. The 10 year moving averages show little movement from the linear trend line. Statistical tests and findings for trends in total annual wet hours are presented in Table 4.12. Of the five gauges tested (Gladwin and Glennie Alcona Dam were excluded due 1-hr record lengths of less than 40 years), Vanderbilt showed a significant negative trend for the t-test and MK, at confidence limits of 95% and 90%, respectively. Grayling showed at negative trend for the t-test at a 90% confidence limit. Based on Levene's test, the

hypothesis that variance did not change could be rejected for the Vanderbilt, Bellaire, and Lake City stations, which are geographically dispersed, suggesting a large range of possible 1-hr AMS.

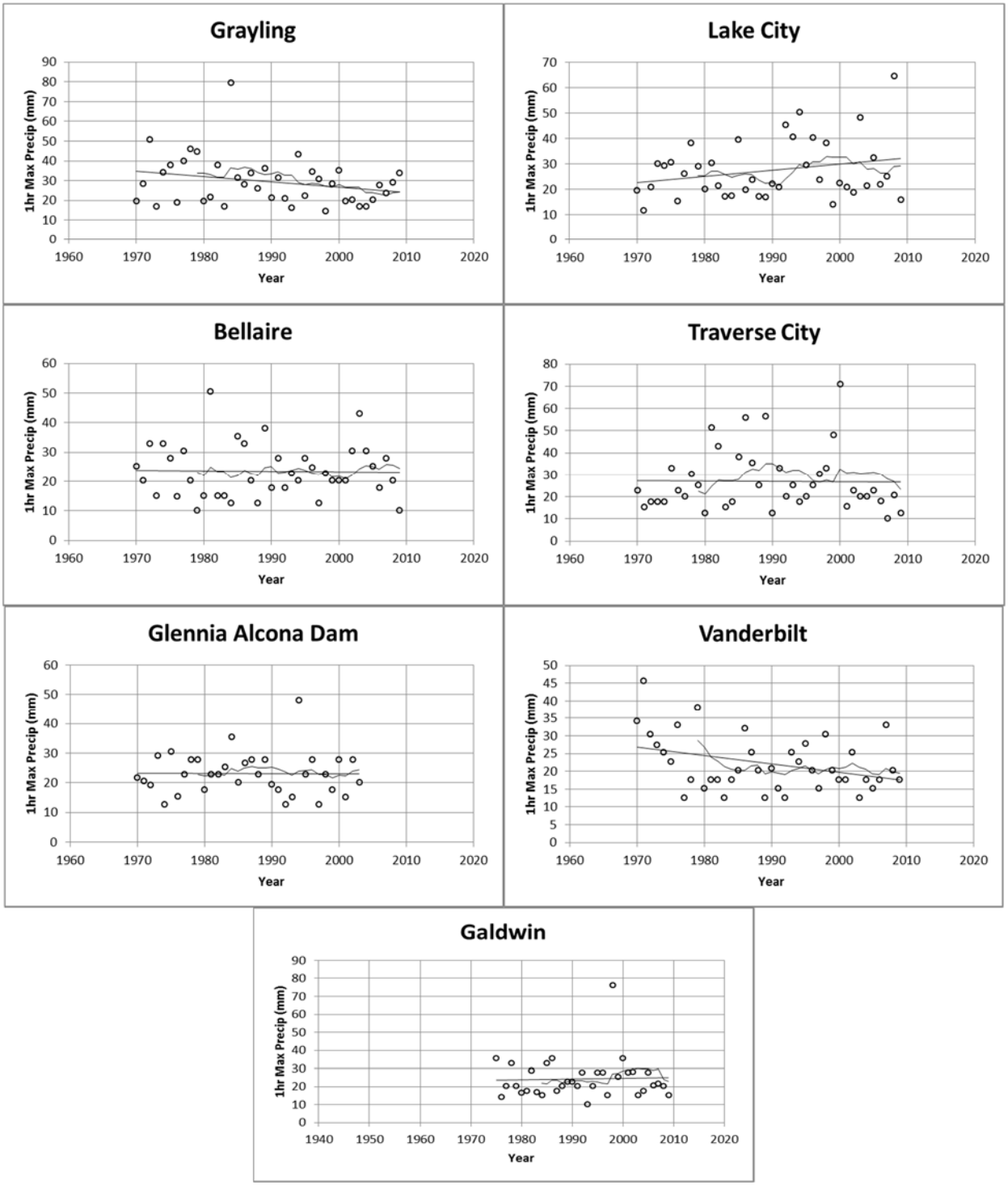

Figure 4.56. 1-hr AMS for several stations in Michigan with linear and 10 year moving average fits

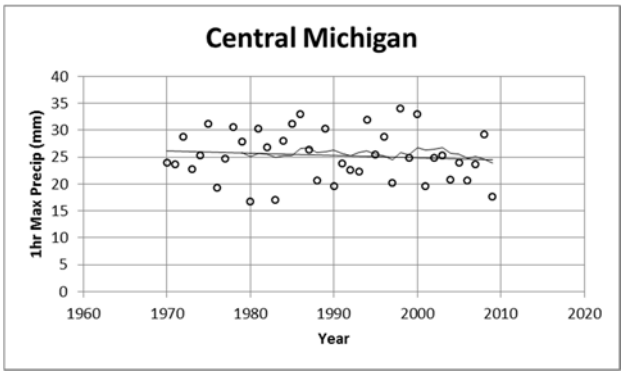

Figure 4.57. 1-hr average AMS for central Michigan region with linear and 10 year moving average fits

Table 4.12. Trend analysis results for 1-hr AMS at individual Michigan stations and of average Michigan region

	Signif Level	AMS 1-hr		
		t-test	MK	Levene
BELLAIRE	95%-5%	NULL	NULL	**HETERO**
	90%-10%			
GAYLORD	95%-5%	-	-	-
	90%-10%			
GLADWIN	95%-5%	-	-	-
	90%-10%			
GRAYLING	95%-5%	NULL	NULL	NULL
	90%-10%	**NEG**		
LAKE CITY EF	95%-5%	NULL	NULL	**HETERO**
	90%-10%			
TRAVERSE CITY	95%-5%	NULL	NULL	NULL
	90%-10%			
VANDERBILT	95%-5%	**NEG**	NULL	**HETERO**
	90%-10%		**NEG**	
HOUGHTON LAKE	95%-5%	-	-	-
	90%-10%			
MICHIGAN AVERAGE	95%-5%	NULL	NULL	NULL
	90%-10%			

Figure 4.58 show total 1-hr AMS for each rain gauge station near Edgar County Illinois (see Section 3.3.6). Figure 4.59 shows total average 1-hr AMS for all 8 gauges (the Charleston, IL gauge station only records daily precipitation data). Paris, IL and Brazil, IN stations show slightly increasing linear trends while Shelbyville Dam, IL and Hustonville Power Plant, IL stations show decreasing linear trends in 1-hr AMS. The other gauging stations show constant linear trends. The 10 year moving average shows nothing of note.

Statistical tests and findings for trends in 1-hr AMS are presented in Table 4.13. Of the five gauges tested (Sullivan, IL and Shelbyville Dam, IL were excluded due 1-hr record lengths of less than 40 years), only Brazil, IN showed a trend for either the t-test and/or MK, but only at a 90% confidence limit. Based on Levene's test, the hypothesis that variance did not change could not be rejected for any stations.

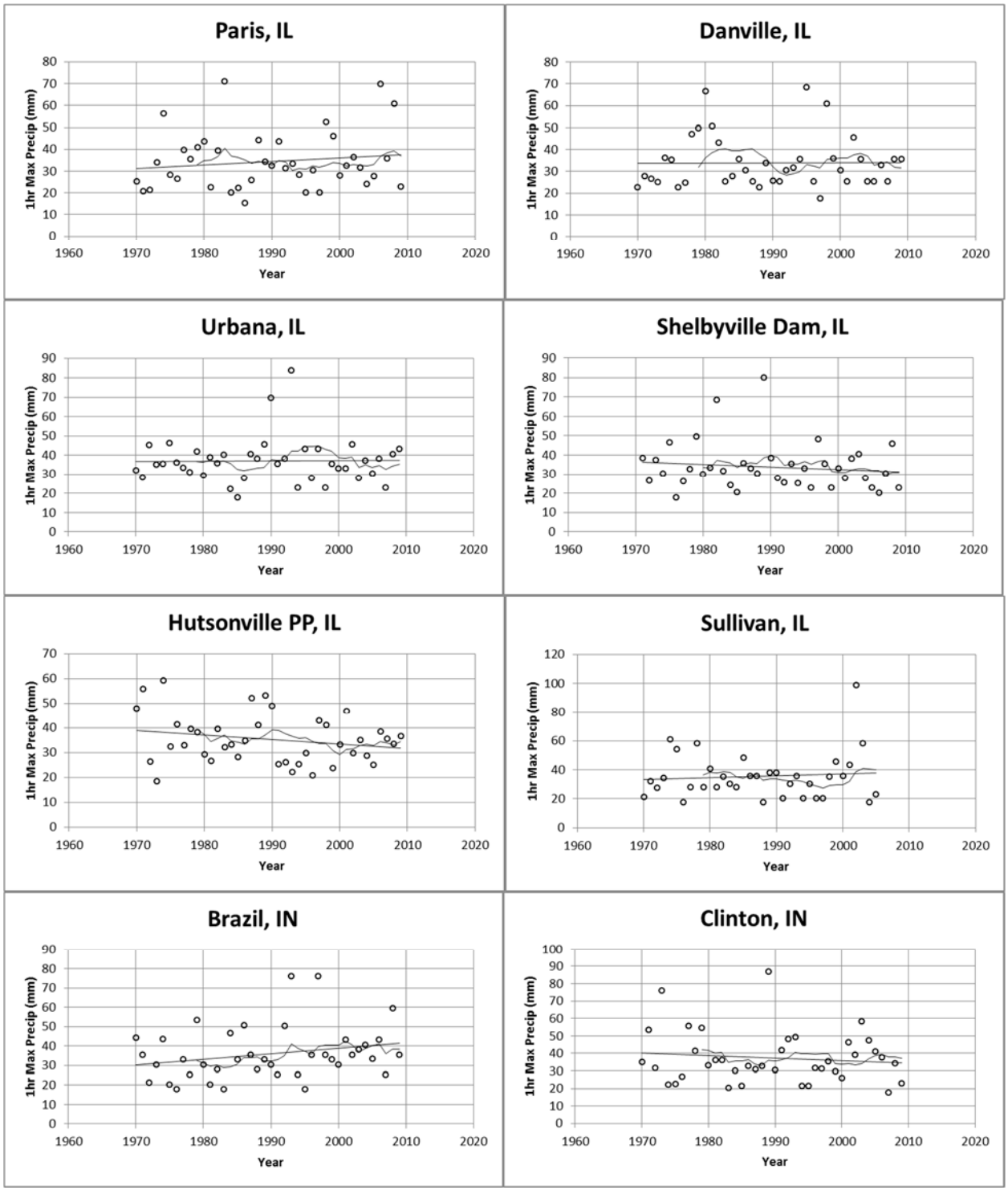

Figure 4.58. 1-hr AMS for several stations in Illinois and Indiana with linear and 10 year moving average fits

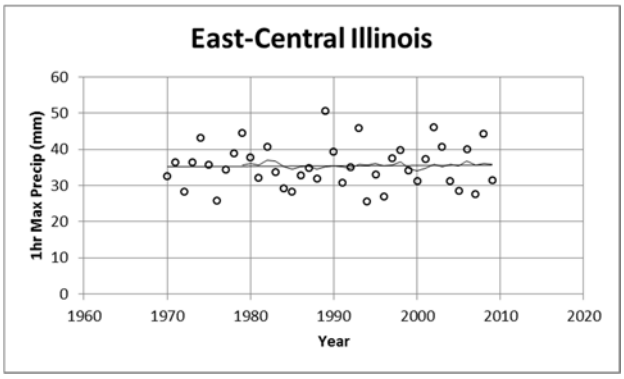

Figure 4.59. 1-hr average AMS for east central Illinois region with linear and 10 year moving average fits

Table 4.13. Trend analysis results for 1-hr AMS at individual Illinois stations and of average Illinois region

	Signif Level	AMS 1-hr		
		t-test	MK	Levene
DANVILLE	95%-5%	NULL	NULL	NULL
	90%-10%			
HUTSONVILLE PP	95%-5%	NULL	NULL	NULL
	90%-10%			
PARIS	95%-5%	NULL	NULL	NULL
	90%-10%			
URBANA	95%-5%	NULL	NULL	NULL
	90%-10%			
BRAZIL, IN	95%-5%	NULL	NULL	NULL
	90%-10%		**POS**	
CLINTON, IN	95%-5%	NULL	NULL	NULL
	90%-10%			
ILLINOIS AVERAGE	95%-5%	NULL	NULL	NULL
	90%-10%			
ILLINOIS AVERAGE	95%-5%	NULL	NULL	NULL
	90%-10%			

Annual Occurrences Greater Than A Given 1-hr Event

In addition to an analysis the 1-hr AMS (the largest event per year), the trend of other large 1-hr events were considered. The annual number of occurrences of 1-hr rain events larger than the gauge recorder's smallest 1-hr AMS were calculated and graphed in a time series. The Indiana, Michigan, and Illinois minimum 1-hr AMS for the gauges were 12.7 mm – 20.3 mm (0.5 in -0.8 in), 10.2 mm -12.7 mm (0.4 in – 0.5 in), and 15.2 mm – 17.8 mm (0.6in - 0.7 in), respectively. The minimum 1-hr AMS for each region corresponds to about half the value of the 1-yr, 24-hr Atlas 14 design storm for each region. In addition to the minimum AMS value for each gauge, the annual number of occurrences great than the 1-yr, 24-hr Atlas 14 design storm for each region was also calculated and graphed in a time series for each gauge. The 1-yr, 24-hr Atlas 14 design storm for the Indiana, Michigan, and Illinois regions are 29 mm (1.14 in), 23.4 mm (0.92 in), and 31 mm (1.22 in), respectively. The number of rainfall occurrences greater than a given amount, can provide insight into the frequency of larger rainstorm events, which analysis of AMS can't provide.

Figure 4.60 and Figure 4.61 show the annual occurrences greater than the smallest 1-hr AMS for each rain gauge station near Camp Atterbury (see Section 3.1.6). Gauge groupings for each figure are consistent with previous sections. Figure 4.62 shows the average number of annual occurrences greater than the smallest 1-hr AMS for all 9 gauges. All the gauge stations except Oolitic Purdue Experimental Farms show a positive linear trend in the number of occurrences greater than the smallest 1-hr AMS. The average number of occurrences is between 5-7, but several stations east and south of Camp Atterbury see up to 10 or more occurrences a year. The region average shows a significant increase at the 90% confidence limit.

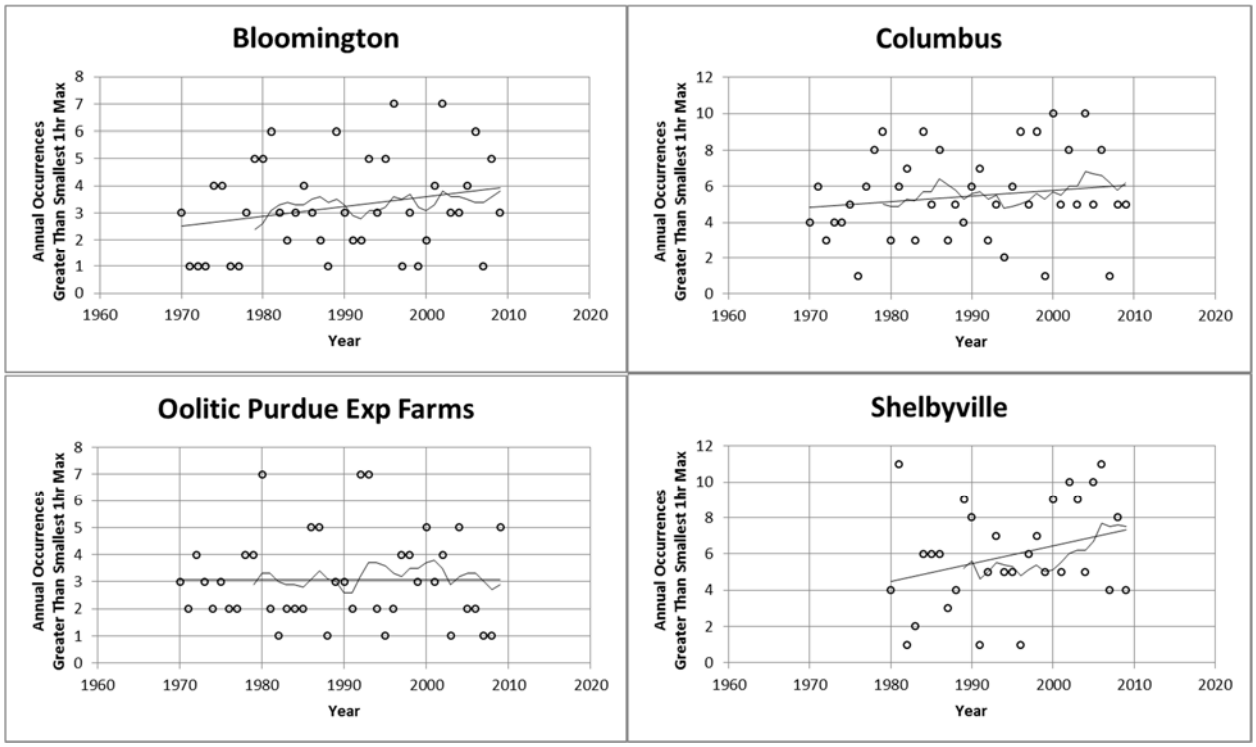

Figure 4.60. Annual occurrences greater than smallest 1-hr AMS for several stations in Indiana with linear and 10 year moving average fits

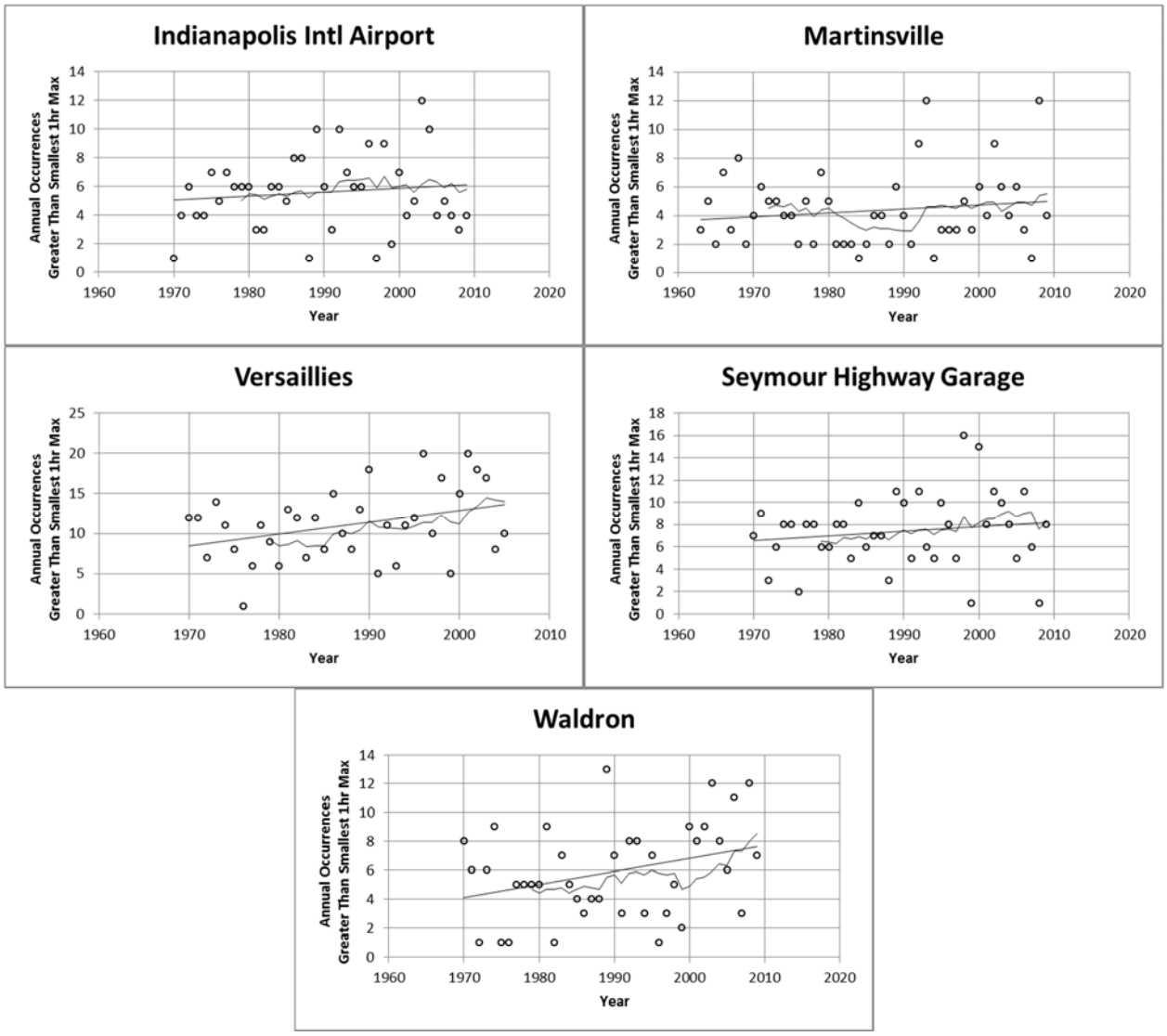

Figure 4.61. Annual occurrences greater than smallest 1-hr AMS for several stations in Indiana with linear and 10 year moving average fits

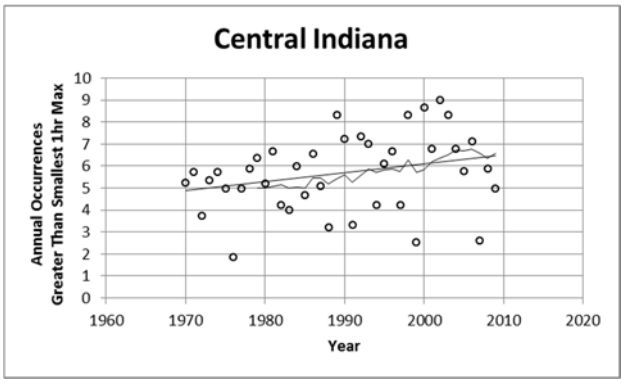

Figure 4.62. Annual average occurrences greater than smallest 1-hr AMS for central Indiana region with linear and 10 year moving average fits

Figure 4.63 and Figure 4.64 show the annual occurrences greater than the applicable 1-yr, 1-hr Atlas 14 design storm for each rain gauge station near Camp Atterbury (see Section 3.1.6). Gauge groupings for each figure are consistent with previous sections. Figure 4.65 shows the average number of annual occurrences greater than the applicable 1-yr, 1-hr Atlas 14 design storm for all 9 gauges. Most of the gauge stations show no change over time in the number of occurrences greater than the 1yr-1hr Atlas 14 design storm. The average number of occurrences per year is expected to be 1 given that reference storm is the 1-year event, which is exactly the number of occurrences seen at most of the gauge stations. Several stations (Shelbyville and Waldron, both in Shelby County) show increasing linear trends due to a higher number of occurrences after 2005, but this seems to be a localized manifestation. The Indiana regional average shows an increasing trend, though not significant.

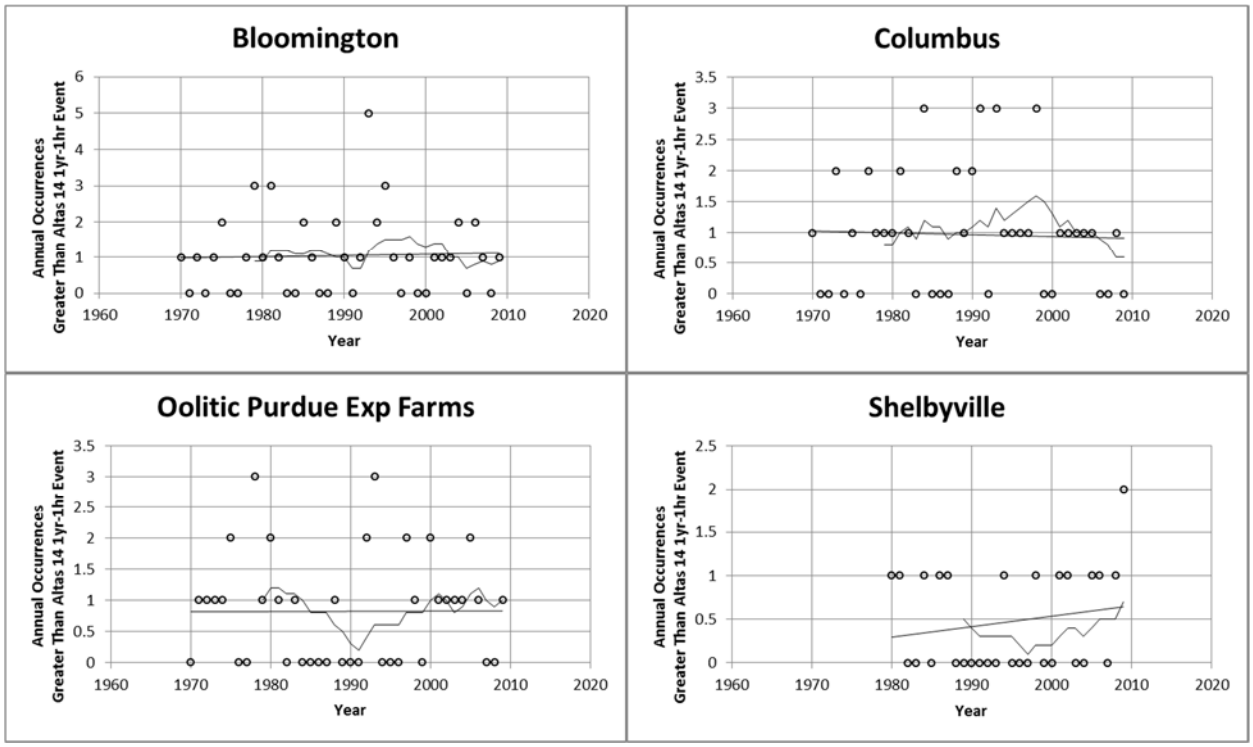

Figure 4.63. Annual occurrences greater than Atlas 14 1yr-1hr event for several stations in Indiana with linear and 10 year moving average fits

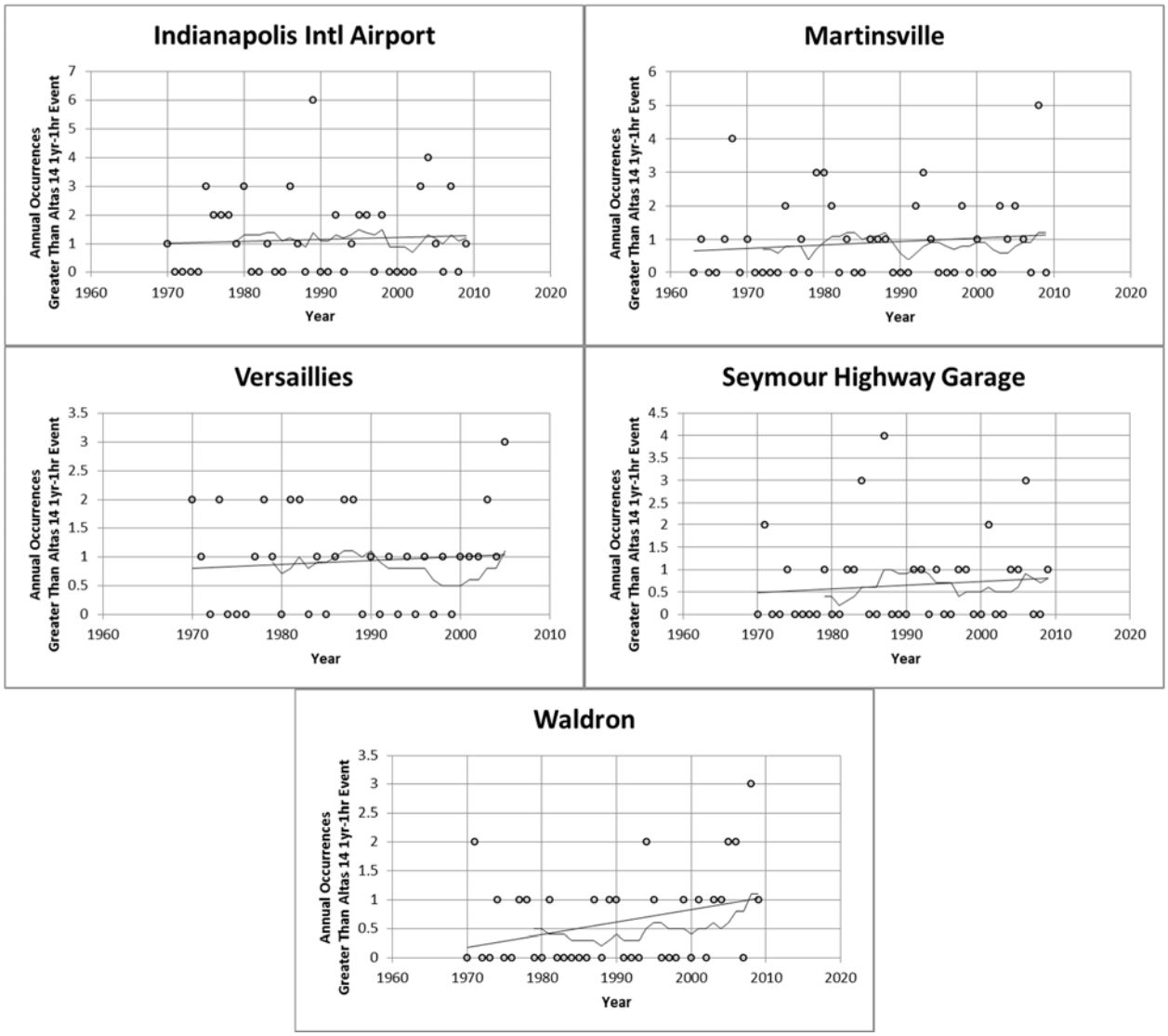

Figure 4.64. Annual occurrences greater than Atlas 14 1yr-1hr event for several stations in Indiana with linear and 10 year moving average fits

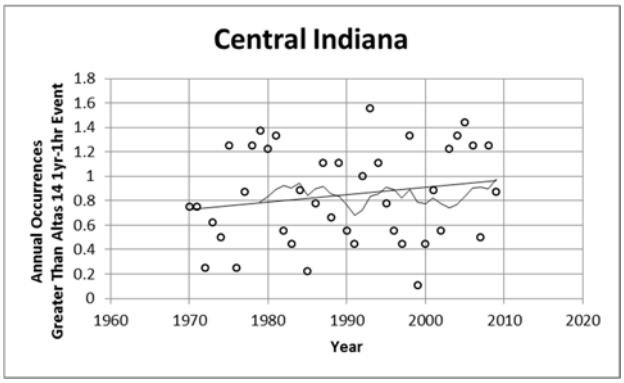

Figure 4.65. Annual average occurrences greater than Atlas 14 1yr-1hr event for central Indiana region with linear and 10 year moving average fits

Figure 4.66 shows the annual occurrences greater than the smallest 1-hr AMS for each rain gauge station near Camp Grayling (see Section 3.2.6). Figure 4.67 shows the average number of annual occurrences greater than the smallest 1-hr AMS for all 9 gauges. Most of the gauge station show a constant or slightly decreasing trend in the number of occurrences greater than the smallest 1-hr AMS. Galdwin station, located the furthest south, is the only station with an increasing trend. The average annual number of occurrences is nearly constant at 6, with a range of 1-20 occurrences. The highest number of occurrences seem to occur at the stations closest to Lake Michigan and at Gladwin (south).

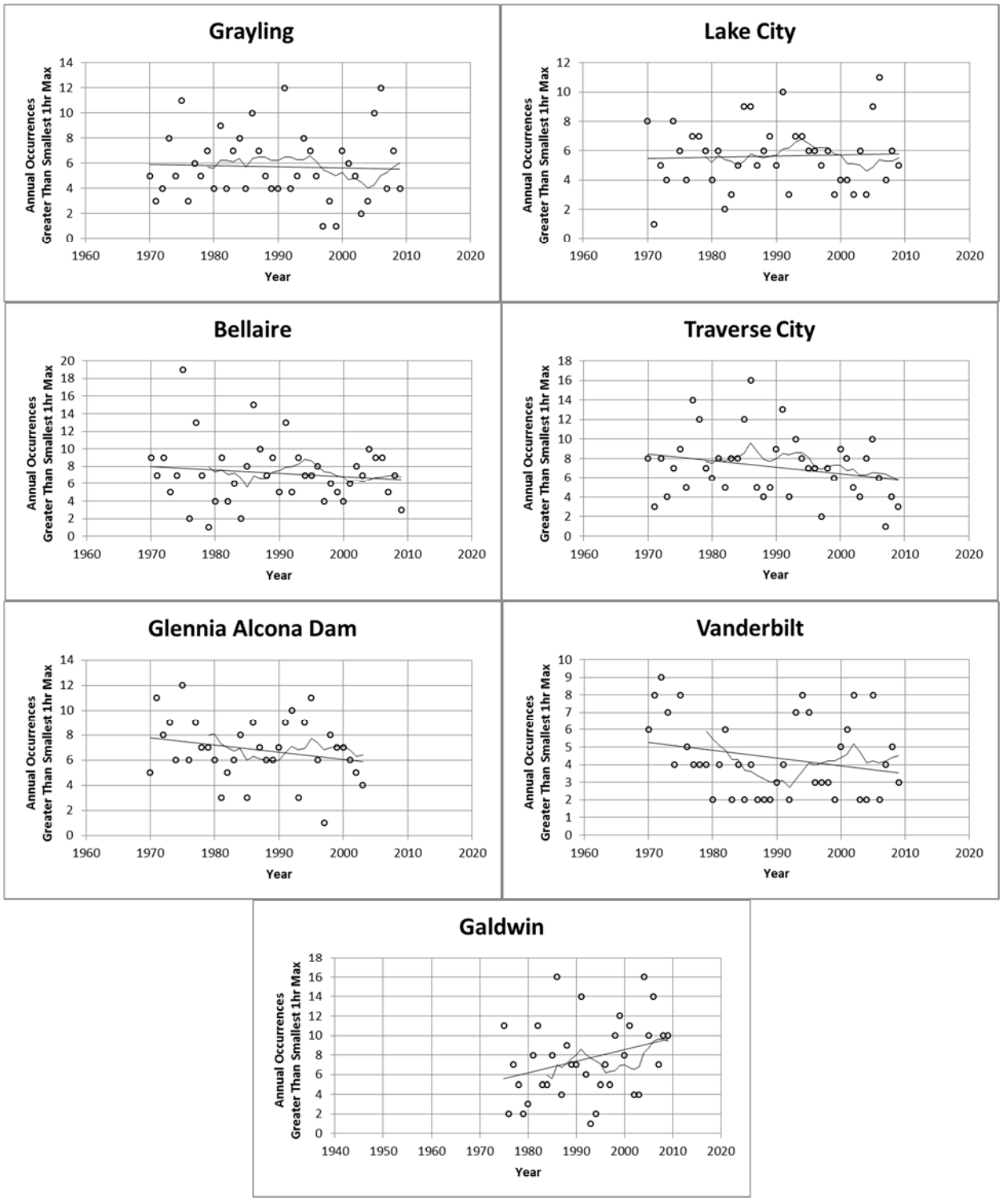

Figure 4.66. Annual occurrences greater than smallest 1-hr AMS for several stations in Michigan with linear and 10 year moving average fits

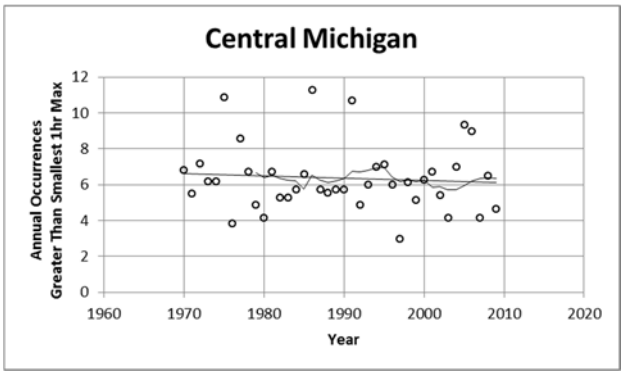

Figure 4.67. Annual average occurrences greater than smallest 1-hr average AMS for central Michigan region with linear and 10 year moving average fits

Figure 4.68 shows the annual occurrences greater than the applicable 1-yr, 1-hr Atlas 14 design storm for each rain gauge station near Camp Grayling (see Section 3.2.6). Figure 4.69 shows the average number of annual occurrences greater than the applicable 1-yr, 1-hr Atlas 14 design storm for all 9 gauges. The region's stations show mostly constant trends in the number of annual occurrences greater than the applicable 1-yr, 1-hr Atlas 14 design storm, with almost all increases or decreases minor. Vanderbilt, the most northern station, shows a more significant decreasing trend. The average number of occurrences per year is expected to be 1 given that reference storm is the 1-year event. However, unlike the Indiana stations, the average number of occurrences a year is closer to 0.6, which holds constant throughout the time series. Grayling station is the only gauge to record an average of 1 occurrence per year, with a range of 0-5 occurrences.

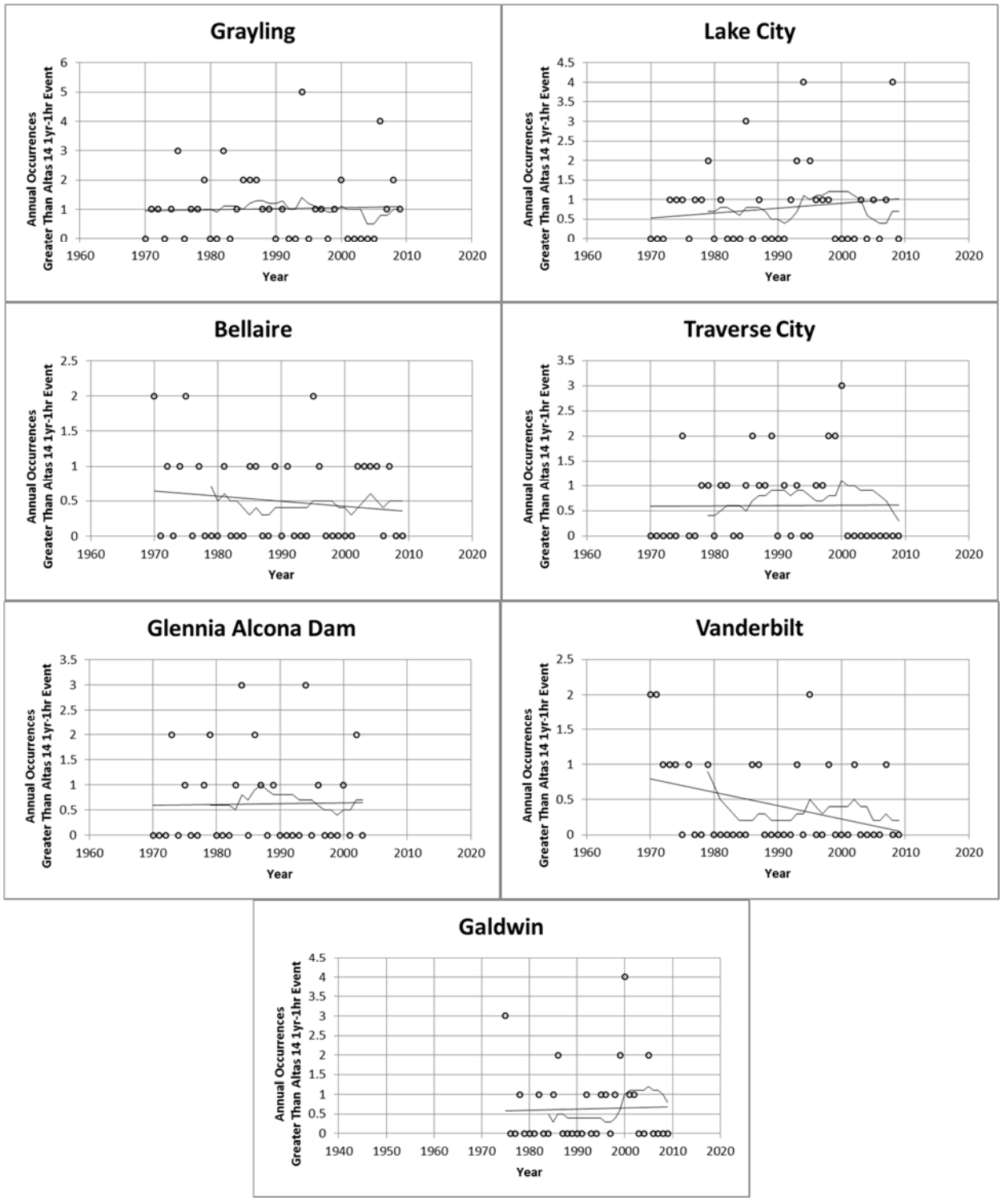

Figure 4.68. Annual occurrences greater than Atlas 14 1yr-1hr event for several stations in Michigan with linear and 10 year moving average fits

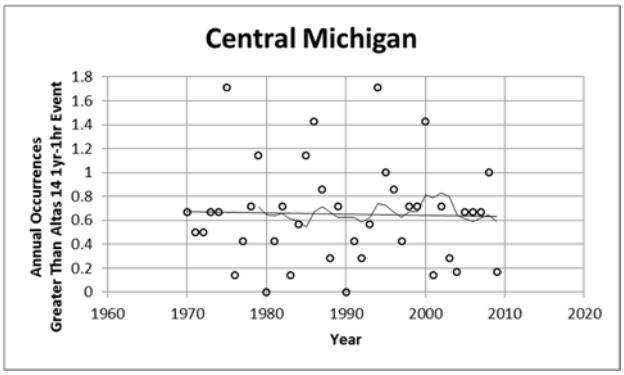

Figure 4.69. Annual average occurrences greater than Atlas 14 1yr-1hr event for central Michigan region with linear and 10 year moving average fits

Figure 4.70 shows the annual occurrences greater than the smallest 1-hr AMS for each rain gauge station near Edgar County Illinois (see Section 3.3.6). Figure 4.71 shows the average annual occurrences greater than the smallest 1-hr AMS for all 8 gauges. Paris, IL, Hutsonville Power Plant, IL, and Brazil, IN show increasing linear trends and are located south and east of Edgar County. The records from Sullivan, IL (to the northwest) shows a decrease in the linear trend, while the remaining gauge records show no trends. In general, the East Central Illinois region shows an increase in the number of annual occurrences greater than the smallest 1-hr AMS, but less significantly than the Indiana region.

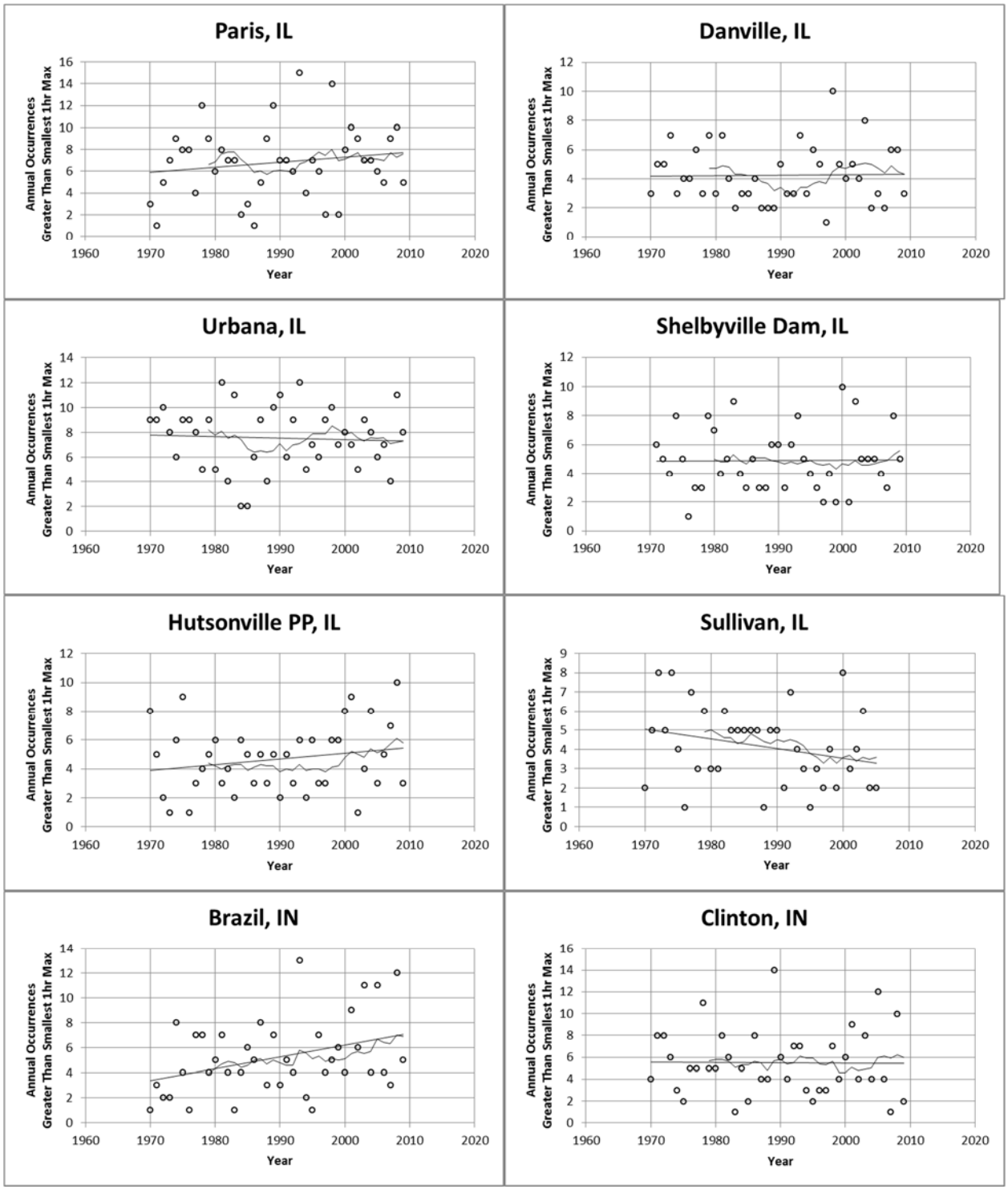

Figure 4.70. Annual occurrences greater than smallest 1-hr AMS for several stations in Illinois with linear and 10 year moving average fits

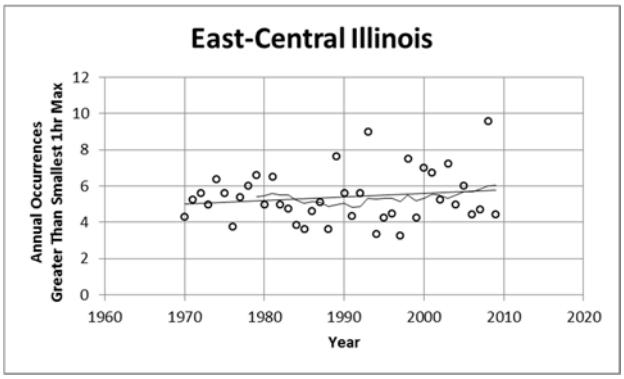

Figure 4.71. Annual average occurrences greater than smallest 1-hr average AMS for east central Illinois region with linear and 10 year moving average fits

Figure 4.72 show the annual occurrences greater than the applicable 1-yr, 1-hr Atlas 14 design storm for each rain gauge station near Edgar County Illinois (see Section 3.3.6). Figure 4.73 shows the average annual occurrences greater than the applicable 1-yr, 1-hr Atlas 14 design storm for all 8 gauges. The linear trends at each station are mixed, with Brazil, IN and Sullivan, IL slightly increasing, Shelbyville Dam, IL slightly decreasing, and the remaining stations hold nearly constant. The average number of occurrences per year is expected to be 1 given that reference storm is the 1-year event, which is seen on average at Paris, IL, Urbana, IL, Hustonville Power Plant, IL, and Clinton, IN. The average number of annual occurrences is constant for the region at 0.9.

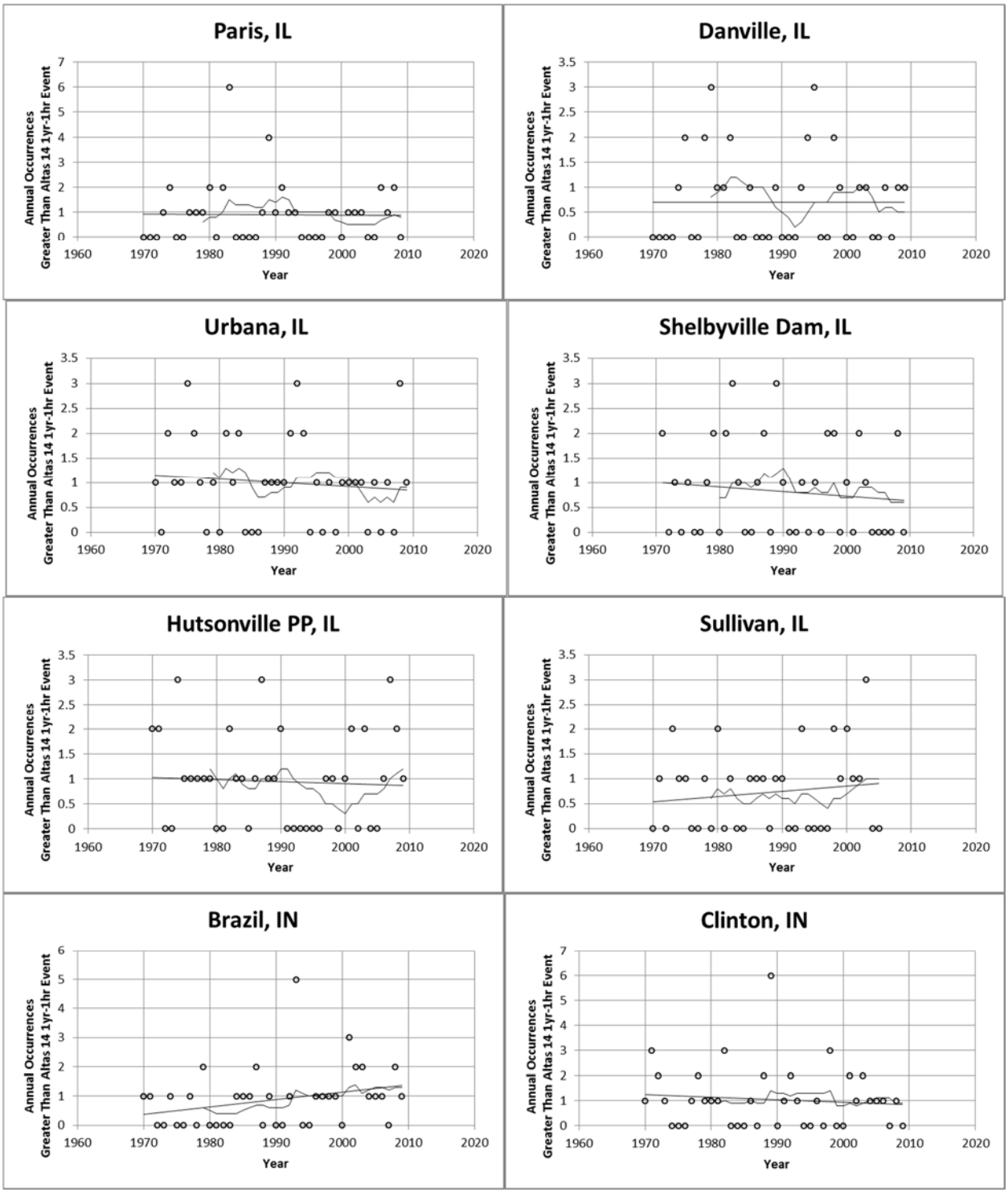

Figure 4.72. Annual occurrences greater than Atlas 14 1yr-1hr event for several stations in Illinois and Indiana with linear and 10 year moving average fits

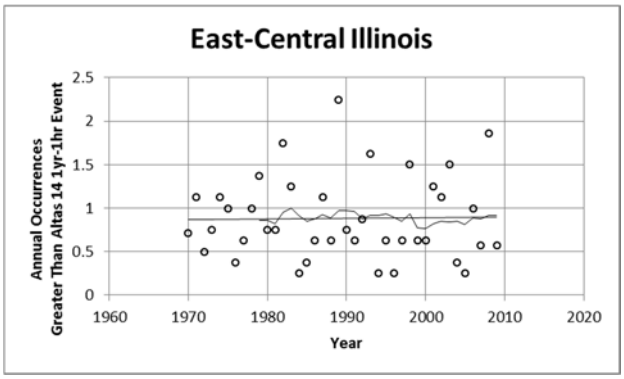

Figure 4.73. Annual average occurrences greater than Atlas 14 1yr-1hr event for east central Illinois region with linear and 10 year moving average fits

4.3.6 Trend Slope Correlation

The statistical trend results for total annual precipitation, total annual wet days, and AMS (1-hr and 24-hr) were compiles into single tables for each region to determine if any correlation between trend slopes is evident. If a trend was detected only by one test (MK or t-test) and only for the 90%-10% confidence interval, the tables report a NULL result but with the trend shown in parentheses. Table 4.14, Table 4.15, and Table 4.16 show that on average total annual precipitation is increasing annually at half or more of the stations in each region. AMS shows no trends or only a slightly positive trend at some locations in Indiana and Illinois while AMS in Michigan is flat or only slightly negative at some locations. Total annual wet hours are trending flat or negative at some locations in all three regions. Correlation between trends in total annual precipitation and trends in AMS and total annual wet hours are not evident. For example, increasing total annual precipitation does not correspond with certain trends in the derived statistics (AMS, total annual wet hours), some are positive, some are negative, but most are null.

Table 4.14. Trend analysis comparison for total annual precipitation, 1-hr AMS, 24-hr AMS, and total annual wet hours at individual Indiana stations and of average central Indiana region

	Total Annual Precip	AMS 1-hr	AMS 24-hr	Total Annual Wet Hours
BLOOMINGTON	**POS**	NULL	NULL	NULL
COLUMBUS	**POS**	NULL	NULL	NULL (neg)
INDIANAPOLIS IA	NULL	NULL	NULL	NULL
MARTINSVILLE	NULL	NULL	NULL	NULL
OOLITIC PURDUE EF	NULL	NULL	NULL	**NEG**
SEYMOUR HG	**POS**	NULL	NULL	NULL
SEYMOUR	**POS**	-	**POS**	-
SHELBYVILLE	NULL	-	NULL	-
WALDRON	**POS**	NULL	NULL	NULL
INDIANA AVERAGE	**POS**	NULL	**POS**	NULL

Table 4.15. Trend analysis comparison for total annual precipitation, 1-hr AMS, 24-hr AMS, and total annual wet hours at individual Michigan stations and of average central Michigan region

	Total Annual Precip	AMS 1-hr	AMS 24-hr	Total Annual Wet Hours
BELLAIRE	NULL	NULL	NULL	NULL (pos)
GAYLORD	**POS**	-	NULL	-
GLADWIN	NULL	-	NULL	-
GRAYLING	NULL	NULL (neg)	NULL	**NEG**
LAKE CITY EF	**POS**	NULL	NULL	-
TRAVERSE CITY	-	NULL	-	NULL
VANDERBILT	NULL	**NEG**	NULL	**NEG**
HOUGHTON LAKE	**POS**	-	NULL	-
MICHIGAN AVERAGE	NULL (pos)	NULL	NULL	**NEG**

Table 4.16. Trend analysis comparison for total annual precipitation, 1-hr AMS, 24-hr AMS, and total annual wet hours at individual Illinois stations and of average east central Illinois region

	Total Annual Precip	AMS 1-hr	AMS 24-hr	Total Annual Wet Hours
CHARLESTON	**POS**	-	NULL	-
DANVILLE	NULL	NULL	NULL	NULL
HUTSONVILLE PP	**POS**	NULL	NULL (pos)	NULL
PARIS	NULL (pos)	NULL	NULL	**NEG**
URBANA	**POS**	NULL	NULL	NULL
BRAZIL, IN	**POS**	NULL (pos)	NULL	**NEG**
CLINTON, IN	-	NULL	-	NULL
ILLINOIS AVERAGE	**POS**	NULL	NULL	NULL (neg)

4.3.7 L-Moment Precipitation Frequency Analysis

Precipitation regional frequency analyses were completed for observed data for each region/site and three time frames using the regional L-Moments method. The three time frames were 1970-1989, 1980-1999, and 1990-2009, for which precipitation magnitudes were found for the following durations (1-, 2-, 3-, 6-, 12-, and 24-hr; and 2-, 5-, and 10-day) and ARIs (0.5-, 1-, 2-, 5-, 10-, 25-, 50-, 100-year). Based on the discordance and heterogeneity measures for the three time frames, it was determined that the regions are homogeneous. The precipitation magnitudes for each duration and ARI were validated with comparisons to published NOAA Atlas 14 values and are provided. All maximum precipitation is adjusted for PDS estimates.

Figure 4.74 and Figure 4.75 shows the maximum precipitation distributions at Columbus, IN for a range of return periods and durations of 1-, 2-, 3-, 6-, 12-, and 24-hr and 2-, 5-, and 10-day, respectively. Columbus, IN is the closest gauge site to Camp Atterbury. The results indicate that for short duration storms of 3 hours or less the most current time frame (1990-2009) experienced maximum storm events of less intensity than previous decades and also below Atlas 14 values. As storm durations increase, the maximum precipitation amounts increase from 1970-1989 to 1980-1999 to 1990-2009. The most recent time frame closely matches Atlas 14 values for all return periods and durations over 12 hours.

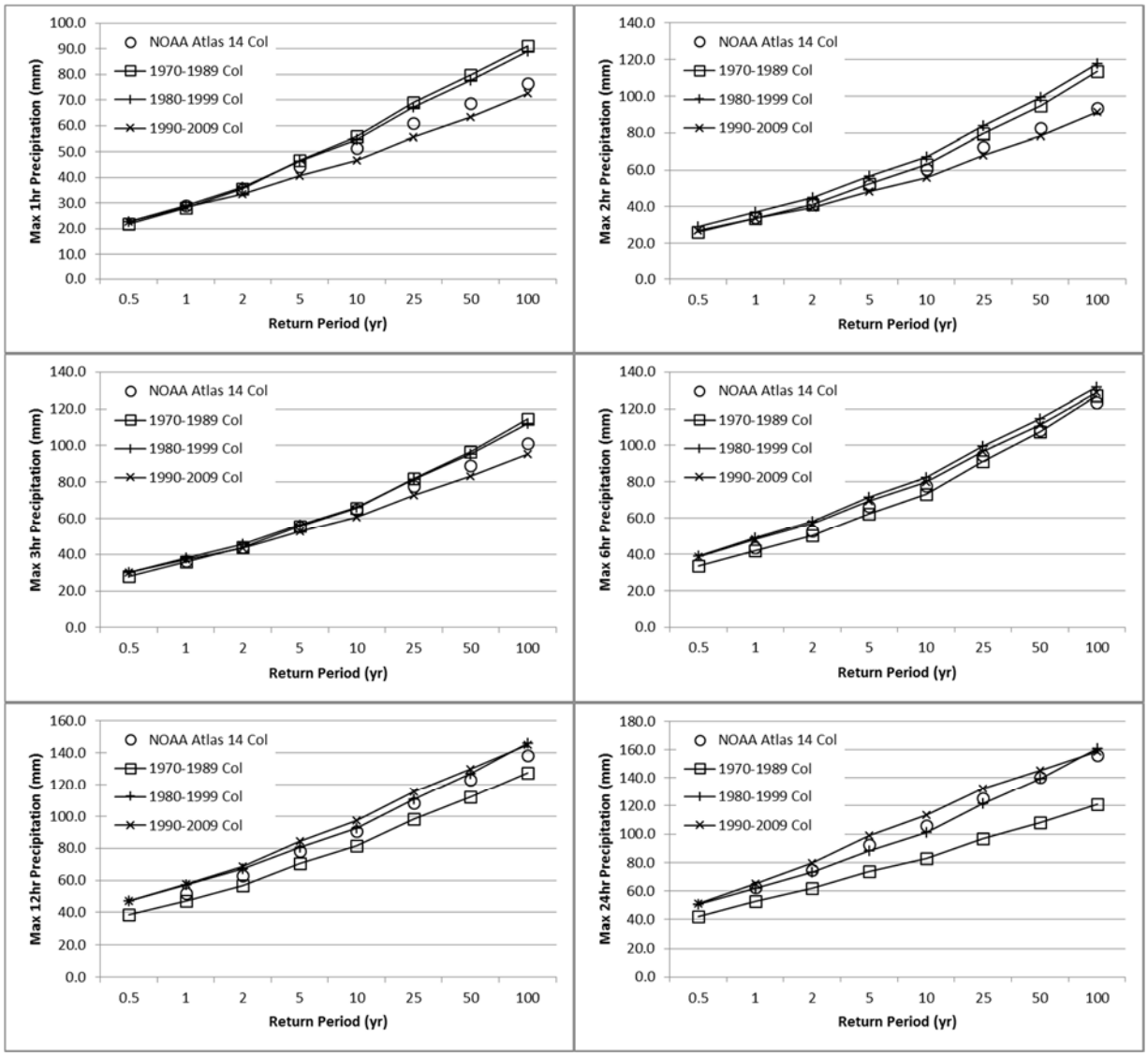

Figure 4.74. Comparison of estimated maximum precipitation for selected durations and return periods for 1970-1989, 1980-1999, and 1990-2009, as determined by L-moments regional frequency analysis at Columbus, Indiana. Atlas 14 values also included.

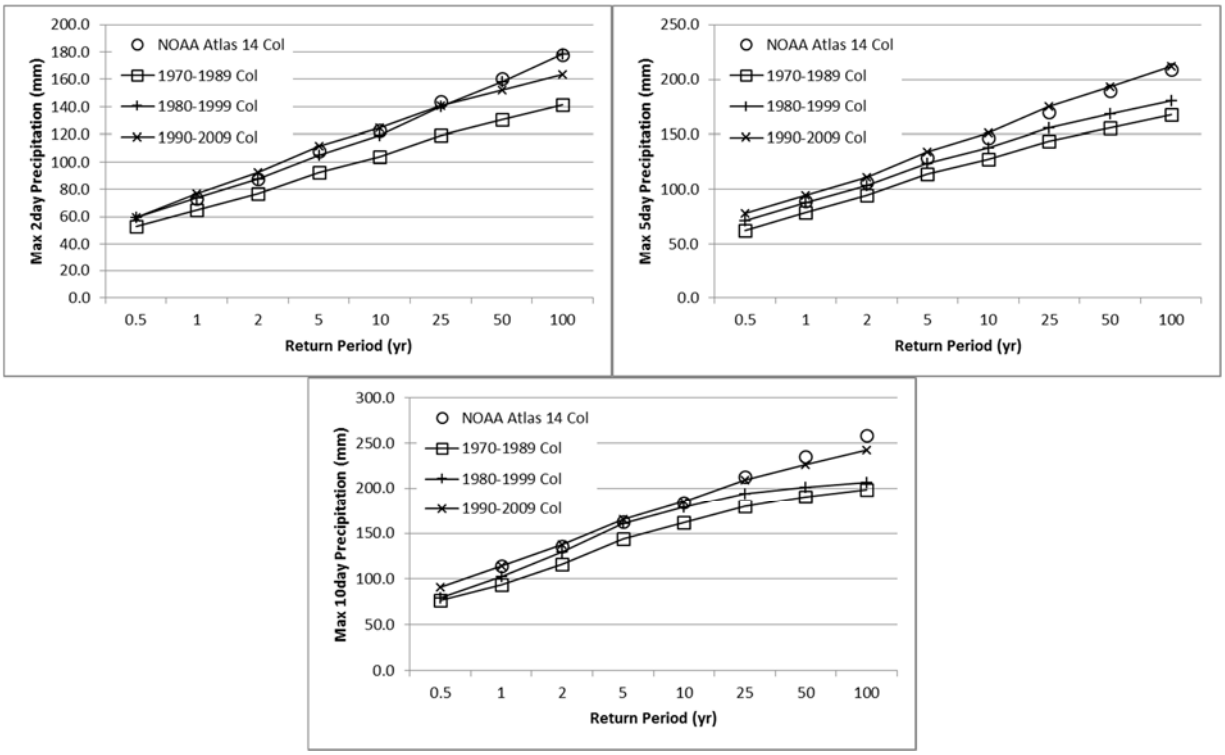

Figure 4.75. Comparison of estimated maximum precipitation for selected durations and return periods for 1970-1989, 1980-1999, and 1990-2009, as determined by L-moments regional frequency analysis at Columbus, Indiana. Atlas 14 values also included.

Table 4.17 shows the percent difference between the maximum 1970-1989 and 1990-2009 precipitations at Columbus, IN for all storm durations and return periods as determined by the L-moments regional frequency analysis. Table 4.18 shows the percent difference between the average maximum 1970-1989 and 1990-2009 precipitations for all gauges in the Indiana region. The highlighted values denote a significant difference as determined by Monte Carlo simulations used to construct confidence limits at a 95% confidence level. The negative values for durations of 1 to 3 hours denotes that the maximum precipitations for the latter time period (1990-2009) are smaller than the previous period. For shorter durations of 1-6 hours the latter time period has maximum precipitation events 23% less than to 14% more than the former period. For durations of 12 hours or more, the latter time period experienced maximum precipitation events 14% to 31% greater than the former time period, for which durations of 24-hrs and 5-days experienced significant differences. See Appendix A for tables showing

the percent difference between the maximum 1990-2009 and 1970-1989 precipitations at the other Indiana gauges.

Table 4.17. Changes in maximum precipitation between 1990-2009 and 1970-1989, as determined by L-moments regional frequency analysis at Columbus, Indiana, expressed as a percent difference.

Columbus, IN	0.5 yr	1 yr	2 yr	5 yr	10 yr	25 yr	50 yr	100 yr
1-hr	4.0%	0.4%	-6.0%	-13.8%	-18.1%	-21.6%	-22.7%	-22.7%
2-hr	4.1%	-0.4%	-4.1%	-8.4%	-11.6%	-15.7%	-18.8%	-21.8%
3-hr	6.3%	2.6%	-0.7%	-4.8%	-7.8%	-11.9%	-15.0%	-18.2%
6-hr	14.3%	13.7%	12.5%	10.5%	8.7%	6.0%	3.7%	1.3%
12-hr	20.1%	20.1%	19.6%	18.5%	17.4%	15.8%	14.4%	13.0%
24-hr	19.3%	21.1%	**25.4%**	**29.7%**	**31.1%**	**30.9%**	29.4%	27.0%
2-day	11.3%	16.6%	18.6%	18.9%	18.2%	16.7%	15.5%	14.3%
5-day	**22.0%**	18.1%	16.3%	16.3%	17.3%	19.4%	21.3%	**23.3%**
10-day	16.4%	20.1%	17.3%	14.0%	13.4%	14.9%	17.1%	19.9%

Table 4.18. Changes in precipitation frequency estimates between 1990-2009 and 1970-1989, as determined by L-moments regional frequency analysis as average of Indiana region stations, expressed as a percent difference.

Indiana Region	0.5 yr	1 yr	2 yr	5 yr	10 yr	25 yr	50 yr	100 yr
1-hr	9.4%	5.8%	-0.5%	-8.3%	-12.7%	-16.2%	-17.3%	-17.3%
2-hr	8.2%	3.8%	0.1%	-4.3%	-7.5%	-11.6%	-14.7%	-17.7%
3-hr	12.6%	8.9%	5.6%	1.5%	-1.5%	-5.6%	-8.7%	-11.9%
6-hr	12.6%	12.1%	10.9%	8.8%	7.0%	4.3%	2.1%	-0.3%
12-hr	14.9%	14.8%	14.3%	13.2%	12.2%	10.5%	9.2%	7.7%
24-hr	11.3%	13.1%	17.4%	**21.7%**	**23.2%**	23.0%	21.5%	19.0%
2-day	13.5%	18.8%	20.8%	21.0%	20.4%	18.9%	17.7%	16.5%
5-day	**21.0%**	17.1%	15.3%	15.2%	16.2%	18.3%	20.2%	**22.3%**
10-day	17.7%	21.4%	18.6%	15.3%	14.7%	16.2%	18.4%	21.2%

Figure 4.76 shows a graphical version of Table 4.17 and Table 4.18 to illustrate the percent difference between the maximum 1970-1989 and 1990-2009 precipitations and average maximum precipitations for different durations and return periods. For short storm durations, the difference in maximum precipitation between time periods is broad between different return periods. For longer durations, the difference in maximum precipitation between time periods is larger but narrower between different

return periods. Maximum precipitation estimates at Columbus, IN are very similar to the Indiana region as a whole with only slight variances in magnitude of the differences between time periods.

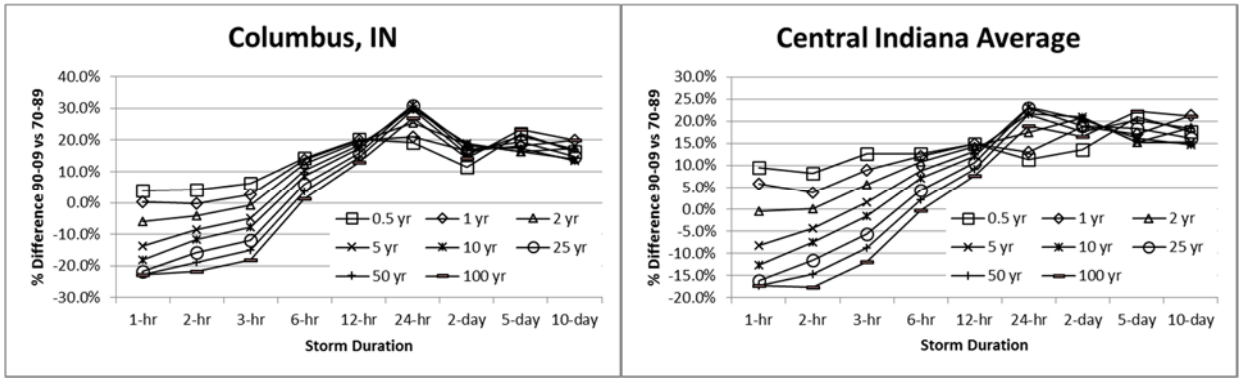

Figure 4.76. Comparison of estimated maximum precipitation for selected durations and return periods between 1990-2009 and 1970-1989, as determined by L-moments regional frequency analysis at Columbus, Indiana and an average of central Indiana region stations.

Figure 4.77 and Figure 4.78 shows the maximum precipitation distributions at Grayling, Mi for a range of return periods and durations of 1-, 2-, 3-, 6-, 12-, and 24-hr and 2-, 5-, and 10-day, respectively. Grayling, MI is the closest gauge site to Camp Grayling. The results indicate that for all storm durations and ARIs less than 25-yrs the most recent time frame (1990-2009) experienced maximum storm events of less intensity than previous decades but in line with Atlas 14 values. As storm durations increase, 1990-2009 maximum precipitation is greater than the 1970-1989 precipitation for ARIs greater than 25-yrs. Results indicate that between 1970-1989 and 1990-2009 the storm intensity of more frequent storms (ARIs less than 25-yrs) has decreased but the intensity of extreme events (ARIs greater than 25-yrs) have become more intense. Maximum precipitation values for the middle time period (1980-1999) are greater than those values from the most recent time period for all durations and return periods.

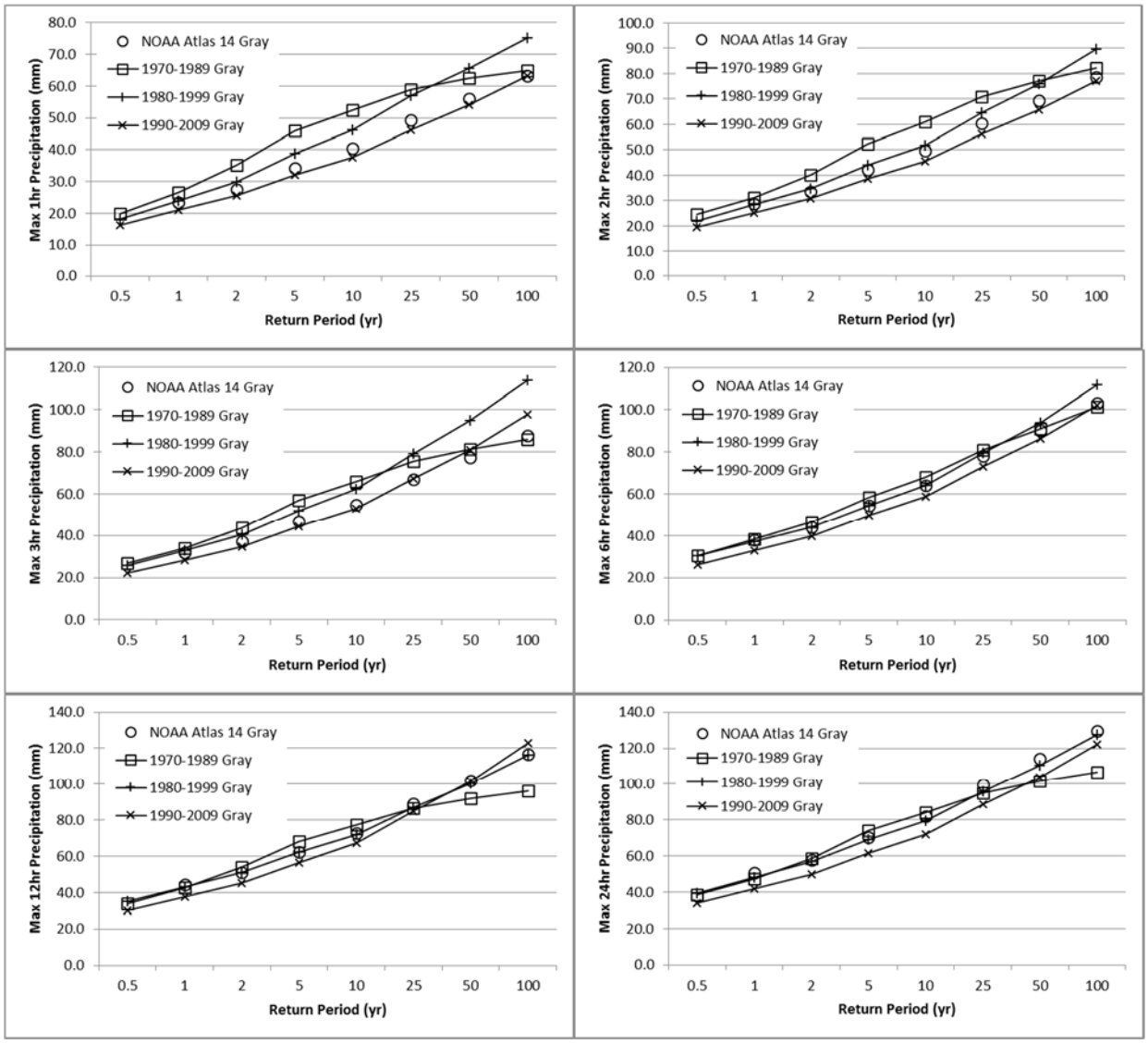

Figure 4.77. Comparison of estimated maximum precipitation for selected durations and return periods for 1970-1989, 1980-1999, and 1990-2009, as determined by L-moments regional frequency analysis at Grayling, Michigan. Atlas 14 values also included.

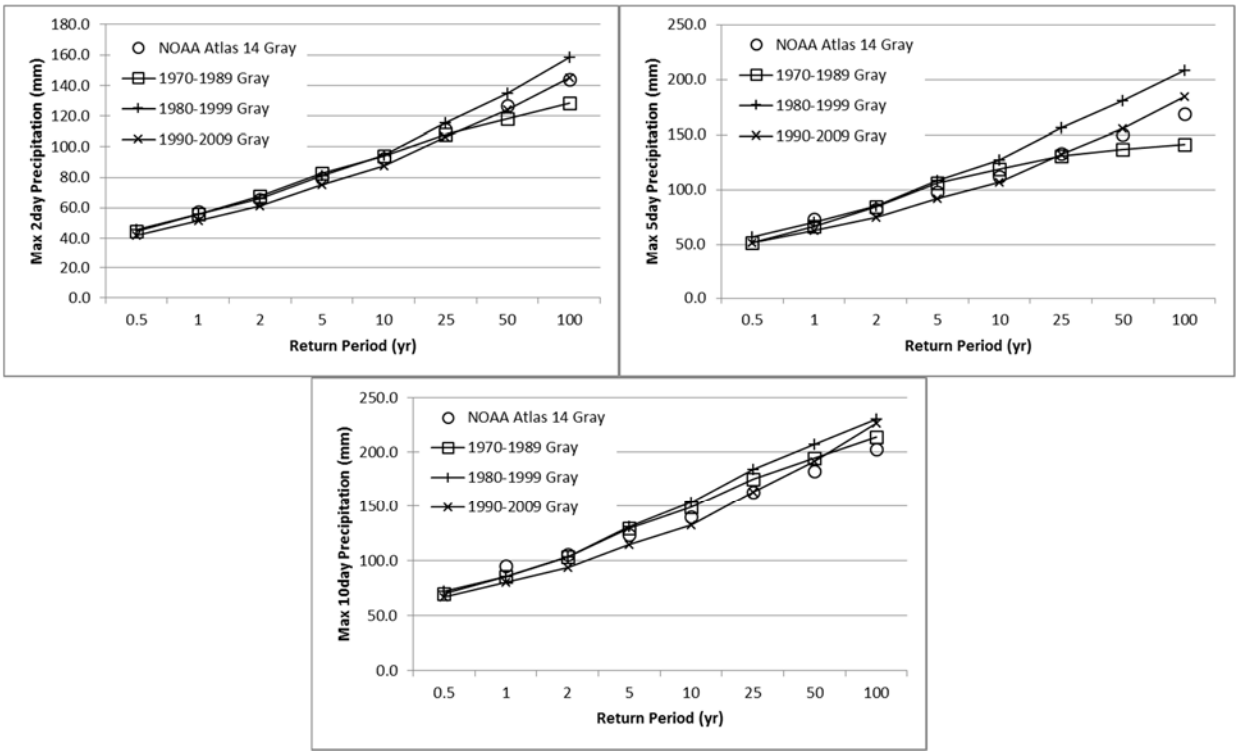

Figure 4.78. Comparison of estimated maximum precipitation for selected durations and return periods for 1970-1989, 1980-1999, and 1990-2009, as determined by L-moments regional frequency analysis at Grayling, Michigan. Atlas 14 values also included.

Table 4.19 shows the percent difference between the maximum 1970-1989 and 1990-2009 precipitations at Grayling, MI for all storm durations and return periods as determined by the L-moments regional frequency analysis. Table 4.20 shows the percent difference between the average maximum 1970-1989 and 1990-2009 precipitations for all gauges in the Michigan region. The highlighted values denote a significant difference as determined by Monte Carlo simulations used to construct confidence limits at a 95% confidence level. The negative values for shorter durations denotes that the maximum precipitation values for the latter time period (1990-2009) are smaller than the previous period. For shorter durations and more frequent storm events maximum precipitation values are up to 35% less than the former period. Several storm events for 1990-2009 with durations of 1-, 2-, and 3-hrs are significantly less than storm events for 1970-1989 with the same ARI. For longer durations and more extreme events, the latter time period experienced maximum precipitation events up to 26%

greater than the former time period, several of which are significantly more. See Appendix A for tables showing the percent difference between the maximum 1990-2009 and 1970-1989 precipitations at the other Michigan gauges.

Table 4.19. Changes in precipitation frequency estimates between1990-2009 and 1970-1989, as determined by L-moments regional frequency analysis at Grayling, Michigan, expressed as a percent difference.

Grayling, MI	0.5 yr	1 yr	2 yr	5 yr	10 yr	25 yr	50 yr	100 yr
1-hr	-19.6%	-23.5%	**-31.7%**	**-35.6%**	**-33.0%**	-24.0%	-14.3%	-2.8%
2-hr	-23.7%	-21.2%	-26.1%	**-30.2%**	**-29.2%**	-23.1%	-15.7%	-6.4%
3-hr	-18.2%	-18.1%	-23.0%	**-25.0%**	-21.5%	-11.3%	-0.4%	12.7%
6-hr	-15.3%	-14.7%	-15.6%	-15.8%	-14.3%	-10.0%	-5.3%	0.7%
12-hr	-11.2%	-12.7%	-17.7%	-18.7%	-14.1%	-2.1%	10.1%	24.4%
24-hr	-13.4%	-12.2%	-16.2%	-18.3%	-15.6%	-7.1%	2.2%	13.4%
2-day	-6.0%	-7.6%	-9.5%	-9.5%	-7.2%	-1.4%	4.8%	12.2%
5-day	-0.7%	-5.6%	-12.7%	-14.7%	-10.3%	1.2%	12.9%	**26.5%**
10-day	-4.4%	-6.2%	-9.8%	-12.3%	-11.5%	-7.0%	-1.4%	6.0%

Table 4.20. Changes in precipitation frequency estimates between 1990-2009 and 1970-1989, as determined by L-moments regional frequency analysis as average of Michigan region stations, expressed as a percent difference.

Michigan Region	0.5 yr	1 yr	2 yr	5 yr	10 yr	25 yr	50 yr	100 yr
1-hr	2.6%	-1.3%	-9.6%	**-13.7%**	-11.0%	-1.9%	7.9%	19.5%
2-hr	-2.6%	0.0%	-5.1%	-9.2%	-8.2%	-2.0%	5.5%	14.8%
3-hr	-3.2%	-3.0%	-8.0%	-10.0%	-6.5%	3.8%	14.7%	27.6%
6-hr	-3.4%	-2.7%	-3.6%	-3.8%	-2.3%	2.0%	6.7%	12.7%
12-hr	-1.7%	-3.3%	-8.3%	-9.3%	-4.6%	7.4%	19.5%	**33.6%**
24-hr	-3.9%	-2.7%	-6.7%	**-8.8%**	-6.1%	2.4%	11.7%	22.9%
2-day	1.7%	0.1%	-1.9%	-1.9%	0.5%	6.3%	12.4%	19.9%
5-day	5.5%	0.6%	-6.5%	-8.5%	-4.1%	7.5%	19.1%	**32.6%**
10-day	1.6%	-0.2%	-3.8%	-6.3%	-5.5%	-1.1%	4.6%	11.9%

Figure 4.79 shows a graphical version of Table 4.19 and Table 4.20 to illustrate the percent difference between the maximum 1970-1989 and 1990-2009 precipitations and average maximum precipitations for different durations and return periods. For the regional averages, the difference between the two time periods is consistent across storm durations. There is little difference for frequent events while

recent extreme storms are expected to be more intense than extreme storms from the 70's and 80's. However, for ARIs of about 5-yrs, recent storms are expected to be less intense than storms from the 70's and 80's. Near Grayling, MI the relationship between return periods is the same as for the region, however, recent extreme storms are expected to be much less intense than extreme storms from the 70's and 80's for shorter duration events.

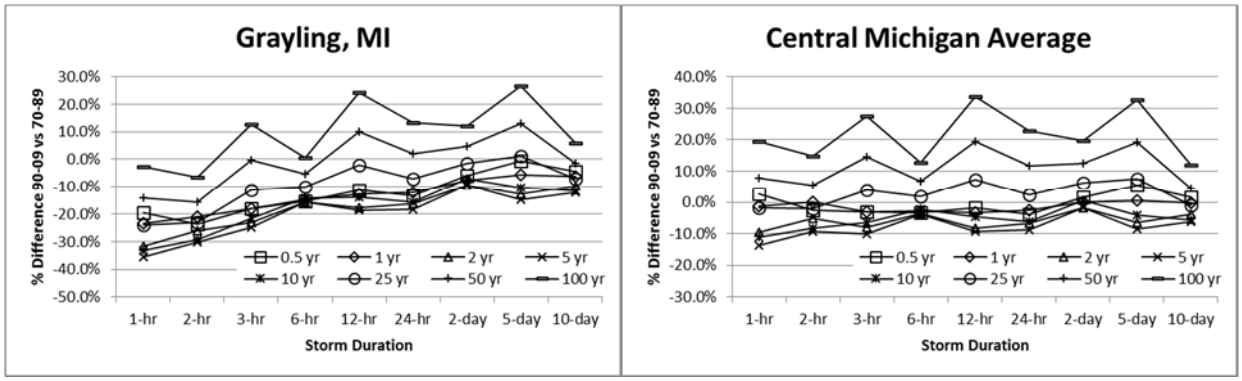

Figure 4.79. Comparison of estimated maximum precipitation for selected durations and return periods between 1990-2009 and 1970-1989, as determined by L-moments regional frequency analysis at Grayling, Michigan and an average of central Michigan region stations.

Figure 4.80 and Figure 4.81 shows the maximum precipitation distributions at Paris, IL for a range of return periods and durations of 1-, 2-, 3-, 6-, 12-, and 24-hr and 2-, 5-, and 10-days, respectively. Paris, IL is the closest gauge site to the study sites within Edgar County. The results indicate little difference in maximum precipitation between all time frames, which are in line with Atlas 14 values. The only notable difference between 1970-1989 and 1990-2009 maximum precipitation occurs during infrequent storms (return periods greater than 25-yrs) of short durations (1-, 2-, and 3-hrs), for which the latter time period saw more intense events.

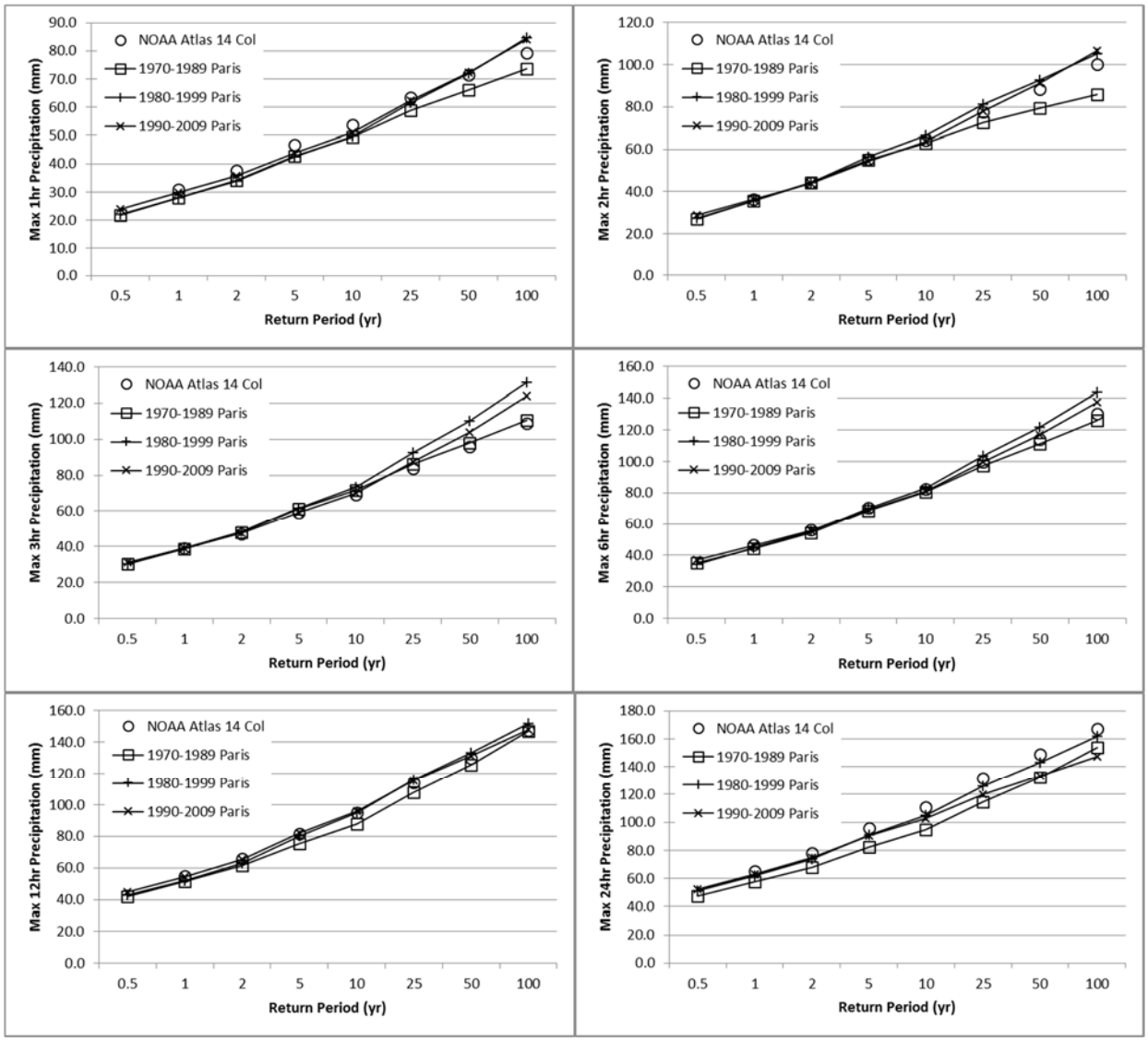

Figure 4.80. Comparison of estimated maximum precipitation for selected durations and return periods for 1970-1989, 1980-1999, and 1990-2009, as determined by L-moments regional frequency analysis at Paris, Illinois. Atlas 14 values also included.

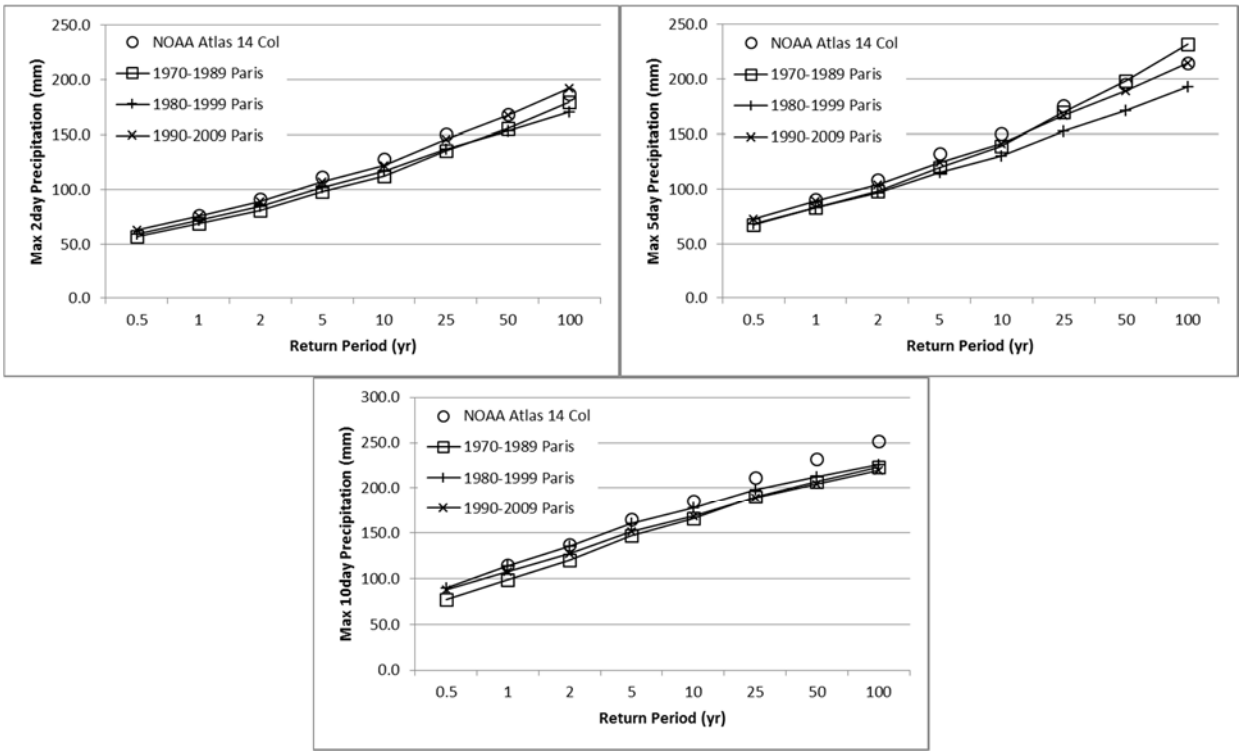

Figure 4.81. Comparison of estimated maximum precipitation for selected durations and return periods for 1970-1989, 1980-1999, and 1990-2009, as determined by L-moments regional frequency analysis at Paris, Illinois. Atlas 14 values also included.

Table 4.21 shows the percent difference between the maximum 1970-1989 and 1990-2009 precipitations at Paris, IL for all storm durations and return periods as determined by the L-moments regional frequency analysis. Table 4.22 shows the percent difference between the average maximum 1970-1989 and 1990-2009 precipitations for all gauges in the Illinois region. The highlighted values denote a significant difference as determined by Monte Carlo simulations used to construct confidence limits at a 95% confidence level. The results show no significant differences in maximum 1970-1989 and 1990-2009 precipitations for Paris, IL or the greater regional average. Except for extreme events with ARIs of 50- or 100-yrs, the differences between time periods are +/- 10%. See Appendix A for tables showing the percent difference between the maximum 1990-2009 and 1970-1989 precipitations at the other Illinois gauges.

Table 4.21. Changes in precipitation frequency estimates between 1990-2009 and 1970-1989, as determined by L-moments regional frequency analysis at Paris, Illinois, expressed as a percent difference.

Paris, IL	0.5 yr	1 yr	2 yr	5 yr	10 yr	25 yr	50 yr	100 yr
1-hr	8.7%	6.7%	4.3%	2.8%	3.2%	5.8%	9.1%	13.6%
2-hr	6.9%	2.0%	-1.1%	-1.3%	1.2%	7.5%	13.9%	21.5%
3-hr	3.0%	1.4%	-1.2%	-2.9%	-2.2%	1.3%	5.7%	11.4%
6-hr	5.6%	4.4%	2.4%	0.6%	0.6%	2.5%	5.2%	9.0%
12-hr	7.2%	5.3%	6.4%	8.2%	8.4%	6.8%	4.3%	0.6%
24-hr	9.5%	9.0%	9.4%	9.2%	7.9%	4.5%	0.7%	-4.1%
2-day	9.8%	9.4%	9.1%	8.6%	8.3%	7.7%	7.3%	6.9%
5-day	7.4%	7.0%	5.7%	3.4%	1.3%	-1.9%	-4.6%	-7.5%
10-day	12.6%	8.6%	5.7%	3.0%	1.4%	-0.1%	-1.1%	-1.9%

Table 4.22. Changes in precipitation frequency estimates between 1990-2009 and 1970-1989, as determined by L-moments regional frequency analysis as average of Illinois region stations, expressed as a percent difference.

Illinois Region	0.5 yr	1 yr	2 yr	5 yr	10 yr	25 yr	50 yr	100 yr
1-hr	2.5%	0.5%	-1.8%	-3.4%	-3.0%	-0.4%	3.0%	7.4%
2-hr	4.1%	-0.8%	-3.9%	-4.2%	-1.6%	4.6%	11.0%	18.7%
3-hr	3.2%	1.6%	-0.9%	-2.7%	-2.0%	1.5%	5.9%	11.7%
6-hr	5.4%	4.3%	2.2%	0.5%	0.5%	2.3%	5.1%	8.8%
12-hr	6.0%	4.1%	5.2%	7.0%	7.2%	5.7%	3.1%	-0.6%
24-hr	7.9%	7.3%	7.7%	7.6%	6.3%	2.9%	-0.9%	-5.7%
2-day	9.7%	9.4%	9.0%	8.6%	8.2%	7.7%	7.3%	6.8%
5-day	13.6%	13.2%	11.9%	9.6%	7.5%	4.3%	1.6%	-1.4%
10-day	13.4%	9.4%	6.5%	3.8%	2.2%	0.7%	-0.3%	-1.1%

Figure 4.76 shows a graphical version of Table 4.17 and Table 4.18 to illustrate the percent difference between the maximum 1970-1989 and 1990-2009 precipitations and average maximum precipitations for different durations and ARIs. For all ARIs less than 50-yrs the difference in maximum precipitation between time periods is -5% to 10%. Maximum precipitation estimates at Paris, IL are very similar to the Illinois region as a whole with only slight variances in magnitude of the differences between time periods.

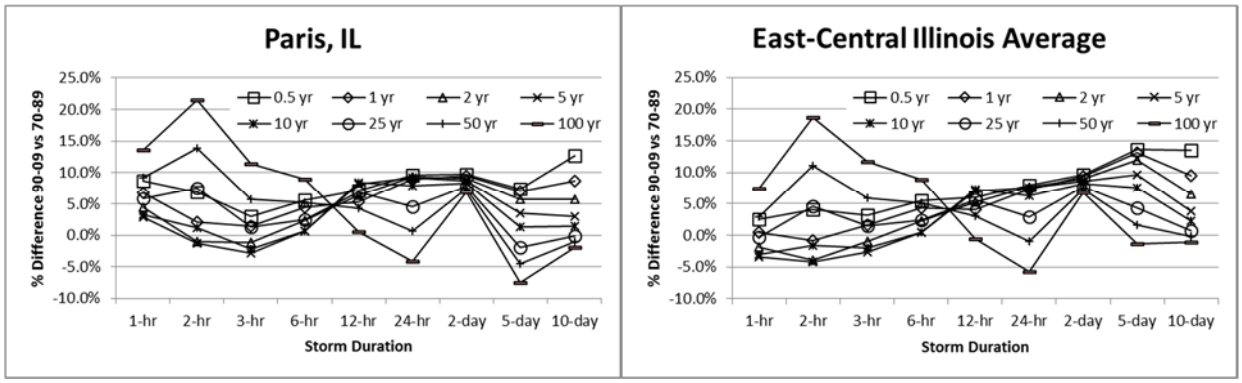

Figure 4.82. Comparison of estimated maximum precipitation for selected durations and return periods between 1990-2009 and 1970-1989, as determined by L-moments regional frequency analysis at Paris, Illinois and an average of east central Illinois region stations.

4.4 Discussion

Total annual precipitation has increased in central Indiana, central Michigan, and east central Illinois by approximately 5%, 7%, and 15% since 1914, 1940, and 1923, respectively. Trend analyses using the t-test and the MK test indicate total annual precipitation is increasing (95% confidence limit) at five out of nine Indiana gauges and four out of six Illinois gauges. The averages of the Indiana and Illinois gauges also show increasing trends. In central Michigan, three out of seven gauges show an increase in total annual precipitation at the 95% or 90% confidence limits. About half of the studied gauges show significant increases in total annual precipitation during the second half of the 20th Century. These results are consistent with findings presented in literature (eg: Karl and Knight, 1998; Melillo et al., 2014; Pryor et al., 2009).

In order to determine if and how rainfall intensity has changed, the temporal distribution of rainfall was investigated. To this end, the number of annual wet days (calendar days) and wet hours (clock hours) were analyzed. Annual wet days at the Indiana gauges average 80 days per year 1914-2009. The linear trend line for most Indiana gauges is completely flat, while two of the gauges with shorter data sets starting after 1945, show slight increasing trends due to above average annual wet days in the 1980's

and early 1990's. On the other hand, average annual wet days in Michigan and Illinois increased 7% and 16% since 1940 and 1923, respectively. Pryor et al. (2009) also reported increasing trends in the number of annual wet days in the Midwest. The regions with the larger increases in total annual precipitation (7% in Michigan and 15% in Illinois) also show increasing trends (7% in Michigan and 16% in Illinois) in annual wet days.

Annual wet hours were also assessed in order to facilitate climate model bias correction with regards to precipitation thresholds and to investigate changes in rainfall occurrences at sub daily durations. Total annual wet hours have no trend to a slightly decreasing trend across all three regions with average decreases of 10%, 16%, and 13% in Indiana, Michigan, and Illinois, 1970-2009. Trend analyses using the t-test and the MK test indicate total annual wet days are decreasing (95% confidence limit) at one out of seven Indiana gauges, one out of five Michigan gauges, and one out of six Illinois gauges. Several decreasing trends were detected only by the t-test at gauges with heterogeneous variance, but were discounted due to the t-test being less reliable under such conditions. Heterogeneous variance was determined at the 90% confidence limit for 4 gauges in Indiana and Illinois and 2 in Michigan. Little literature is available on the historic trends of wet hours or any sub-daily durations.

These analyses suggest total annual precipitation in the three study regions has increased during the last 60 or more years, while the number of wet days has also generally increased. However, the number of wet hours has been the same or slightly decreased, suggesting more rain is falling within a shrinking span of time annually and so the intensity of rainfall is generally increasing. The wet hours are also occurring within more calendar days, which suggests more intense rainfall is occurring more frequently, as a greater volume of rainfall is occurring during slightly fewer hours but spread over more 24 hour

periods. Groisman et al. (2012), Madsen and Figdor (2007), Pryor et al. (2009), and others have attributed the increases in annual precipitation to increases in the frequency of large storm events (durations of 1-7 days) while others (eg. Karl and Knight, 1998; Melillo et al., 2014) determined increases in both the frequency and intensity of large storm everts play a role (durations of 1-7 days).

The AMS (24-hr and 1-hr) was analyzed to determine if the intensity of the largest storm events are increasing. The average 24-hr AMS has increased by 13% and 11% in Indiana and Illinois and decreased by 5% in Michigan since 1914, 1923, and 1940, respectively. The average 1-hr AMS has increased by 2% and Illinois and decreased by 1% and 4% in Indiana and Michigan since 1970. The trend analysis showed the 24-hr AMS increase in Indiana is significant at 1 gauge and for the average of all the gauges and the 1-hr AMS decrease in Michigan is significant at 1 gauge. All other trends were statically steady. Bonnin et al. (2006) determined 82% of tested gauges in Illinois and 84% of tested gauges in Indiana showed no significant trend (95% confidence limit only) when analyzing 24-hr AMS, while 16% and 12% of gauges show increasing trends. Perica et al, (2013) determined 79% and 89% of tested gauges in Michigan show no significant trend (95% confidence limit only) when testing 24-hr and 1-hr AMS, respectively. Positive trends were reported at 21% and 11% of gauges for 24-hr and 1-hr AMS, while no gauges showed a negative trend. The area of Michigan over lapping the study region showed only one gauge with a positive trend for the 24-hr AMS. Given the smaller sample size of the current study, the trend results from the literature generally match the result provided above, however the analysis at the 90% confidence limit reveals a slightly downward trend in the 1-AMS in Michigan that previous studies didn't find.

Numerous studies (eg: Groisman et al., 2005; Groisman et al., 2012; Karl and Knight, 1998; Pryor et al. 2009) have found increases in the frequency of extreme precipitation events, which are usually described as 90th percentile, 95th percentile, or the largest 3% storm events with durations of 1-7 days. For this study, the frequency of rain events larger than or equal to the gauge record's smallest 24-hr AMS was investigated. The smallest 24-hr AMS for each region corresponds to about half the value of the 1-yr, 24-hr Atlas 14 design storm, which are both very close to the 24-hr 95th percentile storm event for each region. A significant average increase in the frequency of events larger than the smallest 24hr-AMS was detected for each region (95$^{\%}$ confidence for Indiana and Michigan and 90% confidence for Illinois), which agrees with the literature. The frequency of larger storm events in each region (greater than the 1-yr, 24-hr Atlas 14 design storm) has increased in Indiana (95% confidence) but has remained stready in Michigan and Illinois. The 1-yr, 24-hr Atlas 14 design storm is greater than or equal (in Indiana) to the 99th percentile storm in all three regions. The results indicate the frequency of extreme events up to the 95th but less than 99th percentile storms are increasing in Michigan and Illinois while the frequency of extreme events up to about the 99th percentile storm are increasing in Indiana.

Analysis of the frequency of 1-hr duration rainfall was also conducted using rain events larger than or equal to the gauge record's smallest 1-hr AMS and greater than the 1-yr, 1-hr Atlas 14 design storm. Again the minimum 1-hr AMS for each region corresponds to about half the value of the 1-yr, 1-hr Atlas 14 design storm for each region and is approximately equal to the 95th percentile 1-hr storm depths. Results show increases in the frequency of both storm events in the Indiana region, with the increase in rain events larger than or equal to the gauge record's smallest 1-hr AMS being significant (90% confidence limit). The average frequency of storm events with 1-hr durations in Michigan and Illinois are steady, though individual gauges show increases and decreases within each region.

Over all, the intensity and frequency of extreme storm events are steady at a majority of gauges in Indiana, Michigan, and Illinois. However, the average intensity of extreme 24-hr events have increased in Indiana and Illinois (though not significantly in the latter) along with an increase in the frequency of such events in all three regions. For the shorter duration of 1-hr, the intensity of extreme events are steady in all regions while the frequency of extreme events is also steady in Illinois and Michigan. However, evidence suggests the frequency of extreme 1-hr events has increased in Indiana.

Precipitation regional frequency analysis was used to estimate how often specific events (for numerous return periods and durations) occur and how they changed between 1970-1989 and 1990-2009. The use of numerous gauges within a region increase robustness and minimize uncertainty due to outliers at a single rain gauge. Monte Carlo simulations are also used to construct confidence limits at a 95% confidence level. Confidence intervals constructed through this approach account for uncertainties in distribution parameters, but not for other sources of uncertainties (for example, distribution selection), that could also significantly impact the total error (Perica et al., 2013). Results indicate a significant increase in the intensity of longer duration (>12hr) events in Indiana for all ARIs while changes in shorter duration events between time periods are more steady. An increase in the intensity of similar long duration storm events was also seen in Illinois, though not significantly, and the changes in shorter duration events between time periods was also steady. In Michigan, the intensity of less frequent events increased (ARIs of 50 – 100 yrs) while the intensity of all other events were steady or slightly decreasing. These results are consistent with the trend analyses provided above.

Huff and Angel (1992) conducted a similar analysis of design storm maximum perception in the Midwest comparing 40-yr periods of 1901-1940 and 1941-1980. They found an increase in rainfall intensity between the two time periods in Illinois and Michigan for 24-hr events while Indiana was steady. The result from Huff and Angel (1992) and this study suggest that the assumption of a stationary time series for fitting statistical distributions to historical precipitation data may be invalid. Huff and Angel (1992) suggest rainfall frequency relations be updated on the order of every 20-yrs to capture any substantial changes in rainfall relations, an idea supported by the current findings.

4.5 Conclusion

The comparison of observed data at the same location over different time frames can validate the assumption of stationarity of precipitation magnitudes and frequencies. The results suggest the assumption that precipitation is stationary over time with regards to total annual rainfall and storm frequency and intensity is not valid for the Midwest generally, or central Indiana, central Michigan, and east central Illinois, specifically. Total annual precipitation has increased over the past century as well as average annual wet days in certain areas, while average annual wet hours have remained steady or slightly decreased in some areas. The intensity of large events has generally stayed steady across the region, but have shown increases and decreases at individual gauges for durations of 24- and 1-hrs, respectively. Finally, the frequency of large storm events has increased across the region, particularly in Indiana. There is no implication in these results that the trends will necessarily continue; however, evidence from some studies suggests that the most recent 5 to 15 years are the best predictor of conditions for the next 1 to 5 years, so current trends are likely to continue at least in the short term (Easterling, Angel, & Kirsch, 1990).

Numerous uncertainties associated with precipitation observations and with their spatial/temporal aggregation can be partially reduced by regional analysis. The use of numerous gauges within a region increase robustness and minimize uncertainty due to outliers at a single rain gauge. Regional frequency analysis was used to estimate how often specific events (for numerous return periods and durations) occur and how they changed between 1970-1989 and 1990-2009. Results indicate the intensity of longer duration events has increased between the two periods while a slight decrease occurred in Michigan for shorter duration events. These results suggest the assumption of a stationary time series for fitting statistical distributions to historical precipitation data may be invalid. Also, since IDF estimates are based on gauge data, the length and time period from which the data was obtained can greatly affect results. The regional frequency analyses showed that the precipitation magnitudes from the 1990-2009 time frame are most similar to the corresponding Atlas 14 values, however, regional frequency analyses showed be updates periodically as newer gauge data becomes available. Updating regional frequency analyses on the order of every 10-20 years will ensure the nonstationary of precipitation is at least partially accounted for, though anticipating future conditions would not be addressed.

References

Bonnin, G. M., Martin, D., Lin, B., Parzybok, T., Yekta, M., & Riley, D. (2006). National Oceanic Atmospheric Administration Atlas 14: precipitation frequency atlas for the United States, Volume 2 Version 3.0: Delaware, District of Columbia, Illinois, Indiana, Kentucky, Maryland, New Jersey, North Carolina, Ohio, Pennsylvania, South Carolina, Tennessee, Virginia, West Virginia. U.S. Department of Commerce. Silver Spring, MD.

Easterling, W. E., Angel, J. R., & Kirsch, S. A. (1990). The appropriate use of climatic information in Illinois natural-gas utility weather normalization techniques. Illinois State Water Survey, Report of Investigation 112.

Groisman, P. Y., Knight, R. W., Easterling, D. R., Karl, T. R., Hegerl, G. C., and Razuvaev, V. H. (2005). Trends in intense precipitation in the climate record. Journal of Climate, 18: 1326-1350.

Groisman, P. Y., Knight, R. W., & Karl, T. R. (2012). Changes in intense precipitation over the central United States. Journal of Hydrometeorology, 13: 47-66.

Haan, C.T. (1977). Statistical Methods in Hydrology, The Iowa State Univ. Press, Ames.

Hershfield, D.M. (1961). Rainfall frequency atlas of the United States for durations from 30 min to 24 h and return periods from 1 to 100 years. Technical Paper No. 40. Weather Bureau, U.S. Department of Commerce, Washington, DC.

Hosking, J. R. M. & J. R. Wallis (1997). Regional Frequency Analysis, an Approach Based on L-Moments. Cambridge University Pres.

Hosking, J. R. M. (1990). L-Moments: Analysis and Estimation of Distributions Using Linear Combinations of Order Statistics, 52(1): 105-124.

Hosking, J. R. M. (2015). Package 'lmomRFA' manual-regional frequency analysis using L-moments, Version 3.0-1, CRAN.

Huff, F. A. & Angel, J. R. (1992). Rainfall frequency atlas of the Midwest (Bulletin 71). Illinois State Water Survey, Champaign, IL.

Karl, T. R., Knight, R.W. (1998). Secular trends of precipitation amount, frequency, and intensity in the United States. Bull Am Meteorol Soc 79,(2):231–241.

Kendall, M. G. (1970) Rank Correlation Methods, 4th ed. London: Griffin

Langbein, W. B. (1949). Annual Floods and the Partial-Duration Flood Series. Transactions American Geophysical Union 30, 879-881.

Levene, H. (1960). In I. Olkin et al. eds., Contributions to Probability and Statistics: Essays in Honor of Harold Hotelling. Stanford University Press, 278-292.

Madsen, T. & Figdor, E. (2007). When it rains, it pours. Global warming and the rising frequency of extreme precipitation in the United States. Environment America Research & Policy Center.

Markus, M., Wuebbles, D. J., Laing, X., Hayhoe, K., Kristovich, D. A. R. (2012). Diagnostic analysis of future climate scenarios applied to urban flooding in the Chicago metropolitan area. Climatic Change, 111: 879-902.

Melillo, J. M., Richmond, T. C., & Yohe, G. W. (Eds.). (2014). Climate change impacts in the United States: The Third National Climate Assessment (NCA). U.S. Global Change Research Program, 841 pp.

Perica, S., Martin, D., Pavlovic, S., Roy, I., St. Laurent, M., Trypaluk, C., Unruh, D., Yekta, M., Bonnin, G. (2013). National Oceanic Atmospheric Administration Atlas 14: precipitation frequency atlas for the United States, Volume 8 Version 2.0: Midwestern States (Colorado, Iowa, Kansas, Michigan, Minnesota, Missouri, Nebraska, North Dakota, Oklahoma, South Dakota, Wisconsin). U.S. Department of Commerce. Silver Spring, MD.

Pryor, S. C., Howe, J. A., & Kunkel, K. E. (2009). How spatially coherent and statistically robust are temporal changes in extreme precipitation in the contiguous USA? Int. J. Climatology, 29: 31–45.

US Environmental Protection Agency (USEPA). (2013). Better assessment science integrating Point and nonpoint sources (BASINS), Version 4.1, User's Manual. Office of Water, EPA-823-B-13-001.

US Army Corps of Engineers (USACE). (2014). Climate change Adaptation plan. Climate Preparedness and Resilience Steering Committee. Department of the Army.

Chapter 5 – CLIMATE CHANGE MODELING AND PROJECTIONS

Abstract

The stationary assumption of total annual precipitation, total annual wet days and wet hours, AMS (1-hr and 24-hr) were tested for regions centered around central Indiana, central Michigan, and east central Illinois using four global climate models (GCMs) from the Coupled Model Intercomparison Project Phase Five (CMIP5). The GCMs were dynamically downscaled to 25 km (15.53 mi) grid spacing and 1-hr time steps according to the representative concentration pathway 8.5 (RCP8.5) scenario using the Abdus Salam International Centre for Theoretical Physics (ICTP) Regional Climate Model Version Four (RegCM4). The four models were bias corrected first by applying a minimum precipitation threshold below which hourly precipitation estimates were set to zero and then by implementing quantile mapping. Precipitation frequency estimates are calculated for the 0.5-, 1-, 2-, 5-, 10-, 25-, 50-, and 100-year ARIs and durations of 1-, 2-, 3-, 6-, 12-, and 24-hr; and 2-, 5-, and 10-days for the model simulation (1980-1999) and projections (2040-2059 and 2080-2099) for the four climate models and compared to the observed data (1980-1999).

The average projected (2080-2099) design storm of the four RCMs across all locations, durations, and return periods is larger than the corresponding observed design storm and usually significantly larger based on the standard deviation of the RCM results, especially for ARIs greater than 1 year. On average the projected (2080-2099) design storms are 51%, 52%, and 34% larger than the observed design storms. The average projected (2040-2059) design storm is also more intense than observed design storms for corresponding return periods and durations. On average the projected (2040-2059) design storms are 6%, 25%, and 31% larger than the observed design storms. The four RCMs provided bias-corrected precipitation output that agreed in general trends, however, the precise levels of precipitation

increases varied substantially, especially for the 2040-2059 projected timeframe. As a result, the inferred changes in precipitation are difficult to distinguish from natural variability and determining specific projected design storms for future hydrology and stormwater infrastructure design is difficult. Nonetheless, the average and upper and lower bounds of RCM projected precipitation can be usefully in studying potential impacts of climate change on watershed hydrology and related infrastructure.

Keywords: Precipitation, quantile mapping, RCMs, climate change, hydrology

5.1 Introduction

Recent studies applying GCMs (IPCC, 2014) project that extreme precipitation events will become more intense and frequent in many regions, including the Midwest. Unfortunately, the typical GCM output grid-cell size is approximately 50×70 miles and the temporal scale in also large, which poorly represent local scale precipitation (IDNR, 2015). GCM data must be downscaled to spatial and temporal increments appropriate for local (or point) precipitation and flood studies (Olsson et al., 2012).
The recent availability of higher spatial and temporal resolution (sub daily) climate data, as produced by RCMs through dynamical downscaling, has facilitated impact assessments (Zhu, 2013). However, dynamically downscaled data often requires bias correction, the aim of which is to correct systematic error in RCM output, such as disparities in the frequency of rain events, total amount of rainfall, and seasonality, and have been found to be an important aspect of using such output for small-scale hydrologic modeling (Fowler et al., 2007).

This study focuses on the Midwest by utilizing climate models provided by the Center for Climate Research at the University of Wisconsin-Madison (Notaro et al., 2015). Four GCMs from the Coupled

Model Intercomparison Project Phase Five (CMIP5) were dynamically downscaled to 25 km (15.53 mi) grid spacing according to the representative concentration pathway 8.5 (RCP8.5) scenario using the Abdus Salam International Centre for Theoretical Physics (ICTP) Regional Climate Model Version Four (RegCM4) (Notaro et al., 2015). RegCM4 is a community RCM developed over several decades (Elguindi et al., 2011; Giorgi et al., 2012). The study included a 25 km (15.53 mi) grid spacing, 28 vertical sigma levels, and 1-hr time step. Care was taken to incorporate the effects of the Great Lakes within the dynamic processes of the model due to the coarse resolution and poor representation of the Great Lakes in the CMIP5 models. Raw precipitation output from the four (RCMs) are bias corrected using the quantile mapping method due to overestimated average annual total precipitation, 1-hr AMS, and total annual wet hours when comparing model simulation data (1980-1999) to observed gauge data (1980-1999).

Following the model bias correction, model precipitation trends (simulations and projections) are compared to observed data trends from Chapter 4. In addition, precipitation frequency estimates are calculated for the 0.5-, 1-, 2-, 5-, 10-, 25-, 50-, and 100-year ARIs and durations of 1-, 2-, 3-, 6-, 12-, and 24-hr; and 2-, 5-, and 10-days for the model simulation (1980-1999) and projections (2040-2059 and 2080-2099) for the four climate models and compared to the observed data (1980-1999). Finally, analyzing four different RCMs provides a range of possible projections (upper and lower bounds based on the highest and lowest model outputs) and an average projection for each design storm to utilize in subsequent hydrologic modeling and engineering design.

5.2 Methods

5.2.1 Climate Models

This study utilizes climate models provided by the Center for Climate Research at the University of Wisconsin-Madison (Notaro et al., 2015). Four GCMs from CMIP5 were dynamically downscaled to 25 km (15.53 mi) grid spacing according to the RCP8.5 scenario using the ICTP RegCM4 (Notaro et al., 2015). RegCM4 is a community RCM developed over several decades (Elguindi et al., 2011; Giorgi et al., 2012). The RegCM modeling system has four components: Terrain and ICBC (preprocessor), RegCM, and the Postprocessor (Elguindi et al., 2011). Terrestrial variables (including elevation, landuse, and sea surface temperature) and three-dimensional isobaric meteorological data are horizontally interpolated from a latitude-longitude mesh to a high-resolution domain. Vertical interpolation from pressure levels to the σ coordinate system of RegCM is also performed. σ surfaces near the ground closely follow the terrain, and the higher-level σ surfaces tend to approximate isobaric surfaces. See Elguindi et al. (2011) and Giorgi et al. (2012) for more detailed of overview and history of the RegCM4 RCM.

The specific application of RegCM4 by the Center for Climate Research at the University of Wisconsin-Madison is detailed in Notaro et al. (2015). The study included a 25 km (15.53 mi) grid spacing and 28 vertical sigma levels. Care was taken to incorporate the effects of the Great Lakes within the dynamic processes of the model due to the coarse resolution and poor representation of the Great Lakes in the CMIP5 models. RegCM4 was interactively coupled to a one-dimensional, energy balance lake model and the Great Lakes were represented by 431 grid cells. Notaro et al. (2015) provides an overview of past studies using RegCM4 in the Great Lake Region, finding that the model has generally produced fair to good fits with temperate, liquid precipitation, and snowfall when run for historic time periods.

The Coupled Model Intercomparison Project Phase Five (CMIP5) are a set of coordinated climate model experiments promoted by the World Climate Research Programme's (WCRP) Working Group on Coupled Modelling (WGCM) (Taylor et al., 2012). Each GCM(s) was standardized with regards to inputs, output formatting, and general experimental setup, but internal processes varied as per the discretion of the corresponding modeling groups and focus of study. Standard inputs included future projection simulations forced with specified CO2 concentrations [referred to as "representative concentration pathways" (RCPs)]. RCP8.5, the high emissions scenario, refers to radiative forcing that increases throughout the twenty-first century before reaching a level of about 8.5 W m−2 at the end of the century (Taylor et al., 2012). RCP8.5 was the only scenario considered for this study as it was the only scenario so far considered by the Center for Climate Research at the University of Wisconsin-Madison for the ongoing modeling efforts due to computational limitations (Figure 5.1). The high emissions scenario is the most extreme scenario with regards to radiative forcing and is often among the first used for modeling efforts to estimate possible future climate projections. There is evidence to suggest that all SRES emissions scenarios underestimate the amount of warming that is already being observed, both in western Europe (Oldenborgh et al., 2008) and globally (Rahmstorf et al., 2007) and so RCP8.5 may be the most accurate going forward. Sanford et al. (2014) reported that recent observed global CO_2 emissions are higher than corresponding RCP8.5 projections, meaning the most extreme pathway may actually underestimate future atmospheric concentrations. The standard outputs included a historical run forced by observed atmospheric composition changes with time-evolving land cover (Taylor et al., 2012). A historical run of 1980-1999 was used for this study.

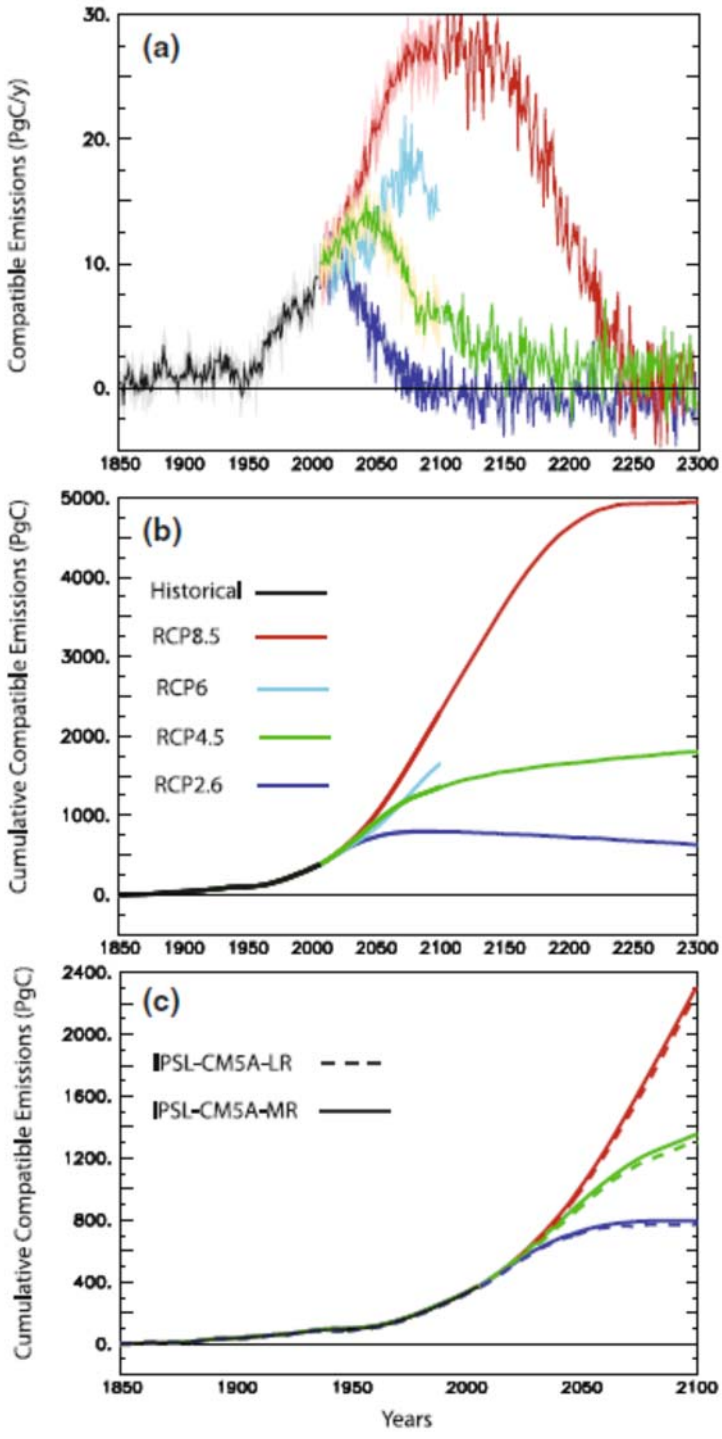

Figure 5.1. Time evolution of the compatible CO_2 emissions (a, in PgC/year) and of the cumulative emissions (b, in PgC) for the historical period (black) and for the RCP 2.6 (blue), the RCP 4.5 (green), the RCP 6.0 (light blue), and the RCP 8.5 (red) scenarios, simulated by the IPSL-CM5A-LR model. The time period is restricted to 1850–2100 in (c) where the results are shown for both the IPSLCM5A-LR and IPSL-CM5A-MR models (Dufresne et al., 2013).

The four CMIP5 GCMs downscale by RegCM4 include the Centre National de Recherches Meteorologiques Coupled Global Climate Model Version Five (CNRM-CM5) (Voldoire et al., 2012), the Model for Interdisciplinary Research on Climate Version Five (MIROC5) (Watanabe et al., 2010), the Institute Pierre Simon Laplace Coupled Model Version Five-Medium Resolution (IPSL-CM5-MR) (Dufresne et al., 2013), and the Meteorological Research Institute Coupled Global Climate Model Version Three (MRI-CGCM3) (Yukimoto et al., 2012). These models are denoted as CNRM, IPSL, MIROC, and MRI, respectively.

See each reference for a detailed overview of model processes and summary of results for each respective GCM. With regards to precipitation, all four model overestimate average global precipitation and show complex regional patterns and slight seasonal variations (eg. Dufresne et al., 2013 and Yukimoto et al., 2012). For the Great Lake region of North America total precipitation is generally bias high but these precipitation biases are common for GCM as discussed in more detail in Section 5.2.2 Bias Correction. Despite the differences among the forcing in each scenario, the pattern of the change in precipitation in 2100 for a given model version is strikingly similar for the different RCPs scenarios (eg. Dufresne et al., 2013 and Yukimoto et al., 2012). In this case, considering only one RCP scenarios with regards to precipitation prior to 2100 is appropriate for this group of models.

5.2.2 Bias Correction

CMIP5 GCMs generally overestimate precipitation and sometimes underestimate extreme precipitation, which are common systematic errors (bias) with regards to hydrologically relevant variables produced by GCM-RCM model chains (Ehret et al., 2012). The biases are often to a degree that precludes their direct interpretation or application for simulation and projection in hydrologic and hydraulic models. To overcome this problem, post-processing of either GCM or RCM output by correcting with and towards

observations has become a standard procedure in climate change impact studies (Ehret et al., 2012). The following section describes the methods used to bias correct the RCM precipitation output for this study.

Precipitation Threshold

The first step in precipitation bias correction is to adjust the frequency of precipitation events to match observed events (Lindau and Simmer, 2012). Many climate models produce precipitation characterized by 'drizzle', where rainfall occurs many days or hours (depending on model timesteps) with very low rainfall totals (Fowler and Kilsby, 2007 and Themeßl et al., 2011). Thresholds are selected below which very low rainfall totals are set to zero so that the average number of wet hours or days matches the observed average number of wet hours or days. Both fixed thresholds and percentile-defined threshold are commonly used, but the former is usually used for relatively homogeneous regions (Groisman et al., 2012). Thresholds are typically between 0.1 mm – 2 mm and depend on the characteristic of both the observed precipitation and model precipitation being compared (eg. Lindau and Simmer, 2012; Rosenburg et al., 2010; and Themeßl et al., 2011). A fixed threshold was used for this study to adjust the average number of annual wet hours for each model to match the average number of observed annual wet hours for each region.

Quantile Mapping

The second step in precipitation bias correction is to adjust the intensity of the climate model rainfall to agree with the observed intensity. Quantile mapping (also sometimes referred to as CDF matching) is an approach which adjusts the mean and variance of a model simulation to agree with the statistical properties of the observations (eg. Themeßl et al., 2011). For this method, the empirical cumulative distribution function (eCDF; Wilks, 2006) of the model output is adjusted to agree with the eCDF of the observations for the historic time period (Wood et al., 2004; Maurer and Hidalgo, 2008). For a given grid

box and corresponding rain gauge a percentile value for the model simulation is found and then replaces the simulated precipitation with the observed precipitation from the same percentile in the (observed) eCDF (Sun et al., 2011). The quintile mapping bias correction function is given as (Li et al., 2010):

$$Y_{t,i}^{val} = ecdf_{t,i}^{obs,cal^{-1}}\left(ecdf_{t,i}^{mod,cal}\left(X_{t,i}^{val}\right)\right)$$

Equation 5.1

Where X^{val} is the raw RCM output corrected to an estimated Y^{val} with $ecdf^{-1}$ (observed) indicating the inverse $ecdf$ (model), and thus a data quantile. This purely empirical quantile mapping only maps modelled values to observed values, so no new extremes (outside the observed range) can be obtained (Themeßl et al., 2011). For applications to future climate simulations, however, some kind of extrapolation beyond the range of observations has to be added to allow for new extremes, for this study the extrapolation is linear.

Li et al. (2010) proposed an approach for future eCDF where the difference over time in the model output (eCDF model projection [future] minus eCDF model simulation [historic]) is preserved in the projection. For the future projection, the eCDFs for the model projection and simulation, and the observations are created and then the corresponding percentile values in the three eCDFs are found. The bias-corrected output is calculated by subtracting the difference between the model simulation and the observations from the model projection at the same percentile. Hence, projected changes in the model output should be preserved (Sun et al., 2011). Quantile mapping has been applied for monthly, daily, and hourly precipitation bias correction (eg. Li et al. 2010; Themeßl et al., 2011; and Rosenberg et al., 2010), respectively, and does a good job of reducing system bias across all percentiles compared to other methods (Gudmundsson et al., 2012). Quantile mapping has also been applied by month so that for a given time frame 12 eCDF (one for each month) are created for model projection and simulation,

and the observations and adjusted separately (Brocca et al., 2011). Both methods were tested for this study.

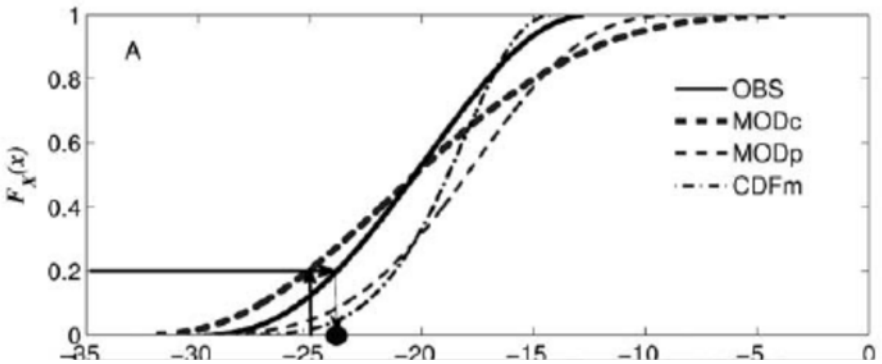

Figure 5.2. Illustration of methodology of quantile mapping using synthetic generated winter time temperature data for a grid point. Solid black line shows observations (OBS). Thick dashed line shows model simulation for current climate (MODc). Thin dashed line shows model simulation for future projection (MODp). Dotted-dashed line shows CDF matching (Li et al., 2010).

5.2.3 Precipitation Frequency Analysis

The same regional precipitation frequency analysis using the L-moments method was used for the RCMs precipitation output data as used for the historic precipitation gauge data in Chapter 4. See Section 4.2.3 Precipitation Frequency Analysis for method description.

5.2.4 Areal Mean and Point Rainfall Ratio

Hershfield (1961) and Huff and Angel (1992) developed area-depth curves for estimating areal mean rainfall frequencies from point rainfall frequencies. RCM precipitation output is provided as the areal mean for each model grid, in this study grids are 25 km x 25 km with an area of 625 km^2 (241.3 mi^2). Applicable ratios were used to convert all RCM precipitation output from areal mean to point rainfall depths for comparison with observed (point) rainfall data gathered at gauge stations.

5.3 Results

5.3.1 Precipitation Threshold and Raw RCM Analyses

Four RCMs were analyzed for the correct precipitation threshold to match observed (1980-1999) and simulated (1980-1999) wet hours. The simulated total annual precipitation, 1-hr AMS, and wet hours for each RCM were compared to observed values by region. Once a precipitation threshold was selected for each model, an analysis of projected (2040-2059 and 2080-2099) total annual precipitation, 1-hr AMS, 24-hr AMS, wet hours, and wet days was completed to determine if subsequent bias correction was needed. A single precipitation threshold was selected for each RCM to simplify subsequent bias correction if needed.

For each RCM simulation, precipitation thresholds of 0.76 mm, 1.02 mm, 1.27 mm, and 1.52 mm (0.03 in, 0.04 in, 0.05 in, and 0.06 in) were applied for which all values below the threshold were set to zero. The RCM simulations overestimated total annual precipitation when no threshold was applied but moved closer to the observed average as larger thresholds were applied. Figure 5.3 shows a box-whisker plot for each region with observed and RCM simulated total annual precipitation, to which the thresholds were applied. Generally, the RCM simulations are more accurate compared to the observed data for the Michigan region, while the difference between observed and simulated total annual precipitation is similarly inaccurate for the Indiana and Illinois regions. MRI overestimates total annual precipitation the most in all three regions, followed by CNRM, and then IPSL and MIROC. However, after thresholds are applied, many of the simulations are not significantly different from observed values.

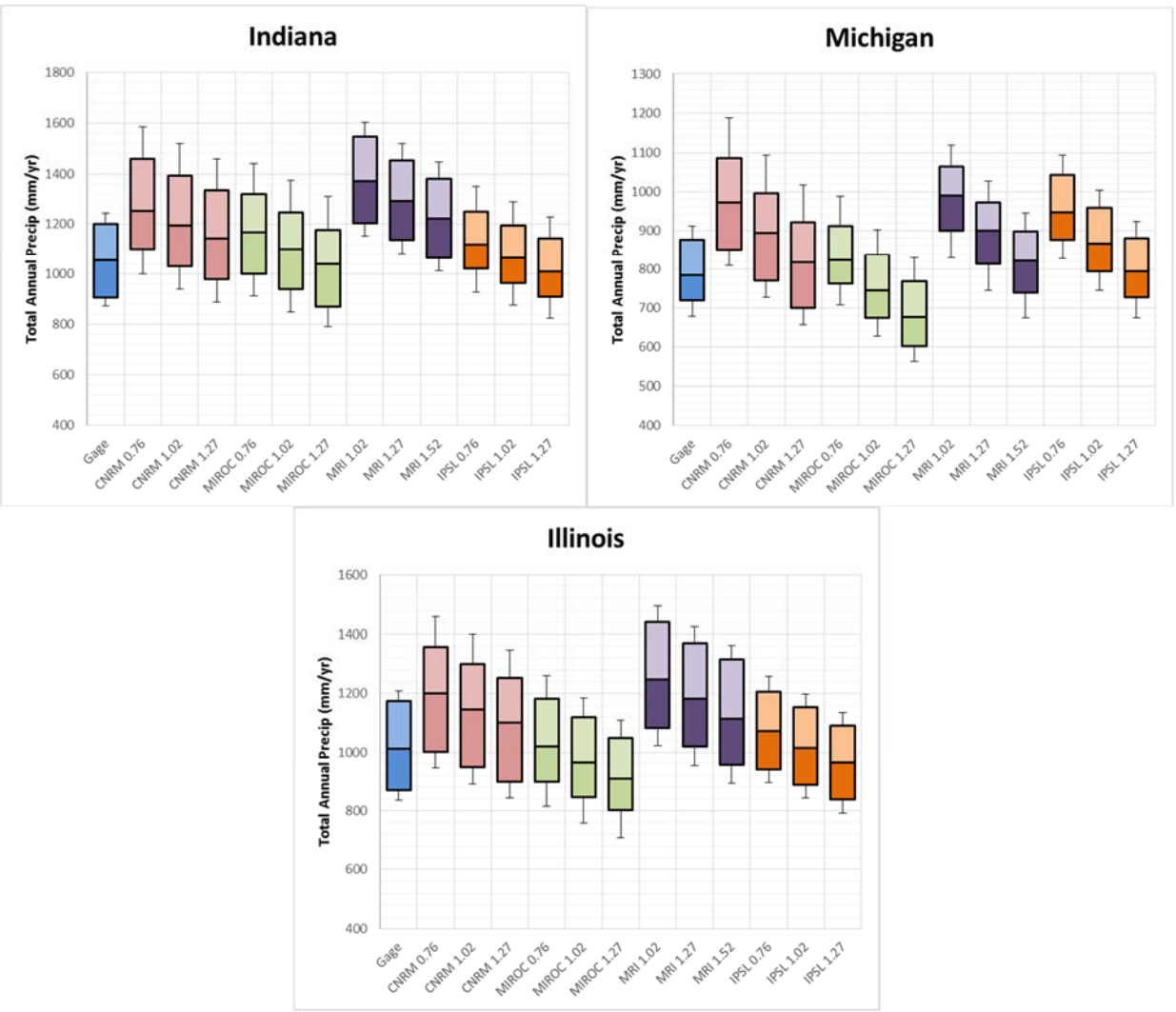

Figure 5.3. Box-whisker plots of observed and modeled (1980-1999) total annual precipitation (mm/yr) for thresholds of 0.76mm, 1.02mm, 1.27mm, and 1.52mm. Solid box denotes 25th to 75th percentiles and middle line denotes median. The whiskers denote the average +/- the standard deviation.

Figure 5.4 shows a box-whisker plot for each region with observed and RCM simulated 1-hr AMS, to which the thresholds were applied. The simulated RCM 1-hr AMS are more accurate compared to the observed data for the Michigan region, while the difference between observed and simulated 1-hr AMS is similarly inaccurate for the Indiana and Illinois regions. For Illinois and Indiana the average simulated 1-hr AMS is 50%-100% larger than the observed while the average simulated Michigan 1-hr AMS is 30%-75% larger than the observed. As expected, small precipitation thresholds have no effect on the annual maximum values.

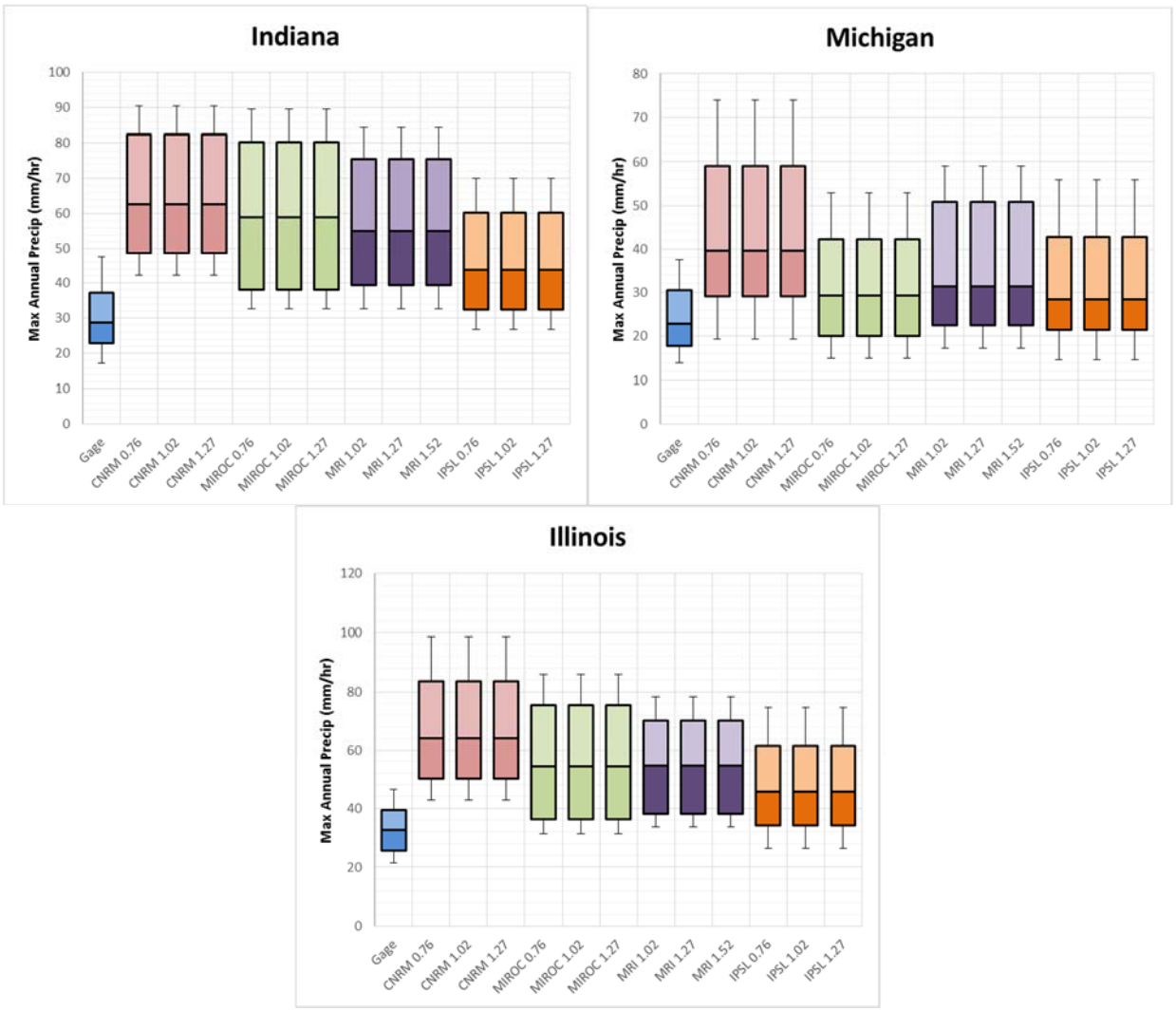

Figure 5.4. Box-whisker plots of observed and modeled (1980-1999) maximum 1hr precipitation (mm/hr) for thresholds of 0.76mm, 1.02mm, 1.27mm, and 1.52mm. Solid box denotes 25th to 75th percentiles and middle line denotes median. The whiskers denote the average +/- the standard deviation.

The first step in precipitation bias correction is to adjust the frequency of precipitation events to match observed events. Figure 5.5 is a box-whisker plot for each region with observed and RCM simulated total annual wet hours, to which the thresholds were applied. A single precipitation threshold was selected for each RCM to simplify subsequent bias correction, if needed. Results indicate that RCMs CNRM, MIROC, and IPSL most closely match observed total annual wet hours when a threshold precipitation of 1.02 mm (0.04 in) is applied. For RCM MRI, the optimum threshold is 1.27 mm (0.05 in).

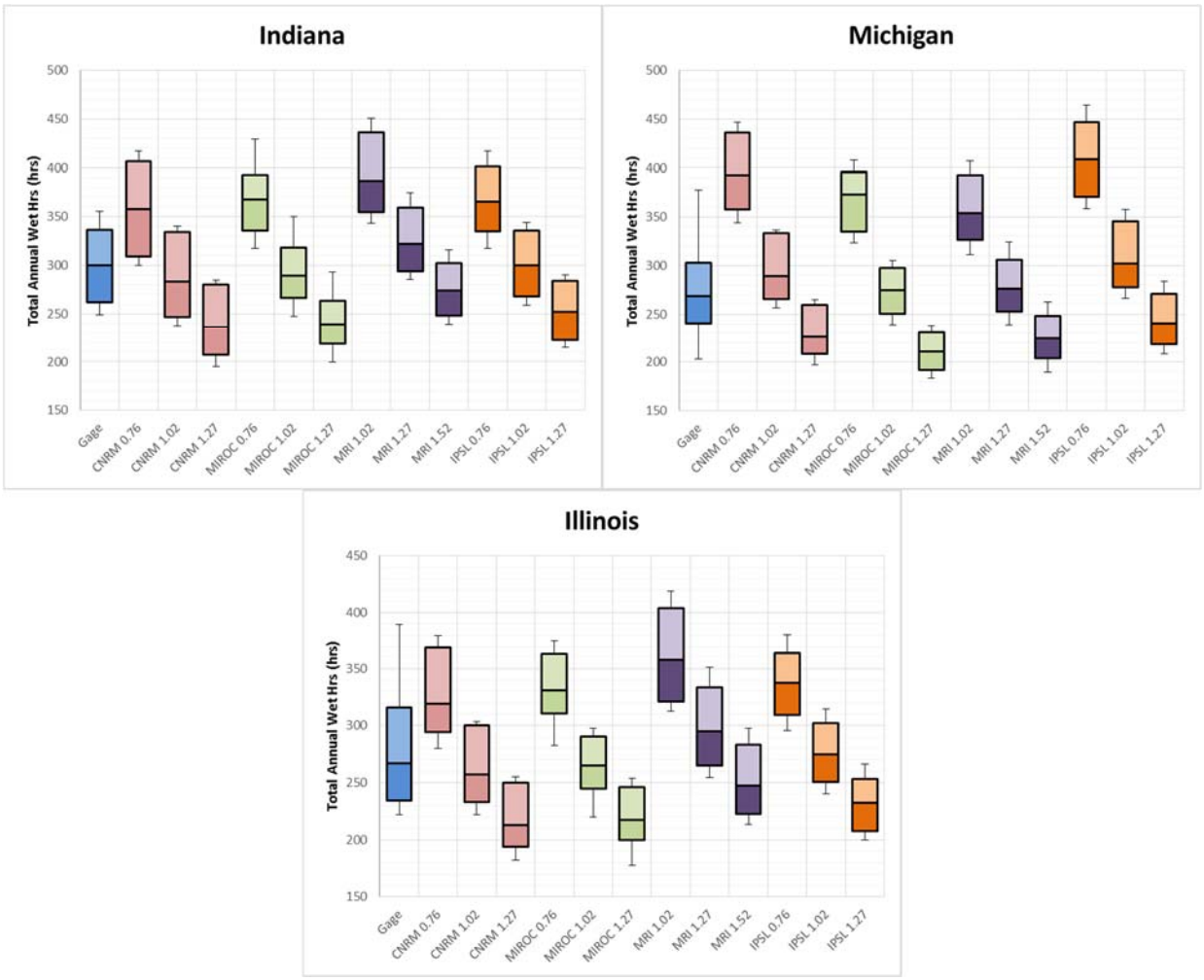

Figure 5.5. Box-whisker plots of observed and modeled (1980-1999) total annual wet hours for thresholds of 0.76mm, 1.02mm, 1.27mm, and 1.52mm. Solid box denotes 25th to 75th percentiles and middle line denotes median. The whiskers denote the average +/- the standard deviation.

Given the precipitation thresholds of 1.02 mm for CNRM, MIROC, and IPSL, and 1.27 mm for MRI, the following analyses of raw (not bias corrected) RCM simulations and projections were completed to determine if further bias correction was needed. Figure 5.6 shows a box-whisker plot for each region with observed and RCM simulated and projected total annual precipitation, to which the final thresholds were applied. The simulated values are generally within range of the observed, CNRM and MRI simulations tend to be higher than observed. The projected total annual precipitation values are all higher than the observed and simulated values, sometimes significantly.

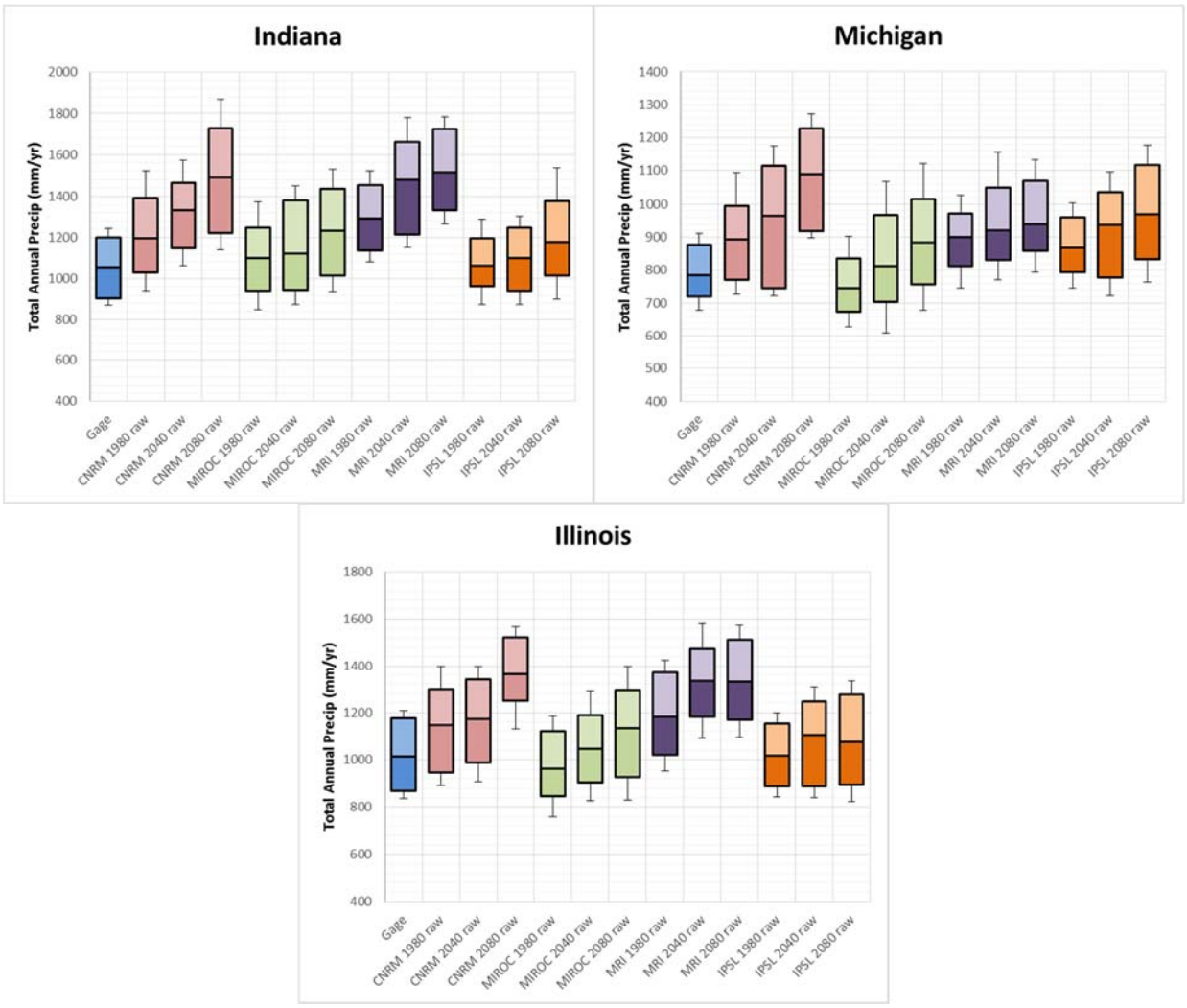

Figure 5.6. Box-whisker plots of observed and modeled (1980-1999, 2040-2059, and 2080-2099) raw total annual precipitation (mm/yr) for a threshold of 1.02mm for CNRM, IPSL, and MIROC, and a threshold of 1.27mm for MRI. Solid box denotes 25th to 75th percentiles and middle line denotes median. The whiskers denote the average +/- the standard deviation.

Figure 5.7 shows a box-whisker plot for each region with observed and RCM simulated and projected 1-hr AMS, to which the final thresholds were applied. The simulated and projected values are significantly higher than observed values for the Illinois and Indiana regions, while simulated values in the Michigan regions are also higher, though not always significantly. The significant difference between observed and RCM simulated 1-hr AMS suggests the RCMs need to be bias corrected so that the intensity of the latter agrees with the intensity of the former.

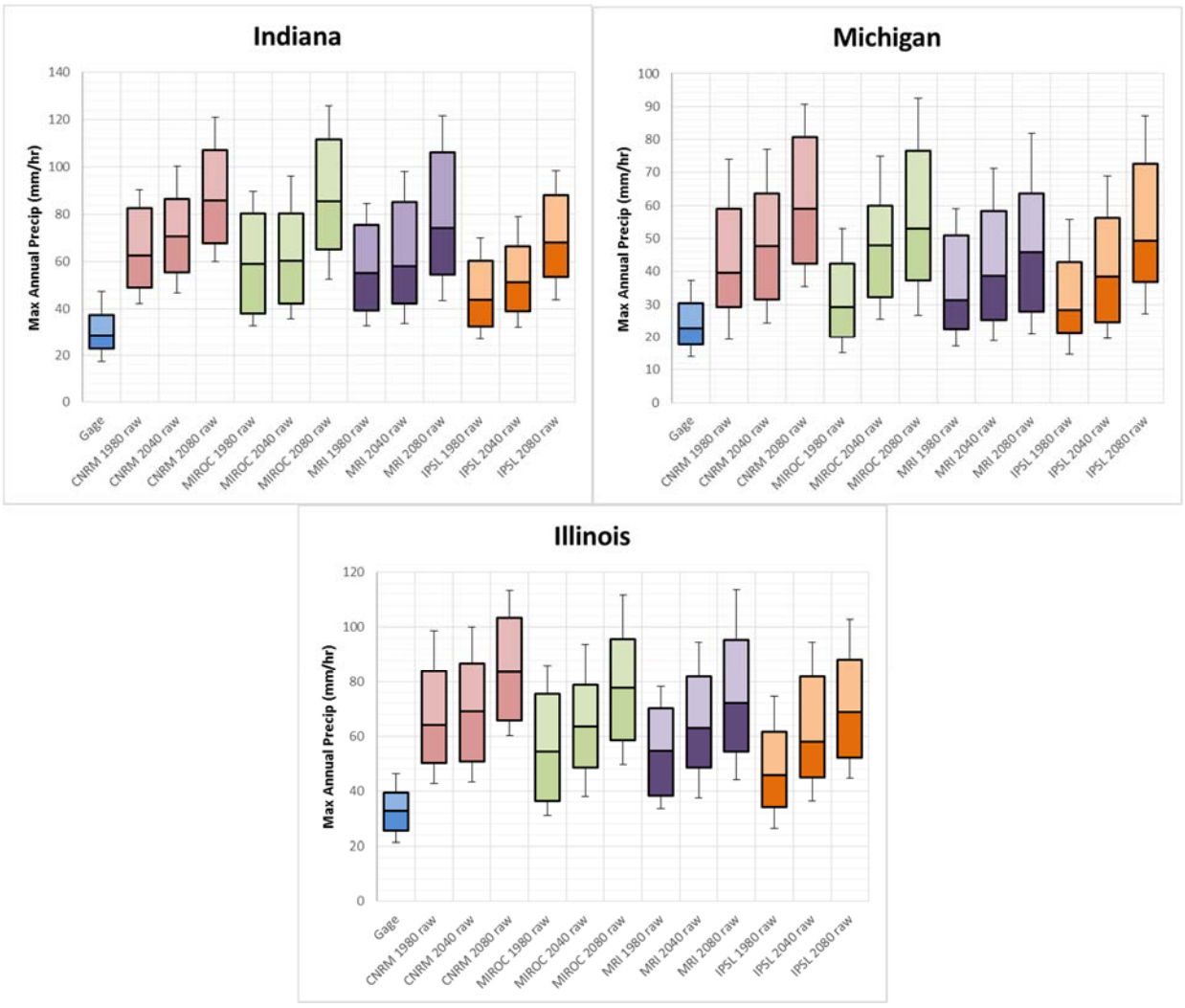

Figure 5.7. Box-whisker plots of observed and modeled (1980-1999, 2040-2059, and 2080-2099) raw maximum 1hr precipitation (mm/yr) for a threshold of 1.02mm for CNRM, IPSL, and MIROC, and a threshold of 1.27mm for MRI. Solid box denotes 25th to 75th percentiles and middle line denotes median. The whiskers denote the average +/- the standard deviation.

In addition to 1-hr AMS, the 24-hr AMS was also analyzed to verify if the RCMs overestimated simulated storm intensity across a range of storm durations when compared to observed intensities of the same durations. The Figure 5.8 shows a box-whisker plot for each region with observed and RCM simulated and projected 24-hr AMS, to which the final thresholds were applied. The simulated and projected values are significantly higher than observed values for all regions. The significant difference between

observed and RCM simulated 24-hr AMS verifies the RCMs need to be bias corrected so that the intensity of the latter agrees with the intensity of the former.

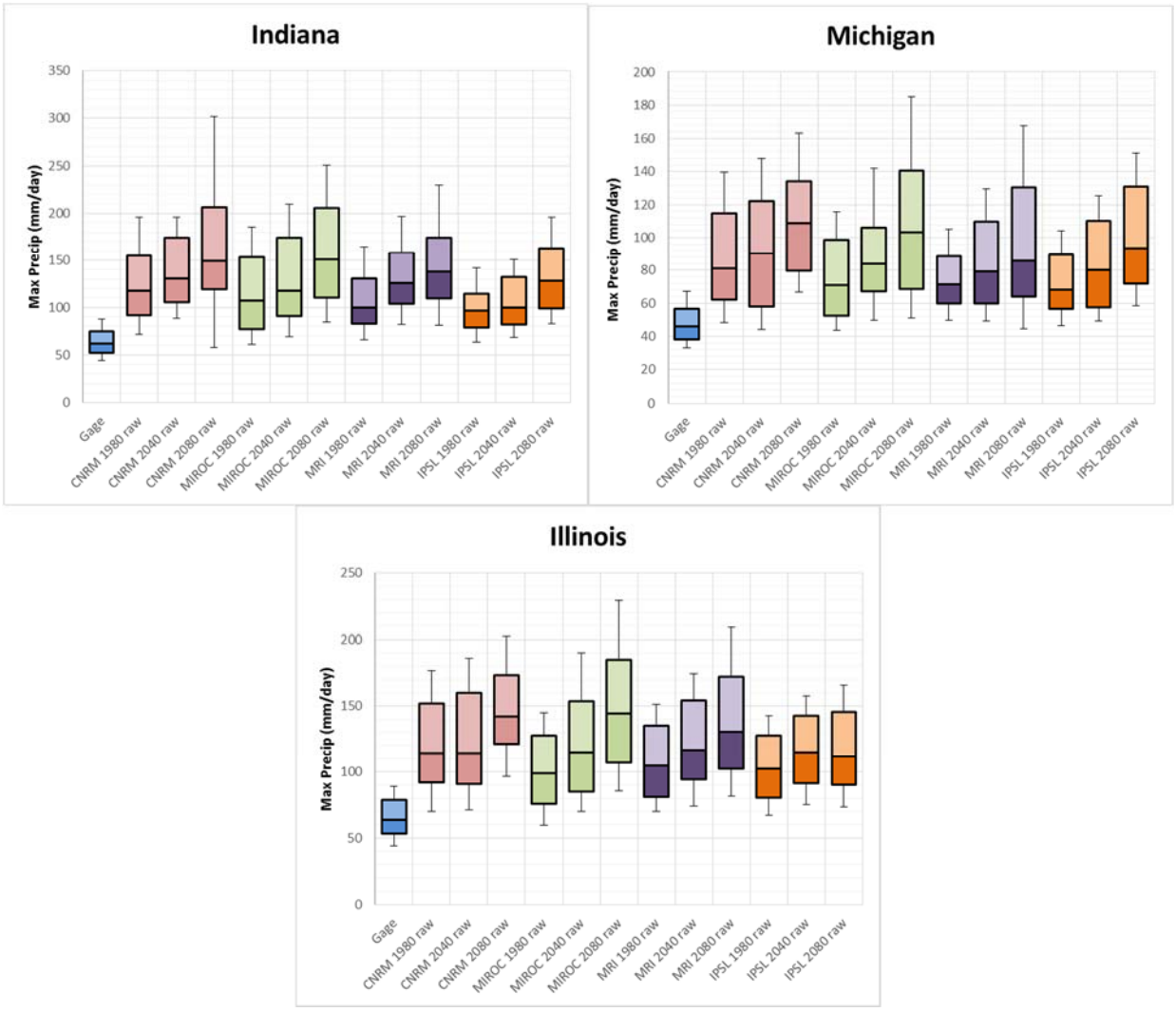

Figure 5.8. Box-whisker plots of observed and modeled (1980-1999, 2040-2059, and 2080-2099) raw maximum 24hr precipitation (mm/day) for a threshold of 1.02mm for CNRM, IPSL, and MIROC, and a threshold of 1.27mm for MRI. Solid box denotes 25th to 75th percentiles and middle line denotes median. The whiskers denote the average +/- the standard deviation.

A final check of total annual wet hours and wet days was completed for RCM simulated and projected precipitation and observed records. Figure 5.9 is a box-whisker plot for each region with observed and RCM simulated and projected total annual wet hours, to which the final thresholds were applied. One

threshold was applied to each RCM across all regions to simplify possible bias correction, but simulated and projected values are generally within range of observed values across all regions. CNRM and MRI suggest fairly constant wet hours through current century while MIROC and IPSL suggest decreasing total annual wet hours.

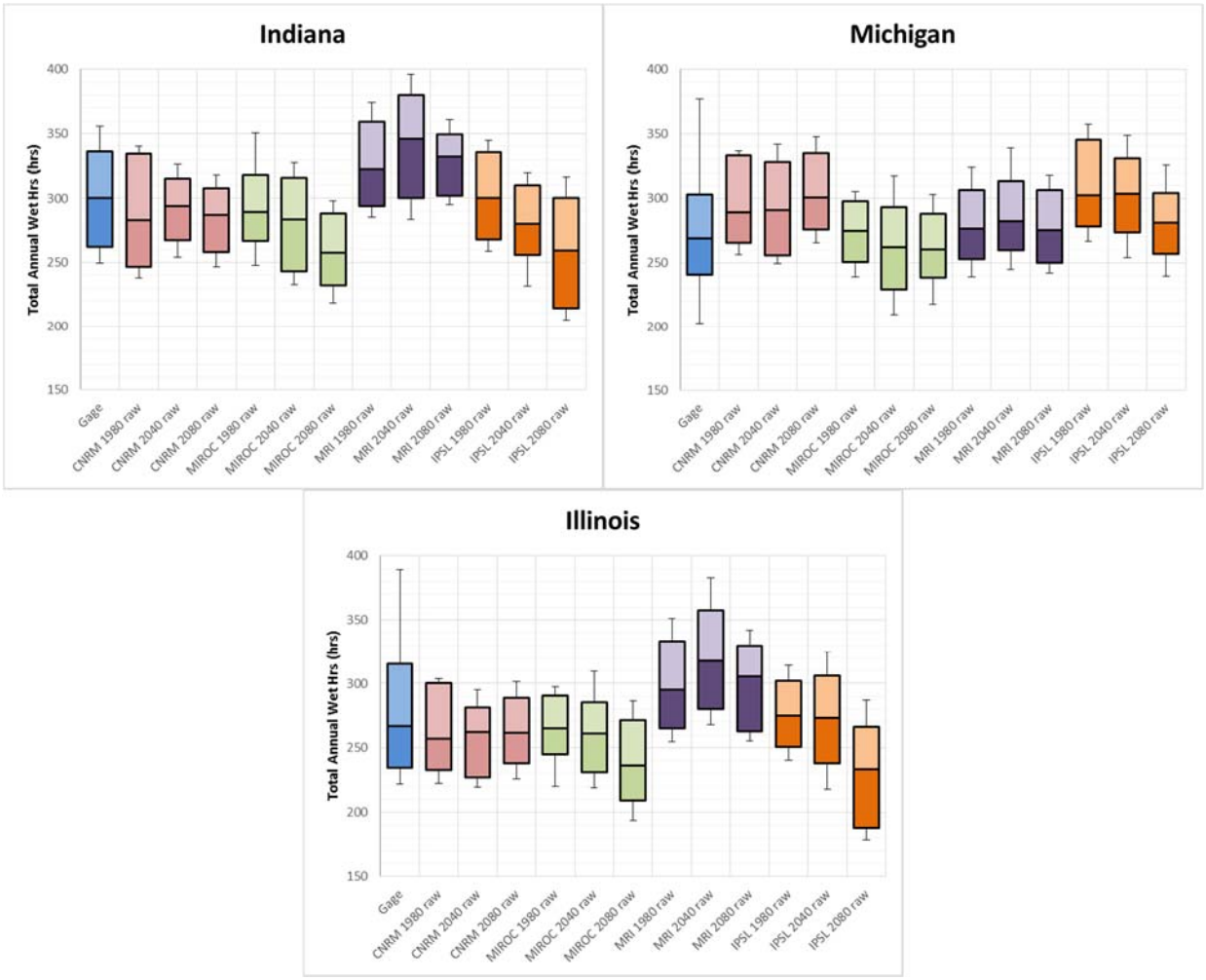

Figure 5.9. Box-whisker plots of observed and modeled (1980-1999, 2040-2059, and 2080-2099) raw total annual wet hours for a threshold of 1.02mm for CNRM, IPSL, and MIROC, and a threshold of 1.27mm for MRI. Solid box denotes 25th to 75th percentiles and middle line denotes median. The whiskers denote the average +/- the standard deviation.

Figure 5.10 is a box-whisker plot for each region with observed and RCM simulated and projected total annual wet days (calendar days), to which the final thresholds were applied. Again, CNRM and MRI suggest fairly constant wet days through current century while MIROC and IPSL suggest decreasing total

annual wet days. CNRM, MIROC, and IPSL underestimate total annual wet days for the Illinois region while MRI matches the observed data well. CNRM and MRI over estimates wet days in the Michigan and Indiana regions, respectively, while the median for the models in each region of within 10% of the observed.

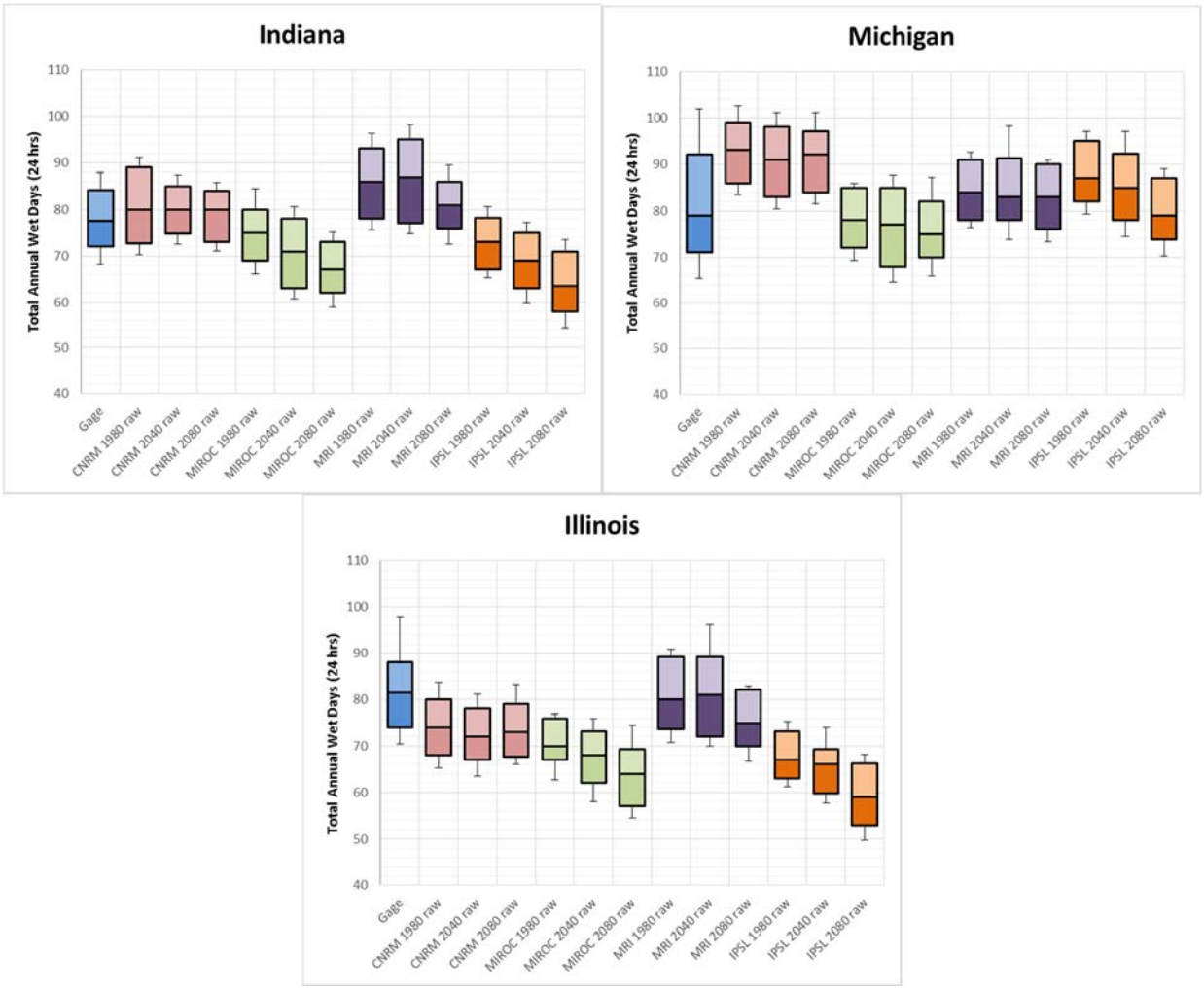

Figure 5.10. Box-whisker plots of observed and modeled (1980-1999, 2040-2059, and 2080-2099) raw total annual wet days (24hrs) for a threshold of 1.02mm for CNRM, IPSL, and MIROC, and a threshold of 1.27mm for MRI. Solid box denotes 25th to 75th percentiles and middle line denotes median. The whiskers denote the average +/- the standard deviation.

5.3.2 Quantile Mapping

The second step in precipitation bias correction is to adjust the intensity of the RCM simulations (1980-1999) to agree with the observed (1980-1999) intensity. Quantile mapping was applied so that the eCDF of the simulations (by grid output) were adjusted to agree with the eCDF of the observations from each corresponding gauge. Each eCDF covered all 20 years of applicable data. The same adjustments (as those applied to the simulations) were then applied to corresponding projected (2040-2059 and 2080-2099) eCDFs. Figure 5.11 shows the eCDF of the observed data at the Paris, IL gauge and the biased and corrected eCDFs of the IPSL simulated data for the corresponding model grid output. See Appendix B for figures of the same eCDFs for the Graying, MI and Columbus, IN gauge stations. The solids lines show the raw (biased) eCDFs of the simulated (blue) and projected (green and red) IPSL output while the observed eCDF is shown in gray. The dashed lines show the unbiased eCDFs, adjusted towards the

observed data.

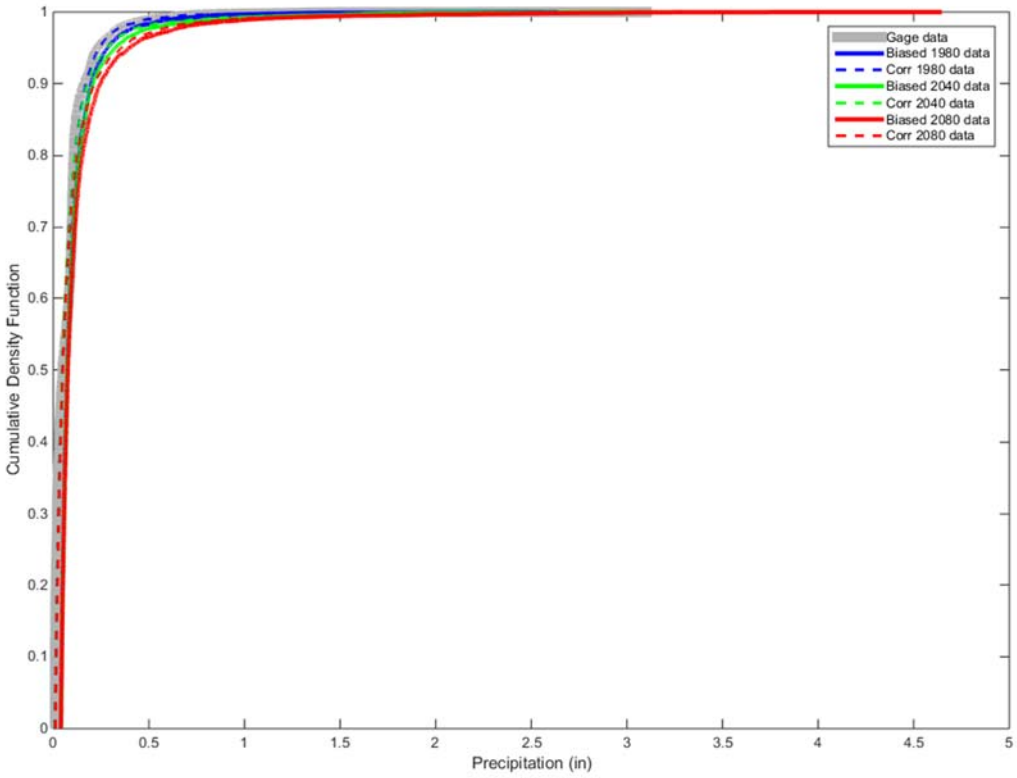

Figure 5.11. eCDFs of observed, and raw and corrected model (IPSL) simulation and model projections at Paris, IL using quantile mapping.

Figure 5.12 shows a zoomed in version of Figure 5.11 at two points to better display how the model output was adjusted towards the observed data. The raw simulatied eCDF (soid blue), to the right of the observed data, shows the overestimated storm intensity of the RCM output compared to the observed storm intensities. The bias corrected simuated eCDF (dash blue) has been shifted to the left and roughly matchs the observed eCDF. The projected eCDFs (solid green and red) were shifted by the same amount as the simulated eCDF to complete the bias correction.

Near the end of observed eCDF, which deontes the most extreme precipitation and the largest ARIs, the simulated eCDF was also adjected to match the observed eCDF. For this example the highest observed

precipitation was 70.9 mm (2.79 in), to which the maximum simulated output was adjusted to 70.1 mm (2.76 in). Accurate quantile mapping enabled RCM simulated precipitation intensities to closely match observed precipitation intensities across the entire eCDFs. Figure 5.13 shows the quantile-quantile (q-q) plot of the observed (black "x"), IPSL simulated (blue, "x" is raw and "o" is bias corrected) and IPSL projected (green and red, "x" is raw and "o" is bias corrected) data at Paris, IL. A q-q plot is a graphical technique for determining if two data sets come from populations with a common distribution. The plot shows that the raw model data overestimates the observed data, especially for higher intensity storms. The bias corrected simulated data matches the observed data well, which is to be expected after the application of quantile mapping. The projected rainfall data, even after bias correction, is more intense than observed data, which means the RCM projects more intense rainfall in the latter half of the 21st century than was recorded at the end of the 20th century.

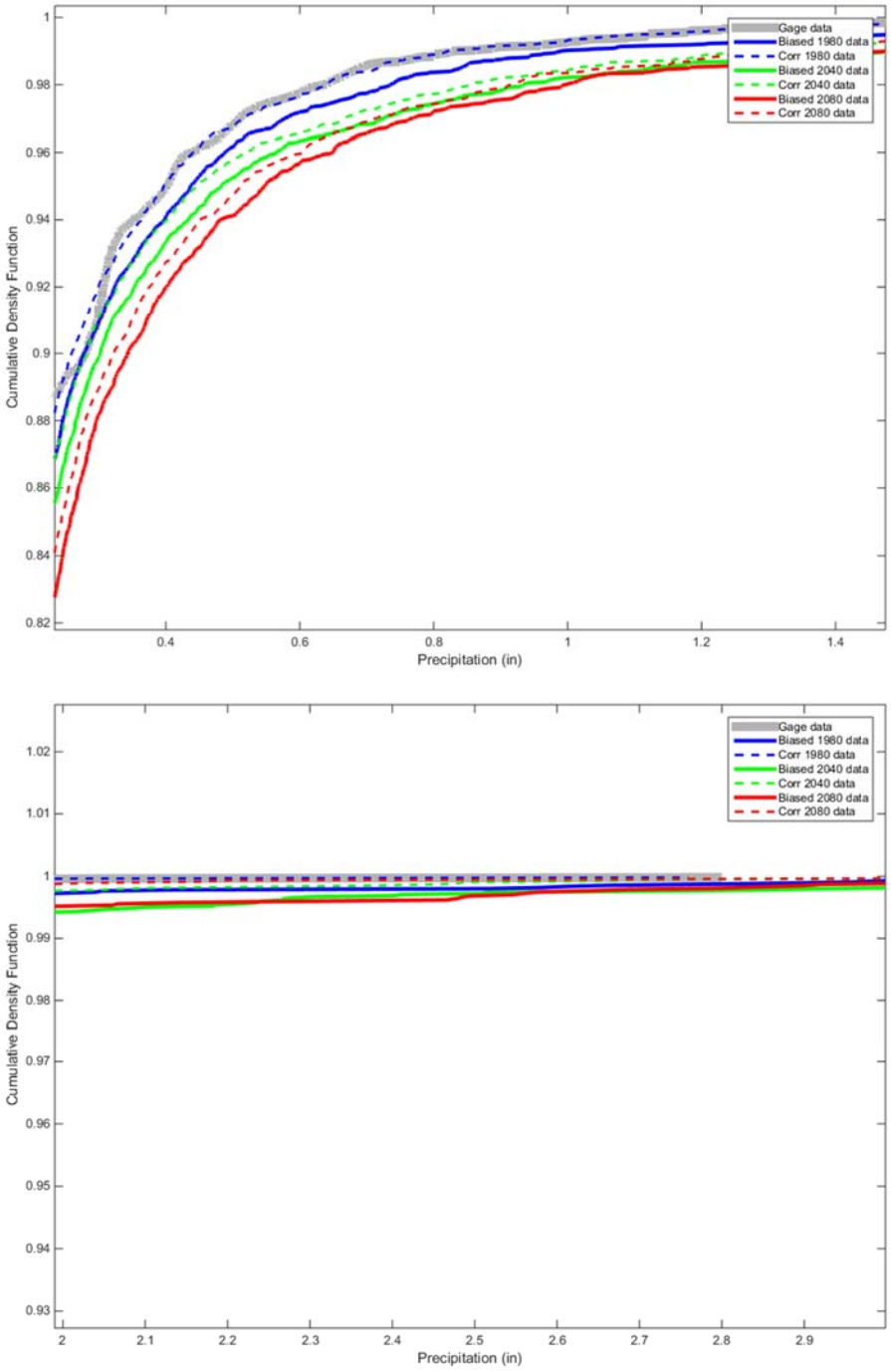

Figure 5.12. Zoomed in eCDFs of observed, and raw and corrected model (IPSL) simulation and model projections at Paris, IL using quantile mapping.

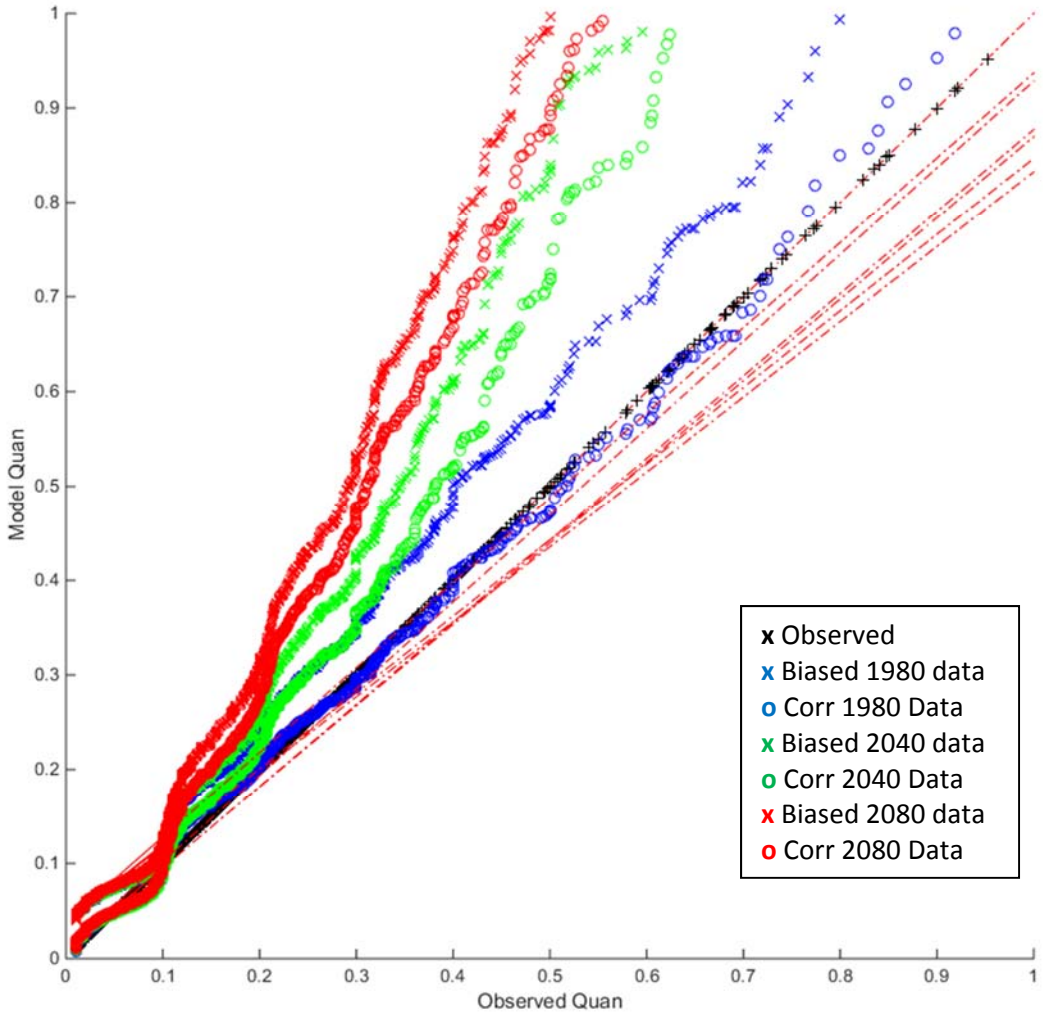

Figure 5.13. Quantile-quantile plot of observed vs raw and corrected model (IPSL) simulation and model projections at Paris, IL using quantile mapping. "X" is biased (raw), "O" is corrected.

Quantile mapping was also applied by month so that for a given time frame (20 years in this study) 12 eCDFs (one for each month) were created for model projection and simulations, and the observations and adjusted separately. Figure 5.14 shows monthly eCDFs for observed and raw and corrected IPSL simulated and projected data at Paris, IL. See Appendix B for figures of the same monthly eCDFs for the Graying, MI and Columbus, IN gauge stations. Due to month to month variations in the RCM simulated data, bias correction often produced extreme maximum precipitation values for projected data. In

some months the simulated model precipitation would severely underestimate observed precipitation, causing projected precipitation to increase greatly in magnitude post bias correction. Figure 5.15 shows a few examples of monthly q-q plots at Grayling, MI which illustrate the variations in monthly modeled precipitation and extreme outliers that persist or are amplified by the quantile mapping process.

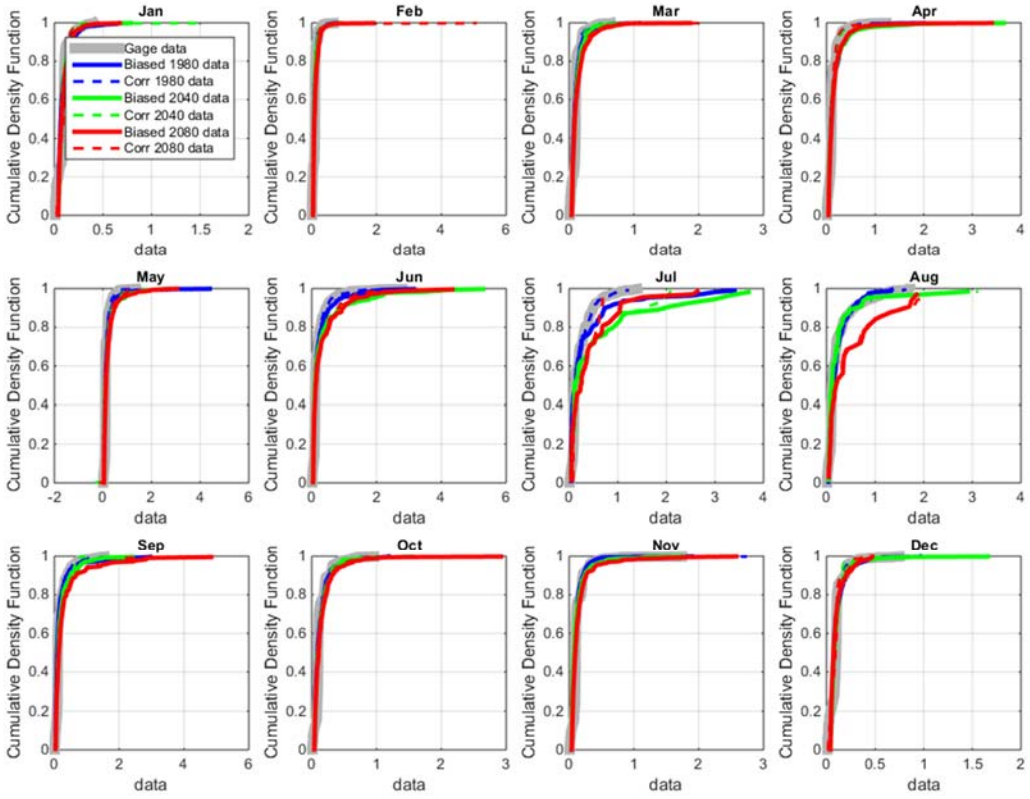

Figure 5.14. Monthly eCDFs of observed, and raw and corrected model (IPSL) simulation and model projections at Paris, IL using quantile mapping.

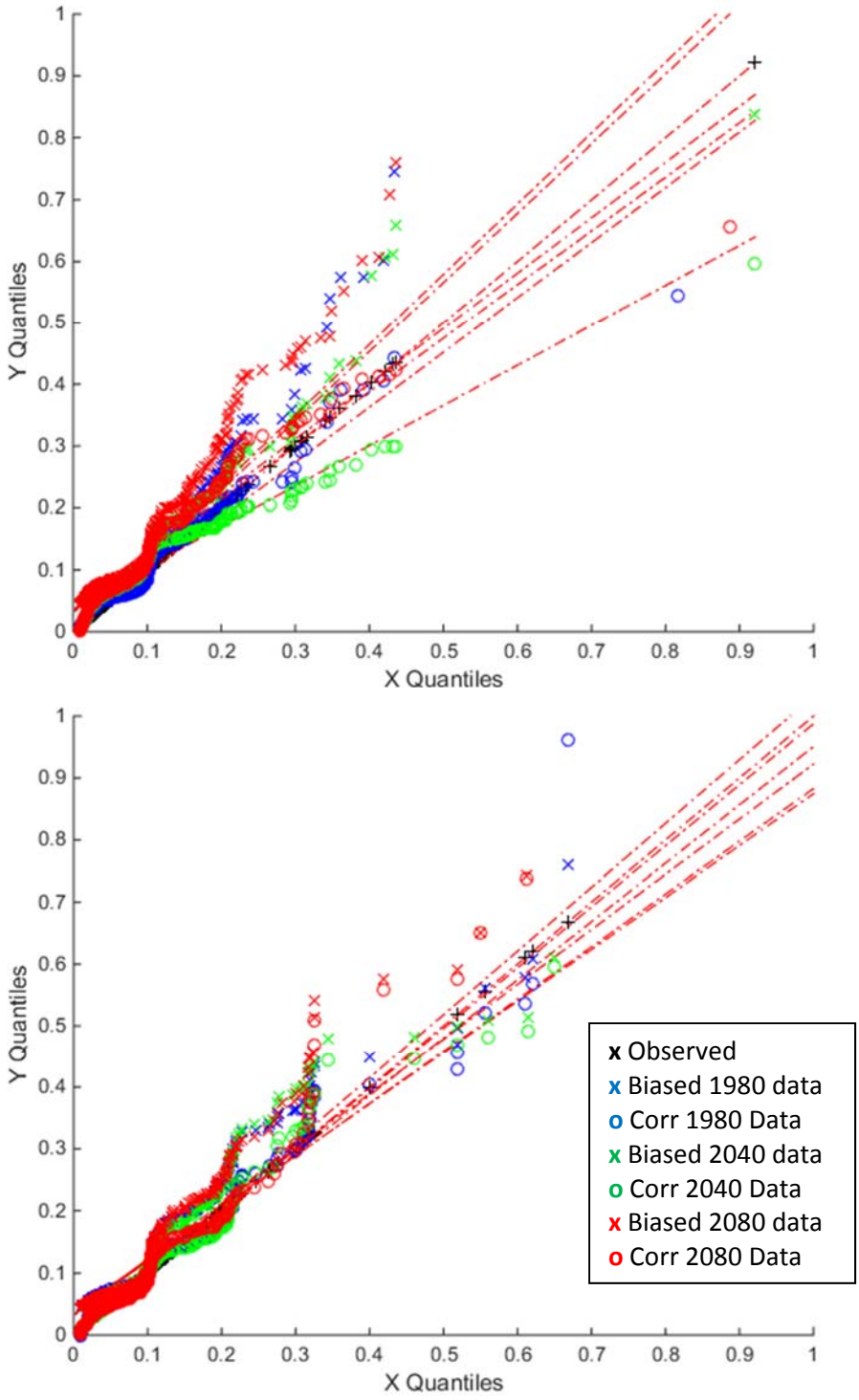

Figure 5.15. Quantile-quantile plots of April and October observed vs raw and corrected model (IPSL) simulation and model projections at Grayling, MI using quantile mapping. "X" is raw, "O" is corrected.

5.3.3 Trend Comparison

After completion of quantile mapping bias correction, RCM precipitation outputs were again compared to observed precipitation to assess post correction trends and ensure the bias correction procedure successfully adjusted precipitation intensities. Figure 5.16 shows a box-whisker plot for each region with observed and bias corrected RCM simulated and projected total annual precipitation. The simulated values are very similar to the observed for all regions and models. The projected total annual precipitation values are all higher than the observed and simulated values, sometimes significantly.

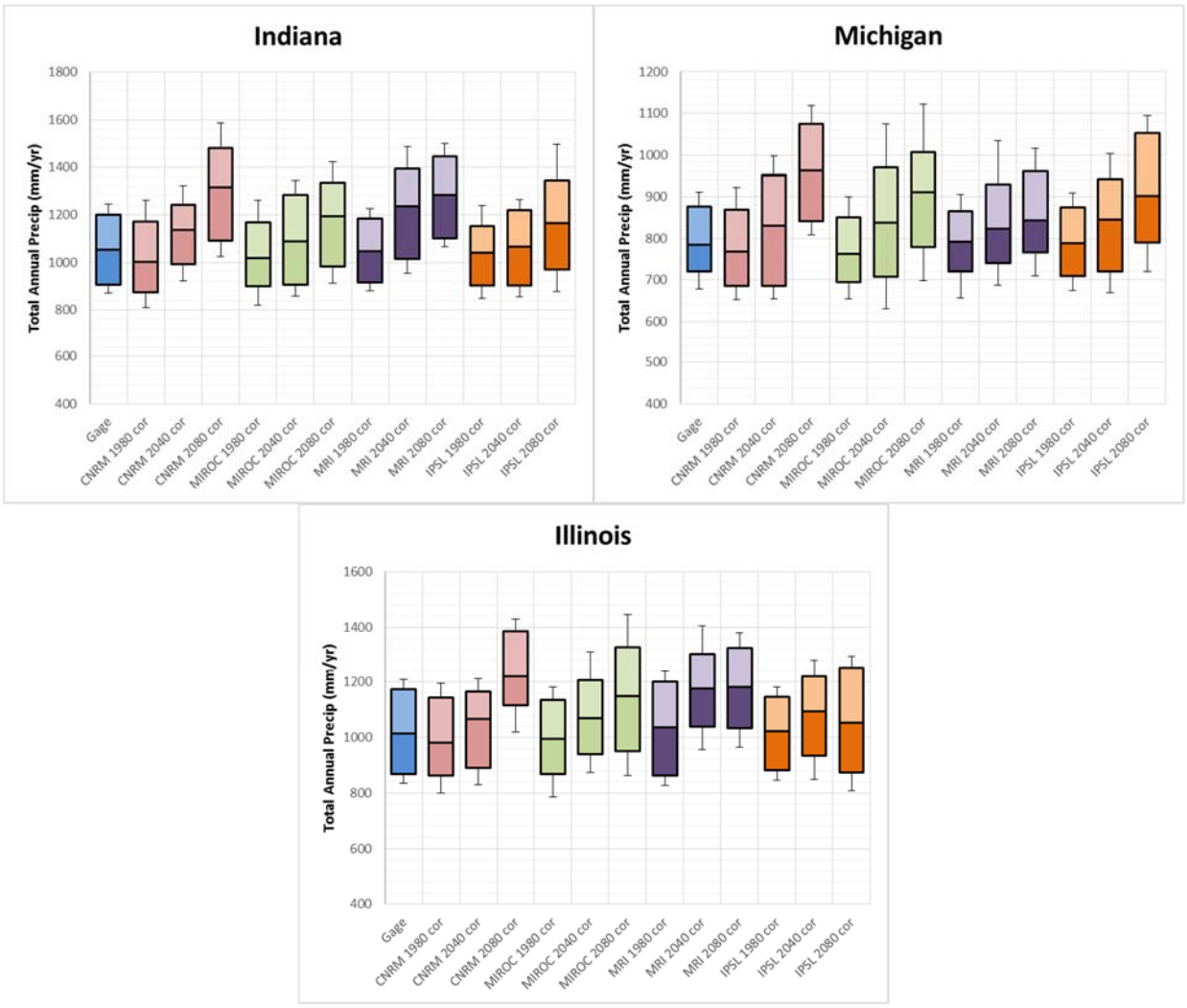

Figure 5.16. Box-whisker plots of observed and modeled (1980-1999, 2040-2059, and 2080-2099) corrected total annual precipitation (mm/yr) for a threshold of 1.02mm for CNRM, IPSL, and MIROC, and a threshold of 1.27mm for MRI. Solid box denotes 25th to 75th percentiles and middle line denotes median. The whiskers denote the average +/- the standard deviation.

Figure 5.17 shows a box-whisker plot for each region with observed and bias corrected RCM simulated and projected 1-hr AMS. The simulated values are consistent with the observed for all regions and models, suggesting bias correction was successful. The 2040-2059 projected 1-hr AMS values are typically marginally higher than the observed/simulated values, while the 2080-2099 projected 1-hr AMS values are mostly significantly higher than the observed/simulated values

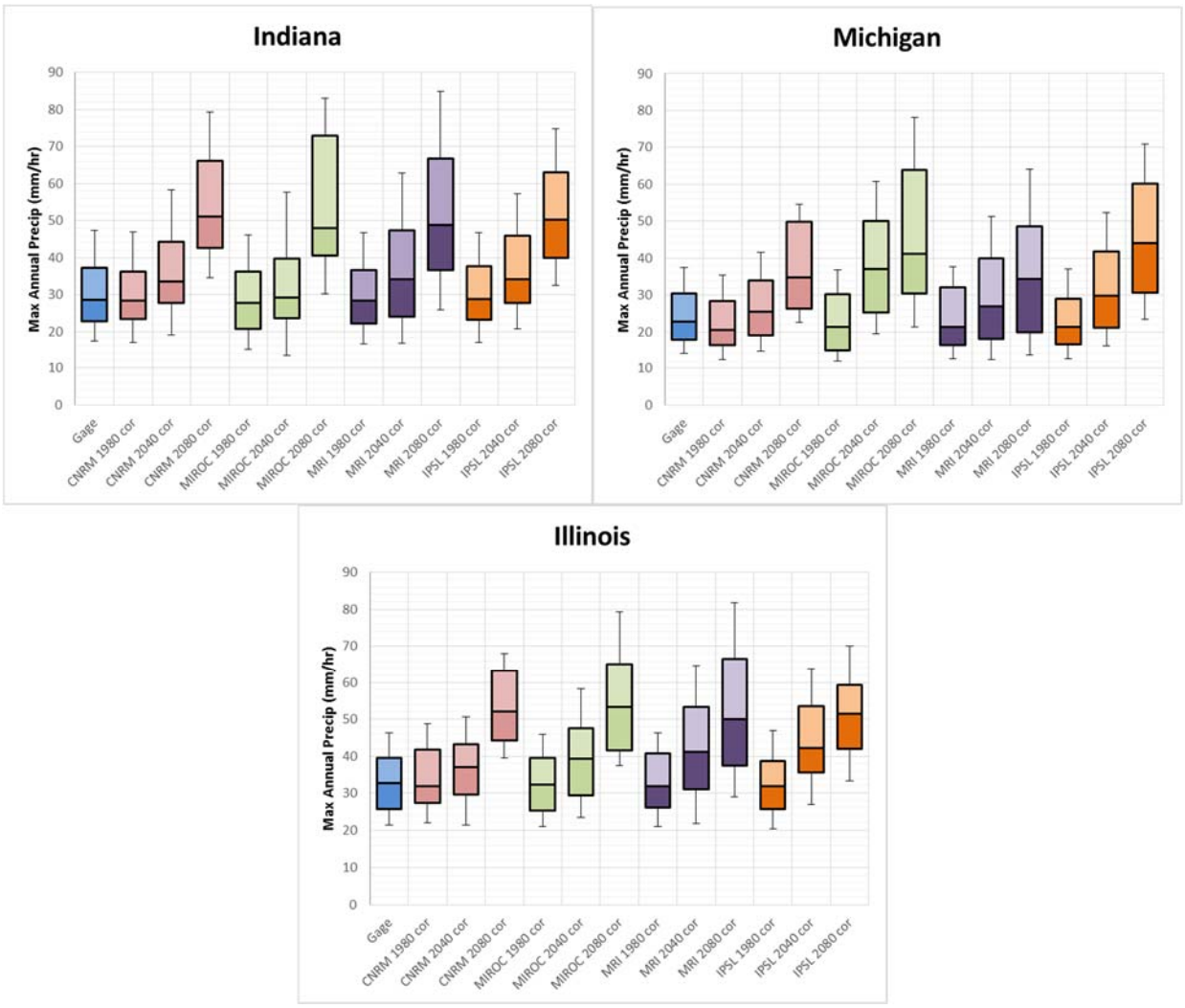

Figure 5.17. Box-whisker plots of observed and modeled (1980-1999, 2040-2059, and 2080-2099) corrected maximum 1hr precipitation (mm/hr) for a threshold of 1.02mm for CNRM, IPSL, and MIROC, and a threshold of 1.27mm for MRI. Solid box denotes 25th to 75th percentiles and middle line denotes median. The whiskers denote the average +/- the standard deviation.

Figure 5.18 shows a box-whisker plot for each region with observed and bias corrected RCM simulated and projected 24-hr AMS. The simulated values are consistent with the observed for all regions and models. The 2040-2059 projected 24-hr AMS values are typically marginally higher than the observed/simulated values, while the 2080-2099 projected 24-hr AMS values are mostly marginally higher than the 2040-2059 values.

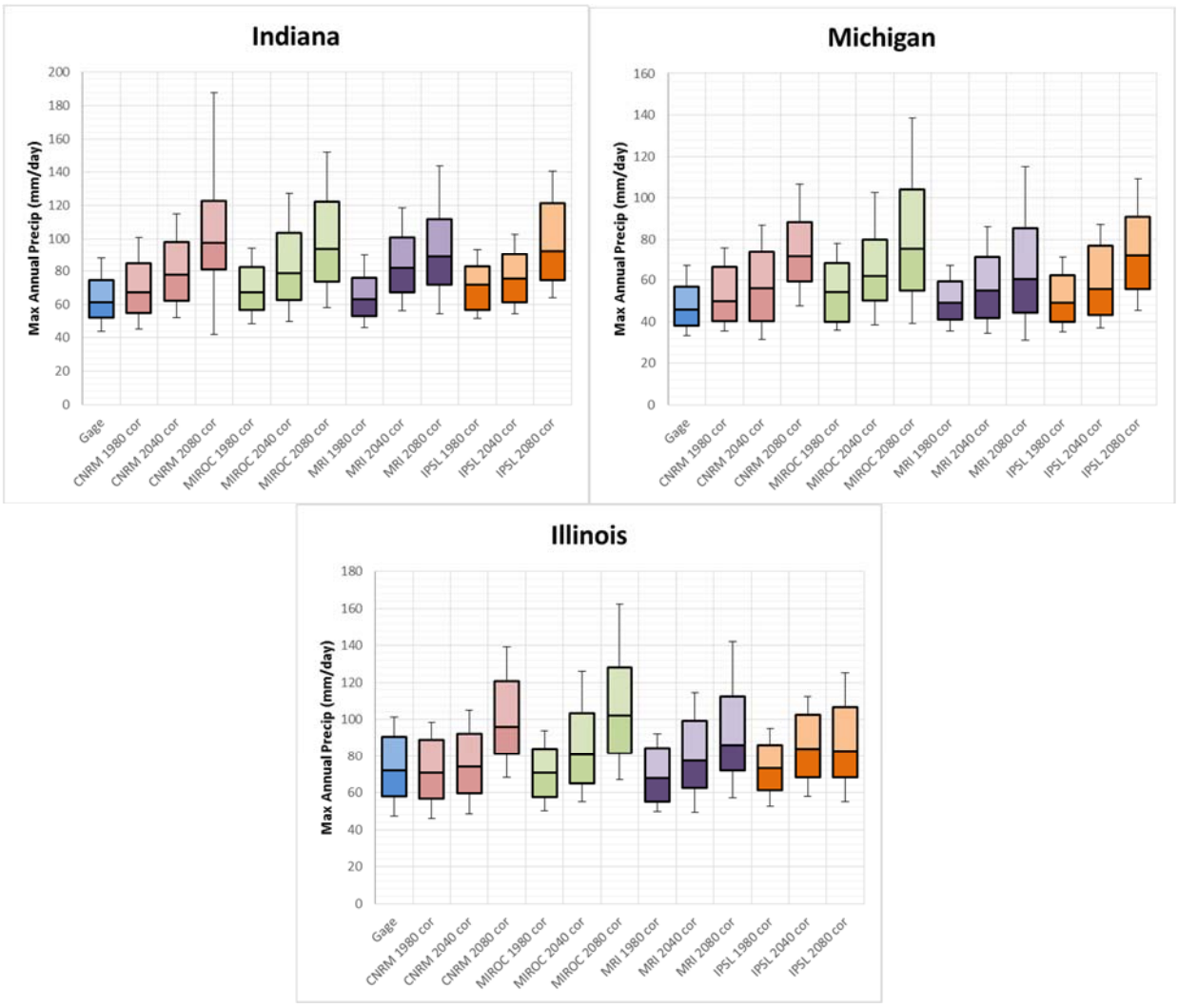

Figure 5.18. Box-whisker plots of observed and modeled (1980-1999, 2040-2059, and 2080-2099) corrected maximum 24hr precipitation (mm/day) for a threshold of 1.02mm for CNRM, IPSL, and MIROC, and a threshold of 1.27mm for MRI. Solid box denotes 25th to 75th percentiles and middle line denotes median. The whiskers denote the average +/- the standard deviation.

In addition comparing bias corrected model output with observed data, the trend of each were compared. Figure 5.19 shows, for each region, the observed average total annual precipitation ("o") and the bias corrected average RCM total annual precipitation ("x") for all four models. The linear trend in observed data (see Figure 4.3, Figure 4.6, and Figure 4.9) is denoted by a dashed line and the linear trend in average RCM data is denoted by a solid line. The trends in total annual precipitation match in slope and magnitude for the Michigan. Trend slope and magnitude are comparable for the Indiana

region, though modeled total annual precipitation rises slightly slower than the averaged observed trend suggests. The averaged observed Illinois trend rises more quickly than the averaged RCM perception.

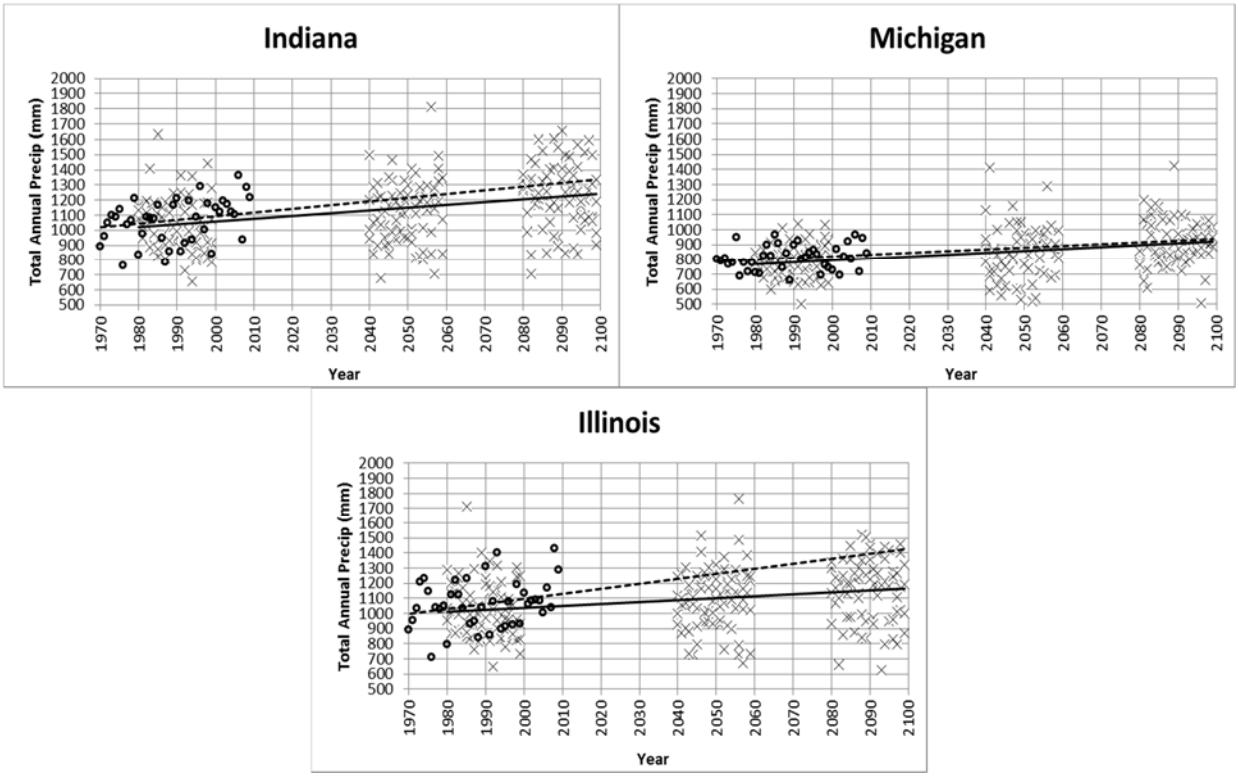

Figure 5.19. Average total annual observed (1970-2007), simulated (1980-1999), and projected (2040-2059 and 2080-2099) precipitation for the Indiana, Michigan, and Illinois regions. Observed is denoted with "o" and model is denoted with "x". Solid line is a linear fit of all modeled data (time frames and RCMs). Dashed line is a linear fit of available average observed data projected forward to the year 2099.

With regards to 1-hr and 24-hr AMS, Figure 5.20 shows, for each region, the observed average 1-hr and 24-hr AMS ("o") and the bias corrected average RCM 1-hr and 24-hr AMS ("x") for all four models. The linear trend in observed data (see Figure 4.21, Figure 4.24, Figure 4.27, Figure 4.55, Figure 4.57, and Figure 4.59) is denoted by a dashed line and the linear trend in RCM data is denoted by a solid line. The observed 1-hr AMS trends in Indiana and Illinois are flat and decreasing insignificantly in Michigan. However, the RCM output trends are all increasing by more than 50% in 100 years. The observed 24-hr AMS trend in Michigan is flat, increasing insignificantly in Illinois, and increasing significantly in Indiana.

By 2099 the differences between observed projections and model projection are about 20 mm/hour and 20-30 mm/day for the 1-hr and 24-hr AMS, respectively.

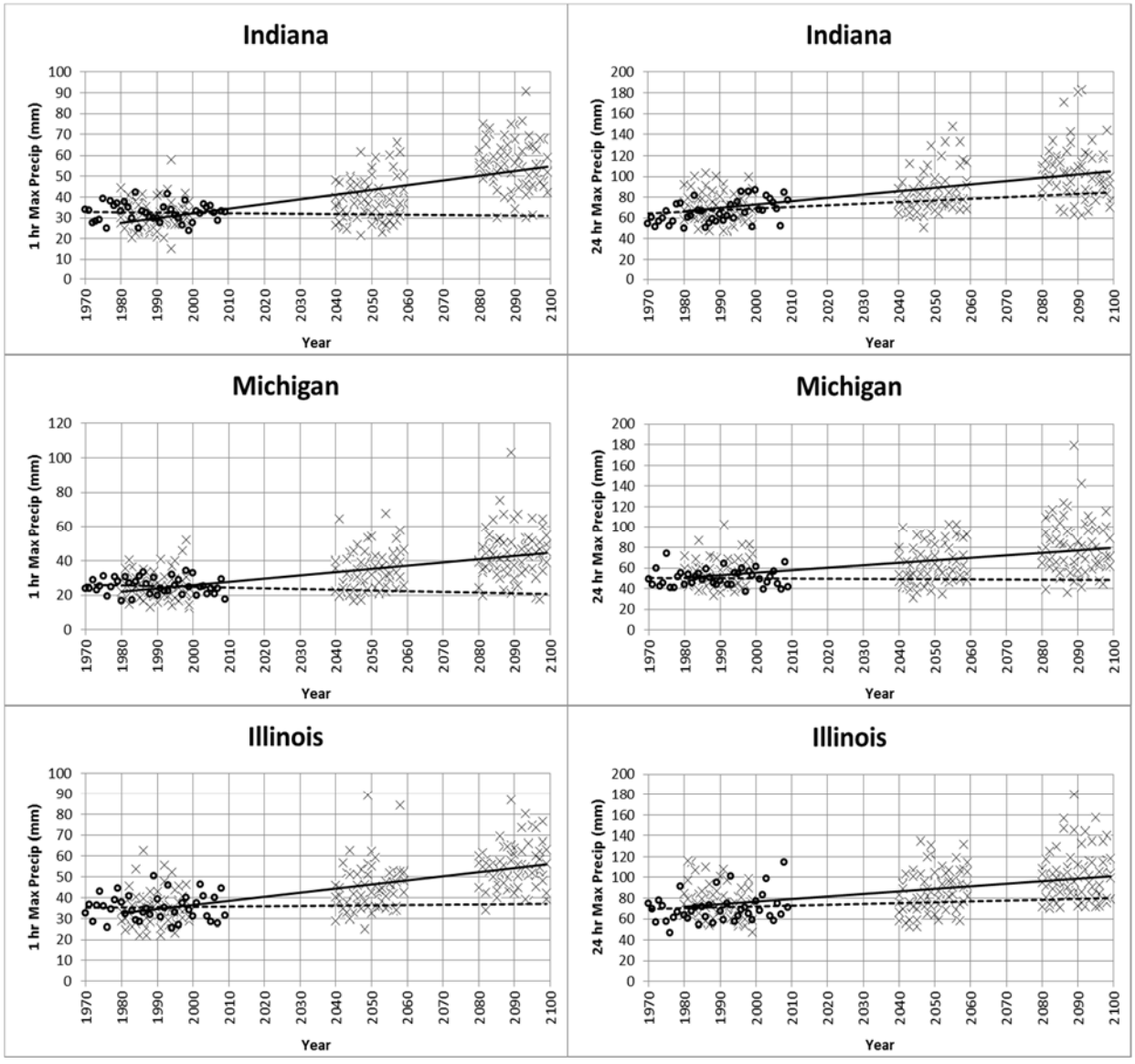

Figure 5.20. Average 1-hr and 24-hr observed (1970-2007), simulated (1980-1999), and projected (2040-2059 and 2080-2099) AMS for the Indiana, Michigan, and Illinois regions. Observed is denoted with "o" and model is denoted with "x". Solid line is a linear fit of all modeled data (time frames and RCMs). Dashed line is a linear fit of available average observed AMS projected forward to the year 2099.

5.3.4 L-Moment Analyses

Precipitation frequency analyses were completed for bias corrected RCM simulations and projections for each region/site using the regional L-Moments method. Precipitation magnitudes were found for the following durations (1-, 2-, 3-, 6-, 12-, and 24-hr; and 2-, 5-, and 10-day) and ARIs (0.5-, 1-, 2-, 5-, 10-, 25-, 50-, 100-year). Based on the discordance and heterogeneity measures it was determined that the regions are homogeneous. The RCM precipitation magnitudes for each duration and return period were compared with observed (1980-1999) data presented in Section 4.3.6.

First, changes in precipitation magnitudes were assessed between pre- and post-bias corrected RCM output compared to observed values. Figure 5.21 shows the percent difference between observed and pre- and post-bias corrected CNRM simulated and projected maximum precipitation distributions at Columbus, IN, Grayling, MI, and Paris, IL for a range of ARIs and durations of 1- and 24-hrs. See Appendix B for the same comparison of MRI, MIROC, and IPSL outputs. For 1-hr duration storms at Columbus, IN, the raw CNRM maximum precipitation was 40%-60% higher than the observed maximum precipitation, across all returns periods. After bias correction the difference was reduced to +/- 2%.

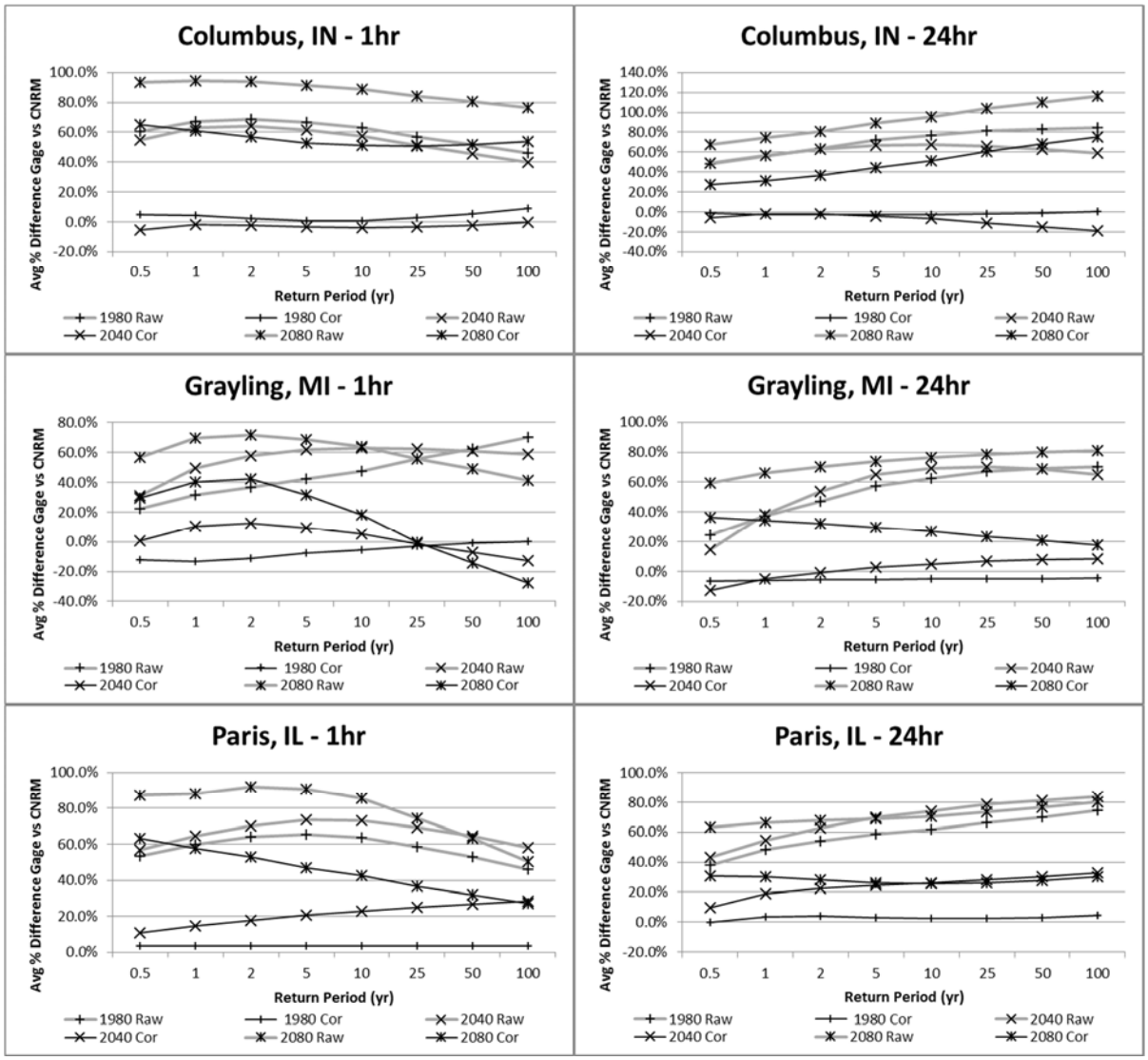

Figure 5.21. Average percent difference between observed (Gauge) and modeled (CNRM) simulation (1980-1999) and projections (2040-2059 and 2080-2099) estimated maximum precipitation for selected durations and return periods as determined by L-moments regional frequency analysis. Gauge data time frame is 1980-1999.

Figure 5.22, Figure 5.23, Figure 5.24, and Figure 5.25 show the maximum bias corrected CNRM, IPSL, MIROC, and MRI precipitation distributions (simulated and projected) at Columbus, IN for a range of ARIs and durations of 1-, 3-, 6-, 12-, and 24-hr and 5-days, respectively. Columbus, IN is the closest gauge site to Camp Atterbury. Observed (1980-1999) and NOAA Atlas 14 values are included for comparison. CNRM and IPSL provide similar results that indicate that for all storm durations the observed, simulated, and projected (2040-2059) values are all similar to Atlas 14 values. MIROC and MRI

return projected (2040-2059) maximum values that are larger than observed values for higher return periods. The projected (2080-2099) maximum precipitation for all four RCMs is significantly higher than observed values for all durations. The simulated values are very close to the observed values, as should be expected following bias correction. See Appendix B for tables showing the percent difference between the observed and projected precipitations at Columbus, IN for all storm durations and return periods as determined by the L-moments regional frequency analysis.

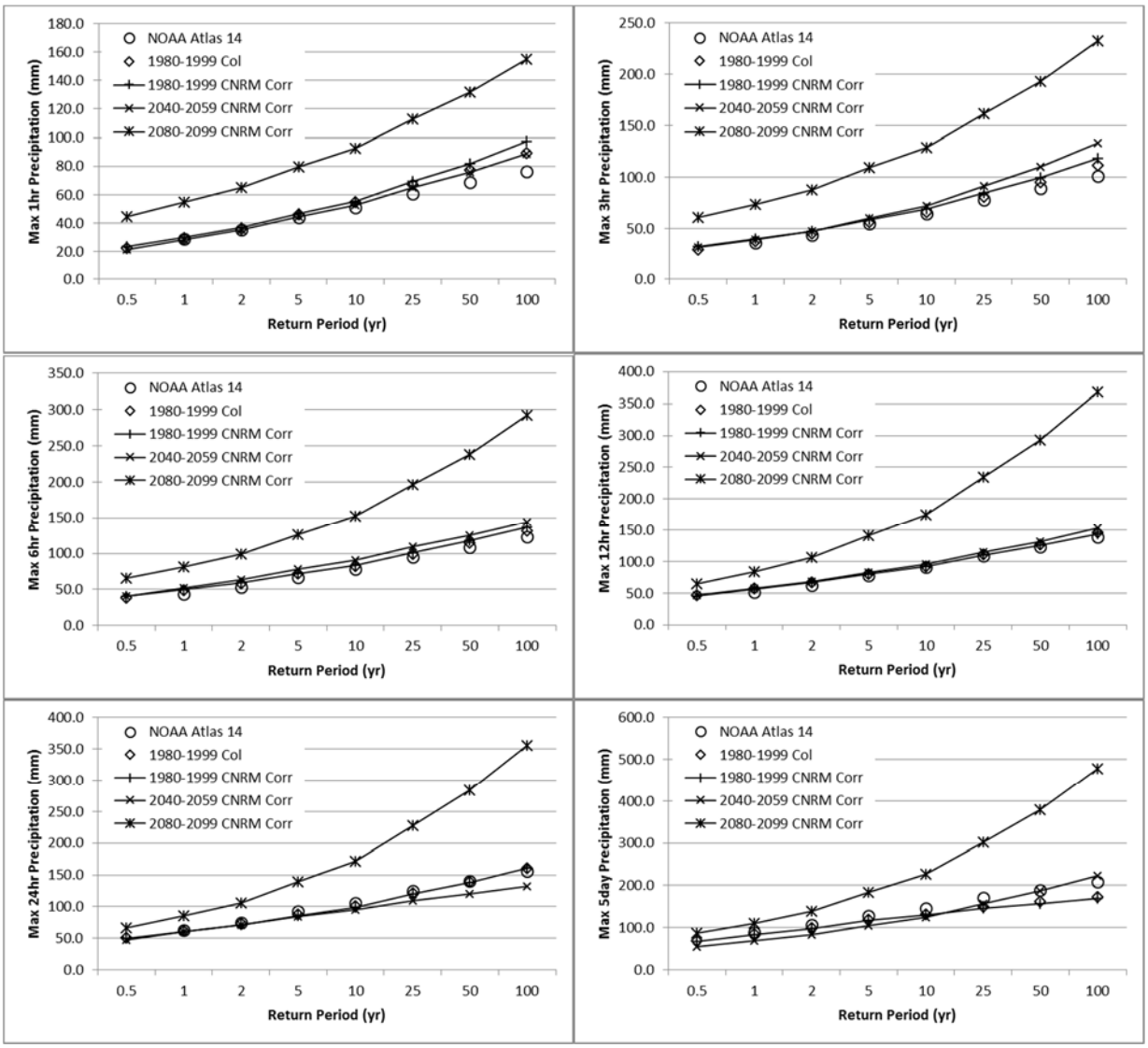

Figure 5.22. Comparison of modeled (CNRM) simulation (1980-1999) and projection (2040-2059 and 2080-2099) estimated maximum precipitation for selected durations and return periods as determined by L-moments regional frequency analysis at Columbus, Indiana. Atlas 14 and observed (1980-1999) values also included.

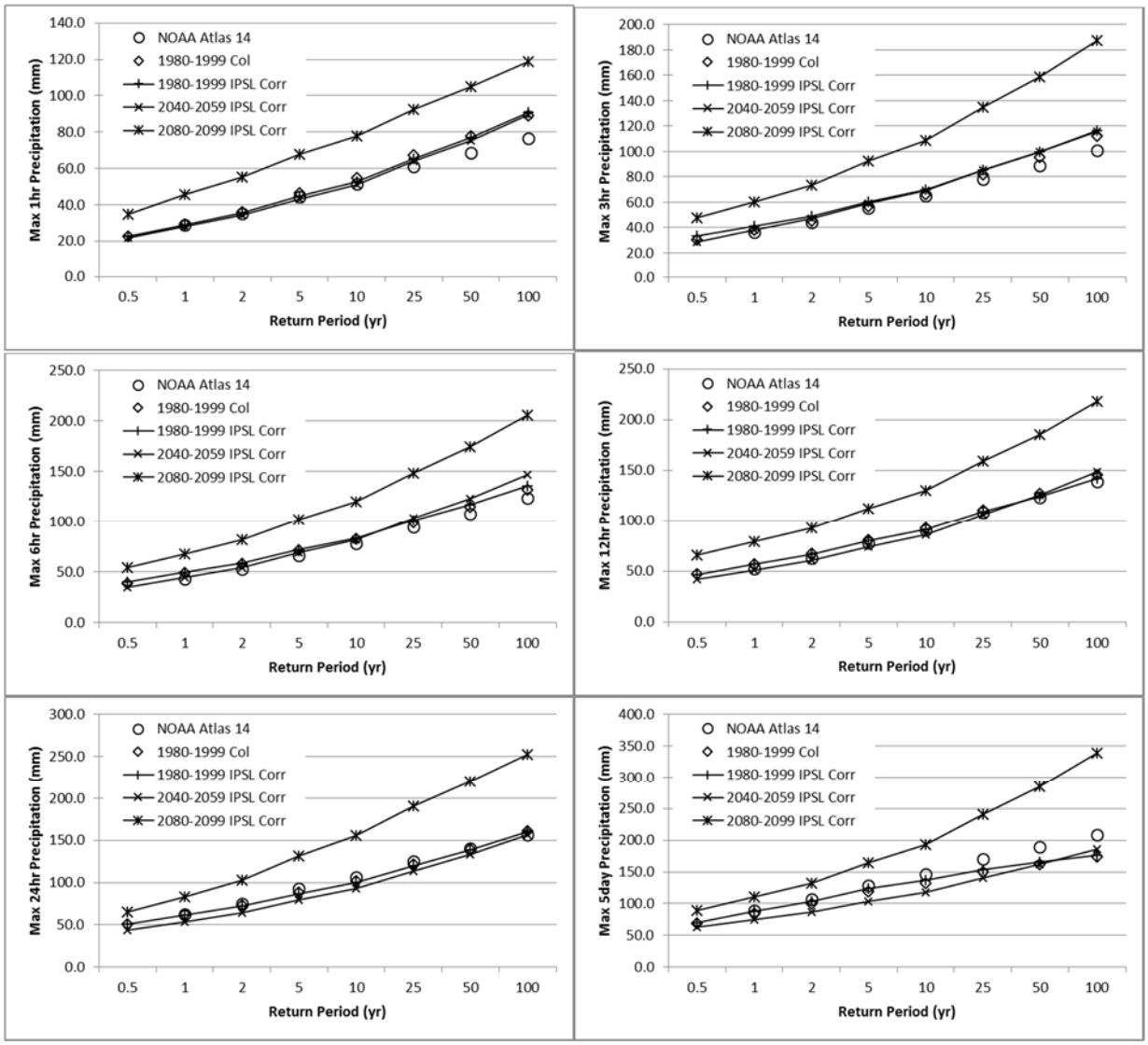

Figure 5.23. Comparison of modeled (IPSL) simulation (1980-1999) and projection (2040-2059 and 2080-2099) estimated maximum precipitation for selected durations and return periods as determined by L-moments regional frequency analysis at Columbus, Indiana. Atlas 14 and observed (1980-1999) values also included.

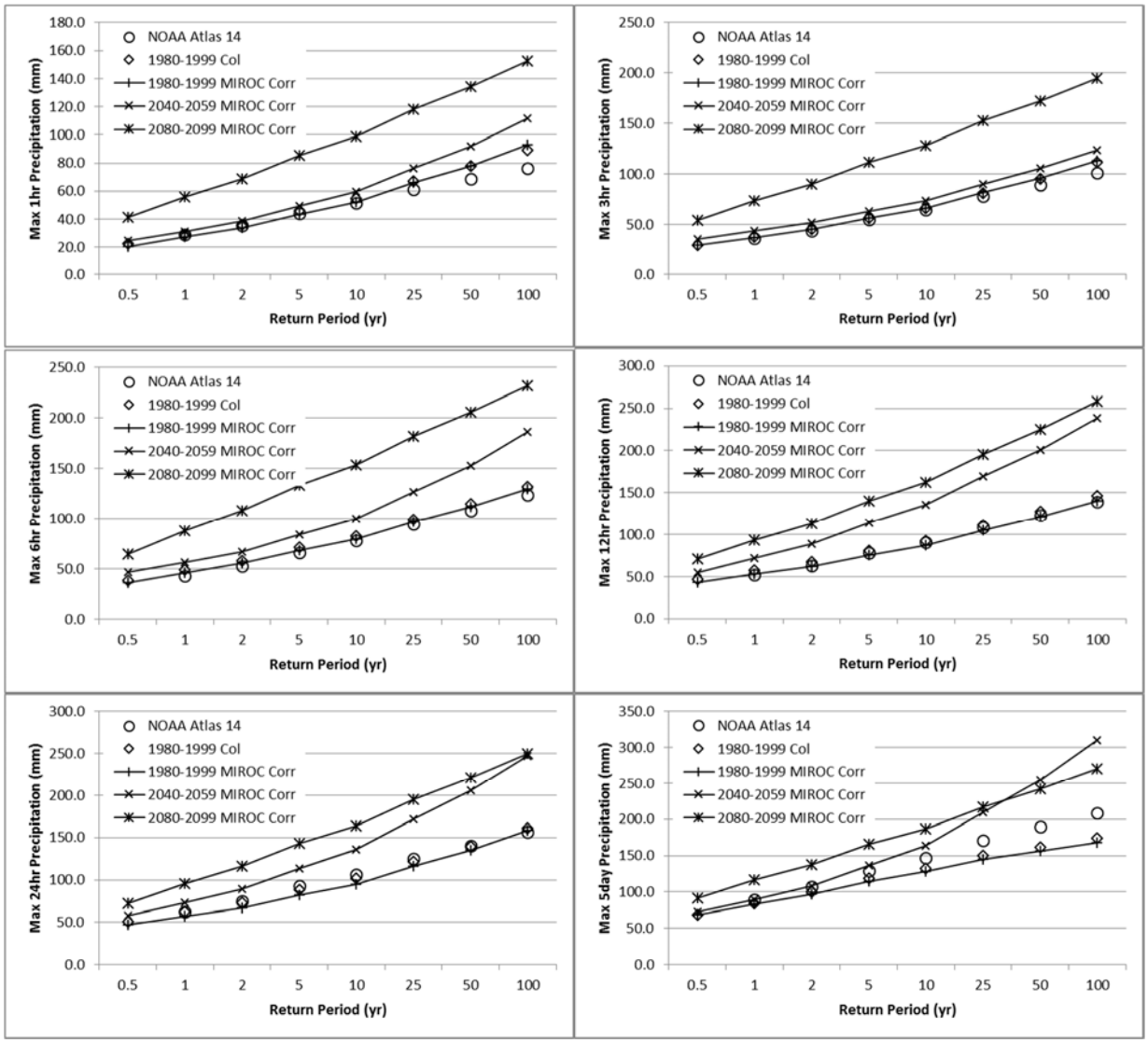

Figure 5.24. Comparison of modeled (MIROC) simulation (1980-1999) and projection (2040-2059 and 2080-2099) estimated maximum precipitation for selected durations and return periods as determined by L-moments regional frequency analysis at Columbus, Indiana. Atlas 14 and observed (1980-1999) values also included.

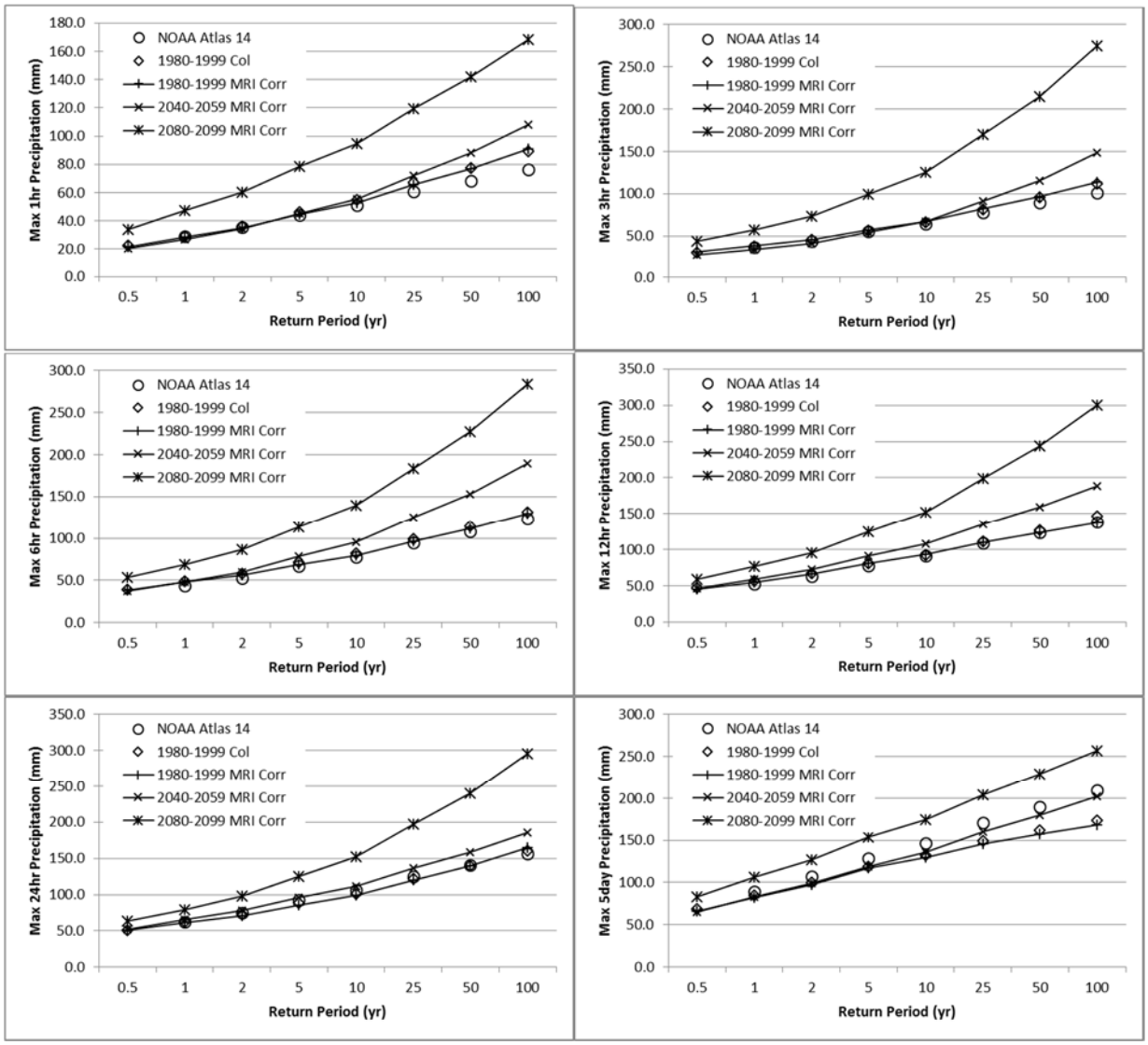

Figure 5.25. Comparison of modeled (MRI) simulation (1980-1999) and projection (2040-2059 and 2080-2099) estimated maximum precipitation for selected durations and return periods as determined by L-moments regional frequency analysis at Columbus, Indiana. Atlas 14 and observed (1980-1999) values also included.

Figure 5.26, Figure 5.27, Figure 5.28, and Figure 5.29 show the maximum bias corrected CNRM, IPSL, MIROC, and MRI precipitation distributions (simulated and projected) at Grayling, MI for a range of ARIs and durations of 1-, 3-, 6-, 12-, and 24-hr and 5-day, respectively. Grayling, MI is the closest gauge site to Camp Grayling. Observed (1980-1999) and NOAA Atlas 14 values are included for comparison. The projected (2080-2099) maximum precipitation for IPSL, MIROC, and MRI is significantly higher than observed values for all durations and ARIs greater than 1 year. IPSL, MIROC, and MRI also provide

similar results for projected (2040-2059) value, which are typically about half way between observed and projected (2080-2099) values. Most projected (2040-2059) values are significantly greater than observed values for these models. CNRM projected maximum precipitation outputs differ from those of the other three models. CNRM projected (2080-2099) maximum values are significantly larger than observed for ARIs less than 25 years while projected (2040-2059) values are not significantly larger than observed for any design storm. Also, projected (2080-2099) values are lower than observed values for ARIs greater than 25 years. The simulated values are very close the observed values, as should be expected following bias correction. See Appendix B for tables showing the percent difference between the observed and projected precipitations at Grayling, MI for all storm durations and return periods as determined by the L-moments regional frequency analysis.

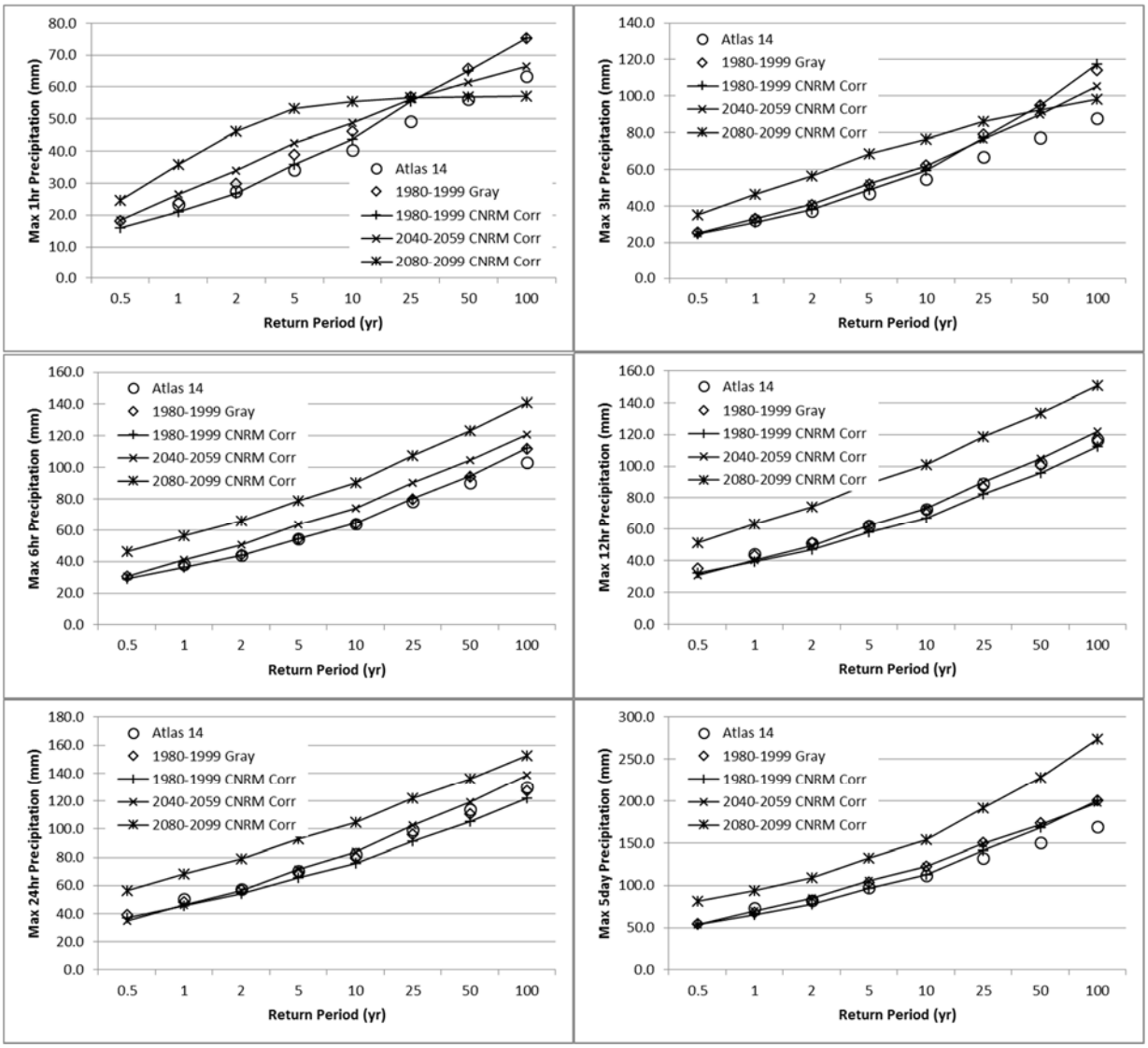

Figure 5.26. Comparison of modeled (CNRM) simulation (1980-1999) and projection (2040-2059 and 2080-2099) estimated maximum precipitation for selected durations and return periods as determined by L-moments regional frequency analysis at Grayling, Michigan. Atlas 14 and observed (1980-1999) values also included.

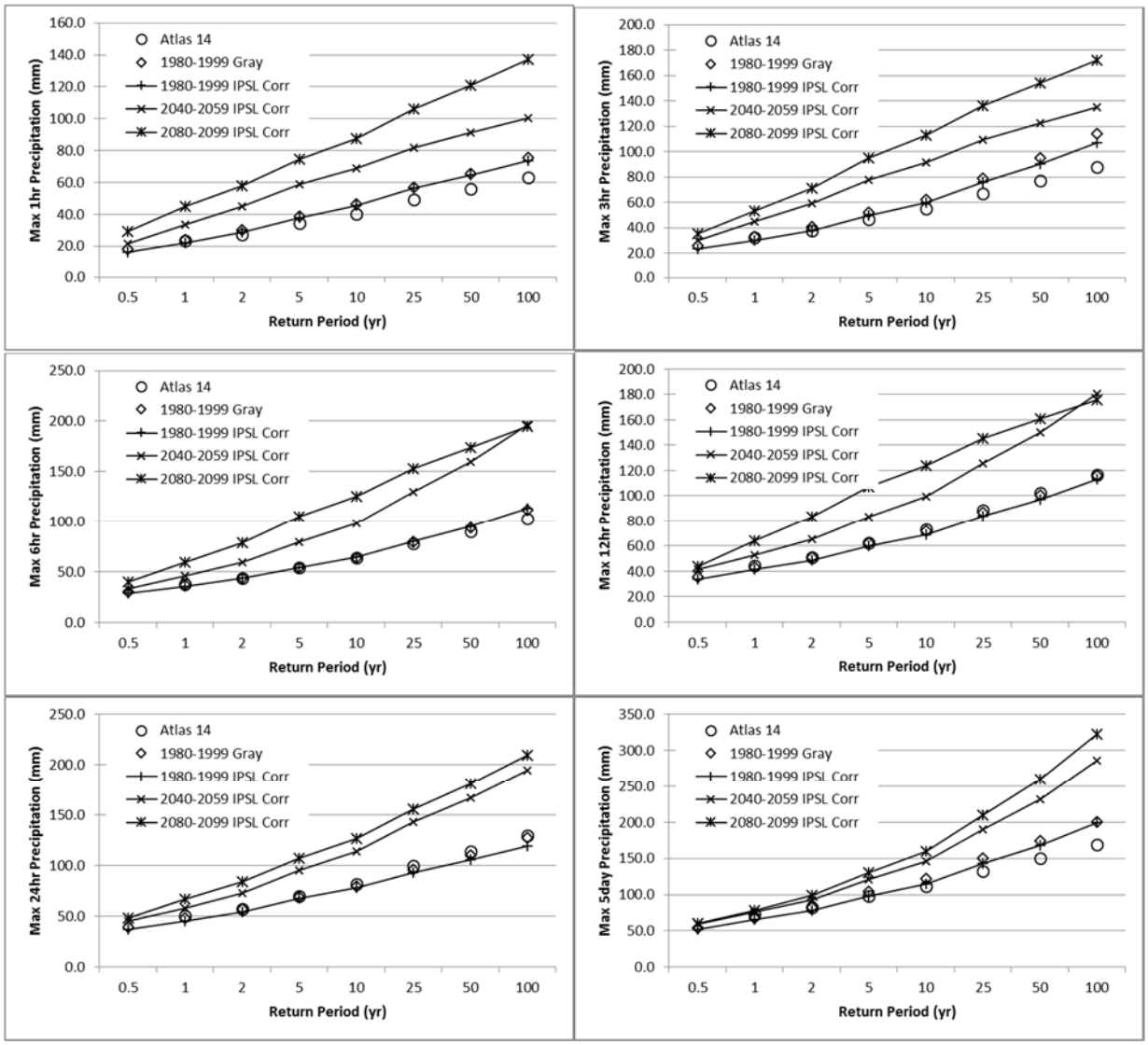

Figure 5.27. Comparison of modeled (IPSL) simulation (1980-1999) and projection (2040-2059 and 2080-2099) estimated maximum precipitation for selected durations and return periods as determined by L-moments regional frequency analysis at Grayling, Michigan. Atlas 14 and observed (1980-1999) values also included.

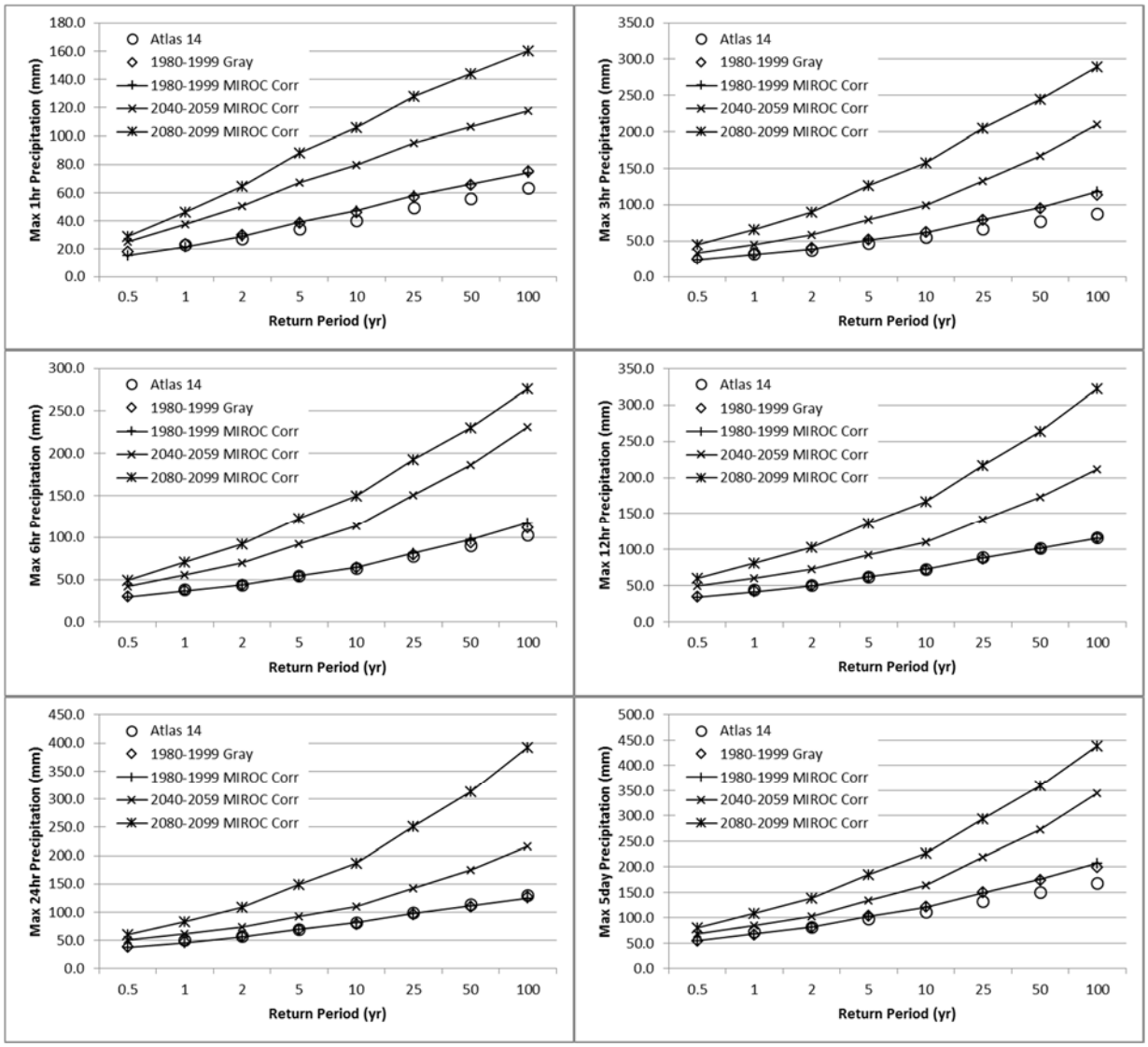

Figure 5.28. Comparison of modeled (MIROC) simulation (1980-1999) and projection (2040-2059 and 2080-2099) estimated maximum precipitation for selected durations and return periods as determined by L-moments regional frequency analysis at Grayling, Michigan. Atlas 14 and observed (1980-1999) values also included.

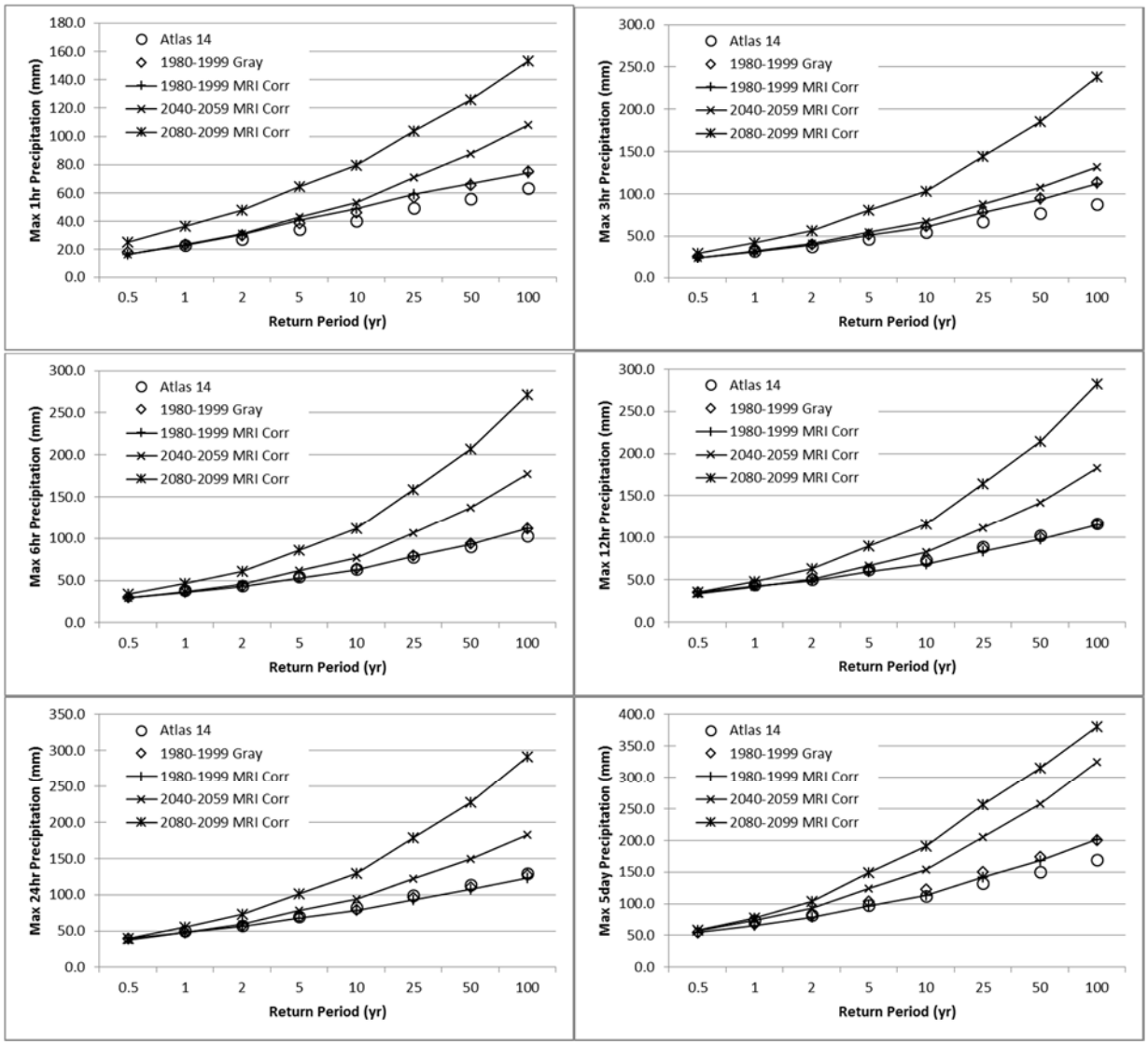

Figure 5.29. Comparison of modeled (MRI) simulation (1980-1999) and projection (2040-2059 and 2080-2099) estimated maximum precipitation for selected durations and return periods as determined by L-moments regional frequency analysis at Grayling, Michigan. Atlas 14 and observed (1980-1999) values also included.

Figure 5.30, Figure 5.31, Figure 5.32, and Figure 5.33 shows the maximum bias corrected CNRM, IPSL, MIROC, and MRI precipitation distributions (simulated and projected) at Paris, IL for a range of return periods and durations of 1-, 3-, 6-, 12-, and 24-hr and 5-day, respectively. The Paris, IL gauge site is located within Edgar County. Observed (1980-1999) and NOAA Atlas 14 values are included for comparison. CNRM, IPSL, and MRI provide similar results for projected (2040-2059) value, which are typically higher than projected (2080-2099) values. CNRM, IPSL, and MRI projected (2040-2059) values

are significantly higher than observed values for shorter duration storms events and closer to observed values for longer duration events. The projected (2080-2099) maximum precipitation for CNRM, IPSL, and MRI is also significantly higher than observed values for shorter duration events, but usually less than projected (2040-2059) values. MIROC projected (2080-2099) maximum values are significantly larger than observed for all return periods while projected (2040-2059) values are significantly larger than observed for return periods less than 25 years, but less than projected (2080-2099) values. The simulated values are very close to the observed values, as should be expected following bias correction. See Appendix B for tables showing the percent difference between the observed and projected precipitations at Paris, IL for all storm durations and return periods as determined by the L-moments regional frequency analysis.

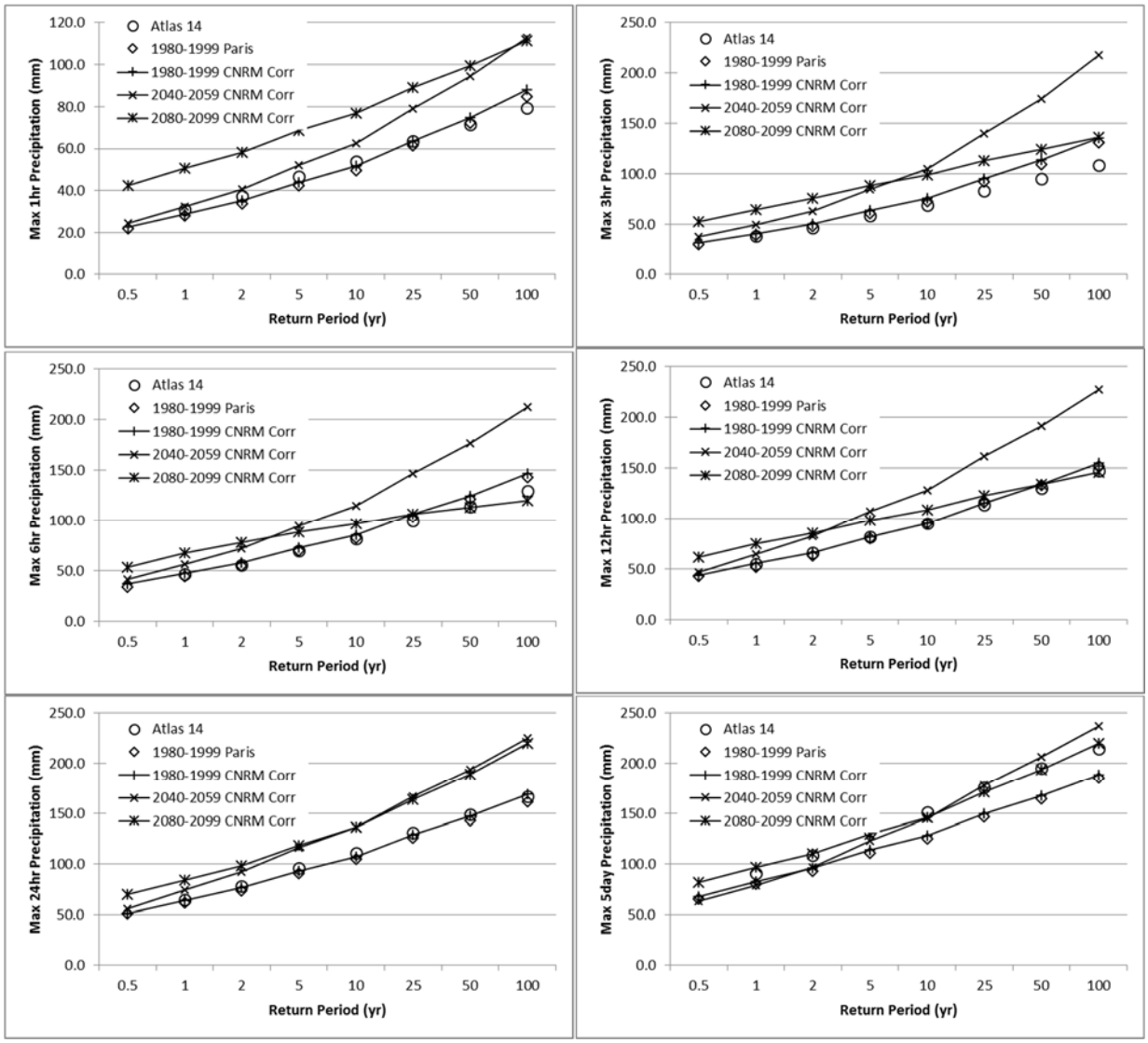

Figure 5.30. Comparison of modeled (CNRM) simulation (1980-1999) and projection (2040-2059 and 2080-2099) estimated maximum precipitation for selected durations and return periods as determined by L-moments regional frequency analysis at Paris, Illinois. Atlas 14 and observed (1980-1999) values also included.

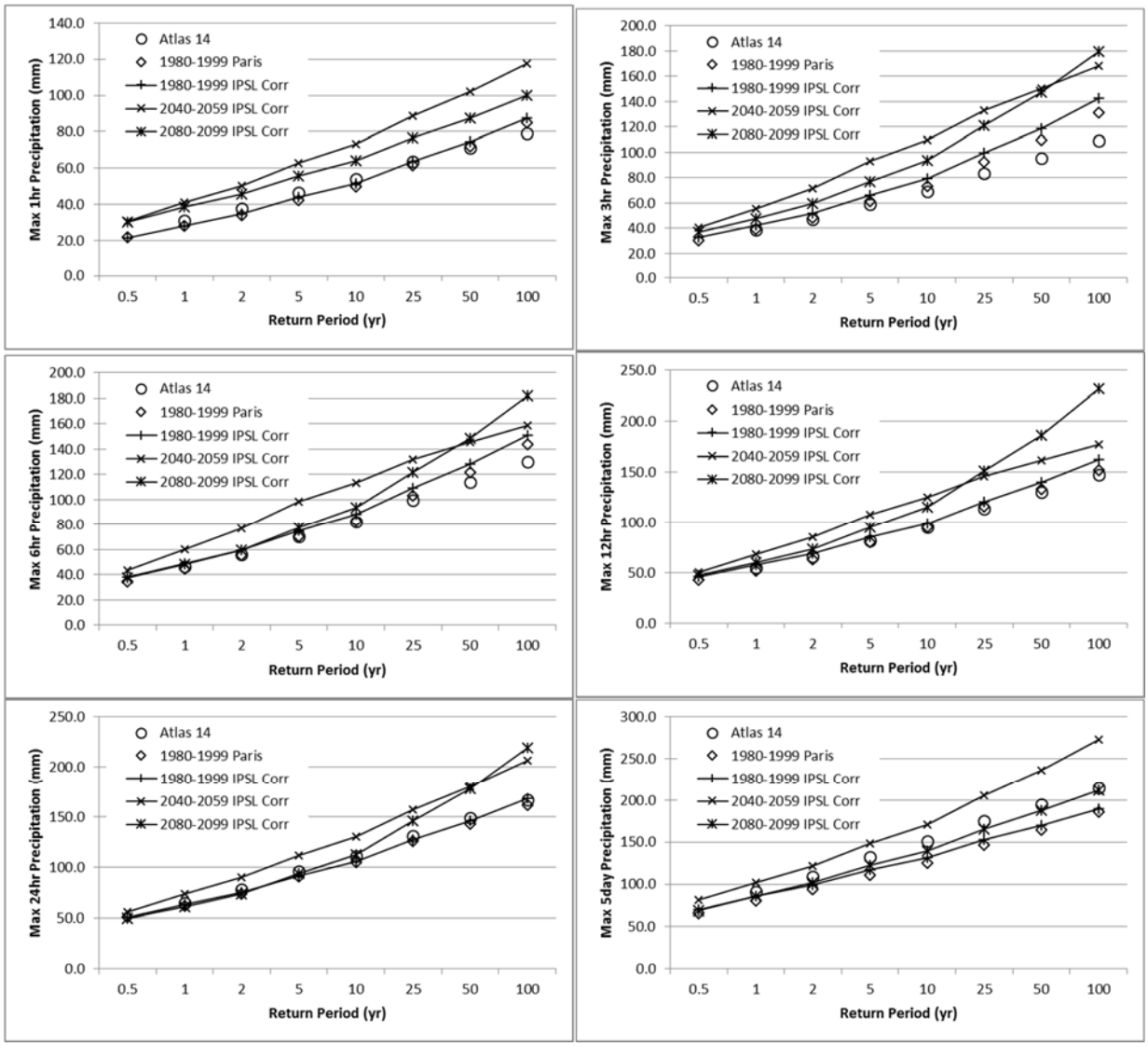

Figure 5.31. Comparison of modeled (IPSL) simulation (1980-1999) and projection (2040-2059 and 2080-2099) estimated maximum precipitation for selected durations and return periods as determined by L-moments regional frequency analysis at Paris, Illinois. Atlas 14 and observed (1980-1999) values also included.

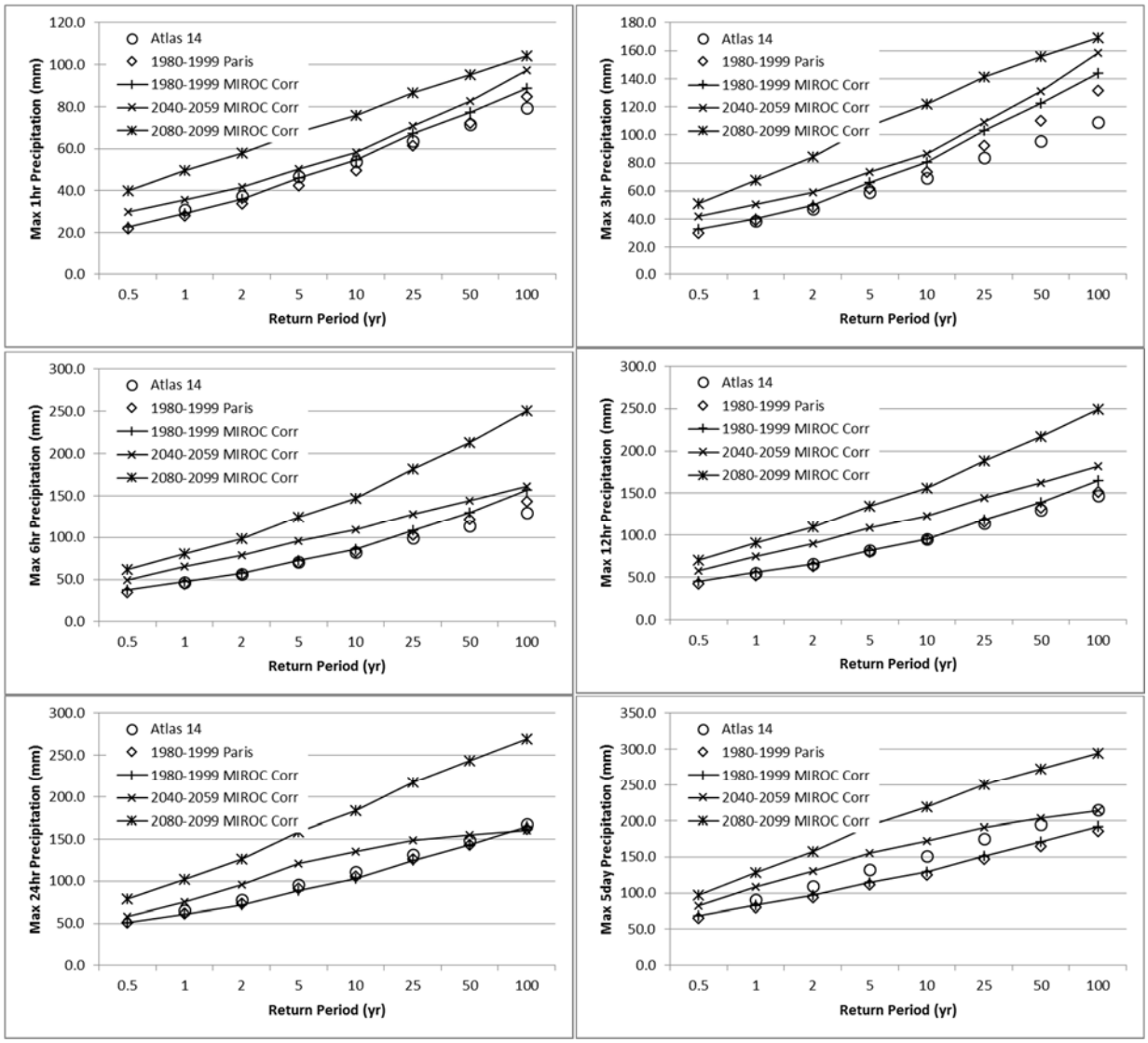

Figure 5.32. Comparison of modeled (MIROC) simulation (1980-1999) and projection (2040-2059 and 2080-2099) estimated maximum precipitation for selected durations and return periods as determined by L-moments regional frequency analysis at Paris, Illinois. Atlas 14 and observed (1980-1999) values also included.

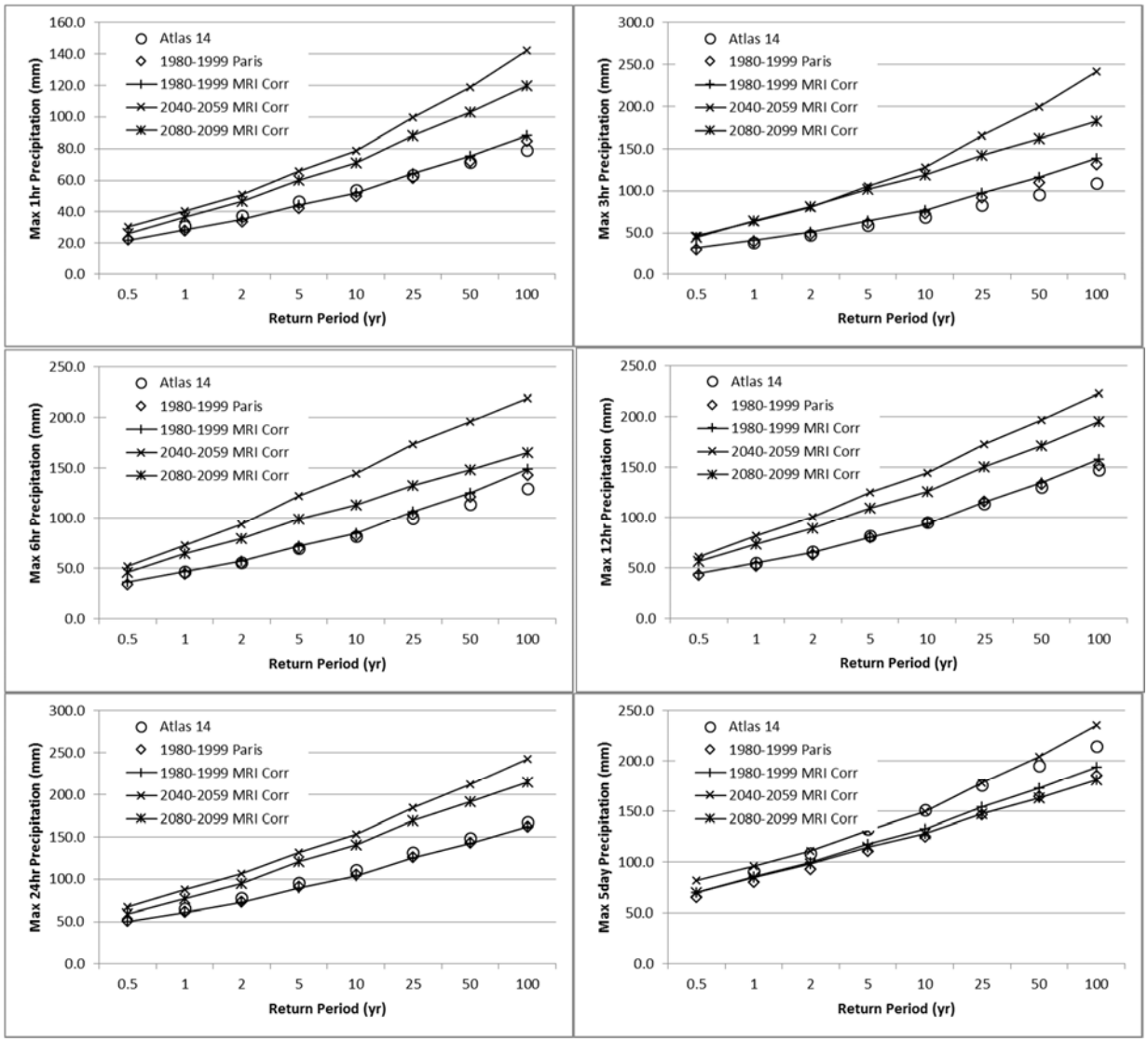

Figure 5.33. Comparison of modeled (MRI) simulation (1980-1999) and projection (2040-2059 and 2080-2099) estimated maximum precipitation for selected durations and return periods as determined by L-moments regional frequency analysis at Paris, Illinois. Atlas 14 and observed (1980-1999) values also included.

Figure 5.34 shows the maximum bias corrected CNRM, IPSL, MIROC, and MRI precipitation distributions (simulated and projected) at Columbus, IN for a range of ARIs and durations of 1-, 3-, 6-, and 24-hr. The observed maximum precipitation distributions and the average RCM values with error bars of +/- one standard deviation are also presented. The variability in RCM output is illustrated in the following figures. For example, MRI provides the highest projected values for shorter duration events but average values for longer durations, with respect to the other three RCMs. CNRM provides maximum values less

than the other three RCMs for most durations for the 2040-2059 projections but the highest values for most durations for the 2080-2099 projections. The overall tends of the RCM average maximum values are consistent across a range of durations and the spread of the values is fairly narrow, except for 2040-2059 projections with durations greater than 12 hours. The uncertainty among results from the four RCM is highest, both in magnitude and as a percentage, for the most extreme events (highest return periods).

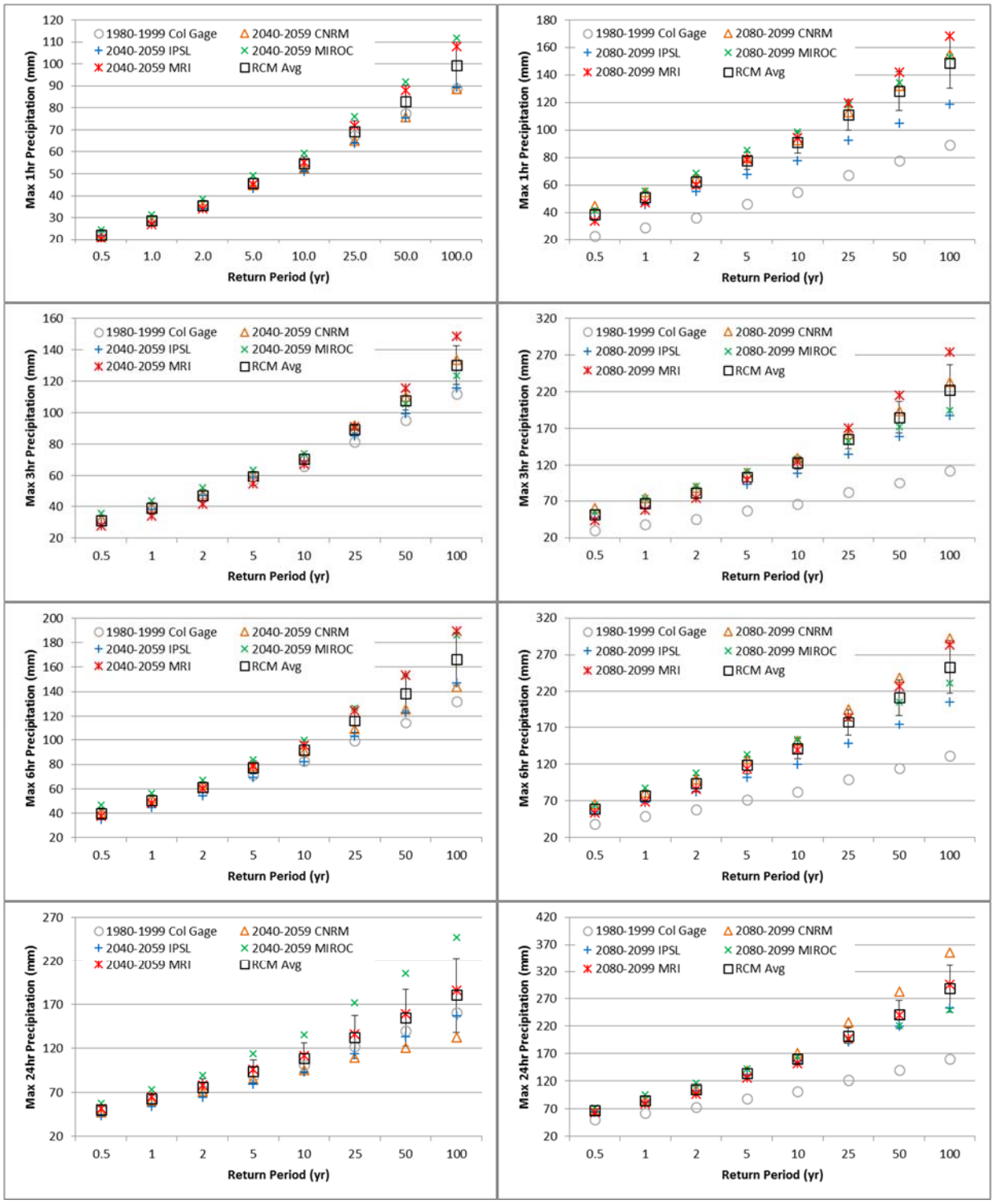

Figure 5.34. Comparison of modeled projection (2040-2059 and 2080-2099) estimated maximum precipitation for selected durations and return periods as determined by L-moments regional frequency analysis at Columbus, Indiana. Observed (1980-1999) values and average of modeled projections with error of +/- 1 standard deviation also included.

Figure 5.35 shows the maximum bias corrected CNRM, IPSL, MIROC, and MRI precipitation distributions (simulated and projected) at Grayling, MI for a range of return periods and durations of 1-, 3-, 6-, and 24-hr. The observed maximum precipitation distributions and the average RCM values with error bars of +/- one standard deviation are also presented. The overall tends of the RCM average maximum values are consistent across a range of durations but the spread of the values are much wider than the other regions. MIROC and CNRM generally return the highest and lowest values, respectively, and can differ by 100%-150% for the larger ARIs. The uncertainty among results from the four RCM is highest, both in magnitude and as a percentage, for the most extreme events (highest return periods). However, the uncertainty for the Michigan region is higher than for Illinois and Indiana.

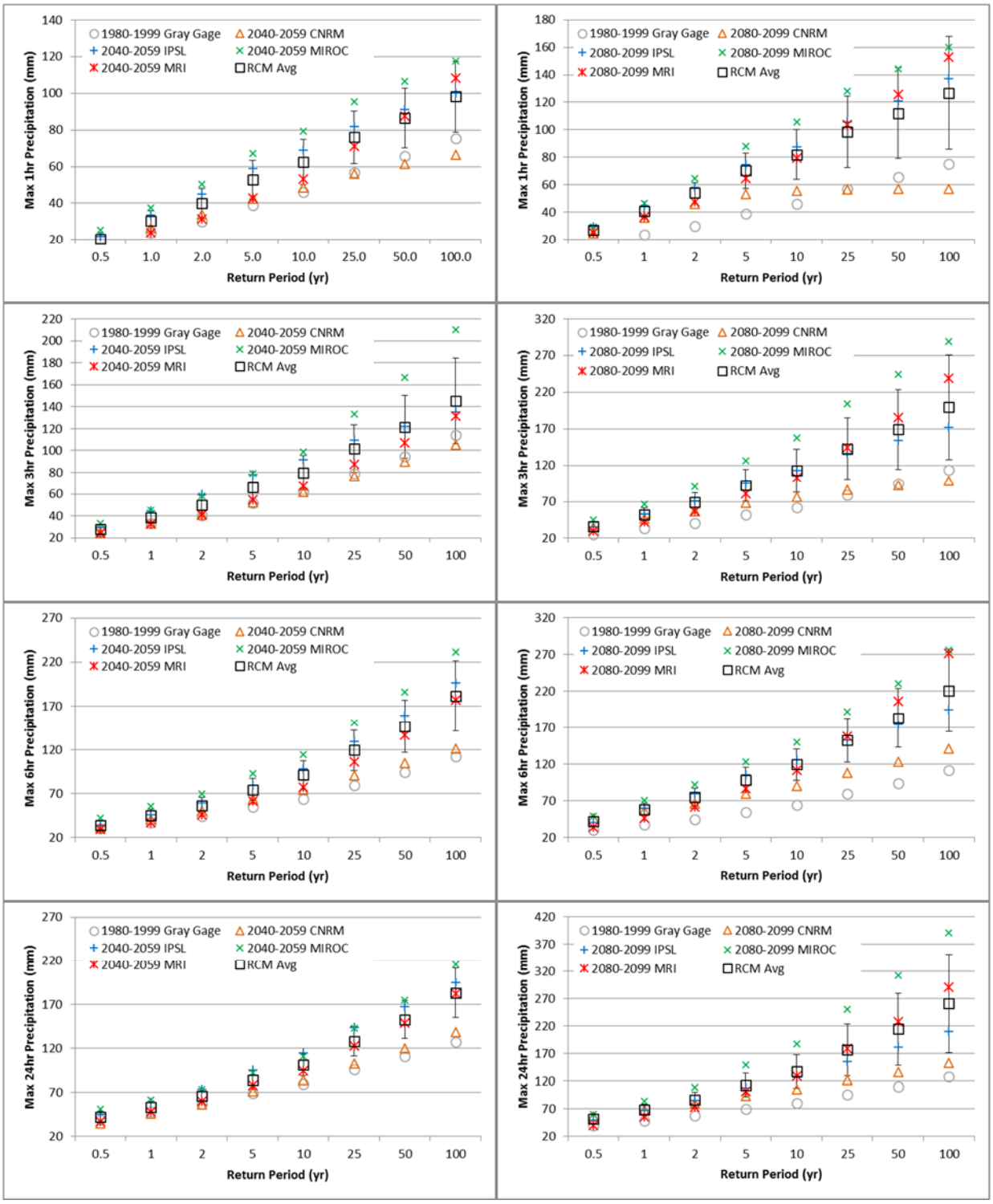

Figure 5.35. Comparison of modeled projection (2040-2059 and 2080-2099) estimated maximum precipitation for selected durations and return periods as determined by L-moments regional frequency analysis at Grayling, Michigan. Observed (1980-1999) values and average of modeled projections with error of +/- 1 standard deviation also included.

Figure 5.36 shows the maximum bias corrected CNRM, IPSL, MIROC, and MRI precipitation distributions (simulated and projected) at Paris, IL for a range of return periods and durations of 1-, 3-, 6-, and 24-hr. The observed maximum precipitation distributions and the average RCM values with error bars of +/- one standard deviation are also presented. The overall tends of the RCM average maximum values are similar to the Columbus, IN results. The trends in averaged values are consistent across a range of durations and the spread of the values is fairly narrow, except for 2080-2099 projections with a duration of 6 hours.

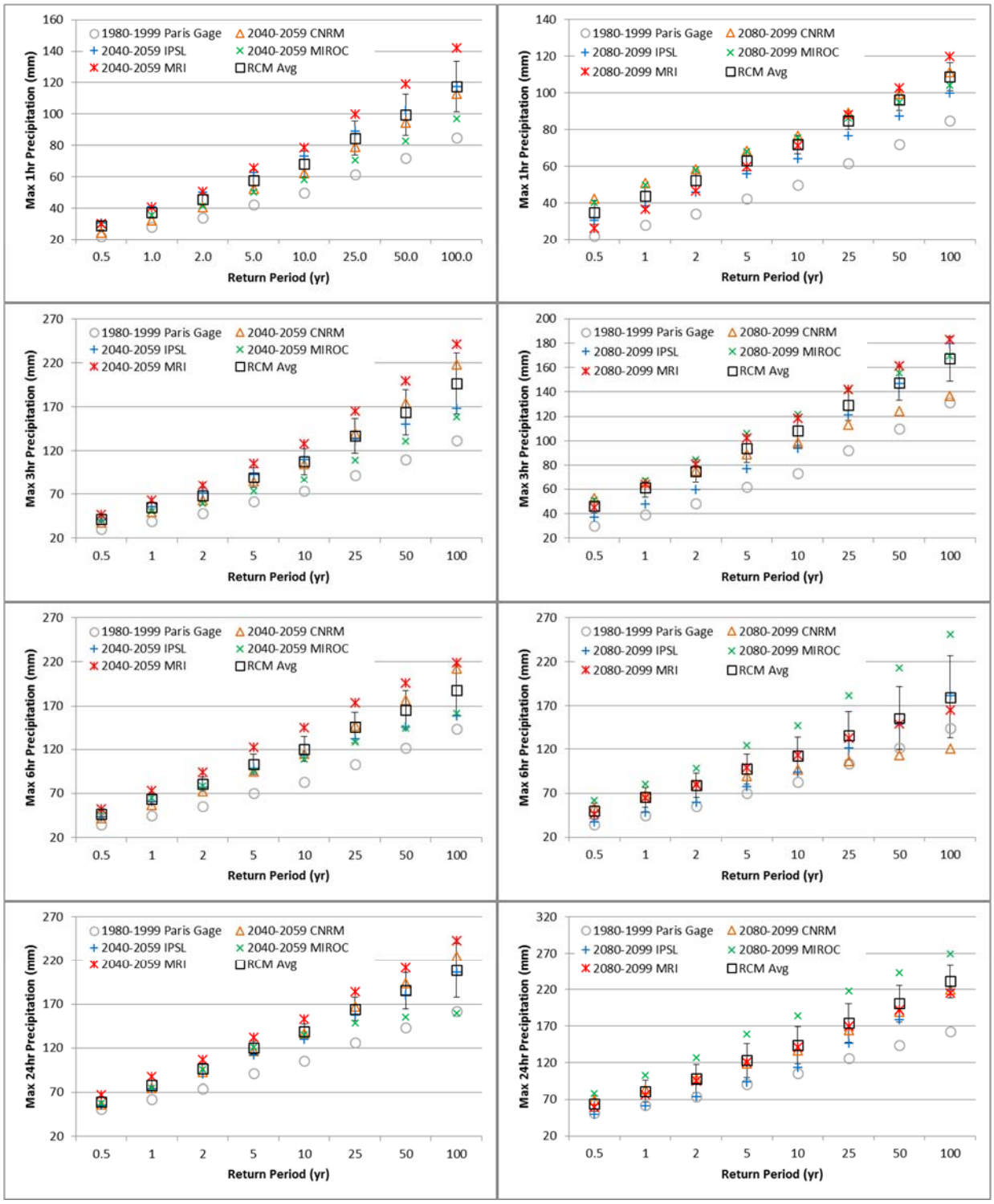

Figure 5.36. Comparison of modeled projection (2040-2059 and 2080-2099) estimated maximum precipitation for selected durations and return periods as determined by L-moments regional frequency analysis at Paris, Illinois. Observed (1980-1999) values and average of modeled projections with error of +/- 1 standard deviation also included.

5.4 Discussion

CMIP5 GCMs generally overestimate precipitation and sometimes underestimate extreme precipitation. Raw precipitation output from the four RCMs (CMIP5 GCMs downscale by RegCM4, see Notaro et al., 2015) overestimated average annual total precipitation, 1-hr AMS, and total annual wet hours when comparing model simulation data to observed gauge data (1980-1999). The RCMs were bias corrected first by applying a minimum precipitation threshold below which hourly precipitation estimates were set to zero and then by implementing quantile mapping. Precipitation thresholds of 1.02 mm for CNRM, MIROC, and IPSL, and 1.27 mm for MRI were used. These values are within an acceptable range given that thresholds are typically between 0.1 mm – 2 mm in literature (eg. Lindau and Simmer, 2012; Rosenburg et al., 2010; and Themeßl et al., 2011).

Following application of the thresholds, average observed total annual wet hours and wet days were compared to the RCMs simulations and projections. Total annual wet hours and wet days are generally natural or decrease (depending on the RCM) during RCM projected timeframes compared to the simulated/observed timeframe (1980-1999) (see Figure 5.9 and Figure 5.10). The RCM outputs are in line with trend results for total annual wet hours from Chapter 4, which found that total annual wet hours have a steady to slightly decreasing trend across all three regions 1970-2009. On the other hand, average annual wet days in Michigan and Illinois increased since 1940 and 1923, respectively, while the trend in Indiana was natural. The RCM output shows steady or decreasing trends in average total annual wet days between simulations and projections (see Figure 5.10), which isn't consistent with observed historic trends. However, the identification of observed trends in total annual wet hours and wet days are no guarantee those trends will continue into the future. The application of thresholds to match

observed and simulated wet hours assumes those thresholds are valid for the predicted RCM timeframes, but makes no assumption to guess future or predicted wet hours.

The second step in precipitation bias correction is to adjust the intensity of the RCM simulations (1980-1999) to agree with the observed (1980-1999) intensity. Quantile mapping was applied for which the eCDF of the simulations (by grid output) were adjusted to agree with the eCDF of the observations from each corresponding gauge. Quantile mapping assumes that the rainfall distribution will be the same in the future as in the observed climate (Folwer and Kilsby, 2007), though there is no guarantee this assumption is true. Quantile mapping was completed in a manor suggested by Li et al. (2010) and Sun et al. (2011). Ideally climate modeling will advance to a point where applying statistical approaches such as quantile mapping bias correction (and the corresponding inherent uncertainties) won't be necessary in order to apply RCM simulations and projections to hydrologic and hydraulic models. In the meantime such methods are necessary to link RCM results to hydrologic impacts on small scale watersheds (Markus et al., 2012).

Post bias-correction analysis of the RCM outputs shows an increase from simulation and projected timeframes for total annual precipitation, 1-hr AMS, and 24-hr AMS. Generally, all four analyzed RCMs behave similarly with regards to the general trend and magnitude of changes between the simulated (1980-1999) and projected (2040-2059 and 2080-2099) timeframes. A comparison of total annual precipitation trend lines between observed (projected to 2099) and RCM output show trend slope and magnitude are comparable for the Michigan and Indiana regions while the averaged projected observed Illinois trend rises more quickly than the averaged RCM perception. Comparisons of 1-hr and 24-hr AMS trend lines between observed (projected to 2099) and RCM output show trend slopes that diverge as

projected RCM 1-hr and 24-hr AMS output increases significantly by 2099. Again, observed trends in total annual precipitation, 1-hr AMS, and 24-hr AMS is no guarantee those trends will continue into the future. In addition, the slope of the observed (projected to 2099) trend lines can be changed depending how much of the observed records were included. The slope of the projected observed trend lines change primarily due to decadal variability, highlighted by decades of significant drought or wetness, so the length and start of the observed data can greatly influence projected observed trend lines.

Precipitation regional frequency analysis was used to estimate how often specific events (for numerous return periods and durations) occur and how they change in the projected timeframes. The RCM precipitation magnitudes (simulated and projected) for each duration and return period were compared with observed (1980-1999) data. Monte Carlo simulations were used to construct confidence limits at a 95% confidence level. Design storms determined from the projected RCM precipitation varied greatly between return periods, between durations, and between RCMs. In general, all four RCMs projected significant increases in precipitation intensity at the end of the twenty first century (2080-2099) compared to the observed values (1980-1999). The increases range from 27% to 102% depending on the location, return period, duration, and RCM. A few significant increases were also seen in precipitation intensity in the middle of the twenty first century (2040-2059) compared to the observed values (1980-1999), though increases were generally minor. The RCMs also showed some projected decreases in precipitation intensity for a few return periods and durations, but the deceases where rarely significant. This general increase in precipitation intensity has been found in other studies (eg: Forsee and Ahmad, 2011 & Vavrus and Behnke, 2014).

RCM uncertainty and the output variability was anticipated and addressed by analyzing four different RCMs to provide a range of possible projections and upper and lower bounds based on the highest and lowest model outputs (eg: Fowler and Kilsby, 2007; Pielke et al., 2012). Only four were available due to the considerable computing resources and time required to downscale one RCM (Notaro et al., 2015). The average projected (2080-2099) design storm of the four RCMs across all locations, durations, and return periods is larger than the corresponding observed design storm and usually significantly larger based on the standard deviation of the RCM results, especially for ARIs greater than 1 year. On average the projected (2080-2099) design storms are 51%, 52%, and 34% larger than the observed design storms for Indiana, Michigan, and Illinois, respectively. The average projected (2040-2059) design storm is also more intense than the observed design storm for the corresponding return periods and durations. On average the projected (2040-2059) design storms are 6%, 25%, and 31% larger than the observed design storms for Indiana, Michigan, and Illinois, respectively. However, for this timeframe, the results from two of the RCMs are generally similar in magnitude to the observed data while the output from the other two RCMs are generally significantly more intense than the observed data. The results of each RCM with relation to the observed data change for each duration, ARI, and location; so one RCM is not constantly at the upper or lower bounds of the four RCM outputs.

The four RCMs provided bias-corrected precipitation output that agreed in general trends but the precise levels of precipitation increases varied substantially, especially for the 2040-2059 projected timeframe. As a result, the inferred changes in precipitation are difficult to distinguish from natural variability given the relatively short simulation periods of twenty years, an issue regularly seen in literature (eg: Rosenburg et al., 2010; Markus et al., 2012). The differences between the four sets of projected precipitation and the observed precipitation are large enough that potential future changes in

design storms and subsequent changes in stream hydrology and stormwater infrastructure design should be considered. The analysis of additional downscaled GCMs to determine a probability distribution of projected precipitation would be beneficial for producing recommended projected design storms. With the limit of four RCMs, the average and upper and lower bounds could only be considered.

5.5 Conclusion

The four CMIP5 GCMs dynamically downscaled by the RegCM4 RCM (Notaro et al., 2015) overestimated average annual total precipitation, 1-hr AMS, 24-hr AMs, and total annual wet hours and wet days when comparing model simulation data to observed gauge data (1980-1999). Application of quantile mapping bias correction was necessary in order to apply RCM simulations and projections to hydrologic and hydraulic models on a watershed-scale. Post bias-correction analysis of the RCM simulation outputs showed successfully adjusted precipitation statistics when comparted to observed data.

The four RCMs provided bias-corrected precipitation output that agreed in general trends but the precise levels of precipitation increases varied substantially, especially for the 2040-2059 projected timeframe. The average projected (2080-2099) design storm of the four RCMs across all locations, durations, and return periods is larger than the corresponding observed design storm and usually significantly larger based on the standard deviation of the RCM results, especially for ARIs greater than 1 year. The average projected (2040-2059) design storm is also more intense than the observed design storm for the corresponding return periods and durations. However, for this timeframe, the results from two of the RCMs are generally similar in magnitude to the observed data while the output from the other two RCMs are generally significantly more intense than the observed data. The results of each RCM with relation to the observed data change for each duration, ARI, and location; so one RCM is not

constantly at the upper or lower bounds of the four RCM outputs. The differences between the four sets of projected precipitation and the observed precipitation are large enough that potential future changes in design storms and subsequent changes in stream hydrology and stormwater infrastructure design should be considered, though the range of projected changes make it difficult to determine specific IDF curve modifications at this time. The averaged RCM projections can be applied to estimate future conditions (ie. stream hydrology) but with the understanding that such projection carry significant uncertainty, as revealed by the upper and lower bounds based on the highest and lowest model outputs.

References

Dufresne, J.-L., et al. (2013). Climate change projections using the IPSL-CM5 Earth System Model: From CMIP3 to CMIP5. Clim. Dyn. 40: 2123-2165.

Ehret, U., Zehe, E., Wulfmeyer, V., Warrach-Sagi, K., & Liebert, J. (2012). "Should we apply bias correction to global and regional climate model data?" Hydrol. Earth Syst. Sci, 16: 3391-3404.

Elguindi, N., et al. (2011). Regional climatic model RegCM user manual version 4.1. The Abdus Salam International Centre for Theoretical Physical Strada Costiera, Trieste.

Forsee, W. J. & Ahmad, S. (2011). Evaluating urban storm-water infrastructure design in response to projected climate change. Journal of Hydrologic Engineering, 16(11): 865-873.

Fowler, H. J., Blenkinsop, S., & Tebaldi, C. (2007). Linking climate change modeling to impacts studies: recent advances in downscaling techniques for hydrological modeling. Int. J. of Climato. 27: 1547-1578.

Fowler, H. J., Kilsby, C. G. (2007). Using regional climate model data to simulate historical and future river flows in northwest England. Climatic Change, 80: 337-367.

Giorgi, F., et al. (2012). RegCM4: model description and preliminary test over multiple CORDEX domains. Clim Res, 52: 7-29.

Groisman, P. Y., Knight, R. W., & Karl, T. R. (2012). Changes in intense precipitation over the central United States. Journal of Hydrometeorology, 13: 47-66.

Hershfield, D.M. (1961). Rainfall frequency atlas of the United States for durations from 30 min to 24 h and return periods from 1 to 100 years. Technical Paper No. 40. Weather Bureau, U.S. Department of Commerce, Washington, DC.

Huff, F. A. & Angel, J. R. (1992). Rainfall frequency atlas of the Midwest (Bulletin 71). Illinois State Water Survey, Champaign, IL.

Illinois Department of Natural Resources (IDNR). (2015). Report for the Urban Flood Awareness Act. Office of Water Resources. Springfield, Illinois. (Winters, B. A., Angel, J., Ballerine, C., Byard, J., Flegel, A., Gambill, D. R., Jenkins, J. P., McConkey, S., Markus, M., Bender, B. A., O'Toole, M. J.)

Intergovernmental Panel on Climate Change (IPCC). (2014) Climate change 2014: synthesis report. Contribution of working groups I, II and III to the fifth assessment report of the Intergovernmental Panel on Climate Change (Pachauri, R. K. & Meyer, L. A. [eds.]). IPCC, Geneva, Switzerland, 151 pp.

Li, H., Sheffield, J., & Wood, E. F. (2010). Bias correction of monthly precipitation and temperature fields from Intergovernmental Panel on Climate Change AR4 models using equidistant quantile matching, J. Geophys. Res. 115: D10101.

Lindau, R. & Simmer, C. (2012). On correction precipitation as simulated by the regional climate model COSMO-CLM with daily rain gauge observations. Meteorol Atmos Phys, 119: 31-42.

Markus, M., Wuebbles, D. J., Laing, X., Hayhoe, K., Kristovich, D. A. R. (2012). Diagnostic analysis of future climate scenarios applied to urban flooding in the Chicago metropolitan area. Climatic Change, 111: 879-902.

Maurer, E. P., & Hidalgo, H. G. (2008). Utility of daily vs. monthly large scale climate data: An intercomparison of two statistical downscaling methods, Hydrol. Earth Syst. Sci., 12: 551–563.

Notaro, M., Bennington, V., & Vavrus, S. (2015). Dynamically Downscaled Projections of Lake-Effect Snow in the Great Lakes Basin. J of Climate, 28: 1661-1684.

Olsson, J., Gidhagen, L., Gamerith, V., Gruber, G., Hoppe, H., & Kutschera, P. (2012). Downscaling of short-term precipitation from regional climate models for sustainable urban planning. Sustainability, 4: 866-887.

Pielke, R. A., Sr., Wilby, R., Niyogi, D., Hossain, F., Dairuku, K., Adegoke, J., Kallos, G., Seastedt, T., & Suding, K. (2012). Dealing with complexity and extreme events using a bottom-up, resource based vulnerability perspective, in Complexity and Extreme Events in Geosciences, Geophys. Monogr. Ser., edited by A. S. Sharma et al., AGU, Washington, D. C., in press.

Rosenberg, E. A., Keys, P. W., Booth, D. B., Hartley, D., Burkey, J., Steinemann, A. C., & Lettenmaier, D. P. (2010). Precipitation extremes and impacts of climate change on stormwater infrastructure in Washington State. Climatic Change, 102: 319-349.

Sanford, T., Frumhoff, P. C., Luers, A., & Gulledge, J. (2014). The climate policy narrative for a dangerously warming world. Nature Climate Change, 4: 164-166.

Sun, F. B., Roderick, M. L., Lim, W. H., & Farquhar, G. D. (2011). Hydroclimatic projections for the Murray-Darling Basin based on an ensemble derived from Intergovernmental Panel on Climate Change AR4 climate models. Water Resour. Res., 47: W00g02.

Taylor, K. E., Stouffer, R. J., & Meehl, G. A. (2012). An overview of CMIP5 and the experiment design. Bull. Am. Meteorol. Soc., 93: 485–498.

Themessl, M. J., Gobiet, A., & Leuprecht, A. (2011). Empirical statistical downscaling and error correction of daily precipitation from regional climate models, Int. J. Climatol., 31: 1530–1544.

Vavrus, S. J. & Behnke, R. J. (2014). A comparison of projected future precipitation in Wisconsin using global and downscaled climate model simulations: implications for public health. Int. J. Climatology, 34: 3106-3124.

Voldoire, A., et al. (2013). The CNRM-CM5.1 global climate model: description and basic evaluation. Clim Dyn, 40: 2091-2121.

Watanabe, M., et al. (2010). Improved climate simulation by MIROC5: Mean states, variability, and climate sensitivity. J of Climate, 23: 6312-6335.

Wilks, DS. (1995). Statistical Methods in Atmospheric Science, Volume 59 of International Geophysics Series. Academic Press: San Diego, London.

Wood, A.W., Leung, L.R., Sridhar, V., & Lettenmaier, D.P. (2004). Hydrologic implications of dynamical and statistical approaches to downscale climate model outputs. Climatic Change, 62: 189–216.

Yukimoto, S., et al. (2012). A New Global Climate Model of the Meteorological Research Institute: MRI-CGCM3 - Model Description and Basic Performance. J of the Meteorological Society of Japan, 90A: 23-64.

Zhu, J. (2013). Impact of climate change on extreme rainfall across the United States. Journal of Hydrologic Engineering, 18: 1301-1309.

Chapter 6 – HYDROLOGIC PROJECTIONS

Abstract

Projected climate model precipitation (from four CMIP5 GCMs dynamically downscaled using RegCM4) was applied to hydrologic models to determine projected first-order stream flow characteristics and compare to observed stream flow characteristics, in order to determine the validity of the assumption that the statistical characteristics of hydrologic time series data are constant through time. The study streams are located in central Indiana, central Michigan, and east central Illinois. Hydrologic models were developed for each study stream within the U.S. Army Corps of Engineers (USACE) Hydrologic Engineering Center-Hydrologic Modeling System (HEC-HMS) Version 4.0 modeling application and regression equation outputs and gauge data from gauges within the same region and with watershed hydrologic features similar to the study streams were used to corroborate HEC-HMS outputs. Design event rainfall data (averaged from all four climate models) was obtained from precipitation frequency analysis of observed (1980-1999 and 1990-2009) records using the regional L-Moments method. The HEC-HMS hydrologic events models were run for the 0.5-, 1-, 2-, 5-, 10-, 25-, 50-, and 100-year events. Continuous 20-year precipitation was also utilized for long-term simulations. Observed precipitation (1980-1999 and 1990-2009 gauge data), simulated precipitation (1980-1999 RCM data), and projected precipitation (2040-2059 and 2080-2099 RCM data) was used to model long-term flow behavior of the study streams.

The result indicate increases in peak flood events across all return periods for the projected timeframes compared to observed conditions. In Indiana and Michigan the projected (2080-2099) peak flow events are larger than the projected (2040-2059) peak flows while in Illinois the projected (2080-2099) peak flow events are larger than or equal to the former events. Analysis of the number of days projected

stream flow exceeds the 0.5-, 1-, and 10-yr design flows during the 20-yr simulation showed a wide range of results between the two models representing the upper and lower bounds of maximum precipitation estimates for a majority of return periods for each projected timeframe at each location. Generally there was an increase in exceedances during the projected timeframes compared to current conditions, but on a yearly average basis the increase were minimal. Only in Michigan, where watershed specific variables contribute to increases in the temporal length of the peak flood events, were the differences in exceedance between present and projected conditions on the order of one week to ten days. The results suggest the magnitude and total length of peak flow events will increase in the future, but high data and modeling uncertainty makes it difficult to exactly quantify the potential future changes in stream hydrology.

Keywords: Precipitation, stream hydrology, peak flood, climate change, riverine flooding

6.1 Introduction

Beyond the question of precipitation, is the issue of how changes in precipitation will impact stream hydrology. Of specific note is the issue of stationarity, or the assumption that the statistical characteristics of hydrologic time series data are constant through time, which enables the use of well-accepted, simplified statistical methods in water resources planning and design. If the magnitude, duration, or frequency of peak floods change in the future compared to current conditions, current engineering design techniques and the resulting built infrastructure may be under or over designed for future conditions. Climate change has shown the assumption of stationarity to be invalid (USACE, 2014).

Wright et al. (2012) used daily precipitation statistics from four climate models and three greenhouse gas (GHG) emissions scenarios (A2, A1B, and B1) to projected changes in streamflow for HUC 8 watersheds across the United States. They found significant increases in flow from the 100-year, 24-hr precipitation event that imply that the entire frequency distribution of flows may shift in the future. For example, what once was a 100-year event may be a 50-year event in the future. The shift of the entire frequency distribution because of climate change could have important implications for the life-cycle costs of maintaining stormwater infrastructure. Fowler and Kilsby (2007) used dynamically downscaled RCM precipitation output as input to hydrological models to simulated daily flow distributions in eight catchments. Results suggested RCM data can be used with some confidence to examine future changes in flow regime and suggested changing seasonality of flow regimes compared to historic observations.

The main purpose of this chapter was to apply projected climate model precipitation to hydrologic models to determine projected stream flow characteristics and compare to present-day stream flow characteristics, generated from observed precipitation data. Hydrologic models were developed for each study stream within the U.S. Army Corps of Engineers (USACE) Hydrologic Engineering Center-Hydrologic Modeling System (HEC-HMS) Version 4.0 modeling application (USACE, 2000). Regression equation outputs and gauge data from gauges within the same region and with watershed hydrologic features similar to the study streams were used to corroborate HEC-HMS outputs. Design event rainfall data (averaged from all four climate models) was obtained from precipitation frequency analysis of observed (1980-1999 and 1990-2009) records using the regional L-Moments method (Hosking and Wallis, 1997). The HEC-HMS hydrologic events models were run for the 0.5-, 1-, 2-, 5-, 10-, 25-, 50-, and 100-year events. Continuous 20-year precipitation was also utilized for long-term simulations. Observed precipitation (1980-1999 and 1990-2009 gauge data), simulated precipitation (1980-1999 RCM data),

and projected precipitation (2040-2059 and 2080-2099 RCM data) was used to model long-term flow behavior of the study streams.

6.2 Methods

6.2.1 Regression Equations

Rao (2006), Holtschlag and Croske (1984), and Soong et al. (2004), developed annual maximum series regression equations for rural streams in Indiana, Michigan, and Illinois, respectively. The regression equations were established by estimating peak discharges using a Log-Pearson Type III distribution. Independent variables in the equations generally include drainage area, channel slope, and a regional factor, where drainage area and main channel slope are determined from a topographic map, and the regional factor is a constant dependent upon the geographical location of the sites within each state. Additional variables include soil permeability for the Illinois equations, degree of urbanization for the Illinois and Indiana equations, and average snowfall for the Michigan equations. Soil permeability is determined from an average soil permeability map (the arithmetic average of the high and low soil permeability values from STATSGO database) (Soil Survey Staff, 2015) and urbanization is determined from the Multi-Resolution Land Characteristics (MRLC) Consortium National Land Cover Database (NLCD 2011) (Homer et al., 2015). Specific equations for each site can be found in the cited reports.

Drainage area, channel slope, and permeability were obtained from StreamStats, a web-based GIS application created by the United States Geological Survey in cooperation with the Environmental Systems Research Institute. Regression equation outputs were used to corroborate HEC-HMS outputs.

6.2.2 Stage Data

The U.S. Geological Survey (USGS) owns and maintains a nationwide network of stream gauges. Although all study streams are ungagged at the point of interest, gauges within the same region and with watershed hydrologic features similar to the study streams were compiled. Peak flow data from the gauged sites were compared to the hydrologic model peak flow values.

6.2.3 HEC-HMS

Hydrologic models were developed for each study stream within the U.S. Army Corps of Engineers (USACE) Hydrologic Engineering Center-Hydrologic Modeling System (HEC-HMS) Version 4.0 modeling application (USACE, 2000).

Precipitation

Design event rainfall data was obtained from precipitation frequency analysis of observed (1980-1999 and 1990-2009) records using the regional L-Moments method (See Section 4.3.6). Design event rainfall depths were used to support design event modeling performed for existing conditions assessments. The observed (1980-1999 and 1990-2009) records were used due to the fact that the former period was used to bias correct the RCM precipitation and the latter is the most recent for representing present-day conditions. Design event rainfall depths from the bias corrected RCM L-moments output (Section 5.3.4 L-Moment Analyses) was also used to model the effects of changes in design storm on design events.

Continuous 20-year precipitation was also utilized for long-term simulations. Observed precipitation (1980-1999 and 1990-2009 gauge data), simulated precipitation (1980-1999 RCM data), and projected precipitation (2040-2059 and 2080-2099 RCM data) was used to model long-term flow behavior of the study streams.

Huff Distribution

Huff (1990) used data from long-term operation of three recording rain gauge networks in Illinois to develop time distribution relationships. Although based upon Illinois data, these relationships should be applicable for other states in the region and other locations of similar precipitation (Huff and Angel, 1992). The Illinois study was undertaken because earlier time distribution models, developed by the Soil Conservation Service (SCS) (1972) and others, were not considered satisfactory for use with the Midwest's heavy rainstorms.

Runoff Volume Calculation

The SCS CN loss model uses the empirical CN parameter to calculate runoff volumes based on landscape characteristics such as soil type, land cover, imperviousness, and land use development. Areas characterized by saturated or poorly infiltrating soils, or impervious development, have higher CN values, converting a greater portion of rainfall volume into runoff. The SCS methodology uses Equation 6.1 to compute stormwater runoff volume for each time step (USDA, 1986):

$$Q = \frac{(P - I_a)^2}{(P - I_a) + S}$$

Equation 6.1

where Q is runoff volume, P is precipitation, S is the storage coefficient, and I_a is the initial abstractions. Rainfall abstractions due to ponding and evapotranspiration can be simulated using an initial abstractions I_a parameter. The commonly used default value of I_a is estimated as 0.2 × S, where S is the storage coefficient for soil in the subbasin. S is related to CN through Equation 6.2:

$$S = \frac{25400}{CN} - 254$$

Equation 6.2

where CN is the curve number. Table 6.1 describes the input data used to develop the CN values throughout the watershed.

Table 6.1. Description of Curve Number Input Data

Variable Used to Determine CN	Approach for Definition of Variable for Rock River Subwatershed Hydrologic Modeling
Ground cover	The 2011 Multi-Resolution Land Characteristics (MRLC) Consortium National Land Cover Database (NLCD 2011) was used. A lookup table was developed to link NLCD categories to categories for which CN values have been estimated.
Soil type	The Natural Resources Conservation Service (NRCS) publishes county soil surveys that include a hydrologic classification of A, B, C, or D. If a soil group's infiltration capacity is affected by a high water table, it is classified as, for instance, "A/D," meaning the drained soil has "A" infiltration characteristics, undrained "D." It was assumed that half of these soil groups (by area) are drained for crop land, undrained for all other land use types.
Antecedent moisture condition	Antecedent Moisture Conditions (AMC) reflect the initial soil storage capacity available for rainfall. For areas within the Midwest it is typical to assume an AMC of II.

The U.S. Department of Agriculture, Natural Resources Conservation Service (NRCS) Soil Survey Geographic (SSURGO) soil data (Soil Survey Staff, 2015) and the Multi-Resolution Land Characteristics (MRLC) Consortium National Land Cover Database (NLCD 2011) (Homer et al., 2015) where used to as inputs to generate CN values. Land cover has a significant effect on basin hydrology, affecting the volume of runoff produced by a given area and the speed of runoff delivered to the receiving system. Impervious areas restrict infiltration and produce more runoff, which is often delivered to receiving systems more rapidly through storm sewer networks. The NLCD data include 16 land cover classifications. The SSURGO soil data includes hydrologic soil group, representing the minimum infiltration rate of the soil after wetting. Table 6.2 summarizes the hydrologic soil groups.

Table 6.2. Hydrologic Soil Groups

Hydrologic Soil Group	Description	Texture	Infiltration Rates (mm/hr)
A	Low runoff potential and high infiltration rates even when wetted	Sand, loamy sand, or sandy loam	>7.62
B	Moderate infiltration rates when wetted	Silt loam or loam	3.81-7.62
C	Low infiltration rates when wetted	Sandy clay loam	1.27-3.81
D	High runoff potential and very low infiltration when wetted	Clay loam, silty clay loam, sandy clay, silty clay or clay	0-1.27

All data from *Technical Release 55, Urban Hydrology for Small Watersheds* (USDA, 1986)

Specific combinations of land use and soil type were linked to CN values using a lookup table based on values recommended in Table 6.3 excerpted from TR-55: Urban Hydrology for Small Watersheds (USDA, 1986). The CN matrix includes assumptions about the imperviousness of land use classes, and therefore, percent impervious does not need to be explicitly considered as the SCS runoff volume calculation.

Table 6.3. Runoff Curve Numbers for Urban Areas

Cover Type and Hydrologic Condition	Avg. % Impervious Area	A	B	C	D
Fully developed urban areas (vegetation established)					
Open Space (lawns, parks, golf courses, cemeteries, etc.)					
Poor condition (grass cover <50%)		68	79	86	89
Fair condition (grass cover 50 to 75%)		49	69	79	84
Good condition (grass cover > 75%)		39	61	74	80
Impervious Areas					
Paved parking lots, roofs, driveways, etc. (excluding right-of-way)		98	98	98	98
Streets and roads					
Paved; curbs and storm sewers (excluding right-of-way)		98	98	98	98
Paved; open ditches (including right-of-way)		83	89	92	93
Gravel (including right-of-way)		76	85	89	91
Dirt (including right-of-way)		72	82	87	89
Western Desert Urban Areas					
Natural desert landscaping (pervious areas only)		63	77	85	88
Artificial desert landscaping (imperious weed barrier, desert shrub with 1- to 2-inch sand or gravel mulch and basin barriers		96	96	96	96
Urban Districts					
Commercial and business	85	89	92	94	95
Industrial	72	81	88	91	93
Residential Districts by Average Lot Size					
1/8 acre or less	65	77	85	90	92
¼ acre	38	61	75	83	87
1/3 acre	30	57	72	81	86
½ acre	25	54	70	80	85
1 acre	20	51	68	79	84
2 acres	12	46	65	77	82
Developing Urban Areas					
Newly Graded Areas (pervious areas only, no vegetation)		77	86	91	94

Note: Average runoff condition, and I_a=0.2S
Note: Table Source is *TR-55: Urban Hydrology for Small Watersheds* (USDA, 1986)

See Chapter 3 for study site specific summaries of land cover, soil, and CN data.

Runoff Hydrograph Production

The runoff volume produced for a subbasin is converted into a basin-specific hydrograph by using a synthetic unit hydrograph. A synthetic unit hydrograph relates the parameters of parametric unit hydrograph model to specific watershed characteristics. The SCS Unit Hydrograph method is used for the study watersheds. The SCS unit hydrograph for developing a unit hydrograph is based on observed

data collected in small, agricultural watersheds in the United States. Rural unit hydrographs derived from gauged rainfall and runoff were averaged to form a single-peaked, dimensionless unit hydrograph. Within the dimensionless unit hydrograph, the discharge (U_t) is expressed as a ratio to the peak discharge (U_p) for any time t, a fraction of T_p (the time of peak discharge). The unit hydrograph peak and time to peak are related by the following expression (USDA, 1986):

$$U_p = C\frac{A}{T_p}$$

Equation 6.3

where A is watershed area C is a conversion constant. The time to peak can be calculated by the expression:

$$T_p = \frac{\Delta t}{2} + t_{lag}$$

Equation 6.4

where Δt is excess precipitation duration and t_{lag} is basin lag, or the time difference between the center of mass of rainfall excess and the peak of the unit hydrograph. In gauged watersheds, the basin lag can be determined through model calibration. For un-gauged watersheds, however, lag time can be calculated as (USACE, 2013):

$$t_{lag} = \frac{(L^{0.8}(\mathrm{S}+1)^{0.7})}{1900 \times Y^{0.5}}$$

Equation 6.5

Where L is the hydraulic length of the watershed, S is the storage coefficient, and Y is the basin slope.

Runoff Routing

The hydrographs created for each subbasin using the SCS Unit Hydrograph method are sometimes routed within HEC-HMS in upstream areas where the resolution of subbasins defined is greater than the hydraulic model extent. The channel routing models compute a downstream hydrograph for each

channel reach when given an upstream hydrograph as an upstream boundary condition. The Muskingum-Cunge method for hydrologic routing was used for the study reaches

Muskingum-Cunge routing is based on the assumption that the storage volume in a stream reach at an instant in time is a linear function of weighted inflow and outflow. The Muskingum-Cunge routing equation is (USACE, 2000):

$$O_t = C_1 I_{t-1} + C_2 I_t + C_3 O_{t-1} + C_4 (q_L \Delta x)$$

Equation 6.6

where O_t, O_{t-1} are outflow hydrograph ordinates at time *t* and *t*-1, I_t, I_{t-1} are inflow hydrograph ordinates at time *t* and *t*-1, q_L is lateral inflow, Δx is the computation distance step, and C_1, C_2, C_3, and C_4 are coefficients.

The Coefficients are:

$$C_1 = \frac{\frac{\Delta t}{K} + 2X}{\frac{\Delta t}{K} + 2(1 - X)}$$

Equation 6.7

$$C_2 = \frac{\frac{\Delta t}{K} - 2X}{\frac{\Delta t}{K} + 2(1 - X)}$$

Equation 6.8

$$C_3 = \frac{2(1 - X) - \frac{\Delta t}{K}}{\frac{\Delta t}{K} + 2(1 - X)}$$

Equation 6.9

$$C_4 = \frac{2\left(\frac{\Delta t}{K}\right)}{\frac{\Delta t}{K} + 2(1 - X)}$$

Equation 6.10

where parameters *K* and *X* are:

$$K = \frac{\Delta x}{c}$$

Equation 6.11

$$X = \frac{1}{2}\left(1 - \frac{Q}{BS_o c \Delta x}\right)$$

Equation 6.12

where Q is flow, B is top width of water surface, S_o is channel slope, and c is wave celerity (speed).

Channel characteristics such as channel shape, reach length, roughness coefficient(s), and energy grade must be specified. HEC-geoHMS calculates reach lengths and estimates energy slopes as computed reach slopes for input for HEC-HMS. Channel shape and roughness were determined from a combination of aerial imagery, survey data, and site photos.

Watershed and Subwatershed Delineation

Terrain preprocessing and watershed delineation were completed using the HEC-geoHMS v10.1 toolkit for ArcGIS 10.1. The topographic data for each study watershed was developed from light detection and ranging (LiDAR) data. See Chapter 3 for details.

Occasionally, the elevation data contains constructed structures that do not represent surface hydrology, for instance, raised roadways that do not restrict overland flow. The delineation in these areas was modified to best represent surface hydrology. Storm-sewer networks were also considered in the delineation of some areas, particularly in low gradient areas where ground slope was slight or inconclusive and the required data was available. The watersheds for each studied stream were divided into subbasins based upon consideration of the direction of steepest descent from local elevation maxima. The size of subbasins varied based upon the drainage network density and proximity to the hydraulically modeled waterway. Subbasin boundaries were modified is determined necessary, for example, when retention ponds or lakes were encountered. Boundaries were defined to most

accurately represent the actual area tributary to specific modeled elements. GIS data was developed for all subbasins delineated and used for hydrologic model data development.

6.3 Results

6.3.1 Nineveh Creek (Camp Atterbury, IN)

The following section provides HEC-HMS model overview and hydrologic results for Nineveh Creek at Camp Atterbury. See Section 3.1 for applicable HEC-HMS input datasets.

HEC-HMS Model

Figure 6.1 is a schematic of the HEC-HMS model for the Nineveh watershed upstream of the Impact Area at Camp Atterbury. Table 6.4 lists the subbasin name, the sub-basin area, the time of concentration, and the average curve number for each sub-basin.

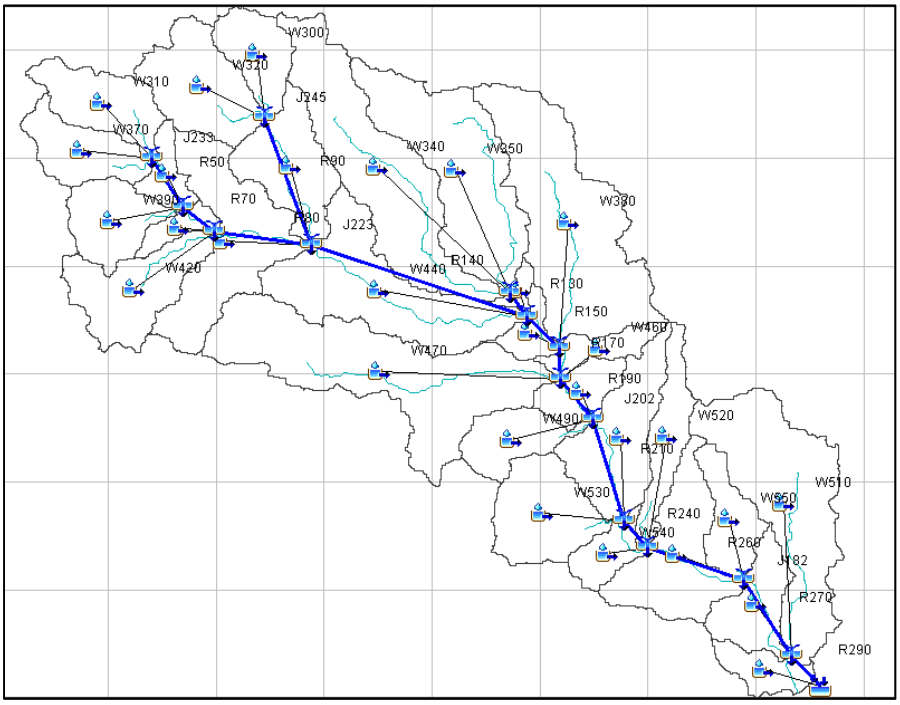

Figure 6.1. Schematic of the HMS model for Nineveh Creek

Table 6.4. Major properties of the sub-watersheds for the Nineveh Creek

Sub-basin name	*Sub-basin area (km^2)*	*Time of Concentration (MIN)*	*Curve number*	*Sub-basin name*	*Sub-basin area (km^2)*	*Time of Concentration (MIN)*	*Curve number*
W580	0.41113	68.958	70.1	W430	0.12	38.389	71.2
W570	1.4125	73.795	73.6	W420	1.1717	45.592	80.7
W560	0.7471	69.611	73.3	W410	1.8282	51.292	79.6
W550	0.64096	63.187	76.2	W400	0.25368	26.196	73.8
W540	0.41264	62.176	70.3	W390	0.80857	39.533	82.1
W530	1.1532	57.334	70.6	W380	2.9305	145.15	76.7
W520	0.70545	103.74	80.4	W370	0.78413	45.349	84.2
W510	2.4667	141.37	69.4	W360	0.32674	25.815	78.9
W500	1.342	117.92	72.9	W350	2.2934	110.96	78.7
W490	0.66178	63.983	69.2	W340	2.4993	102.98	84.1
W480	0.49947	55.569	72.9	W330	1.1362	36.836	84.4
W470	3.1586	99.964	77.8	W320	1.2126	42	86.3
W460	0.37762	62.957	74.1	W310	0.89716	49.503	86.2
W450	0.28718	55.539	67.8	W300	0.67975	31.703	90.1
W440	2.1702	73.799	78.7				

Critical Duration Analysis

A critical-duration analysis was performed to determine the storm duration that generally results in higher flow rate estimates for Nineveh Creek. Storm ARIs of 1-, 10-, and 100-yrs (observed 1990-2009 precipitation) was analyzed with a range of storm durations to determine estimated flow rates in HEC-HMS. Two locations were chosen, near the LWCs and near the bridge structures; these locations are denoted by HEC-HMS element names and correspond roughly to HEC-RAS river stations (RS). The results for Nineveh Creek are summarized in Table 6.5. The highest flow rate at each river station location is highlighted.

Table 6.5. Nineveh Creek critical duration analysis

Location	Rainfall Distribution and Duration	Drainage Area (sq km)	1yr-Flow Rate (cms)	10yr-Flow Rate (cms)	100yr-Flow Rate (cms)
J193	Huff, 1hr	26.6	9.3	27.8	65
	Huff, 2hr		14.1	38.4	100.2
	Huff, 3hr		15.5	39.8	97.9
	Huff, 6hr		***21***	***54.2***	***127.7***
	Huff,12hr		20.4	50.5	94.7
J215	Huff, 1hr	16.2	9.7	33.2	70.4
	Huff, 2hr		12.9	30.4	95.1
	Huff, 3hr		13.8	40.2	90.4
	Huff, 6hr		***17.7***	***48.4***	***106.2***
	Huff,12hr		15.6	38	67.5

If no single storm can be identified as a critical duration for every location in the watershed it is desirable and common practice to select one duration storm event to use for comprehensive watershed planning efforts. The results of the Nineveh Creek analysis support selecting the 6-hour duration storm.

Hydrologic Analysis-Peak Flood

Model calibration and verifications was not possible for the Nineveh Creek HEC-HMS model directly, because no long term gauging station is located within or near the study reach. HEC-HMS peak flow results using observed (1990-2009) precipitation values were compared to StreamStats values for two locations on Nineveh Creek (Table 6.6). At the upstream location the flow rates for ARIs of 2-50 years are within 10% of StreamStats flow while for remaining ARIs the model flow rates are higher than those produced by StreamStats. At the downstream location, model flows are less than StreamStats for ARIs less than 50 years and more than StreamStats for ARIs greater than 50 years.

Table 6.6. Published and simulated HEC-HMS peak flood comparison for different return periods

Return Period	HMS-J193	StreamStats	
(yr)	(m^3/s)	(m^3/s)	% diff
1	21	18.9	11%
2	27.3	32.3	-17%
5	40.2	50.0	-22%
10	54.2	63.1	-15%
25	76.6	81.0	-6%
50	98.1	94.9	3%
100	127.7	107.9	17%
500	161.2	138.8	15%

Return Period	HMS-J215	StreamStats	
(yr)	(m^3/s)	(m^3/s)	% diff
1	17.7	13.3	29%
2	25.5	24.8	3%
5	37.4	39.9	-7%
10	48.4	51.5	-6%
25	66.7	66.5	0%
50	85.2	78.2	9%
100	106.2	89.5	17%
500	132.4	116.4	13%

HMS peak flows using observed (1990-2009) precipitation values (considered present conditions) were also compared to peak stream flow data from a USGS gauge station (03354500) on Beanblossom Creek, located west of Camp Atterbury in Brown County. Beanblossom Creek watershed is similar to Nineveh Creek watershed, in land cover, topography, and size, with a drainage area of 37.8 km^2 at the gauge station. The USGS 03354500 station has 42 years of data, ending operation in 1993. Table 6.7 shows peak stream flow comparisons, taking into account the difference in drainage area between the two watersheds. The peak flow rate are within +/- 15% for ARIs of 1-25 years.

Table 6.7. Nineveh Creek and Beanblossom Creek peak flood comparison for different return periods

Return Period	HMS-J193 Nineveh Cr	Beanblossom Cr	
(yr)	(m^3/s)	(m^3/s)	% diff
1	21	18.1	14.8%
2	27.3	26.3	3.7%
5	40.2	35.4	12.8%
10	54.2	52.5	3.3%
25	76.6	86.9	-12.6%

HMS peak floods using present conditions (observed, 1990-2009) inputs were also compared to peak floods generated from average projected RCM precipitation values (See Section 5.3.4). The results (Table 6.8) show the difference between presents and projected (2040-2059) peak flows to be 7%-40%. The projected peak flow are larger than present conditions for all ARIs, and are larger in magnitude for larger return periods. Projected (2080-2099) peak flows are also larger than present conditions by 80%-95%.

Table 6.8. Peak floods comparison between present conditions (1990-2009) and average RCM projections (2040-2059 and 2080-2099) for different return periods

Return Period (yr)	Present (m^3/s)	Avg RCM 2040 (m^3/s)	Avg RCM 2080 (m^3/s)	Percent Diff Present-RCM 2040	Percent Diff Present-RCM 2080
0.5	12.4	13.6	30.0	9.2%	83.0%
1	21	22.5	48.2	6.9%	78.6%
2	27.3	32.0	73.5	15.9%	91.7%
5	40.2	49.3	111.0	20.3%	93.7%
10	54.2	70.8	150.3	26.6%	94.0%
25	76.6	105.8	196.7	32.0%	87.9%
50	98.1	146.0	255.9	39.2%	89.2%
100	127.7	178.0	331.5	32.9%	88.8%

Figure 6.2 shows Nineveh Creek hydrographs for ARIs of 0.5-, 1-, 2-, 5-, 10-, 25-, 50-, and 100-years for present conditions and average RCM projections, and includes published flood peaks (StreamStats) at the LWCs. Present and projected (2040-2059) peak floods are similar for low ARIs, but the projected peaks are larger than present peaks as ARI increases. Projected (2080-2099) peak flood are noticeably larger than the other flood scenarios.

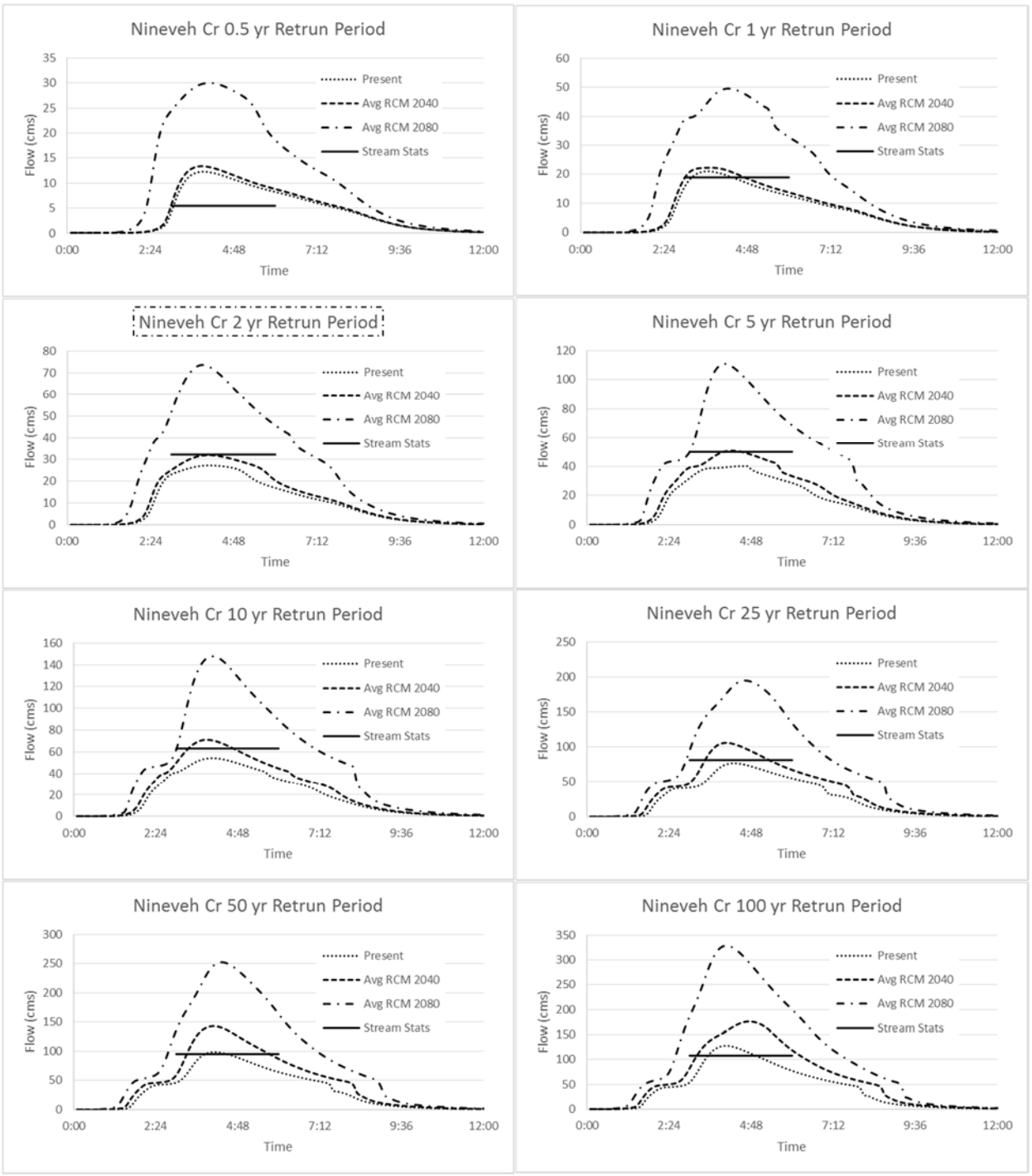

Figure 6.2. Hydrographs for various return periods at Nineveh Creek (J193) for the present time, projected times (2040-2059 and 2080-2099), and published peak floods.

Hydrologic Analysis-Continuous Simulation

Continuous 20-year simulations were also run through the Nineveh Creek HEC-HMS model. The hydrologic outputs resulting from observed precipitation input (1980-1999) was compared to outputs produced by RCM simulation precipitation from the MRI and IPSL models. MRI and IPSL produced the largest and smallest projected estimated maximum precipitation values for Columbus, IN, respectively, so a comparison of their results show the range of RCM projections (see Section 5.3.4). Table 6.9 shows the number of days Nineveh Creek exceeds the 0.5-, 1-, and 10-yr design flows during the 20-yr simulation given precipitation inputs of observed (1980-1999 and 1990-2009) values and simulated MRI and IPSL (1980-1999) values. The difference between the four scenarios is minimal, while the occurrences of flow exceedance for ARIs of 0.5 and 1 years are larger than expected. However, the number of days the flow is greater than the various design flows denotes that total time interval of high flows, not the number of high flow events or individual exceedances. Also, the difference between observed scenarios is larger than the differences between observed and simulated scenarios.

Table 6.9. Comparison of the number of days Nineveh Creek is above various design flows given precipitation inputs of present conditions (1980-1999) and RCM simulations (1980-1999) for IPSL and MRI. Continuous simulation of 20 years.

Return Period (yr)	Present (1980-1999) days	IPSL (1980-1999) days	MRI (1980-1999) days	Present (1990-2009) days	Percent Diff Pres 1980 - IPSL 1980	Percent Diff Pres 1980 - MRI 1981	Percent Diff Pres 1980 - Pres 1990
0.5	120.1	131.9	119.9	140.1	9.3%	-0.2%	15.4%
1	45.0	48.8	44.9	48.8	8.0%	-0.3%	8.0%
10	1.75	1.63	1.75	1.25	-7.4%	0.0%	-33.3%

Table 6.10 shows the number of days Nineveh Creek exceeds the 0.5-, 1-, and 10-yr design flows during the 20-yr simulation given precipitation inputs of observed (1990-2009) values (assumed to be present conditions) and projected MRI and IPSL (2040-2059) values. The difference between present conditions and IPSL and MRI projected (2040-2059) conditions is relatively minor. IPSL projects slightly fewer days

of flow greater than the 0.5-yr design flow while both RCMs project more days of flow greater than the 1-yr design flow. Both RCMs project fewer days greater than the 10-yr design flow.

Table 6.10. Comparison of the number of days Nineveh Creek is above various design flows given precipitation inputs of present conditions (1990-2009) and RCM projections (2040-2059) for IPSL and MRI. Continuous simulation of 20 years.

Return Period (yr)	Present (1990-2009) Total days	IPSL (2040-2059) Total days	MRI (2040-2059) Total days	Percent Diff Pres 1990 - IPSL 2040	Percent Diff Pres 1990 - MRI 2040
0.5	140.1	132.4	144.3	-5.7%	2.9%
1	48.8	53.1	55.0	8.6%	12.0%
10	1.25	0.75	1.00	-50.0%	-22.2%

Table 6.11 shows the number of days Nineveh Creek exceeds the 0.5-, 1-, and 10-yr design flows during the 20-yr simulation given precipitation inputs of observed (1990-2009) values (assumed to be present conditions) and projected MRI and IPSL (2080-2099) values. The difference between present conditions and IPSL and MRI projected (2080-2099) conditions is large, especially for return periods greater than 0.5-yrs. IPSL and MRI project an average of 19, 25, and 7 more days than present conditions of flow greater than the ARI design flows of 0.5-, 1-, and 10-yrs.

Table 6.11. Comparison of the number of days Nineveh Creek is above various design flows given precipitation inputs of present conditions (1990-2009) and RCM projections (2080-2099) for IPSL and MRI. Continuous simulation of 20 years.

Return Period (yr)	Present (1990-2009) Total days	IPSL (2080-2099) Total days	MRI (2080-2099) Total days	Percent Diff Pres 1990 - IPSL 2080	Percent Diff Pres 1990 - MRI 2080
0.5	140.1	152.4	165.5	8.4%	16.6%
1	48.8	75.0	72.6	42.4%	39.3%
10	1.25	9.25	7.4	152.4%	142.0%

6.3.2 East Branch Au Sable (Camp Grayling)

The following section provides HEC-HMS model overview and hydrologic results for East Branch Au Sable River near Camp Grayling, Michigan. See Section 3.1 for applicable HEC-HMS input datasets.

HEC-HMS Model

Figure 6.3 is a schematic of the HEC-HMS model for the East Branch Au Sable watershed upstream of the confluence with the Au Sable River. Table 6.12 lists the subbasin name, the sub-basin area, the time of concentration, and the average curve number for each sub-basin.

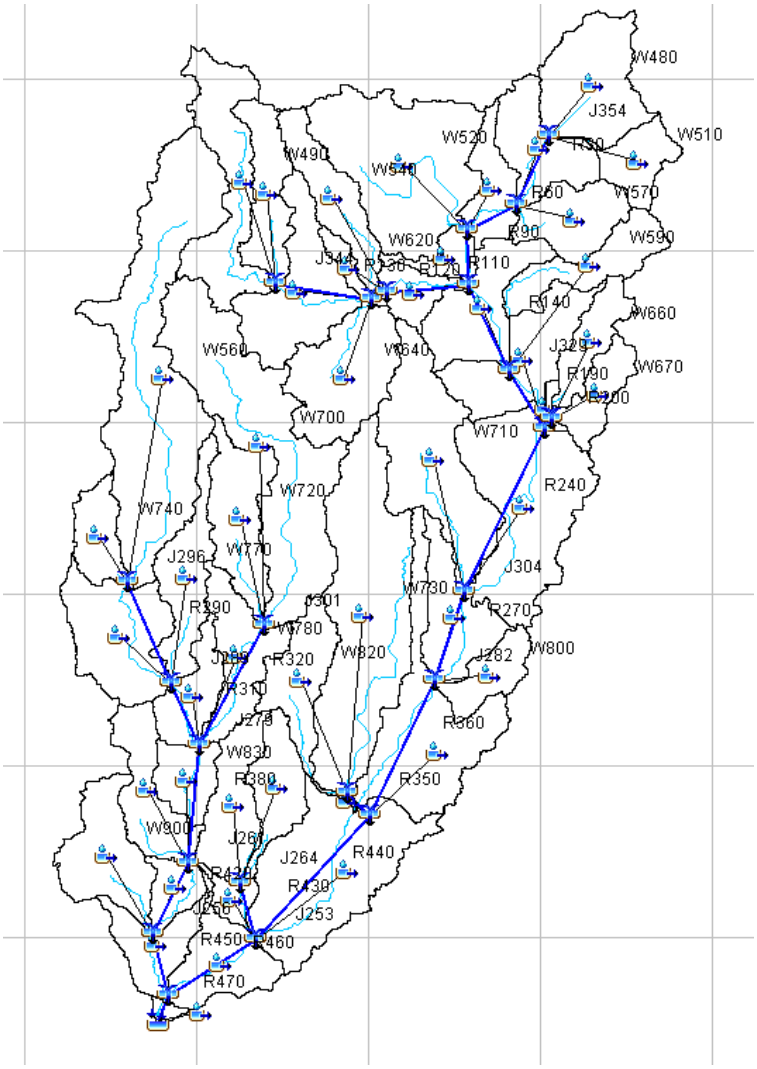

Figure 6.3. Schematic of the HMS model for East Branch Au Sable River

Table 6.12. Major properties of the sub-watersheds for the East Branch Au Sable River

Sub-basin name	*Sub-basin area (km^2)*	*Time of Concentration (MIN)*	*Curve number*	*Sub-basin name*	*Sub-basin area (km^2)*	*Time of Concentration (MIN)*	*Curve number*
W940	0.25	169.25	49.38	W700	10.74	451.35	43.02
W930	3.04	300.45	42.79	W690	8.13	302.04	44.97
W920	2.25	292.48	54.28	W680	0.23	74.07	40.74
W910	0.77	465.69	46.70	W670	1.80	171.13	32.74
W900	3.76	281.22	35.20	W660	1.90	263.34	31.84
W890	1.43	207.43	50.95	W650	4.31	282.40	38.35
W880	2.95	289.37	32.48	W640	4.91	223.80	33.50
W870	2.44	232.06	45.73	W630	4.89	248.17	37.20
W860	3.18	239.99	49.18	W620	0.64	164.40	32.67
W850	8.25	394.09	42.57	W610	3.85	248.75	43.39
W840	0.05	98.69	63.82	W600	1.38	171.83	33.78
W830	1.83	185.04	35.06	W590	2.77	348.97	32.52
W820	3.09	304.69	37.54	W580	1.04	196.40	43.59
W810	2.16	225.12	33.49	W570	2.83	284.49	32.10
W800	1.77	201.59	35.25	W560	13.16	524.36	35.59
W790	6.76	418.74	43.56	W550	2.89	243.50	44.32
W780	3.29	282.36	34.41	W540	2.89	275.66	38.73
W770	3.25	304.94	39.15	W530	2.04	271.55	34.71
W760	3.20	290.30	50.15	W520	8.78	272.91	41.34
W750	4.82	236.39	33.18	W510	1.89	223.83	31.82
W740	1.84	205.29	33.55	W500	3.20	273.60	31.35
W730	10.83	600.00	42.24	W490	5.11	417.80	37.97
W720	3.74	275.74	37.37	W480	4.76	215.32	34.02
W710	6.92	325.47	38.53				

Critical Duration Analysis

A critical-duration analysis was performed to determine the storm duration that generally results in higher flow rate estimates for East Branch Au Sable River. Storm ARIs of 1-, 10-, and 100-yrs (observed 1990-2009 precipitation) was analyzed with a range of storm durations to determine estimated flow rates in HEC-HMS. Two locations were chosen, near the LWC and upstream of the confluence with the

Au Sable River; these locations are denoted by HEC-HMS element names and correspond roughly to HEC-RAS river stations (RS). The results for East Branch Au Sable River are summarized in Table 6.13. The highest flow rate at each river station location is highlighted.

Table 6.13. East Branch Au Sable River critical duration analysis

Location	Rainfall Distribution and Duration	Drainage Area (sq km)	1yr-Flow Rate (cms)	10yr-Flow Rate (cms)	100yr-Flow Rate (cms)
Outlet	Huff, 6hr	176.0	1.1	2.4	6.2
	Huff, 12hr		***1.3***	2.8	10.5
	Huff, 24hr		***1.3***	2.8	10
	Huff, 48hr		1.1	3.1	13.2
	Huff, 120hr		1	***3.9***	***16.5***
R440	Huff, 6hr	102.9	1.1	2.4	5.2
	Huff, 12hr		***1.3***	***2.7***	***7.3***
	Huff, 24hr		***1.3***	2.6	6.6
	Huff, 48hr		1.1	2.4	6.8
	Huff, 120hr		1	2.4	7.2

If no single storm can be identified as a critical duration for every location in the watershed it is desirable and common practice to select one duration storm event to use for comprehensive watershed planning efforts. The results of the East Branch Au Sable River analysis support selecting the 12-hour duration storm, which is the critical duration for the LWC of interest for this study.

Hydrologic Analysis-Peak Flood

Model calibration and verifications was possible for the East Branch Au Sable River HEC-HMS model directly, due to a long term gauging station being located near the study reach. USGS 04135600 gauging station has 26 years of data, ending operation in 1994. The station was located upstream of the confluence with the Au Sable River, near the HEC-HMS model output. Table 6.14 shows HEC-HMS peak flow results using observed (1990-2009) precipitation values were compared to gauge derived values for

the East Branch Au Sable River. The flow rates for ARIs of 1-50 years are within 15% of gauge peak flows.

Table 6.14. Gauge and simulated HEC-HMS peak flood comparison for different return periods

Return Period	East Br Au Sable Gauge	HEC-HMS at Outlet	
(yr)	(m^3/s)	(m^3/s)	% diff
1	2.1	2.3	8.2%
2	2.8	2.6	-8.4%
5	3.7	3.2	-14.5%
10	4.2	3.8	-11.0%
25	4.9	5.2	6.3%
50	5.3	6.3	16.4%
100	5.8	7.5	25.8%

HMS peak flows using observed (1990-2009) precipitation values for the LWC (CG4) location was also compared to the peak stream flows derived from the USGS gauge data, after adjusting the peak flows based on a ratio of the watershed area at the LWC site comparted to the total watershed area. Table 6.15 shows peak stream flow comparisons, taking into account the difference in drainage area between the two watersheds. The peak flow rate are within +/- 28% for ARIs of 1-50 years but reasonably similar when considering the total magnitudes of the peak flows.

Table 6.15. Gauge (adjusted for watershed area) and simulated HEC-HMS peak flood comparison for different return periods

Return Period	East Br Au Sable Gauge	HEC-HMS at R440	
(yr)	(m^3/s)	(m^3/s)	% diff
1	1.6	1.3	-20.4%
2	2.1	1.6	-28.4%
5	2.8	2.2	-23.6%
10	3.2	2.7	-16.8%
25	3.7	3.8	3.2%
50	4.0	5.1	23.5%
100	4.4	6.3	36.5%

HMS peak floods using present conditions (observed, 1990-2009) inputs were also compared to peak floods generated from average projected RCM precipitation values (See Section 5.3.4). The results (Table 6.16) show the difference between present and projected (2040-2059) peak flows to be 32%-57%. The projected peak flow are larger than present conditions for all ARIs, and are larger in magnitude for larger return periods. Projected (2080-2099) peak flows are also larger than present conditions by 57%-97%.

Table 6.16. Peak floods comparison between present conditions (1990-2009) and average RCM projections (2040-2059 and 2080-2099) for different return periods

Return Period (yr)	Present (m^3/s)	Avg RCM 2040 (m^3/s)	Avg RCM 2080 (m^3/s)	Precent Diff Present-RCM 2040	Precent Diff Present-RCM 2080
0.5	1	1.4	1.8	33.3%	57.1%
1	1.3	1.8	2.6	32.3%	66.7%
2	1.6	2.3	3.5	35.9%	74.5%
5	2.2	3.2	5.4	37.0%	84.2%
10	2.7	4.2	7.0	43.5%	88.9%
25	3.8	6.7	10.2	55.2%	91.1%
50	5.1	7.8	13.0	42.3%	87.4%
100	6.6	11.9	19.0	57.9%	97.1%

Figure 6.4 shows East Branch Au Sable hydrographs for ARIs of 0.5-, 1-, 2-, 5-, 10-, 25-, 50-, and 100-years for present conditions and average RCM projections, and includes USGS gauge flood peaks. Present, projected (2040-2059), and projected (2080-2099) peak floods increase in a linearly across all return intervals.

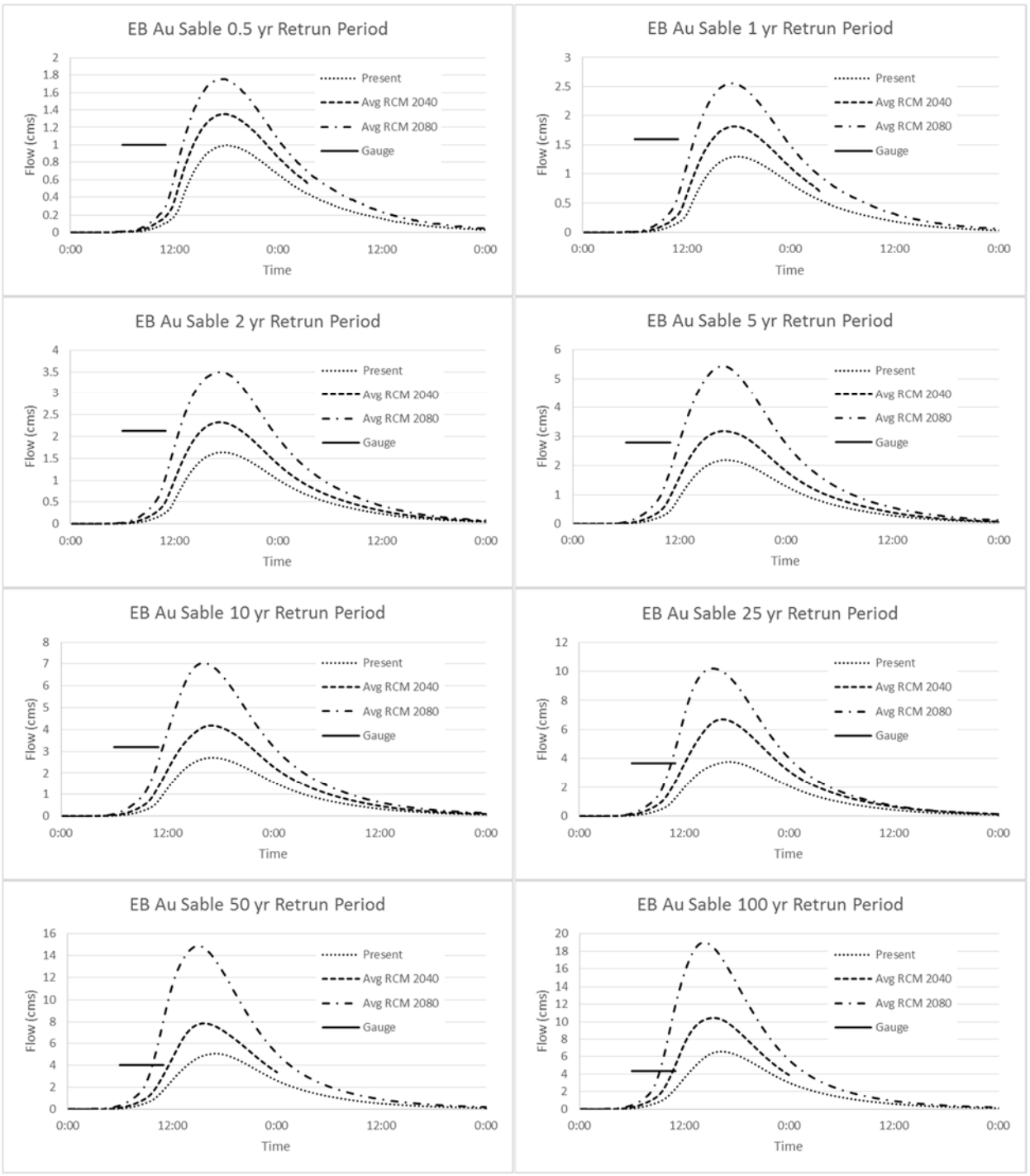

Figure 6.4. Hydrographs for various return periods at East Branch Au Sable River (J440) for the present time, projected times (2040-2059 and 2080-2099), and USGS gauge peak floods.

Hydrologic Analysis-Continuous Simulation

Continuous 20-year simulations were also run through the East Branch Au Sable River HEC-HMS model. The hydrologic outputs resulting from observed precipitation input (1980-1999) was compared to outputs produced by RCM simulation precipitation from the CNRM and MIROC models. CNRM and MIROC produced the smallest and largest projected estimated maximum precipitation values for Grayling, MI, respectively, so a comparison of their results show the range of RCM projections (see Section 5.3.4). Table 6.17 shows the number of days East Branch Au Sable River exceeds the 0.5-, 1-, and 10-yr design flows during the 20-yr simulation given precipitation inputs of observed (1980-1999 and 1990-2009) values and simulated CNRM and MIROC (1980-1999) values. The difference between the four scenarios is minimal, while the occurrences of flow exceedance for ARIs of 0.5 and 1 years are larger than expected. However, the number of days the flow is greater than the various design flows denotes that total time interval of high flows, not the number of high flow events or individual exceedances.

Table 6.17. Comparison of the number of days East Branch Au Sable River is above various design flows given precipitation inputs of present conditions (1980-1999) and RCM simulations (1980-1999) for CNRM and MIROC. Continuous simulation of 20 years.

Return Period (yr)	Present (1980-1999) days	CNRM (1980-1999) days	MIROC (1980-1999) days	Present (1990-2009) days	Percent Diff Pres 1980 - CNRM 1980	Percent Diff Pres 1980 - MIROC 1981	Percent Diff Pres 1980 - Pres 1990
0.5	758.0	735.0	721.0	720.0	-3.1%	-5.0%	-5.1%
1	522.0	506.5	503.5	489.0	-3.0%	-3.6%	-6.5%
10	244.5	239.5	246.0	224.5	-2.1%	0.6%	-8.5%

Table 6.18 shows the number of days East Branch Au Sable River exceeds the 0.5-, 1-, and 10-yr design flows during the 20-yr simulation given precipitation inputs of observed (1990-2009) values (assumed to be present conditions) and projected CNRM and MIROC (2040-2059) values. The difference between

present conditions and CNRM and MIROC projected (2040-2059) conditions is relatively minor. Both models project slightly more days of flow greater than the present design flow for all return periods.

Table 6.18. Comparison of the number of days East Branch Au Sable River is above various design flows given precipitation inputs of present conditions (1990-2009) and RCM projections (2040-2059) for CNRM and MIROC. Continuous simulation of 20 years.

Return Period (yr)	Present (1980-1999) days	CNRM (2040-2059) days	MIROC (2040-2059) days	Percent Diff Pres 1990 - CNRM 2040	Percent Diff Pres 1990 - MIROC 2040
0.5	720.0	809.5	773.5	11.7%	7.2%
1	489.0	560.0	551.0	13.5%	11.9%
10	224.5	275.0	279.5	20.2%	21.8%

Table 6.19 shows the number of days East Branch Au Sable River exceeds the 0.5-, 1-, and 10-yr design flows during the 20-yr simulation given precipitation inputs of observed (1990-2009) values (assumed to be present conditions) and projected CNRM and MIROC (2080-2099) values. The difference between present conditions and CNRM projected (2080-2099) conditions is large for all return periods. MIROC projects slight few days than present conditions of flow greater than the ARI design flows of 0.5- and 1-yr.

Table 6.19. Comparison of the number of days East Branch Au Sable River is above various design flows given precipitation inputs of present conditions (1990-2009) and RCM projections (2080-2099) for CNRM and MIROC. Continuous simulation of 20 years.

Return Period (yr)	Present (1980-1999) days	CNRM (2080-2099) days	MIROC (2080-2099) days	Percent Diff Pres 1990 - CNRM 2080	Percent Diff Pres 1990 - MIROC 2080
0.5	720.0	951.5	660.0	27.7%	-8.7%
1	489.0	713.5	486.5	37.3%	-0.5%
10	224.5	383.0	283.0	52.2%	23.1%

6.3.3 Portage Creek (Camp Grayling)

The following section provides HEC-HMS model overview and hydrologic results for Portage Creek near Camp Grayling, Michigan. See Section 3.1 for applicable HEC-HMS input datasets.

HEC-HMS Model

Figure 6.5 is a schematic of the HEC-HMS model for the Portage Creek watershed upstream of the confluence with the Manistee River. Table 6.20 lists the subbasin name, the sub-basin area, the time of concentration, and the average curve number for each sub-basin.

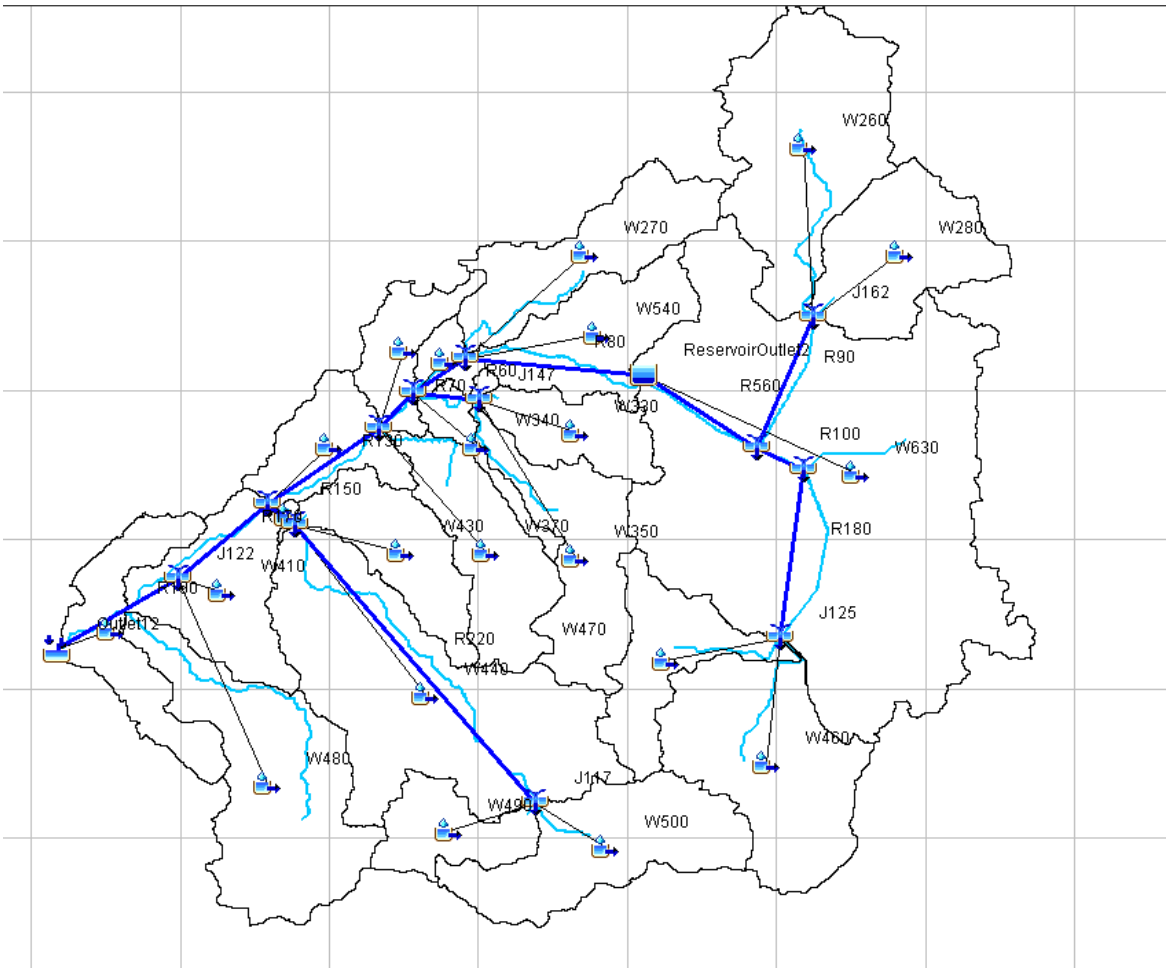

Figure 6.5. Schematic of the HMS model for Portage Creek

Table 6.20. Major properties of the sub-watersheds for the Portage Creek

Sub-basin name	*Sub-basin area (km^2)*	*Time of Concentration (MIN)*	*Curve number*	*Sub-basin name*	*Sub-basin area (km^2)*	*Time of Concentration (MIN)*	*Curve number*
W630	21.0	1440.0	78.0	W370	3.1	184.0	61.8
W500	4.2	133.8	49.5	W360	2.0	342.0	46.7
W490	1.8	165.3	35.6	W350	3.4	164.8	53.4
W480	5.9	218.8	44.5	W340	0.9	236.8	77.0
W470	2.6	184.7	37.7	W330	1.9	195.0	76.5
W460	5.3	137.7	53.6	W320	1.5	388.4	48.4
W450	2.7	238.5	47.1	W310	0.6	188.3	57.1
W440	9.0	270.0	42.1	W540	3.0	281.0	64.1
W430	2.6	215.1	67.5	W280	3.6	151.9	68.8
W420	0.1	53.2	77.9	W270	3.3	196.6	67.2
W410	3.2	269.9	62.2	W260	6.0	163.9	57.2

Critical Duration Analysis

A critical-duration analysis was performed to determine the storm duration that generally results in higher flow rate estimates for Portage Creek. Storm ARIs of 1-, 10-, and 100-yrs (observed 1990-2009 precipitation) was analyzed with a range of storm durations to determine estimated flow rates in HEC-HMS. Three locations were chosen, near the three LWCs; these locations are denoted by HEC-HMS element names and correspond roughly to HEC-RAS river stations (RS). The results for Portage Creek are summarized in Table 6.21. The highest flow rate at each river station location is highlighted.

Table 6.21. Portage Creek critical duration analysis

Location	Rainfall Distribution and Duration	Drainage Area (sq km)	1yr-Flow Rate (cms)	10yr-Flow Rate (cms)	100yr-Flow Rate (cms)
Outlet	3hr	87.8	0.1	0.5	4.8
	6hr		0.1	0.7	4.9
	12hr		0.1	1.2	***8.3***
	24hr		0.2	1.3	7.2
	48hr		***0.3***	***1.8***	7.5
	120hr		0.2	1.5	6.8
R170	3hr	76.0	0.1	0.6	4.3
	6hr		0.1	0.8	4.1
	12hr		0.1	1.2	***6.4***
	24hr		0.2	1.3	5.5
	48hr		***0.3***	***1.5***	5.3
	120hr		0.2	1.4	5.0
R80	3hr	38.6	0.1	0.2	0.6
	6hr		0.1	0.2	0.6
	12hr		0.1	0.3	1.0
	24hr		0.1	0.3	1.0
	48hr		***0.2***	***0.5***	***1.4***
	120hr		***0.2***	0.4	1.2

If no single storm can be identified as a critical duration for every location in the watershed it is desirable and common practice to select one duration storm event to use for comprehensive watershed planning efforts. The results of the Portage Creek analysis support selecting the 48-hour duration storm, which is the critical duration for return intervals of 1- and 10-yrs at all three LWCs and the critical duration of the 100-yr return interval at LWC GC4, located just downstream of Lake Margrethe.

Hydrologic Analysis-Peak Flood

Model calibration and verifications was not possible for the Portage Creek HEC-HMS model directly, due to no long term gauging station being located near the study reach. In addition, the presents of Lake Margrethe within the watershed precluded the application of regional regression equations to

determine peak flow rates. The Portage Creek watershed and stream channel below Lake Margrethe are similar to the East Branch Au Sable watershed and upper stream channel. The changes applied to the latter HEC-HMS model during the calibration step were also applied to the Portage Creek model in a similar manner. In addition, the 2008 study of the Lake Margrethe outlet dam and water levels, conducted by the Northwest Design Group of Petoskey, Michigan, was incorporated into the HEC-HMS model. The peak flow rate from the Lake Margrethe outlet structure, as determined in the 2008 study, matches the peak, 100-yr flow rate determined from the HEC-HMS model. Annual operation of the Lake Margrethe outlet gates, as determined from conversations with the Lake Margrethe Property Owner's Association, who operate the dam, were also incorporated into the model. Table 6.22 shows HEC-HMS peak flow results using observed (1990-2009) precipitation values for all three LWC locations.

Table 6.22. Simulated HEC-HMS peak floods for different return periods

Return Period	HEC-HMS at Outlet	HEC-HMS at R170	HEC-HMS at R80
(yr)	(m^3/s)	(m^3/s)	(m^3/s)
0.5	0.1	0.1	0.1
1	0.3	0.3	0.2
2	0.6	0.6	0.2
5	1.1	1	0.4
10	1.8	1.5	0.5
25	3.4	2.6	0.7
50	5.1	3.8	1
100	7.5	5.3	1.4

HMS peak floods using present conditions (observed, 1990-2009) inputs were also compared to peak floods generated from average projected RCM precipitation values (See Section 5.3.4). The results (Table 6.23 and Table 6.24) show the difference between present and projected peak flows at LWCs CG1 (near confluence with Manistee River) and CG3 (just downstream of Lake Margrethe), respectively. The projected peak flows are larger than present conditions for all ARIs, and are larger in magnitude for

larger return periods. For smaller return periods the difference in flow is on the order of several tenths of a cubit meter per second, so the differences in magnitude are very small.

Table 6.23. Peak floods comparison between present conditions (1990-2009) and average RCM projections (2040-2059 and 2080-2099) for different return periods at LWC GC1 near the confluence with the Manistee River.

Return Period (yr)	Present (m^3/s)	Avg RCM 2040 (m^3/s)	Avg RCM 2080 (m^3/s)	Precent Diff Present-RCM 2040	Precent Diff Present-RCM 2080
0.5	0.1	0.2	0.4	66.7%	120.0%
1	0.3	0.5	1.0	50.0%	107.7%
2	0.6	1.0	2.2	50.0%	114.3%
5	1.1	2.3	4.9	70.6%	126.7%
10	1.8	4.0	7.8	75.9%	125.0%
25	3.4	7.5	13.1	75.2%	117.6%
50	5.1	11.5	18.4	77.1%	113.2%
100	7.5	16.8	25.4	76.5%	108.8%

Table 6.24. Peak floods comparison between present conditions (1990-2009) and average RCM projections (2040-2059 and 2080-2099) for different return periods at LWC GC3 just downstream of Lake Margethe.

Return Period (yr)	Present (m^3/s)	Avg RCM 2040 (m^3/s)	Avg RCM 2080 (m^3/s)	Precent Diff Present-RCM 2040	Precent Diff Present-RCM 2080
0.5	0.1	0.1	0.2	0.0%	66.7%
1	0.2	0.2	0.3	0.0%	40.0%
2	0.2	0.3	0.6	40.0%	100.0%
5	0.4	0.6	1.0	40.0%	85.7%
10	0.5	0.8	1.5	46.2%	100.0%
25	0.7	1.4	2.3	66.7%	106.7%
50	1.0	2.1	3.3	71.0%	107.0%
100	1.4	3.0	4.6	72.7%	106.7%

Figure 6.6 and Figure 6.7 shows Portage Creek hydrographs for ARIs of 0.5-, 1-, 2-, 5-, 10-, 25-, 50-, and 100-years for present conditions and average RCM projections near confluence with Manistee River

(outlet) and just downstream of Lake Margrethe (R80), respectively. Present, projected (2040-2059), and projected (2080-2099) peak floods increase in a linearly across all return intervals.

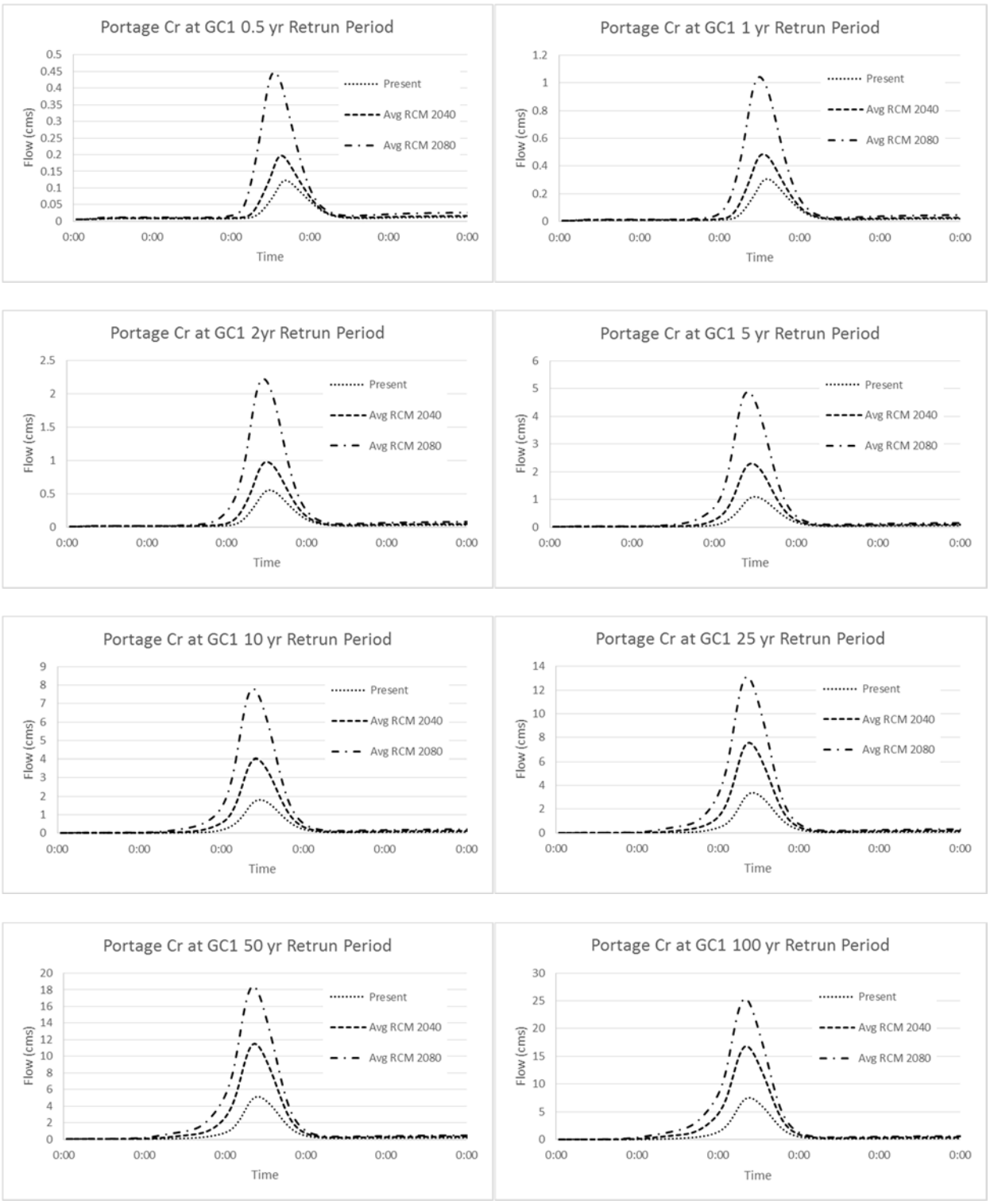

Figure 6.6. Hydrographs for various return periods at Portage Creek (outlet) for the present time, projected times (2040-2059 and 2080-2099), and USGS gauge peak floods.

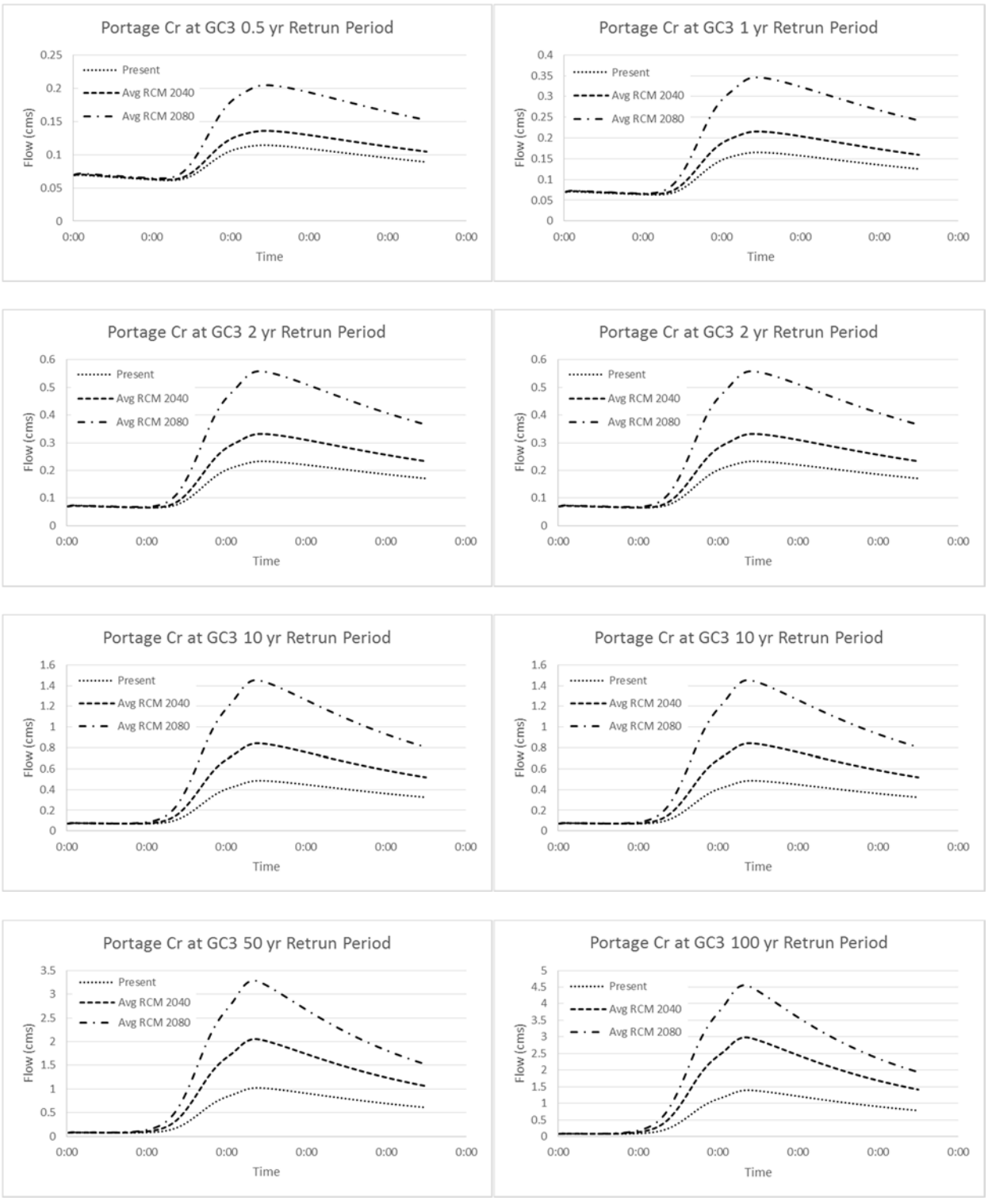

Figure 6.7. Hydrographs for various return periods at Portage Creek (R80) for the present time, projected times (2040-2059 and 2080-2099), and USGS gauge peak floods.

Hydrologic Analysis-Continuous Simulation

Continuous 20-year simulations were also run through the Portage Creek HEC-HMS model. The hydrologic outputs resulting from observed precipitation input (1980-1999) was compared to outputs produced by RCM simulation precipitation from the CNRM and MIROC models. CNRM and MIROC produced the smallest and largest projected estimated maximum precipitation values for Grayling, MI, respectively, so a comparison of their results show the range of RCM projections (see Section 5.3.4). Table 6.25 and Table 6.26 show the number of days Portage Creek exceeds the 0.5-, 1-, and 10-yr design flows during the 20-yr simulation given precipitation inputs of observed (1980-1999 and 1990-2009) values and simulated CNRM and MIROC (1980-1999) values, near confluence with Manistee River (outlet) and just downstream of Lake Margrethe (R80), respectively. The difference between the four scenarios is minimal. However, the number of days the flow is greater than the various design flows denotes that total time interval of high flows, not the number of high flow events or individual exceedances.

Table 6.25. Comparison of the number of days Portage Creek near the confluence with Manistee River (outlet) is above various design flows given precipitation inputs of present conditions (1980-1999) and RCM simulations (1980-1999) for CNRM and MIROC. Continuous simulation of 20 years.

Return Period (yr)	Present (1980-1999) days	CNRM (1980-1999) days	MIROC (1980-1999) days	Present (1990-2009) days	Percent Diff Pres 1980 - CNRM 1980	Percent Diff Pres 1980 - MIROC 1981	Percent Diff Pres 1980 - Pres 1990
0.5	903.6	902.0	862.8	864.0	-0.2%	-4.6%	-4.5%
1	768.4	763.2	739.2	724.4	-0.7%	-3.9%	-5.9%
10	330.0	337.0	335.0	307.0	2.1%	1.5%	-7.2%

Table 6.26. Comparison of the number of days Portage Creek downstream of Lake Margrethe (R80) is above various design flows given precipitation inputs of present conditions (1980-1999) and RCM simulations (1980-1999) for CNRM and MIROC. Continuous simulation of 20 years.

Return Period (yr)	Present (1980-1999) days	CNRM (1980-1999) days	MIROC (1980-1999) days	Present (1990-2009) days	Percent Diff Pres 1980 - CNRM 1980	Percent Diff Pres 1980 - MIROC 1981	Percent Diff Pres 1980 - Pres 1990
0.5	1154.3	1090.5	1075.0	1161.2	-5.7%	-7.1%	0.6%
1	1009.8	929.3	906.5	1020.7	-8.3%	-10.8%	1.1%
10	417.0	419.0	375.0	395.7	0.5%	-10.6%	-5.3%

Table 6.27 and Table 6.28 show the number of days Portage Creek exceeds the 0.5-, 1-, and 10-yr design flows during the 20-yr simulation given precipitation inputs of observed (1990-2009) values (assumed to be present conditions) and projected CNRM and MIROC (2040-2059) values, near confluence with Manistee River (outlet) and just downstream of Lake Margrethe (R80), respectively. At the Lake Margrethe outlet, the difference between present conditions and both RCM projected (2040-2059) conditions are minimal due to the storage capacity of the lake. Both models project more days of flow greater than the present design flow for all return periods, especially the 10-yrs ARI.

Table 6.27. Comparison of the number of days Portage Creek near the confluence with Manistee River (outlet) is above various design flows given precipitation inputs of present conditions (1990-2009) and RCM projections (2040-2059) for CNRM and MIROC. Continuous simulation of 20 years.

Return Period (yr)	Present (1980-1999) days	CNRM (2040-2059) days	MIROC (2040-2059) days	Percent Diff Pres 1990 - CNRM 2040	Percent Diff Pres 1990 - MIROC 2040
0.5	864.0	947.6	889.2	9.2%	2.9%
1	724.4	811.6	769.2	11.4%	6.0%
10	307.0	381.0	410.0	21.5%	28.7%

Table 6.28. Comparison of the number of days Portage Creek downstream of Lake Margrethe (R80) is above various design flows given precipitation inputs of present conditions (1990-2009) and RCM projections (2040-2059) for CNRM and MIROC. Continuous simulation of 20 years.

Return Period (yr)	Present (1980-1999) days	CNRM (2040-2059) days	MIROC (2040-2059) days	Percent Diff Pres 1990 - CNRM 2040	Percent Diff Pres 1990 - MIROC 2040
0.5	1161.2	1090.5	1105.8	-6.3%	-4.9%
1	1020.7	932.5	955.3	-9.0%	-6.6%
10	395.7	434.0	419.3	9.2%	5.8%

Table 6.29 and Table 6.30 show the number of days Portage Creek exceeds the 0.5-, 1-, and 10-yr design flows during the 20-yr simulation given precipitation inputs of observed (1990-2009) values (assumed to be present conditions) and projected CNRM and MIROC (2080-2099) values, near confluence with Manistee River (outlet) and just downstream of Lake Margrethe (R80), respectively. At the Lake Margrethe outlet, the difference between present conditions and both RCM projected (2080-2099) conditions are minimal due to the storage capacity of the lake. Both models project more days of flow greater than the present design flow for all return periods, especially the 10-yrs ARI.

Table 6.29. Comparison of the number of days Portage Creek near the confluence with Manistee River (outlet) is above various design flows given precipitation inputs of present conditions (1990-2009) and RCM projections (2080-2099) for CNRM and MIROC. Continuous simulation of 20 years.

Return Period (yr)	Present (1980-1999) days	CNRM (2080-2099) days	MIROC (2080-2099) days	Percent Diff Pres 1990 - CNRM 2080	Percent Diff Pres 1990 - MIROC 2080
0.5	864.0	992.4	958.8	13.8%	10.4%
1	724.4	863.2	848.4	17.5%	15.8%
10	307.0	542.0	544.0	55.4%	55.7%

Table 6.30. Comparison of the number of days Portage Creek downstream of Lake Margrethe (R80) is above various design flows given precipitation inputs of present conditions (1990-2009) and RCM projections (2080-2099) for CNRM and MIROC. Continuous simulation of 20 years.

Return Period (yr)	Present (1980-1999) days	CNRM (2080-2099) days	MIROC (2080-2099) days	Percent Diff Pres 1990 - CNRM 2080	Percent Diff Pres 1990 - MIROC 2080
0.5	1161.2	1126.5	1114.7	-3.0%	-4.1%
1	1020.7	997.3	966.2	-2.3%	-5.5%
10	395.7	508.5	460.0	25.0%	15.0%

6.3.4 North Fork Embarras River (Edgar County)

The following section provides HEC-HMS model overview and hydrologic results for North Fork Embarras River in Edgar County, Illinois. See Section 3.1 for applicable HEC-HMS input datasets.

HEC-HMS Model

Figure 6.8 is a schematic of the HEC-HMS model for the North Fork Embarras River watershed upstream of N 200th Street. Table 6.31 lists the subbasin name, the sub-basin area, the time of concentration, and the average curve number for each sub-basin.

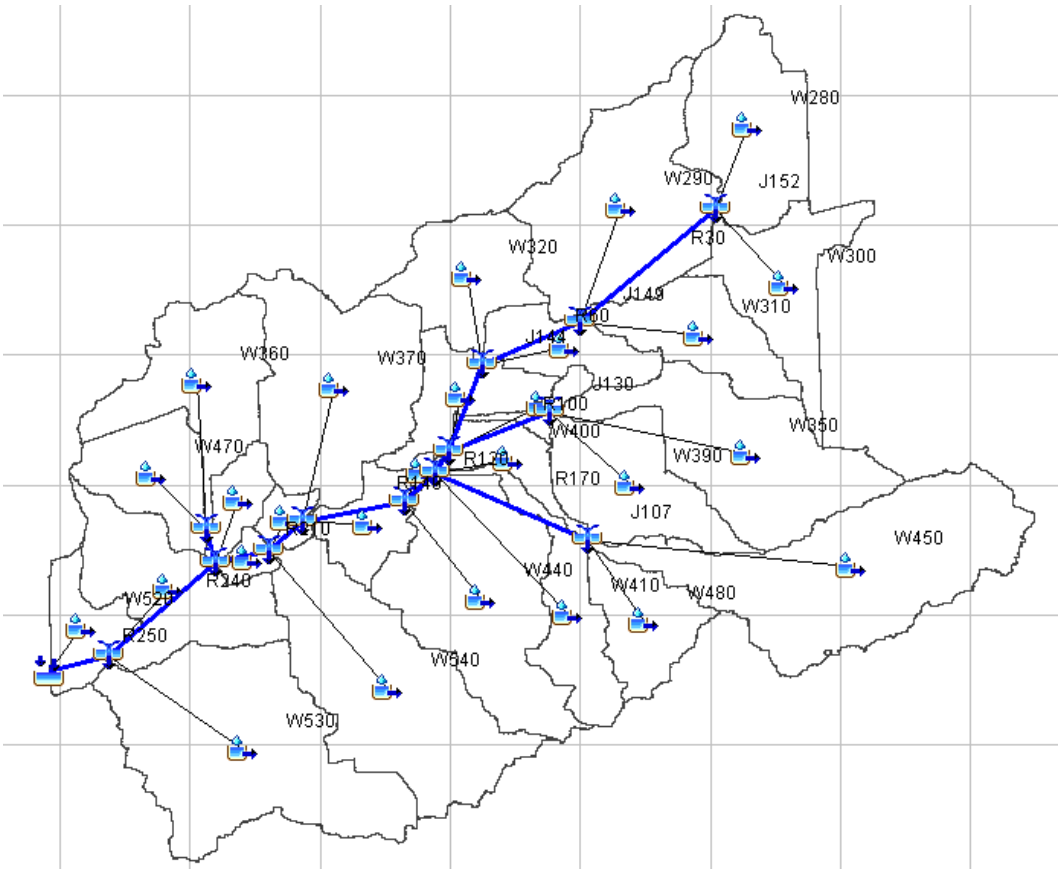

Figure 6.8. Schematic of the HMS model for North Fork Embarras River

Table 6.31. Major properties of the sub-watersheds for the North Fork Embarras River

Sub-basin name	*Sub-basin area (km^2)*	*Time of Concentration (MIN)*	*Curve number*	*Sub-basin name*	*Sub-basin area (km^2)*	*Time of Concentration (MIN)*	*Curve number*
W540	0.89	48.05	84.38	W400	0.15	27.57	88.42
W530	1.04	44.24	84.16	W390	0.44	43.32	81.06
W520	0.19	20.13	82.48	W380	0.07	24.85	84.04
W510	0.52	36.62	79.74	W370	0.76	36.46	85.86
W500	0.12	23.77	86.73	W360	0.48	32.73	86.20
W490	0.05	14.74	72.84	W350	0.71	52.93	80.50
W480	0.28	27.47	79.12	W340	0.25	29.87	85.73
W470	0.30	25.72	86.71	W330	0.24	32.23	85.51
W460	0.07	11.69	82.66	W320	0.36	24.95	84.25
W450	1.04	56.27	81.59	W310	0.33	46.34	86.65
W440	0.80	38.34	85.76	W300	0.41	45.72	87.25
W430	0.19	19.05	84.27	W290	0.80	34.23	85.53
W420	0.02	7.36	87.17	W280	0.51	29.69	85.75
W410	0.31	37.52	85.86				

Critical Duration Analysis

A critical-duration analysis was performed to determine the storm duration that generally results in higher flow rate estimates for North Fork Embarras River. Storm ARIs of 1-, 10-, and 100-yrs (observed 1990-2009 precipitation) was analyzed with a range of storm durations to determine estimated flow rates in HEC-HMS. The LWC location was used; this location is denoted by a HEC-HMS element name (outlet) and corresponds roughly to HEC-RAS river stations (RS). The results for North Fork Embarras River are summarized in Table 6.32 The highest flow rate at each river station location is highlighted.

Table 6.32. North Fork Embarras River critical duration analysis

Location	Rainfall Distribution and Duration	Drainage Area (sq km)	1yr-Flow Rate (cms)	10yr-Flow Rate (cms)	100yr-Flow Rate (cms)
Outlet	Huff, 1hr	11.4	6.4	28.2	71.4
	Huff, 2hr		10.3	36.5	89.2
	Huff, 3hr		10.1	***37.5***	***98.4***
	Huff, 6hr		***10.9***	35.4	84.5

If no single storm can be identified as a critical duration for every location in the watershed it is desirable and common practice to select one duration storm event to use for comprehensive watershed planning efforts. The results of the North Fork Embarras River analysis support selecting the 3-hour duration storm.

Hydrologic Analysis-Peak Flood

Model calibration and verifications was not possible for the North Fork Embarras River HEC-HMS model directly, because no long term gauging station is located within or near the study reach. HEC-HMS peak flow results using observed (1990-2009) precipitation values were compared to StreamStats values for one location on North Fork Embarras River (Table 6.33). The flow rates for ARIs of 0.5-50 years are within 10% of StreamStats flow.

Table 6.33. Published and simulated HEC-HMS peak flood comparison for different return periods

Return Period	HMS-Outlet	StreamStats	
(yr)	(m^3/s)	(m^3/s)	% diff
0.5	5.2	5.1	2%
1	10.1	9.6	5%
2	16.4	15.3	7%
5	26.7	24.9	7%
10	37.5	34.3	9%
25	55.1	50.3	9%
50	73.7	66.8	10%
100	98.4	87.9	11%

HMS peak flows using observed (1990-2009) precipitation values (considered present conditions) were also compared to peak stream flow data from a USGS gauge station (03344500) on Range Creek, located southwest of Edgar County in Cumberland County. Range Creek watershed is similar to the North Fork Embarras River, in land cover, topography, and size, with a drainage area of 19.7 km^2 at the gauge station. The USGS 03344500 station has 32 years of data, ending operation in 1983. Table 6.34Table 6.7 shows peak stream flow comparisons, taking into account the difference in drainage area between the two watersheds. The peak flow rate are within +/- 15% for ARIs of 2-50 years.

Table 6.34. North Fork Embarras River and Range Creek peak flood comparison for different return periods

Return Period	Ranch Cr	NorthFork Embarras R	
(yr)	(m^3/s)	(m^3/s)	% diff
2	14.7	16.4	11.1%
5	26.5	26.7	0.7%
10	36.3	37.5	3.1%
25	50.9	55.1	7.9%
50	63.4	73.7	15.1%
100	77.3	98.4	24.0%

HMS peak floods using present conditions (observed, 1990-2009) inputs were also compared to peak floods generated from average projected RCM precipitation values (See Section 5.3.4). The results (Table 6.35) show the difference between presents and projected (2040-2059) peak flows to be 66%-79%. The projected peak flow are larger than present conditions for all ARIs, and are larger in magnitude for small return periods. Projected (2080-2099) peak flows are also larger than present conditions by 45%-100%.

Table 6.35. Peak floods comparison between present conditions (1990-2009) and average RCM projections (2040-2059 and 2080-2099) for different return periods

Return Period (yr)	Present (m^3/s)	Avg RCM 2040 (m^3/s)	Avg RCM 2080 (m^3/s)	Percent Diff Atlas 14-RCM 2040	Percent Diff Atlas 14-RCM 2080
0.5	5.2	12.0	15.7	79.1%	100.5%
1	10.1	23.2	28.5	78.7%	95.3%
2	16.4	36.0	42.7	74.8%	89.0%
5	26.7	57.0	61.7	72.4%	79.2%
10	37.5	77.8	78.9	69.9%	71.1%
25	55.1	115.0	105.7	70.4%	62.9%
50	73.7	150.5	128.8	68.5%	54.4%
100	98.4	196.3	155.1	66.4%	44.7%

Figure 6.9 shows North Fork Embarras River hydrographs for ARIs of 0.5-, 1-, 2-, 5-, 10-, 25-, 50-, and 100-years for present conditions and average RCM projections, and includes published flood peaks (StreamStats). Both projected (2040-2059 & 2080-2099) peak floods are similar for all ARIs and larger than present peaks.

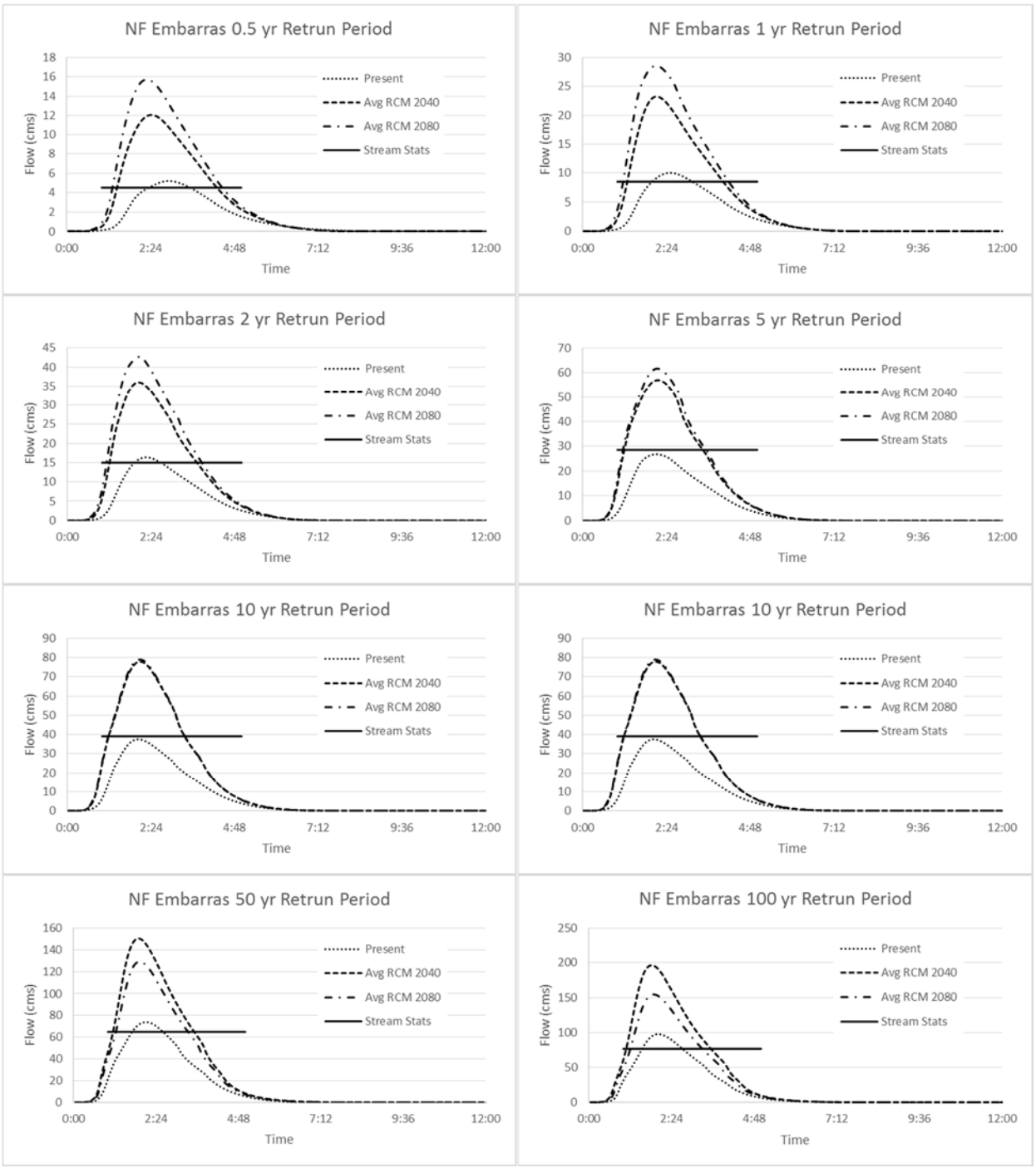

Figure 6.9. Hydrographs for various return periods at North Fork Embarras River (output) for the present time, projected times (2040-2059 and 2080-2099), and published peak floods.

Hydrologic Analysis-Continuous Simulation

Continuous 20-year simulations were also run through the North Fork Embarras River HEC-HMS model. The hydrologic outputs resulting from observed precipitation input (1980-1999) was compared to outputs produced by RCM simulation precipitation from the MRI and IPSL models. MRI and IPSL produced the largest and smallest projected estimated maximum precipitation values for Paris, IL, respectively, so a comparison of their results show the range of RCM projections (see Section 5.3.4). Table 6.36 shows the number of days the North Fork Embarras River exceeds the 0.5-, 1-, and 10-yr design flows during the 20-yr simulation given precipitation inputs of observed (1980-1999 and 1990-2009) values and simulated MRI and IPSL (1980-1999) values. The difference between the four scenarios is minimal. The number of days the flow is greater than the various design flows denotes that total time interval of high flows, not the number of high flow events or individual exceedances.

Table 6.36. Comparison of the number of days North Fork Embarras River is above various design flows given precipitation inputs of present conditions (1980-1999) and RCM simulations (1980-1999) for IPSL and MRI. Continuous simulation of 20 years.

Return Period (yr)	Present (1980-1999) days	IPSL (1980-1999) days	MRI (1980-1999) days	Present (1990-2009) days	Percent Diff Pres 1980 - IPSL 1980	Percent Diff Pres 1980 - MRI 1981	Percent Diff Pres 1990
0.5	141.8	142.3	135.5	149.7	0.4%	-4.5%	5.4%
1	44.6	46.6	48.6	51.5	4.4%	8.6%	14.4%
10	1.8	1.6	1.8	1.6	-14.6%	-4.7%	-14.6%

Table 6.37 shows the number of days the North Fork Embarras River exceeds the 0.5-, 1-, and 10-yr design flows during the 20-yr simulation given precipitation inputs of observed (1990-2009) values (assumed to be present conditions) and projected MRI and IPSL (2040-2059) values. The difference between present conditions and IPSL and MRI projected (2040-2059) conditions is relatively minor.

Table 6.37. Comparison of the number of days the North Fork Embarras River is above various design flows given precipitation inputs of present conditions (1990-2009) and RCM projections (2040-2059) for IPSL and MRI. Continuous simulation of 20 years.

Return Period (yr)	Present (1990-2009) days	IPSL (2040-2059) days	MRI (2040-2059) days	Percent Diff Pres 1990 - IPSL 2040	Percent Diff Pres 1990 - MRI 2040
0.5	149.7	153.8	168.6	2.7%	11.9%
1	51.5	58.7	57.7	13.0%	11.3%
10	1.6	4.8	2.7	100.0%	51.0%

Table 6.38 shows the number of days the North Fork Embarras River exceeds the 0.5-, 1-, and 10-yr design flows during the 20-yr simulation given precipitation inputs of observed (1990-2009) values (assumed to be present conditions) and projected MRI and IPSL (2080-2099) values. The difference between present conditions and IPSL and MRI projected (2080-2099) conditions is large, especially for return periods greater than 0.5-yrs. IPSL and MRI project an average of 12 and 3 more days than present conditions of flow greater than the ARI design flows of 1- and 10-yrs.

Table 6.38. Comparison of the number of days the North Fork Embarras River is above various design flows given precipitation inputs of present conditions (1990-2009) and RCM projections (2080-2099) for IPSL and MRI. Continuous simulation of 20 years.

Return Period (yr)	Present (1990-2009) days	IPSL (2080-2099) days	MRI (2080-2099) days	Percent Diff Pres 1990 - IPSL 2080	Percent Diff Pres 1990 - MRI 2080
0.5	149.7	151.4	160.4	1.2%	6.9%
1	51.5	64.6	63.4	22.5%	20.7%
10	1.6	4.0	4.9	86.6%	102.6%

6.3.5 East Fork Big Creek (Edgar County)

The following section provides HEC-HMS model overview and hydrologic results for East Fork Big Creek within Edgar County, IL. See Section 3.1 for applicable HEC-HMS input datasets.

HEC-HMS Model

Figure 6.10 is a schematic of the HEC-HMS model for the East Fork Big Creek watershed. Table 6.39 lists the subbasin name, the sub-basin area, the time of concentration, and the average curve number for each sub-basin.

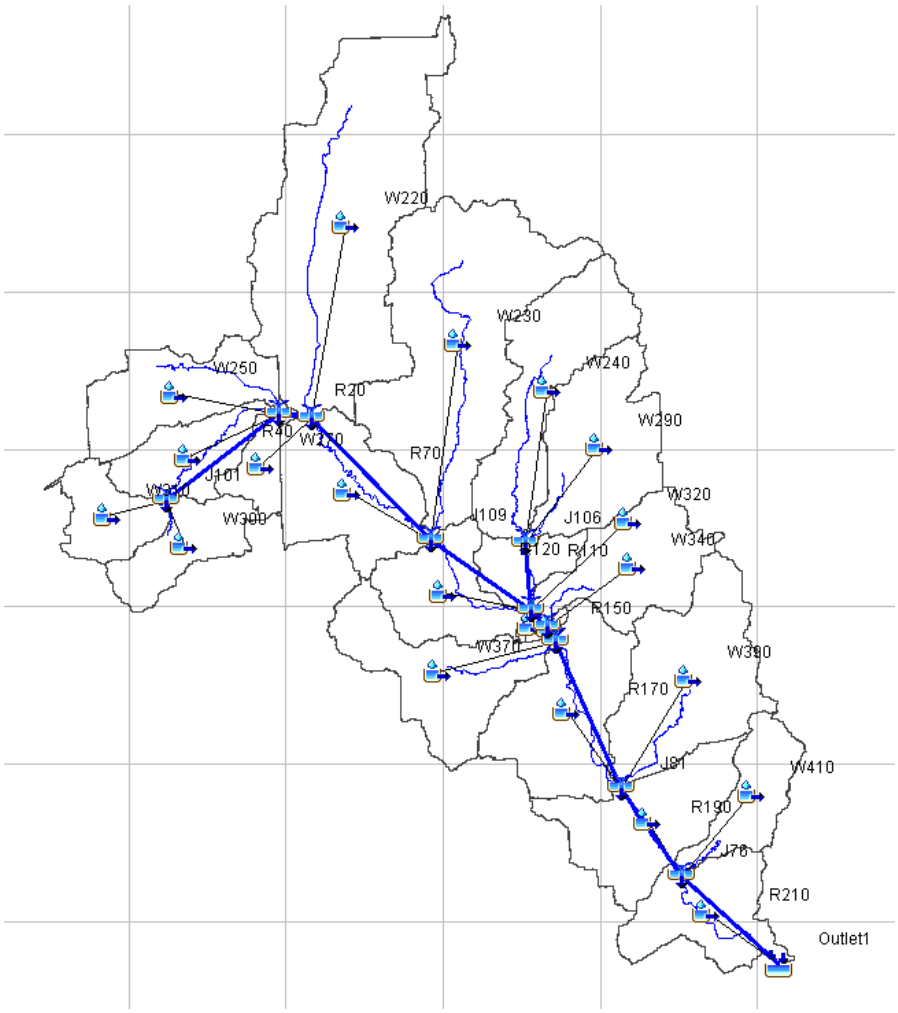

Figure 6.10. Schematic of the HMS model for East Fork Big Creek

Table 6.39. Major properties of the sub-watersheds for the East Fork Big Creek

Sub-basin name	*Sub-basin area (km^2)*	*Time of Concentration (MIN)*	*Curve number*	*Sub-basin name*	*Sub-basin area (km^2)*	*Time of Concentration (MIN)*	*Curve number*
W420	1.38	48.25	73.31	W310	0.83	43.29	85.19
W410	0.95	54.22	75.93	W300	0.94	45.22	80.89
W400	1.81	49.91	74.53	W290	1.99	60.75	81.91
W390	2.45	59.08	73.99	W280	1.87	54.66	73.31
W380	2.06	55.57	65.35	W270	0.48	29.19	79.51
W370	1.85	52.75	80.31	W260	1.01	59.09	72.39
W360	0.06	9.95	68.21	W250	1.53	62.35	82.44
W350	0.06	11.99	74.43	W240	2.14	73.83	83.62
W340	1.58	44.22	77.43	W230	4.42	89.84	83.34
W330	1.27	48.27	69.93	W220	5.38	103.80	86.02
W320	0.61	31.80	73.94				

Critical Duration Analysis

A critical-duration analysis was performed to determine the storm duration that generally results in higher flow rate estimates for East Fork Big Creek. Storm ARIs of 1-, 10-, and 100-yrs (observed 1990-2009 precipitation) was analyzed with a range of storm durations to determine estimated flow rates in HEC-HMS. The LWC location was used; this location is denoted by a HEC-HMS element name (outlet) and corresponds roughly to HEC-RAS river stations (RS). The results for East Fork Big Creek are summarized in Table 6.40. The highest flow rate at each river station location is highlighted.

Table 6.40. East Fork Big Creek critical duration analysis

Location	Rainfall Distribution and Duration	Drainage Area (sq km)	1yr-Flow Rate (cms)	10yr-Flow Rate (cms)	100yr-Flow Rate (cms)
Outlet	Huff, 1hr	34.7	5.5	30.8	78.4
	Huff, 2hr		12.1	51.3	123.8
	Huff, 3hr		14.4	56.8	***152.7***
	Huff, 6hr		***17.4***	***60***	149.1
	Huff, 12hr		13.1	54.5	131.7

If no single storm can be identified as a critical duration for every location in the watershed it is desirable and common practice to select one duration storm event to use for comprehensive watershed planning efforts. The results of the East Fork Big Creek analysis support selecting the 6-hour duration storm.

Hydrologic Analysis-Peak Flood

Model calibration and verifications was possible for the East Fork Big Creek HEC-HMS model directly, because a long term gauging station is located within the study reach. HMS peak flows using observed (1990-2009) precipitation values (considered present conditions) were compared to peak stream flow data from a USGS gauge station (03341700) on Tributary to East Fork Big Creek, located southwest of Paris, IL in Edgar County. The gauged watershed location corresponds to the HMS model junction J115, with a drainage area of 2.8 km^2 at the gauge station. The USGS 03341700 station has 15 years of data, ending operation in 1975. Table 6.41 shows peak stream flow comparisons. The peak flow rate are within +/- 13% for ARIs of 1-100 years.

Table 6.41. East Fork Big Creek gauge and HMS peak flood comparison for different return periods

Return Period	East Fork Big Creek-HMS J115	East Fork Big Creek-USGS Gauge	
(yr)	(m^3/s)	(m^3/s)	% diff
1	2.7	3.1	13.3%
2	5.2	5	-3.6%
5	8.3	8.2	-1.2%
10	10.6	11.4	7.1%
25	13.8	12.8	-7.7%
50	16.4	14.4	-13.0%
100	19.1	19	-0.6%

In addition, HEC-HMS peak flow results using observed (1990-2009) precipitation values were compared to StreamStats values at the LWC location (Table 6.42). The flow rates for ARIs of 2-50 years are within

10% of StreamStats flow while for remaining ARIs the model flow rates are higher than those produced by StreamStats.

Table 6.42. Published and simulated HEC-HMS peak flood comparison for different return periods

Return Period	HMS-Outlet	StreamStats	
(yr)	(m^3/s)	(m^3/s)	% diff
0.5	9.1	7.4	21%
1	17.4	11.7	39%
2	27.7	26.8	3%
5	44.9	49.6	-10%
10	60	66.5	-10%
25	87.2	89.8	-3%
50	115.7	107.9	7%
100	149.1	126.9	16%

HMS peak floods using present conditions (observed, 1990-2009) inputs were also compared to peak floods generated from average projected RCM precipitation values (See Section 5.3.4). The results (Table 6.43) show the difference between present and projected (2040-2059) peak flows to be 50-75%. The projected peak flow are larger than present conditions for all ARIs, and are smaller in magnitude for larger return periods. Projected (2080-2099) peak flows are also larger than present conditions by 40-80%.

Table 6.43. Peak floods comparison between present conditions (1990-2009) and average RCM projections (2040-2059 and 2080-2099) for different return periods

Return Period (yr)	Present (m^3/s)	Avg RCM 2040 (m^3/s)	Avg RCM 2080 (m^3/s)	Precent Diff Atlas 14-RCM 2040	Precent Diff Atlas 14-RCM 2080
0.5	9.1	17.7	20.9	64.2%	78.7%
1	17.4	37.8	39.5	73.9%	77.7%
2	27.7	59.4	58.0	72.8%	70.7%
5	44.9	92.2	83.8	69.0%	60.5%
10	60	121.1	107.8	67.5%	57.0%
25	87.2	159.2	145.9	58.4%	50.4%
50	115.7	198.1	179.0	52.5%	43.0%
100	149.1	246.5	228.9	49.2%	42.2%

Figure 6.11 shows East Fork Big Creek hydrographs for ARIs of 0.5-, 1-, 2-, 5-, 10-, 25-, 50-, and 100-years for present conditions and average RCM projections, and includes published flood peaks (StreamStats). Both projected (2040-2059 & 2080-2099) peak floods are similar for all ARIs and larger than present peaks.

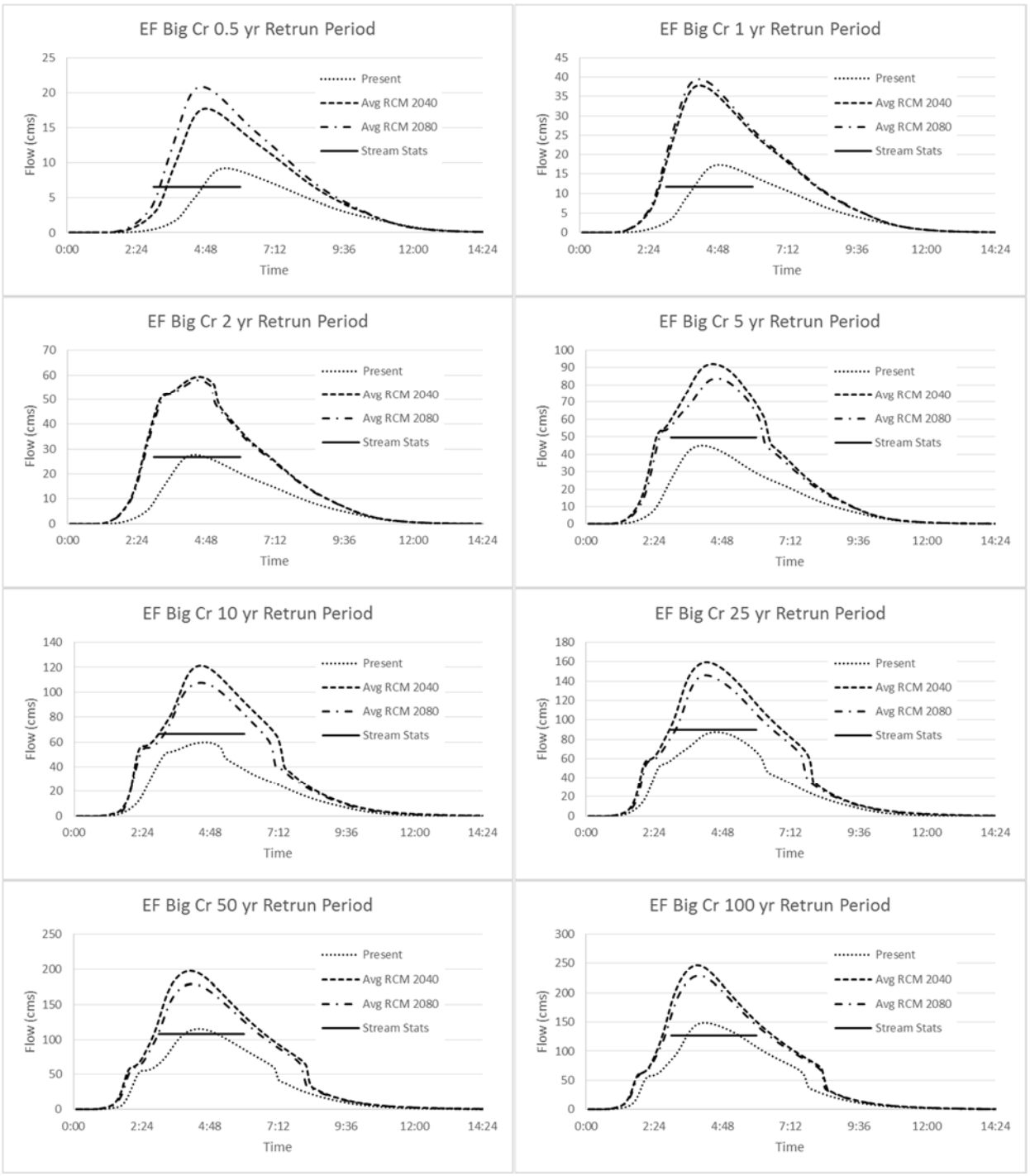

Figure 6.11. Hydrographs for various return periods at East Fork Big Creek (output) for the present time, projected times (2040-2059 and 2080-2099), and published peak floods.

Hydrologic Analysis-Continuous Simulation

Continuous 20-year simulations were also run through the East Fork Big Creek HEC-HMS model. The hydrologic outputs resulting from observed precipitation input (1980-1999) was compared to outputs produced by RCM simulation precipitation from the CNRM and MIROC models. CNRM and MIROC produced the largest and smallest projected estimated maximum precipitation values for Paris, IL, respectively, so a comparison of their results show the range of RCM projections (see Section 5.3.4). Table 6.44 shows the number of days East Fork Big Creek exceeds the 0.5-, 1-, and 10-yr design flows during the 20-yr simulation given precipitation inputs of observed (1980-1999 and 1990-2009) values and simulated CNRM and MIROC (1980-1999) values. The difference between the four scenarios is minimal. However, the number of days the flow is greater than the various design flows denotes that total time interval of high flows, not the number of high flow events or individual exceedances.

Table 6.44. Comparison of the number of days East Fork Big Creek is above various design flows given precipitation inputs of present conditions (1980-1999) and RCM simulations (1980-1999) for CNRM and MIROC. Continuous simulation of 20 years.

Return Period (yr)	Present (1980-1999) days	CNRM (1980-1999) days	MIROC (1980-1999) days	Present (1990-2009) days	Percent Diff Pres 1980 - CNRM 1980	Percent Diff Pres 1980 - MIROC 1980	Percent Diff Pres 1980 - Pres 1990
0.5	180.5	167.9	162.3	192.9	-7.2%	-10.6%	6.6%
1	63.4	68.0	54.8	68.0	7.0%	-14.6%	7.0%
10	2.13	1.63	2.63	2.25	-26.7%	21.1%	5.7%

Table 6.45 shows the number of days East Fork Big Creek exceeds the 0.5-, 1-, and 10-yr design flows during the 20-yr simulation given precipitation inputs of observed (1990-2009) values (assumed to be present conditions) and projected CNRM and MIROC (2040-2059) values. The difference between present conditions and CNRM and MIROC projected (2040-2059) conditions is minor. CNRM projects

slightly fewer days of flow greater than the 0.5- and 1-yr design flows while both RCMs project more days of flow greater than the 10-yr design flow.

Table 6.45. Comparison of the number of days East Fork Big Creek is above various design flows given precipitation inputs of present conditions (1990-2009) and RCM projections (2040-2059) for CNRM and MIROC. Continuous simulation of 20 years.

Return Period (yr)	Present (1990-2009) days	CNRM (2040-2059) days	MIROC (2040-2059) days	Percent Diff Pres 1990 - CNRM 2040	Percent Diff Pres 1990 - MIROC 2040
0.5	192.9	179.3	169.4	-7.3%	-13.0%
1	68.0	61.0	72.4	-10.9%	6.2%
10	2.25	4.63	5.63	69.1%	85.7%

Table 6.46 shows the number of days East Fork Big Creek exceeds the 0.5-, 1-, and 10-yr design flows during the 20-yr simulation given precipitation inputs of observed (1990-2009) values (assumed to be present conditions) and projected CNRM and MIROC (2080-2099) values. The difference between present conditions and CNRM and MIROC projected (2080-2099) conditions is small considering average days per year. CNRM and MIROC project an average of 13 and 7 more days than present conditions of flow greater than the ARI design flows of 1- and 10-yrs.

Table 6.46. Comparison of the number of days East Fork Big Creek is above various design flows given precipitation inputs of present conditions (1990-2009) and RCM projections (2080-2099) for CNRM and MIROC. Continuous simulation of 20 years.

Return Period (yr)	Present (1990-2009) days	CNRM (2080-2099) days	MIROC (2080-2099) days	Percent Diff Pres 1990 - CNRM 2080	Percent Diff Pres 1990 - MIROC 2080
0.5	192.9	208.8	180.5	7.9%	-6.6%
1	68.0	85.9	82.75	23.2%	19.6%
10	2.25	7.63	11.25	108.9%	133.3%

6.4 Discussion

This study applied projected climate model precipitation to hydrologic models to determine projected first-order stream flow characteristics and compare to observed stream flow characteristics. Flood peak frequency analysis of existing conditions and average future climate projection from the four RCMs were compared. In addition, continuous 20-year simulations were run through the HEC-HMS models using observed precipitation and projected precipitation from two of the four RCMs. The two models utilized for the continuous simulations were those models that represented the upper and lower bounds of maximum precipitation estimates for a majority of return periods for each projected timeframe at each location.

The HEC-HMS hydrologic events models were run for the 0.5-, 1-, 2-, 5-, 10-, 25-, 50-, and 100-year events. In Indiana, the difference between present and projected (2040-2059) peak flows were an increase of 7%-40%. Projected (2080-2099) peak flows are also larger than present conditions by 80%-95%. The differences in peak flow were larger as a percent difference for larger return periods.
In Illinois, the difference between present and projected (2040-2059) peak flows were an increase of 66%-79% and 50%-75% for the two studied streams. Projected (2080-2099) peak flows are also larger than present conditions by 45%-100% and 40%-80% for the two studied streams. The differences in peak flow were larger as a percent difference for more frequent return periods, which is the opposite of the Indiana stream.

In Michigan, the difference between present and projected (2040-2059) peak flows were an increase of 32%-57% for the East Branch Au Sable River. Projected (2080-2099) peak flows are also larger than present conditions by 57%-97%. The differences in peak flow were larger as a percent difference for

larger return periods. For Portage Creek, the difference between present and projected peak flow were on the order of 75% and 100%, however, differences in peak flows for return periods less than 10 years are on the order of several tenths of a cubit meter per second, so the differences in magnitude are very small.

Generally, for each region the projected (2080-2099) peak flow events are larger or equal to the projected (2040-2059) peak flows and both are larger than present conditions. These findings are similar to the projected increases in rainfall intensity of extreme storms for each region. However, relatively small increases in the projected precipitation design storms caused relatively larger increases in the projected peak floods. In Michigan, the watersheds are swampy, the soils are sandy, and there are numerous inline ponds and lakes, causing significant hydrograph attenuation. As a result the peak floods are smaller relative to the drainage areas of the watershed when compared to the Indiana and Illinois watersheds. While the percent differences between observed and projected peak floods are similar to Indiana and Illinois, the magnitudes of the peak floods and the differences are much smaller in Michigan. These watershed specific variables increase uncertainty with regards to the peak flood magnitude.

The frequency of potential exceedances of current peak flood events was also investigated using continuous 20-yr simulations. The number of days the flow is greater than the various design flows denotes the total time interval of high flows, not the number of high flow events or individual exceedances (negative numbers denote fewer projected days at a given flow than present days). For more common peak floods (0.5- and 1-yr return period) the number of days Nineveh Creek (Indiana) exceeds the current design flows during projected (2040-2059) scenarios is -6–4 days for the 0.5-yr

event and 4-6 days for the 1-yr event. The number of days Nineveh Creek (Indiana) exceeds the observed design flows during projected (2080-2099) scenarios is 12-26 days from the 0.5-yr event and 26-73 days for the 1-yr event. In Illinois the number of days the streams exceed the observed design flows during projected (2040-2059) scenarios is 4-19 days and -13-23 days for the 0.5-yr event and 6-7 days and -7-4 for the 1-yr event. The number of days the Illinois streams exceed the observed design flows during projected (2080-2099) scenarios is 2-10 days and -12-16 days for the 0.5-yr event and 12-13 days and 15-18 days for the 1-yr event. The exceedance days listed are for the entire 20-yr continuous simulation, so average annual exceedances (0.5-, 1-, and 10-yr events) are on the order of -0.5-4 days per year or -0.1% to 1% of the year. So, the projected exceedances of current peak flood events in Illinois and Indiana are minimal.

In Michigan the number of days the streams exceed the observed design flows during projected (2040-2059) scenarios is 54-90 days and -71-84 days for the 0.5-yr event and 62-71 days and -88-87 days for the 1-yr event. The number of days the Michigan streams exceed the observed design flows during projected (2080-2099) scenarios is -60-231 days and -47-128 days for the 0.5-yr event and -2-225 days and -55-139 days for the 1-yr event. The exceedance days listed are for the entire 20-yr continuous simulation, so average annual exceedances (0.5-, 1-, and 10-yr events) are on the order of -4-11 days per year or -1% to 3% of the year. The significant hydrograph attenuation in the Michigan watersheds increases the temporal length of the peak flood events as the inline waterbodies and swamps slowly drain. As a result, the range and length of exceedances compared to observed conditions is greater in Michigan that in Indiana and Illinois, primarily as a result of watershed specific variables as opposed to differences in projected precipitation between the three regions.

Mailhot et al. (2007), Markus et al. (2012), Vavrus and Behnke (2014), and Zhu (2013) used downscaled climate models to project changes in IDF curves and design storm depth for Southern Quebec, Chicago IL, Wisconsin, and several US urban centers, respectively. The projected precipitation was applied within various hydrology models, including HEC-HMS, to determine the effects of climate change on urban and natural drainage systems. The studies, like this study, found that peak discharges will increase in magnitude, though not always statistically significantly. The studies that investigated projected exceedances generally found the frequency of potential exceedances of observed peak flows will increase as well. Again, like this study, the increases in flow exceedances were not typically statistically significant.

The flood peak frequency analysis between existing and projected conditions was completed using the average future climate projection from the four RCMs, and so does not explicitly included the uncertainty due to the range of RCM projections. The 20-yr continuous simulations utilized the two models representing the upper and lower bounds of maximum precipitation estimates for a majority of return periods for each projected timeframe at each location, thereby revealing the range of projected exceedances (or lack of exceedances) and resulting uncertainty. The results range 10 to 225 days between the upper and lower RCMs, signifying a large amount of uncertainty, but generally the projected peak floods are larger in magnitude and the frequency of exceedances are greater than observed conditions (especially for the 10yr events at the end of the twenty-first century), though not necessarily significantly.

6.5 Conclusion

The main purpose of this chapter was to apply projected climate model precipitation to hydrologic models to determine projected first-order stream flow characteristics and compare to observed stream flow characteristics. Hydrologic models were developed for each study stream within the U.S. Army Corps of Engineers (USACE) Hydrologic Engineering Center-Hydrologic Modeling System (HEC-HMS) Version 4.0 modeling application (USACE, 2000). Regression equation outputs and gauge data from gauges within the same region and with watershed hydrologic features similar to the study streams were used to corroborate HEC-HMS outputs. Design event rainfall data (averaged from all four climate models) was obtained from precipitation frequency analysis of observed (1980-1999 and 1990-2009) records using the regional L-Moments method. The HEC-HMS hydrologic events models were run for the 0.5-, 1-, 2-, 5-, 10-, 25-, 50-, and 100-year events. Continuous 20-year precipitation was also utilized for long-term simulations. Observed precipitation (1980-1999 and 1990-2009 gauge data), simulated precipitation (1980-1999 RCM data), and projected precipitation (2040-2059 and 2080-2099 RCM data) was used to model long-term flow behavior of the study streams.

The results indicate increases in peak flood events across all return periods for the projected timeframes compared to observed conditions. In Indiana and Michigan the projected (2080-2099) peak flow events are larger than the projected (2040-2059) peak flows while in Illinois the projected (2080-2099) peak flow events are larger than or equal to the former events. Analysis of the number of days projected stream flow exceeds the 0.5-, 1-, and 10-yr design flows during the 20-yr simulation showed a wide range of results between the two models representing the upper and lower bounds of maximum precipitation estimates for a majority of return periods for each projected timeframe at each location. Generally there was an increase in exceedances during the projected timeframes compared to current

conditions, but on a yearly average the increase were minimal. Only in Michigan, where watershed specific variables contribute to increases the temporal length of the peak flood events, were the differences in exceedance between present and projected conditions on the order of one week to ten days. The results suggest the magnitude and total length of peak flow events will increase in the future, but high data and modeling uncertainty makes it difficult to exactly quantify the potential future changes in stream hydrology. Generally, the projected (2080-2099) 1-yr and 10-yr peak flood events are approximately equal to the present 10-yr and 50-yr peak flood event, respectively.

References

Bonnin, G. M., Martin, D., Lin, B., Parzybok, T., Yekta, M., & Riley, D. (2006). National Oceanic Atmospheric Administration Atlas 14: precipitation frequency atlas for the United States, Volume 2 Version 3.0: Delaware, District of Columbia, Illinois, Indiana, Kentucky, Maryland, New Jersey, North Carolina, Ohio, Pennsylvania, South Carolina, Tennessee, Virginia, West Virginia. U.S. Department of Commerce. Silver Spring, MD.

Fowler, H. J., & Kilsby, C. G. (2007). Using regional climate model data to simulate historical and future river flows in northwest England. Climatic Change, 80: 337-367.

Holtschlag, D. J. & Croskey, H. M. (1984). Statistical models for estimating flow characteristics of Michigan streams, U.S. Geological Survey Water-Resources Investigations Report 84-4207.

Homer, C.G., Dewitz, J.A., Yang, L., Jin, S., Danielson, P., Xian, G., Coulston, J., Herold, N.D., Wickham, J.D., & Megown, K. (2015). Completion of the 2011 National Land Cover Database for the conterminous United States-Representing a decade of land cover change information. Photogrammetric Engineering and Remote Sensing, 81(5): 345-354

Hosking, J. R. M. & J. R. Wallis (1997). Regional Frequency Analysis, an Approach Based on L-Moments. Cambridge University Pres.

Huff, F.A. 1990. Time Distributions of Heavy Rainstorms in Illinois. Illinois State Water Survey Circular 173, 18 p.

Huff, F. A. & Angel, J. R. (1992). Rainfall frequency atlas of the Midwest (Bulletin 71). Illinois State Water Survey, Champaign, IL.

Mailhot, A., Dushesne, S., Caya, D., & Talbot, G. (2007). Assessment of future change in intensity–duration–frequency (IDF) curves for Southern Quebec using the Canadian Regional Climate Model (CRCM). Journal of Hydrology, 347: 197-210.

Markus, M., Wuebbles, D. J., Laing, X., Hayhoe, K., Kristovich, D. A. R. (2012). Diagnostic analysis of future climate scenarios applied to urban flooding in the Chicago metropolitan area. Climatic Change, 111: 879-902.

Perica, S., Martin, D., Pavlovic, S., Roy, I., St. Laurent, M., Trypaluk, C., Unruh, D., Yekta, M., Bonnin, G. (2013). National Oceanic Atmospheric Administration Atlas 14: precipitation frequency atlas for the United States, Volume 8 Version 2.0: Midwestern States (Colorado, Iowa, Kansas, Michigan, Minnesota, Missouri, Nebraska, North Dakota, Oklahoma, South Dakota, Wisconsin). U.S. Department of Commerce. Silver Spring, MD.

Roa, A. R. (2006). Flood frequency relationships for Indiana. Federal Highway Administration, Joint Transportation Research Program, FHWA/IN/JTRP-2005/18.

Soil Survey Staff, Natural Resources Conservation Service, United States Department of Agriculture. U.S. General Soil Map (STATSGO2). Available online at http://sdmdataaccess.nrcs.usda.gov/. Accessed [12/29/2015].

Soong, D. T., Ishii, A. L., Sharpe, J. B., & Avery, C. F. (2004). Estimating Flood-Peak Discharge Magnitudes and Frequencies for Rural Streams in Illinois, U.S. Geological Survey Science Investigations Report 2004-5103.

United States Department of Agriculture (USDA), Natural Resource Conservation Service. (1986). Urban Hydrology for Small Watersheds. Technical Release No. 55.

United States Army Corps of Engineers (USACE). (2000). Hydrologic Modeling System HEC-HMS Technical Reference Manual, Report Number CPD-74B.

USACE. (2014). Climate change Adaptation plan. Climate Preparedness and Resilience Steering Committee. Department of the Army.

USACE. (2013). HEC-GeoHMS geospatial hydrologic modeling extension Version 10.1, Report Number CPD-77, (Fleming, M. J. & Doan, J. H.).

Wright, L., Chinowsky, P., Strzepek, K., Jones, R., Streeter, R., Smith, J. B., Mayotte, J., Powell, A., Jantarasami, L., & Perkins, W. (2012). Estimated effects of climate change on flood vulnerability of U.S. bridges. Mitig Adapt Strateg Glob Change, 17: 939-955.

Zhu, J. (2013). Impact of climate change on extreme rainfall across the United States. Journal of Hydrologic Engineering, 18: 1301-1309.

Chapter 7 – HYDRAULIC PROJECTIONS

Abstract

The resiliency and safety of low water crossing with regards to changes in projected stream flow regimes caused by climate change is unknown. This study analyzed low water crossing with regards to overtopping flow depth, overtopping flow velocity, and scour under present (1980-1999 & 1990-2009), simulated (1980-1999), and projected (2040-2059) and (2080-2099) design flow values. Hydraulic models were developed within the Hydrologic Engineering Center-River Analysis System (HEC-RAS) Version 4.1.0. Peak flow rates developed from gauge (existing conditions) and average future climate projection precipitation data were used as hydraulic model imputes. Steady state HEC-RAS models were implemented for design storms with ARIs of 0.5-, 1-, 2-, 5-, 10-, 25-, 50-, and 100-years for all scenarios. Continuous 20-year simulations were modeled using rating curves developed from the HEC-RAS models. Climate models used for the continuous simulations were the two climate models representing the upper and lower bounds of maximum precipitation estimates for a majority of return periods for each projected timeframe at each location.

The results indicate the riverine crossing structures considered for this study are projected to see an increase in the magnitude and frequency of high flow events by the end of this century. The projected (2080-2099) 10-yr event is on the order of the present 50-yr (sometimes 25-yr or 100-yr) event for many of the studied streams, suggesting possible future conditions should be considered when designing new infrastructure. Unfortunately the uncertainty inherent in the climate modeling makes it difficult to determine specific recommendations on how to revise current LWC design criteria with regards to climate change in the study regions. The continuous model simulations and projections proved to underestimate average yearly flow durations for small flow events with very frequent return periods.

Special care must be taken when using and applying frequent events from dynamically downscaled RCM precipitation data. An investigation into the timing and intensity of very frequent observed and simulated precipitation events could be needed before applying similar climate model data to hydrologic and hydraulic models.

Keywords: Stream hydrology, peak flood, climate change, low water crossing, hydraulics

7.1 Introduction

Runoff from increased precipitation intensity and quantity may have a significant impact of related infrastructure (Huff and Angel, 1992). With regards to riverine crossing structures, increases in the frequency and quantity of high flow events will increase bridge/culvert capacity exceedances (causing upstream flooding to occur), increase overtopping and scouring problems to structures, increase flood plain inundatation occurrences, and increase the occurrences of culvert blockage by debris (Scottish Executive, 2005; USDOT, 2014). The Transportation Research Board (TRB, 2008) suggested low-lying bridges will be more susceptible to flooding, thousands of culverts could be undersized, and runoff from increased precipitation levels will also affect stream flow and sediment delivery in some locations, with potentially adverse effects to bridge foundations. Therefore, it may be necessary to account for the nonstationary nature of precipitation and flooding when estimating the magnitudes and frequencies of future events and design stream crossing structures accounting (IDNR, 2015 & Mailhot and Duschesne, 2010).

This study routed observed and projected steady flow hydrographs through hydraulic models to determine usability and sustainability of current structures and feasibility of alternative designs for

projected flow regimes. The peak flood hydrographs were developed from HEC-HMS models of the study watersheds from existing conditions and average future climate projection data. Continuous 20-year simulations were run through the HEC-HMS models using observed precipitation and projected precipitation from two of the four RCMs. The two models utilized for the continuous simulations were those models that represented the upper and lower bounds of maximum precipitation estimates for a majority of return periods for each projected timeframe at each location. Hydraulic models were developed within the Hydrologic Engineering Center-River Analysis System (HEC-RAS) Version 4.1.0 (USACE, 2010). Steady state HEC-RAS models were implemented for design storms with ARIs of 0.5-, 1-, 2-, 5-, 10-, 25-, 50-, and 100-years for scenarios including present conditions and average RCM projections. The resiliency and safety of all LWCs and applicable bridges were tested with regards to overtopping flow depth, overtopping flow velocity, and scour under present, simulated, and projected (2040-2059) and (2080-2099) design flow values. The usability of all LWCs and applicable bridges were also tested using all applicable continuous 20-yr simulations, which were analyzed using rating curves

7.2 Methods

7.2.1 HEC-RAS

Hydraulic models were developed within the Hydrologic Engineering Center-River Analysis System (HEC-RAS) Version 4.1.0 (USACE, 2010). Steady flow routing methodologies were used within HEC-RAS.

Cross-sections and Hydraulic Structures

Hydraulic model data was developed through field surveys with some additional definition of channel overbank areas and roadway crests using the topographic data described in Chapter 3. Cross section locations were developed in HEC-GeoRAS and surveyed channel geometry was inserted into topographically generated cross-sectional data. Cross-sectional data was surveyed by the US Army Corps

of Engineers (USACE). Surveys of the open channel of each tributary and all crossings were performed to characterize the channel and near overbank geometry. Cross-sectional geometry in the non-surveyed overbank area was obtained using the topographic data described in Sections 3.1.5, 3.2.5, and 3.3.5 combined with the surveyed channel cross section.

Bridges, culverts, LWCs, and hydraulic structures were also surveyed. In a few cases, information from construction plans was used to supplement survey data. Ineffective flow areas were placed at cross sections upstream and downstream of crossings, generally assuming a contraction ratio of 1:1 and an expansion ratio of 2:1. Contraction and expansion coefficients generally were increased to 0.3 and 0.5, respectively, at cross sections adjacent to structures.

Channel Roughness

Channel and overbank roughness characteristics were determined from photographs taken during the field surveys. The photographs were combined with information from aerial photography to assign modeled Manning's 'n' roughness coefficients along the modeled stream length. Chow (1959) was used to determine the proper Manning's coefficients for each stream channel and overbank area.

Discharge Input and Boundary Conditions

Steady state peak flow data and unsteady state long term flow data was obtained from the HEC-HMS hydrologic models as described in 0. Downstream boundary conditions were determined assumed to be normal depth.

7.2.2 In-stream Processes

Bed shear stress

Sediment deposition and scour was evident upstream and downstream of the LWC in Edgar Co, IL. To analyze this issue stream bed topography within the study reach was surveyed to estimate local bed shear stress as needed. The dimensionless bed shear stress is computed as (Shields, 1936):

$$\tau_b^* = \frac{\tau_b}{(\rho_s - \rho)gD}$$

Equation 7.1

where τ_b^* is dimensionless bed shear stress, τ_b is bed shear stress, ρ_s is the density of the sediment, ρ is the density of water, g is acceration due to gravity, and D is the diameter of the sediment. The bed shear stress was computed as:

$$\tau_b = \rho g h S$$

Equation 7.2

where h is the depth of water (m) and S is the average bed slope of the reach. The dimensionless bed shear stress was computed along the reach at the peak flow depth of several design storms. These calculations did not account for local changes in the stream bed slope, such as at the riffle-pool structures or at LWC structures.

Articulating Concrete Block (ACB) Design Guidelines

ACB armored LWCs were studied at two locations along Nineveh Creek at Camp Atterbury. The stability of a single block is a function of the applied hydraulic conditions (velocity and shear stress), the angle of the inclined surface on which it rests, and the weight and geometry of the block (FHWA, 2009). The safety factor (SF) for a single block in an ACB matrix is defined as the ratio of restraining moments to overturning moments:

$$SF = \frac{\left({}^{l_2}/_{l_1}\right) a_\theta}{\cos\beta\sqrt{(1-a_\theta)^2} + \eta_1\left({}^{l_2}/_{l_1}\right) + \frac{(l_3 F'_D \cos\delta + l_4 F'_L)}{l_1 W_s}}$$

Equation 7.3

where l_1, l_2, l_3, and l_4 are moment arms of the proposed block, W_s is the submerged weight of the block, a_θ is the projection of W_s into the subgrade beneath the block, β is the angle of block projection once in motion, η_1 is the stability number for a sloped surface, is F'_D additional drag, and F'_L is additional lift. Equations for finding all variables can be found in HEC 23 Section 8.3 (FHWA, 2009). The design shear stress and critical shear stress for a block on the streambed must be known in order to find the factor of safety given in Equation 7.3. The design shear stress is found from Equation 7.2 while the critical shear stress is given by the Cable-Concrete manufactures (see Appendix C). A typical FS for stream revetment projects is 1.5 while a FS of 2.0 is considered for protection around bridge abutments and pier.

Pier Scour Mitigation

Riprap protection around bridge piers to protect against scour during high flow events is a common practice (FHWA, 2009). The standard Isbash (1936) formula for sizing riprap on a channel bed is:

$$d_{50} = \frac{0.692(V_{des})^2}{(S_g - 1)2g}$$

Equation 7.4

Where d_{50} is the required median stone diameter (m), S_g is specific gravity of riprap (usually 2.65), g is acceleration due to gravity, and V_{des} is the design flow velocity on the pier given as:

$$V_{des} = K_1 K_2 V_{pier}$$

Equation 7.5

Where K_1 is a pier shape factor (1.5 for round-nose piers and 1.7 for square-faced piers), K_2 is velocity adjustment for pier location in channel (0.9 near the bank of straight reach and up to 1.7 for pier located

in the main current of flow around a sharp bend), and V_{pier} is maximum velocity in main channel upstream of pier.

Culvert Design Guidelines

The usability of all LWCs and applicable bridge were tested under present, simulated, and projected (2040-2059) and (2080-2099) using continuous 20-yr simulations. The usability of a crossing for both vehicles and pedestrians were considered with regards to public safety and typical responses of the general public to flooded roadways. With regards to vehicles, Balke et al. (2011) reports it only takes about 0.62 m (2 ft) of water to float most cars and, in some cases, less. Many smaller cars will float in as little as 0.31 m (1 ft) of water (Federal Emergency Management Agency, 2013). For this study LWCs used strictly by military vehicles were judged to be usable for overtopping flow depths less than 0.62 m. LWCs used by military vehicles and/or the general public were considered usable for overtopping flow depths less than 0.31 m. The duration of all overtopping flow, regardless of depth, was also considered due to the guidance given by FEMA and others to turn around and not drive across any water covered stream crossing if the depth of the water can't be determined (FEMA, 2013).

For pedestrians, Abt et al. (1989) and Jonkman and Penning-Rowsell (2008) found human instability, when wading through flowing water, to occur across varying depth-velocity combinations. At a depth of 1 m, flow velocity of 0.5 m/s can cause instability, while at a depth of 0.31 m, flow velocity of 3 m/s can cause instability. Other factors such as stream bottom characterizes (riprap, algae, muck), water characteristics (debris, temperature), and human variables (clothing, footwear, health, age, fatigue) can affect human stability in flowing water. For this study, an overtopping flow velocity of 0.62 m/s was considered with regards to LWC usability and safety in addition to the flow depth.

7.3 Results

7.3.1 Nineveh Creek (Camp Atterbury, IN)

HEC-RAS Model

Figure 7.1 is a schematic of the HEC-RAS model for Nineveh Creek. The stream channel contains two improved fords and two bridges. The modeled stream length for Nineveh Creek is 4.4 km. Figure 7.2 shows the stream profile and flood profiles for the present and projected (2040-2059 and 2080-2099) 100yr peak flows.

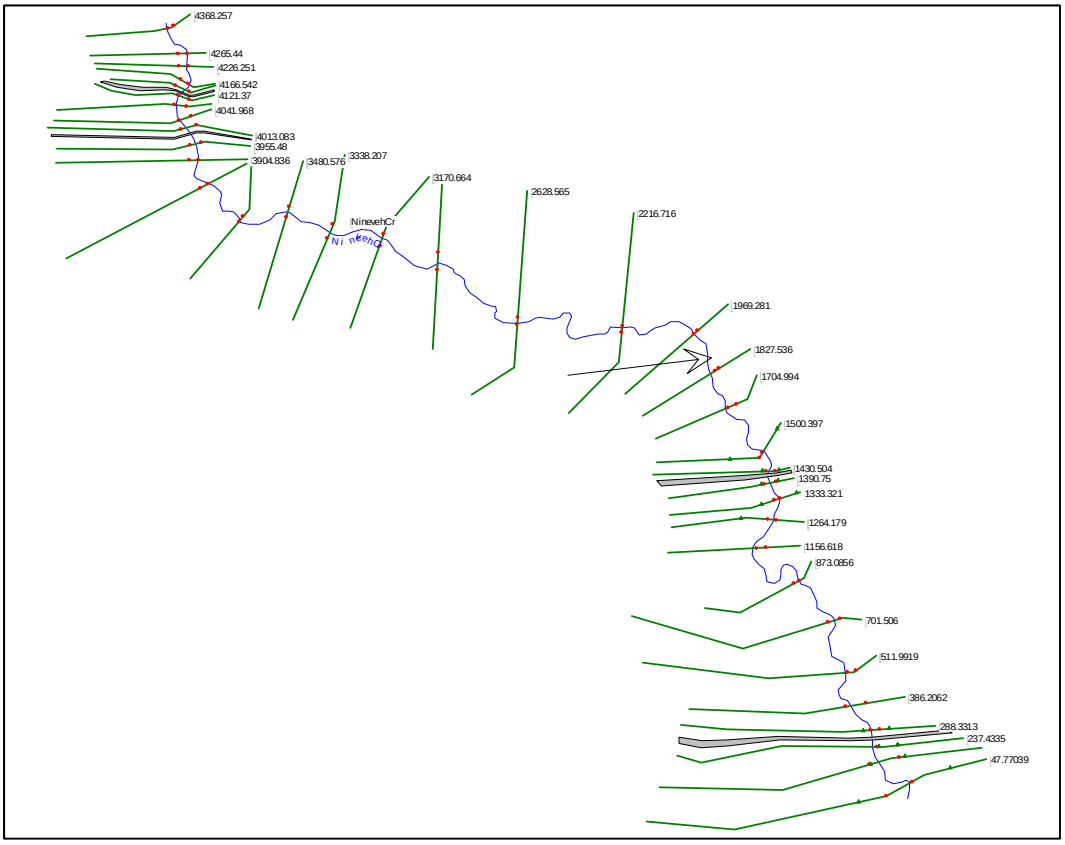

Figure 7.1. Schematic of the HEC-RAS model for the Nineveh Creek

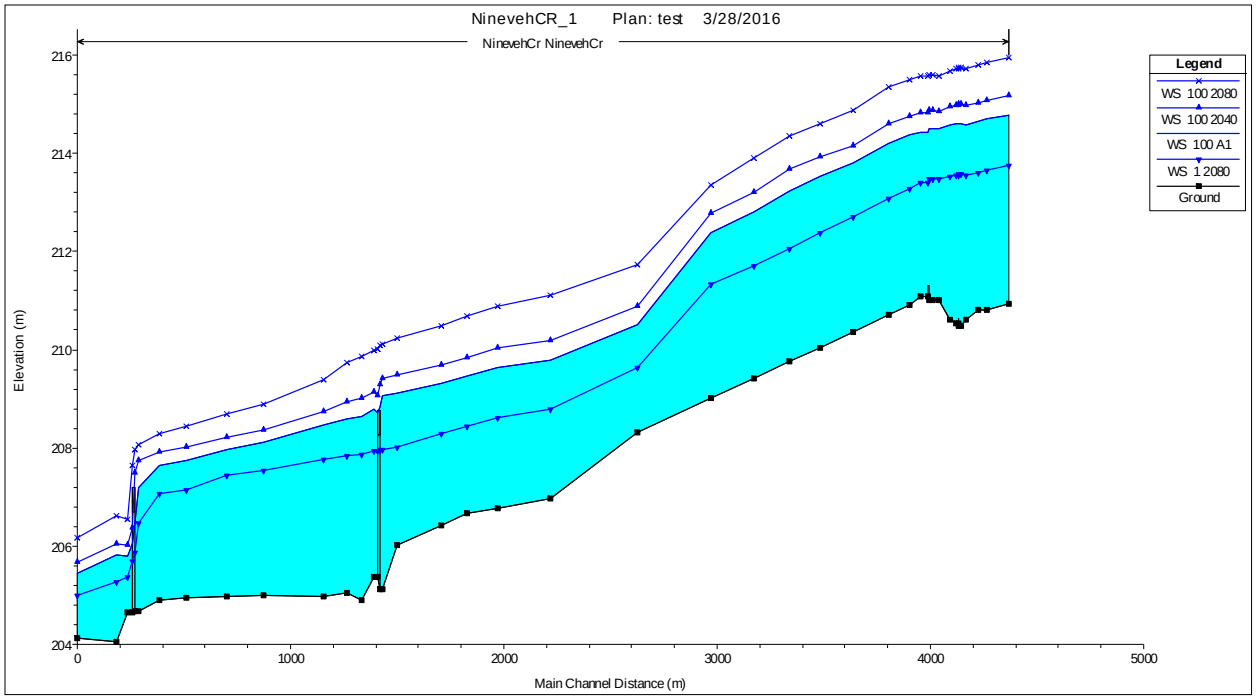

Figure 7.2. Profile of the HEC-RAS model for the Nineveh Creek

Nineveh Creek Low Water Crossings

The steady state HEC-RAS model was implemented for design storms with ARIs of 0.5-, 1-, 2-, 5-, 10-, 25-, 50-, and 100-years for scenarios including present conditions and average RCM projections determined in Chapter 6. Table 7.1 shows the maximum flow depth at the two improved fords for a range of return periods and scenarios. LWC CA4, the upstream most crossing, experiences deeper maximum flow depths for all scenarios and ARIs due to its location on the stream profile. Projected (2040-2059) flow depths are 2%-12% deeper than present conditions over the range of return periods and projected (2080-2099) flow depths are 25%-34% deeper than present conditions. LWC CA3, downstream of CA4, experiences smaller maximum depths but the differences between projected (2040-2059) and projected (2080-2099) vs. present conditions are 4%-14% and 30%-45%, respectively.

Table 7.1. Maximum flow depth for different scenarios and return periods at Nineveh Creek LWCs

	CA4 - North LWC					CA3 - South LWC				
Return Period	Present	Avg RCM 2040	Avg RCM 2080	Precent Diff	Precent Diff	Present	Avg RCM 2040	Avg RCM 2080	Precent Diff	Precent Diff
(yr)	(m)	(m)	(m)	Present - RCM 2040	Present- RCM 2080	(m)	(m)	(m)	Present - RCM 2040	Present- RCM 2080
0.5	1.83	1.89	2.5	3.2%	30.9%	1.12	1.18	1.77	5.2%	45.0%
1	2.19	2.24	2.94	2.3%	29.2%	1.47	1.53	2.21	4.0%	40.2%
2	2.41	2.55	3.38	5.6%	33.5%	1.69	1.83	2.64	8.0%	43.9%
5	2.77	2.97	3.84	7.0%	32.4%	2.04	2.24	3.09	9.3%	40.9%
10	3.06	3.34	4.2	8.7%	31.4%	2.33	2.6	3.45	11.0%	38.8%
25	3.42	3.79	4.52	10.3%	27.7%	2.68	3.04	3.75	12.6%	33.3%
50	3.7	4.16	4.85	11.7%	26.9%	2.96	3.41	4.07	14.1%	31.6%
100	4	4.4	5.18	9.5%	25.7%	3.25	3.64	4.39	11.3%	29.8%

Table 7.2 shows the maximum velocity over the LWCs for a range of return periods and scenarios. The maximum velocities are greater over LWC CA3 due to the smaller depths for each return period and the location of the stream profile. The differences in maximum flow velocities between projected (2040-2059) and projected 2080-2099) vs present conditions for LWXs CA4 and CA3 are 2%-19%, 40%-48%, 2%-19%, and 28%-47%, respectively.

Table 7.2. Maximum flow velocities for different scenarios and return periods at Nineveh Creek LWCs

	CA4 - North LWC					CA3 - South LWC				
Return Period	Present	Avg RCM 2040	Avg RCM 2080	Precent Diff	Precent Diff	Present	Avg RCM 2040	Avg RCM 2080	Precent Diff	Precent Diff
(yr)	(m/s)	(m/s)	(m/s)	Present - RCM 2040	Present- RCM 2080	(m/s)	(m/s)	(m/s)	Present - RCM 2040	Present- RCM 2080
0.5	0.28	0.29	0.43	3.5%	42.3%	0.4	0.41	0.53	2.5%	28.0%
1	0.36	0.37	0.54	2.7%	40.0%	0.47	0.48	0.62	2.1%	27.5%
2	0.41	0.44	0.66	7.1%	46.7%	0.51	0.54	0.73	5.7%	35.5%
5	0.49	0.54	0.8	9.7%	48.1%	0.58	0.62	0.88	6.7%	41.1%
10	0.57	0.65	0.93	13.1%	48.0%	0.65	0.72	1.02	10.2%	44.3%
25	0.67	0.78	1.07	15.2%	46.0%	0.75	0.86	1.17	13.7%	43.8%
50	0.76	0.92	1.22	19.0%	46.5%	0.83	1	1.33	18.6%	46.3%
100	0.86	1.01	1.4	16.0%	47.8%	0.94	1.11	1.52	16.6%	47.2%

The improved LWCs were analyzed for stability using the factor of safety method detailed in Section 7.2.2 (Table 7.3). Design flow with ARIs of 10-, 25-, and 100-yrs were considered for each scenario [present conditions, projected (2040-2059), and projected (2080-2099)]. A FS of 1.5 is typical for stream

revetment projects. Results indicated the existing armor, 45 lb/ft^2 cable-concrete (45s), is sufficient to withstand flows with ARIs greater than 100-yrs under present conditions but insufficient for flows greater the ARIs of 25-yrs and 10-yrs under projected (2040-2059) and (2080-2099) conditions, respectively. An analysis of 70 lb/ft^2 cable-concrete (70s) was also completed (Table 7.4). 70s are sufficient to withstand all present and projected peak floods other than the 100-yr, projected (2080-2099) event.

Table 7.3. Factor of safety of existing (45 lb/ft^2) Nineveh Creek cable concrete LWCs for different scenarios and return periods

CC 45			
FS for Design Storm	Present	Avg RCM 2040	Avg RCM 2080
10 yr	3.30	2.68	1.39
25 yr	2.51	1.92	1.07
100 yr	1.61	1.18	0.64

Table 7.4. Factor of safety of alternative (70 lb/ft^2) Nineveh Creek cable concrete LWCs for different scenarios and return periods

CC 70			
FS for Design Storm	Present	Avg RCM 2040	Avg RCM 2080
10 yr	5.52	4.59	2.51
25 yr	4.33	3.40	1.96
100 yr	2.89	2.16	1.20

Rating curves for maximum flow depth and flow velocity vs flow rate were developed for a wide range of flow rates for each LWC. See Figure 7.3. These rating curves were used to analyze the continuous 20yr simulations: present (1990-2009) and MRI and IPSL (2040-2059 and 2080-2099).

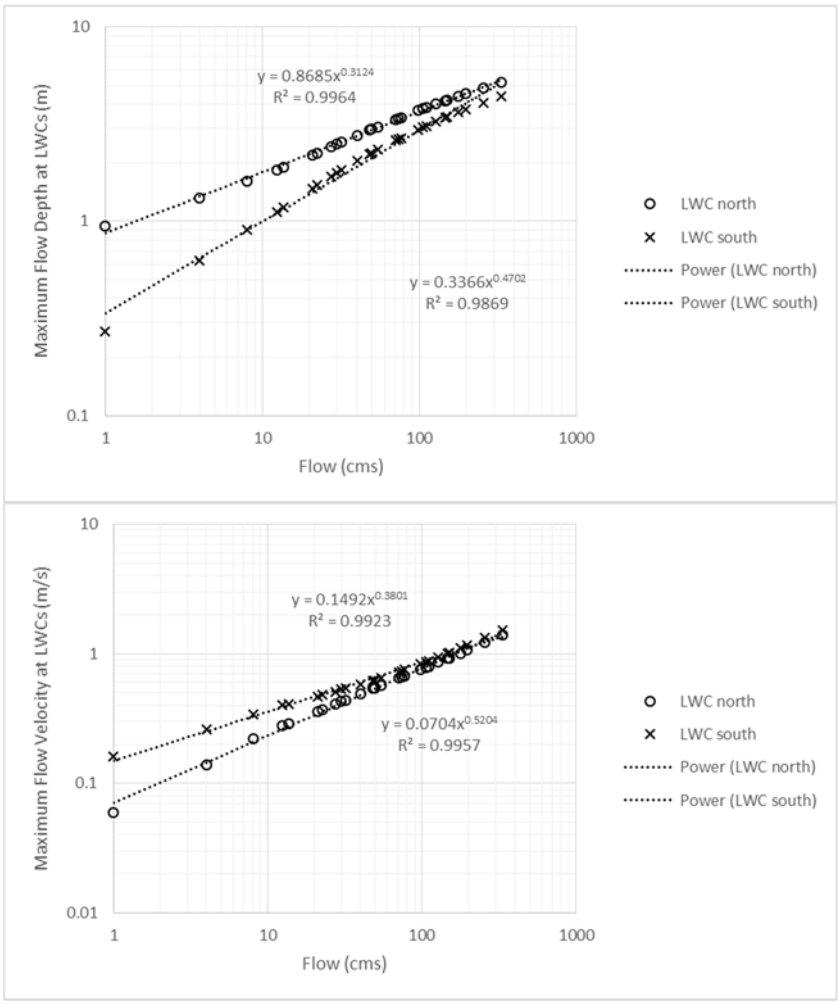

Figure 7.3. Rating curves for maximum depth vs flow rate and channel velocity vs flow rate at Nineveh Creek LWCs

The continuous simulations were analyzed using rating curves to determine the amount of time over each 20yr simulations the LWCs would be unusable due to flow depths greater than 0.62 m or flow velocities greater than 0.62 m/s (Table 7.5 and Table 7.6). A depth of 0.31 m is typically used to determine if a LWC is passible, but 0.62 m was used due to the height and robustness of military vehicles. A flow depth of 0.62 m corresponds to a flow rate well less than the 0.5-yr event. Results indicates flow depth at CA4 is greater than 0.62m 19% of the time under present conditions and 13%-17% of the time under projected simulations. For CA3, the flow depths is greater than 0.62 m 8% of the time under present conditions and 6%-7% under projected simulations. Flow velocity at CA4 is again

generally slower than at CA3 and the amount of time velocity is greater than 0.62 m/s is 0%-0.1% for the former and 0.1%-0.3% for the later.

Table 7.5. Amount of time (%) for different scenarios over a 20yr period that water depth at Nineveh Creek LWCs is greater than 0.62 m

CA4 - North LWC - Depth > 0.62m					CA3 - South LWC - Depth > 0.62m				
Present	IPSL	IPSL	MRI	MRI	Present	IPSL	IPSL	MRI	MRI
1990	2040	2080	2040	2080	1990	2040	2080	2040	2080
19.3%	12.6%	14.0%	16.5%	15.7%	7.6%	6.2%	6.0%	7.4%	7.0%

Table 7.6. Amount of time (%) for different scenarios over a 20yr period that water velocity at Nineveh Creek LWCs is greater than 0.62 m/s

CA4 - North LWC - Vel > 0.62 m/s					CA3 - South LWC - Vel > 0.62 m/s				
Present	IPSL	IPSL	MRI	MRI	Present	IPSL	IPSL	MRI	MRI
1990	2040	2080	2040	2080	1990	2040	2080	2040	2080
0.0%	0.0%	0.1%	0.0%	0.1%	0.1%	0.1%	0.3%	0.1%	0.3%

The comparisons between present (1990-2009) conditions and projected (2040-2059 and 2080-2099) conditions seems to indicate that the hydrographs of IPSL are more compressed (shorter) than the peak hydrographs of the gauge data and MRI during continuous simulations. The projected peak flows are greater than the 1990-2009 peak flows, but the IPSL projected amount of time the LWCs experience a given depth is less than current conditions. Table 7.7 shows a comparison of time over each 1980-1999 scenario (observed and simulation) the LWCs would be unusable due to flow depths greater than 0.62 m or flow velocities greater than 0.62 m/s. Results indicate that the IPSL simulations may underestimate the length of time high flows persist compared to observed values, which means the timing of IPSL precipitation events are also shorter than observed events, though the magnitudes are similar as per Q-Q mapping.

Table 7.7. Amount of time (%) for 1980-1999 simulations that water depth and velocity at Nineveh Creek LWCs is greater than 0.31 m and 0.62 m/s, respectively, with percent differences

CA4 - North LWC					CA3 - South LWC				
Depth > 0.62m			Precent Diff	Precent Diff	Depth > 0.62m			Precent Diff	Precent Diff
Obs	IPSL	MRI	Obs-IPSL	Obs-MRI	Obs	IPSL	MRI	Obs-IPSL	Obs-MRI
1980	1980	1980	1980	1980	1980	1980	1980	1980	1980
18.6%	14.0%	16.1%	-28.1%	-14.4%	6.7%	6.5%	6.8%	-2.9%	1.7%
CA4 - North LWC					CA3 - South LWC				
Vel > 0.15 m/s			Precent Diff	Precent Diff	Vel > 0.15 m/s			Precent Diff	Precent Diff
Gage	IPSL	MRI	Obs-IPSL	Obs-MRI	Gage	IPSL	MRI	Obs-IPSL	Obs-MRI
1980	1980	1980	1980	1980	1980	1980	1980	1980	1980
6.1%	5.8%	6.0%	-3.7%	-0.5%	13.6%	11.3%	12.6%	-18.0%	-7.7%

Nineveh Creek Bridges

The steady state HEC-RAS model was implemented with for design storms with ARIs of 0.5-, 1-, 2-, 5-, 10-, 25-, 50-, and 100-years for scenarios including present conditions and average RCM projections determined in Chapter 6. Table 7.8 shows the maximum flow depth at the two bridges for a range of return periods and scenarios. Bridge CA2, the upstream bridge, experiences deeper maximum flow depths for all scenarios and ARIs due to its location on the stream profile. Projected (2040-2059) flow depths are 3%-15% deeper than present conditions over the range of return periods and projected (2080-2099) flow depths are 24%-34% deeper than present conditions. Bridge CA1, downstream of CA1 at the Impact Area boundary, experiences smaller maximum depths but the differences between projected (2040-2059) and projected (2080-2099) vs. present conditions are 2%-19% and 29%-48%, respectively.

Table 7.8. Maximum depths for different scenarios and return periods at Nineveh Creek Bridges (gray denotes overtopping flow)

	CA2 - North Bridge					CA1 - South Bridge				
Return Period	Present	Avg RCM 2040	Avg RCM 2080	Precent Diff	Precent Diff	Present	Avg RCM 2040	Avg RCM 2080	Precent Diff	Precent Diff
(yr)	(m)	(m)	(m)	Present - RCM 2040	Present- RCM 2080	(m)	(m)	(m)	Present - RCM 2040	Present- RCM 2080
0.5	1.74	1.81	2.46	3.9%	34.3%	1.04	1.06	1.39	1.9%	28.8%
1	2.15	2.21	2.85	2.8%	28.0%	1.18	1.21	1.81	2.5%	42.1%
2	2.38	2.52	3.23	5.7%	30.3%	1.33	1.45	2.16	8.6%	47.6%
5	2.7	2.86	3.74	5.8%	32.3%	1.66	1.84	2.43	10.3%	37.7%
10	2.94	3.16	4.14	7.2%	33.9%	1.91	2.13	2.65	10.9%	32.5%
25	3.27	3.67	4.38	11.5%	29.0%	2.18	2.43	3.1	10.8%	34.8%
50	3.55	4.11	4.65	14.6%	26.8%	2.39	2.63	3.26	9.6%	30.8%
100	3.93	4.29	4.98	8.8%	23.6%	2.53	3.07	3.39	19.3%	29.1%

Table 7.9 shows the maximum velocity under the bridges for a range of return periods and scenarios. The maximum velocities are greater under bridge CA1 due to the smaller depths for each return period. The differences in maximum flow velocities between projected (2040-2059) and projected 2080-2099) vs present conditions for bridges CA2 and CA1 are 2%-17%, 17%-48%, 0%-7%, and 4%-41%, respectively. Note that for CA1, at a flow rate near 115 cms water begins to overtop the road embankments and substantial flow conveyance begins in the floodplain upstream and downstream of the structure. As a result, flow velocity begins to decrease for flows over 115 cms.

Table 7.9. Maximum flow velocities for different scenarios and return periods at Nineveh Creek Bridges (gray denotes drop in main channel flow velocity due to significant overland flow in the floodplains)

	CA2 - North Bridge					CA1 - South Bridge				
Return Period	Present	Avg RCM 2040	Avg RCM 2080	Precent Diff	Precent Diff	Present	Avg RCM 2040	Avg RCM 2080	Precent Diff	Precent Diff
(yr)	(m/s)	(m/s)	(m/s)	Present - RCM 2040	Present- RCM 2080	(m/s)	(m/s)	(m/s)	Present - RCM 2040	Present- RCM 2080
0.5	0.66	0.67	0.78	1.5%	16.7%	1.93	2.03	2.93	5.1%	41.2%
1	0.72	0.73	0.94	1.4%	26.5%	2.65	2.76	2.9	4.1%	9.0%
2	0.76	0.8	1.15	5.1%	40.8%	2.89	2.92	3	1.0%	3.7%
5	0.87	0.95	1.22	8.8%	33.5%	2.89	2.89	3.43	0.0%	17.1%
10	1	1.15	1.34	14.0%	29.1%	2.9	3	2.8	3.4%	-3.5%
25	1.17	1.2	1.58	2.5%	29.8%	3.04	3.27	1.97	7.3%	-42.7%
50	1.3	1.32	1.82	1.5%	33.3%	3.14	2.79	2.12	-11.8%	-38.8%
100	1.26	1.49	2.06	16.7%	48.2%	2.8	1.88	2.38	-39.3%	-16.2%

The bridges were analyzed for pier scour countermeasure requirements as in Section 7.2.2 (Table 7.10). Design flow with ARIs of 25-, 50-, and 100-yrs were considered for each scenario (present conditions, projected (2040-2059), and projected (2080-2099). Typically, riprap is sized as d_{50} of 150-, 200-, 400-, 550-, 650-, and 750-mm. Riprap with a d_{50} of 150mm is required for CA2 under present and projected (2040-2059) conditions, and 200mm under projected (2080-2099) conditions. CA1 requires riprap with a d_{50} of 550mm for under present and projected (2040-2059) conditions, and 650mm under projected (2080-2099) conditions. Note that at CA1 the maximum velocity is projected to occur more often (lower ARIs) under projected conditions than under present conditions.

Table 7.10. Required d_{50} (m) for pier scour protection at Nineveh Creek Bridges for different scenarios and return periods

CA2 - North Bridge - d_{50} (mm)				CA1 - South Bridge - d_{50} (mm)			
Design Storm	Present	Avg RCM 2040	Avg RCM 2080	Design Storm	Present	Avg RCM 2040	Avg RCM 2080
25	66	69	120	5	402	402	566
50	81	84	159	10	404	433	
100	76	107	204	25	444	514	
				50	474		

A rating curve for maximum flow depth vs flow rate was developed for a wide range of flow rates for each bridge. See Figure 7.4. The rating curve was used to analyze the continuous 20yr simulations: present (1990-2009) and MRI and IPSL (2040-2059 and 2080-2099).

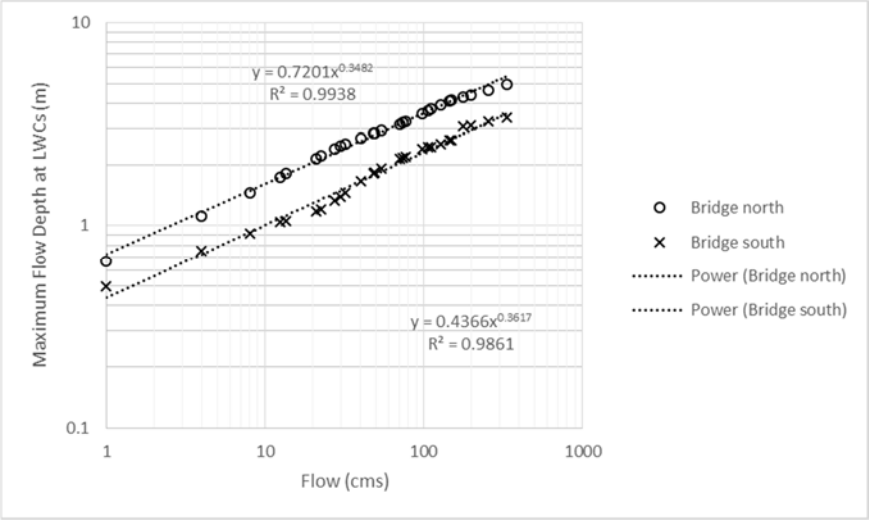

Figure 7.4. Rating curves for maximum depth vs flow rate and channel velocity vs flow rate at Nineveh Creek Bridges

Bridges usually remain open during high flow events unless the water surface reaches either the lower cord or the road surface. The continuous simulations were analyzed using rating curves to determine the amount of time over each 20yr simulations the water surface reached the lower cord of each bridge (Table 7.11). The results indicate that the water surface only reaches the lower cords during the projected (2080-2099) simulations and only during one event for each.

Table 7.11. Amount of time (%) for different scenarios over a 20yr period that water depth at Nineveh Creek Bridges up to the lower cord

CA2 - North Bridge - WSE at low cord					CA1 - South Bridge - WSE at low cord				
Present	IPSL	IPSL	MRI	MRI	Present	IPSL	IPSL	MRI	MRI
	2040	2080	2040	2080		2040	2080	2040	2080
0.0%	0.0%	0.1%	0.0%	0.1%	0.0%	0.0%	0.1%	0.0%	0.1%

7.3.2 East Branch Au Sable River (Camp Grayling, MI)

HEC-RAS Model

Figure 7.5 is a schematic of the HEC-RAS model for East Branch Au Sable River at LWC CG4. The stream channel contains one vented LWC. The modeled stream length for Nineveh Creek is 680 m. Figure 7.6 shows the stream profile and flood profiles for the present and projected (2040-2059 and 2080-2099) 100yr peak flows.

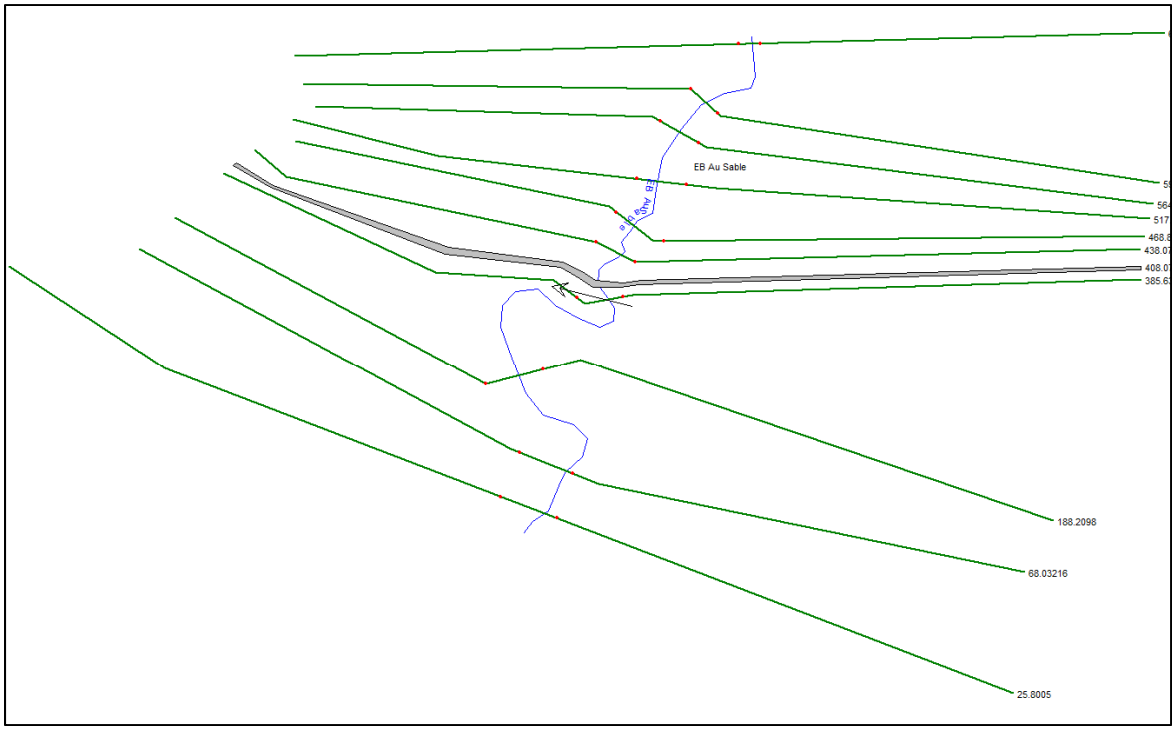

Figure 7.5. Schematic of the HEC-RAS model for the East Branch Au Sable River

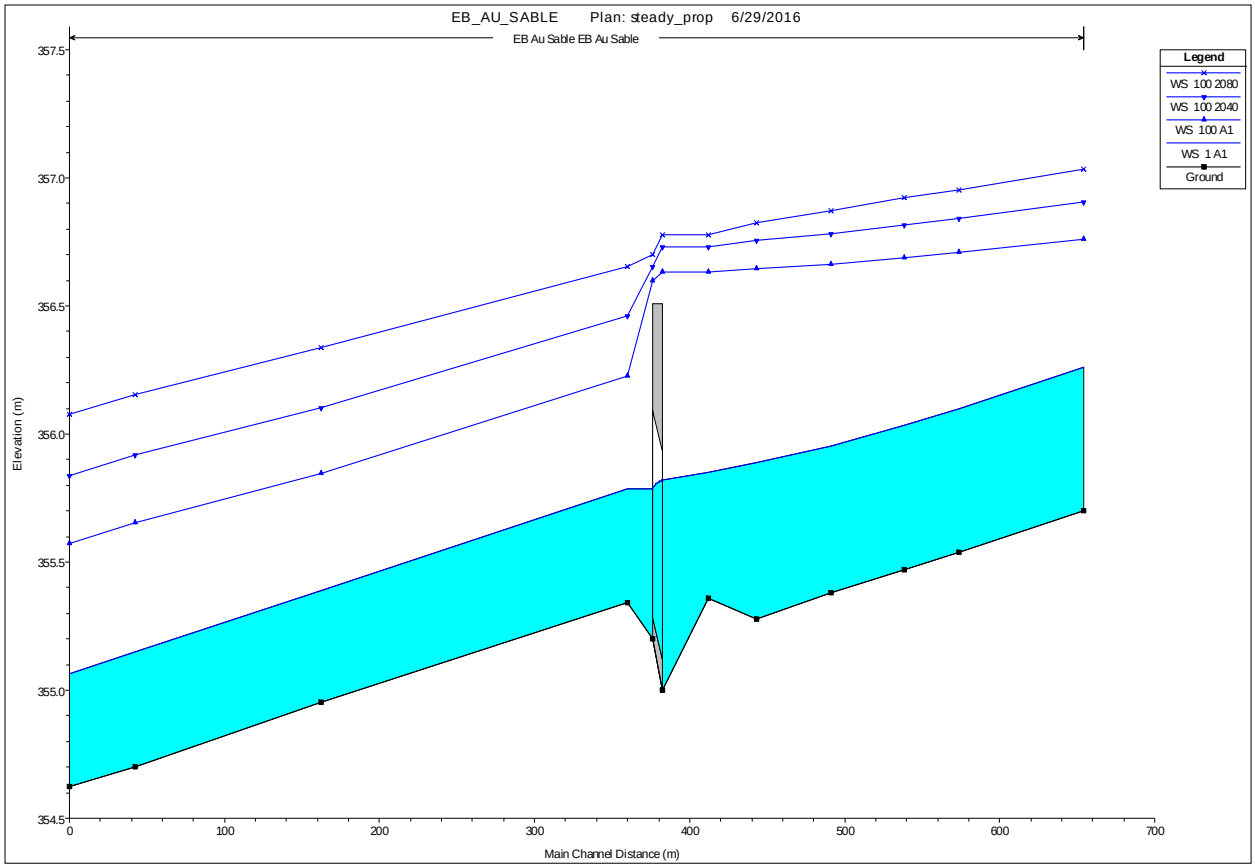

Figure 7.6. Profile of the HEC-RAS model for East Branch Au Sable River

East Branch Au Sable Low Water Crossing

The steady state HEC-RAS model was implemented for design storms with ARIs of 0.5-, 1-, 2-, 5-, 10-, 25-, 50-, and 100-years for scenarios including present conditions and average RCM projections determined in Chapter 6. Table 7.12 shows the maximum flow depth over the roadway at the vented ford for a range of return periods and scenarios. LWC CG4 experiences overtopping fow during the 50 year event and the overtopping flow is 0.13m deep during the 100 yr event. Overtopping flow occurs during the 25 yr and 5 yr design storms for the Projected (2040-2059) and projected (2080-2099) conditions.

Table 7.12. Maximum overtopping flow depth for different scenarios and return periods at East Branch Au Sable LWC

	CG 4- LWC - Weir Flow Depth				
Return Period	Present	Avg RCM 2040	Avg RCM 2080	Precent Diff	Precent Diff
(yr)	(m)	(m)	(m)	Present - RCM 2040	Present- RCM 2080
0.5	0	0	0	-	-
1	0	0	0	-	-
2	0	0	0	-	-
5	0	0	0.09	-	200.0%
10	0	0	0.14	-	200.0%
25	0	0.13	0.21	200.0%	200.0%
50	0.07	0.16	0.24	78.3%	109.7%
100	0.13	0.23	0.31	55.6%	81.8%

Table 7.13 shows the maximum overtopping velocity over the LWC for a range of return periods and scenarios. The maximum overtopping velocities are 0.6-0.7 m/s during over topping flow, but with minimal water depths. The differences in maximum flow velocities between projected (2040-2059) and projected 2080-2099) vs present conditions are minimal, but the projected scenario overtopping flow depths are greater can under present conditions.

Table 7.13. Maximum overtopping flow velocities for different scenarios and return periods at East Branch Au Sable LWC

	CG 4 - LWC - Weir Flow Vel				
Return Period	Present	Avg RCM 2040	Avg RCM 2080	Precent Diff	Precent Diff
(yr)	(m/s)	(m/s)	(m/s)	Present - RCM 2040	Present- RCM 2080
0.5	0.00	0.00	0.00	-	-
1	0.00	0.00	0.00	-	-
2	0.00	0.00	0.00	-	-
5	0.00	0.00	0.62	-	200.0%
10	0.00	0.00	0.64	-	200.0%
25	0.00	0.63	0.67	200.0%	200.0%
50	0.61	0.65	0.69	6.3%	12.3%
100	0.63	0.68	0.73	7.6%	14.7%

Rating curves for maximum overtopping flow depth and flow velocity vs flow rate were developed for a wide range of flow rates at the LWC. See Figure 7.7. These rating curves were used to analyze the continuous 20yr simulations: present (1990-2009) and CNRM and MIROC (2040-2059 and 2080-2099).

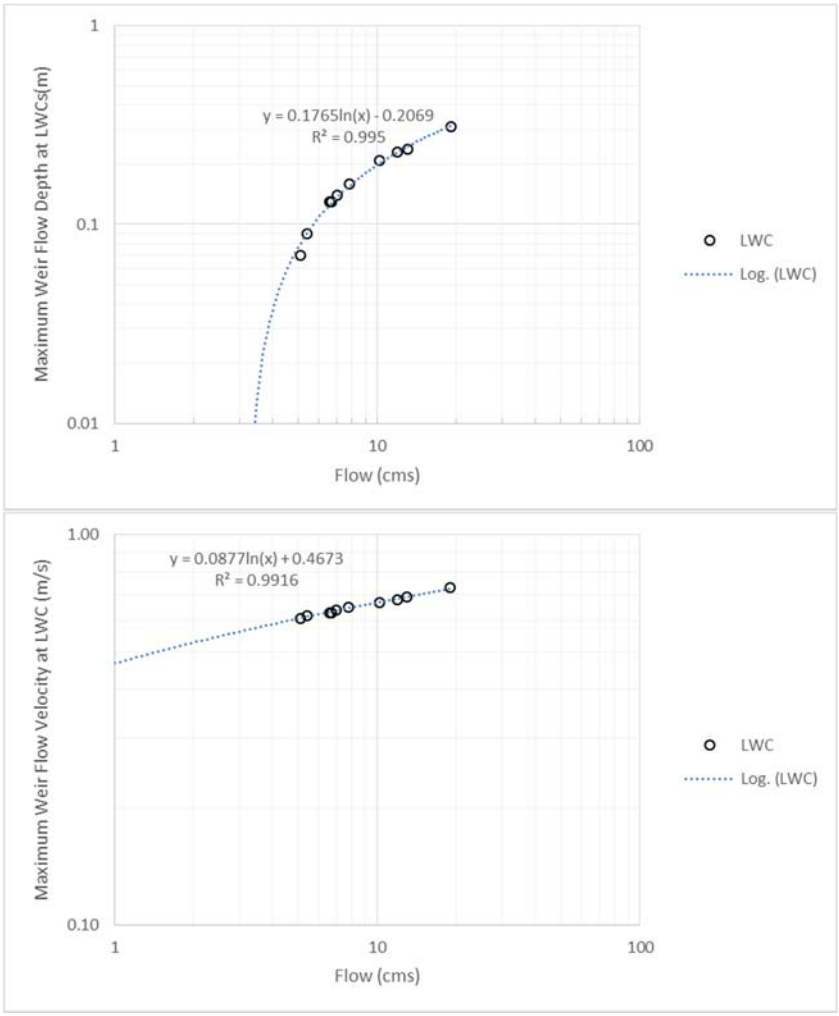

Figure 7.7. Rating curves for maximum depth vs flow rate and channel velocity vs flow rate at East Branch Au Sable LWC

The continuous simulations were analyzed using rating curves to determine the amount of time over each 20yr simulations the LWC would be unusable due to flow depths greater than 0.31 m or flow velocities greater than 0.62 m/s (Table 7.14 and Table 7.15). A depth of 0.31 m is typically used to determine if a LWC is passible, which was applicable for this structure since it is used by the general

public in addition to use by military vehicles. The amount of time over each 20yr simulations the LWC would be overtopped (depth > 0.01 m) was also determined, due to the fact that many drivers will not cross a road that is overtopped, regardless of depth. Results indicates flow depth at CG4 is greater than 0.01m 1.6% of the time under present conditions and 2%-3% of the time under projected simulations. Flow depth rarely reaches 0.31m and only during the projected (2080-2099) simulations. Overtopping flow velocity at CG4 is rarely greater than 0.62 m/s, less than 0.7% of the time under all scenarios.

Table 7.14. Amount of time (%) for different scenarios over a 20yr period that weir water depth at East Branch Au Sable LWC is greater than 0.01 m and 0.31 m

CG4 - EB Au Sable LWC									
Overtopping - Depth > 0.01m					Depth > 0.31m				
Present 1990	CNRM 2040	CNRM 2080	MIROC 2040	MIROC 2080	Present 1990	CNRM 2040	CNRM 2080	MIROC 2040	MIROC 2080
1.6%	2.1%	3.3%	2.5%	2.5%	0.0%	0.0%	0.0%	0.1%	0.1%

Table 7.15. Amount of time (%) for different scenarios over a 20yr period that water velocity at East Branch Au Sable LWC is greater than 0.62 m/s

CG4 - EB Au Sable LWC - Vel > 0.62 m/s				
Present 1990	CNRM 2040	CNRM 2080	MIROC 2040	MIROC 2080
0.8%	1.3%	2.2%	1.7%	1.8%

The comparisons between present (1990-2009) conditions and projected (2040-2059 and 2080-2099) conditions indicate that the projected peak flows are greater than the 1990-2009 peak flows and the roadway will be over topped more under projected conditions than under present conditions. To determine the validity of projected conditions Table 7.16 shows a comparison of time over each 1980-1999 scenario (observed and simulation) the LWCs would be unusable due to flow depths greater than 0.01 m and 0.31 m or flow velocities greater than 0.62 m/s. Results indicate that the simulations match the length of time high flows persist compared to observed values.

Table 7.16. Amount of time (%) for 1980-1999 simulations that water depth and velocity at East Branch Au Sable LWC is greater than 0.01 m or 0.31 m and 0.62 m/s, respectively, with percent differences

CG4 - EB Au Sable LWC									
Overtopping - Depth > 0.01m			Precent Diff	Precent Diff	Depth > 0.31m			Precent Diff	Precent Diff
Obs	CNRM	MIROC	Obs-CNRM	Obs-MIROC	Obs	CNRM	MIROC	Obs-CNRM	Obs-MIROC
1980	1980	1980	1980	1980	1980	1980	1980	1980	1980
1.8%	1.8%	1.8%	0.0%	0.0%	0.0%	0.0%	0.0%	0.0%	0.0%

Vel < 0.62 m/s			Precent Diff	Precent Diff
Obs	CNRM	MIROC	Obs-CNRM	Obs-MIROC
1980	1980	1980	1980	1980
1.1%	1.0%	1.1%	-10.0%	15.0%

Given the above analysis, the EB Au Sable LWC could be considered a high VAR LWC, since all flow passes through the vents for design events less than 50-yrs under present conditions. The existing structure also passes the average RCM projected (2080-2099) design events less than 5-yrs. A proposed LWC design, for which the vented area was reduced by half, was analyzed to determine usability under current and projected conditions. Results (Table 7.17) indicates flow depth at the proposed CG4 LWC is greater than 0.01m 7.3% of the time under present conditions and 7%-10% of the time under projected simulations. Flow depth rarely reaches 0.31m and only during the projected (2080-2099) simulations. Overtopping flow velocity at the proposed CG4 LWC is unchanged from the existing LWC.

Table 7.17. Amount of time (%) for different scenarios over a 20yr period that weir water depth at East Branch Au Sable LWC (Proposed) is greater than 0.01 m and 0.31 m or water velocity at East Branch Au Sable LWC is greater than 0.62 m/s

CG4 - EB Au Sable LWC - Proposed									
Overtopping - Depth > 0.01m					Depth > 0.31m				
Present	CNRM	CNRM	MIROC	MIROC	Present	CNRM	CNRM	MIROC	MIROC
1990	2040	2080	2040	2080	1990	2040	2080	2040	2080
7.3%	8.3%	10.4%	8.2%	7.1%	0.0%	0.0%	0.0%	0.1%	0.1%

CG4 - EB Au Sable LWC - Vel > 0.62 m/s				
Present	CNRM	CNRM	MIROC	MIROC
1990	2040	2080	2040	2080
0.6%	0.9%	1.7%	1.3%	1.5%

7.3.3 Portage Creek (Camp Grayling, MI)

HEC-RAS Model

Figure 7.8 is a schematic of the HEC-RAS model for Portage Creek. The stream channel contains two vented fords and one bridge. The modeled stream length for Nineveh Creek is 11.9 km. Figure 7.9 shows the stream profile and flood profiles for the present and projected (2040-2059 and 2080-2099) 100yr peak flows.

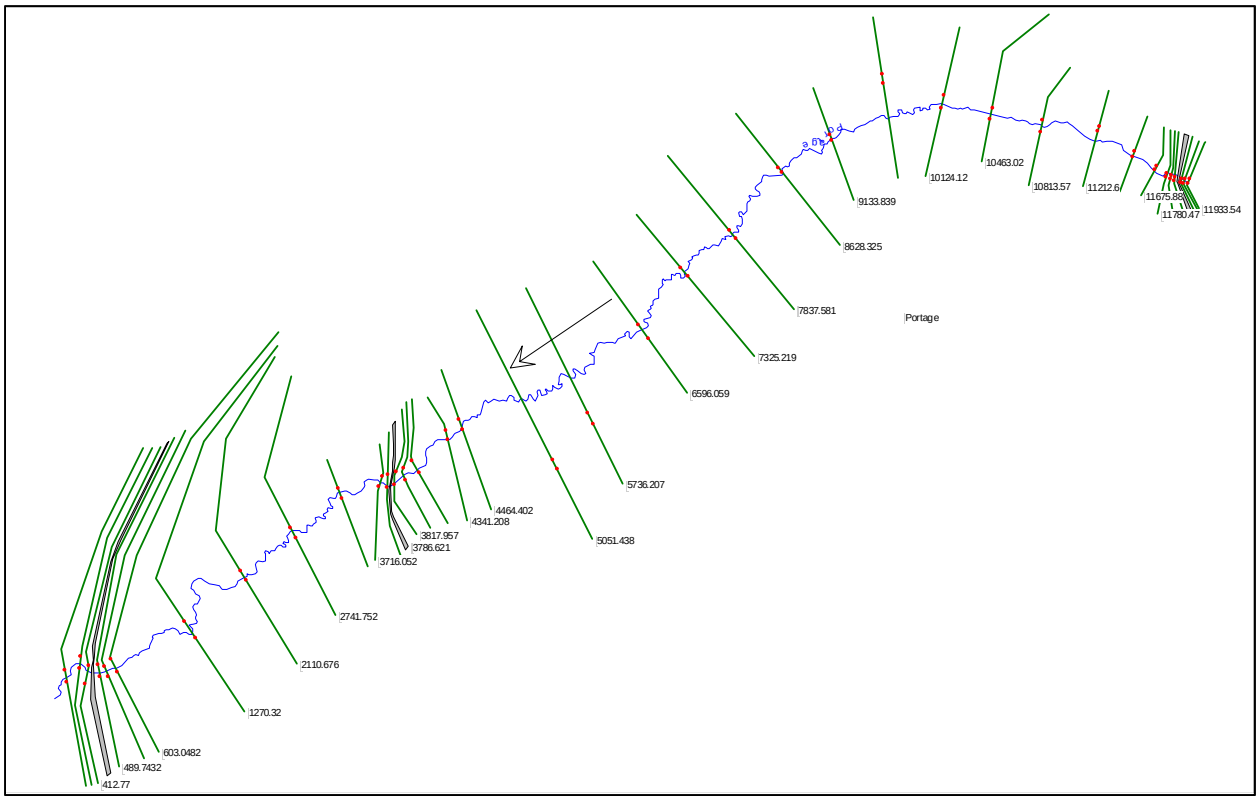

Figure 7.8. Schematic of the HEC-RAS model for Portage Creek

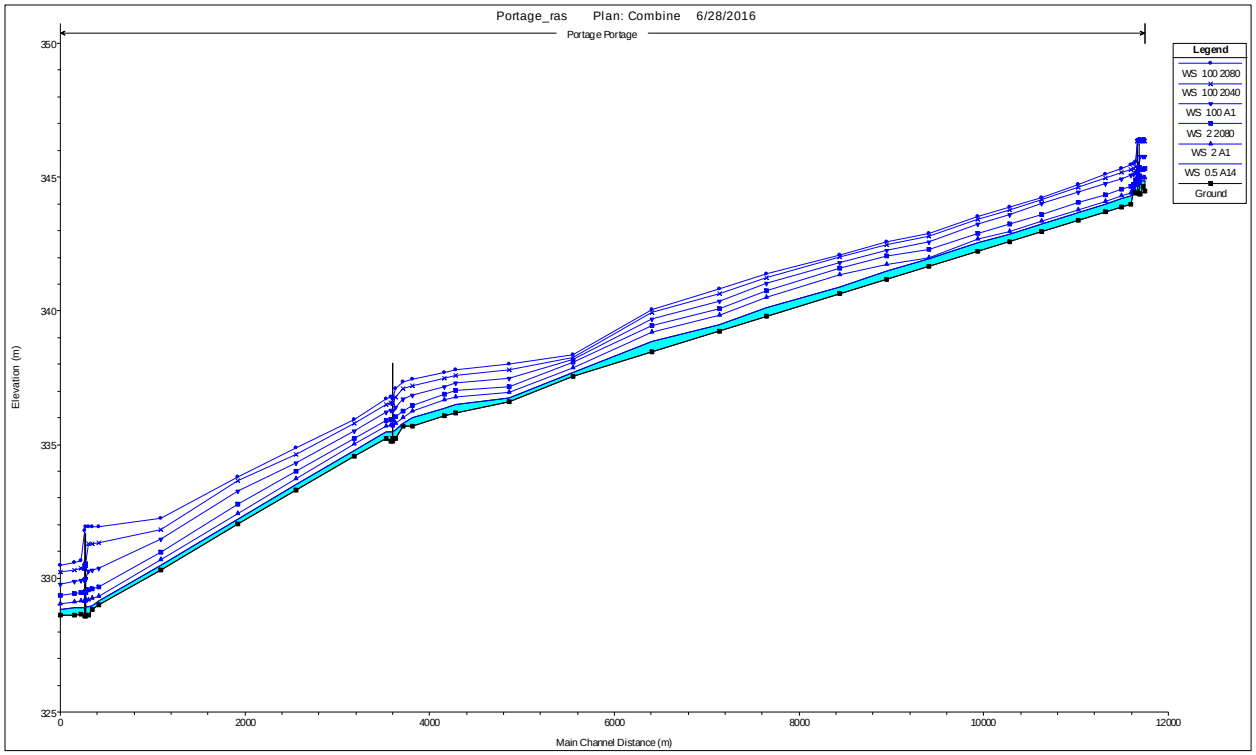

Figure 7.9. Profile of the HEC-RAS model for Portage Creek

Portage Creek Low Water Crossing

The steady state HEC-RAS model was implemented for design storms with ARIs of 0.5-, 1-, 2-, 5-, 10-, 25-, 50-, and 100-years for scenarios including present conditions and average RCM projections determined in Chapter 6. Table 7.18 shows the maximum overtopping flow depth at the two vented fords for a range of return periods and scenarios. LWC CG3, the upstream most crossing, is not overtopped under current conditions. Projected (2040-2059) 50-yr and 100-yr flow events overtop the road as do projected (2080-2099) 25-yr to 100-yr flow events. Maximum overtopping depths are 0.15 and 0.24 m for the upstream and downstream LWC, respectively. LWC CG1 is only overtopped during the projected (2080-2099) 100-yr flow event.

Table 7.18. Maximum flow depth for different scenarios and return periods at Portage Creek LWCs

	CG 3- LWC - Weir Flow Depth						CG 1- LWC - Weir Flow Depth				
Return Period	Present	Avg RCM 2040	Avg RCM 2080	Precent Diff	Precent Diff		Present	Avg RCM 2040	Avg RCM 2080	Precent Diff	Precent Diff
(yr)	(m)	(m)	(m)	Present - RCM 2040	Present- RCM 2080		(m)	(m)	(m)	Present - RCM 2040	Present- RCM 2080
0.5	0	0	0	-	-		0	0	0	-	-
1	0	0	0	-	-		0	0	0	-	-
2	0	0	0	-	-		0	0	0	-	-
5	0	0	0	-	-		0	0	0	-	-
10	0	0	0	-	-		0	0	0	-	-
25	0	0	0.06	-	200.0%		0	0	0	-	-
50	0	0.04	0.11	200.0%	200.0%		0	0	0	-	-
100	0	0.1	0.15	200.0%	200.0%		0	0	0.24	-	200.0%

Table 7.19 shows the maximum overtopping velocity over the LWCs for a range of return periods and scenarios. The maximum velocities are 0.56 and 0.66 m/s for the upstream and downstream LWC, respectively.

Table 7.19. Maximum flow velocities for different scenarios and return periods at Portage Creek LWCs

	CG 3 - LWC - Weir Flow Vel						CG 1 - LWC - Weir Flow Vel				
Return Period	Present	Avg RCM 2040	Avg RCM 2080	Precent Diff	Precent Diff		Present	Avg RCM 2040	Avg RCM 2080	Precent Diff	Precent Diff
(yr)	(m/s)	(m/s)	(m/s)	Present - RCM 2040	Present- RCM 2080		(m/s)	(m/s)	(m/s)	Present - RCM 2040	Present- RCM 2080
0.5	0.00	0.00	0.00	-	-		0	0	0	-	-
1	0.00	0.00	0.00	-	-		0	0	0	-	-
2	0.00	0.00	0.00	-	-		0	0	0	-	-
5	0.00	0.00	0.00	-	-		0	0	0	-	-
10	0.00	0.00	0.00	-	-		0	0	0	-	-
25	0.00	0.00	0.49	-	200.0%		0	0	0	-	-
50	0.00	0.48	0.53	200.0%	200.0%		0	0	0	-	-
100	0.00	0.51	0.56	200.0%	200.0%		0	0	0.66	-	200.0%

Rating curves for maximum overtopping flow depth and flow velocity vs flow rate were developed for a wide range of flow rates for each LWC. See Figure 7.10. These rating curves were used to analyze the continuous 20yr simulations: present (1990-2009) and CNRM and MIROC (2040-2059 and 2080-2099).

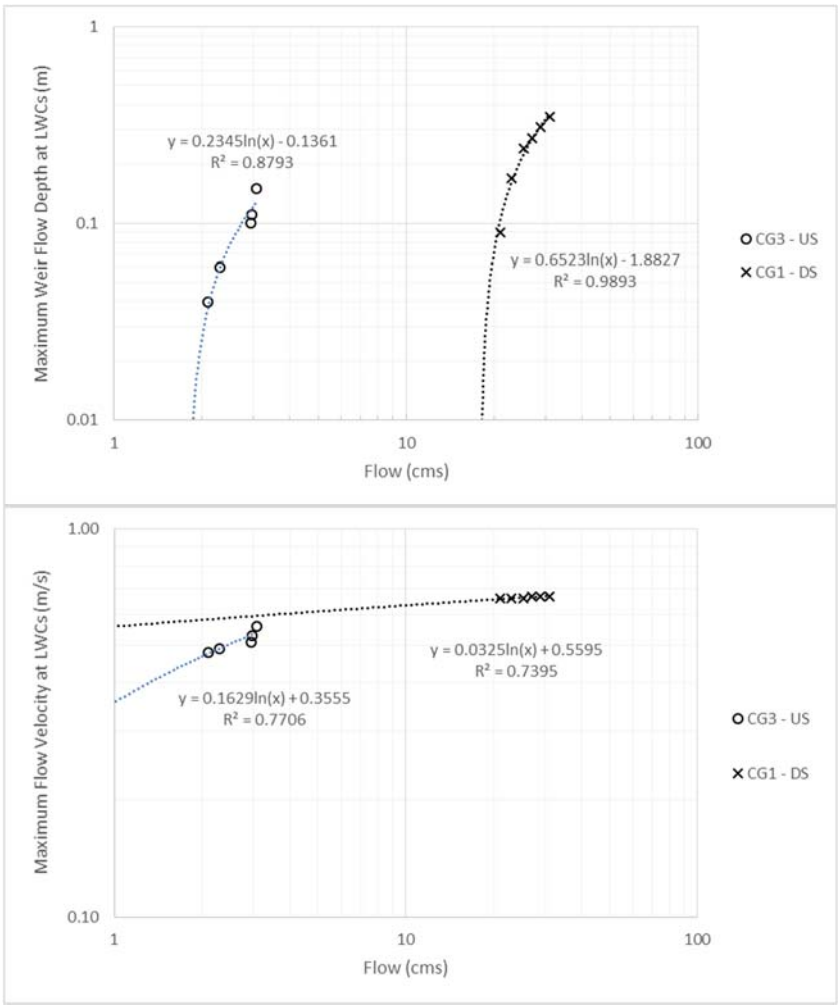

Figure 7.10. Rating curves for maximum depth vs flow rate and channel velocity vs flow rate at Nineveh Creek LWCs

The continuous simulations were analyzed using rating curves to determine the amount of time over each 20yr simulation the LWC would be unusable due to flow depths greater than 0.31 m or flow velocities greater than 0.62 m/s (Table 7.20 and Table 7.21). A depth of 0.31 m is typically used to determine if a LWC is passible, which was applicable for this structure since it is used by the general public in addition to use by military vehicles. The amount of time over each 20yr simulations the LWC would be overtopped (depth > 0.01 m) was also determined, due to the fact that many drivers will not cross a road that is overtopped, regardless of depth. Results indicates that CG3 is overtopped 1.6% of the time under present conditions and 2%-3% of the time under projected simulations. Flow depth

rarely reaches 0.31m and only during the projected (2080-2099) simulations. Overtopping flow velocity at CG4 is rarely greater than 0.62 m/s, less than 0.2% of the time under all scenarios. The downstream LWC (CG1) is only overtopped during the projected (2080-2099) MIROC simulation and only for 0.03% of the 20yr period. Overtopping flow at CG1 never exceeds 0.62 m/s.

Table 7.20. Amount of time (%) for different scenarios over a 20yr period that weir water depth at Portage Creek LWCs is greater than 0.01 m and 0.31 m

CG3 - Portage Creek, US LWC									
Overtopping - Depth > 0.01m					Depth > 0.31m				
Present	CNRM	CNRM	MIROC	MIROC	Present	CNRM	CNRM	MIROC	MIROC
1990	2040	2080	2040	2080	1990	2040	2080	2040	2080
0.3%	0.3%	1.3%	1.3%	2.3%	0.0%	0.0%	0.0%	0.0%	0.1%
CG1 - Portage Creek, DS LWC									
Overtopping - Depth > 0.01m					Depth > 0.31m				
Present	CNRM	CNRM	MIROC	MIROC	Present	CNRM	CNRM	MIROC	MIROC
1990	2040	2080	2040	2080	1990	2040	2080	2040	2080
0.0%	0.0%	0.0%	0.0%	0.03%	0.0%	0.0%	0.0%	0.0%	0.0%

Table 7.21. Amount of time (%) for different scenarios over a 20yr period that water velocity at Portage Creek LWCs is greater than 0.62 m/s

CG3 - US LWC - Vel > 0.62 m/s				
Present	IPSL	IPSL	MRI	MRI
1990	2040	2080	2040	2080
0.0%	0.0%	0.0%	0.0%	0.2%
CG4 - DS LWC - Vel > 0.62 m/s				
Present	IPSL	IPSL	MRI	MRI
1990	2040	2080	2040	2080
0.0%	0.0%	0.0%	0.0%	0.0%

The comparisons between present (1990-2009) conditions and projected (2040-2059 and 2080-2099) conditions indicate that the projected peak flows are greater than the 1990-2009 peak flows and the roadway will be over topped slightly more under projected conditions than under present conditions. To determine the validity of projected conditions Table 7.22 shows a comparison of time over each 1980-1999 scenario (observed and simulation) the LWCs would be unusable due to flow depths greater

than 0.01 m and 0.31 m or flow velocities greater than 0.62 m/s. Results indicate that the simulations estimate the LWC will be overtopped 1 day per year on average while the observed resulted in 2.5 days of overtopping per year. The percent difference is large but the magnitude of the difference is very small.

Table 7.22. Amount of time (%) for 1980-1999 simulations that water depth and velocity at Portage Creek LWC CG3 is greater than 0.01 m or 0.31 m and 0.62 m/s, respectively, with percent differences

CG3 - Portage Creek, US LWC									
Overtopping - Depth > 0.01m			Precent Diff	Precent Diff	Depth > 0.31m			Precent Diff	Precent Diff
Obs	CNRM	MIROC	Obs-CNRM	Obs-MIROC	Obs	CNRM	MIROC	Obs-CNRM	Obs-MIROC
1980	1980	1980	1980	1980	1980	1980	1980	1980	1980
0.7%	0.3%	0.3%	-89.9%	14.6%	0.0%	0.0%	0.0%	0.0%	0.0%

Vel < 0.62 m/s			Precent Diff	Precent Diff
Obs	CNRM	MIROC	Obs-CNRM	Obs-MIROC
1980	1980	1980	1980	1980
0.0%	0.0%	0.0%	0.0%	0.0%

Given the above analysis, the Portage Creek LWCs could be considered a high VAR LWCs, since all flow passes through the vents for design events greater than the 100-yr ARI under present conditions. The existing structures also pass the average RCM projected (2080-2099) design events less than 25-yrs or 100-yrs for CG3 and CG1, respectively. Proposed LWC designs, for which the vented areas were reduced and road profiles were lowered was analyzed to determine usability under current and projected conditions. The proposed design for CG3 consists of 2 CMP culvers each 0.5 m is diameter and the road profile lowered 1 m. The proposed design for CG1 consists of 2 CMP culvers each 1 m is diameter and the road profile lowered 1 m. Results (Table 7.23) indicates the proposed CG3 LWC would be overtopped 23% of the time under present conditions and 26%-32% of the time under projected simulations. Overtopping flow depth rarely reaches 0.31m under any simulation. Overtopping flow velocity at the proposed CG3 LWC is unchanged from the existing LWC.

Table 7.23. Amount of time (%) for different scenarios over a 20yr period that weir water depth at Portage Creek CG3 (upstream) LWC (Proposed) is greater than 0.01 m and 0.31 m or water velocity is greater than 0.62 m/s

CG3 - Portage Creek, US LWC									
Overtopping - Depth > 0.01m					Depth > 0.31m				
Present	CNRM	CNRM	MIROC	MIROC	Present	CNRM	CNRM	MIROC	MIROC
1990	2040	2080	2040	2080	1990	2040	2080	2040	2080
22.6%	25.9%	32.3%	25.8%	28.8%	0.0%	0.0%	0.1%	0.2%	0.6%

CG3 - US LWC - Vel > 0.62 m/s				
Present	CNRM	CNRM	MIROC	MIROC
1990	2040	2080	2040	2080
0.0%	0.0%	0.0%	0.0%	0.0%

Results (Table 7.24) indicates the proposed CG1 LWC would be overtopped 2% of the time under present conditions and 2%-7% of the time under projected simulations. Overtopping flow depth never reaches 0.31m under any simulation. Overtopping flow velocity at the proposed CG1 LWC only exceeds 0.61 m/s during the project (2080-2099) MIROC simulation.

Table 7.24. Amount of time (%) for different scenarios over a 20yr period that weir water depth at Portage Creek CG1 (downstream) LWC (Proposed) is greater than 0.01 m and 0.31 m or water velocity is greater than 0.62 m/s

CG1 - Portage Creek, DS LWC									
Overtopping - Depth > 0.01m					Depth > 0.31m				
Present	CNRM	CNRM	MIROC	MIROC	Present	CNRM	CNRM	MIROC	MIROC
1990	2040	2080	2040	2080	1990	2040	2080	2040	2080
2.0%	2.0%	8.0%	7.0%	12.0%	0.0%	0.0%	0.0%	0.0%	0.2%

CG1 - DS LWC - Vel > 0.62 m/s				
Present	CNRM	CNRM	MIROC	MIROC
1990	2040	2080	2040	2080
0.0%	0.0%	0.0%	0.0%	0.1%

Bridge

The bridge (CG2) over Portage Creek is a single span structure with spill-thru abutments. No flow scenario reaches the low cord of the bridge nor are the bridge approaches overtopped. The bridge is

not at risk of scour due to the lack of a pier and protected spill-thru abutments. No further analysis was performed.

7.3.4 North Fork Embarras River (Edgar County, IL)

HEC-RAS Model

Figure 7.11 is a schematic of the HEC-RAS model for North Fork Embarras River in Edgar County, IL. The stream channel contains one vented ford. The modeled stream length for Nineveh Creek is 380 m. Figure 7.12 shows the stream profile and flood profiles for the present and projected (2040-2059 and 2080-2099) 100yr peak flows.

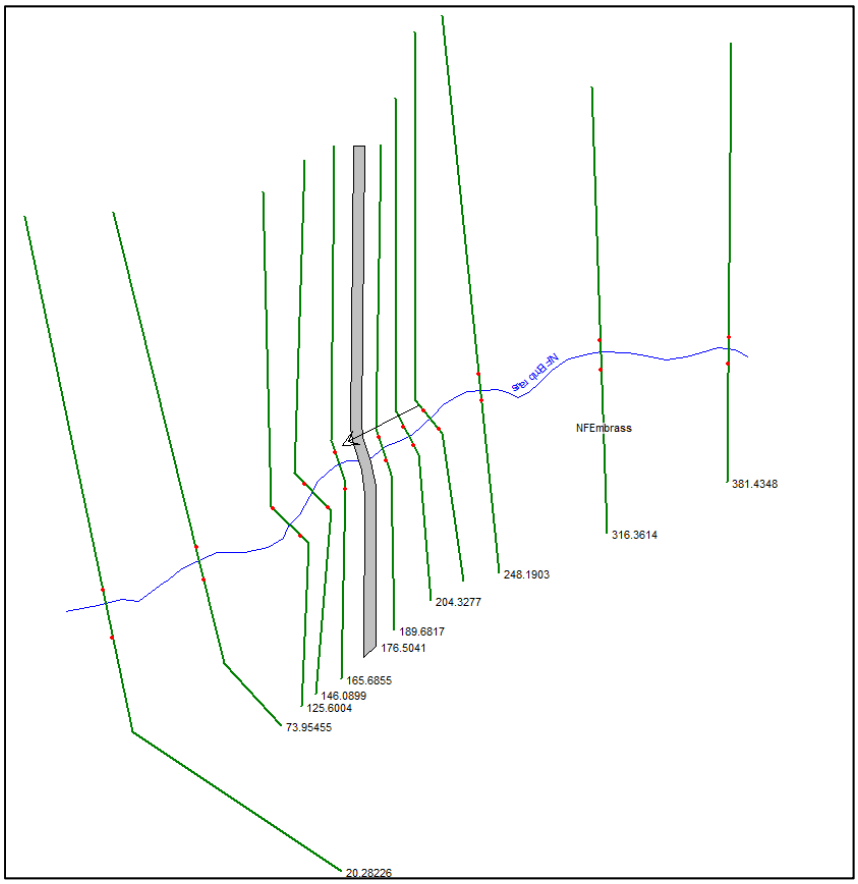

Figure 7.11. Schematic of the HEC-RAS model for the North Fork Embarras Rive

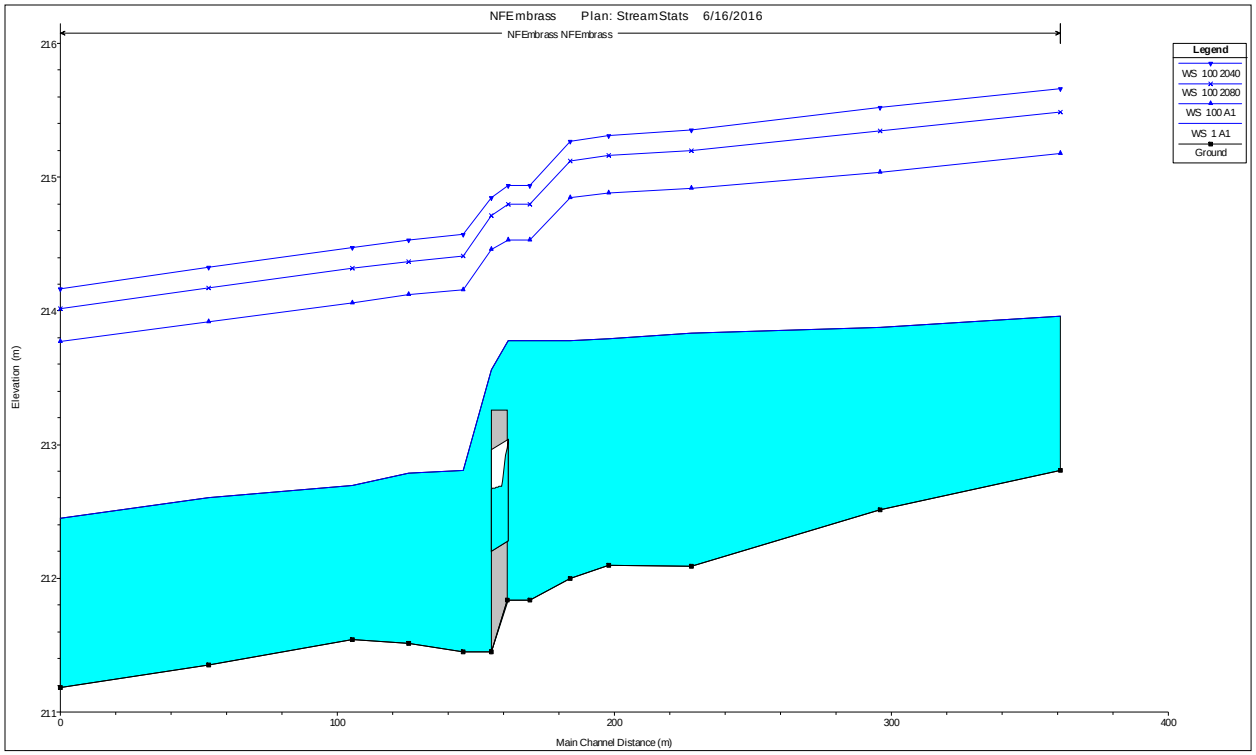

Figure 7.12. Profile of the HEC-RAS model for the North Fork Embarras River

North Fork Embarras River Low Water Crossing

The steady state HEC-RAS model was implemented for design storms with ARIs of 0.5-, 1-, 2-, 5-, 10-, 25-, 50-, and 100-years for scenarios including present conditions and average RCM projections determined in Chapter 6. Table 7.25 shows the maximum flow depth over the roadway at the vented ford for a range of return periods and scenarios. LWC Edgar 1 experiences overtopping for during all studied events and ranges from 0.23 m – 1.87 m. Overtopping flow is deeper during projected (2040-2059) events greater than the 20-yr ARI and deeper during projected (2080-2099) events less than the 10-yr ARI.

Table 7.25. Maximum overtopping flow depth for different scenarios and return periods at North Fork Embarras River LWC

	Edgar 1 - LWC - Weir Flow Depth				
Return Period	Present	Avg RCM 2040	Avg RCM 2080	Precent Diff	Precent Diff
(yr)	(m)	(m)	(m)	Present - RCM 2040	Present- RCM 2080
0.5	0.23	0.64	0.76	94.3%	107.1%
1	0.54	0.92	0.99	52.1%	58.8%
2	0.78	1.07	1.14	31.4%	37.5%
5	0.97	1.25	1.28	25.2%	27.6%
10	1.09	1.38	1.38	23.5%	23.5%
25	1.23	1.56	1.52	23.7%	21.1%
50	1.35	1.71	1.62	23.5%	18.2%
100	1.48	1.87	1.72	23.3%	15.0%

Table 7.26 shows the maximum overtopping velocity over the LWC for a range of return periods and scenarios. The maximum overtopping velocities are 2.88 m/s – 3.46 m/s during over topping flow. The differences in maximum flow velocities between projected (2040-2059) and projected 2080-2099) vs present conditions are 5% - 70% depending on the event return period.

Table 7.26. Maximum overtopping flow velocities for different scenarios and return periods at North Fork Embarras River LWC

	Edgar 1 - LWC - Weir Flow Vel				
Return Period	Present	Avg RCM 2040	Avg RCM 2080	Precent Diff	Precent Diff
(yr)	(m/s)	(m/s)	(m/s)	Present - RCM 2040	Present- RCM 2080
0.5	0.40	0.70	0.84	54.5%	71.0%
1	0.62	1.11	1.29	56.6%	70.2%
2	0.86	1.52	1.71	55.5%	66.1%
5	1.23	2.27	3.00	59.4%	83.7%
10	1.54	2.78	2.85	57.4%	59.7%
25	2.09	2.85	2.88	30.8%	31.8%
50	2.81	3.18	2.95	12.4%	4.9%
100	2.88	3.46	3.24	18.3%	11.8%

Rating curves for maximum overtopping flow depth and flow velocity vs flow rate were developed for a wide range of flow rates at the LWC. See Figure 7.13. These rating curves were used to analyze the continuous 20yr simulations: present (1990-2009) and IPSL and MRI (2040-2059 and 2080-2099).

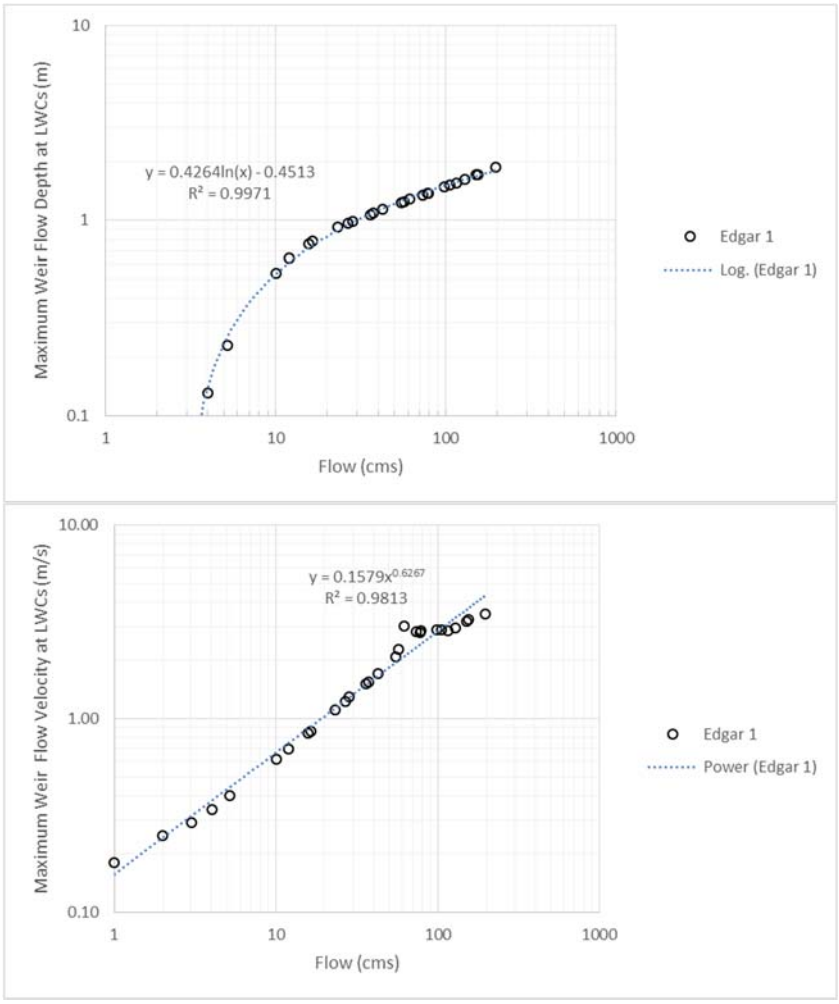

Figure 7.13. Rating curves for maximum depth vs flow rate and channel velocity vs flow rate at North Fork Embarras River

The continuous simulations were analyzed using rating curves to determine the amount of time over each 20yr simulations the LWC would be unusable due to flow depths greater than 0.31 m or flow velocities greater than 0.62 m/s (Table 7.27 and Table 7.28). A depth of 0.31m is typically used to determine if a LWC is passible, which was applicable for this structure since it is used by the general public. The amount of time over each 20yr simulations the LWC would be overtopped (depth > 0.01 m)

was also determined, due to the fact that many drivers will not cross a road that is overtopped, regardless of depth. Results indicates flow depth at Edgar 1 is greater than 0.01m 4% of the time under present conditions and 3%-4% of the time under projected simulations. Flow depth reaches 0.31m slightly less than 2% of the time under all simulations. Overtopping flow velocity at Edgar 1 is rarely greater than 0.62 m/s, about 1% of the time under all scenarios.

Table 7.27. Amount of time (%) for different scenarios over a 20yr period that weir water depth at North Fork Embarras River LWC is greater than 0.01 m and 0.31 m

Edgar 1 -NF Embarras LWC									
Overtopping - Depth > 0.01 m					Depth > 0.31m				
Present 1990	IPSL 2040	IPSL 2080	MRI 2040	MRI 2080	Present 1990	IPSL 2040	IPSL 2080	MRI 2040	MRI 2080
4.0%	3.6%	3.4%	4.1%	3.8%	1.7%	1.8%	1.8%	1.9%	1.8%

Table 7.28. Amount of time (%) for different scenarios over a 20yr period that water velocity at North Fork Embarras River LWC is greater than 0.62 m/s

Edgar 1 - Vel > 0.62 m/s				
Present 1990	IPSL 2040	IPSL 2080	MRI 2040	MRI 2080
0.9%	1.0%	1.1%	1.1%	1.1%

The comparisons between present (1990-2009) conditions and projected (2040-2059 and 2080-2099) conditions indicate that the projected peak flows are greater than the 1990-2009 peak flows while the roadway will be over topped about the same projected conditions as under present conditions. To determine the validity of projected conditions Table 7.29 shows a comparison of time over each 1980-1999 scenario (observed and simulation) the LWCs would be unusable due to flow depths greater than 0.01 m and 0.31 m or flow velocities greater than 0.62 m/s. Results indicate that the simulations approximately match the length of time high flows persist compared to observed values.

Table 7.29. Amount of time (%) for 1980-1999 simulations that water depth and velocity at North Fork Embarras River LWC is greater than 0.01 m or 0.31 m and 0.62 m/s, respectively, with percent differences

Edgar 1 -NF Embarras LWC									
Depth > 0.01m			Precent Diff	Precent Diff	Depth > 0.31m			Precent Diff	Precent Diff
Obs	IPSL	MRI	Obs-IPSL	Obs-MRI	Obs	IPSL	MRI	Obs-IPSL	Obs-MRI
1980	1980	1980	1980	1980	1980	1980	1980	1980	1980
3.8%	3.5%	3.6%	-7.9%	-7.1%	1.6%	1.6%	1.6%	4.6%	-0.7%

Vel < 0.62 m/s			Precent Diff	Precent Diff
Obs	IPSL	MRI	Obs-IPSL	Obs-MRI
1980	1980	1980	1980	1980
0.8%	0.9%	0.9%	1.6%	0.4%

Given the above analysis, the NF Embarras LWC could be considered a Low VAR LWC, since the crossing is overtopped during the 0.5-yr flow event under present conditions. The crossing is overtopped numerous times a year (totaling about 14 days) but the duration of any single overtopping is relatively short. The existing vent is perched 0.31 m above the upstream streambed, eliminating aquatic organism passage at base flow and causing scour downstream of the culvert. A proposed LWC design, for which the same vent was lowered to the stream bed was analyzed to determine usability under current and projected conditions. Results (Table 7.30) indicate the lowering of the vent would reduce the length of overtopping events by about a third, while the different between present projected conditions is minor. The duration of overtopping flow depth greater than 0.31m is the same between the existing and proposed structures and between present and projected scenarios.

Table 7.30. Amount of time (%) for different scenarios over a 20yr period that weir water depth at North Fork Embarras River LWC (Proposed) is greater than 0.01 m and 0.31 m or water velocity at North Fork Embarras River LWC is greater than 0.62 m/s

Edgar 1 -NF Embarras LWC									
Overtopping - Depth > 0.01 m					Depth > 0.31m				
Present 1990	IPSL 2040	IPSL 2080	MRI 2040	MRI 2080	Present 1990	IPSL 2040	IPSL 2080	MRI 2040	MRI 2080
2.6%	2.6%	2.5%	2.9%	2.7%	1.6%	1.6%	1.7%	1.8%	1.7%

Edgar 1 - Vel > 0.62 m/s				
Present 1990	IPSL 2040	IPSL 2080	MRI 2040	MRI 2080
1.0%	1.1%	1.2%	1.1%	1.1%

7.3.5 East Fork Big Creek (Edgar County, IL)

HEC-RAS Model

Figure 7.1 is a schematic of the HEC-RAS model for East Fork Big Creek. The stream channel contains one vented ford. The modeled stream length for East Fork Big Creek is 340 m. Figure 7.15 shows the stream profile and flood profiles for the present and projected (2040-2059 and 2080-2099) 100yr peak flows.

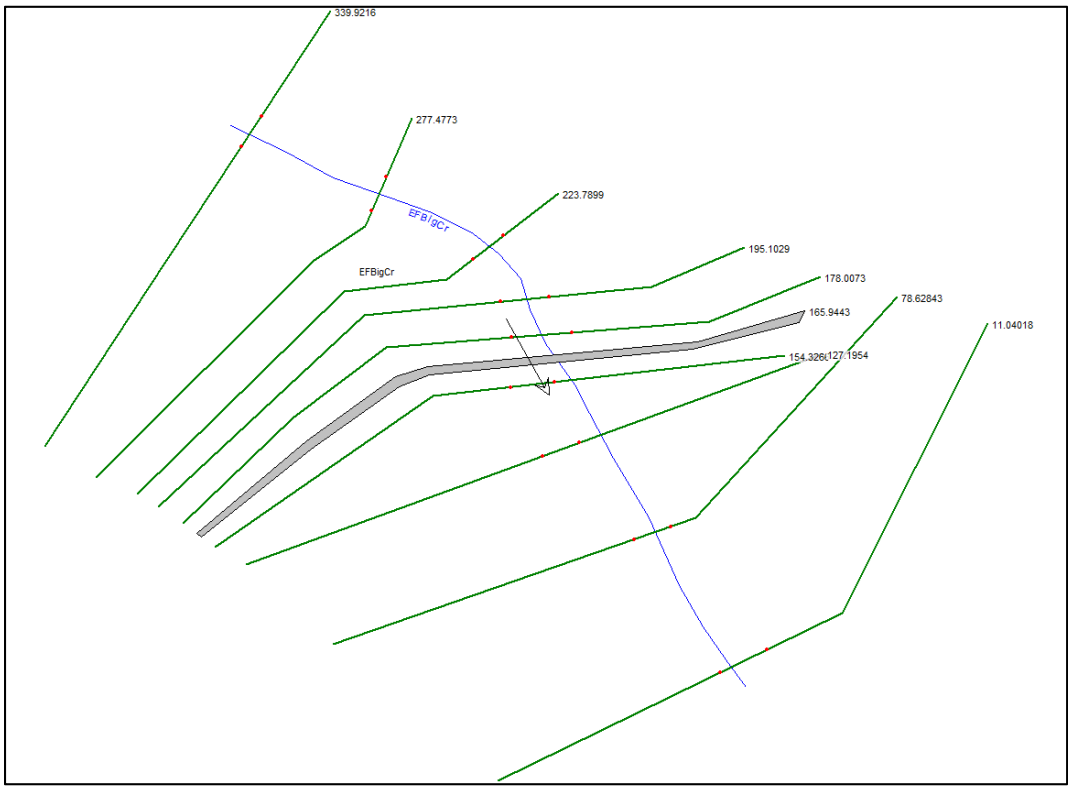

Figure 7.14. Schematic of the HEC-RAS model for the East Fork Big Creek

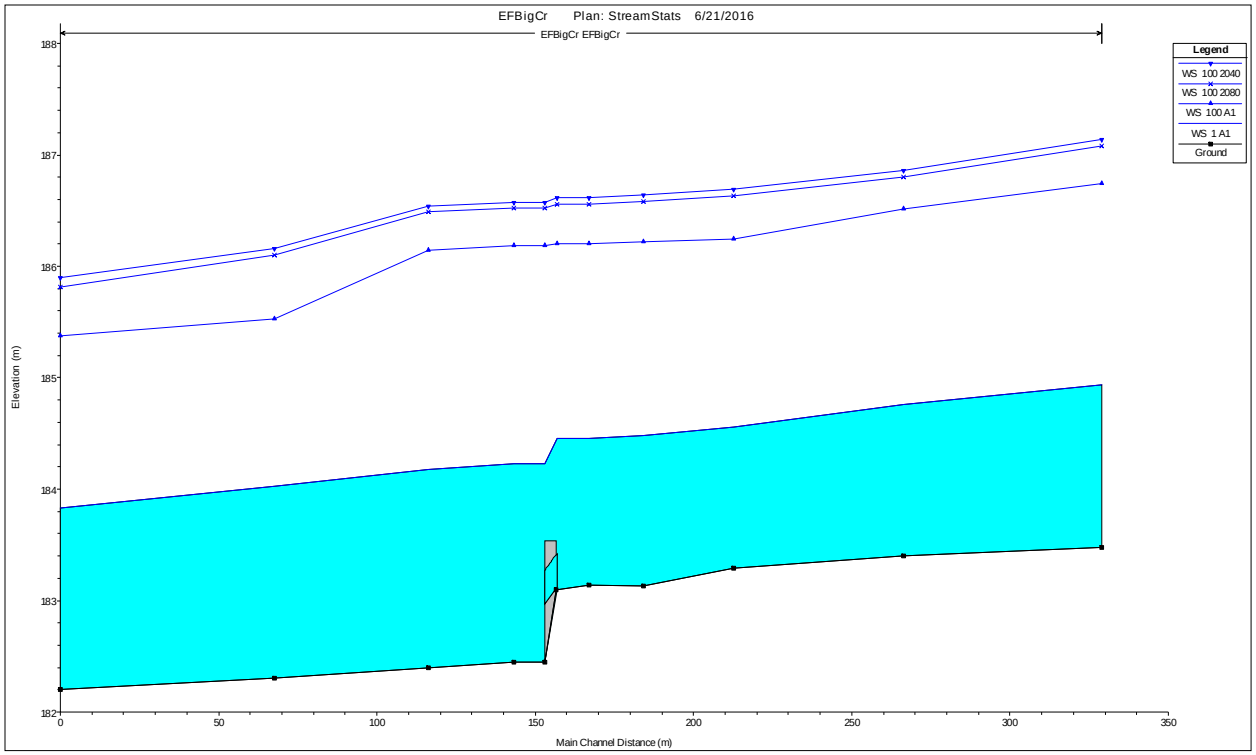

Figure 7.15. Profile of the HEC-RAS model for the East Fork Big Creek

East Fork Big Creek Low Water Crossing

The steady state HEC-RAS model was implemented for design storms with ARIs of 0.5-, 1-, 2-, 5-, 10-, 25-, 50-, and 100-years for scenarios including present conditions and average RCM projections determined in Chapter 6. Table 7.31 shows the maximum flow depth over the roadway at the vented ford for a range of return periods and scenarios. LWC Edgar 3 experiences overtopping for during all studied events and ranges from 0.69 m – 3.18 m. Overtopping flow is similar is depth between projected (2040-2059) events projected (2080-2099) events.

Table 7.31. Maximum overtopping flow depth for different scenarios and return periods at East Fork Big Creek LWC

	Edgar 3 - LWC - Weir Flow Depth				
Return Period	Present	Avg RCM 2040	Avg RCM 2080	Precent Diff	Precent Diff
(yr)	(m)	(m)	(m)	Present - RCM 2040	Present- RCM 2080
0.5	0.69	0.98	1.07	34.7%	43.2%
1	0.97	1.49	1.53	42.3%	44.8%
2	1.25	1.92	1.9	42.3%	41.3%
5	1.65	2.36	2.26	35.4%	31.2%
10	1.93	2.63	2.52	30.7%	26.5%
25	2.3	2.9	2.8	23.1%	19.6%
50	2.59	3.06	3	16.6%	14.7%
100	2.82	3.23	3.18	13.6%	12.0%

Table 7.32 shows the maximum overtopping velocity over the LWC for a range of return periods and scenarios. The maximum overtopping velocities are 1.98 m/s – 2.15 m/s during over topping flow. The differences in maximum flow velocities between projected (2040-2059) and projected 2080-2099) vs present conditions are 1% - 35% depending on the event return period, but the magnitude of the differences is small. The difference between the projected scenarios is also small.

Table 7.32. Maximum overtopping flow velocities for different scenarios and return periods at East Fork Big Creek LWC

	Edgar 3 - LWC - Weir Flow Vel				
Return Period	Present	Avg RCM 2040	Avg RCM 2080	Precent Diff	Precent Diff
(yr)	(m/s)	(m/s)	(m/s)	Present - RCM 2040	Present- RCM 2080
0.5	0.72	1.02	1.11	34.5%	42.6%
1	1.01	1.42	1.45	33.7%	35.8%
2	1.23	1.67	1.65	30.3%	29.2%
5	1.52	1.94	1.90	24.3%	22.2%
10	1.67	1.97	1.96	16.5%	16.0%
25	1.92	1.95	1.98	1.6%	3.1%
50	1.94	2.07	1.98	6.5%	2.0%
100	1.98	2.20	2.15	10.5%	8.2%

Rating curves for maximum overtopping flow depth and flow velocity vs flow rate were developed for a wide range of flow rates at the LWC. See Figure 7.13. These rating curves were used to analyze the continuous 20yr simulations: present (1990-2009) and CNRM and MIROC (2040-2059 and 2080-2099).

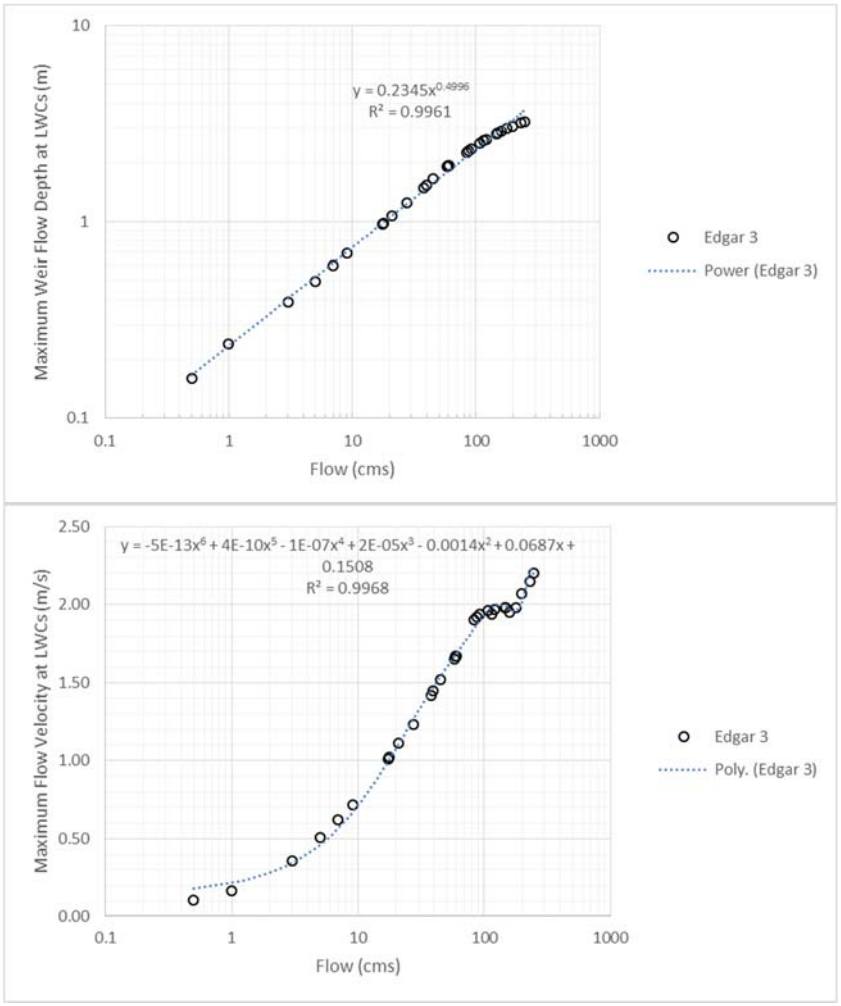

Figure 7.16. Rating curves for maximum depth vs flow rate and channel velocity vs flow rate at East Fork Big Creek

The continuous simulations were analyzed using rating curves to determine the amount of time over each 20yr simulations the LWC would be unusable due to flow depths greater than 0.31 m or flow velocities greater than 0.62 m/s (Table 7.33 and Table 7.34). A depth of 0.31 m is typically used to determine if a LWC is passible, which was applicable for this structure since it is used by the general public. The amount of time over each 20yr simulations the LWC would be overtopped (depth > 0.01 m)

was also determined, due to the fact that many drivers will not cross a road that is overtopped, regardless of depth. Results indicates flow depth at Edgar 3 is greater than 0.01m 18% of the time under present conditions and 11%-14% of the time under projected simulations. Flow depth reaches 0.31m more than 11% of the time under present conditions and 8% - 9% of the time for projected scenarios. Overtopping flow velocity at Edgar 3 is greater than 0.62 m/s about 3% of the time under all scenarios.

Table 7.33. Amount of time (%) for different scenarios over a 20yr period that weir water depth at East Fork Big Creek LWC is greater than 0.01 m and 0.31 m

Edgar 3 - EF Big Creek LWC									
Overtopping - Depth > 0.01 m					Depth > 0.31m				
Present 1990	CNRM 2040	CNRM 2080	MIROC 2040	MIROC 2080	Present 1990	CNRM 2040	CNRM 2080	MIROC 2040	MIROC 2080
18.4%	13.4%	13.7%	12.4%	11.3%	10.6%	8.9%	9.3%	8.5%	7.8%

Table 7.34. Amount of time (%) for different scenarios over a 20yr period that water velocity at East Fork Big Creek LWC is greater than 0.62 m/s

Edgar 3 - Vel > 0.62 m/s				
Present 1990	CNRM 2040	CNRM 2080	MIROC 2040	MIROC 2080
3.1%	3.0%	3.4%	2.8%	2.9%

The comparisons between present (1990-2009) conditions and projected (2040-2059 and 2080-2099) conditions indicate that the projected peak flows are greater than the 1990-2009 peak flows while the roadway will be overtopped less under projected conditions (total time) than under present conditions. To determine the validity of projected conditions Table 7.35 shows a comparison of time over each 1980-1999 scenario (observed and simulation) the LWCs would be unusable due to flow depths greater than 0.01 m and 0.31 m or flow velocities greater than 0.62 m/s. Results indicate that the simulations underestimate the length of time high flows persist compared to observed values, especially for flow

rates with short ARIs. Results from Section 6.3.5 also indicated the CNRM and MIROC models under estimated the duration of specific design flows compared to observed records.

Table 7.35. Amount of time (%) for 1980-1999 simulations that water depth and velocity at East Fork Big Creek LWC is greater than 0.01 m or 0.31 m and 0.62 m/s, respectively, with percent differences

Edgar 3 - EF Big Creek LWC									
Depth > 0.01m			Precent Diff	Precent Diff	Depth > 0.31m			Precent Diff	Precent Diff
Obs	CNRM	MIROC	Obs-CNRM	Obs-MIROC	Obs	CNRM	MIROC	Obs-CNRM	Obs-MIROC
1980	1980	1980	1980	1980	1980	1980	1980	1980	1980
18.1%	13.6%	13.2%	-28.2%	-31.1%	10.4%	9.2%	9.0%	-11.4%	-14.1%

Vel < 0.62 m/s			Precent Diff	Precent Diff
Obs	IPSL	MRI	Obs-IPSL	Obs-MRI
1980	1980	1980	1980	1980
2.9%	2.9%	2.7%	-2.5%	-4.5%

Given the above analysis, the EF Big Creek LWC could be considered a Low VAR LWC, since the crossing is overtopped during well less than the 0.5-yr flow event under present conditions. The crossing is overtopped for almost any flow larger than base flow but the duration of any single overtopping is relatively short. The existing vents are 0.31 m (1 ft) in diameter and partially plugged with sediment, eliminating aquatic organism passage at base flow and sediment deposition upstream of the LWC. An analysis of the upstream reach (Figure 7.17) shows the dimensionless shields stress for sand (primarily deposited upstream of the LWC) is large enough to indicate sediment transport along the reach absent the sediment trap created by the LWC roadway, which operates effectively as a perched improved ford. The average particle Reynolds Number for the upstream reach is less than 100.

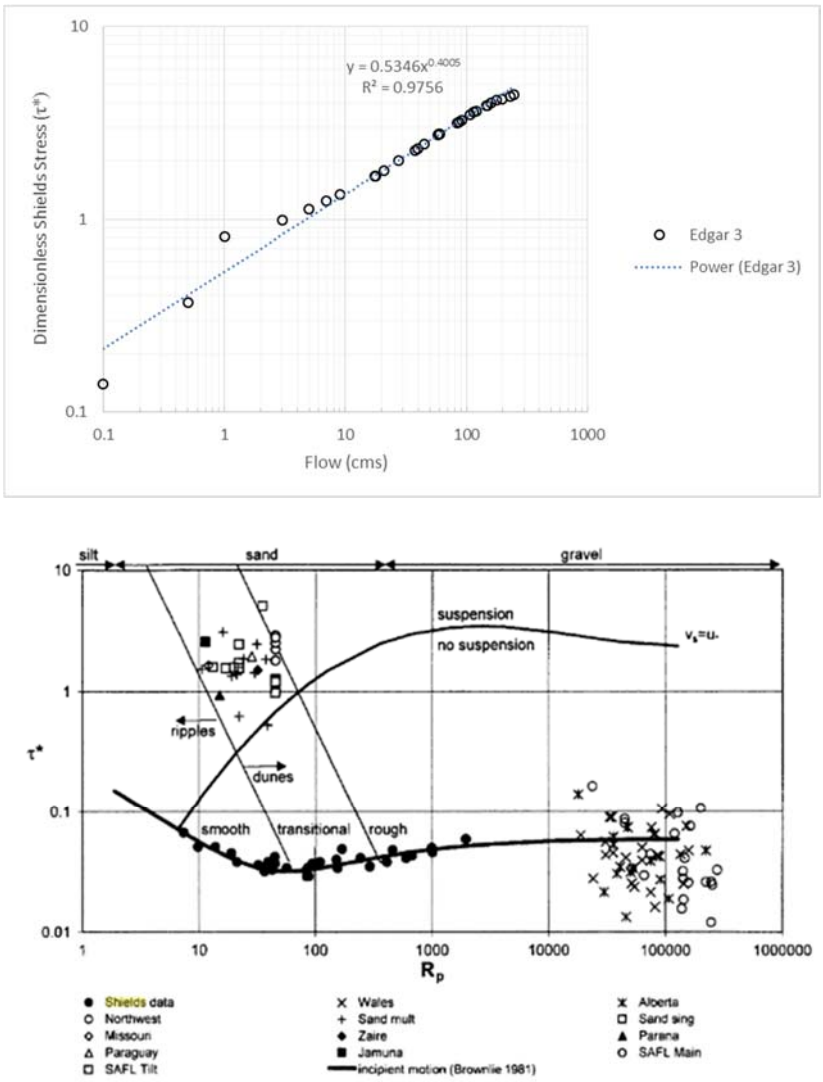

Figure 7.17. Dimensionless Shields parameter for the upstream reach for a range of flows with the Shields Regime diagram (Garcia, 2008).

A proposed LWC design, provided by the Illinois Department of Transportation, for which the roadway was raised 1.46 m to make room for a 2.44 m (H) by 1.22 m (V) box culvert was analyzed to determine usability under current and projected conditions. The larger culvert opening would allow sediment and aquatic organism passage. Results (Table 7.36) indicate the new profile with box culvert vent would reduce the length of overtopping events from 11% - 17% to 2% - 3%, while the different between present and projected conditions is also reduced. The duration of overtopping flow depth greater than 0.31m is reduced from 8% - 11% to 1% - 2%, while the different between present and projected

conditions is also reduced. The duration of overtopping flow velocity greater than 0.62 m/s is reduced by about 1%, or 3.5 days per year.

Table 7.36. Amount of time (%) for different scenarios over a 20yr period that weir water depth at East Fork Big Creek LWC (Proposed) is greater than 0.01 m and 0.31 m or water velocity at East Fork Big Creek LWC is greater than 0.62 m/s

Edgar 3 - EF Big Creek LWC									
Overtopping - Depth > 0.01 m					Depth > 0.31m				
Present 1990	CNRM 2040	CNRM 2080	MIROC 2040	MIROC 2080	Present 1990	CNRM 2040	CNRM 2080	MIROC 2040	MIROC 2080
2.5%	2.3%	2.7%	2.2%	2.4%	1.4%	1.3%	1.7%	1.4%	1.6%

Edgar 3 - Vel > 0.62 m/s				
Present 1990	CNRM 2040	CNRM 2080	MIROC 2040	MIROC 2080
2.5%	2.3%	2.7%	2.2%	2.3%

7.4 Discussion

This study routed steady flow hydrographs, developed from observed and projected rainfall data, through hydraulic models to determine usability and sustainability of current structures and feasibility of alternative designs for projected flow regimes. The peak flood hydrographs were developed from HEC-HMS models of the study watersheds from existing conditions and average future climate projection data. Continuous 20-year simulations were run through the HEC-HMS models using observed precipitation and projected precipitation from two of the four RCMs. The two models utilized for the continuous simulations were those models that represented the upper and lower bounds of maximum precipitation estimates for a majority of return periods for each projected timeframe at each location. Hydraulic models were developed within HEC-RAS. Steady state HEC-RAS models were implemented for design storms with ARIs of 0.5-, 1-, 2-, 5-, 10-, 25-, 50-, and 100-years for scenarios including present conditions and average RCM projections. Continuous 20-yr simulations were analyzed using rating curves.

The resiliency and safety of all LWCs and applicable bridges were tested with regards to overtopping flow depth, overtopping flow velocity, and scour under present, simulated, and projected (2040-2059) and (2080-2099) design flow values. The usability of all LWCs and applicable bridges were also tested using all applicable continuous 20-yr simulations. In Indiana, two improved fords and two 3-span bridges were modeled. The results show overtopping flow depth and velocity during the present 100-yr flood events is about equal to the overtopping flow depth and velocity during the projected (2080-2099) 10-yr flood event. Analysis of the existing cable-concrete LWCs show they are designed appropriately for the present 100-yr flood event, but are insufficient to withstand the projected (2080-2099) 10-yr flood event. For the bridges, overtopping flow will occur during the projected (2080-2099) 10-yr flood event but only occurs during the 100-yr event under existing conditions. At the Indiana structures, the current 100-yr flood event is about equal to the projected 10-yr event at the end of the twenty-first century.

In Illinois, two vented fords were modeled. The results show overtopping flow depth during the present 100-yr flood events is about equal to the overtopping flow depth during the projected (2080-2099) 25-yr flood event. The LWC over East Fork Big Creek has two small vents and acts more like an improved ford than a vented ford. In Michigan three vented fords and a single span bridge were modeled. The results show overtopping flow depth during the present 100-yr flood events is about equal to the overtopping flow depth during the projected (2080-2099) 10-yr to 50-yr flood events, depending on the stream and the location of the structures with regards to instream lakes.

With regards to usability and safety, the Indiana fords are impassable under current conditions during events less than the 0.5-yr event, which accounts for 8% or 19% of the year. Projected simulation

indicate the LWCs will be impassable 6%-17% of the year, so the difference between present and projected usability is -2%, or about 7 days more days under projected conditions. The Illinois vented fords are impassable during events at or less than the 0.5-yr event, which accounts for 2%-11% of the year. Projected simulations indicate the LWCs will be impassable 2%-9% of the year, so the difference between present and projected usability is - 2%, or about 7 days more days under projected conditions. The Michigan fords are impassable under current conditions during events larger than 50-yr event, which accounts for less than 1% of the year. Projected flows indicate the LWCs will be impassable 0.1%-2% of the year, so the difference between present and projected usability is 1%, or about 3 days. Given the relatively large vented opening compared to the current and projected peak flood, the Michigan LWC could be considered to have high vented-area ratio, and so are unusable only during infrequent conditions.

The improved fords at Camp Atterbury and the vented LWC over East Fork Big Creek in Edgar Co, IL are overtopped during base flow or very frequent (small) flood events, respectively. The analyses of LWCs with regards to the amount of time they are impassable show that when very small flood events are considered, the climate model simulations underestimate the observed data (see Table 7.7 and Table 7.35). These results indicate that the simulations underestimate the length of time, on a yearly basis, flows persist compared to observed values, especially for events with very short ARIs. One possible explanation is that the average individual simulated precipitation events are of a shorter duration than the average individual observed events, causing slightly shorter (temporally) hydrographs for low flow events. A review of the Q-Q mapping (Section 5.3) shows that total annual wet hours are similar between the observed and simulated data (1980-1999) after threshold applications (see Figure 5.9), but this doesn't necessarily indicate that the average hyetographs for the observed and simulated data are

identical (either in length or magnitude). When comparing the observed data to the climate model projections (2040-2059 and 2080-2099) to determine impassable conditions, the latter also underestimate the former (See Table 7.5 and Table 7.33) despite a projected shift in IDF curves and a corresponding increase in magnitude of projected peak floods. A partial explanations may be that for models MIROC and IPSL, the projected precipitation suggests decreasing total annual wet hours by 2080-2099, meaning there are fewer low flow flood events to overtop the LWCs (see Figure 5.9). Nonetheless, the other two models, CNRM and MRI, also underestimate the occurrence of overtopping compared to observed data.

When larger flow events are considered the discrepancy between observed and simulated and projected data lessens or disappears completely. For East Fork Big Creek (Table 7.35), the occurrence of overtopping flow was compared between observed and simulated scenarios for two water depths, 0.01m and 0.31m. When only larger flows are considered (depth greater than 0.31m) the difference between the overserved and simulated scenarios is less than half as large as when including very small flows (depth greater than 0.01m). A proposed LWC design was also analyzed for East Fork Big Creek (Table 7.36), which would have a larger vented area than the existing structure. The overtopping analysis only included much larger flows as a results. In this case the projected scenarios don't underestimate the yearly temporal occurrence of flows compared to the observed scenarios, suggesting that only the temporal occurrence of very low flow is underestimated for the climate model scenarios.

The riverine crossing structures considered for this study are projected to see an increase in the magnitude and frequency of high flow events by the end of this century, similar to findings from other studies (eg: Wright et al., 2012). The projected (2080-2099) 10-yr event is on the order of the present

50-yr (sometimes 25-yr or 100-yr) event for many of the studied streams, suggesting possible future conditions should be considered when designing new infrastructure. Mailhot and Duschesne (2010) and Scottish Executive (2005) provide examples of methods to revise the current design criteria to meet projected conditions. For example, a LWC typically designed for the 25-yr peak flow event should instead be designed to the present-day 50-yr event. Unfortunately the uncertainty inherent in the climate modeling and sampling variability, as discussed previously, makes it difficult to develop specific recommendations on how to revise current LWC design criteria with regards to climate change in the study regions. Nonetheless, the projected increases in peak flow, and the resulting increases in channel scour, capacity exceedances, and overtopping flow depth and velocity will increase the LWCs' susceptibility for failure (Scottish Executive, 2005; USDOT, 2014; Wright et al., 2012). For examples, the improved fords at Camp Atterbury are projected to be susceptible to scour by the end of the century.

The average yearly flow duration of model simulations and projections proved to be uncertain, especially for small flow events with very small ARIs. The two models utilized for the continuous simulations, representing the upper and lower bounds of maximum precipitation estimates, produced wide ranges of flow duration estimates, and underestimated observed duration estimates for small flow events with very small ARIs. In Iowa, an exceedance probability of 2% or about 7 days is recommended (McDonald and Anderson-Wilk, 2003). The range of flow exceedance between the models is on the order of 3.5-7 days and the different between the observed and simulated scenarios is 7-14 days for those LWC overtopped during small flow events. Such uncertainty currently prevents flow duration from being used to determine the usability of LWCs under projected conditions. Additional analysis of frequent observed and simulated precipitation events is needed with regards to the frequency,

magnitudes, and durations of such events. Previous studies have focused on extreme events, precipitation and flow, so limited work has focused on small events.

7.5 Conclusion

The main purpose of this chapter was to route projected design flow and continuous stream flow hydrographs through hydraulic models to determine usability and sustainability of current structures and feasibility of alternative designs for projected flow regimes. The peak flood hydrographs were developed from HEC-HMS models of the study watersheds from existing conditions and average future climate projection data. Continuous 20-year simulations were run through the HEC-HMS models using observed precipitation and projected precipitation the two models representing the upper and lower bounds of maximum precipitation estimates for a majority of return periods for each projected timeframe at each location. Hydraulic models were developed within HEC-RAS. Steady state HEC-RAS models were implemented for design storms with ARIs of 0.5-, 1-, 2-, 5-, 10-, 25-, 50-, and 100-years for scenarios including present conditions and average RCM projections.

The results revealed the riverine crossing structures considered for this study are projected to see an increase in the magnitude and frequency of high flow events by the end of this century. The projected (2080-2099) 10-yr event is on the order of the present 50-yr (sometimes 25-yr or 100-yr) event for many of the studied streams, suggesting possible future conditions should be considered when designing new infrastructure. Unfortunately the uncertainty inherent in the climate modeling and sampling variability makes it difficult to develop specific recommendations on how to revise current LWC design criteria with regards to climate change in the study regions. The continuous model simulations and projections proved to underestimate average yearly flow durations for small flow events with very small ARIs. Up to

this point published literature has focused mainly on large precipitation and flow events with large return periods and durations, usually 10-yr or 100-yr return periods and long durations on the order of 24-hrs to 7-days. This study shows additional bias correction is needed for dynamically downscaled RCM precipitation data if that data is to be used to project frequent flood events, which are caused by the more frequent (generally short in duration and smaller in total volume) precipitation events.

References

Abt, S. R, Wittler, R. J., & Love, D. J. (1989). Human stability in a high flood hazard zone. Water Resources Bulletin, 25(4): 881-890.

Balke, K., Higgins, L., Chrysler, S., Pesti, G., Chaudhary, N., & Brydia, R. (2011). Signing strategies for low-water and flood-prone highway crossings. Report 0-6262-1. Texas Transportation Institute, Texas A&M University.

Chow, V.T. (1959). Open Channel Hydraulics, McGraw-Hill Book Company, NY.

Federal Emergency Management Agency (FEMA). (2013). Turn around don't drown, Fact Sheet, Portsmouth, N.H. Accessed on July 15, 2016 at http://www.fema.gov/news-release/2013/06/28/turn-around-dont-drownr-0

Federal Highway Administration (FHWA). (2009). Bridge scour and stream instability countermeasures. US Department of Transportation. Publication No. FHWA-NHI-01-003, HEC 23. (Lagasse, P.F, Clopper, P.E., Pagán-Ortiz, J.E., Zevenbergen, L.W., Arneson, L.A., Schall, J.D., & Girard, L.G.).

Garcia, M.H. 2008. Sediment Transport and Morphodynamics. In: M.H. Garica (Ed), Ch 2 in sedimentation Engineering, ASCE Manuals and Reports on Engineering Practice No. 110.

Huff, F. A. & Angel, J. R. (1992). Rainfall frequency atlas of the Midwest (Bulletin 71). Illinois State Water Survey, Champaign, IL.

Illinois Department of Natural Resources (IDNR). (2015). Report for the Urban Flood Awareness Act. Office of Water Resources. Springfield, Illinois. (Winters, B. A., Angel, J., Ballerine, C., Byard, J., Flegel, A., Gambill, D. R., Jenkins, J. P., McConkey, S., Markus, M., Bender, B. A., O'Toole, M. J.)

Isbash, S.V. (1936). Construction of dams by depositing rock in running water, Transactions, Second Congress on Large Dams, Washington, D.C. USA.

Jonkman, S. N. & Penning-Rowsell, E. (2008). Human instability in flood flows. Journal of the American Water Resources Association, 44(4): 1-11.

Mailhot, A. & Duchesne, S. (2010). Design criteria of urban drainage infrastructure under climate change. J. Water Resour. Plann. Manage., 136(2): 201-208.

McDonald, T. & Anderson-Wilk, M. (2003). Low water crossings in Iowa a section and design guide. Center for Transportation Research and Education, Iowa State University.

Scottish Executive. (2005). Scottish road network climate change study. (Galbraith, R. M., Price, D. J., & Shackman, L.).

Shields, A. (1936). Application of similarity mechanics and turbulence research on shear flow. *Mitteilungen der Preußischen Versuchsanstalt für Wasserbau **26**. Berlin: Preußische Versuchsanstalt für Wasserbau.*

Transportation Research Board (TRB). (2008). Potential impacts of climate change of U.S. transportation. National Research Council. Special Report 290, Washington D.C.

United States Army Corps of Engineers (USACE). (2010). HEC-RAS river analysis system hydraulic reference manual, Version 4.1. Report Number CPD-69, (Brunner, G. W.).

USACE. (2012). HEC-GeoRAS GIS tools for support of HEC-RAS using ArcGIS 10, extension Version 10.1, Report Number CPD-83, (Ackerman, C. T.).

US Department of Tranportation (USDOT). (2014). Climate adaption plan ensuring transportation infrastructure and system resilience. Washington, DC.

Wright, L., Chinowsky, P., Strzepek, K., Jones, R., Streeter, R., Smith, J. B., Mayotte, J., Powell, A., Jantarasami, L., & Perkins, W. (2012). Estimated effects of climate change on flood vulnerability of U.S. bridges. Mitig Adapt Strateg Glob Change, 17: 939-955.

Chapter 8 – SUMMARY AND FUTURE STEPS

8.1 Summary

Overall objective of this study is to determine if, and to what degree, regional climate model precipitation projections can be used as inputs to stream hydrologic models to determine subsequent impacts at stream crossing structures. To make this determination, four specific objectives were evaluated: 1) examine trends in historic precipitation data with regards to total annual precipitation, total annual wet days and wet hours, and regional frequency analysis for a range of design storms and extreme events, 2) bias correct and analyze projected precipitation data from four climate models with regards to total annual precipitation, total annual wet days and wet hours, and regional frequency analysis for a range of design storms and extreme events and compare findings to analyses of historic precipitation data, 3) apply projected climate model precipitation to hydrologic models to determine projected stream flow characteristics and compare to current stream flow characteristics, and 4) route projected design flow and continuous stream flow hydrographs through hydraulic models to determine usability and sustainability of current structures and feasibility of alternative designs for projected flow regimes.

To meet these objectives, gauge data from regions centered on central Indiana, central Michigan, and east central Illinois were tested for historic trends. This study utilized climate models provided by the Center for Climate Research at the University of Wisconsin-Madison (Notaro et al., 2015). The RCMs were bias corrected first by applying a minimum precipitation threshold below which hourly precipitation estimates were set to zero and then by implementing quantile mapping. Lastly, the historic precipitation and projected climate model precipitation data was applied to hydrologic models

to determine projected stream flow characteristics and compare to observed stream flow characteristics and then the flows were applied to hydraulic models to determine usability and sustainability of current LWC structures and feasibility of alternative designs for projected flow regimes.

Analysis and evaluation of historic and projected precipitation and subsequent hydrologic and hydraulic modeling leads to the following main conclusions:

- Results suggest the assumption that precipitation is stationary over time with regards to total annual rainfall and storm frequency and intensity is not valid for the three Midwest regions. Total annual precipitation has increased over the past century as well as average annual wet days in Michigan and Illinois, while average annual wet hours have remained steady or slightly decreased in some areas. The intensity of large events has generally stayed steady while the frequency of large storm events (24-hr duration) has increased. The frequency of 1-hr duration extreme events have increased in Indiana, but are natural in the other regions.

- The average projected (2080-2099) design storm of the four RCMs across all locations, durations, and return periods is larger than the corresponding observed (1980-1999) design storm and usually significantly larger based on the standard deviation of the RCM results, especially for ARIs greater than 1 year. The four RCMs provided bias-corrected precipitation output that agreed in general trends, however, the precise levels of precipitation increases varied substantially, especially for the 2040-2059 projected timeframe. As a result, the inferred changes in precipitation are difficult to distinguish from natural variability and determining specific projected design storms for future hydrology and stormwater infrastructure design is

difficult due to the substantial range of model outputs. Nonetheless, the average and upper and lower bounds of RCM projected precipitation can be usefully in studying potential impacts of climate change on watershed hydrology and related infrastructure.

- The results indicate increases in peak flood events across all return periods for the projected timeframes compared to observed conditions. In Indiana and Michigan the projected (2080-2099) peak flow events are larger than the projected (2040-2059) peak flows while in Illinois the projected (2080-2099) peak flow events are larger than or equal to the former events. Analysis of the number of days projected stream flow exceeds the 0.5-, 1-, and 10-yr design flows during the 20-yr simulation showed a wide range of results between the two models representing the upper and lower bounds of maximum precipitation estimates for a majority of return periods for each projected timeframe at each location.

- The projected (2080-2099) 10-yr flow event is on the order of the present 50-yr (sometimes 25-yr or 100-yr) event for many of the studied streams, suggesting possible future conditions should be considered when designing new infrastructure. Unfortunately the uncertainty inherent in the climate modeling (and subsequent hydrologic modeling) makes it difficult to develop specific recommendations on how to revise current LWC design criteria with regards to climate change in the study regions. The continuous model simulations and projections proved to underestimate average yearly flow durations for small flow events with very frequent return periods. Special care must be taken when using and applying frequent events from dynamically downscaled RCM precipitation data.

8.2 Future Steps

The current study contributes to the understanding of precipitation stationarity and the application of regional climate model precipitation projections for use as inputs to stream hydrologic models to determine subsequent impacts at stream crossing structures. After discovering the conclusions in this study, several areas for further analysis are identified:

- A review of frequent historic and projected precipitation events is need to better apply such events for hydrologic and hydraulic models to study impacts on LWCs. The two models utilized for the continuous simulations underestimated observed duration estimates for small flow events with very small ARIs. Additional analysis of frequent observed and simulated precipitation events is needed with regards to the frequency, magnitudes, and durations of such events.

- The 2007 Energy Independence and Security Act (EISA) Section 438 calls upon federal facilities to "maintain or restore, to the maximum extent technically feasible, the predevelopment hydrology of the property" affected by "development or redevelopment project involving a Federal facility with a footprint that exceeds 5,000 square feet". A key provision of the act requires the use of low impact development (LID) stormwater facilities where applicable. Such facilities are required to hold the runoff volume of all storms less than the 95th percentile, 24-hour event. Using hourly climate model projections to develop projected 95th percentile, 24-hour precipitation events would contribute to the design of sustainable LID and traditional stormwater infrusturue on Federal facilities.

- Several of the LWCs in this study, especially the vented ford over East Fork Big Creek in Illinois, act as sediment traps and generally alter the fluvial geomorphic balance of the study reaches. In addition, numerous studies have been done looking at how LWCs effect aquatic organism passage. Collecting three dimensional velocity vector and stream wise velocity field data at existing LWCs and using that data to calibrate three dimensional fluid dynamics models would inform LWC design and installation with regards to sediment and aquatic organism passage.

8.3 A Note on Uncertainty

Numerous uncertainties in climate scenarios, modeling, and data are associated with projecting future precipitation. When available some studies will use numerous emissions scenarios as a way to deal with climate uncertainty. For this study, only the highest emissions scenario (RCP8.5) was available. The high emissions scenario is the most extreme scenario with regards to radiative forcing and is often among the first used for modeling efforts to estimate possible future climate projections. There is evidence to suggest that all SRES emissions scenarios underestimate the amount of warming that is already being observed, both in western Europe (Oldenborgh et al., 2008) and globally (Rahmstorf et al., 2007) and so RCP8.5 may be the most accurate going forward. Also, the climate model used for this study incorporated the effects of the Great Lakes within the dynamic processes of the model, which are poorly represented in the CMIP5 models. The four RCMs provided bias-corrected precipitation output that agreed in general trends but the precise levels of precipitation increases varied substantially, especially for the 2040-2059 projected timeframe. The analysis of additional downscaled GCMs to determine a probability distribution of projected precipitation would be beneficial for producing recommended projected design storms. With the limit of four RCMs, the average and upper and lower bounds could only be considered.

Decadal variability is another source of uncertainty. The length and timing of historical data used to determine historic trends can greatly impact the magnitude and even the slope of the trend in question. Also, the frequency analyses used 20 years of observed data to estimate rare events with return periods of 25-100 years. Finally, observed data for a 20 year period and the corresponding statistics were used to bias correct RCM projections with several assumptions made about the stationarity of certain variables and statistics. As suggested by Markus et al. (2012), decadal variability could be minimized by generating longer future climate datasets or by including analysis of numerous models

In general, the changes in hydrologic flows were constant with changes in projected precipitation. However, watershed specific variables, such as those found in Michigan, can add a great deal of uncertainty to modeling results. In addition, the analysis of frequent storm events and flow hydrographs revealed an apparent underestimate of average yearly flow durations. Modeling uncertainty could be partially minimized by modeling watersheds with long-term stream gauge records. Unfortunately small watersheds appropriate for LWCs are infrequently gauged, and larger watersheds, such as those in central Michigan, include so much hydrograph attenuation that small storm events and the resulting flow hydrographs are unhelpful.

References

Abt, S. R, Wittler, R. J., & Love, D. J. (1989). Human stability in a high flood hazard zone. Water Resources Bulletin, 25(4): 881-890.

Arisz, H. & Burrell, B. C. (2006). Urban drainage infrastructure planning and design considering climate change. EIC Climate Change Technology, 2006 IEEE: 1-9.

Balke, K., Higgins, L., Chrysler, S., Pesti, G., Chaudhary, N., & Brydia, R. (2011). Signing strategies for low-water and flood-prone highway crossings. Report 0-6262-1. Texas Transportation Institute, Texas A&M University.

Barnard, R. J., Johnson, J. , Brooks, P., Bates, K. M., Heiner, B., Klavas, J. P., Ponder, D. C., Smith, P. D., & Powers, P.D.(2013). Water Crossings Design Guideline. Washington Department of Fish and Wildlife, Olympia, Washington.

Bonnin, G. M., Martin, D., Lin, B., Parzybok, T., Yekta, M., & Riley, D. (2006). National Oceanic Atmospheric Administration Atlas 14: precipitation frequency atlas for the United States, Volume 2 Version 3.0: Delaware, District of Columbia, Illinois, Indiana, Kentucky, Maryland, New Jersey, North Carolina, Ohio, Pennsylvania, South Carolina, Tennessee, Virginia, West Virginia. U.S. Department of Commerce. Silver Spring, MD.

Bouska, W. W., Keane, T., & Paukert, C. P. (2014). The effects of road crossings on prairie stream habitat and function. Journal of Freshwater Ecology, 25(4): 499-506.

Bouska, W. W., & Paukert, C. P. (2010). Road crossing designs and their impact on fish assemblages of Great Plains streams. Transactions of the American Fisheries Society, 139: 214-222.

Brown, K. J. (1994). River-bed sedimentation caused by off-road vehicles at river fords in the Victorian Highlands, Australia. Journal of the American Water Resources Association, 30(2): 239-250.

Brown, K. R., Aust, W. M., & McGuire, K. J. (2013). Sediment delivery from bare and gravel forest road stream crossings approaches in the Virginia Piedmont. Forest Ecology and Management, 310: 836-846.

Carstens, R. L., & Woo, R. Y. H. (1981). Liability and traffic control considerations for low water stream crossings: final report. Ames, IA: Department of Civil Engineering, Engineering Research Institute, Iowa State University.

Castro, C. L., Pielke, R. A., Sr., & Leoncini, G. (2005), Dynamical downscaling: assessment of value retained and added using the Regional Atmospheric Modeling System (RAMS), J. Geophys. Res., 110, D05108, doi:10.1029/2004JD004721.

Castro, J. (2003). Geomorphologic impacts of culvert replacement and removal: avoiding channel incision. U.S. Fish and Wildlife Service. Oregon Fish and Wildlife Office.

Chinowsky, P. S., Price, J. C., & Neumann, J. E. (2013). Assessment of climate change adaptation costs of the U.S. road network. Global Environmental Change, 23:764-773.

Chow, V.T. (1959). Open Channel Hydraulics, McGraw-Hill Book Company, NY.

Cocchiglia, L., Purcell, P. J., & Kelly-Quinn, M. (2012). A critical review of the effects of motorway river-crossing construction on the aquatic environment. Freshwater Reviews, 5: 141-168.

Denault, C., Millar, R. G., & Lence, B. J. (2006). Assessmeht of possible impacts of climate change in an urban catchment. Journal of the American Water Resources Associatation, 42: 685–697.

Department of the Army. 1997. Environmental enhancement and protection (AR 200-1). Headquarters, Department of the Army, Washinton, D.C. Retrieved June 15, 2006, from http://www.army.mil/usapa/epubs/pdf/r00_1.pdf.

Dewar, J.A. & Wachs, M. (2006). Transportation planning, climate change, and decision making under uncertainty: Commissioned paper for Committee on Climate Change and U.S. Department of Transportation, Transportation Research Board.

Dufresne, J.-L., et al. (2013). Climate change projections using the IPSL-CM5 Earth System Model: From CMIP3 to CMIP5. Clim. Dyn. 40: 2123-2165.

Easterling, W. E., Angel, J. R., & Kirsch, S. A. (1990). The appropriate use of climatic information in Illinois natural-gas utility weather normalization techniques. Illinois State Water Survey, Report of Investigation 112.

Ehret, U., Zehe, E., Wulfmeyer, V., Warrach-Sagi, K., & Liebert, J. (2012). “Should we apply bias correction to global and regional climate model data?” Hydrol. Earth Syst. Sci, 16: 3391-3404.

Elguindi, N., et al. (2011). Regional climatic model RegCM user manual version 4.1. The Abdus Salam International Centre for Theoretical Physical Strada Costiera, Trieste.

Exec. Order No. 13,514, (2009). 3 C. F. R. 74(194): 52117-52127.

Exec. Order No. 13,514, (2013). 3 C. F. R. 78(215): 66819-66824.

Federal Emergency Management Agency (FEMA). (2013). Turn around don't drown, Fact Sheet, Portsmouth, N.H. Accessed on July 15, 2016 at http://www.fema.gov/news-release/2013/06/28/turn-around-dont-drownr-0

Federal Highway Administration (FHWA). (2009). Bridge scour and stream instability countermeasures. US Department of Transportation. Publication No. FHWA-NHI-01-003, HEC 23. (Lagasse, P.F, Clopper, P.E., Pagán-Ortiz, J.E., Zevenbergen, L.W., Arneson, L.A., Schall, J.D., & Girard, L.G.).

FHWA. (2003). User's Manual for FESWMS FST2DH, Two-dimensional Depth-averaged Flow and Sediment Transport Model. Release 3, Report No. FHWA-RD-03-053, University of Kentucky Research Foundation, Lexington, KY. (Froehlich, D.C.).

FHWA. (2012a). Evaluating scour at bridges. US Department of Transportation, Publication No. FHWA-HIF-12-003, HEC 18. (Arneson, L. A., Zenenbergen, L. W., Lagasse, P. F., & Clopper, P. E.).

FHWA. (2012b). Hydraulic design of highway culverts. US Department of Transportation, Publication No. FHWA-HIF-12-026, HDS 5. (Schall, J. D., Thompson, P. L., Zerges, S. M., Kilgore, R. T., & Morris, J. L.).

FHWA. (2012c). Hydraulic design of safe bridges. US Department of Transportation, Publication No. FHWA-HIF-12-018, HDS 7. (Zevenbergen, L. W., Arneson, L. A., & Miller, A. C.).

FHWA. (2012d). Stream stability at highway structures. US Department of Transportation, Publication No. FHWA-HIF-12-004, HEC 20. (Lagasse, P. F., Zevenbergen, L. W., Spitz, W. J., & Arneson, L. A.).

Forsee, W. J. & Ahmad, S. (2011). Evaluating urban storm-water infrastructure design in response to projected climate change. Journal of Hydrologic Engineering, 16(11): 865-873.

Fortier, C. & Mailhot, A. (2015). Climate change impact on combined sewer overflows. J. Water *Resour. Plann. Manage.*,, 141(5): 04014073.

Fowler, H. J., Blenkinsop, S., & Tebaldi, C. (2007). Linking climate change modeling to impacts studies: recent advances in downscaling techniques for hydrological modeling. Int. J. of Climato. 27: 1547-1578.

Fowler, H. J., & Kilsby, C. G. (2003). A regional frequency analysis of United Kingdom extreme rainfall from 1961 to 2000. Int J Climatology, 23:1313–1334.

Fowler, H. J., & Kilsby, C. G. (2007). Using regional climate model data to simulate historical and future river flows in northwest England. Climatic Change, 80: 337-367.

Fowler, H. J., & Wilby, R. L. (2010), Detecting changes in seasonal precipitation extremes using regional climate model projections: Implications for managing fluvial flood risk. Water Resour. Res., 46, W03525, doi:10.1029/2008WR007636.

Frederick, R. H., Myers, V. A., & Auciello, E. P. (1977). Five- to 60-minute precipitation frequency of the eastern and central United States. National Oceanic and Atmospheric Administration, Technical Memorandum NWS Hydro-35. Silver Spring, Md.

Garcia, M.H. 2008. Sediment Transport and Morphodynamics. In: M.H. Garica (Ed), Ch 2 in sedimentation Engineering, ASCE Manuals and Reports on Engineering Practice No. 110.

Giorgi, F., et al. (2012). RegCM4: model description and preliminary test over multiple CORDEX domains. Clim Res, 52: 7-29.

Groisman, P. Y., Knight, R. W., Easterling, D. R., Karl, T. R., Hegerl, G. C., and Razuvaev, V. H. (2005). Trends in intense precipitation in the climate record. Journal of Climate, 18: 1326-1350.

Groisman, P. Y., Knight, R. W., & Karl, T. R. (2012). Changes in intense precipitation over the central United States. Journal of Hydrometeorology, 13: 47-66.

Haan, C.T. (1977). Statistical Methods in Hydrology, The Iowa State Univ. Press, Ames.

Hennegriff, W. (2007). Climate change and floods-finding and adaptation strategies for flood protection in Baden-Wurttemberg. Water Science & Technology, 56(4): 35-44.

Hershfield, D.M. (1961). Rainfall frequency atlas of the United States for durations from 30 min to 24 h and return periods from 1 to 100 years. Technical Paper No. 40. Weather Bureau, U.S. Department of Commerce, Washington, DC.

Holtschlag, D. J. & Croskey, H. M. (1984). Statistical models for estimating flow characteristics of Michigan streams, U.S. Geological Survey Water-Resources Investigations Report 84-4207.

Hosking, J. R. M. & J. R. Wallis (1997). Regional Frequency Analysis, an Approach Based on L-Moments. Cambridge University Pres.

Hosking, J. R. M. (1990). L-Moments: Analysis and Estimation of Distributions Using Linear Combinations of Order Statistics, 52(1): 105-124.

Hosking, J. R. M. (2015). Package 'lmomRFA' manual-regional frequency analysis using L-moments, Version 3.0-1, CRAN.

Huff, F.A. 1990. Time Distributions of Heavy Rainstorms in Illinois. Illinois State Water Survey Circular 173, 18 p.

Huff, F. A. & Angel, J. R. (1989). Rainfall distributions and hydroclimatic characteristics of heavy rainstorms in Illinois (Bulletin 70). Illinois State Water Survey, Champaign, IL.

Huff, F. A. & Angel, J. R. (1992). Rainfall frequency atlas of the Midwest (Bulletin 71). Illinois State Water Survey, Champaign, IL.

Illinois Department of Natural Resources (IDNR). (2015). Report for the Urban Flood Awareness Act. Office of Water Resources. Springfield, Illinois. (Winters, B. A., Angel, J., Ballerine, C., Byard, J., Flegel, A., Gambill, D. R., Jenkins, J. P., McConkey, S., Markus, M., Bender, B. A., O'Toole, M. J.)

Intergovernmental Panel on Climate Change (IPCC). (2014) Climate change 2014: synthesis report. Contribution of working groups I, II and III to the fifth assessment report of the Intergovernmental Panel on Climate Change (Pachauri, R. K. & Meyer, L. A. [eds.]). IPCC, Geneva, Switzerland, 151 pp.

IPCC. (2000). Special Report on Emissions Scenarios. A Special Report of Working Group III of the Intergovernmental Panel on Climate Change. (Nakicenovic, N. & Swart, R [eds.]) Cambridge University Press: Cambridge, 570 pp.

Isbash, S.V. (1936). Construction of dams by depositing rock in running water, Transactions, Second Congress on Large Dams, Washington, D.C. USA.

Janssen E., Wuebbles, D. J., Kunkel, K. E., Olsen, S. C., & Goodman, A. (2014). Observational- and model-based trends and projections of extreme precipitation over the contiguous United States. Earth's Future 2: 99–113.

Jonkman, S. N. & Penning-Rowsell, E. (2008). Human instability in flood flows. Journal of the American Water Resources Association, 44(4): 1-11.

Karl, T. R., Knight, R.W. (1998). Secular trends of precipitation amount, frequency, and intensity in the United States. Bull Am Meteorol Soc 79,(2):231–241.

Kendall, M. G. (1970) Rank Correlation Methods, 4th ed. London: Griffin

Kidd, K. R., Aust, W. M., Copenheaver, C. A. (2014). Recreational stream crossing effects on sediment delivery and macroinvertebrates in southwestern Virginia, USA. Environmental Management, 54: 505-516.

Kirk, R. E. (1996). Practical significance: a concept whose time has come. Educational and Psychological Measurements, 56(5): 746-759.

Kirshen, P., Caputo, L., Vogel, R., Mathisen, P., Rosner, A., & Renaud, T. (2015). Adapting urban infrastructure to climate change: a drainage case study. J. Water Resour. Plann. Manage., 141(4), 04014064.

Kunkel, K.E., Andsager, K., Easterling, D.R. (1999). Long-term trends in extreme precipitation events over the conterminous United States and Canada. J Clim, 12:2515–2527.

Kunkel, K. E., Easterling, D. R., Redmond, K., Hubbard, K. (2003). Temporal variations of extreme precipitation events in the United States: 1895–2000. Geophys Res Lett, 30(17):1900.

Lane, P. N., & Sheridan, G. J. (2002). Impact of an unsealed forest road stream crossing: Water quality and sediment sources. Hydrological Processes, 16(13): 2599-2612.

Langbein, W. B. (1949). Annual Floods and the Partial-Duration Flood Series. Transactions American Geophysical Union 30, 879-881.

Leahy, T. K. (2014). Hydrologic modeling of low water crossing design performance at Camp Atterbury Joint Maneuver Training Center, Indiana. M.S. Thesis. Department of Agricultural and Biological Engineering, University of Illinois, Urbana, Illinois.

Levene, H. (1960). In I. Olkin et al. eds., Contributions to Probability and Statistics: Essays in Honor of Harold Hotelling. Stanford University Press, 278-292.

Li, H., Sheffield, J., & Wood, E. F. (2010). Bias correction of monthly precipitation and temperature fields from Intergovernmental Panel on Climate Change AR4 models using equidistant quantile matching, J. Geophys. Res. 115: D10101.

Lindau, R. & Simmer, C. (2012). On correction precipitation as simulated by the regional climate model COSMO-CLM with daily rain gauge observations. Meteorol Atmos Phys, 119: 31-42.

Lohnes, R. A., Gu, R. R., McDonald, T., & Jha, M. K. (2001). Low water stream crossings: design and construction recommendations. Center for Transportation Research and Education, Iowa State University.

Leopold, L.B. (1994). A View of the River. Harvard University Press. Cambridge, MA.

Lucero, O. A. (1998). Invariance of the design storm in a region under a rainfall climate change at mid-latitudes. Atmospheric Research, 49: 11-20.

Madsen, H., Arnbjerg-Nielsen, K., & Mikkelsen, P. S. (2009). Update of regional intensity-duration-frequency curves in Denmark: tendency towards increased storm intensities. Atmospheric Research, 92: 343-349.

Madsen, T. & Figdor, E. (2007). When it rains, it pours. Global warming and the rising frequency of extreme precipitation in the United States. Environment America Research & Policy Center.

Mailhot, A. & Duchesne, S. (2010). Design criteria of urban drainage infrastructure under climate change. J. Water Resour. Plann. Manage., 136(2): 201-208.

Mailhot, A., Dushesne, S., Caya, D., & Talbot, G. (2007). Assessment of future change in intensity–duration–frequency (IDF) curves for Southern Quebec using the Canadian Regional Climate Model (CRCM). Journal of Hydrology, 347: 197-210.

Malinga, G.A. (2007). Analyzing the effects of low water fords on stream stability at Fort Riley, Kansas. M.S. Thesis. Department of Biological and Agricultural Engineering, Kansas State University, Manhattan, Kansas.

Markus, M., Wuebbles, D. J., Laing, X., Hayhoe, K., Kristovich, D. A. R. (2012). Diagnostic analysis of future climate scenarios applied to urban flooding in the Chicago metropolitan area. Climatic Change, 111: 879-902.

Maurer, E. P., & Hidalgo, H. G. (2008). Utility of daily vs. monthly large scale climate data: An intercomparison of two statistical downscaling methods, Hydrol. Earth Syst. Sci., 12: 551–563.

McCuen, R. H. (2016). Assessment of hydrological and statistical significance. J. Hydrol. Eng., 02516001: 1-2.

McDonald, T. & Anderson-Wilk, M. (2003). Low water crossings in Iowa a section and design guide. Center for Transportation Research and Education, Iowa State University.

Melillo, J. M., Richmond, T. C., & Yohe, G. W. (Eds.). (2014). Climate change impacts in the United States: The Third National Climate Assessment (NCA). U.S. Global Change Research Program, 841 pp.

Moglen, G. & Rios Vidal, G. (2014). Climate change and storm water infrastructure in the Mid-Atlantic Region: design mismatch coming? Journal of Hydrologic Engineering, 19(11), 04014026.

Motayed, A. K., Chang, F. M., & Mukherjee, D. K. (1983). Design and Construction of Low Water Stream Crossings. U.S. Department of Transportation, Federal Highway Administration Report No. FHWA/RD-83/015.

Neumann, J. E., Price, J. C., Chinowsky, P., Wright, L., Ludwig, L., Streeter, R., Jones, R., Smith, J. B., Perkins, W., Jantarasami, L., & Martinich, J. (2014). Climate change risks to US infrastructure: impacts on roads, bridges, coastal development, and urban drainage. Climate Change, 131(1): 97-109.

Notaro, M., Bennington, V., & Vavrus, S. (2015). Dynamically Downscaled Projections of Lake-Effect Snow in the Great Lakes Basin. J of Climate, 28: 1661-1684.

Office of the Undersecretary of Defense (OUSD). (2013). High-level climate change vulnerability assessment. Office of the Deputy Undersecretary of Defense for Installations and Environment, Department of Defence, Washington, DC. (Hayden, T. J., Goran, W. D., Case, M. P., Burks-Copes, K., Loechl, P. M., Pranger, S., Dain-Owens, A., Sweeney, S. C., & Weatherly, J. W.) Retrieved July, 2015, from http://www.asaie.army.mil/Public/ES/doc/ArmyHigh-LevelClimateChangeVulnerabilityAssessment2013final.pdf.

OUSD. (2014). Department of Defense base structure report. Office of the Deputy Undersecretary of Defense for Installations and Environment, Department of Defence, Washington, DC. Retrieved July, 2015, from http://www.acq.osd.mil/ie/download/bsr/Base%20Structure%20Report%20FY14.pdf.

Oldenborgh, G. J., van Drijfhout, S. S., van Ulden, A., Haarsma, R., Sterl, A., Severijns, C., Hazeleger, W., & Dijkstra, H. (2008). Western Europe is warming much faster than expected, Clim. Past Discuss., 4: 897–928.

Olsson, J., Gidhagen, L., Gamerith, V., Gruber, G., Hoppe, H., & Kutschera, P. (2012). Downscaling of short-term precipitation from regional climate models for sustainable urban planning. Sustainability, 4: 866-887.

Perica, S., Martin, D., Pavlovic, S., Roy, I., St. Laurent, M., Trypaluk, C., Unruh, D., Yekta, M., Bonnin, G. (2013). National Oceanic Atmospheric Administration Atlas 14: precipitation frequency atlas for the United States, Volume 8 Version 2.0: Midwestern States (Colorado, Iowa, Kansas, Michigan, Minnesota, Missouri, Nebraska, North Dakota, Oklahoma, South Dakota, Wisconsin). U.S. Department of Commerce. Silver Spring, MD.

Pielke, R. A., Sr., (2002). Overlooked issues in the U.S. national climate and IPCC assessments, Clim. Change, 52(1-2), 1–11, doi:10.1023/A:1017473207687.

Pielke, R. A., Sr. & Wilby, R. L. (2012). Regional climate downscaling: what's the point? EOS, 93(5): 52-53, doi:10.1029/2012EO050008.

Pielke, R. A., Sr., Wilby, R., Niyogi, D., Hossain, F., Dairuku, K., Adegoke, J., Kallos, G., Seastedt, T., & Suding, K. (2012). Dealing with complexity and extreme events using a bottom-up, resource based vulnerability perspective, in Complexity and Extreme Events in Geosciences, Geophys. Monogr. Ser., edited by A. S. Sharma et al., AGU, Washington, D. C., in press.

Pryor, S. C., Howe, J. A., & Kunkel, K. E. (2009). How spatially coherent and statistically robust are temporal changes in extreme precipitation in the contiguous USA? Int. J. Climatology, 29: 31–45.

R Core Team. 2014. R: A language and environment for statistical computing. R Foundation for Statistical Computing, Vienna, Austria. URL http://www.R-project.org/.

Rahmstorf, S., Cazenave, A, Church, J. A., Hansen, J. E., Keeling, R. F., Parker, D. E., and Somerville, R. C. J. (2007). Recent Climate Observations Compared to Projections. Science, 316, 709, doi:10.1126/science.1136843.

Roa, A. R. (2006). Flood frequency relationships for Indiana. Federal Highway Administration, Joint Transportation Research Program, FHWA/IN/JTRP-2005/18.

Rosenberg, E. A., Keys, P. W., Booth, D. B., Hartley, D., Burkey, J., Steinemann, A. C., & Lettenmaier, D. P. (2010). Precipitation extremes and impacts of climate change on stormwater infrastructure in Washington State. Climatic Change, 102: 319-349.

Sample, L. J., Steichen, J., & Kelley, J. R. (1998). Water quality impacts from low water fords on military training lands. Journal of the American Water Resources Association, 34(4): 939-949.

Sanford, T., Frumhoff, P. C., Luers, A., & Gulledge, J. (2014). The climate policy narrative for a dangerously warming world. Nature Climate Change, 4: 164-166.

Savonis, M. J., Burkett, V. R., Potter, J. R., Kafalenos, R., Hyman, R., & Leonard, K. (2009). The impact of climate change on transportation in the Gulf Coast. TCLEE 2009: 1-11.

Scottish Executive. (2005). Scottish road network climate change study. (Galbraith, R. M., Price, D. J., & Shackman, L.).

Shields, A. (1936). Application of similarity mechanics and turbulence research on shear flow. *Mitteilungen der Preußischen Versuchsanstalt für Wasserbau **26**. Berlin: Preußische Versuchsanstalt für Wasserbau.*

Soil Survey Staff, Natural Resources Conservation Service, United States Department of Agriculture. U.S. General Soil Map (STATSGO2). Available online at http://sdmdataaccess.nrcs.usda.gov/. Accessed [12/29/2015].

Soong, D. T., Ishii, A. L., Sharpe, J. B., and Avery, C. F. (2004). Estimating Flood-Peak Discharge Magnitudes and Frequencies for Rural Streams in Illinois, U.S. Geological Survey Science Investigations Report 2004-5103.

Sun, F. B., Roderick, M. L., Lim, W. H., & Farquhar, G. D. (2011). Hydroclimatic projections for the Murray-Darling Basin based on an ensemble derived from Intergovernmental Panel on Climate Change AR4 climate models. Water Resour. Res., 47: W00g02.

Svendsen, N. G. 2005. Erosion and water quality assessment military training lands at Camp Atterbury Joint Maneuver Training Center, M.S. thesis. Department of Agricultural and Biological Engineering, University of Illinois, Urbana, IL.

Taylor, K. E., Stouffer, R. J., & Meehl, G. A. (2012). An overview of CMIP5 and the experiment design. Bull. Am. Meteorol. Soc., 93: 485–498.

Themessl, M. J., Gobiet, A., & Leuprecht, A. (2011). Empirical statistical downscaling and error correction of daily precipitation from regional climate models, Int. J. Climatol., 31: 1530–1544.

Transportation Research Board (TRB). (2008). Potential impacts of climate change of U.S. transportation. National Research Council. Special Report 290, Washington D.C.

US Department of Agriculture (USDA). (2006). Low-water crossings: geomorphic, biological, and engineering design considerations. Forest Service, National Technology and Development Program. (Clarkin, K., Keller, G., Warhol, T., & Hixson, S.).

United States Department of Agriculture (USDA), Natural Resource Conservation Service. (1986). Urban Hydrology for Small Watersheds. Technical Release No. 55.

United States Army Corps of Engineers (USACE). (2000). Hydrologic Modeling System HEC-HMS Technical Reference Manual, Report Number CPD-74B.

USACE. (2006a). Defilade, stationary target and moving target embankment, low water crossing, and course road designs for soil loss prevention. ERDC/CERL TR-06-31. Champaign, IL: U.S. Army Engineer Research and Development Center. (Svendsen, N.G., Kalita, P. K., Gebhart, D. L., & Denight, M. L.)

USACE. (2006b). Lessons learned: streambank stabilization on army training lands. Public Work Technical Bulletin 200-3-41. Washington, DC. (Howard, H. R., Svendsen, N. G.., Hargrave, M. L., Gambill, D. R., Erhart, L. K., Ochsner, W. R., Schneck, B. D., Carmany, K. M., & McLeod, M. E.).

USACE. (2009). Users Guide to RMA2 WES Version 4.5. (Donnell, B.P., Letter, J.V., McAnally, W.H., & Thomas, W.A.).

USACE. (2010). HEC-RAS, River Analysis System Hydraulic Reference Manual. Report No. CPD-69. (Brunner, G.W.).

USACE. (2011). Low-water crossings: Lessons Learned. Public Work Technical Bulletin 200-1-115. Washington, DC. (Howard, H., Svendsen, N., Holmes, J., & Holscher, J.)

USACE. (2012). HEC-GeoRAS GIS tools for support of HEC-RAS using ArcGIS 10, extension Version 10.1, Report Number CPD-83, (Ackerman, C. T.).

USACE. (2013). HEC-GeoHMS geospatial hydrologic modeling extension Version 10.1, Report Number CPD-77, (Fleming, M. J. & Doan, J. H.).

USACE. (2014). Climate change Adaptation plan. Climate Preparedness and Resilience Steering Committee. Department of the Army.

US Department of Tranportation (USDOT). (2014). Climate adaption plan ensuring transportation infrastructure and system resilience. Washington, DC.

US Environmental Protection Agency (USEPA). (2013). Better assessment science integrating Point and nonpoint sources (BASINS), Version 4.1, User's Manual. Office of Water, EPA-823-B-13-001.

US Geological Survey (USGS). (1959). Flow-duration curves. Water-Supply Paper 1542-A. (Searcy, J. K.).

USGS. (2002). Effects of hardened low-water crossings on stream habitat, water quality, and periphyton in four streams at the Fort Polk Military Reservation, Vernon Parish, Louisiana, October 1998 through November 1999. Water-Resources Investigations Report No. 02-4291. Baton Rouge, LA. (Tollett, R. W., Bryan, B. W., & Bryan, C. F.).

USGS. (2007). Effects of hardened low-water crossings on periphyton and water quality in select streams at the Fort Polk Military Reservation, Louisiana, 1998-99 and 2003-04. Scientific Investigations Report 2007-5279. Baton Rouge, LA. (Bryan, B. W., Bryan ,C. F., Lovelace, J. K., &Tollett, R. W.).

US Water Resources Council (USWRC). (1981). Guidelines for determining flood flow frequency. Bulletin No. 17B, the Hydrology Committee, Washington, D.C.

Vavrus, S. J. & Behnke, R. J. (2014). A comparison of projected future precipitation in Wisconsin using global and downscaled climate model simulations: implications for public health. Int. J. Climatology, 34: 3106-3124.

Voldoire, A., et al. (2013). The CNRM-CM5.1 global climate model: description and basic evaluation. Clim Dyn, 40: 2091-2121.

Wang, J., Edwards, P. J., & Wood, F. (2013). Turbidity and suspended-sediment changes from stream-crossing construction on a forest haul road in West Virginia, USA. International Journal of Forest Engineering, 24(1): 76-90.

Warren Jr, M. L., and M. G. Pardew. 1998. Road crossings as barriers to small-stream fish movement. Transactions of the American Fisheries Society, 127: 637-644.

Watt, E. & Marsalek, J. (2013). Critical review of the evolution of the design storm event concept. Can. J. Civ. Eng., 40: 105-113.

Wear, L. A., Aust, W. M, Bolding, M. C., Strahm, B. D., & Dolloff, C. A. (2013). Effectiveness of best management practices for sediment reduction at operational forest stream crossings. Forest Ecology and Mangement, 289: 551-561.

Wilby, R. L., & Fowler, H. L. (2010), Regional climate downscaling, in Modelling the Impact of Climate Change on Water Resources, edited by C. F. Fung, A. Lopez, and M. New, chap. 3, pp. 34–85, Wiley-Blackwell, Chichester, U. K.

Wilks, DS. (1995). Statistical Methods in Atmospheric Science, Volume 59 of International Geophysics Series. Academic Press: San Diego, London.

Wood, A.W., Leung, L.R., Sridhar, V., & Lettenmaier, D.P. (2004). Hydrologic implications of dynamical and statistical approaches to downscale climate model outputs. Climatic Change, 62: 189–216.

Wright, L., Chinowsky, P., Strzepek, K., Jones, R., Streeter, R., Smith, J. B., Mayotte, J., Powell, A., Jantarasami, L., & Perkins, W. (2012). Estimated effects of climate change on flood vulnerability of U.S. bridges. Mitig Adapt Strateg Glob Change, 17: 939-955.

Wuebbles, D., Meehl, G., Hayhoe, K., Karl, T., Kunkel, K., Santer, B., Wehner, M., Colle, B., Fishcer, E., Fu, R., Goodman, A., Janssen, E., Kharin, V., Lee, H., Li, W., Long, L., Olsen, S., Pan, Z., Seth. A., Sheffield, J., & Sun, L. (2014). CMIP5 climate model analysis, Am. Meteorol. Soc., 95(4): 571–583.

Yukimoto, S., et al. (2012). A New Global Climate Model of the Meteorological Research Institute: MRI-CGCM3 - Model Description and Basic Performance. J of the Meteorological Society of Japan, 90A: 23-64.

Zhu, J. (2013). Impact of climate change on extreme rainfall across the United States. Journal of Hydrologic Engineering, 18: 1301-1309.

Appendix A: Additional Data from Chapter 4

Table A.1. Changes in 1-hr maximum precipitation between 1970-1989 and 1990-2009, at various Indiana gauges, expressed as a percent difference.

1-hr	0.5 yr	1 yr	2 yr	5 yr	10 yr	25 yr	50 yr	100 yr
BLOOM	17.0%	13.4%	7.1%	-0.7%	-5.1%	-8.6%	-9.8%	-9.8%
COLUM	4.0%	0.4%	-6.0%	-13.8%	-18.1%	-21.6%	-22.7%	-22.7%
IND AP	2.7%	-0.9%	-7.2%	-15.0%	-19.3%	-22.8%	-24.0%	-24.0%
MARTIN	13.4%	9.8%	3.5%	-4.3%	-8.7%	-12.2%	-13.3%	-13.4%
OOL EF	5.8%	2.3%	-4.1%	-11.9%	-16.2%	-19.7%	-20.9%	-20.9%
SEY HG	6.7%	3.2%	-3.2%	-11.0%	-15.3%	-18.8%	-20.0%	-20.0%
SHELBY	3.3%	-0.3%	-6.7%	-14.4%	-18.8%	-22.3%	-23.4%	-23.4%
VER WW	13.0%	9.5%	3.1%	-4.7%	-9.1%	-12.6%	-13.7%	-13.7%
WALD	19.3%	15.8%	9.4%	1.6%	-2.7%	-6.3%	-7.4%	-7.4%
Avg	9.4%	5.8%	-0.5%	-8.3%	-12.7%	-16.2%	-17.3%	-17.3%

Table A.2. Changes in 2-hr maximum precipitation between 1970-1989 and 1990-2009, at various Indiana gauges, expressed as a percent difference.

2-hr	0.5 yr	1 yr	2 yr	5 yr	10 yr	25 yr	50 yr	100 yr
BLOOM	14.1%	9.7%	6.0%	1.6%	-1.5%	-5.7%	-8.7%	-11.8%
COLUM	4.1%	-0.4%	-4.1%	-8.4%	-11.6%	-15.7%	-18.8%	-21.8%
IND AP	-4.9%	-9.4%	-13.1%	-17.4%	-20.5%	-24.6%	-27.7%	-30.7%
MARTIN	18.0%	13.6%	9.9%	5.6%	2.4%	-1.7%	-4.8%	-7.9%
OOL EF	11.3%	6.9%	3.2%	-1.2%	-4.3%	-8.4%	-11.5%	-14.6%
SEY HG	10.5%	6.1%	2.4%	-2.0%	-5.1%	-9.3%	-12.3%	-15.4%
SHELBY	2.2%	-2.2%	-5.9%	-10.3%	-13.4%	-17.5%	-20.6%	-23.6%
VER WW	3.4%	-1.1%	-4.8%	-9.1%	-12.3%	-16.4%	-19.4%	-22.5%
WALD	16.1%	11.7%	8.0%	3.6%	0.5%	-3.6%	-6.7%	-9.8%
Avg	8.2%	3.8%	0.1%	-4.3%	-7.5%	-11.6%	-14.7%	-17.7%

Table A.3. Changes in 3-hr maximum precipitation between 1970-1989 and 1990-2009, at various Indiana gauges, expressed as a percent difference.

3-hr	0.5 yr	1 yr	2 yr	5 yr	10 yr	25 yr	50 yr	100 yr
BLOOM	13.5%	9.7%	6.5%	2.4%	-0.7%	-4.7%	-7.8%	-11.0%
COLUM	6.3%	2.6%	-0.7%	-4.8%	-7.8%	-11.9%	-15.0%	-18.2%
IND AP	13.0%	9.3%	6.0%	2.0%	-1.1%	-5.1%	-8.3%	-11.4%
MARTIN	15.5%	11.8%	8.5%	4.5%	1.4%	-2.6%	-5.8%	-8.9%
OOL EF	14.6%	10.9%	7.6%	3.6%	0.5%	-3.6%	-6.7%	-9.8%
SEY HG	8.6%	4.9%	1.6%	-2.5%	-5.5%	-9.6%	-12.7%	-15.8%
SHELBY	4.0%	0.2%	-3.1%	-7.1%	-10.2%	-14.2%	-17.3%	-20.5%
VER WW	14.9%	11.2%	7.9%	3.8%	0.8%	-3.3%	-6.4%	-9.6%
WALD	23.3%	19.6%	16.3%	12.3%	9.2%	5.2%	2.1%	-1.1%
Avg	12.6%	8.9%	5.6%	1.5%	-1.5%	-5.6%	-8.7%	-11.9%

Table A.4. Changes in 6-hr maximum precipitation between 1970-1989 and 1990-2009, at various Indiana gauges, expressed as a percent difference.

6-hr	0.5 yr	1 yr	2 yr	5 yr	10 yr	25 yr	50 yr	100 yr
BLOOM	11.4%	10.9%	9.7%	7.7%	5.8%	3.1%	0.9%	-1.5%
COLUM	14.3%	13.7%	12.5%	10.5%	8.7%	6.0%	3.7%	1.3%
IND AP	8.8%	8.2%	7.0%	5.0%	3.2%	0.5%	-1.8%	-4.2%
MARTIN	16.4%	15.9%	14.7%	12.6%	10.8%	8.1%	5.9%	3.5%
OOL EF	8.2%	7.6%	6.4%	4.4%	2.6%	-0.1%	-2.4%	-4.8%
SEY HG	15.2%	14.7%	13.5%	11.5%	9.7%	7.0%	4.7%	2.3%
SHELBY	-0.2%	-0.7%	-1.9%	-4.0%	-5.8%	-8.5%	-10.7%	-13.1%
VER WW	14.7%	14.1%	12.9%	10.9%	9.1%	6.4%	4.1%	1.7%
WALD	25.4%	24.9%	23.7%	21.7%	19.9%	17.2%	15.0%	12.6%
Avg	12.6%	12.1%	10.9%	8.8%	7.0%	4.3%	2.1%	-0.3%

Table A.5. Changes in 12-hr maximum precipitation between 1970-1989 and 1990-2009, at various Indiana gauges, expressed as a percent difference.

12-hr	0.5 yr	1 yr	2 yr	5 yr	10 yr	25 yr	50 yr	100 yr
BLOOM	10.4%	10.3%	9.8%	8.7%	7.7%	6.0%	4.7%	3.2%
COLUM	20.1%	20.1%	19.6%	18.5%	17.4%	15.8%	14.4%	13.0%
IND AP	6.8%	6.7%	6.2%	5.1%	4.0%	2.4%	1.0%	-0.5%
MARTIN	21.4%	21.4%	20.9%	19.8%	18.7%	17.1%	15.7%	14.3%
OOL EF	7.0%	6.9%	6.4%	5.3%	4.3%	2.6%	1.3%	-0.2%
SEY HG	14.2%	14.2%	13.7%	12.6%	11.5%	9.8%	8.5%	7.0%
SHELBY	9.5%	9.4%	8.9%	7.8%	6.7%	5.1%	3.7%	2.3%
VER WW	19.5%	19.4%	18.9%	17.8%	16.8%	15.1%	13.8%	12.3%
WALD	**26.4%**	**26.4%**	**25.9%**	24.8%	23.7%	22.1%	20.8%	19.3%
Avg	14.9%	14.8%	14.3%	13.2%	12.2%	10.5%	9.2%	7.7%

Table A.6. Changes in 24-hr maximum precipitation between 1970-1989 and 1990-2009, at various Indiana gauges, expressed as a percent difference.

24-hr	0.5 yr	1 yr	2 yr	5 yr	10 yr	25 yr	50 yr	100 yr
BLOOM	6.8%	8.6%	12.9%	17.3%	18.8%	18.6%	17.1%	14.6%
COLUM	19.3%	21.1%	**25.4%**	**29.7%**	**31.1%**	**30.9%**	29.4%	27.0%
IND AP	5.0%	6.8%	11.1%	15.5%	17.0%	16.8%	15.3%	12.8%
MARTIN	19.5%	21.3%	**25.6%**	**29.9%**	**31.4%**	**31.1%**	29.7%	27.2%
OOL EF	-0.3%	1.5%	5.8%	10.2%	11.7%	11.5%	10.0%	7.5%
SEY HG	10.5%	12.3%	16.7%	**21.0%**	**22.5%**	22.3%	20.8%	18.3%
SHELBY	6.3%	8.1%	12.4%	16.8%	18.3%	18.0%	16.5%	14.0%
VER WW	16.3%	18.0%	**22.4%**	**26.7%**	**28.1%**	**27.9%**	26.4%	24.0%
WALD	19.4%	21.2%	**25.5%**	**29.8%**	**31.3%**	**31.0%**	29.6%	27.1%
Avg	11.3%	13.1%	17.4%	**21.7%**	**23.2%**	23.0%	21.5%	19.0%

Table A.7. Changes in 2-day maximum precipitation between 1970-1989 and 1990-2009, at various Indiana gauges, expressed as a percent difference.

2-day	0.5 yr	1 yr	2 yr	5 yr	10 yr	25 yr	50 yr	100 yr
BLOOM	9.6%	14.8%	16.9%	17.1%	16.4%	15.0%	13.8%	12.5%
COLUM	11.3%	16.6%	18.6%	18.9%	18.2%	16.7%	15.5%	14.3%
IND AP	12.1%	17.3%	19.3%	19.6%	18.9%	17.5%	16.3%	15.0%
MARTIN	**24.8%**	**30.0%**	**32.0%**	**32.3%**	**31.6%**	**30.2%**	**29.0%**	27.7%
OOL EF	5.7%	11.0%	13.0%	13.3%	12.6%	11.2%	9.9%	8.7%
SEY HG	9.4%	14.7%	16.7%	17.0%	16.3%	14.9%	13.6%	12.4%
SHELBY	11.4%	16.6%	18.7%	18.9%	18.2%	16.8%	15.6%	14.3%
VER WW	17.8%	**23.0%**	**25.1%**	**25.3%**	**24.6%**	23.2%	22.0%	20.7%
WALD	21.4%	**26.6%**	**28.6%**	**28.8%**	**28.1%**	**26.7%**	25.5%	24.3%
Avg	13.5%	18.8%	20.8%	21.0%	20.4%	18.9%	17.7%	16.5%

Table A.8. Changes in 5-day maximum precipitation between 1970-1989 and 1990-2009, at various Indiana gauges, expressed as a percent difference.

5-day	0.5 yr	1 yr	2 yr	5 yr	10 yr	25 yr	50 yr	100 yr
BLOOM	17.8%	13.9%	12.2%	12.1%	13.1%	15.2%	17.1%	19.1%
COLUM	22.0%	18.1%	16.3%	16.3%	17.3%	19.4%	21.3%	23.3%
IND AP	14.8%	10.9%	9.1%	9.1%	10.1%	12.2%	14.1%	16.1%
MARTIN	**34.2%**	**30.4%**	**28.6%**	**28.5%**	**29.5%**	**31.6%**	**33.4%**	**35.5%**
OOL EF	11.4%	7.4%	5.6%	5.6%	6.6%	8.7%	10.6%	12.6%
SEY HG	15.4%	11.5%	9.7%	9.6%	10.6%	12.7%	14.6%	16.7%
SHELBY	14.4%	10.5%	8.7%	8.6%	9.6%	11.7%	13.7%	15.7%
VER WW	**30.4%**	**26.6%**	**24.8%**	**24.7%**	**25.7%**	**27.8%**	**29.7%**	31.7%
WALD	**29.1%**	**25.2%**	**23.5%**	**23.4%**	**24.4%**	26.4%	28.3%	30.3%
Avg	21.0%	17.1%	15.3%	15.2%	16.2%	18.3%	20.2%	22.3%

Table A.9. Changes in 10-day maximum precipitation between 1970-1989 and 1990-2009, at various Indiana gauges, expressed as a percent difference.

10-day	0.5 yr	1 yr	2 yr	5 yr	10 yr	25 yr	50 yr	100 yr
BLOOM	18.3%	**22.1%**	19.3%	15.9%	15.4%	16.9%	19.1%	**21.9%**
COLUM	16.4%	**20.1%**	17.3%	14.0%	13.4%	14.9%	17.1%	**19.9%**
IND AP	10.8%	14.5%	11.7%	8.4%	7.8%	9.3%	11.5%	14.3%
MARTIN	**27.3%**	**30.9%**	**28.2%**	24.9%	24.3%	**25.8%**	**28.0%**	**30.7%**
OOL EF	16.0%	**19.7%**	16.9%	13.6%	13.1%	14.5%	16.7%	**19.5%**
SEY HG	16.4%	**20.1%**	17.3%	14.0%	13.5%	14.9%	17.1%	**19.9%**
SHELBY	8.5%	12.2%	9.4%	6.0%	5.5%	7.0%	9.2%	12.0%
VER WW	**23.3%**	**27.0%**	**24.2%**	20.9%	20.4%	21.8%	**24.0%**	**26.8%**
WALD	**22.3%**	**26.0%**	23.2%	19.9%	19.4%	20.9%	**23.1%**	**25.8%**
Avg	17.7%	**21.4%**	18.6%	15.3%	14.7%	16.2%	18.4%	**21.2%**

Table A.10. Changes in 1-hr maximum precipitation between 1970-1989 and 1990-2009, at various Michigan gauges, expressed as a percent difference.

1-hr	0.5 yr	1 yr	2 yr	5 yr	10 yr	25 yr	50 yr	100 yr
BELL	4.1%	0.1%	-8.2%	-12.3%	-9.6%	-0.4%	9.4%	20.9%
GLAD	14.4%	10.4%	2.1%	-2.0%	0.7%	9.9%	19.6%	**31.0%**
GLENN	0.6%	-3.4%	-11.7%	-15.7%	-13.0%	-3.9%	5.9%	17.5%
GRAY	-19.6%	-23.5%	**-31.7%**	**-35.6%**	**-33.0%**	-24.0%	-14.3%	-2.8%
LAKE EF	**33.7%**	**29.9%**	21.7%	17.6%	20.3%	29.4%	**38.8%**	**49.9%**
TRAVE	-5.9%	-9.9%	-18.1%	-22.2%	-19.5%	-10.4%	-0.6%	11.0%
VAND	-8.7%	-12.6%	-20.9%	-24.9%	-22.2%	-13.1%	-3.4%	8.2%
Avg	2.6%	-1.3%	-9.6%	**-13.7%**	-11.0%	-1.9%	7.9%	19.5%

Table A.11. Changes in 2-hr maximum precipitation between 1970-1989 and 1990-2009, at various Michigan gauges, expressed as a percent difference.

2-hr	0.5 yr	1 yr	2 yr	5 yr	10 yr	25 yr	50 yr	100 yr
BELL	1.2%	3.8%	-1.3%	-5.4%	-4.3%	1.9%	9.3%	18.6%
GLAD	7.6%	10.1%	5.1%	1.0%	2.0%	8.2%	15.6%	24.8%
GLENN	-7.2%	-4.6%	-9.6%	-13.7%	-12.7%	-6.5%	0.9%	10.2%
GRAY	-23.7%	-21.2%	-26.1%	**-30.2%**	**-29.2%**	-23.1%	-15.7%	-6.4%
LAKE EF	**32.3%**	**34.8%**	29.9%	25.9%	26.9%	33.0%	**40.1%**	**49.0%**
TRAVE	-11.1%	-8.5%	-13.5%	-17.6%	-16.6%	-10.4%	-3.0%	6.3%
VAND	-16.4%	-13.8%	-18.8%	-22.9%	-21.9%	-15.8%	-8.3%	1.0%
Avg	-2.6%	0.0%	-5.1%	-9.2%	-8.2%	-2.0%	5.5%	14.8%

Table A.12. Changes in 3-hr maximum precipitation between 1970-1989 and 1990-2009, at various Michigan gauges, expressed as a percent difference.

3-hr	0.5 yr	1 yr	2 yr	5 yr	10 yr	25 yr	50 yr	100 yr
BELL	-2.9%	-2.7%	-7.7%	-9.7%	-6.2%	4.1%	15.0%	**27.9%**
GLAD	7.5%	7.7%	2.7%	0.7%	4.2%	14.5%	25.3%	**38.0%**
GLENN	-7.7%	-7.6%	-12.6%	-14.6%	-11.0%	-0.7%	10.2%	23.1%
GRAY	-18.2%	-18.1%	-23.0%	**-25.0%**	-21.5%	-11.3%	-0.4%	12.7%
LAKE EF	**33.1%**	**33.3%**	28.4%	26.4%	29.9%	**39.9%**	**50.2%**	**62.2%**
TRAVE	-16.4%	-16.3%	-21.3%	**-23.2%**	-19.7%	-9.5%	1.4%	14.5%
VAND	-16.7%	-16.5%	-21.5%	**-23.5%**	-20.0%	-9.7%	1.2%	14.2%
Avg	-3.2%	-3.0%	-8.0%	-10.0%	-6.5%	3.8%	14.7%	27.6%

Table A.13. Changes in 6-hr maximum precipitation between 1970-1989 and 1990-2009, at various Michigan gauges, expressed as a percent difference.

6-hr	0.5 yr	1 yr	2 yr	5 yr	10 yr	25 yr	50 yr	100 yr
BELL	-5.5%	-4.9%	-5.8%	-6.0%	-4.5%	-0.2%	4.6%	10.5%
GLAD	2.7%	3.4%	2.5%	2.3%	3.8%	8.1%	12.8%	18.7%
GLENN	-1.6%	-0.9%	-1.8%	-2.0%	-0.5%	3.8%	8.5%	14.4%
GRAY	-15.3%	-14.7%	-15.6%	-15.8%	-14.3%	-10.0%	-5.3%	0.7%
LAKE EF	22.6%	23.3%	22.3%	22.2%	23.6%	27.9%	32.5%	38.3%
TRAVE	-13.9%	-13.2%	-14.2%	-14.3%	-12.9%	-8.6%	-3.8%	2.1%
VAND	-11.8%	-11.2%	-12.1%	-12.3%	-10.8%	-6.5%	-1.7%	4.2%
Avg	-3.4%	-2.7%	-3.6%	-3.8%	-2.3%	2.0%	6.7%	12.7%

Table A.14. Changes in 12-hr maximum precipitation between 1970-1989 and 1990-2009, at various Michigan gauges, expressed as a percent difference.

12-hr	0.5 yr	1 yr	2 yr	5 yr	10 yr	25 yr	50 yr	100 yr
BELL	-4.3%	-5.8%	-10.9%	-11.8%	-7.2%	4.8%	17.0%	**31.2%**
GLAD	1.3%	-0.3%	-5.3%	-6.3%	-1.6%	10.3%	22.5%	**36.5%**
GLENN	4.5%	3.0%	-2.1%	-3.0%	1.6%	13.6%	25.7%	**39.7%**
GRAY	-11.2%	-12.7%	-17.7%	-18.7%	-14.1%	-2.1%	10.1%	24.4%
LAKE EF	10.2%	8.6%	3.6%	2.6%	7.3%	19.2%	**31.2%**	**45.1%**
TRAVE	-0.6%	-2.1%	-7.2%	-8.2%	-3.5%	8.5%	20.6%	**34.7%**
VAND	-12.4%	-14.0%	-19.0%	-20.0%	-15.3%	-3.4%	8.8%	23.1%
Avg	-1.7%	-3.3%	-8.3%	-9.3%	-4.6%	7.4%	19.5%	**33.6%**

Table A.15. Changes in 24-hr maximum precipitation between 1970-1989 and 1990-2009, at various Michigan gauges, expressed as a percent difference.

24-hr	0.5 yr	1 yr	2 yr	5 yr	10 yr	25 yr	50 yr	100 yr
BELL	-7.1%	-5.9%	-10.0%	-12.0%	-9.3%	-0.8%	8.5%	19.7%
GLAD	2.0%	3.2%	-0.9%	-2.9%	-0.2%	8.3%	17.6%	**28.7%**
GLENN	2.4%	3.6%	-0.5%	-2.6%	0.1%	8.7%	17.9%	**29.0%**
GRAY	-13.4%	-12.2%	-16.2%	-18.3%	-15.6%	-7.1%	2.2%	13.4%
LAKE EF	6.6%	7.8%	3.7%	1.7%	4.4%	12.9%	22.1%	**33.2%**
TRAVE	-2.1%	-0.9%	-4.9%	-7.0%	-4.3%	4.3%	13.5%	24.7%
VAND	-16.6%	-15.4%	-19.4%	-21.5%	-18.8%	-10.3%	-1.0%	10.3%
Avg	-3.9%	-2.7%	-6.7%	**-8.8%**	-6.1%	2.4%	11.7%	22.9%

Table A.16. Changes in 2-day maximum precipitation between 1970-1989 and 1990-2009, at various Michigan gauges, expressed as a percent difference.

2-day	0.5 yr	1 yr	2 yr	5 yr	10 yr	25 yr	50 yr	100 yr
BELL	-0.5%	-2.2%	-4.1%	-4.1%	-1.8%	4.0%	10.2%	17.6%
GLAD	6.0%	4.3%	2.4%	2.4%	4.7%	10.5%	16.7%	24.0%
GLENN	5.0%	3.3%	1.4%	1.4%	3.7%	9.5%	15.7%	23.1%
GRAY	-6.0%	-7.6%	-9.5%	-9.5%	-7.2%	-1.4%	4.8%	12.2%
LAKE EF	9.6%	8.0%	6.1%	6.1%	8.4%	14.2%	20.3%	27.7%
TRAVE	0.3%	-1.3%	-3.3%	-3.3%	-1.0%	4.9%	11.0%	18.4%
VAND	-3.1%	-4.8%	-6.7%	-6.7%	-4.4%	1.5%	7.6%	15.0%
Avg	1.7%	0.1%	-1.9%	-1.9%	0.5%	6.3%	12.4%	19.9%

Table A.17. Changes in 5-day maximum precipitation between 1970-1989 and 1990-2009, at various Michigan gauges, expressed as a percent difference.

5-day	0.5 yr	1 yr	2 yr	5 yr	10 yr	25 yr	50 yr	100 yr
BELL	6.7%	1.8%	-5.3%	-7.3%	-2.9%	8.6%	20.3%	**33.7%**
GLAD	1.6%	-3.2%	-10.4%	-12.4%	-8.0%	3.6%	15.3%	**28.8%**
GLENN	15.8%	10.9%	3.8%	1.8%	6.2%	17.7%	**29.3%**	**42.5%**
GRAY	-0.7%	-5.6%	-12.7%	-14.7%	-10.3%	1.2%	12.9%	**26.5%**
LAKE EF	9.9%	5.0%	-2.1%	-4.1%	0.3%	11.9%	23.5%	**36.9%**
TRAVE	3.6%	-1.2%	-8.3%	-10.3%	-6.0%	5.6%	17.3%	**30.8%**
VAND	2.2%	-2.6%	-9.7%	-11.8%	-7.4%	4.2%	15.9%	**29.4%**
Avg	5.5%	0.6%	-6.5%	-8.5%	-4.1%	7.5%	19.1%	**32.6%**

Table A.18. Changes in 10-day maximum precipitation between 1970-1989 and 1990-2009, at various Michigan gauges, expressed as a percent difference.

10-day	0.5 yr	1 yr	2 yr	5 yr	10 yr	25 yr	50 yr	100 yr
BELL	-0.7%	-2.5%	-6.0%	-8.6%	-7.8%	-3.3%	2.3%	9.7%
GLAD	3.0%	1.2%	-2.4%	-4.9%	-4.1%	0.3%	6.0%	13.3%
GLENN	10.7%	8.9%	5.4%	2.9%	3.6%	8.1%	13.7%	21.0%
GRAY	-4.4%	-6.2%	-9.8%	-12.3%	-11.5%	-7.0%	-1.4%	6.0%
LAKE EF	13.3%	11.5%	7.9%	5.4%	6.2%	10.7%	16.3%	23.6%
TRAVE	-8.1%	-9.9%	-13.5%	-16.0%	-15.2%	-10.8%	-5.1%	2.2%
VAND	-2.9%	-4.7%	-8.3%	-10.8%	-10.0%	-5.6%	0.1%	7.4%
Avg	1.6%	-0.2%	-3.8%	-6.3%	-5.5%	-1.1%	4.6%	11.9%

Table A.19. Changes in 1-hr maximum precipitation between 1970-1989 and 1990-2009, at various Illinois gauges, expressed as a percent difference.

1-hr	0.5 yr	1 yr	2 yr	5 yr	10 yr	25 yr	50 yr	100 yr
DAN	2.0%	-0.1%	-2.4%	-4.0%	-3.6%	-1.0%	2.4%	6.8%
HUT PP	-13.2%	-15.3%	-17.6%	-19.1%	-18.8%	-16.2%	-12.8%	-8.4%
PARIS	8.7%	6.7%	4.3%	2.8%	3.2%	5.8%	9.1%	13.6%
SHELBY	-12.1%	-14.2%	-16.5%	-18.0%	-17.6%	-15.0%	-11.7%	-7.3%
SULL	5.3%	3.2%	0.9%	-0.7%	-0.3%	2.3%	5.7%	10.1%
URB	12.6%	10.5%	8.2%	6.6%	7.0%	9.6%	13.0%	17.4%
BRAZIL	22.5%	20.5%	18.2%	16.6%	17.0%	19.6%	22.9%	27.3%
CLIN	-6.3%	-8.4%	-10.7%	-12.2%	-11.8%	-9.2%	-5.9%	-1.5%
Avg	2.5%	0.5%	-1.8%	-3.4%	-3.0%	-0.4%	3.0%	7.4%

Table A.20. Changes in 2-hr maximum precipitation between 1970-1989 and 1990-2009, at various Illinois gauges, expressed as a percent difference.

2-hr	0.5 yr	1 yr	2 yr	5 yr	10 yr	25 yr	50 yr	100 yr
DAN	5.1%	0.2%	-2.9%	-3.1%	-0.6%	5.7%	12.1%	19.8%
HUT PP	-6.3%	-11.2%	-14.3%	-14.5%	-12.0%	-5.7%	0.7%	8.4%
PARIS	6.9%	2.0%	-1.1%	-1.3%	1.2%	7.5%	13.9%	21.5%
SHELBY	-7.2%	-12.1%	-15.1%	-15.4%	-12.9%	-6.6%	-0.2%	7.5%
SULL	-0.2%	-5.1%	-8.2%	-8.4%	-5.9%	0.3%	6.8%	14.5%
URB	23.6%	18.8%	15.7%	15.5%	18.0%	24.2%	30.5%	**38.0%**
BRAZIL	23.4%	18.6%	15.5%	15.3%	17.8%	24.0%	30.3%	**37.8%**
CLIN	-12.3%	-17.2%	-20.2%	-20.4%	-18.0%	-11.7%	-5.3%	2.4%
Avg	4.1%	-0.8%	-3.9%	-4.2%	-1.6%	4.6%	11.0%	18.7%

Table A.21. Changes in 3-hr maximum precipitation between 1970-1989 and 1990-2009, at various Illinois gauges, expressed as a percent difference.

3-hr	0.5 yr	1 yr	2 yr	5 yr	10 yr	25 yr	50 yr	100 yr
DAN	2.9%	1.3%	-1.3%	-3.0%	-2.3%	1.2%	5.6%	11.3%
HUT PP	-4.7%	-6.3%	-8.9%	-10.6%	-9.9%	-6.4%	-2.0%	3.7%
PARIS	3.0%	1.4%	-1.2%	-2.9%	-2.2%	1.3%	5.7%	11.4%
SHELBY	-7.2%	-8.8%	-11.3%	-13.1%	-12.4%	-8.9%	-4.5%	1.3%
SULL	3.4%	1.9%	-0.7%	-2.4%	-1.8%	1.8%	6.2%	11.9%
URB	19.1%	17.6%	15.0%	13.3%	14.0%	17.5%	21.8%	27.5%
BRAZIL	19.9%	18.4%	15.8%	14.1%	14.8%	18.3%	22.6%	28.3%
CLIN	-10.8%	-12.4%	-14.9%	-16.7%	-16.0%	-12.5%	-8.1%	-2.3%
Avg	3.2%	1.6%	-0.9%	-2.7%	-2.0%	1.5%	5.9%	11.7%

Table A.22. Changes in 6-hr maximum precipitation between 1970-1989 and 1990-2009, at various Illinois gauges, expressed as a percent difference.

6-hr	0.5 yr	1 yr	2 yr	5 yr	10 yr	25 yr	50 yr	100 yr
DAN	6.3%	5.1%	3.1%	1.4%	1.4%	3.2%	5.9%	9.7%
HUT PP	3.1%	1.9%	-0.1%	-1.9%	-1.9%	0.0%	2.7%	6.5%
PARIS	5.6%	4.4%	2.4%	0.6%	0.6%	2.5%	5.2%	9.0%
SHELBY	-2.6%	-3.8%	-5.9%	-7.6%	-7.6%	-5.7%	-3.0%	0.7%
SULL	-1.9%	-3.1%	-5.1%	-6.9%	-6.9%	-5.0%	-2.3%	1.4%
URB	23.4%	22.3%	20.3%	18.5%	18.5%	20.4%	23.1%	26.7%
BRAZIL	19.4%	18.2%	16.2%	14.5%	14.5%	16.3%	19.0%	22.7%
CLIN	-9.0%	-10.1%	-12.2%	-13.9%	-13.9%	-12.0%	-9.3%	-5.6%
Avg	5.4%	4.3%	2.2%	0.5%	0.5%	2.3%	5.1%	8.8%

Table A.23. Changes in 12-hr maximum precipitation between 1970-1989 and 1990-2009, at various Illinois gauges, expressed as a percent difference.

12-hr	0.5 yr	1 yr	2 yr	5 yr	10 yr	25 yr	50 yr	100 yr
DAN	7.9%	6.1%	7.2%	8.9%	9.2%	7.6%	5.0%	1.4%
HUT PP	-0.6%	-2.5%	-1.3%	0.4%	0.7%	-0.9%	-3.5%	-7.2%
PARIS	7.2%	5.3%	6.4%	8.2%	8.4%	6.8%	4.3%	0.6%
SHELBY	-1.0%	-2.9%	-1.8%	0.0%	0.2%	-1.4%	-3.9%	-7.6%
SULL	-1.3%	-3.2%	-2.0%	-0.3%	0.0%	-1.6%	-4.2%	-7.9%
URB	12.9%	11.0%	12.1%	13.9%	14.1%	12.6%	10.0%	6.3%
BRAZIL	**28.2%**	**26.3%**	**27.5%**	**29.2%**	29.4%	27.9%	25.4%	21.7%
CLIN	-6.3%	-8.2%	-7.0%	-5.3%	-5.0%	-6.6%	-9.2%	-12.9%
Avg	6.0%	4.1%	5.2%	7.0%	7.2%	5.7%	3.1%	-0.6%

Table A.24. Changes in 24-hr maximum precipitation between 1970-1989 and 1990-2009, at various Illinois gauges, expressed as a percent difference.

24-hr	0.5 yr	1 yr	2 yr	5 yr	10 yr	25 yr	50 yr	100 yr
DAN	10.3%	9.7%	10.1%	10.0%	8.7%	5.3%	1.5%	-3.3%
HUT PP	-0.9%	-1.4%	-1.0%	-1.2%	-2.5%	-5.9%	-9.7%	-14.5%
PARIS	9.5%	9.0%	9.4%	9.2%	7.9%	4.5%	0.7%	-4.1%
SHELBY	1.9%	1.3%	1.7%	1.5%	0.3%	-3.2%	-7.0%	-11.8%
SULL	3.0%	2.5%	2.8%	2.7%	1.4%	-2.0%	-5.8%	-10.6%
URB	15.7%	15.2%	15.5%	15.4%	14.1%	10.7%	6.9%	2.1%
BRAZIL	**21.8%**	**21.3%**	**21.6%**	**21.5%**	20.2%	16.8%	13.1%	8.3%
CLIN	0.9%	0.3%	0.7%	0.6%	-0.7%	-4.1%	-7.9%	-12.7%
Avg	7.9%	7.3%	7.7%	7.6%	6.3%	2.9%	-0.9%	-5.7%

Table A.25. Changes in 2-day maximum precipitation between 1970-1989 and 1990-2009, at various Illinois gauges, expressed as a percent difference.

2-day	0.5 yr	1 yr	2 yr	5 yr	10 yr	25 yr	50 yr	100 yr
DAN	8.4%	8.1%	7.8%	7.3%	6.9%	6.4%	6.0%	5.6%
HUT PP	10.0%	9.7%	9.4%	8.9%	8.5%	8.0%	7.6%	7.2%
PARIS	9.8%	9.4%	9.1%	8.6%	8.3%	7.7%	7.3%	6.9%
SHELBY	7.6%	7.3%	6.9%	6.5%	6.1%	5.6%	5.2%	4.8%
SULL	1.5%	1.2%	0.9%	0.4%	0.0%	-0.5%	-0.9%	-1.3%
URB	11.3%	11.0%	10.6%	10.2%	9.8%	9.3%	8.9%	8.5%
BRAZIL	**28.9%**	**28.6%**	**28.2%**	**27.8%**	27.4%	26.9%	26.5%	26.1%
CLIN	-1.5%	-1.8%	-2.2%	-2.6%	-3.0%	-3.5%	-3.9%	-4.4%
Avg	9.7%	9.4%	9.0%	8.6%	8.2%	7.7%	7.3%	6.8%

Table A.26. Changes in 5-day maximum precipitation between 1970-1989 and 1990-2009, at various Illinois gauges, expressed as a percent difference.

5-day	0.5 yr	1 yr	2 yr	5 yr	10 yr	25 yr	50 yr	100 yr
DAN	6.0%	5.6%	4.3%	2.0%	-0.1%	-3.3%	-6.0%	-9.0%
HUT PP	**25.3%**	**24.9%**	23.7%	21.4%	19.3%	16.1%	13.4%	10.5%
PARIS	7.4%	7.0%	5.7%	3.4%	1.3%	-1.9%	-4.6%	-7.5%
SHELBY	5.7%	5.3%	4.1%	1.8%	-0.4%	-3.6%	-6.3%	-9.2%
SULL	1.9%	1.5%	0.3%	-2.0%	-4.1%	-7.4%	-10.1%	-13.0%
URB	19.6%	19.2%	17.9%	15.6%	13.5%	10.3%	7.6%	4.7%
BRAZIL	**34.7%**	**34.3%**	**33.1%**	**30.9%**	28.8%	25.6%	23.0%	20.1%
CLIN	4.6%	4.2%	3.0%	0.7%	-1.4%	-4.7%	-7.4%	-10.3%
Avg	13.6%	13.2%	11.9%	9.6%	7.5%	4.3%	1.6%	-1.4%

Table A.27. Changes in 10-day maximum precipitation between 1970-1989 and 1990-2009, at various Illinois gauges, expressed as a percent difference.

10-day	0.5 yr	1 yr	2 yr	5 yr	10 yr	25 yr	50 yr	100 yr
DAN	9.4%	10.4%	8.9%	6.1%	4.2%	2.1%	0.8%	-0.3%
HUT PP	**21.0%**	**21.9%**	20.4%	17.7%	15.8%	13.7%	12.4%	11.3%
PARIS	-0.5%	0.4%	-1.1%	-3.9%	-5.8%	-7.9%	-9.2%	-10.3%
SHELBY	-2.6%	-1.6%	-3.2%	-5.9%	-7.8%	-9.9%	-11.3%	-12.4%
SULL	-4.0%	-3.1%	-4.6%	-7.3%	-9.3%	-11.4%	-12.7%	-13.8%
URB	7.0%	7.9%	6.4%	3.7%	1.8%	-0.4%	-1.7%	-2.8%
BRAZIL	**25.0%**	**25.9%**	**24.4%**	21.7%	19.9%	17.7%	16.4%	15.3%
CLIN	2.0%	2.9%	1.4%	-1.3%	-3.2%	-5.4%	-6.7%	-7.8%
Avg	7.4%	8.3%	6.8%	4.1%	2.2%	0.0%	-1.3%	-2.4%

Appendix B: Additional Data from Chapter 5

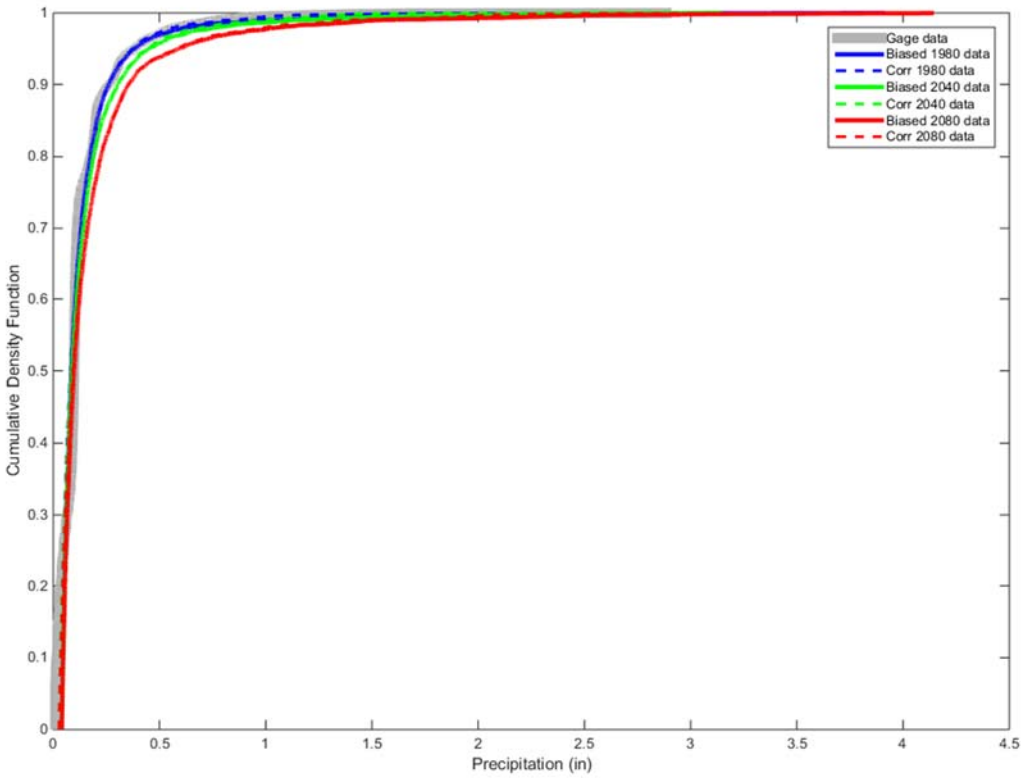

Figure B.1. eCDFs of observed, and raw and corrected model (IPSL) simulation and model projections at Columbus, IN using quantile mapping.

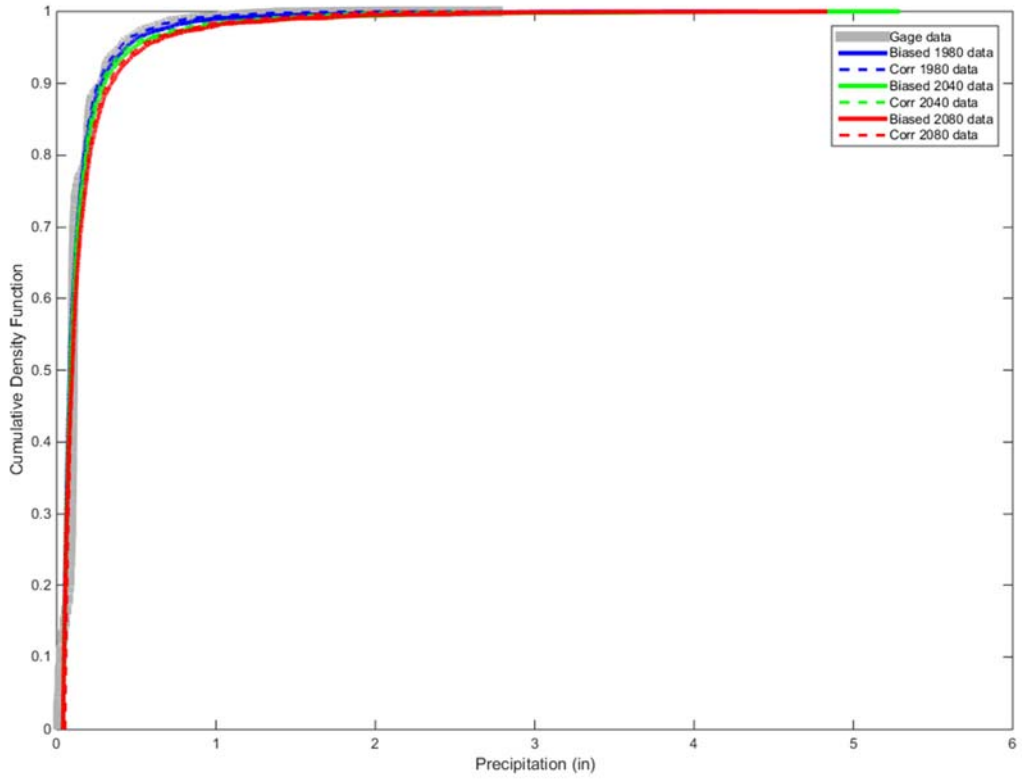

.

Figure B.2. eCDFs of observed, and raw and corrected model (IPSL) simulation and model projections at Grayling, MI using quantile mapping.

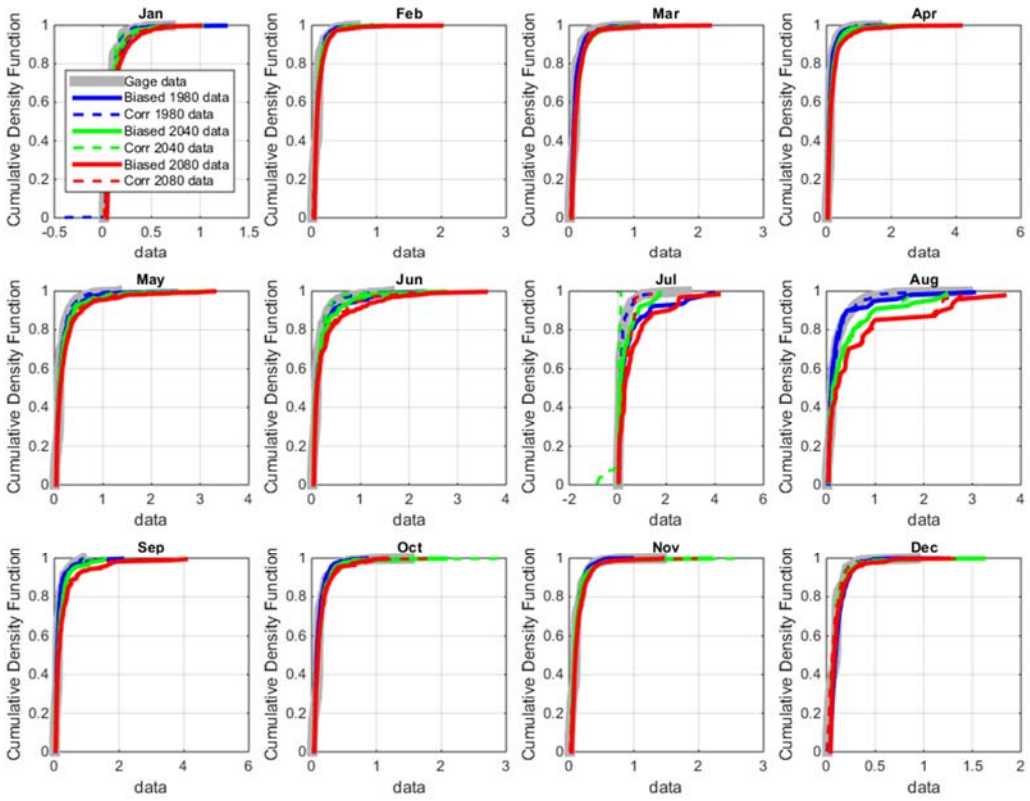

Figure B.3. Monthly eCDFs of observed, and raw and corrected model (IPSL) simulation and model projections at Columbus, IN using quantile mapping.

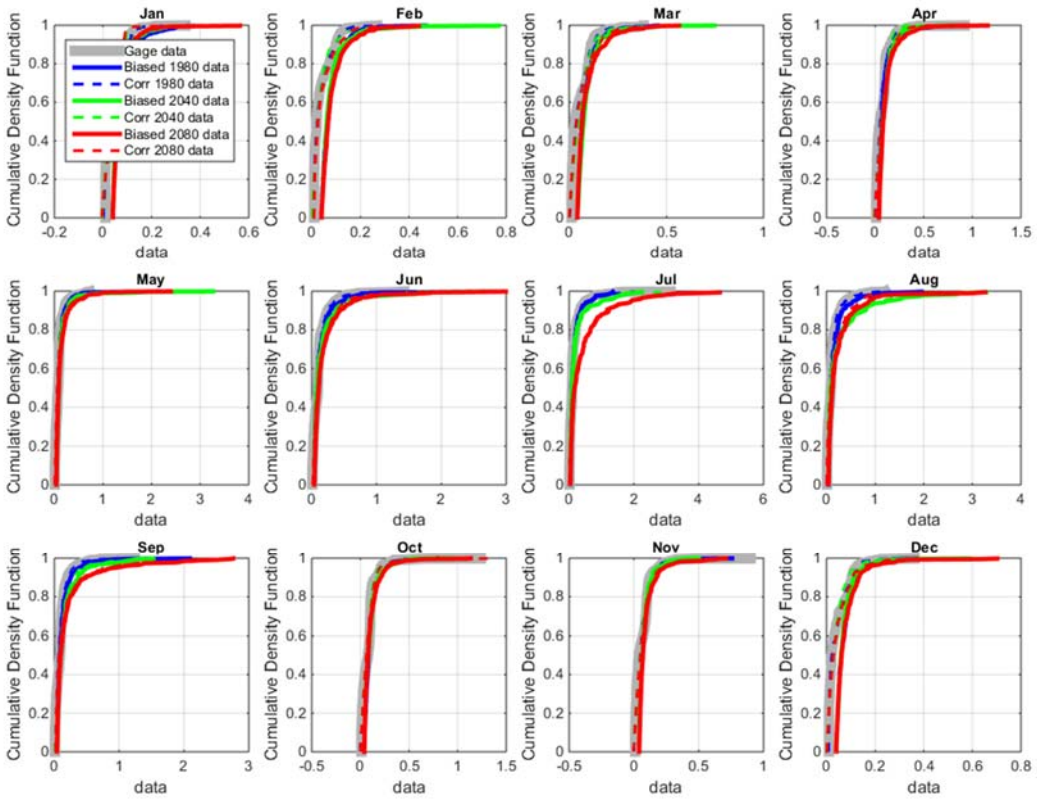

Figure B.4. Monthly eCDFs of observed, and raw and corrected model (IPSL) simulation and model projections at Grayling, MI using quantile mapping.

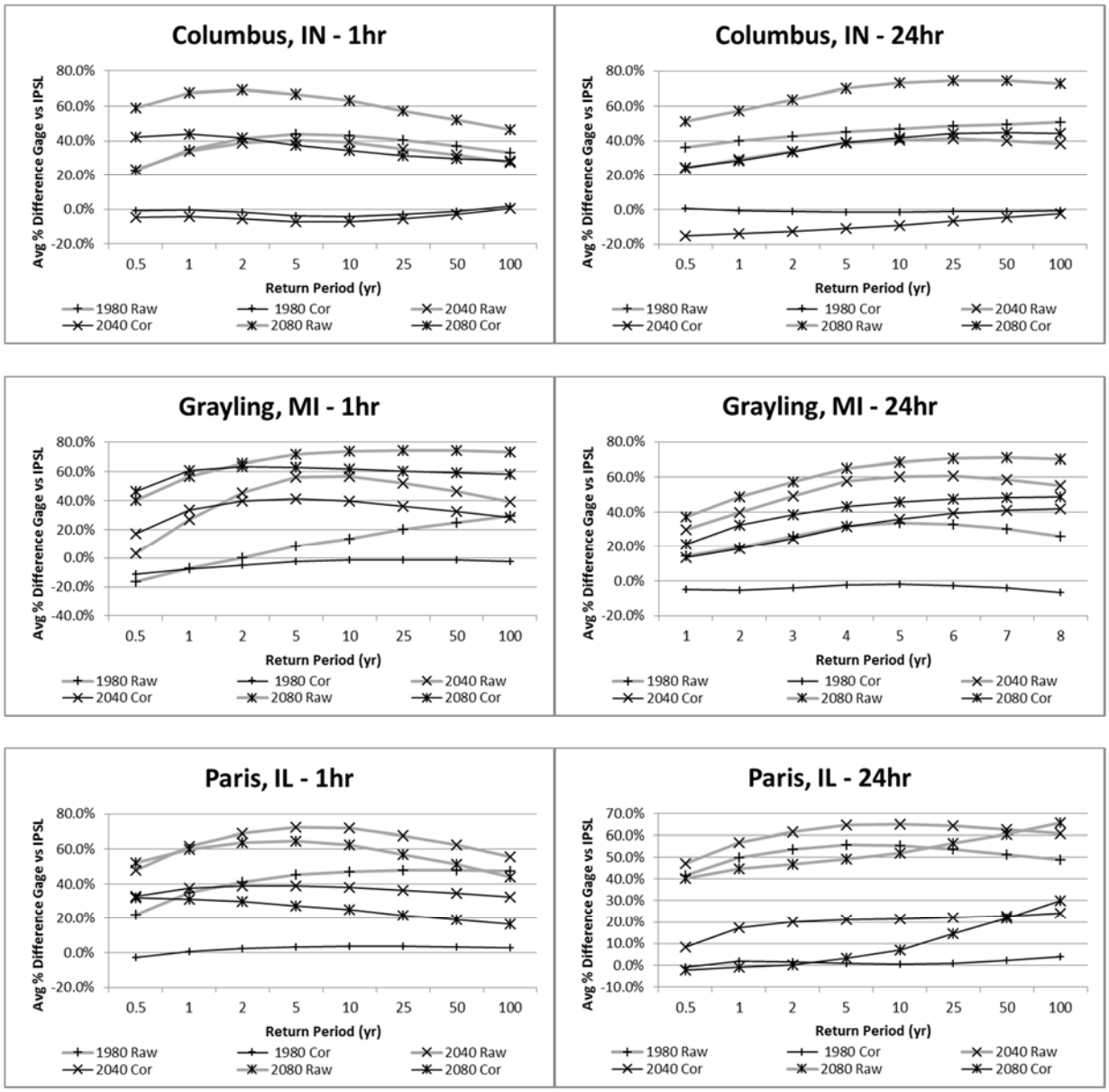

Figure B.5. Average percent difference between observed (Gauge) and modeled (IPSL) simulation (1980-1999) and projections (2040-2059 and 2080-2099) estimated maximum precipitation for selected durations and return periods as determined by L-moments regional frequency analysis. Gauge data time frame is 1980-1999.

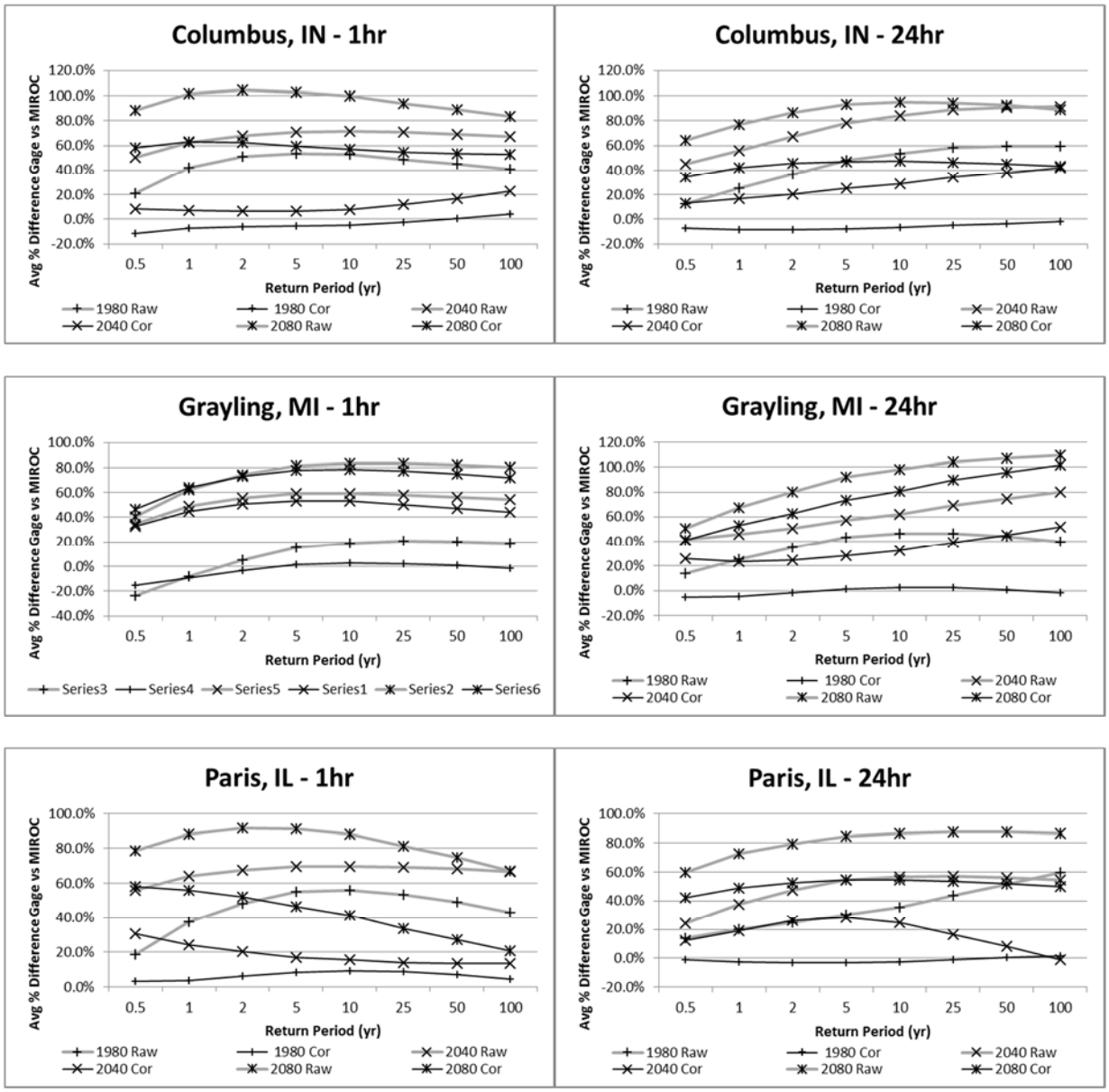

Figure B.6. Average percent difference between observed (Gauge) and modeled (MIROC) simulation (1980-1999) and projections (2040-2059 and 2080-2099) estimated maximum precipitation for selected durations and return periods as determined by L-moments regional frequency analysis. Gauge data time frame is 1980-1999.

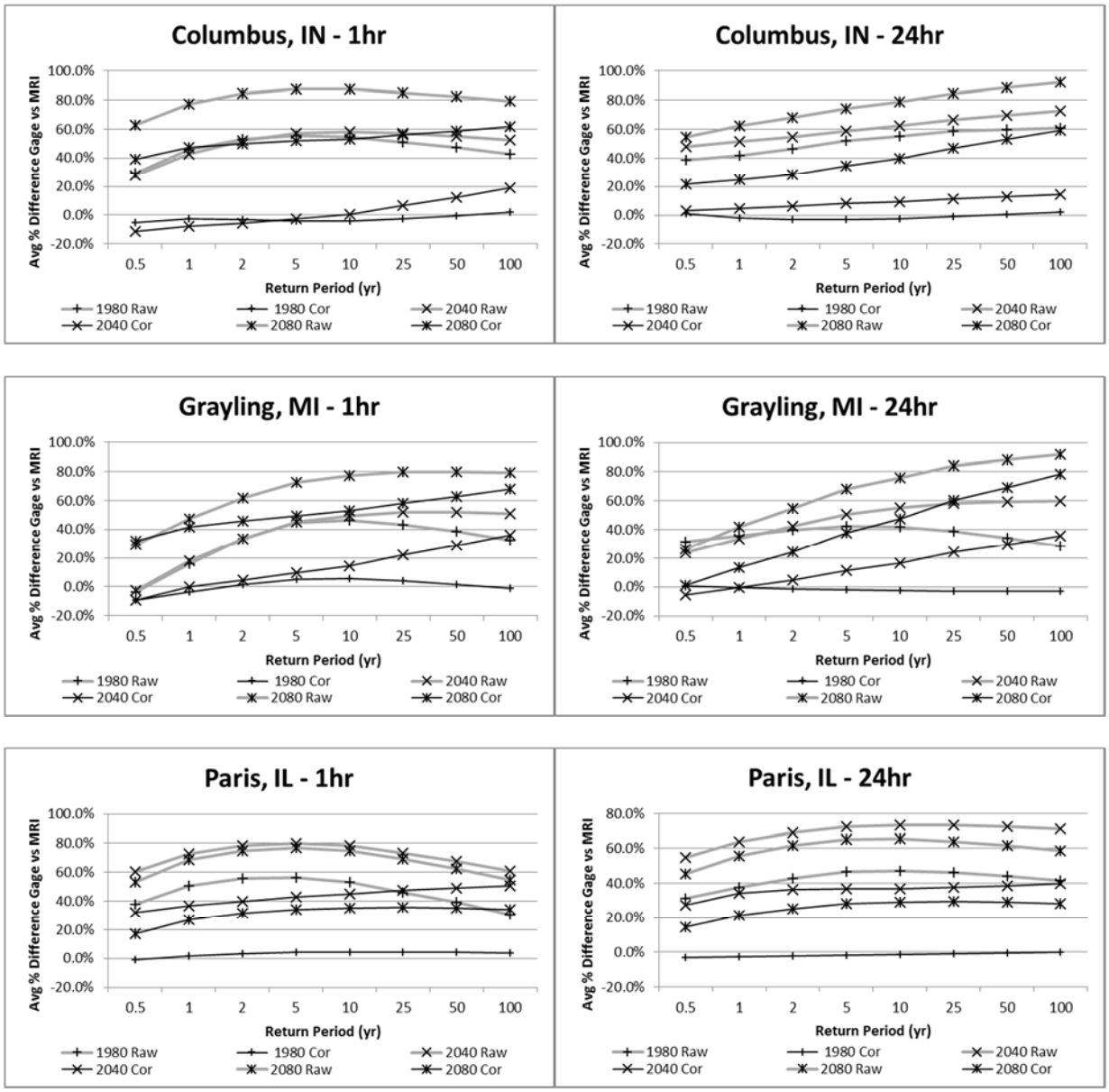

Figure B.7. Average percent difference between observed (Gauge) and modeled (MRI) simulation (1980-1999) and projections (2040-2059 and 2080-2099) estimated maximum precipitation for selected durations and return periods as determined by L-moments regional frequency analysis. Gauge data time frame is 1980-1999.

Table B.1. Changes in precipitation frequency estimates between observed (1980-1999) and projected CNRM (2040-2059 and 2080-2099) values, as determined by L-moments regional frequency analysis for Columbus, IN, expressed as a percent difference. Highlighted values are significant.

2040-2059								
Columbus, IN	0.5 yr	1 yr	2 yr	5 yr	10 yr	25 yr	50 yr	100 yr
1-hr	-5.7%	-2.1%	-2.3%	-3.6%	-4.1%	-3.6%	-2.3%	-0.4%
2-hr	4.5%	2.5%	2.0%	2.5%	3.4%	5.1%	6.8%	8.7%
3-hr	5.7%	4.7%	5.1%	6.8%	8.7%	11.8%	14.6%	17.6%
6-hr	4.3%	7.1%	8.4%	9.2%	9.4%	9.4%	9.1%	8.7%
12-hr	-0.1%	0.9%	1.6%	2.3%	2.9%	3.5%	4.0%	4.4%
24-hr	-6.1%	-2.3%	-2.1%	-4.1%	-6.6%	-10.9%	-14.8%	-19.2%
2-day	-18.6%	-14.9%	-11.6%	-9.4%	-9.5%	-11.8%	-14.8%	-18.8%
5-day	-23.3%	-20.3%	-17.2%	-11.4%	-5.4%	5.0%	14.2%	24.6%
10-day	-3.9%	-2.3%	-5.3%	-3.3%	3.3%	17.0%	**29.4%**	**43.0%**
2080-2099								
Columbus, IN	0.5 yr	1 yr	2 yr	5 yr	10 yr	25 yr	50 yr	100 yr
1-hr	**65.2%**	**61.1%**	**56.9%**	**52.7%**	**51.0%**	**50.7%**	**51.8%**	**53.9%**
2-hr	**68.1%**	**64.4%**	**62.0%**	**59.9%**	**58.8%**	**57.7%**	**57.1%**	**56.8%**
3-hr	**67.6%**	**64.7%**	**63.6%**	**63.7%**	**64.4%**	**66.2%**	**67.9%**	**70.0%**
6-hr	**50.7%**	**50.2%**	**51.9%**	**55.8%**	**59.5%**	**65.4%**	**70.3%**	**75.5%**
12-hr	32.3%	**38.4%**	**45.1%**	**54.3%**	**61.6%**	**71.4%**	**78.9%**	**86.5%**
24-hr	27.3%	31.3%	**36.6%**	**44.6%**	**51.3%**	**60.7%**	**68.0%**	**75.6%**
2-day	28.0%	30.2%	**35.6%**	**44.7%**	**52.7%**	**64.4%**	**73.6%**	**83.1%**
5-day	23.8%	27.3%	**32.7%**	**42.7%**	**52.4%**	**67.7%**	**80.3%**	**93.4%**
10-day	**33.2%**	**36.2%**	**36.5%**	**42.4%**	**50.7%**	**64.2%**	**75.0%**	**85.8%**

Table B.2. Changes in precipitation frequency estimates between observed (1980-1999) and projected CNRM (2040-2059 and 2080-2099) values, as determined by L-moments regional frequency analysis for Grayling, MI, expressed as a percent difference. Highlighted values are significant.

2040-2059								
Grayling, MI	0.5 yr	1 yr	2 yr	5 yr	10 yr	25 yr	50 yr	100 yr
1-hr	0.8%	10.5%	12.2%	9.3%	5.2%	-1.4%	-6.9%	-12.6%
2-hr	3.2%	11.0%	14.8%	15.2%	12.6%	6.3%	-0.1%	-7.8%
3-hr	-2.2%	0.7%	1.2%	0.4%	-0.8%	-3.2%	-5.3%	-7.8%
6-hr	1.0%	9.8%	13.4%	15.0%	14.7%	12.8%	10.6%	7.7%
12-hr	-13.6%	-7.0%	-3.2%	0.1%	1.8%	3.5%	4.3%	4.9%
24-hr	-12.7%	-5.1%	-0.8%	2.9%	4.9%	6.7%	7.7%	8.4%
2-day	-13.4%	-3.1%	2.1%	5.6%	6.9%	7.3%	6.8%	5.8%
5-day	-2.0%	3.3%	3.6%	1.9%	0.5%	-0.8%	-1.3%	-1.3%
10-day	-13.2%	0.0%	5.3%	8.4%	10.3%	13.2%	15.7%	18.5%
2080-2099								
Grayling, MI	0.5 yr	1 yr	2 yr	5 yr	10 yr	25 yr	50 yr	100 yr
1-hr	29.6%	**40.4%**	**42.4%**	**31.4%**	18.4%	-0.4%	-14.3%	**-27.5%**
2-hr	**40.7%**	**43.9%**	**43.8%**	**39.6%**	**33.8%**	23.3%	13.6%	2.5%
3-hr	**31.6%**	**33.9%**	**32.9%**	**27.5%**	20.7%	8.5%	-2.5%	-14.9%
6-hr	**41.8%**	**41.0%**	**39.3%**	**36.4%**	**33.9%**	30.0%	26.7%	23.2%
12-hr	**37.4%**	**37.8%**	**37.1%**	**35.4%**	**33.6%**	30.8%	28.4%	25.7%
24-hr	**36.0%**	**34.3%**	**32.3%**	**29.4%**	**27.1%**	23.6%	20.9%	18.0%
2-day	**40.3%**	**35.6%**	**32.1%**	**28.6%**	26.4%	23.8%	22.2%	20.8%
5-day	**39.0%**	**33.0%**	28.1%	23.9%	22.8%	24.0%	26.8%	31.1%
10-day	23.0%	**27.1%**	25.9%	24.3%	25.2%	29.8%	**35.5%**	**42.9%**

Table B.3. Changes in precipitation frequency estimates between observed (1980-1999) and projected CNRM (2040-2059 and 2080-2099) values, as determined by L-moments regional frequency analysis for Paris, IL, expressed as a percent difference. Highlighted values are significant.

2040-2059								
Paris, IL	0.5 yr	1 yr	2 yr	5 yr	10 yr	25 yr	50 yr	100 yr
1-hr	10.7%	14.9%	17.8%	20.8%	22.8%	25.1%	26.7%	28.3%
2-hr	6.8%	10.5%	12.8%	16.4%	20.4%	27.6%	34.2%	**41.8%**
3-hr	22.1%	24.2%	27.2%	31.8%	35.6%	41.0%	**45.2%**	**49.6%**
6-hr	19.2%	23.4%	26.4%	29.7%	32.0%	34.8%	36.8%	38.8%
12-hr	9.2%	21.8%	26.2%	28.5%	30.1%	32.9%	35.9%	39.6%
24-hr	9.4%	18.8%	22.4%	24.6%	26.0%	28.2%	30.2%	32.7%
2-day	1.9%	10.7%	15.8%	21.2%	25.5%	32.2%	**37.9%**	**44.3%**
5-day	-3.6%	-1.3%	3.5%	10.1%	14.5%	19.4%	22.2%	24.4%
10-day	2.2%	-6.5%	-3.5%	6.8%	15.1%	25.2%	31.8%	37.6%
2080-2099								
Paris, IL	0.5 yr	1 yr	2 yr	5 yr	10 yr	25 yr	50 yr	100 yr
1-hr	**63.3%**	**57.8%**	**53.0%**	**47.0%**	**42.6%**	**36.5%**	31.9%	27.1%
2-hr	**54.5%**	**49.2%**	**43.3%**	**36.4%**	**32.5%**	**28.9%**	27.4%	26.6%
3-hr	**54.2%**	**50.0%**	**44.5%**	**36.4%**	**29.8%**	20.1%	12.3%	3.9%
6-hr	**44.3%**	**40.6%**	**34.0%**	**23.9%**	15.3%	2.9%	-7.1%	-17.6%
12-hr	**36.6%**	**35.6%**	**29.8%**	20.3%	13.5%	5.4%	0.3%	-4.2%
24-hr	**30.9%**	**30.3%**	**28.4%**	**26.3%**	25.7%	26.3%	27.9%	30.3%
2-day	**26.3%**	22.6%	20.4%	20.3%	22.5%	28.4%	34.9%	43.0%
5-day	22.0%	18.4%	16.7%	15.6%	15.3%	15.6%	16.1%	16.9%
10-day	23.1%	17.5%	15.6%	17.5%	21.6%	29.9%	**37.8%**	**46.7%**

Table B.4. Changes in precipitation frequency estimates between observed (1980-1999) and projected IPSL (2040-2059 and 2080-2099) values, as determined by L-moments regional frequency analysis for Columbus, IN, expressed as a percent difference. Highlighted values are significant.

2040-2059								
Columbus, IN	0.5 yr	1 yr	2 yr	5 yr	10 yr	25 yr	50 yr	100 yr
1-hr	-4.5%	-4.2%	-5.6%	-7.0%	-7.0%	-5.3%	-2.9%	0.5%
2-hr	-8.5%	-9.6%	-9.4%	-8.2%	-6.8%	-4.5%	-2.4%	0.0%
3-hr	-4.3%	0.6%	2.9%	4.3%	4.7%	4.5%	4.0%	3.2%
6-hr	-10.0%	-8.8%	-6.7%	-3.3%	-0.4%	3.8%	7.3%	10.9%
12-hr	-10.7%	-11.3%	-10.6%	-8.8%	-7.0%	-4.0%	-1.4%	1.6%
24-hr	-15.2%	-14.2%	-12.8%	-10.8%	-9.1%	-6.6%	-4.5%	-2.4%
2-day	-19.5%	-21.8%	-16.6%	-8.5%	-4.1%	-1.1%	-0.7%	-1.6%
5-day	-9.5%	-12.3%	-14.0%	-13.6%	-11.4%	-5.9%	-0.2%	6.7%
10-day	-1.8%	-10.0%	-14.8%	-13.1%	-7.9%	1.5%	9.2%	17.0%
2080-2099								
Columbus, IN	0.5 yr	1 yr	2 yr	5 yr	10 yr	25 yr	50 yr	100 yr
1-hr	**42.2%**	**44.1%**	**41.8%**	**37.5%**	**34.6%**	31.5%	29.8%	28.6%
2-hr	**38.7%**	**40.4%**	**40.4%**	**39.1%**	**37.7%**	35.1%	32.8%	30.3%
3-hr	**44.6%**	**46.1%**	**47.0%**	**48.0%**	**48.7%**	**49.4%**	**49.9%**	**50.4%**
6-hr	**33.1%**	**33.0%**	**33.8%**	**35.5%**	**37.1%**	**39.5%**	**41.6%**	43.9%
12-hr	**33.4%**	**32.1%**	**32.0%**	**32.7%**	**33.8%**	**35.6%**	**37.4%**	39.4%
24-hr	24.5%	**28.6%**	**33.5%**	**39.0%**	**42.0%**	**44.3%**	44.9%	44.6%
2-day	27.3%	**32.5%**	**41.1%**	**51.7%**	**58.1%**	**64.4%**	**67.7%**	**69.9%**
5-day	**26.3%**	**26.5%**	**27.8%**	**32.0%**	**37.2%**	**46.5%**	**55.0%**	**64.4%**
10-day	**44.4%**	**42.8%**	**41.7%**	**45.2%**	**50.7%**	**59.5%**	**66.4%**	**73.2%**

Table B.5. Changes in precipitation frequency estimates between observed (1980-1999) and projected IPSL (2040-2059 and 2080-2099) values, as determined by L-moments regional frequency analysis for Grayling, MI, expressed as a percent difference. Highlighted values are significant.

2040-2059								
Grayling, MI	0.5 yr	1 yr	2 yr	5 yr	10 yr	25 yr	50 yr	100 yr
1-hr	17.3%	**33.8%**	**39.8%**	**41.2%**	**39.7%**	35.9%	32.4%	28.4%
2-hr	18.9%	30.8%	**35.0%**	**36.4%**	**35.9%**	33.8%	31.4%	28.4%
3-hr	14.9%	30.1%	**37.3%**	**39.9%**	**38.2%**	32.2%	25.4%	16.8%
6-hr	10.5%	21.7%	29.4%	37.3%	**42.2%**	**47.8%**	51.6%	55.0%
12-hr	16.2%	20.4%	24.2%	28.7%	32.1%	36.6%	39.9%	43.3%
24-hr	13.6%	18.7%	24.7%	**31.7%**	**35.7%**	**39.4%**	41.1%	41.9%
2-day	12.2%	19.2%	25.1%	**30.7%**	**32.9%**	33.5%	32.3%	30.0%
5-day	8.9%	11.4%	12.7%	15.0%	17.8%	23.3%	28.7%	35.1%
10-day	8.9%	23.0%	29.3%	33.9%	37.0%	41.5%	45.2%	49.3%
2080-2099								
Grayling, MI	0.5 yr	1 yr	2 yr	5 yr	10 yr	25 yr	50 yr	100 yr
1-hr	**46.4%**	**60.8%**	**63.7%**	**63.0%**	**61.8%**	**60.1%**	**59.1%**	**58.2%**
2-hr	**45.6%**	**57.9%**	**64.4%**	**67.6%**	**67.1%**	**63.4%**	**58.7%**	52.5%
3-hr	31.2%	**46.7%**	**54.6%**	**58.3%**	**57.7%**	**53.2%**	**47.7%**	40.5%
6-hr	27.2%	**46.0%**	**56.5%**	**63.4%**	**64.9%**	**63.2%**	**59.6%**	54.3%
12-hr	21.7%	**38.7%**	**47.8%**	**52.9%**	**53.2%**	**50.3%**	**46.2%**	40.7%
24-hr	21.5%	**32.6%**	**38.6%**	**43.3%**	**45.6%**	**47.6%**	**48.5%**	48.9%
2-day	8.2%	17.4%	27.3%	**35.9%**	**38.6%**	**38.0%**	34.9%	30.1%
5-day	10.2%	15.1%	18.3%	22.4%	26.4%	33.3%	39.6%	46.7%
10-day	16.2%	21.2%	22.0%	23.8%	27.7%	36.8%	**46.1%**	**57.1%**

Table B.6. Changes in precipitation frequency estimates between observed (1980-1999) and projected IPSL (2040-2059 and 2080-2099) values, as determined by L-moments regional frequency analysis for Paris, IL, expressed as a percent difference. Highlighted values are significant.

2040-2059								
Paris, IL	0.5 yr	1 yr	2 yr	5 yr	10 yr	25 yr	50 yr	100 yr
1-hr	**32.9%**	**37.4%**	**38.9%**	**39.0%**	**38.2%**	36.4%	34.6%	32.4%
2-hr	**36.1%**	**44.2%**	**45.8%**	**43.6%**	**40.3%**	**34.8%**	30.2%	25.4%
3-hr	29.6%	**34.9%**	**39.0%**	**41.0%**	**40.1%**	35.9%	30.9%	24.6%
6-hr	23.6%	29.4%	**32.9%**	**33.4%**	**30.9%**	24.5%	17.9%	10.0%
12-hr	16.3%	26.8%	30.1%	29.5%	27.2%	23.0%	19.2%	15.2%
24-hr	8.4%	17.2%	20.0%	21.0%	21.3%	22.0%	22.9%	24.1%
2-day	3.4%	10.9%	13.6%	15.4%	16.7%	19.0%	21.3%	24.0%
5-day	21.6%	**23.8%**	**25.9%**	**28.6%**	**30.6%**	**33.5%**	35.6%	37.9%
10-day	20.2%	17.4%	20.0%	**26.8%**	**32.8%**	**41.2%**	**47.3%**	**53.4%**
2080-2099								
Paris, IL	0.5 yr	1 yr	2 yr	5 yr	10 yr	25 yr	50 yr	100 yr
1-hr	**31.9%**	**31.2%**	**29.7%**	27.2%	25.1%	21.9%	19.2%	16.4%
2-hr	22.2%	21.1%	17.6%	13.1%	10.6%	8.7%	8.2%	8.5%
3-hr	20.3%	20.2%	21.0%	22.7%	24.3%	26.8%	28.9%	31.1%
6-hr	8.3%	6.9%	7.6%	10.0%	12.4%	16.4%	19.8%	23.6%
12-hr	10.8%	13.8%	14.7%	16.6%	19.6%	26.4%	33.2%	41.5%
24-hr	-2.2%	-1.0%	0.3%	3.3%	7.1%	14.6%	21.7%	30.1%
2-day	-10.5%	-7.4%	-5.0%	-0.7%	3.9%	12.0%	19.5%	28.2%
5-day	3.8%	6.5%	8.2%	9.8%	10.8%	12.0%	12.7%	13.4%
10-day	0.7%	1.6%	1.5%	2.6%	4.7%	9.0%	13.0%	17.5%

Table B.7. Changes in precipitation frequency estimates between observed (1980-1999) and projected MIROC (2040-2059 and 2080-2099) values, as determined by L-moments regional frequency analysis for Columbus, IN, expressed as a percent difference. Highlighted values are significant.

2040-2059								
Columbus, IN	0.5 yr	1 yr	2 yr	5 yr	10 yr	25 yr	50 yr	100 yr
1-hr	8.1%	7.4%	6.4%	6.4%	7.9%	12.2%	16.9%	22.7%
2-hr	5.8%	6.7%	7.3%	7.8%	8.1%	8.4%	8.6%	8.7%
3-hr	16.9%	14.3%	12.8%	11.5%	10.9%	10.3%	10.1%	10.0%
6-hr	18.1%	14.5%	14.2%	16.2%	19.0%	24.1%	**28.8%**	**34.1%**
12-hr	16.4%	23.4%	28.4%	33.9%	37.5%	42.0%	45.1%	48.2%
24-hr	13.0%	16.6%	20.2%	25.1%	28.8%	34.1%	38.1%	42.3%
2-day	4.4%	5.8%	8.2%	11.9%	15.1%	19.9%	23.7%	27.8%
5-day	5.5%	5.8%	8.1%	14.2%	21.3%	33.5%	44.3%	56.4%
10-day	4.7%	4.4%	1.0%	1.2%	4.8%	12.4%	19.1%	26.1%
2080-2099								
Columbus, IN	0.5 yr	1 yr	2 yr	5 yr	10 yr	25 yr	50 yr	100 yr
1-hr	**58.2%**	**62.9%**	**62.2%**	**59.3%**	**57.2%**	**54.8%**	**53.6%**	**52.7%**
2-hr	**61.2%**	**66.9%**	**68.7%**	**68.7%**	**67.6%**	**65.2%**	**62.9%**	**60.0%**
3-hr	**58.0%**	**64.3%**	**66.0%**	**65.5%**	**63.9%**	**60.7%**	**57.6%**	**53.9%**
6-hr	**49.8%**	**57.1%**	**59.7%**	**60.6%**	**60.2%**	**58.7%**	**57.0%**	**54.9%**
12-hr	**41.3%**	**47.8%**	**51.1%**	**53.7%**	**54.7%**	**55.5%**	**55.6%**	**55.3%**
24-hr	**34.5%**	**42.1%**	**45.4%**	**47.0%**	**47.2%**	**46.3%**	**45.1%**	**43.4%**
2-day	**26.9%**	**32.0%**	**38.1%**	**44.5%**	**47.6%**	**49.6%**	**49.8%**	**49.1%**
5-day	**28.7%**	**31.8%**	**32.2%**	**32.8%**	**34.0%**	**36.9%**	**39.9%**	**43.5%**
10-day	16.0%	**23.9%**	**26.4%**	**24.5%**	21.9%	18.6%	16.6%	15.1%

Table B.8. Changes in precipitation frequency estimates between observed (1980-1999) and projected MIROC (2040-2059 and 2080-2099) values, as determined by L-moments regional frequency analysis for Grayling, MI, expressed as a percent difference. Highlighted values are significant.

2040-2059								
Grayling, MI	0.5 yr	1 yr	2 yr	5 yr	10 yr	25 yr	50 yr	100 yr
1-hr	**33.0%**	**44.6%**	**50.8%**	**53.5%**	**53.0%**	**50.4%**	**47.5%**	**44.0%**
2-hr	**39.3%**	**51.4%**	**60.4%**	**67.5%**	**69.9%**	**69.9%**	**68.0%**	**64.8%**
3-hr	**26.1%**	**31.0%**	**35.6%**	**41.2%**	**45.5%**	**51.0%**	**55.2%**	**59.3%**
6-hr	**32.4%**	**39.5%**	**45.2%**	**51.6%**	**56.1%**	**61.7%**	**65.7%**	**69.5%**
12-hr	**33.1%**	**33.1%**	**35.0%**	**38.8%**	**42.5%**	**48.2%**	**53.0%**	**58.2%**
24-hr	**25.6%**	**23.8%**	**24.8%**	**28.5%**	**32.5%**	**39.2%**	**45.1%**	**51.6%**
2-day	22.8%	19.2%	19.0%	21.7%	**25.5%**	**32.3%**	**38.5%**	**45.6%**
5-day	22.2%	22.3%	22.9%	**25.6%**	**29.5%**	**37.1%**	**44.4%**	**52.9%**
10-day	11.7%	16.0%	21.9%	**28.5%**	**32.2%**	**35.7%**	**37.6%**	**39.0%**
2080-2099								
Grayling, MI	0.5 yr	1 yr	2 yr	5 yr	10 yr	25 yr	50 yr	100 yr
1-hr	**46.5%**	**64.1%**	**73.0%**	**77.7%**	**78.4%**	**76.9%**	**74.8%**	**72.0%**
2-hr	**52.2%**	**71.0%**	**82.3%**	**89.3%**	**90.7%**	**88.8%**	**85.4%**	**80.4%**
3-hr	**54.4%**	**67.1%**	**76.0%**	**83.5%**	**86.7%**	**88.5%**	**88.2%**	**86.8%**
6-hr	**46.7%**	**62.2%**	**70.5%**	**77.0%**	**80.2%**	**82.9%**	**84.1%**	**84.7%**
12-hr	**51.7%**	**60.7%**	**67.4%**	**74.7%**	**79.6%**	**85.6%**	**89.9%**	**94.0%**
24-hr	**41.2%**	**53.2%**	**62.7%**	**73.2%**	**80.4%**	**89.4%**	**95.7%**	**101.9%**
2-day	**46.4%**	**53.0%**	**58.7%**	**65.6%**	**70.5%**	**76.9%**	**81.6%**	**86.3%**
5-day	**38.3%**	**47.0%**	**51.6%**	**56.0%**	**59.5%**	**64.8%**	**69.5%**	**74.6%**
10-day	**36.9%**	**47.0%**	**49.2%**	**50.2%**	**52.2%**	**57.0%**	**62.3%**	**68.8%**

Table B.9. Changes in precipitation frequency estimates between observed (1980-1999) and projected MIROC (2040-2059 and 2080-2099) values, as determined by L-moments regional frequency analysis for Paris, IL, expressed as a percent difference. Highlighted values are significant.

Paris, IL	0.5 yr	1 yr	2 yr	5 yr	10 yr	25 yr	50 yr	100 yr
1-hr	**30.7%**	**24.2%**	20.3%	17.0%	15.4%	14.1%	13.7%	13.6%
2-hr	**22.8%**	**20.6%**	17.5%	14.4%	13.4%	14.0%	15.8%	18.5%
3-hr	**32.4%**	**24.8%**	**20.7%**	17.7%	16.8%	16.7%	17.5%	18.8%
6-hr	**36.1%**	**36.6%**	**34.7%**	**30.8%**	**27.2%**	21.6%	16.9%	11.7%
12-hr	**30.1%**	**35.9%**	**34.6%**	**29.9%**	**26.2%**	22.1%	19.8%	18.0%
24-hr	12.4%	18.9%	**26.1%**	**28.2%**	**24.9%**	16.3%	8.0%	-1.3%
2-day	8.3%	18.0%	**26.8%**	**29.2%**	**25.7%**	17.2%	9.2%	0.5%
5-day	22.5%	**29.5%**	**33.1%**	**33.6%**	**31.6%**	**26.2%**	20.7%	14.0%
10-day	17.2%	21.0%	**21.5%**	**22.5%**	**24.1%**	**27.2%**	**30.1%**	**33.3%**
2080-2099								
Paris, IL	0.5 yr	1 yr	2 yr	5 yr	10 yr	25 yr	50 yr	100 yr
1-hr	**57.9%**	**55.9%**	**52.2%**	**46.3%**	**41.2%**	**33.6%**	**27.4%**	20.6%
2-hr	**59.8%**	**58.7%**	**55.0%**	**49.9%**	**46.7%**	**43.7%**	**42.3%**	**41.6%**
3-hr	**51.1%**	**53.3%**	**54.7%**	**53.3%**	**49.7%**	**42.0%**	**34.4%**	**25.3%**
6-hr	**57.0%**	**56.5%**	**56.1%**	**55.7%**	**55.4%**	**55.0%**	**54.7%**	**54.4%**
12-hr	**48.7%**	**53.9%**	**53.5%**	**50.9%**	**49.1%**	**47.8%**	**47.8%**	**48.5%**
24-hr	**42.1%**	**49.0%**	**52.6%**	**54.4%**	**54.4%**	**53.3%**	**51.8%**	**49.8%**
2-day	**35.9%**	**42.6%**	**46.1%**	**49.9%**	**53.1%**	**58.3%**	**63.0%**	**68.2%**
5-day	**38.3%**	**45.8%**	**50.9%**	**54.1%**	**54.3%**	**52.3%**	**49.2%**	**45.1%**
10-day	**27.7%**	**35.2%**	**39.9%**	**44.0%**	**46.2%**	**48.5%**	**49.8%**	**51.0%**

Table B.10. Changes in precipitation frequency estimates between observed (1980-1999) and projected MRI (2040-2059 and 2080-2099) values, as determined by L-moments regional frequency analysis for Columbus, IN, expressed as a percent difference. Highlighted values are significant.

2040-2059								
Columbus, IN	0.5 yr	1 yr	2 yr	5 yr	10 yr	25 yr	50 yr	100 yr
1-hr	-11.5%	-7.5%	-5.4%	-2.6%	0.6%	6.7%	12.4%	19.1%
2-hr	-14.7%	-14.3%	-11.5%	-6.1%	-1.0%	6.7%	13.1%	19.9%
3-hr	-9.1%	-11.1%	-9.3%	-3.9%	1.8%	11.1%	19.2%	**28.0%**
6-hr	-3.2%	-1.0%	2.8%	9.1%	14.6%	22.6%	**29.0%**	**35.8%**
12-hr	-2.4%	3.3%	7.5%	12.2%	15.4%	19.4%	22.2%	**25.0%**
24-hr	2.9%	4.6%	6.1%	8.0%	9.5%	11.5%	13.0%	14.5%
2-day	1.1%	2.2%	3.6%	5.7%	7.5%	10.1%	12.1%	14.3%
5-day	-5.2%	-1.8%	-0.9%	0.4%	2.4%	6.4%	10.4%	15.0%
10-day	0.4%	-2.6%	-7.4%	-7.8%	-4.3%	3.5%	10.4%	17.9%
2080-2099								
Columbus, IN	0.5 yr	1 yr	2 yr	5 yr	10 yr	25 yr	50 yr	100 yr
1-hr	**38.9%**	**47.2%**	**50.0%**	**51.8%**	**53.2%**	**55.9%**	**58.5%**	**61.6%**
2-hr	**38.2%**	**43.6%**	**48.4%**	**54.2%**	**58.5%**	**64.0%**	**68.1%**	**72.1%**
3-hr	**36.5%**	**41.2%**	**46.9%**	**55.0%**	**61.4%**	**70.3%**	**77.1%**	**84.0%**
6-hr	**32.3%**	**34.5%**	**38.7%**	**45.4%**	**51.2%**	**59.5%**	**66.2%**	**73.1%**
12-hr	22.3%	**28.6%**	**34.7%**	**42.6%**	**48.7%**	**56.8%**	**62.9%**	**69.2%**
24-hr	21.8%	24.6%	**28.5%**	**34.6%**	**39.8%**	**47.1%**	**53.0%**	**59.2%**
2-day	19.4%	23.4%	**27.6%**	**33.1%**	**37.4%**	**43.3%**	**47.9%**	**52.6%**
5-day	19.1%	23.1%	24.1%	**25.5%**	**27.3%**	**30.9%**	**34.5%**	**38.7%**
10-day	20.8%	17.7%	13.4%	14.9%	20.7%	**32.0%**	**41.8%**	**52.2%**

Table B.11. Changes in precipitation frequency estimates between observed (1980-1999) and projected MRI (2040-2059 and 2080-2099) values, as determined by L-moments regional frequency analysis for Grayling, MI, expressed as a percent difference. Highlighted values are significant.

2040-2059								
Grayling, MI	0.5 yr	1 yr	2 yr	5 yr	10 yr	25 yr	50 yr	100 yr
1-hr	-9.1%	-0.3%	4.5%	9.8%	14.4%	22.0%	**28.6%**	**35.9%**
2-hr	-12.8%	-3.4%	5.3%	16.0%	23.9%	**34.3%**	**42.0%**	**49.7%**
3-hr	-6.4%	-1.8%	1.6%	5.1%	7.5%	10.3%	12.2%	14.1%
6-hr	-3.2%	-0.5%	4.2%	12.0%	18.8%	**28.9%**	**36.9%**	**45.3%**
12-hr	-5.6%	-4.9%	-1.1%	6.6%	13.9%	**25.1%**	**34.4%**	**44.4%**
24-hr	-5.5%	-0.4%	4.7%	11.5%	16.8%	**24.1%**	**29.7%**	**35.5%**
2-day	-4.8%	-0.7%	5.0%	13.6%	20.9%	**31.4%**	**39.7%**	**48.2%**
5-day	3.6%	8.6%	12.3%	17.6%	22.6%	**31.1%**	**38.7%**	**47.2%**
10-day	-0.2%	14.2%	17.6%	18.4%	19.5%	22.9%	**26.8%**	**31.7%**
2080-2099								
Grayling, MI	0.5 yr	1 yr	2 yr	5 yr	10 yr	25 yr	50 yr	100 yr
1-hr	**32.0%**	**41.5%**	**45.7%**	**49.6%**	**52.9%**	**58.2%**	**62.9%**	**68.1%**
2-hr	23.1%	**33.9%**	**43.7%**	**55.6%**	**64.2%**	**75.2%**	**83.2%**	**91.0%**
3-hr	15.5%	25.2%	**33.4%**	**43.0%**	**49.7%**	**58.3%**	**64.6%**	**70.6%**
6-hr	11.0%	22.0%	**32.2%**	**45.0%**	**54.3%**	**66.3%**	**74.9%**	**83.4%**
12-hr	-0.7%	10.3%	21.4%	**36.1%**	**47.2%**	**61.9%**	**72.6%**	**83.2%**
24-hr	0.9%	13.4%	**24.5%**	**37.9%**	**47.6%**	**60.2%**	**69.3%**	**78.3%**
2-day	3.7%	15.0%	**26.2%**	**39.5%**	**48.0%**	**57.3%**	**62.9%**	**67.6%**
5-day	7.0%	14.2%	23.8%	**35.9%**	**43.8%**	**52.4%**	**57.6%**	**62.0%**
10-day	8.4%	19.3%	**26.3%**	**33.3%**	**38.2%**	**44.6%**	**49.4%**	**54.1%**

Table B.12. Changes in precipitation frequency estimates between observed (1980-1999) and projected MRI (2040-2059 and 2080-2099) values, as determined by L-moments regional frequency analysis for Paris, IL, expressed as a percent difference. Highlighted values are significant.

2040-2059								
Paris, IL	0.5 yr	1 yr	2 yr	5 yr	10 yr	25 yr	50 yr	100 yr
1-hr	**32.0%**	**36.7%**	**39.9%**	**43.1%**	**45.1%**	**47.4%**	**49.0%**	**50.5%**
2-hr	**33.7%**	**38.4%**	**40.5%**	**43.3%**	**46.3%**	**51.7%**	**56.8%**	**62.7%**
3-hr	**42.7%**	**47.1%**	**50.0%**	**52.8%**	**54.5%**	**56.5%**	**57.8%**	**59.0%**
6-hr	**40.8%**	**47.6%**	**52.0%**	**54.5%**	**54.1%**	**50.9%**	**46.9%**	**41.6%**
12-hr	**34.8%**	**44.6%**	**45.7%**	**43.5%**	**41.5%**	**39.4%**	**38.4%**	**37.9%**
24-hr	**27.3%**	**34.4%**	**36.4%**	**36.8%**	**37.0%**	**37.7%**	**38.6%**	**40.0%**
2-day	23.2%	**28.2%**	**29.8%**	**30.7%**	**31.7%**	**33.9%**	**36.2%**	**39.1%**
5-day	21.9%	18.3%	17.0%	16.9%	17.6%	19.4%	21.3%	**23.6%**
10-day	18.1%	15.8%	14.9%	14.7%	14.7%	15.0%	15.2%	15.4%
2080-2099								
Paris, IL	0.5 yr	1 yr	2 yr	5 yr	10 yr	25 yr	50 yr	100 yr
1-hr	17.0%	**26.8%**	**31.3%**	**34.3%**	**35.3%**	**35.5%**	**35.1%**	**34.3%**
2-hr	**26.3%**	**36.4%**	**41.6%**	**44.8%**	**45.7%**	**45.9%**	**45.4%**	**44.6%**
3-hr	**39.1%**	**48.7%**	**50.9%**	**49.8%**	**47.3%**	**42.6%**	**38.0%**	**32.8%**
6-hr	**28.7%**	**35.9%**	**36.6%**	**34.1%**	**30.8%**	**25.1%**	20.0%	14.3%
12-hr	**27.3%**	**34.0%**	**33.7%**	**30.6%**	**28.2%**	**26.0%**	25.1%	24.8%
24-hr	14.6%	21.3%	**25.3%**	**28.1%**	**29.1%**	**29.3%**	**28.9%**	**28.2%**
2-day	16.5%	22.5%	**24.1%**	**24.3%**	**24.5%**	**25.4%**	**26.6%**	**28.2%**
5-day	6.6%	5.8%	4.8%	3.3%	2.1%	0.4%	-0.9%	-2.4%
10-day	11.2%	7.6%	5.8%	4.6%	4.2%	4.1%	4.2%	4.4%

Appendix C: Additional Data from Chapter 7

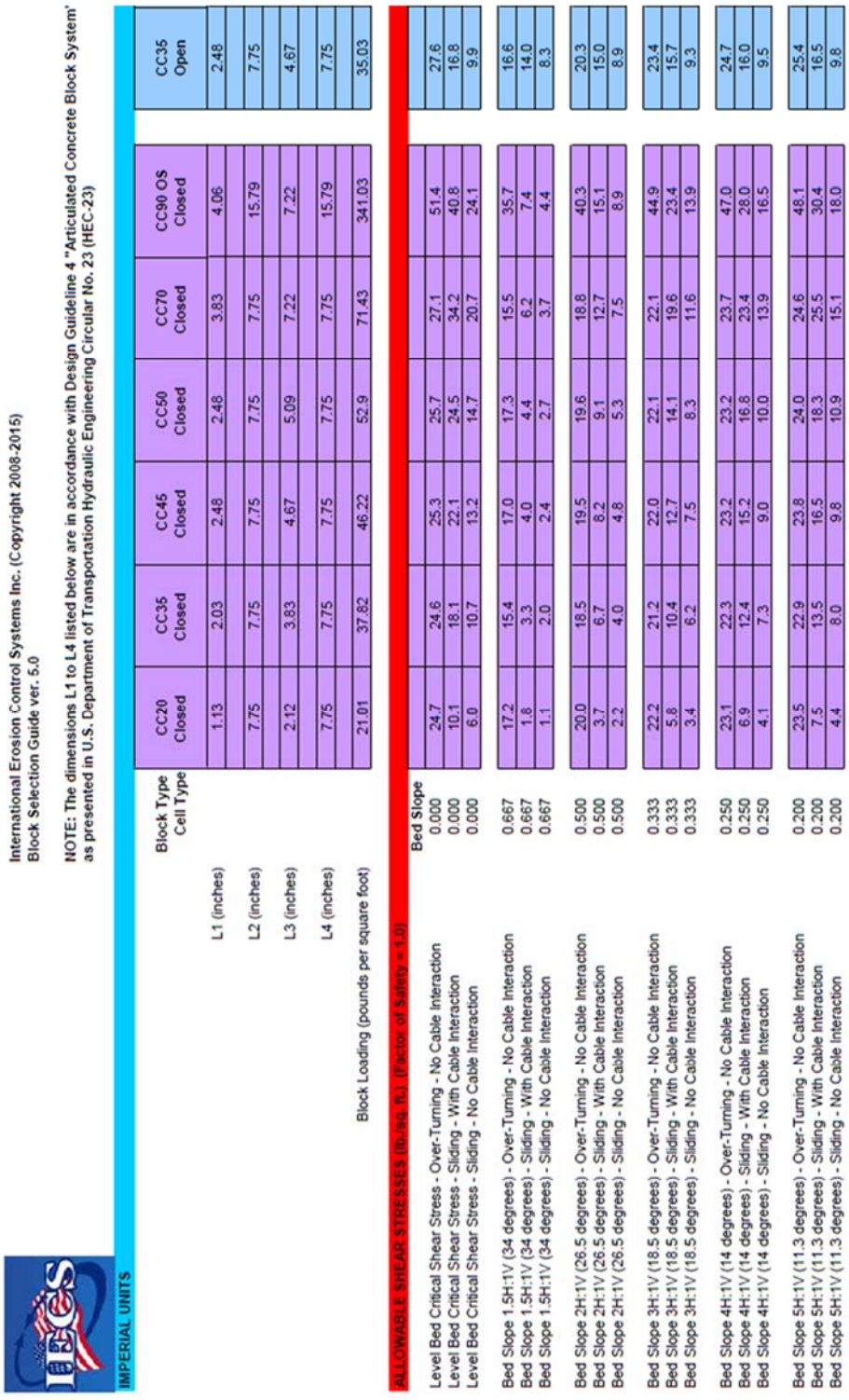

International Erosion Control Systems Inc. (Copyright 2008-2015)
Block Selection Guide ver. 5.0

NOTE: The dimensions L1 to L4 listed below are in accordance with Design Guideline 4 "Articulated Concrete Block System" as presented in U.S. Department of Transportation Hydraulic Engineering Circular No. 23 (HEC-23)

IMPERIAL UNITS

Block Type / Cell Type	CC20 Closed	CC35 Closed	CC45 Closed	CC50 Closed	CC70 Closed	CC90 OS Closed	CC35 Open
L1 (inches)	1.13	2.03	2.48	2.48	3.83	4.06	2.48
L2 (inches)	7.75	7.75	7.75	7.75	7.75	15.79	7.75
L3 (inches)	2.12	3.83	4.67	5.09	7.22	7.22	4.67
L4 (inches)	7.75	7.75	7.75	7.75	7.75	15.79	7.75
Block Loading (pounds per square foot)	21.01	37.82	46.22	52.9	71.43	341.03	35.03
ALLOWABLE SHEAR STRESSES (lb./sq. ft.) (Factor of Safety = 1.0)	**Bed Slope**						
Level Bed Critical Shear Stress - Over-Turning - No Cable Interaction	0.000	24.7	24.6	25.3	25.7	27.1	51.4	27.6
Level Bed Critical Shear Stress - Sliding - With Cable Interaction	0.000	10.1	18.1	22.1	24.5	34.2	40.8	16.8
Level Bed Critical Shear Stress - Sliding - No Cable Interaction	0.000	6.0	10.7	13.2	14.7	20.7	24.1	9.9
Bed Slope 1.5H:1V (34 degrees) - Over-Turning - No Cable Interaction	0.667	17.2	15.4	17.0	17.3	15.5	35.7	16.6
Bed Slope 1.5H:1V (34 degrees) - Sliding - With Cable Interaction	0.667	1.8	3.3	4.0	4.4	6.2	7.4	14.0
Bed Slope 1.5H:1V (34 degrees) - Sliding - No Cable Interaction	0.667	1.1	2.0	2.4	2.7	3.7	4.4	8.3
Bed Slope 2H:1V (26.5 degrees) - Over-Turning - No Cable Interaction	0.500	20.0	18.5	19.5	19.6	18.8	40.3	20.3
Bed Slope 2H:1V (26.5 degrees) - Sliding - With Cable Interaction	0.500	3.7	6.7	8.2	9.1	12.7	15.1	15.0
Bed Slope 2H:1V (26.5 degrees) - Sliding - No Cable Interaction	0.500	2.2	4.0	4.8	5.3	7.5	8.9	8.9
Bed Slope 3H:1V (18.5 degrees) - Over-Turning - No Cable Interaction	0.333	22.2	21.2	22.0	22.1	22.1	44.9	23.4
Bed Slope 3H:1V (18.5 degrees) - Sliding - With Cable Interaction	0.333	5.8	10.4	12.7	14.1	19.6	23.4	15.7
Bed Slope 3H:1V (18.5 degrees) - Sliding - No Cable Interaction	0.333	3.4	6.2	7.5	8.3	11.6	13.9	9.3
Bed Slope 4H:1V (14 degrees) - Over-Turning - No Cable Interaction	0.250	23.1	22.3	23.2	23.2	23.7	47.0	24.7
Bed Slope 4H:1V (14 degrees) - Sliding - With Cable Interaction	0.250	6.9	12.4	15.2	16.8	23.4	28.0	16.0
Bed Slope 4H:1V (14 degrees) - Sliding - No Cable Interaction	0.250	4.1	7.3	9.0	10.0	13.9	16.5	9.5
Bed Slope 5H:1V (11.3 degrees) - Over-Turning - No Cable Interaction	0.200	23.5	22.9	23.8	24.0	24.6	48.1	25.4
Bed Slope 5H:1V (11.3 degrees) - Sliding - With Cable Interaction	0.200	7.5	13.5	16.5	18.3	25.5	30.4	16.5
Bed Slope 5H:1V (11.3 degrees) - Sliding - No Cable Interaction	0.200	4.4	8.0	9.8	10.9	15.1	18.0	9.8

Figure C.1. Cable-Concrete block selection guide.